



**UNIVERSIDADE TÉCNICA DE LISBOA
INSTITUTO SUPERIOR TÉCNICO**



**HYDROMECHANICAL BEHAVIOUR OF CONCRETE DAM
FOUNDATIONS. *IN SITU* TESTS AND NUMERICAL MODELLING**

Maria Luísa Mendes de Vasconcelos Braga Farinha
(Mestre)

Dissertação elaborada no Laboratório Nacional de Engenharia Civil para
obtenção do Grau de Doutor em Engenharia Civil pela Universidade Técnica de
Lisboa no âmbito do protocolo de cooperação entre o IST e o LNEC

Orientador: Doutor José Antero Senra Vieira de Lemos
Co-Orientador: Doutor Emanuel Leandro Maranhã das Neves

Júri

Presidente: Presidente do Conselho Científico do IST

Vogais: Doutor Eduardo Alonso Péres de Ágreda
Doutor Emanuel Leandro Maranhã das Neves
Doutor João José Rio Tinto de Azevedo
Doutora Laura Maria Mello Saraiva Caldeira
Doutor José Antero Senra Vieira de Lemos
Engenheiro Carlos Alberto de Brito Pina
Doutor António Manuel Barbot Campos e Matos

Abril 2010

Título: Comportamento hidromecânico de fundações de barragens de betão. Ensaios *in situ* e modelação numérica

Nome: Maria Luísa Mendes de Vasconcelos Braga Farinha

Doutoramento em Engenharia Civil

Orientador: Doutor José Vieira de Lemos

Co-orientador: Professor Doutor Emanuel Maranha das Neves

Resumo

Apresenta-se um estudo sobre o comportamento de fundações de barragens de betão na fase de exploração normal das obras desenvolvido com o objectivo de validar e fundamentar a aplicação de modelos numéricos de análise do comportamento hidromecânico de maciços rochosos, tendo em vista generalizar a sua utilização e tornar mais eficaz a observação e controlo de segurança destas obras.

Foi estudada a representação em modelos numéricos da cortina de impermeabilização e do sistema de drenagem e das condições geológico-geotécnicas concretas das zonas de fundação analisadas, tendo em conta, nomeadamente, os problemas computacionais associados a modelos tridimensionais. Foram realizados ensaios de afluência de água em duas grandes barragens portuguesas, uma gravidade e uma abóbada, que se verificou serem fundamentais para caracterizar o escoamento no maciço, complementando a informação obtida com o sistema de observação. Desenvolveram-se modelos hidráulicos e hidromecânicos do comportamento das fundações destas barragens, que no caso da barragem gravidade foram utilizados no estudo de cenários de rotura.

Apresentam-se conclusões sobre a adequação e limitação dos modelos numéricos utilizados, sobre os parâmetros essenciais para calibrar e aplicar esses modelos, e propõem-se métodos de planeamento e utilização dos sistemas de observação de fundações de barragens, de modo a melhorar o controlo de segurança.

Palavras chave: barragens de betão; fundações rochosas; ensaios de afluência de água; modelação numérica; comportamento hidromecânico; controlo/avaliação da segurança.

Title: Hydromechanical behaviour of concrete dam foundations. *In situ* tests and numerical modelling

Abstract

A study on the behaviour of concrete dam foundations in normal operating conditions was carried out with a view to validating and justifying the application of numerical models of hydromechanical analysis of rock masses, so that their use may become effective to make the analysis of the monitoring data and safety control of these structures more efficient.

Appropriate ways to model both grout curtains and drainage systems were analysed, as well as ways to represent the geological and geotechnical conditions of the foundation areas studied, namely taking into account the computational difficulties of three-dimensional models. *In situ* tests were carried out in two large Portuguese concrete dams, one gravity and one arch, which proved to be essential to provide detailed information on the hydraulic activity in the foundation, supplementing the available monitoring data. Hydraulic and hydromechanical models of both dams' foundation behaviour were developed, and used in the analysis of failure scenarios in the case of the gravity dam.

Conclusions are drawn about the suitability and limitations of the numerical models developed and the key parameters necessary to calibrate and use these models. Methods to design and use the foundation monitoring systems are proposed, for improvement of safety assessment.

Keywords: concrete dams; rock foundations; borehole water-inflow tests; numerical modelling; hydromechanical behaviour; safety assessment.

ACKNOWLEDGEMENTS

I would like to express my sincere thanks and gratitude to the President of the National Laboratory for Civil Engineering, Researcher Carlos Matias Ramos, to the Director of the Concrete Dams Department, Researcher Carlos Alberto de Brito Pina, and to the Head of the Monitoring Division, Dr. António Lopes Batista, for granting the time and team necessary to carry out this study, and to the following people, without whose help and support it would not have been possible:

Dr. José Vieira de Lemos, thesis supervisor, for his invaluable guidance and advice at all times, for always being available to discuss both the problems and the results, and for his continued encouragement and constructive criticism. I greatly appreciate not only his professional input and opinions, but also his friendship and personal support.

Professor Emanuel Maranha das Neves, thesis co-adviser, for giving me the benefit of his vast experience in geotechnical research in valuable advice and suggestions, and for his continued encouragement and kindness.

Technician Manuel Andrade, for his immeasurable and generous assistance on many occasions, for his untiring dedication and enthusiasm with the experimental work and for making *in situ* testing such an enjoyable experience, despite the difficult conditions.

Dr. António Tavares de Castro, for the fruitful discussions, for providing a second opinion on so many issues, and for his continued interest and friendship.

Julie Robinson, for her friendship and continued support, for her endless patience answering the same questions over and over, for always keeping me confident and for so many laughs at lunch time.

Dr. Laura Caldeira, Dr. José Muralha, Dr. Luís Lamas and Dr. João Bilé Serra for lending me various books and for providing valuable information, which made a significant contribution; Researcher António Silva Gomes, for the helpful discussions; and Dr. João Casaca, for his interest and encouragement.

Technicians Fernando Marques, Ricardo Oliveira and Francisco Morganho, with whom I spent weeks in dam drainage galleries without seeing the sunlight; technician Hernâni Brum for his precious support with the 3D drawings; and technician Maria Teresa Pereira, for her numerous visits to the library to get copies of journals.

My colleagues and friends Noemi Leitão, Jorge Pereira Gomes, Romano Câmara, Nuno Monteiro Azevedo, Eduardo Bretas, Sérgio Oliveira, Paulo Mendes, Ricardo Resende, José Mora Ramos, Juan Tomé Mata, José Piteira Gomes, João Amante, Fernando Garcia, António Tavares, Pedro Pavia Moreira, José Moreira, Hélder Vitória, Carlos Resende, José Carlos Nunes, Jorge Gião, Ana Vieira, Ana Cristina Ferreira, Madalena Barroso and Celeste Jorge, for their continued encouragement.

I would also like to thank EDIA, Empresa de Desenvolvimento e Infra-Estruturas do Alqueva, SA, for the permission to carry out *in situ* tests in both Alqueva and Pedrógão dams and to publish data relative to the monitoring of these dams.

Finally, I deeply thank my husband Luís and our children, Eduardo, Rodrigo and Miguel, for their tolerance and understanding over the last few years. I dedicate my work to them.

TABLE OF CONTENTS

1	Introduction	1
1.1	The role of the foundation in the safety of concrete dams	2
1.2	Objectives.....	4
1.3	Thesis outline	5
2	Concrete dam foundations. Hydromechanical behaviour and analysis.....	9
2.1	Introduction	9
2.2	Characterization of rock masses.....	9
2.2.1	Geological and hydrogeological investigations	10
2.2.2	Geotechnical investigations.....	15
2.3	Fundamentals of fluid flow in continuum media	15
2.3.1	Hydraulic head and hydraulic gradient	15
2.3.2	Extension of Darcy’s experimental law to three-dimensional flows	17
2.3.3	Laplace equation in homogeneous media	17
2.4	Hydromechanical behaviour of rock joints	19
2.4.1	Fluid flow in a single joint	19
2.4.2	Hydromechanical behaviour during joint normal closure.....	21
2.4.3	Hydromechanical behaviour during shear displacement	23
2.5	Specific features of concrete dam foundations	24
2.5.1	Grout curtains and drainage systems.....	25
2.5.2	Flow regime in concrete dam foundations	26
2.5.3	Main problems usually found in the behaviour of concrete dam foundations .	32
2.6	Numerical modelling.....	37
2.6.1	Continuum equivalent and discontinuum models	37
2.6.2	Models to study the hydraulic and hydromechanical behaviour of dam foundations.....	37
2.6.2.1	Analytical solutions and experimental techniques	37
2.6.2.2	Hydraulic models	39
2.6.2.3	Hydromechanical models.....	41
2.6.3	Numerical codes used in this study	43
3	Collection and evaluation of data on the behaviour of dam foundations	47
3.1	Introduction	47
3.2	Safety control criteria	49
3.3	Foundation monitoring	52

3.4	Methodologies used in the collecting and evaluation of the monitoring data.....	55
3.4.1	Collecting and collating of the monitoring data.....	55
3.4.2	Evaluation of the monitoring data.....	55
3.4.3	Quantitative interpretation methods.....	56
3.5	Quantitative interpretation of recorded discharges	60
3.5.1	Previous studies.....	60
3.5.2	This study	63
3.5.3	Variations in discharges due to variations in the reservoir level.....	64
3.5.4	Quantitative interpretation of discharges recorded in Alto Lindoso dam	68
3.5.4.1	Main characteristics of Alto Lindoso dam	68
3.5.4.2	Monitoring and hydraulic behaviour of the dam foundation	69
3.5.4.3	Quantitative interpretation of discharges recorded in a single drain.....	70
3.5.4.4	Quantitative interpretation of discharges recorded in seepage measuring weirs	78
3.5.5	Quantitative interpretation of discharges recorded in Alqueva dam.....	78
3.5.5.1	Main characteristics of Alqueva dam.....	78
3.5.5.2	Quantitative interpretation of discharges	78
3.6	Summary and conclusions.....	88
4	Borehole water-inflow tests	93
4.1	Introduction	93
4.2	Borehole water-inflow tests	94
4.2.1	Main aim and brief description of tests.....	94
4.2.2	Testing equipment.....	95
4.2.3	Preparation of tests and test procedures	96
4.2.4	Analysis of test results.....	98
4.2.5	Previous use of borehole water-inflow tests in Portuguese dams	100
4.2.5.1	Beliche dam.....	100
4.2.5.2	Santa Águeda dam (Marateca dam)	101
4.2.5.3	Funcho dam	101
4.3	Main characteristics of the dams where tests were carried out	102
4.3.1	Alqueva dam	103
4.3.1.1	General description of the dam	103
4.3.1.2	Geological-geotechnical conditions	106
4.3.1.3	Foundation treatment.....	109
4.3.1.4	Foundation behaviour monitoring.....	112
4.3.2	Pedrógão dam.....	114
4.3.2.1	General description of the dam	114
4.3.2.2	Geological-geotechnical conditions	114

4.3.2.3	Foundation treatment.....	116
4.3.2.4	Monitoring of foundation behaviour	117
4.3.2.5	Foundation hydraulic behaviour.....	119
4.4	Tests carried out in Pedrógão dam foundation.....	121
4.4.1	Preparation of tests	121
4.4.1.1	Area where tests were carried out	121
4.4.1.2	Analysis of geological and geotechnical information	122
4.4.1.3	Variation of discharges and water pressures	122
4.4.1.4	Stability analysis	125
4.4.2	Summary of experimental activity	125
4.4.3	Tests in drain D14	125
4.4.4	Tests in drain D18	133
4.4.5	Main difficulties found whilst carrying out tests	137
4.4.6	Conclusions drawn from tests carried out in Pedrógão dam foundation.....	137
4.5	Tests carried out in Alqueva dam foundation	138
4.5.1	Preparation of tests	138
4.5.1.1	Area where tests were carried out and variation of discharges and water pressures	138
4.5.1.2	Analysis of geological and geotechnical information	139
4.5.2	Summary of experimental activity	140
4.5.3	Tests in drain D25 D	141
4.5.4	Tests in piezometer PZB 13-2.....	145
4.5.5	Tests in drain D26 D	145
4.5.6	Tests in drain D27 D	146
4.5.7	Tests in drain D20 D	146
4.5.8	Additional tests.....	147
4.5.8.1	Water electrical conductivity analyses.....	147
4.5.8.2	Tests in drains located in the floor of the downstream drainage gallery branch excavated in the rock mass (GDJD).....	150
4.5.8.3	Closure of all the drains and piezometers located in block 17-18	152
4.5.8.4	Survey of piezometers	153
4.5.9	Conclusions drawn from tests carried out in Alqueva dam foundation	153
4.6	Summary and conclusions drawn from tests carried out <i>in situ</i>	154
5	Numerical modelling of seepage in concrete dam foundations	157
5.1	Introduction	157
5.2	Validation tests of the codes FLAC and 3DEC.....	158
5.2.1	Radial flow to a single well.....	158
5.2.1.1	Analytical solution	158

5.2.1.2	Geometry and boundary conditions	158
5.2.1.3	Axisymmetric model	159
5.2.1.4	Results analysis	162
5.2.1.5	Influence of the radius beyond which the drain has no influence	163
5.2.1.6	Influence of the drain diameter	163
5.2.2	Two-dimensional horizontal model of seepage in a concrete dam foundation	165
5.2.2.1	Analytical solution	166
5.2.2.2	Geometry and boundary conditions	168
5.2.2.3	Results analysis	169
5.2.3	Seepage in a horizontal layer	172
5.2.3.1	Influence of mesh size	172
5.2.3.2	Comparison between the results of 2D and 3D models	174
5.2.4	Unconfined steady state flow	176
5.3	Three-dimensional hydraulic models of concrete dam foundations	179
5.3.1	Introduction	179
5.3.2	Model characteristics.....	179
5.3.3	Influence of grout curtain permeability in a foundation with no drainage system	181
5.3.4	Influence of drainage.....	182
5.3.5	Influence of boundary conditions.....	185
5.3.6	Influence of grout curtain permeability.....	191
5.3.7	Influence of model size	192
5.3.8	Influence of mesh size.....	194
5.3.9	Comparison between the results of 2D and 3D models	195
5.3.10	Comparison between the average hydraulic head at the line of the drains calculated with the 3D model and with the 2D horizontal model.....	196
5.4	Conclusions	200
6	Analysis of seepage in Alqueva dam foundation	203
6.1	Introduction	203
6.2	Two-dimensional model of a vertical cross section at the bottom of the valley	204
6.2.1	Model description.....	204
6.2.2	Hydraulic boundary conditions and numerical results.....	205
6.2.3	Influence of the boundary distances used in the numerical model	213
6.3	Detailed three-dimensional model of a local area.....	215
6.3.1	Model description.....	215
6.3.2	Hydraulic boundary conditions and numerical results.....	218
6.3.3	Influence of mesh size.....	219

6.3.4	Use of single/double precision version	222
6.4	Numerical modelling of borehole water-inflow tests.....	225
6.4.1	Introduction	225
6.4.2	Numerical modelling of tests carried out in drain D25 D	226
6.4.2.1	Introduction	226
6.4.2.2	Hydraulic boundary conditions	228
6.4.2.3	Numerical experiments	228
6.4.2.4	Effect of local surface topography	237
6.4.3	Numerical modelling of tests carried out in drain D20 D	238
6.4.3.1	Introduction	238
6.4.3.2	Hydraulic boundary conditions	240
6.4.3.3	Numerical experiments	240
6.4.4	Conclusions	246
6.5	Parameter studies.....	247
6.5.1	Introduction	247
6.5.2	Influence of rock mass permeability	247
6.5.3	Influence of grout curtain permeability.....	249
6.5.4	Influence of higher rock mass permeability upstream from the dam.....	250
6.5.5	Influence of the permeability of the horizontal layers upstream from the drains.....	253
6.5.6	Influence of the width of higher permeability layers upstream from the drains.....	256
6.5.7	Influence of total or partial clogging of drain D24 D	259
6.5.8	Conclusions	260
6.6	Global three-dimensional hydraulic model	261
6.6.1	Model description.....	261
6.6.2	Hydraulic boundary conditions	265
6.6.3	Results analysis	265
6.7	Hydromechanical interaction in the foundation of Alqueva dam	272
6.7.1	Introduction	272
6.7.2	Comparison of numerical and recorded discharges with the reservoir at different elevations.....	273
6.7.3	Numerical mechanical model.....	276
6.7.3.1	Model description.....	276
6.7.3.2	Material properties	278
6.7.3.3	Sequence of analysis	280
6.7.3.4	Results analysis	283
6.7.3.5	Comparison of monitored and numerical results	291

6.7.4	Hydromechanical interaction	297
6.7.4.1	Introduction	297
6.7.4.2	Correlation between stress and permeability	297
6.7.4.3	Correlation between permeability and local rock mass deformability.....	306
6.7.4.4	Discussion	307
6.7.4.5	Summary and conclusions.....	309
6.8	Piezometric measurements in concrete dam foundations	311
6.8.1	Introduction	311
6.8.2	Model description.....	314
6.8.3	Hydraulic boundary conditions	316
6.8.4	Results analysis	316
6.8.4.1	Analysis of discharges and hydraulic heads.....	316
6.8.4.2	Analysis of flow through discontinuity networks	333
6.8.5	Conclusions and discussion.....	337
6.9	Summary and conclusions.....	341
7	Analysis of seepage and stability assessment – the case study of Pedrógão dam ...	345
7.1	Introduction	345
7.2	Two-dimensional model of vertical cross sections based on the hypothesis of an equivalent continuum media.....	346
7.2.1	Model description.....	346
7.2.2	Hydraulic boundary conditions and numerical results.....	347
7.3	Two-dimensional discontinuum model.....	351
7.3.1	Fluid flow analysis with UDEC	351
7.3.2	Model description.....	352
7.3.3	Sequence of analysis	353
7.3.4	Results analysis	356
7.3.4.1	Stresses and displacements due to both rock mass and dam weight.....	356
7.3.4.2	Hydrostatic loading	356
7.3.4.3	Fluid flow analysis	358
7.3.4.4	Normal displacements and hydraulic aperture along the dam/foundation joint	361
7.3.4.5	Water pressures along the dam/foundation joint and along the joint of higher permeability	366
7.3.4.6	Joint dilatancy	367
7.3.5	Comparison of monitored and numerical hydraulic heads at the piezometers located underneath the stilling basin.....	370
7.4	Stability analysis	374
7.4.1	Introduction	374

7.4.2	Main accident scenarios of different dam types	374
7.4.2.1	Gravity dams	374
7.4.2.2	Buttress dams	375
7.4.2.3	Arch dams	376
7.4.2.4	Other types of dams.....	376
7.4.3	Stability analysis methods for gravity dams	377
7.4.4	Stability analysis of Pedrógão dam	380
7.4.4.1	Limit equilibrium approach.....	380
7.4.4.2	Strength reduction method	386
7.4.4.3	Comparison of the UDEC results with those obtained using the limit equilibrium method	390
7.5	Conclusions	394
8	Conclusions	397
8.1	Summary and conclusions.....	397
8.2	Further developments	403
	References	405
	Appendix 1	427
A1.1	Equipment required to carry out borehole water-inflow tests	427
A1.2	Equipment geometry. Total length of pipes in each test interval	429
A1.3	Test procedures.....	431
A1.4	Measurements taken while carrying out borehole water-inflow tests in both Pedrógão and Alqueva dams	435
A1.5	Electrical conductivity of water and temperature profiles	453
A1.6	Measurements taken when all the drains and piezometers located in block 17-18 were closed.....	475

LIST OF FIGURES

Figure 2.1 – Intervals, symbols and descriptive terms used in the Basic Geotechnical Description of Rock Masses (BGD) (ISRM 1981).	11
Figure 2.2 – Weathering classification (adapted from ISRM 1978).	11
Figure 2.3 – Typical mechanical (a) and hydromechanical (b) fracture responses under normal closure. Effects of sample size is indicated with the laboratory sample response (dashed lines) compared with in-situ fracture response (1 m ² size) (adapted from Rutqvist and Stephansson 2003).	22
Figure 2.4 – Typical mechanical (a) and hydromechanical (b) fracture responses under shear stress. Effects of sample size is indicated with the laboratory sample response (dashed lines) compared with in-situ fracture response (1 m ² size) (adapted from Rutqvist and Stephansson 2003).	23
Figure 2.5 – Grout curtains and drainage systems in concrete dam foundations.	25
Figure 2.6 – Laws for 1-dimensional flow in a fissure, presented by Louis (1969) (after Goodman et al. 1983).	27
Figure 2.7 – Transition from laminar to turbulent flow (after Franciss 1970).	28
Figure 2.8 – Flow through a slope. Comparison of the results from a model test and from computations: a) distribution of piezometric head; b) flow conditions; and c) seepage water discharges (after Wittke 1990).	29
Figure 2.9 – Flow into a tunnel. Comparison of the results from a model test and from computations: a) details of problem; b) distribution of piezometric head; and c) states of flow (after Wittke 1990).	30
Figure 2.10 - Failure at the Malpasset dam, in France, in 1959: a) Londe’s hypothesis (after Rutqvist and Stephansson 2003), and b) Wittke’s modified hypothesis (after Wittke 1990).	33
Figure 2.11 – Portuguese dams which had problems due to foundation deterioration.	35
Figure 3.1 – Monitoring deformations in concrete dam rock foundations (after ICOLD 2005).	53
Figure 3.2 – Monitoring seepage flow and water pressures in concrete dam rock foundations (after ICOLD 2005).	54
Figure 3.3 - Results of quantitative interpretation of discharges in drains located in a) Cabril dam and b) Venda Nova dam, and comparison with recorded discharges (adapted from Gomes and Matos 1985).	61
Figure 3.4 - Comparison of the discharges recorded close to the Itaipu dam spillway with the results of a quantitative interpretation (adapted from Guedes and Coelho 1985).	62
Figure 3.5 – Model of a concrete gravity dam on a jointed rock foundation.	65

Figure 3.6 – Variations in discharges due to variations in the water level in the reservoir, taking into account the coupled hydromechanical behaviour of foundation rock masses, for different discontinuities’ normal stiffness: a) numerical discharges; b) numerical discharges divided, in each case, by the highest discharge.	66
Figure 3.7 – Adjustment of polynomial curves to the numerical results.	67
Figure 3.8 - Variations in discharges during a load/unload cycle.	68
Figure 3.9 – Drainage and piezometric systems in the foundation of Alto Lindoso dam.	70
Figure 3.10 – Variation in the reservoir level and recorded discharges in the measuring weirs.	70
Figure 3.11 – Recorded discharges and water pressures in the foundation of block 10-11.	71
Figure 3.12 – Quantitative interpretation of discharges in drain D10/11.1 (first interpretation).	73
Figure 3.13 – Quantitative interpretation of discharges in drain D10/11.1 (second interpretation).	74
Figure 3.14 – Quantitative interpretation of discharges in drain D10/11.1 (third interpretation).	75
Figure 3.15 – Quantitative interpretation of discharges in drain D10/11.1 (fourth interpretation).	76
Figure 3.16 – Quantitative interpretation of discharges in drain D10/11.1 (fifth interpretation).	77
Figure 3.17 – Quantitative interpretation of discharges recorded in seepage measuring weir 3 (first interpretation).	79
Figure 3.18 – Quantitative interpretation of discharges recorded in seepage measuring weir 3 (second interpretation).	80
Figure 3.19 – Quantitative interpretation of discharges recorded in seepage measuring weir 3 (third interpretation).	81
Figure 3.20 – Quantitative interpretation of discharges recorded in seepage measuring weir 3 (fourth interpretation).	82
Figure 3.21 – Recorded discharges in the bottom of the valley and in drain D25 D.	83
Figure 3.22 – Quantitative interpretation of discharges in drain D25 D.	84
Figure 3.23 – Quantitative interpretation of discharges in the valley bottom (first interpretation).	85
Figure 3.24 – Quantitative interpretation of discharges in the valley bottom (second interpretation).	86
Figure 3.25 – Quantitative interpretation of discharges in the valley bottom (third interpretation).	87
Figure 3.26 – Variations in both reservoir level and total discharges recorded with an automated system (a) and comparison of the total discharges with the part due to variations in hydrostatic pressure obtained in a quantitative interpretation (b).	89

Figure 4.1 – Positioning of packers in the successive steps of borehole water-inflow tests...	94
Figure 4.2 – Common difficulties when carrying out hydraulic tests: a) leakage at the packer; b) flow around the packer (adapted from Wittke 1990).....	97
Figure 4.3 – Main parts of the equipment.	97
Figure 4.4 – Portuguese dams where borehole water-inflow tests were carried out.....	101
Figure 4.5 – Layout of Alqueva dam.	104
Figure 4.6 – Alqueva dam. Downstream view from the left abutment.....	104
Figure 4.7 – Upstream elevation of Alqueva dam.	105
Figure 4.8 – Central cross section of Alqueva dam.	105
Figure 4.9 – Foundation plinth and peripheral joint at the heel of blocks in the valley bottom.....	105
Figure 4.10 – Average position of the main sets of rock joints in relation to the dam.	108
Figure 4.11 – Faults in Alqueva dam foundation.....	108
Figure 4.12 – Treatment of fault 22 (design drawings): a) layout of treatment (areas to be treated and access paths); b) cross sections in the upstream-downstream direction; c) cross section along the dam axis (adapted from Liberal et al. 2002).....	109
Figure 4.13 – Drainage system in Alqueva dam foundation.....	111
Figure 4.14 – Inverted plumb-lines in Alqueva dam.	113
Figure 4.15 – Borehole (rod) and incremental extensometers in Alqueva dam foundation.	113
Figure 4.16 – Piezometric network in Alqueva dam foundation.	113
Figure 4.17 – Pedrógão dam. Upstream and downstream view from the left side of the uncontrolled spillway.	115
Figure 4.18 – Downstream elevation and plan of Pedrógão dam.	115
Figure 4.19 – Average position of the main sets of rock joints in relation to the dam.	117
Figure 4.20 – Areas of weak geomechanical properties and of highest permeability in the foundation of Pedrógão dam.	118
Figure 4.21 – Cross sections of Pedrógão dam.	118
Figure 4.22 – Partial and total flow rates through the foundation.....	120
Figure 4.23 – Discharges and average value of the percentage of hydraulic head in the foundation (04.04.2006, $H_{\text{reservoir}} = 84.71\text{m}$).	120
Figure 4.24 – Water pressures along the upstream-downstream direction recorded on 04.04.2006.....	121
Figure 4.25 – Location of drains and piezometric boreholes in the foundation of block 6-7 and of block 7-8, close to dam vertical joint 7.....	123
Figure 4.26 – Recorded discharges in the foundation of block 6-7.	124
Figure 4.27 – Recorded water pressures in piezometers and piezodrains located in the foundation of block 6-7.....	124

Figure 4.28 – Test steps in borehole D14.....	127
Figure 4.29 – Borehole water inflow tests.	130
Figure 4.30 – Discharges in the equipment placed in drain D14’s area of influence during the water-inflow tests.	131
Figure 4.31 – Water pressures in the equipment placed in drain D14’s area of influence during the water-inflow tests.....	131
Figure 4.32 – Discharge flowing into each of drain’s D14 test intervals (a) and accumulated discharge from the bottom to the head of the borehole (b), compared with the reference discharge.....	132
Figure 4.33 – Discharge coming into the borehole section between the packer and the drain head (a) and variation of water pressure along drain D14 (b).	132
Figure 4.34 – Test steps in borehole D18.....	134
Figure 4.35 – Discharge flowing into each of borehole’s D18 test intervals (a) and accumulated discharge from the bottom to the head of the borehole (b), compared with the reference discharge.....	135
Figure 4.36 – Discharge coming into the borehole section between the packer and the drain head (a) and variation of water pressure along borehole D18 (b).....	135
Figure 4.37 – Recorded discharges and water pressures in the foundation of block 17-18..	138
Figure 4.38 – Location of drains and piezometric boreholes in the foundation of blocks 16-17, 17-18 and 18-19.	139
Figure 4.39 – Electrical conductivity of water and temperature profiles along drain D25 D.	143
Figure 4.40 – Water pressure variation at the different test intervals after being closed.....	143
Figure 4.41 – Inserting the conductivity probe inside the borehole and a clogged borehole.	148
Figure 4.42 – Inflow of water into each borehole in the bottom of the valley and in the first two blocks at the base of the slope, on the right bank.	149
Figure 4.43 – Top of the extension of the downstream drainage gallery towards the right bank.	150
Figure 4.44 – Geological-geotechnical characterization of GDJD’s floor (adapted from EDP 2006), with an approximate location of tested boreholes.	151
Figure 5.1 – Radial flow in a horizontal aquifer confined between impervious strata (artesian flow) (adapted from USACE 1993).	159
Figure 5.2 – Meshes adopted for numerical analysis with FLAC (axisymmetric model). ...	160
Figure 5.3 – Piezometric heads in the radial direction. Numerical values (×) compared to the analytical solution (.....).	161
Figure 5.4 – Drain modelled by its diameter. Difference between numerical discharge and the analytical solution with an increase in the number of mesh elements.....	162
Figure 5.5 – Seepage in a dam foundation: numerical model (after Andrade 1982).	167

Figure 5.6 – Cross section of Alqueva dam central cantilever (assuming a vertical drainage curtain). Horizontal plane in which flow is analysed.	168
Figure 5.7 – Complete mesh and detail of meshes in the vicinity of the drain for numerical analysis of the horizontal plane flow problem.	169
Figure 5.8 – Variations in the hydraulic head along five lines (meshes a) and c)): 1 – line of drains; 2 – line perpendicular to line of drains, that crosses one drain; 3 – line perpendicular to line of drains, midway between drains; 4 – line parallel to line of drains, about 1 m upstream; 5 – line parallel to line of drains, about 1 m downstream.	170
Figure 5.9 – Horizontal seepage flow: a) mesh used in the 2D model and b) schematic view of the domain in the 3D model (division into blocks and internal mesh).	173
Figure 5.10 – Comparison between variations in the hydraulic head along the line of drains in the 2D and 3D models.	174
Figure 5.11 – Comparison between variations in the hydraulic head along the line perpendicular to the line of drains, which crosses one drain, in the 2D and 3D models.	175
Figure 5.12 – Comparison between variations in the hydraulic head along the line perpendicular to the line of drains, midway between drains, in the 2D and 3D models.	175
Figure 5.13 – The Dupuit assumptions. Unconfined steady state flow between two reservoirs (after Bear 1988).	177
Figure 5.14 – Different meshes used in the analysis of unconfined steady state flow: a) and b) standard meshes generated from the average edge length of the tetrahedral-shaped zones; c) and d) regular meshes, generated from the number of divisions along each axis.	178
Figure 5.15 – 3D <i>small model</i> . Division into blocks and internal mesh.	180
Figure 5.16 – 3D <i>large model</i> . Division into blocks and internal mesh.	180
Figure 5.17 – <i>Small model</i> . Comparison of hydraulic head contours with and without drainage.	184
Figure 5.18 – <i>Small model</i> . Different boundary conditions.	185
Figure 5.19 – Hydraulic head contours with two different boundary conditions and different $k_{\text{grout curtain}}/k_{\text{rock mass}}$	187
Figure 5.20 – <i>Small model</i> . Variation in hydraulic head along 50 m long vertical lines for the two different boundary conditions (assuming that the grout curtain permeability is 10 times lower than that of the rock mass).	188
Figure 5.21 – Schematic representation of boundary conditions and hydraulic head contours for $H_u = 143.0$ m and $H_d = 75.0$ m, with $k_{\text{grout curtain}} = 0.01 k_{\text{rock mass}}$	190
Figure 5.22 – Variation of the hydraulic head along 50 m long vertical lines assuming that the lateral and bottom boundaries and the dam/foundation interface are impervious. .	191
Figure 5.23 – 3D model. Hydraulic head contours ($H_{\text{upstream}} = 143.0$ m; $H_{\text{downstream}} = 75.0$ m).	192

Figure 5.24 – Hydraulic head at the drainage line.	197
Figure 6.1 – Foundation numerical model.	205
Figure 6.2 – Detail of the foundation numerical model. Geometry, materials and gridpoints with fixed water pressure (boundary conditions).	206
Figure 6.3 – Hydraulic head contours ((m) for $H_{\text{upstream}} = 145.01$ m and $H_{\text{downstream}} = 80.60$ m).	208
Figure 6.4 – Seepage velocity in the foundation ((m/s) for $H_{\text{upstream}} = 145.01$ m and $H_{\text{downstream}} = 80.60$ m).	208
Figure 6.5 – Variations of piezometric head along the line where the piezometers are positioned at the base of the central cantilever.	209
Figure 6.6 – Hydraulic head contours ((m) for $H_{\text{upstream}} = 145.01$ m and $H_{\text{downstream}} = 80.60$ m and with the grout curtains' hydraulic conductivity 10 times lower than the hydraulic conductivity of the foundation's most pervious area).	210
Figure 6.7 – Seepage velocity in the foundation ((m/s) for $H_{\text{upstream}} = 145.01$ m and $H_{\text{downstream}} = 80.60$ m and with the grout curtains' hydraulic conductivity 10 times lower than the hydraulic conductivity of the foundation's most pervious area).	210
Figure 6.8 – Variations of piezometric head along the line where the piezometers are positioned at the base of the central cantilever (grout curtains' hydraulic conductivity 10 times lower than the hydraulic conductivity of the foundation's most pervious area).	211
Figure 6.9 – Hydraulic head contours ((m) for $H_{\text{upstream}} = 145.01$ m and $H_{\text{downstream}} = 80.60$ m and with the grout curtains' hydraulic conductivity 20 times lower than the hydraulic conductivity of the foundation's most pervious area).	211
Figure 6.10 – Seepage velocity in the foundation ((m/s) for $H_{\text{upstream}} = 145.01$ m and $H_{\text{downstream}} = 80.60$ m and with the grout curtains' hydraulic conductivity 20 times lower than the hydraulic conductivity of the foundation's most pervious area).	212
Figure 6.11 – Variations of piezometric head along the line where the piezometers are positioned at the base of the central cantilever (grout curtains' hydraulic conductivity 20 times lower than the hydraulic conductivity of the foundation's most pervious area).	212
Figure 6.12 – Meshes used to study the distance from the dam area at which boundaries should be located.	214
Figure 6.13 – Position of the foundation model 9.0 m wide in the area where the bottom of the valley meets the right hand side abutment.	217
Figure 6.14 – Face in the upstream-downstream direction of the three-dimensional model of the foundation. Division into blocks and internal mesh, and hydraulic boundary conditions.	218
Figure 6.15 – Regions defined in the 3D model of the foundation of Alqueva dam.	218
Figure 6.16 – Hydraulic head contours for $H_u = 143.0$ m and $H_d = 75.0$ m, with $k_{\text{grout curtain}} = 0.01 k_{\text{rock mass}}$	219

Figure 6.17 – Fine mesh and very coarse mesh: details at the drain’s upper and lower areas.....	221
Figure 6.18 – Hydraulic head (fine mesh) and differences in percentage in hydraulic head (fine mesh and very coarse mesh) along horizontal lines 40 m long at various elevations.....	223
Figure 6.19 - 3D model of the foundation of Alqueva dam. Division into blocks and internal mesh of a 1.5 m wide vertical strip. Very coarse mesh.	224
Figure 6.20 – Inflow of water into each borehole in the area where the bottom of the valley meets the right hand side abutment.	225
Figure 6.21 – Perspective of the three-dimensional AUTOCAD drawing developed to represent the various models’ assumed hypotheses.	227
Figure 6.22 – Situations to be considered to simulate tests carried out in drain D25 D.	227
Figure 6.23 – Steps of model elaboration.	229
Figure 6.24 – Seepage model in the vicinity of drain D25 D (Figure 6.23 - Step 6). Model parameters.....	235
Figure 6.25 – Recorded and numerical discharge flowing into each of drain’s D25 D water-inflow test intervals (a) and accumulated discharge from the bottom to the head of the borehole (b).	236
Figure 6.26 – Hydraulic head contours around the drains for a homogeneous rock mass and for the heterogeneous model: a) view from above; b) cut through drain D25 D, in the upstream-downstream direction.	236
Figure 6.27 – Seepage model to study the effect of local surface topography.	237
Figure 6.28 – Situations to be considered to simulate tests carried out in drain D20 D.	239
Figure 6.29 – Seepage model in the vicinity of drain D20 D. Model parameters.....	242
Figure 6.30 – Recorded and numerical discharge flowing into each of drain’s D20 D water-inflow test intervals (a) and accumulated discharge from the bottom to the head of the borehole (b).	244
Figure 6.31 – Alternative model. Seepage model in the vicinity of drain D20 D (assuming that the grout curtain is partially inefficient in the area where it is crossed by the upper layer of higher permeability). Model parameters.	245
Figure 6.32 – Variation of discharges in each drain and in the water pressure at drain D25 D when closed, with different rock mass permeability values.....	248
Figure 6.33 – Variation of discharges in each drain and in the water pressure at drain D25 D when closed, with different grout curtain permeability values.	250
Figure 6.34 – Variation of discharges in each drain and in the water pressure at drain D25 D when closed, with different permeability values of the rock mass upstream from the dam.	251

Figure 6.35 – Variations in hydraulic head along a horizontal line 40 m long that crosses drain D25 D in the upstream-downstream direction in the main model (reference values) and in a model where there is no area of higher permeability upstream from the dam.	253
Figure 6.36 – Variation of discharges in each drain and in the water pressure at drain D25 D when closed, with the different permeability values for the horizontal layers upstream from the drains.	255
Figure 6.37 - Variations in hydraulic head along a horizontal line 40 m long that crosses drain D25 D in the upstream-downstream direction in the main model and in a model where the permeability of the horizontal layers upstream from the drains is 2.0×10^{-7} m/s.	255
Figure 6.38 – Models with different widths of the horizontal layers upstream from the drains.	257
Figure 6.39 – Variation of discharges in each drain and in the water pressure at drain D25 D when closed, with different widths of the higher permeability layers upstream from the drains.	259
Figure 6.40 – Downstream and upstream views of the 20-node finite element mesh of Alqueva dam.	263
Figure 6.41 – Modelling steps, using 3DEC’s Arch Dam Module.	263
Figure 6.42 – Generation of polyhedral blocks (left) matching FE block faces (right).	264
Figure 6.43 – Internal mesh of the global foundation model.	264
Figure 6.44 - Upstream elevation of Alqueva dam. Location of the area of higher permeability upstream from the dam assumed in the hydraulic model of the dam foundation.	266
Figure 6.45 – Global foundation model: perspective (a), cross section with simulated grout and drainage curtains (b) and detail showing the grout curtain representation (c).	267
Figure 6.46 – Recorded discharges in the foundation of each dam block and comparison with numerical results.	269
Figure 6.47 – Hydraulic head contours (m) in the global hydraulic model of Alqueva dam foundation (for $H_u = 143.6$ m; $H_d = 81.95$ m).	271
Figure 6.48 – Hydraulic head contours (m) in three cuts parallel and in one cut perpendicular to the main river channel, shown in their relative positions (for $H_u = 143.6$ m; $H_d = 81.95$ m).	271
Figure 6.49 – Recorded discharges in the foundation of each dam block and comparison with numerical results for different water levels (numerical model calibrated for the reservoir at 143.6 m and tailwater at 81.95 m; H_u – reservoir level; H_d – tailwater level).	274
Figure 6.50 – Numerical discharges in the foundation of each dam block for different reservoir levels (H_u – reservoir level; H_d – tailwater level).	275
Figure 6.51 - Global mechanical model: perspective (a) and cross section (b).	277

Figure 6.52 – Collated worldwide in situ stress data: vertical stress components (after Hoek and Brown 1980).	281
Figure 6.53 – Collated worldwide in situ stress data: mean horizontal stress component (after Hoek and Brown 1980).....	281
Figure 6.54 - <i>In situ</i> principal stresses. Vertical cross section ($z = 3$ m).	284
Figure 6.55 – Displacements at crest elevation ($y = 154$ m) due to dam weight.	284
Figure 6.56 – Central cross section. Displacements (a) and principal stresses (b) due to dam weight.	284
Figure 6.57 – Displacements at crest elevation ($y = 154$ m) due to hydrostatic loading for the reservoir at 154.0 m (highest reservoir level).....	286
Figure 6.58 – Central cross section. Displacements (a) and principal stresses (b) due to hydrostatic loading for the reservoir at 154.0 m (highest reservoir level).	286
Figure 6.59 – Horizontal radial displacements and vertical displacements at the crest of the central cantilever due to increase in reservoir level.	287
Figure 6.60 – Normal joint displacement vectors for the reservoir at 154.0 m.	288
Figure 6.61 - Shear joint displacement vectors for the reservoir at a) 132.2 m, and b) 143.6 m.	289
Figure 6.62 - Average total vertical stresses in the foundation blocks below the heel of the dam which, in the hydraulic model, simulate conductive joints, with the reservoir at 154.0 m.....	290
Figure 6.63 – Variations in average total vertical stresses in the foundation blocks below the heel of the central cantilever and of block 20-21 which, in the hydraulic model, simulate conductive joints, with changes in reservoir level.....	290
Figure 6.64 – Location of joint gauges in the peripheral joint at the base of the central cantilever.	292
Figure 6.65 – Recorded vertical displacements at three points located in the peripheral joint at the base of the central cantilever.....	292
Figure 6.66 – Rod extensometers below the central cantilever.....	293
Figure 6.67 – Recorded strains in rod extensometer GEF4.	294
Figure 6.68 – Foundation blocks below the central cantilever used to determine average vertical strains to compare with those determined from readings taken in rod extensometer GEF4.....	295
Figure 6.69 – Recorded discharges in the foundation of each dam block with the reservoir at different elevations.....	298
Figure 6.70 – Variation in the permeability of the horizontal layers which simulate water conductive joints with the reservoir level.....	300
Figure 6.71 - Variations in average vertical stresses in the foundation blocks below the heel of the dam with changes in reservoir level.	300

Figure 6.72 – Variation of the permeability of the horizontal layers which simulate conductive joints below the heel of different dam blocks with vertical stress. Adjustment of exponential and logarithmic curves.....	301
Figure 6.73 – Variation of the permeability of the horizontal layers which simulate conductive joints below the heel of different dam blocks with vertical stress.....	303
Figure 6.74 - Variation of the permeability of the horizontal layers which simulate conductive joints below the heel of block 8-9 and 19-20 with vertical stress and with the aperture of a single discontinuity.	303
Figure 6.75 – Recorded discharges in the foundation of each dam block with different reservoir levels and comparison with the results of a model calibrated for water levels on the different dates and with those of the uncoupled hydromechanical model (arrows indicate dam blocks in which the hydromechanical effect was considered).	304
Figure 6.76 – Recorded discharges in the foundation of each dam block with different reservoir levels and comparison with the results of a model calibrated for water levels on the different dates and with those of the uncoupled hydromechanical model (arrows indicate dam blocks in which the hydromechanical effect was considered).	305
Figure 6.77 – Estimated Young’s modulus in the foundation of different dam blocks based on the stress-permeability curves.	307
Figure 6.78 – Seepage models in the five different situations.	313
Figure 6.79 – Lateral face of the simplified 3D model of the foundation of Alqueva dam. Division into blocks and internal mesh.	315
Figure 6.80 – Relative position of the horizontal layers of higher permeability upstream from the piezometer.	316
Figure 6.81 – Situation 1: variations in boreholes’ discharges and in percentage of hydraulic head at the piezometer for different relative permeability values.....	317
Figure 6.82 – Situation 1: hydraulic head contours with the link a) 5 times less pervious than the main layer and b) as pervious as the main layer. Horizontal cut through the middle of the pervious layers, in the upstream-downstream direction.	319
Figure 6.83 – Situation 1: variations in the piezometric head in the middle of the pervious layers along horizontal lines which cross the piezometer a) in the upstream-downstream direction and b) along the plane of the boreholes.....	319
Figure 6.84 – Situation 2: variations in boreholes’ discharges and in percentage of hydraulic head at the piezometer for different values of $k_{lower\ layer}/k_{upper\ layer}$, assuming an impervious rock mass.	321
Figure 6.85 – Situation 2: variations in the piezometric head in the middle of the pervious layers along horizontal lines which cross the piezometer a) in the upstream-downstream direction and b) along the boreholes.....	321

Figure 6.86 – Situation 2: hydraulic head contours with $k_{lower\ layer}/k_{upper\ layer} = 0.2$ and with $k_{lower\ layer}/k_{upper\ layer} = 10.0$. Horizontal cuts through the middle of the pervious layers, in the upstream-downstream direction.	322
Figure 6.87 – Situation 2: variations in boreholes' discharges and in percentage of hydraulic head at the piezometer for different values of $k_{lower\ layer}/k_{upper\ layer}$, assuming a pervious rock mass.	323
Figure 6.88 – Situation 3: variations in boreholes' discharges and in percentage of hydraulic head at the piezometer for different values of $k_{link}/k_{upper\ layer}$, assuming an impervious rock mass.	324
Figure 6.89 – Length of piezometric chambers: i) long single chamber; ii) two long chambers located 3.0 m apart; iii) two long chambers located 5.0 m apart; iv) two chambers 3.0 m long.	325
Figure 6.90 – Situation 4: variations in discharge and in percentage of hydraulic head at the piezometer in the second phase of analysis for different values of $k_{lower\ layer}/k_{upper\ layer}$	326
Figure 6.91 – Situation 4: comparison of variations in percentage of hydraulic head at a long single chamber and those at chambers of different lengths.....	326
Figure 6.92 – Situation 4: hydraulic head along the borehole assuming different piezometers.....	327
Figure 6.93 – Variations in percentage of hydraulic head at the piezometer for different values of $k_{upper\ layer}/k_{rock\ mass}$ and $k_{lower\ layer}/k_{upper\ layer}$	328
Figure 6.94 – Situation 4 ($k_{lower\ layer} = k_{upper\ layer}$): comparison of variations in percentage of hydraulic head in a long single chamber and those in chambers of different lengths...	329
Figure 6.95 – Situation 4 ($k_{lower\ layer}/k_{upper\ layer} = 20$): comparison of variations in percentage of hydraulic head in a long single chamber and those in chambers of different lengths.	329
Figure 6.96 – Situation 5: variations in boreholes' discharges and in percentage of hydraulic head at the piezometer for different values of k_{link}/k_{layer}	330
Figure 6.97 – Situation 5: hydraulic head contours in a vertical cut through the piezometer.	331
Figure 6.98 – Situation 5: hydraulic head contours in horizontal cuts through the middle of both the link and the pervious layer.	331
Figure 6.99 – Situation 5: variations in percentage of hydraulic head at a piezometer either with a long single chamber or with two long chambers, for different values of k_{link}/k_{layer}	332
Figure 6.100 – Flow at a network node (after Hudson and Harrison 2000)	334
Figure 6.101 – Set of discontinuities simulated in situation 1.	335

Figure 6.102 – Comparison of the hydraulic head at the piezometer obtained with the 3D model and with the simplified model shown in Figure 6.101 (Equation 6.24).....	335
Figure 6.103 – Set of discontinuities simulated in situation 1. Width of the horizontal layer of higher permeability upstream from the piezometer.	335
Figure 6.104 – Comparison of the hydraulic head at the piezometer obtained with the 3D model and with the simplified model shown in Figure 6.101 assuming an equivalent permeability in branches 2 and 3.....	336
Figure 6.105 - Set of discontinuities simulated in situations 2, 3 and 5. Hydraulic head at each node and at the piezometer.....	338
Figure 6.106 – Comparison of the hydraulic head at the piezometer obtained with the 3D model and with the simplified models shown in Figure 6.105.	339
Figure 6.107 – Situation 5 assuming an impervious rock mass: comparison of the hydraulic head at the piezometer obtained with the 3D model and with the simplified model shown in Figure 6.105.....	339
Figure 7.1 – Detail of meshes below the dam for three different models.	349
Figure 7.2 – Hydraulic head contours and seepage velocity in the foundation for the three different models shown in Figure 7.1.....	350
Figure 7.3 – Relation between hydraulic aperture, a , and joint normal stress, σ_n , in UDEC (after Itasca 2004).....	352
Figure 7.4 – UDEC model of Pedrógão dam foundation.	353
Figure 7.5 – Principal stresses due to both rock mass and dam weight.	357
Figure 7.6 – Displacements due to both dam weight and the weight of the upper part of the rock mass, downstream from the stilling basin.....	357
Figure 7.7 – Principal stresses after hydrostatic loading.....	358
Figure 7.8– Displacements due to hydrostatic loading.	358
Figure 7.9 – Domain water pressures for full reservoir with a) constant joint aperture, b) hydromechanical interaction with drainage system and c) without drainage system (pressure is proportional to line thickness).	360
Figure 7.10 – Flow rates for full reservoir (flow rate is proportional to line thickness; flow rates below 3.0×10^{-6} (m ³ /s)/m (0.18 (l/min)/m) are not represented).....	361
Figure 7.11 – Block deformation (magnified 3000 times) due to: a) both dam weight and the weight of the upper part of the rock mass, downstream from the stilling basin; b) hydrostatic loading and flow; c) both effects shown together.....	362
Figure 7.12 – Joints at shear limit (green), joints with zero normal force or stress (blue) and magnitude of joint separation (red), for rock masses with different deformability (joint separation is proportional to line thickness).....	363
Figure 7.13 - Joints at shear limit (green), joints with zero normal force or stress (blue) and magnitude of joint separation (red), for rock masses with different deformability, with no drainage system (joint separation is proportional to line thickness).....	364
Figure 7.14 – Normal displacement along the dam/foundation joint.....	365

Figure 7.15 – Hydraulic aperture of the dam/foundation joint.	366
Figure 7.16 - Water pressure along the a) dam/foundation joint and b) joint of higher permeability.....	368
Figure 7.17 – Comparison of water pressures along the dam/foundation joint with both bi-linear and linear distribution of water pressures.....	369
Figure 7.18 – Models for joint dilation: a) the dilation increases indefinitely; b) UDEC model.....	369
Figure 7.19 – Drain discharges during the filling of the reservoir both without and with joint dilation effect for two different joint friction angles.	370
Figure 7.20 – Hydraulic heads at the piezometers located underneath the stilling basin (mid-height level of piezometric chambers shown in brackets).	371
Figure 7.21 – Variations in the hydraulic head at the piezometers located underneath the stilling basin in relation to the reservoir level (mid-height level of piezometric chambers shown in brackets).	372
Figure 7.22 – Location of the piezometric chambers in the foundation of block 6A-6B, in the downstream area, underneath the stilling basin.	372
Figure 7.23 – Physical model tests of a gravity dam on a discontinuous foundation. Failure mechanisms: a) same friction angle on all joints; and b) reduced friction on lower joint (after Pereira Gomes et al. 1997).	379
Figure 7.24 – Water static loads on block 6-7 of Pedrógão dam.	381
Figure 7.25 – Hydrodynamic pressures. Westergaard simplified model.	382
Figure 7.26 – Construction of Pedrógão dam stilling basin.	385
Figure 7.27 – Analysed failure modes.	387
Figure 7.28 – Variation in crest horizontal displacement due to reduction of the friction angle on highlighted joints, for failure modes a), b), and c), shown in Figure 7.27.	389
Figure 7.29 – Failure mode through the dam construction joint shown in Figure 7.27 d): horizontal displacement at crest for a) decreasing friction angle and b) increasing water pressure at the dam joint.....	389
Figure 7.30 – Variation in crest horizontal displacement due to reduction of the friction angle on the dam/foundation interface, for failure mode e) shown in Figure 7.27.....	390
Figure 7.31 – Joints at shear limit (green), joints with zero normal force or stress (blue) and magnitude of joint separation (red), for failure mode b) (joint separation is proportional to line thickness).....	390
Figure 7.32 – Variation in crest horizontal displacement due to reduction of the friction angle on highlighted joints, for failure modes a), b), and c), shown in Figure 7.27.	392
Figure 7.33 – Variation in crest horizontal displacement due to reduction of the friction angle on the dam/foundation interface, for failure mode e) shown in Figure 7.27.....	392
Figure 7.34 – Comparison of water pressures along the dam/foundation joint obtained in the UDEC analysis with the linear distribution of water pressures.	395

LIST OF TABLES

Table 2.1 - Formulas suggested by Moye (1967) and Hoek and Bray (1981) for analysis of water pressure tests.	14
Table 2.2 – Types of boundaries in seepage analysis problems associated with embankment dams or concrete dam foundations.	19
Table 4.1 – Average cohesion and friction angle of discontinuities (LNEC 1984).	106
Table 4.2 – Discharges and water pressures in the equipment placed in drain D14’s area of influence during the borehole water-inflow test.	127
Table 4.3 – Information about the boreholes where tests were carried out.	142
Table 4.4 – Water pressure and discharges measured by piezometers installed in blocks 8-9 and 13-14.	153
Table 5.1 – Axisymmetric model. Numerical discharges and comparison with the analytical solution.	160
Table 5.2 – Drain modelled by its axis ($R = 100$ m). Numerical discharges and comparison to the analytical solution.	164
Table 5.3 – Drain modelled by its axis. Most suitable dimension of the element close to the drain, in order to obtain a drain discharge as close as possible to the analytical solution.	164
Table 5.4 – Drain modelled by its axis ($R = 100$ m). Numerical discharges and comparison to the analytical solution (drain diameter $\phi_1 = 2 \times 0.076 = 0.152$ m).	164
Table 5.5 – Drain modelled by its axis ($R = 100$ m). Numerical discharges and comparison to the analytical solution (drain diameter $\phi_2 = 10 \times 0.076 = 0.76$ m).	165
Table 5.6 – Drain modelled by its axis ($R = 100$ m). Ratio between the most suitable dimension of the element close to the drain and the drain diameter.	165
Table 5.7 – Two-dimensional horizontal model. <i>FLAC</i> results and comparison to analytical solution (error in brackets).	170
Table 5.8 – Geometric characteristics of the different 3D meshes. Calculated discharges and comparison with the analytical solution (in brackets).	173
Table 5.9 – Steady state unconfined flow between two reservoirs. Comparison between numerical discharges and analytical solution.	178
Table 5.10 – Foundation with grout curtain but without drainage. Numerical discharges for different $k_{\text{grout curtain}}/k_{\text{rock mass}}$	181
Table 5.11 – Foundation with both grout and drainage curtains. Numerical discharges for different $k_{\text{grout curtain}}/k_{\text{rock mass}}$	183
Table 5.12 – <i>Small model</i> . Discharges for different boundary conditions and different relationships between the grout curtain and rock mass permeability.	186
Table 5.13 – Numerical discharges for different boundary conditions (see Figure 5.21).	191

Table 5.14 – Numerical discharges for $k_{\text{grout curtain}}/k_{\text{rock mass}} = 0.1; 0.01$ and 0.001	192
Table 5.15 – Influence of model size. Numerical discharges when the hydraulic head is assumed either on the foundation surface upstream and downstream from the dam or on the lateral boundaries ($k_{\text{grout curtain}}/k_{\text{rock mass}} = 0.01$).	193
Table 5.16 – Influence of mesh size. Numerical discharges with different meshes.	195
Table 5.17 – Numerical discharges with 3D and 2D models.	196
Table 5.18 – Comparison between the average hydraulic head at the line of the drains calculated with the 3D model and with the 2D horizontal model.	197
Table 5.19 – Comparison between the average hydraulic head at the drainage line obtained with the 3D model and with the 2D horizontal model (Andrade 1982), with the drains located 3.0 m apart.	199
Table 5.20 – Comparison between the average hydraulic head at the drainage line obtained with the 3D model and with the 2D horizontal model (Andrade 1982), with the drains located 6.0 m apart.	199
Table 6.1 – Results of hydraulic conductivity tests (in Lugeon Units) carried out in the foundation of Alqueva dam, after dam construction but before grouting.	206
Table 6.2 – Average value of the recorded discharges and comparison to numerical results.	206
Table 6.3 - Average value of the recorded discharges and comparison to numerical results (grout curtains' hydraulic conductivity 10 and 20 times lower than the hydraulic conductivity of the foundation's most pervious area).	209
Table 6.4 – Drained foundation. Numerical discharges and comparison with the discharge obtained with the model which has the furthest boundaries.	215
Table 6.5 - Foundation with no drainage curtain. Numerical discharges and comparison with the discharge obtained with the model which has the furthest boundaries	215
Table 6.6 – Influence of mesh size. Numerical discharges with different meshes.	221
Table 6.7 – Influence of mesh size. Number of steps to reach steady state conditions and run times.	221
Table 6.8 – Numerical value of the discharges with single and double-precision versions.	224
Table 6.9 – Number of steps to reach steady state conditions and run times with single and double-precision versions.	224
Table 6.10 – Discharges and water pressures measured in drains D24 D, D25 D and D26 D both in normal operating conditions and with drain D25 D closed.	227
Table 6.11 – Observed discharges in both drain D25 D and its area of influence, and water pressure at the drain head when it is closed.	230
Table 6.12 – Numerical discharges for different rock mass hydraulic conductivity values (model shown in Figure 6.23 - Step 1 (with a single strip 1.5 m wide)).	232
Table 6.13 – Numerical discharges in models where a small area of higher permeability upstream from the dam is considered ($k_{\text{near surface area upstream from the dam}} = 10.0 \times 10^{-7}$ m/s) (Figure 6.23 - Step 2).	232

Table 6.14 - Numerical discharges for different hydraulic conductivity values of the horizontal layer upstream from the drains (model shown in Figure 6.23- Step 3 (with a single strip 1.5 m wide)).	233
Table 6.15 – Numerical discharges for different widths of the horizontal layer upstream from the drains (model shown in Figure 6.23 - Steps 4 and 5 (that takes into account curvatures of the dam where it meets the foundation)).	234
Table 6.16 – Recorded discharges and water pressures and comparison to numerical results (shown in red).	235
Table 6.17 – Distribution of discharges between the drains due to model geometry.	238
Table 6.18 – Discharges and water pressures measured in drains D19 D, D20 D and D21 D in four different situations (September 2007, $H_{\text{reservoir}} = 148.0$ m; $H_{\text{downstream}} = 84.2$ m).	239
Table 6.19 – Recorded discharges and water pressures and comparison to numerical results (shown in red).	243
Table 6.20 – Numerical discharges. Percentage of the quantity of water that flows into the model (in brackets).	244
Table 6.21 – Alternative model. Recorded discharges and water pressures and comparison to numerical results (shown in red).	245
Table 6.22 – Numerical discharges and water pressures for different rock mass permeability values in normal operating conditions and with drain D25 D closed.	248
Table 6.23 - Numerical discharges and water pressures for different grout curtain permeability values in normal operating conditions and with drain D25 D closed.	249
Table 6.24 - Numerical discharges and water pressures for different rock mass permeability values upstream from the dam in normal operating conditions and with drain D25 D closed.	251
Table 6.25 - Numerical discharges and water pressures for different permeability values of the horizontal layers upstream from the drains, in normal operating conditions and with drain D25 D closed.	254
Table 6.26 - Numerical discharges and water pressures for different widths of the horizontal layers upstream from the drains, in normal operating conditions and with drain D25 D closed.	258
Table 6.27 – Discharges with drain D24 D completely blocked from 6.75 m downwards and partially clogged for 0.5 m, both in normal operating conditions and with drain D25 D closed.	260
Table 6.28 – Sensitivity to higher permeabilities.	266
Table 6.29 – Assumed permeability of the horizontal layers between the near-surface area of higher permeability upstream from the dam and the drainage curtain.	269
Table 6.30 – Error analysis: mean error, mean absolute error and mean squared error.	269
Table 6.31 – Material properties.	279
Table 6.32 – Joint mechanical properties in each of the three different models.	279

Table 6.33 – Comparison of radial displacements at the crest of the central cantilever due to increase in reservoir level obtained with the dam simulated as a single block and with the dam simulated as a group of FE elastic blocks separated by joints (y-axis vertical; z-axis towards upstream).....	287
Table 6.34 – Radial displacements at the crest of the central cantilever due to increase in reservoir level (y-axis vertical; z-axis towards upstream).	287
Table 6.35 – Maximum joint aperture for different reservoir levels.....	288
Table 6.36 – Maximum shear joint displacement for different reservoir levels.	288
Table 6.37 – Recorded strains in rod extensometer GEF4 for different reservoir levels.....	294
Table 6.38 – Variations in strains recorded in rod extensometer GEF4, using readings recorded on 2004.02.03 as reference.....	294
Table 6.39 – Average vertical stresses in foundation blocks below the central cantilever for different reservoir levels.	295
Table 6.40 – Variations in numerical stresses and estimated variations in rock mass vertical strains (percentages of recorded strains shown in brackets).	295
Table 6.41 – Variations in apertures of horizontal water conductive discontinuities below dam block 17-18 due to variations in average vertical stresses (numerical values).	296
Table 6.42 – Equivalent permeability of the horizontal layers which simulate water conductive joints for different reservoir levels.	299
Table 6.43 – Hydraulic aperture of a single discontinuity which simulates the horizontal layers of higher permeability below the heel of different dam blocks with the reservoir at 144.8 m.....	303
Table 7.1 - Numerical discharges for the three models of Figure 7.1 and comparison to observed value.....	349
Table 7.2 – Material properties.	353
Table 7.3 – Mechanical properties of discontinuities.	353
Table 7.4 – Joint permeability factor in discontinuities.	355
Table 7.5 – Equivalent deformability of the assumed rock masses.	357
Table 7.6 – Difference between numerical hydraulic heads at the lower and upper piezometric chambers for different permeabilities of the downstream area of the dam/foundation joint.	373
Table 7.7 – Loading combinations to take into account in the safety assessment against dam sliding for both usual and failure scenarios.....	383
Table 7.8 – Safety assessment against sliding at the dam/foundation interface for both usual and failure scenarios.	383
Table 7.9 – Minimum values of the friction angle in discontinuities close to the dam/foundation interface which ensure safety against sliding.....	384
Table 7.10 – Force due to uplift pressures acting upwards on the stilling basin/foundation interface and comparison with the weight of the stilling basin.....	385

Table 7.11 – Limit equilibrium method. Minimum values of the friction angle in discontinuities close to the dam/foundation interface which ensure safety against sliding, and corresponding safety factors. 391

Table 7.12 – UDEC analysis. Friction angle in discontinuities close to the dam/foundation interface which ensure safety against sliding and for which failure occurs, and corresponding safety factors (failure scenarios shown in Figure 7.27)..... 393

Table 7.13 – Comparison between the UDEC results and those from the limit equilibrium method. 395

LIST OF SYMBOLS

a	contact hydraulic aperture [L]
a_0	joint aperture at nominal zero normal stress [L]
Δa	joint normal displacement, taken as positive in opening [L]
a	spacing between drains [L]
a	horizontal acceleration of the dam foundation [LT^{-2}]
A	cross sectional area of flow [L^2]
a	spacing between drains [L]
a	fracture aperture; fracture hydraulic aperture [L]
a_i, b_j and c_k	coefficients
a_{max}	maximum hydraulic aperture [L]
a_{res}	residual aperture [L]
a_s	horizontal acceleration of the dam foundation [LT^{-2}]
b	distance from the drainage curtain to the toe of the dam [L]
c	cohesion [$L^{-1}MT^{-2}$]
c	conductance [L^2T^{-2}]
c	base width of the dam [L]
c_m	coefficient dependent on the slope of the upstream face of the dam
d	spacing of discontinuities [L]
D	aquifer thickness [L]
d	distance between the upstream face of the dam and the drainage curtain [L]
D_h	hydraulic diameter of the fissure [L]
e	width of peripheral joint [L]
e	fracture hydraulic aperture [L]
e	equivalent width [L]
E	Young's modulus; deformability modulus; modulus of deformation [$L^{-1}MT^{-2}$]
E	mechanical joint aperture [L]
E	total energy [L]
E_R	modulus of deformation of the rock matrix [$L^{-1}MT^{-2}$]
E_{RM}	modulus of deformation of the rock mass [$L^{-1}MT^{-2}$]
F_b	inertia force due to the seismic load on the concrete [LMT^{-2}]

f_i	function of level
F_p	passive force in the area of the downstream face below the river bottom [LMT ⁻²]
F_w	horizontal resultant of the hydrostatic pressure on the upstream face of the dam [LMT ⁻²]
F_{wd}	horizontal resultant of the hydrostatic pressure on the downstream face of the dam [LMT ⁻²]
F_{ws}	hydrodynamic pressure on the upstream face of the dam [LMT ⁻²]
g	acceleration due to gravity [LT ⁻²]
g_j	function of temperature
H	water height above the dam base [L]
H	total hydraulic head [L]
h	total hydraulic head, which is the elevation head plus the pressure head ($h = z + p/(\rho_w g)$) [L]
h	height [L]
h	hydraulic head [L]
H_0	increase in head compared with that at rest [L]
H_1	highest hydraulic head [L]
H_2	lowest hydraulic head [L]
H_d	height of the tailwater above a given horizontal plane [L]
H_d	height of the water in the downstream area [L]
$H_{\text{downstream}}$	tailwater level [L]
H_{drain}	hydraulic head at the drain [L]
$H_{\text{piezometer}}$	hydraulic head at the piezometer [L]
$H_{\text{reservoir}}$	reservoir level [L]
H_u	height of the reservoir above a given horizontal plane [L]
H_u	height of the water in the upstream area [L]
H_{upstream}	reservoir level [L]
i	hydraulic gradient [LL ⁻¹]
I_G	global index [-]
I_P	pressure index [-]
I_q	unitary discharge index [-]
I_Q	global discharge index [-]
J	hydraulic gradient
k	independent term (constant)

k	hydraulic conductivity; equivalent hydraulic conductivity [LT^{-1}]
\mathbf{K}	hydraulic conductivity matrix [LT^{-1}]
k	intrinsic permeability; permeability [L^2]
k	independent term
k	absolute roughness of the fissure walls; asperity height [L]
k_e	equivalent hydraulic conductivity [LT^{-1}]
$k_{equivalent}$	equivalent permeability [LT^{-1}]
k_f	joint coefficient of permeability [LT^{-1}]
k_f	fracture hydraulic conductivity [LT^{-1}]
$k_{grout\ curtain}$	equivalent permeability of the grout curtain [LT^{-1}]
k_H	Darcy's coefficient of permeability; hydraulic conductivity [LT^{-1}]
$k_{horizontal}$	equivalent hydraulic conductivity in the horizontal direction [LT^{-1}]
k_i	permeability factor used in UDEC (either a point contact permeability factor (k_c) or a joint permeability factor (k_j))
\mathbf{K}_{ij}	permeability tensor
k_j	joint permeability factor used in UDEC, whose theoretical value is $1/(12\ \mu)$ [$LM^{-1}T$]
k_n	fracture normal stiffness; joint normal stiffness [$L^{-2}MT^{-2}$]
k_{n0}	fracture normal stiffness at zero normal stress [$L^{-2}MT^{-2}$]
k_{ni}	fracture normal stiffness at an initial effective stress [$L^{-2}MT^{-2}$]
k_r	equivalent permeability perpendicular to the borehole [LT^{-1}]
k_{ref}	reference equivalent permeability [LT^{-1}]
$k_{rock\ mass}$	equivalent permeability of the rock mass [LT^{-1}]
k_s	fracture shear stiffness; joint shear stiffness [$L^{-2}MT^{-2}$]
k_w	bulk modulus of the fluid [$L^{-1}MT^{-2}$]
k_z	equivalent permeability parallel to the borehole [LT^{-1}]
L	distance; length [L]
l	length [L]
n_i	direction cosines of the normal to the surface
p	drain perimeter [L]
p	fluid pressure [$L^{-1}MT^{-2}$]
P_d	pressure at the drain, given by the distance from the drain head to a given plane [L]
p_k	function of time
Q	quantity of discharge [L^3]

q	rate of discharge; flow rate [L^3T^{-1}]
Q	flow rate [$L^3 T^{-1}$]
Q_0	total recorded discharge [L^3T^{-1}]
$q_{0 \max}$	maximum recorded discharge per metre along the drainage line [L^2T^{-1}]
q_d	portion of the total discharge that flows towards downstream [L^3T^{-1}]
q_{drain}	portion of the total discharge that flows to the drains [L^3T^{-1}]
q_{\max}	maximum allowable discharge per metre [L^2T^{-1}]
Q_{\max}	maximum global discharge [L^3T^{-1}]
q_{trench}	portion of the total discharge that flows to a hypothetical continuous trench [L^3T^{-1}]
q_u	portion of the total discharge that flows into the domain from upstream [L^3T^{-1}]
R	radius of influence [L]
r	radius [L]
Re	Reynolds number [-]
r_i	deviation between the value observed on date i and the result of the quantitative interpretation model
r_w	radius of the borehole [L]
s	number of days starting 1st January
s	fracture spacing [L]
S	hydraulic head [L]
S_d	average value of the hydraulic head at the line of the drains [L]
s_n^2	mean squared error
t	time [T]
T	transmissivity of aquifer [L^2T^{-1}]
T	fracture transmissivity [L^2T^{-1}]
T_0	transmissivity at zero shear displacement [L^2T^{-1}]
T_r	residual transmissivity at high compressive stress [L^2T^{-1}]
$U_h(h)$	elastic effect due to variations in reservoir water level
$U_i(h_i, \theta_i, t_i)$	observed effect observed on date i , which depends on the hydrostatic pressure, the temperature and the moment when the data is collected
u_n	joint normal displacement [L]
u_n^d	normal displacement due to dilation [L]
u_s	joint shear displacement [L]
u_s	shear displacement [L]
$U_i(t)$	time effect

$U_{\theta}(\theta)$	elastic effect due to thermal variations
v	discharge velocity [LT^{-1}]
V	volume [L^3]
V	domain volume [L^3]
V	resultant of uplift pressures at the dam/foundation interface [LMT^{-2}]
v_x, v_y, v_z	components of discharge velocity along x, y and z axis [LT^{-1}]
W	weight of the concrete cross-section [LMT^{-2}]
y	depth [L]
y	thickness [L]
z	height from the base [L]
z	distance from some arbitrary datum [L]
z_{dil}	shear displacement for zero dilation [L]
α	coefficient
β	coefficient
γ	Unit (or specific) weight [$L^{-2}MT^{-2}$]
γ_c	safety factor relative to cohesion of the concrete/rock mass interface
γ_c	unit (or specific) weight of concrete [$L^{-2}MT^{-2}$]
γ_r	unit (or specific) weight of the rock mass [$L^{-2}MT^{-2}$]
γ_w	unit (or specific) weight of water [$L^{-2}MT^{-2}$]
γ_{ϕ}	safety factor relative to the peak friction angle of the concrete/rock mass interface
$\gamma_{\phi r}$	safety factor relative to the residual friction angle of the concrete/rock mass interface
Δt	timestep [T]
Δt_f	fluid timestep [T]
Δu	variation in the discontinuity aperture [L]
Δu_n	fracture normal displacement [L]
Δu_n^d	normal displacement increment due to dilation [L]
Δu_s	fracture shear displacement [L]
$\Delta \epsilon_{yy}$	strain variation in the y direction [-]
$\Delta \sigma_{yy}$	stress variation in the y direction [$L^{-1}MT^{-2}$]
ϵ	strain [-]
ϵ_{yy}	strain in the y direction [-]
λ	coefficient to correct the permeability in the line of drains

μ	dynamic viscosity of the fluid [$L^{-1}MT^{-1}$]
ν	kinematic viscosity of the fluid [L^2T^{-1}]
ρ_w	water density [$L^{-3}M$]
σ	stress [$L^{-1}MT^{-2}$]
σ_H	stress in the horizontal direction [$L^{-1}MT^{-2}$]
σ_n	fracture normal stress [$L^{-1}MT^{-2}$]
σ'_n	effective fracture normal stress [$L^{-1}MT^{-2}$]
σ'_{ni}	effective fracture normal stress at initial conditions [$L^{-1}MT^{-2}$]
σ'_{zz}	effective stress [$L^{-1}MT^{-2}$]
σ_s	shear stress [$L^{-1}MT^{-2}$]
σ_s^{Peak}	peak shear stress [$L^{-1}MT^{-2}$]
σ_t	tensile strength [$L^{-1}MT^{-2}$]
σ_v	stress in the vertical direction [$L^{-1}MT^{-2}$]
$\sigma_{vertical}$	stress in the vertical direction [$L^{-1}MT^{-2}$]
$\sigma_x, \sigma_y, \sigma_z$	stress in the x, y and z directions, respectively [$L^{-1}MT^{-2}$]
σ_{yy}	stress in the y direction [$L^{-1}MT^{-2}$]
σ_{zz}	total vertical stress [$L^{-1}MT^{-2}$]
ν	Poisson's ratio [-]
φ	friction angle
ϕ	borehole diameter [L]
ϕ	total head; piezometric head; hydraulic potential; head [L]
$\Phi_{0\ max}$	maximum percentage of hydraulic head recorded along the drainage line
Φ_{max}	maximum hydraulic head allowed along the drainage line, expressed in percentage of hydraulic head
φ_r	residual friction angle
\bar{x}	average value of x
$ x $	absolute value of x

OFFICIAL BODIES

ASCE	American Society of Civil Engineers
CFBR	Comité Français des Barrages et Réservoirs
EDF	Électricité de France
EDIA	Empresa de Desenvolvimento e Infra-Estruturas do Alqueva
EDP	Electricidade de Portugal
EPRI	Electric Power and Research Institute
FERC	Federal Energy Regulatory Commission
ICOLD	International Commission on Large Dams
INAG	Instituto da Água
INESC-ID	Instituto de Engenharia de Sistemas e Computadores, Investigação e Desenvolvimento
ISRM	International Society for Rock Mechanics
LNEC	Laboratório Nacional de Engenharia Civil
SCD	Swiss Committee on Dams
USACE	United States Army Corps of Engineers
USBR	United States Bureau of Reclamation

ABBREVIATIONS

2D	Two dimensional
3D	Three dimensional
ADAS	Automated Data Acquisition System
BEM	Boundary element method
BPM	Bonded particle method
DDA	Discontinuity deformation analysis
DEM	Discrete element method
DFN	Discrete fracture network
F	Safety factor
FDM	Finite difference method

FE	Finite element
FEM	Finite element method
HM	Hydromechanical
JRC	Joint roughness coefficient
LU	Lugeon unit
MDE	Maximum design earthquake
OBE	Operational basis earthquake
UCS	Uniaxial compressive strength

1 Introduction

For centuries dams have been constructed all over the world to perform a variety of functions such as flood control, irrigation and water supply, hydropower production, protection of estuaries against flooding tides and improvement of navigation along rivers. Moreover, reservoirs are nowadays increasingly used for recreation, which can attract tourists and thus benefit the local economy. In spite of this, however, the future of dams is currently the subject of much debate, as a large number of people claim that dams are damaging the environment and that their construction has undesirable social effects.

The fact that a large number of dams are a source of renewable energy, which is generated without polluting the atmosphere, is a major advantage in meeting increasing electricity needs. Hydroelectricity today provides almost 20 % of the world's power, and although other renewable energy sources, such as solar and eolic energy, have potential for increased use, they also have limiting characteristics as they can not provide the continuous, reliable supply which is needed. Therefore, multipurpose developments, which include more than one dam and in which the water may be pumped from a downstream to an upstream reservoir in the hours of lower power consumption are increasingly being built to fulfil this necessity.

In European countries such as Spain, Italy and Portugal, a significant period of construction of concrete dams took place in the 1950s along with the economic recovery that followed the end of the 2nd World War, and the main emphasis was on the exploitation of hydroelectric resources for local economic development. Several concrete dams were also built during the 1980s in Portugal, and indeed at present the trend is for increasing construction. Four 20-35 m high concrete dams were built in Portugal in the last three years (Fumadinha, Ferradosa, Olgas and Pretarouca dams), there are currently two large dams under construction (Baixo Sabor dams), and the tender for the construction of three more dams has recently been opened (new Alto Ceira dam, Ribeiradio and Ermida dams). The first four were constructed for water supply, while the others are mainly for energy production. In addition, in 2007, the Portuguese Water Institute (INAG – Instituto da Água) launched the “National Programme for Dams with High Hydroelectric Potential” with the aim of identifying and defining priorities for investments in hydroelectric developments until 2020, to increase the national hydroelectric capacity from the current 5000 MW up to 7000 MW, in order to decrease energy dependency and reduce the carbon dioxide emissions. Thanks to this programme, eight large dams will be built, mainly for energy production (Foz Tua, Padroselos, Alto Tâmega, Daivões, Gouvães, Fridão, Alvito and Girabolhos dams), only one of which is less than 70 m high.

1.1 The role of the foundation in the safety of concrete dams

Concrete dams are built with their foundations in rock masses, which are discontinuous and, in most cases, heterogeneous and anisotropic. Accidents at Malpasset dam, in France in 1959, and Vajont, in Italy in 1963, among others, highlighted the significance of the characteristics of these rock masses. In fact, the foundation rock mass is part of a structural system which includes the dam, the foundation and the reservoir, and is a crucial element when considering safety, as can be concluded from the results of various statistical studies of dam deterioration carried out by the International Commission on Large Dams (ICOLD).

The identification and analysis, on a worldwide scale, of the main accident and incident scenarios that have taken place in concrete, masonry and embankment dams, has been the subject of study of numerous working groups, among which the studies carried out by several ICOLD committees are highlighted. In order to get the largest amount of information possible about accidents and/or incidents in dams ICOLD has already sent out three questionnaires to which a large number of countries responded. Among the studies presented by ICOLD committees it is worth mentioning the following bulletins:

- Lessons from dam incidents (ICOLD 1974);
- Deterioration of dams and reservoirs. Examples and their analysis (ICOLD 1983);
- Ageing of dams and appurtenant works. Review and recommendations (ICOLD 1994);
- Dam failures. Statistical analysis (ICOLD 1995).

The conclusion was drawn that the main cause of accidents in concrete and embankment dams was overtopping due to floods greater than predicted in the design stage or due to operating faults of appurtenant works, followed by faulty behaviour of dam body and foundation.

In concrete dams, not including issues related with the appurtenant works, the majority of recorded failures were due to problems in the foundation rock mass such as erosion and internal dissolving of rock masses, which often lead to a loss of strength, and lack of shear resistance in weak planes of unfavourable direction.

The safety control of dams throughout their lifetime, which includes the phases of design, construction, first filling of the reservoir, operation, and decommissioning, has always been a major concern, especially for those structures of which the failure has the potential for loss of human life and economic consequences. Dams are therefore systematically equipped with a large number of monitoring instruments, of which the results enable the continuing evaluation

of dam behaviour. In addition, there are nowadays, in a great number of countries, regulations, guidelines and codes of practice, which have been continuously updated in order to reduce the risk of accidents. This is the case in Portugal, where the first Regulation for the Safety of Dams, published in 1990, was recently revised (RSB 2007).

The safety control of concrete dams has improved significantly in recent years, with the increasing use of numerical models not only in the analysis of the dam's actual performance but also in the prediction of its behaviour. However, these developments have been mainly restricted to the study of the concrete super-structure. The great complexity of concrete dam foundations, not only due to the existence of discontinuities and heterogeneities but also to the foundation treatment necessary to improve mechanical and hydraulic properties, has always made both the mechanical and hydraulic characterization and the analysis of its behaviour difficult.

Seepage through the rock mass in a concrete dam foundation is a crucial factor and it is well known that there is a significant interdependence between the mechanical and hydraulic behaviour. In fact, in a rock mass the majority of the flow takes place through a complex interconnecting system of discontinuities, whose aperture may vary with variations in stresses and/or strains within the foundation, due, for instance, to changes in the reservoir level. Even slight changes in apertures can lead to significant changes in the quantity of water flowing through the discontinuities. Changes in flow patterns cause changes in mechanical loads, which, in turn, are responsible for changes in the state of stress. A comprehensive review of hydromechanical couplings in fractured rock masses as a result of or directly connected with human activities, can be found in Rutqvist and Stephansson (2003).

The effects of water pressures in both the dam body and its foundation were recognized in the late 1800s, and started to be studied in a scientific way after the concept of effective pressure was introduced by Terzaghi, in 1923. In dam foundations, hydromechanical behaviour began to receive wide attention in the early 1960s, during the investigation of the Malpasset dam failure. Some of the first studies on coupled hydromechanical behaviour in fractured rocks were related to dam foundations (Londe and Sabarly 1966; Louis 1969; Louis and Maini 1970), and since then it has been the subject of extensive laboratory and *in situ* research (e.g. Cappa et al. 2005; 2006; Cornet et al. 2003; Giacomini et al. 2008; Kovari and Koppel 1987; Noorishad et al. 1992; Olsson and Barton 2001; Rutqvist et al. 1992). However, as mentioned in Rutqvist and Stephansson (2003), during the past two decades most of the research and development on hydromechanical coupling in fractured rocks and most applications of hydromechanical coupled analysis have been conducted as part of oil and gas exploration, hot-dry rock geothermal energy investigations, and studies for nuclear waste disposal. Thus, the application of research results to the field conditions of dam foundations is still difficult.

Regarding the dam foundation rock mass, in particular the hydromechanical behaviour, the available numerical techniques are not commonly used to support the analysis of the monitoring data or the safety control, even though there are currently various numerical methods of mechanical and hydromechanical analysis of rock masses which can be effectively used for this purpose, which are systematically presented in Jing and Hudson (2002) and in Jing (2003). These may be divided into two different approaches: continuum and discontinuum modelling, and include different numerical techniques such as the finite element, finite difference and boundary element methods (FEM, FDM and BEM), in continuum analysis, or the discrete element method (DEM), the discontinuous deformation analysis (DDA) and the bonded particle method (BPM), in discontinuum analysis.

1.2 Objectives

The main aim of this research is to validate and justify the application of numerical models for the analysis of hydromechanical behaviour so that their use may become effective, in order to improve our ability to analyse the monitoring data of concrete dam foundations, to make the safety assessment of these structures more efficient. For this, it is essential to carry out systematic and comprehensive work to verify the computational codes, to validate the hypotheses assumed in the numerical codes by comparison of numerical results with both experimental and field data, and to develop methodologies to calibrate the model for the specific geological and geotechnical conditions of a given dam foundation.

The information which is commonly available regarding the hydraulic activity in concrete dam foundations is the quantity of water collected in drainage systems, and water pressures recorded in piezometers located in the various dam blocks. Although essential for the assessment of both dam behaviour and safety, this information is not sufficient to develop accurate hydraulic models, which require the location of seepage paths to be known. *In situ* water-inflow tests are proposed, which are capable of providing more complete information on the foundation's hydraulic behaviour.

Dam performance is often assessed using statistical methods, based on previously collected monitoring results. These simplified methods have been regularly employed in the analysis of dam displacements but are seldom used in the analysis of hydraulic behaviour. An attempt is made to apply these methods in the analysis of drainage data.

Concerning numerical modelling, the first studies of the hydraulic behaviour of rock masses used equivalent continuum models. There are more advanced discontinuum models (fracture flow models), which accurately simulate rock masses' hydromechanical behaviour, however, these models require data which is not usually available, such as that regarding the complex jointing pattern or the joint hydraulic properties. One of the purposes of this study is to

develop a methodology for the application of equivalent continuum models, which can be effectively used in practice, based on data that can be easily obtained from both monitoring and *in situ* tests. Although not practical to study dam's hydraulic behaviour, discontinuum models are commonly used for safety evaluation, and the simpler equivalent continuum models can also provide relevant information to be used in these more complex models.

Some practical issues merit further attention, mainly regarding the use of three-dimensional (3D) numerical models, required to accurately simulate the behaviour of dam foundations, especially arch dams. Large 3D global models of dam foundations are not feasible without simplified representations of both the grout and drainage systems, which have to be properly addressed and justified. It is necessary to develop, test and validate this type of model, which must not only simulate flow correctly, but also be computationally efficient.

1.3 Thesis outline

The thesis is composed of eight chapters. In this chapter 1 the role of the foundation in the safety of concrete dams is highlighted, the subject's relevance is justified and the main aims of the thesis are presented.

Chapter 2 focuses on the behaviour and analysis of concrete dam foundations. It starts by describing main aspects related to rock mass characterization, fluid flow through rock mass discontinuities, and hydromechanical behaviour of rock joints. The specific features of concrete dam foundations are presented, namely the sealing and drainage treatment measures, and the influence that both grout and drainage systems have on the foundation's hydraulic activity is highlighted. The main cases of foundation deterioration observed in Portugal are briefly referred to. A review of previous studies is presented along with a reference to the main numerical methods available to simulate or interpret the hydromechanical behaviour of dam foundations. The factors that influence the choice between equivalent continuum and discontinuous models are outlined and the fundamentals of fluid flow in either continuum or discontinuum media are presented. Finally, a reference is made to the numerical codes used in this study.

Chapter 3 addresses the observation and analysis of concrete dam foundation behaviour. A reference is made to: i) the measures usually taken to fulfil both safety and serviceability requirements; ii) the monitoring equipment to measure the main loads, the factors which define seepage in the foundation (uplift and discharges) and those which must be known to define the states of stress and strain of the foundation rock mass (displacements, strains and stresses); and iii) the methodologies currently used in the collecting and collating of the monitoring data. Simplified methods, such as quantitative interpretation, are traditionally used to interpret recorded data and thus a brief review of these methods is presented. However, due

to the non-linear behaviour of the foundation rock mass the principle of superposition of effects is not valid, making the application of these methods in the analysis of recorded discharges and water pressures difficult. A method is proposed for the analysis of the recorded discharges which takes into account the non-linear hydromechanical behaviour, due to the influence of stress and strain on the permeability.

The study carried out included a series of field tests, which proved to be essential to provide detailed information on the hydraulic activity in the foundation rock mass, supplementing the available monitoring data. Tests were carried out with a view to understanding the way in which flow occurs in specific areas of the foundation and validating numerical models so that their use may become effective. Borehole water-inflow tests, which allow measurement of discharges and water pressures in isolated sections of boreholes, were conducted in the foundation of two large Portuguese concrete dams, one gravity and one arch. As there are no pre-established testing methods, these were developed within this study to provide information which can be useful in the analysis and safety assessment of any dam foundation. Chapter 4 presents a thorough description of these tests, the main characteristics of the dams where tests were carried out, with emphasis on those related with the foundation, and analysis of tests results. Additional tests were carried out and despite some difficulties found whilst testing *in situ*, which are pointed out in order to be avoided in future studies, the tests provided valuable information without which the hydraulic and hydromechanical models presented in the subsequent chapters could not have been developed.

Although rock masses are discontinuous structures, the most widely used tool to study the hydraulic behaviour of concrete dam foundations are models based on the assumption of an equivalent continuum medium. Chapter 5 starts by presenting validation tests of two of the numerical codes used in this study in hydraulic analysis against analytical solutions. Conclusions drawn from these tests regarding the representation of the drain and suitable mesh sizes in the study of seepage flow provided the basis to develop a three dimensional model of a restricted area of the foundation of one of the dams where borehole water-inflow tests were carried out, and this 3D model was used to study the influence of different factors, such as the influence of drainage, boundary conditions, grout curtain permeability, model size and mesh size. The flow in fractured rock masses is mainly three-dimensional but 2D models can sometimes be used, with the advantage of being much simpler, and therefore results of 2D and 3D models were compared.

Conclusions drawn in chapter 5 were essential to develop and justify the application of both 2D and 3D models presented in chapters 6 and 7, in which two case studies of Portuguese dams are examined. In both chapters, the validity of the used numerical models of the dam-foundation structural system is assessed by comparing the numerical results to the monitoring

data and special attention is given to the foundation's hydraulic and hydromechanical behaviour.

The study presented in chapter 6 included the development of a series of numerical models to simulate the hydraulic and hydromechanical behaviour of the studied arch dam foundation, which were progressively validated and calibrated against field data. Borehole water-inflow tests were simulated, and the knowledge of both seepage patterns around particular boreholes and of the key parameters was essential to develop an effective application of a simplified global model of the dam foundation, which provided a good match of both average recorded discharges and water pressures. Global hydraulic models of dam foundations are useful not only for the assessment of the behaviour of operating dams but also to determine water pressure distributions for safety analysis. A simple methodology was developed, which, with an uncoupled mechanical-hydraulic analysis, can be used to establish rules that allow the calculation of discharges for different reservoir levels.

Chapter 7 links analysis of seepage and hydromechanical behaviour of the studied gravity dam foundation with stability assessment. Borehole water-inflow test results were again of major importance in the development of numerical models which properly simulate dam behaviour. Both two-dimensional equivalent continuum and discontinuum models were developed, and the latter was used to assess water pressures within the foundation and to evaluate the safety for different possible failure scenarios involving either the foundation or the dam body.

In the last chapter, a critical discussion of the results obtained and a summary of the main conclusions are presented. Conclusions are drawn about the suitability and limitations of the numerical models developed to interpret and forecast the behaviour of the foundation rock masses and the key parameters necessary to calibrate and use these models. Methods to design and use the foundation monitoring systems are proposed, for improvement of safety assessment. Finally, suggestions for further research are proposed.

2 Concrete dam foundations. Hydromechanical behaviour and analysis

2.1 Introduction

The mechanical and hydraulic processes in rock masses are not independent. Fluid flow influences the mechanical behaviour since changes in water flow cause variations in seepage forces and in hydraulic uplift. These mechanical loads change the stress field, thus inducing deformations in the fractured rock mass. These deformations, in turn, cause changes in permeability and consequently changes in water flow. This is called a coupled hydromechanical process and the coupling mechanisms are between the fracture aperture, rock porosity/permeability, fluid pressure and rock stress (Jing and Stephansson 2007).

This chapter focuses on the behaviour and analysis of concrete dam foundations. It starts by describing main aspects related to rock mass characterization, followed by a summary of the governing equations both in continuum media and through rock mass discontinuities. The main aspects related to hydromechanical behaviour of rock joints are referred to. The specific features of concrete dam foundations are presented, namely the sealing and drainage treatment measures, and the influence that both grout and drainage systems have on the foundation's hydraulic activity is highlighted. The main cases of foundation deterioration observed in Portugal are briefly referred to. A review of previous studies is presented along with a reference to the main numerical methods available to simulate or interpret the hydromechanical behaviour of dam foundations. Finally, a reference is made to the numerical codes used in this study.

2.2 Characterization of rock masses

The foundation of any dam is always a complex structure that requires a well designed and comprehensive site and laboratory investigation programme. The results of this investigation should provide sufficient knowledge of the foundation to help and justify the design of both the super-structure and the foundation treatment, and to predict the response of the foundation to the physical conditions that are going to be imposed by dam construction and subsequent loading. There is extensive literature on characterization of rock masses, which includes geological, geotechnical and foundation materials investigations (e.g. Hudson and Cosgrove 1997; ICOLD 2005; ISRM 2007; USACE 1984) so only the most relevant matters for the study presented here are addressed below.

Laboratory and *in situ* tests are carried out in order to characterize strength, deformability, state of stress and hydraulic properties. The size of the samples tested in the laboratory is not usually large enough to be representative of the rock mass with regard to heterogeneity and

jointing. In most cases, there is also a scale effect, which makes it difficult to use laboratory data to estimate the properties of fractured rock masses. *In situ* tests are often required but they typically involve a small area of the foundation and thus the results may not be representative. Therefore, despite all the investigation carried out prior to and during dam construction, it is well acknowledged and should always be kept in mind that the foundation geology, geomechanics and hydromechanical behaviour can never be fully known.

2.2.1 Geological and hydrogeological investigations

Mapping of the foundation surface geology is the first activity undertaken to acquire a basic knowledge of the geology. Different types of surface geological maps may be drawn, depending on the information required, but they should employ engineering rock description terms in order to be useful for engineering practice. ICOLD (2005) highlights that the map must emphasize features that are relevant to the identification of geological concerns affecting design, project safety and performance. In this regard, the identification of discontinuities (including measurement and orientation), such as faults, joints and bedding planes, is essential for geological mapping, because discontinuities usually govern the performance of the rock mass. Geological cross-sections along and perpendicular to the dam axis are also of major importance.

Among the various guides that have been suggested to prepare geological maps, which give the terminology and symbols to be used, are those presented by the International Society for Rock Mechanics (ISRM 1978, 1981). The first document suggests methods for the quantitative description of rock masses and discontinuities, and the second provides qualitative and quantitative descriptive elements for characterizing the mechanical behaviour of rock masses. In the latter, five characteristics are taken into account: the rock name, with a simplified geological description; two structural characteristics of the rock mass: layer thickness and fracture intercept; and two mechanical characteristics: the uniaxial compressive strength (UCS) of the rock material and the angle of friction of the fractures. The simplified geological description should include a reference to: i) the geological structure of the rock mass; ii) the fracturing of the rock mass; iii) colour, texture and mineral composition of the rock material; and iv) the degree of weathering. Figure 2.1 shows the five different intervals within which each one of the characteristics is described. The terms and symbols used to classify the degree of weathering are shown in Figure 2.2.

Regarding hydrogeological investigations it is not only important to understand the groundwater conditions prior to dam construction, but also to identify springs and seepages that occur in the dam area. Springs that appear during excavation should be treated and the water properly diverted to the downstream area. One of the most important hydrogeological parameters is the permeability of the rock mass, which is controlled by the characteristics of

the discontinuities, because their permeability is usually several orders higher than that of the unweathered rock.

Intervals (cm)	Symbols	Descriptive terms	
> 200	L ₁	Very large	
		L _{1,2}	Large
60 – 200	L ₂	Large	
20 – 60	L ₃	Moderate	Moderate
6 – 20	L ₄	Small	
		L _{4,5}	Small
< 6	L ₅	Very small	

Intervals (cm)	Symbols	Descriptive terms	
> 200	F ₁	Very wide	
		F _{1,2}	Wide
60 – 200	F ₂	Wide	
20 – 60	F ₃	Moderate	Moderate
6 – 20	F ₄	Close	
		F _{4,5}	Close
< 6	F ₅	Very close	

Layer thickness			
Intervals (MPa)	Symbols	Descriptive terms	
> 200	S ₁	Very high	
		S _{1,2}	High
60 – 200	S ₂	High	
20 – 60	S ₃	Moderate	Moderate
6 – 20	S ₄	Low	
		S _{4,5}	Low
< 6	S ₅	Very low	

Fracturing intercept			
Intervals (°)	Symbols	Descriptive terms	
> 45	A ₁	Very high	
		A _{1,2}	High
35 – 45	A ₂	High	
25 – 45	A ₃	Moderate	Moderate
15 – 25	A ₄	Low	
		A _{4,5}	Low
< 15	A ₅	Very low	

Uniaxial compressive strength of the rock			
Intervals (MPa)	Symbols	Descriptive terms	
> 200	S ₁	Very high	
		S _{1,2}	High
60 – 200	S ₂	High	
20 – 60	S ₃	Moderate	Moderate
6 – 20	S ₄	Low	
		S _{4,5}	Low
< 6	S ₅	Very low	

Angle of friction of the fractures			
Intervals (°)	Symbols	Descriptive terms	
> 45	A ₁	Very high	
		A _{1,2}	High
35 – 45	A ₂	High	
25 – 45	A ₃	Moderate	Moderate
15 – 25	A ₄	Low	
		A _{4,5}	Low
< 15	A ₅	Very low	

Figure 2.1 – Intervals, symbols and descriptive terms used in the Basic Geotechnical Description of Rock Masses (BGD) (ISRM 1981).

Term	Description	Symbols
Fresh	No visible sign of rock material weathering; perhaps slight discolouration on major discontinuity surfaces.	W1
Slightly weathered	Discolouration indicates weathering of rock material and discontinuity surfaces. All the rock material may be discoloured by weathering and may be somewhat weaker than in its fresh condition.	W2
Moderately weathered	Less than half of the rock material is decomposed and/or disintegrated to a soil. Fresh or discoloured rock is present either as a discontinuous framework or as core stones.	W3
Highly weathered	More than half of the rock material is decomposed and/or disintegrated to a soil. Fresh or discoloured rock is present either as a discontinuous framework or as core stones.	W4
Completely weathered	All rock material is decomposed and/or disintegrated to soil. The original mass structure is still largely intact.	W5

Figure 2.2 – Weathering classification (adapted from ISRM 1978).

Although rock masses are fissured media, the groundwater flow is usually studied assuming a porous media conceptual model, and is therefore governed by Darcy's law. The results of a series of laboratory experiments conducted by Henry Darcy to study flows of water in vertical homogeneous sand filters, the results of which he published in 1856, indicated that, macroscopically, the velocity of a fluid through porous media is directly proportional to the pressure gradient acting on the fluid:

$$v = k_H i \quad (2.1)$$

or, since the discharge per unit time (rate of discharge or flow rate) is given by $q = v A$

$$q = k_H i A \quad (2.2)$$

The quantity of discharge in a period of time equal to t is given by:

$$Q = k_H i A t \quad (2.3)$$

In the previous equations: v = discharge velocity (m/s); k_H = Darcy's coefficient of permeability or hydraulic conductivity (m/s); i = hydraulic gradient (head loss / length over which head loss occurs (m/m)); q = rate of discharge (discharge on a unit time (m³/s)); A = cross-sectional area of flow (m²); Q = quantity of discharge (m³); t = time of flow (s).

Darcy's law only applies to linear flow (adjacent flow lines are locally straight and parallel), thus for high seepage velocities, Darcy's law does not hold. The upper limit on the range of validity of Darcy's law is given by the Reynolds number (R_e), a dimensionless number which, in steady-state conditions, expresses the ratio of inertial to viscous (frictional) forces during flow.

Darcy's coefficient of permeability, also known as hydraulic conductivity or simply permeability is expressed as a velocity and is usually given in m/s. In fact, the "hydraulic conductivity" is a measure of permeability that includes both the properties of the medium and of the fluid (i.e. density (ρ) and viscosity (μ), or, in the combined form of kinematic viscosity ($\nu = \mu/\rho$)), while "permeability" is an intrinsic property of the medium that is independent of the properties of any fluid (usually expressed in cm² or Darcys). Permeability (k) can be converted to hydraulic conductivity (k_H) with knowledge of the fluid properties:

$$k_H = \frac{\gamma}{\mu} k = \frac{\rho g}{\mu} k = \frac{k g}{\nu} \quad (2.4)$$

where γ = unit weight of the fluid; μ = dynamic viscosity of the fluid; ρ = fluid density; g = gravity acceleration; and ν = kinematic viscosity of the fluid. In practice, however, the

term permeability is often used instead of hydraulic conductivity. Permeability calculated on the basis of Darcy's law is limited to the conditions of laminar flow and complete saturation of the media. When equivalent continuum models are used to study flow in dam foundation rock masses, permeability should be referred to as equivalent permeability.

The hydraulic conductivity of concrete dam foundation rock masses is commonly evaluated with constant-head tests, known as "Lugeon type tests" (Houlsby 1976). These tests are systematically carried out i) during geological investigations, ii) when drilling grout and drainage boreholes, and, iii) with the dam already built, when opening piezometric holes. During geological investigations the results of these tests give important data which is used in the design of seepage control measures. During the initial phase of dam use, structural weight and hydrostatic loads acting simultaneously lead to great stress changes in the rock mass, with a consequent change in joint apertures and fluid flow. The repetition of these tests in drains and piezometric holes during the structure's lifetime can allow the detection of seepage changes.

The well known Lugeon test was originally proposed by Maurice Lugeon, in order to establish a simple empirical criterion to design grouting in dam foundations (Lugeon 1932), and since then it has been widely used to estimate the permeability of rock masses. The test involves isolating a section of a borehole with the aid of packers and injecting water under pressure into that section until the flow rate for any given pressure is constant. The original test was conducted at a pressure of 1 MPa (10 bar), and the results were expressed in Lugeon units (LU), 1 LU being defined as the water take of 1 litre / minute per metre length of test section, at an effective pressure of 1 MPa (Houlsby 1976). Over the years several changes have been suggested to improve the tests, such as adapting the test interval length to the joint pattern of the rock mass, considering various pressure stages; and adapting pressure values to the rock mass characteristics, the test depth, and the maximum water pressures expected during the dam's lifetime.

Injection tests in boreholes lead to scalar values of hydraulic conductivity. However, the rock mass permeability can be highly anisotropic and the differences in the permeability in different directions can be of various orders (Rocha and Franciss 1977). To take into account the anisotropy in the rock mass permeability, i.e. to determine its hydraulic conductivity tensor (or permeability tensor), various methods have been proposed by different authors (e.g. Louis 1969; Serafim and Del Campo 1965; Snow 1965). Rocha and Franciss (1977) suggested a method that had the great advantage, compared to the previously devised methods, of allowing the determination of the permeability tensor at a point from a single integral sample, provided it was representative of the fracturing. However, Wittke (1990) is of the opinion that this method is only a supplementary method to determine permeability, as integral samples have small dimensions and are rarely representative of permeability. Wang et

al. (2002) presented a new methodology based on the numerical simulation of a few hydraulic tests carried out *in situ*, using a discrete fracture flow model. Despite these attempts, Lugeon type tests remain the most widely used tool to evaluate the equivalent permeability of concrete dam foundations.

Permeability values can be expressed either in Lugeon units or in m/s. This allows the comparison of the permeability of a heterogeneous and fractured rock mass with that of a homogeneous medium which has the same water take at a pressure of 10 bar. It is usually assumed that 1 LU is equivalent to 1.3×10^{-7} m/s, or more frequently simply to 1.0×10^{-7} m/s (Fell et al. 2005; Houlsby 1976; Lancaster-Jones 1975; Wyllie 1999). This value may be obtained using the solution for steady-state laminar flow in homogeneous and isotropic media around a test well. Hvorslev and the U.S. Bureau of Reclamation, in 1951, Moye, in 1967, and Hoek and Bray, in 1981, suggested the use of different formulas for analysis of water pressure tests (Bulut et al. 1996; Hoek and Bray 1981; Hvorslev 1951; Moye 1967). Hamm et al. (2007) show that the equations suggested by the first two above-mentioned authors are mathematically the same, and that those suggested by the last two (Table 2.1) are simplified cases of the Hvorslev formula.

Lugeon type tests are usually carried out in 5.0 m long test sections in boreholes with a diameter of 76 mm. In this case, according to Moye’s formula 1 LU is equivalent to 1.4×10^{-7} m/s. Hoek and Bray (1981) suggest that for most applications the ratio between the equivalent permeability perpendicular to the borehole and that in the parallel direction (k_r/k_z) is about 10^6 . This implies that there are no fractures parallel to the hole, and in most rock masses this would not be a reasonable approximation (Fell et al. 2005). If it is assumed that $k_r/k_z = 10$ then 1 LU is equivalent to 1.6×10^{-7} m/s. In homogeneous isotropic conditions $k_r = k_z$ and thus $m = (k_r/k_z)^{1/2} = 1$, and 1 LU is equivalent to 1.3×10^{-7} m/s.

Moye (1967)	$k_e = \frac{Q}{12 \pi L H_0} \left[1 + \ln \left(\frac{L}{2 r_w} \right) \right]$	k_e = equivalent hydraulic conductivity (m/s)
	Remark : based on the assumption of radial laminar flow in a homogeneous isotropic rock mass	Q = flow rate (m ³ /s) r_w = radius of the borehole (m) L = length of the test section (m) H_0 = increase in head compared with that at rest (m)
Hoek and Bray (1981)	$k_e = \frac{Q \ln \left(\frac{m L}{r_w} \right)}{12 \pi L H_0} \quad \text{where } m = \left(\frac{k_r}{k_z} \right)^{1/2}$	k_r = equivalent permeability perpendicular to the borehole k_z = equivalent permeability parallel to the borehole
	Remark : based on the assumption of ellipsoidal symmetrical flow about the axis of the borehole test section (simplified case of the Hvorslev equation when $m L > 10 \times 2 r_w$).	

Table 2.1 - Formulas suggested by Moye (1967) and Hoek and Bray (1981) for analysis of water pressure tests.

2.2.2 Geotechnical investigations

Field investigations include the collecting of information from test pits and trenches (and if necessary from adits and shafts), examination of cored boreholes, and various tests carried out in order to evaluate: i) the permeability and the deformability of the different areas of the dam foundation, ii) the shear strength parameters of intact rock and discontinuities, and iii) the *in situ* state of stress. The different methods for investigating dam foundation rock masses are presented in detail in ICOLD (1993). It is important to highlight that the majority of the tests involve relatively small volumes of the rock mass and thus test results must be carefully analysed and interpreted in order to give useful information for both dam design and analysis of dam foundation performance.

Empirical rock mass classification systems for engineering purposes have been developed, such as the RMR (rock mass rating) system of Bieniawski and the Q (or NGI) system of Barton. These systems were originally established for the design of tunnels. Although extensions of the RMR have been proposed to cover the case of dam foundations and slopes (e.g. Romana 2004), their use in dam foundations is rare. In this respect, however, the percentage of core recovery, employed to classify cored boreholes, is a basic index of the quality of the rock mass which is extensively used.

Laboratory investigations include rock classification tests, such as saturation water content, bulk density and porosity; the stress-strain and strength properties of intact rock; and the deformation and strength properties of rock joints. Tests can also be carried out to measure the hydraulic conductivity of both rock joints and intact rock.

2.3 Fundamentals of fluid flow in continuum media

In the majority of the analyses presented in this study it is assumed that flow takes place in an equivalent continuum media under steady-state conditions, thus the fundamental equations which describe flow under these conditions are presented below.

2.3.1 Hydraulic head and hydraulic gradient

Water moves from areas of higher energy to areas of lower energy. The total energy of a fluid element with a unit weight is given by (Louis 1969):

$$E = z + \frac{p}{\gamma} + \frac{v^2}{2g} \quad (2.5)$$

where: z = distance from some arbitrary datum [L]; p = fluid pressure at a certain point M [$L^{-1} M T^{-2}$]; γ = unit (or specific) weight of the fluid [$L^{-2} M T^{-2}$]; v = velocity of the fluid at M [$L T^{-1}$]; and g = acceleration due to gravity [$L T^{-2}$].

The total energy per unit weight [L] can be divided in two parts:

i) total head
$$\phi = z + \frac{p}{\gamma} \quad (2.6)$$

ii) velocity head
$$\frac{v^2}{2g} \quad (2.7)$$

The total head, ϕ , also known as piezometric head, as hydraulic potential, as hydraulic head, or simply head, is usually represented by h . According to Equation 2.6 the total head is the sum of the elevation head (distance from some arbitrary datum) and the pressure head (fluid pressure divided by the unit weight of the fluid). The pressure head represents the height of a fluid column capable, by its weight, of imposing pressure p . The velocity head represents the kinetic energy per weight unit, which means that it represents the height from which a fluid element should fall, in vacuum, to attain velocity v . The velocity head may usually be neglected, and thus the total head provides a good approximation to the energy head (Wittke 1990).

The hydraulic potential and the kinetic energy vary from one point to another in a fluid. If it is assumed that flow takes place in steady-state conditions, they can be described as a function of space only. In a system of arbitrary coordinates (x,y,z) , the total head of a fluid can thus be written as:

$$\phi(x, y, z) = z(x, y, z) + \frac{p(x, y, z)}{\gamma} \quad (2.8)$$

The hydraulic gradient \vec{J} is defined as minus the gradient of the hydraulic head:

$$\vec{J} = -g \vec{rad} \phi(x, y, z) \quad (2.9)$$

or, in index notation

$$J_i = - \frac{\partial \phi}{\partial x_i} \quad (i = 1, 2, 3) \quad (2.10)$$

If function $\phi(x, y, z)$ is known, then the hydraulic head contours (which are surfaces in three dimensional problems, and lines in two-dimensional problems) can be represented by:

$$\phi(x, y, z) = \text{const.} \quad (2.11)$$

2.3.2 Extension of Darcy's experimental law to three-dimensional flows

Darcy's laboratory experiments were carried out with unidirectional flows. However, the experimental law may be extended to three-dimensional flows in anisotropic and non-homogeneous domains. In this case Darcy's law is written, in vector form, as (Bear 1988):

$$\bar{v} = -\mathbf{K} \text{ grad} \left(z + \frac{p}{\gamma} \right) = -\mathbf{K} \text{ grad } \phi \quad (2.12)$$

or, in index notation:

$$v_i = -K_{ij} \frac{\partial \phi}{\partial x_j} \quad (i, j = 1, 2, 3) \quad (2.13)$$

where v_i are the components of Darcy velocity along x , y and z axis, and \mathbf{K} is the hydraulic conductivity matrix, which is symmetrical and is expressed as a velocity. There is a system of orthogonal axis, known as principal axis, for which $K_{ij} = 0$ for $i \neq j$.

2.3.3 Laplace equation in homogeneous media

In an isotropic media the hydraulic conductivity matrix \mathbf{K} becomes a single scalar ($K_{11} = K_{22} = K_{33} = k_H$) and the extended Darcy's law (Equation 2.12) is written as:

$$v = k_H i$$

$$\bar{v} = -k_H \text{ grad } \phi = -\text{grad } k_H \phi \quad (2.14)$$

Given that v_x , v_y , and v_z are the components of Darcy velocity along x , y and z axis:

$$v_x = -k_H \frac{\partial \phi}{\partial x}; \quad v_y = -k_H \frac{\partial \phi}{\partial y}; \quad v_z = -k_H \frac{\partial \phi}{\partial z} \quad (2.15)$$

Using the equation of continuity, which represents conservation of mass:

$$\frac{\partial v_x}{\partial x} + \frac{\partial v_y}{\partial y} + \frac{\partial v_z}{\partial z} = 0 \quad \text{or} \quad \text{div } \bar{v} = 0 \quad (2.16)$$

the Laplace equation is obtained; this expresses water movement in a homogeneous porous media:

$$\frac{\partial^2 \phi}{\partial x^2} + \frac{\partial^2 \phi}{\partial y^2} + \frac{\partial^2 \phi}{\partial z^2} = 0 \quad \Leftrightarrow \quad \nabla^2 \phi = 0 \quad (2.17)$$

When formulating Laplace equation it is assumed that: i) flow takes place in steady-state conditions; ii) water is incompressible; iii) the media is incompressible and homogeneous; and iv) flow is laminar. The assumption of incompressibility of water is acceptable under typical subsurface conditions because, as the compressibility of water is only 4.9×10^{-10} /Pa, a pressure change of 1 MPa (10 bar) changes the density by only 0.05 % (Zimmerman and Bodvarsson 1996). The assumption that flow is laminar is also adequate, as is going to be shown in section 2.5.2.

From the analysis of Equation 2.17 it can be seen that the hydraulic conductivity k_H is not in the Laplace equation, which means that in an isotropic media the total piezometric head is independent of permeability, being dependent only on the domain geometry and boundary conditions.

According to Harr (1962), seepage analysis problems associated with embankment dams or concrete dam foundations involve four possible types of boundaries (Table 2.2): i) impervious boundary; ii) entrances and exits; iii) seepage face; and iv) free surface. Therefore, boundary conditions can be defined by the hydraulic head value, ϕ , by the discharge, or by a free surface condition. When the boundary condition is defined by the hydraulic head, the latter can be constant:

$$\phi_{\text{boundary1}} = h_1 \quad (2.18)$$

or it can vary along the boundary:

$$\phi_{\text{boundary2}} = f(x_i) \quad (i = 1, 2, 3) \quad (2.19)$$

The seepage face is a particular case of this type of boundary condition, in which pressure is zero, and thus the hydraulic head equals the elevation head.

If the boundary condition is defined by the discharge:

$$\phi_{\text{boundary3}} = k_{i,j} \frac{\partial \phi}{\partial x_j} n_i \quad (i, j = 1, 2, 3) \quad (2.20)$$

where n_i are the direction cosines of the normal to the surface. An impervious boundary is a particular case of this boundary condition, where the discharge is zero.

Boundary condition	Remarks
Impervious	The interface between the foundation and adjacent materials with very low permeability, such as concrete or a very low permeability soil, is simulated as an impervious boundary. As no flow takes place across an impervious boundary flow in the pervious media next to the impervious boundary is parallel to that boundary.
Entrances and exits	The lines defining the area where water enters or leaves the pervious domain are known as entrances and exits. Along these lines the hydraulic head is the same, regardless of their direction or shape. Flow is perpendicular to any entrance or exit.
Seepage face	In embankment dams, the saturated pervious soil mass may have a boundary exposed to the atmosphere and allows water to escape along this boundary. Pressure along this surface is atmospheric. This boundary condition does not occur in concrete dams.
Free surface	This boundary, as for an impervious boundary, is not crossed by flow

Table 2.2 – Types of boundaries in seepage analysis problems associated with embankment dams or concrete dam foundations.

A free surface condition (or phreatic condition) is established by simultaneously imposing the hydraulic head (which is equal to the elevation head) and the value of the discharge (discharge null):

$$\begin{aligned} \phi_{\text{boundary}} &= z & (p = 0) & \quad (2.21) \\ k_{ij} \frac{\partial \phi}{\partial x_j} n_i &= 0 & (i, j = 1, 2, 3) & \end{aligned}$$

The location of a free surface is *a priori* unknown and is part of the required solution.

The solution of a flow problem in a continuum media involves determining the distribution of the hydraulic head in the domain under analysis in such a way that the equation of continuity and the boundary conditions are satisfied, which enables the evaluation of other flow factors and the mechanical effects of flow (Carmo Vaz 1979).

2.4 Hydromechanical behaviour of rock joints

2.4.1 Fluid flow in a single joint

It is essential to understand how fluid flows in rock joints in order to address the complex hydromechanical behaviour of concrete dam foundations, and this has been the subject of extensive research. The most commonly applied conceptual model for flow through a single fracture, known as the parallel plate model, represents the fracture as the void space between two parallel smooth plates (Louis 1969; Louis and Maini 1970; Snow 1965). The solution for steady state laminar incompressible flow in such fracture geometry gives the mean velocity as:

$$v = k_f i \quad (2.22)$$

where i = hydraulic gradient applied to the fluid (m/m), and the fracture hydraulic conductivity is given by

$$k_f = \frac{a^2 g}{12 \nu} \quad (2.23)$$

where a = fracture aperture (m); ν = kinematic viscosity of the fluid (m²/s); and g = acceleration of gravity (m/s²). The flow rate per unit width is thus expressed by the cubic law:

$$q = \nu a = \frac{a^3 g}{12 \nu} i \quad (2.24)$$

Thus, the laminar discharge of parallel-plate openings is proportional to the cube of aperture, which means that it is extremely sensitive to the size of the aperture.

Natural rock fractures are neither smooth nor parallel and thus several studies have been carried out in order to establish whether the parallel plate model is adequate for the prediction of flow in natural fractures. Louis (1969) showed that the cubic law is essentially valid for laminar flow in rock joints but proposed an empirical correction factor for this law in order to account for fracture roughness. Lomitze, in 1951, and Barton and de Quadros (1997) also suggested the use of an extra roughness coefficient, and similar formulas were proposed by these researchers, with different correction factors due to the different samples of fractures that were used: Lomitze used smooth glass plates with variable roughness, achieved by glueing sand grains to the surface, while Louis and Barton and de Quadros used different rock fractures.

Most of the studies suggested that better predictions could be obtained if the joint wall roughness and the regions where the joint walls touch were taken into account. The joint wall roughness leads to spatial variations in aperture and the contact between both fracture walls leads to partial obstruction of the flow. Witherspoon et al. (1980) stated that the apparent reduction in flow due to deviations from the parallel plate geometry could be incorporated into the cubic law by multiplying the flow rate by a linear correction factor. Tsang and Witherspoon (1981) developed a physical model where the single fracture is represented by a collection of voids and the closure of the fracture results from a deformation of these voids. This model enabled fracture roughness to be characterized from a relationship between the stress-displacement measurements of intact rock and those of jointed rock, and these researchers thus proposed the use of a weighted average aperture in the cubic law that leads to flow rate as a function of normal stress. Predicted flow rates using this model were close to

results from laboratory data on granite and basalt. Neuzil and Tracy (1981) developed a different model for flow in a fracture, where the fracture is represented by a set of parallel plate openings with different apertures, and they presented theoretical relationships between mean aperture and flow rate. They suggested the use of an aperture frequency distribution for the fracture. Barton et al. (1985) suggested that a rock fracture has both a mechanical and a hydraulic aperture with an empirical relation that considers the joint roughness coefficient (JRC) and stated that the hydraulic aperture should be used in the cubic law.

The concepts of mechanical and hydraulic aperture are particularly relevant. Olsson and Barton (2001) defined the mechanical joint aperture (E) as the average point-to-point distance between two rock joint surfaces, perpendicular to a selected plane. A single value can be used to define the aperture, but it can also be described stochastically. The aperture distribution is only valid at a certain state of stress and pore pressure. The mechanical aperture is usually determined from a two dimensional (2D) joint section, which is only a part of the real 3D surface. The hydraulic aperture (e) is measured by analysing the fluid flow and can be determined both from laboratory fluid flow experiments and borehole pumping tests in the field. Barton et al. (1985) proposed a nonlinear empirical correlation between hydraulic and mechanical aperture.

According to Liu (2005) the assumption that the hydraulic and mechanical apertures are equal has been shown to be a good approximation for a high flow rate and large apertures, but laboratory data and numerical experiments suggest that the approximation breaks down as the stress acting perpendicular to the fracture plane results in fracture apertures approaching the scale of the surface roughness. The hydraulic aperture is always less than the mechanical aperture and their ratio depends crucially on the fracture roughness.

2.4.2 Hydromechanical behaviour during joint normal closure

The influence of normal stress on the aperture and flow behaviour of rock joints has been the subject of extensive research (e.g. Barton and de Quadros 1997; Barton et al. 1985; Cammarata et al. 2007; Cook 1992; Gale et al. 1994; Hans and Boulon 2003; Kulatilake et al. 2008; Li et al. 2008; Londe and Sabarly 1966; Lopez et al. 2007; Marache et al. 2008; Neuzil and Tracy 1981; Noorishad et al. 1992; Pyrak-Nolte and Morris 2000; Rutqvist et al. 1992; Sisavath et al. 2003; Tsang and Witherspoon 1981; Witherspoon et al. 1980).

The typical mechanical and hydromechanical behaviour of rock joints under normal stress is shown in Figure 2.3. The normal deformation is non-linear (Figure 2.3 a) and the rate of deformation is greater at low normal stress, which means that fracture stiffness increases with increasing effective normal stress. The same figure shows there is a scale effect and that the maximum joint closure increases with sample size (Yoshinaka et al. 1993).

Regarding the hydromechanical behaviour, experimental results show that there is a decrease in fracture transmissivity with normal stress, but there is an apparent residual transmissivity (T_r) at high stress when the fracture appears to be mechanically compressed (Figure 2.3 b). The transmissivity (T) of a fracture with an aperture a and hydraulic conductivity k_f is given by:

$$T = k_f a \quad (2.25)$$

The residual transmissivity indicates that the fluid flow at high stress may be dominated by tube-like flow channels, which cannot be closed easily (Rutqvist and Stephansson 2003). This effect led Witherspoon et al. (1980) to introduce the concept of “residual hydraulic aperture”. The phenomenon of size effect for normal closure, which indicates that fracture hydraulic conductivity increases with specimen size, has been suggested by several researchers based both on experimental data (Witherspoon et al. 1980; Yoshinaka et al. 1993) and on theoretical studies (e.g. Neuzil and Tracy 1981).

Several constitutive models that simulate joint normal closure have been developed, (Bandis et al. 1983; Barton et al. 1985; Goodman 1974) of which the most commonly applied is the hyperbolic function developed by Bandis.

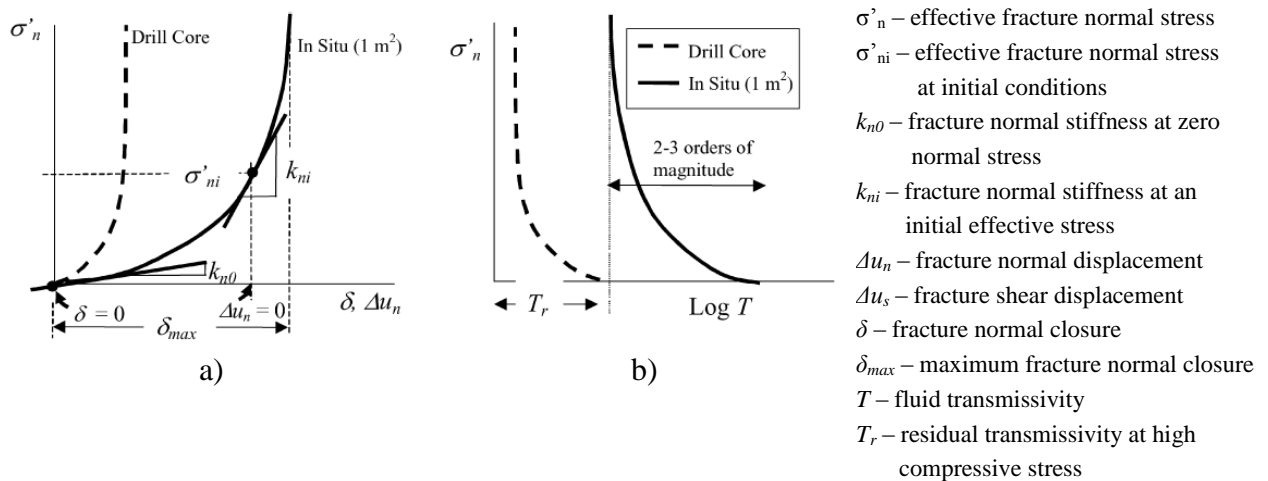


Figure 2.3 – Typical mechanical (a) and hydromechanical (b) fracture responses under normal closure. Effects of sample size is indicated with the laboratory sample response (dashed lines) compared with in-situ fracture response (1 m² size) (adapted from Rutqvist and Stephansson 2003).

2.4.3 Hydromechanical behaviour during shear displacement

The inherent roughness of rock mass discontinuities gives rise to the phenomenon of dilatancy, described by Plesha (1987) as a tendency of two contacting bodies to separate during relative tangential motion due to the sliding of rough surfaces of one body on those of the other. This separation during shear displacement causes an increase in joint hydraulic apertures and consequently an increase in joint permeability. This effect on joint permeability has been analysed both theoretically (e.g. Barton et al. 1985; Bawden et al. 1980) and experimentally (e.g. Chen et al. 2000; Esaki et al. 1999; Olsson and Barton 2001; Yeo et al. 1998).

Figure 2.4 shows the typical mechanical and hydromechanical behaviour of clean, rough, dilatant rock joints under constant normal stress. Regarding the mechanical behaviour, there is a rapid increase in shear stress up to a peak, followed by a loss in load-carrying capacity. The shear displacement is accompanied by shear dilation, as shown in the lower curves of Figure 2.4 a). During elastic deformation of the fracture, there is minimum dilation. The onset of rapid dilation occurs when asperities begin to slide against each other. The rate of dilation (slope of Δu_n curve) increases and reaches a maximum, which is known as the peak shear stress (Barton et al 1985). There is also a scale effect: for a larger sample, the peak shear stress is smaller and takes place after a larger shear displacement. The onset of shear dilation is delayed in larger samples because a larger displacement is required to reach peak shear stress.

Concerning the hydromechanical behaviour, laboratory experiments show that decreases in hydraulic conductivity during shear displacement are a result of gouge production, which

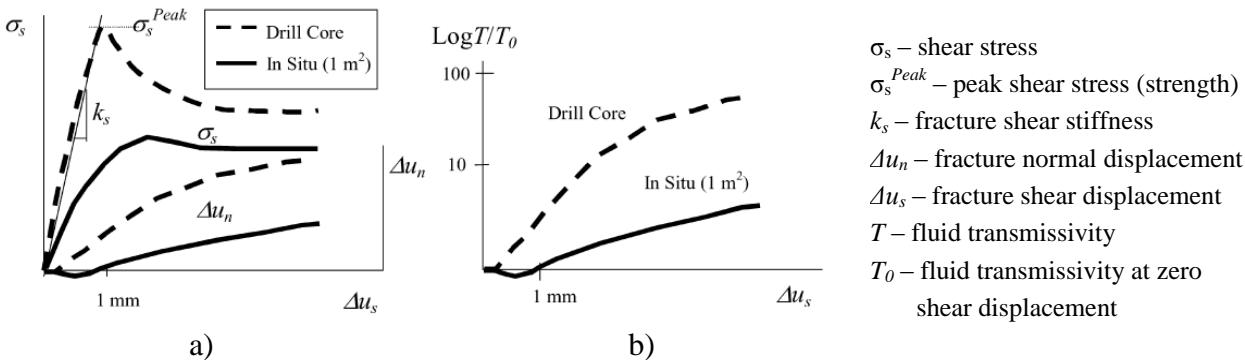


Figure 2.4 – Typical mechanical (a) and hydromechanical (b) fracture responses under shear stress. Effects of sample size is indicated with the laboratory sample response (dashed lines) compared with in-situ fracture response (1 m² size) (adapted from Rutqvist and Stephansson 2003).

tends to block flow paths. The increase in aperture due to dilatancy has the opposite effect. The tests carried out on granite by Esaki et al. (1999) and by Olsson and Barton (2001) show that the joint transmissivity starts to increase after about 1 mm of shear displacement and then increases rapidly by about 1-2 orders of magnitude up to 5 mm. Afterwards, curves tend to be flat and any further shear displacement may give rise to relatively small changes in permeability (Figure 2.4 b). It is worth noting that little experimental work exists on the effect of shear deformation on rock joints' hydraulic conductivity due to difficulties involved in carrying out this kind of test.

Constitutive models for hydromechanical coupling during shear displacement of rock joints, with the hydraulic aperture given as a function of the real mechanical aperture and the joint roughness coefficient (JRC), were developed by Barton et al. (1985) and by Olsson and Barton (2001).

2.5 Specific features of concrete dam foundations

Concrete dam foundation rock masses usually need treatment to satisfy the requirements of stability, deformation and low permeability. Ground improvement works depend significantly on the type and size of the dam, and are essential to the structure's safety. Different measures are available to: i) increase foundation shear strength, stability of abutments and foundation stiffness; ii) improve the contact between the dam concrete and the foundation rock mass, and iii) reduce both the quantity of water flowing through the foundation and uplift pressures. A detailed description of available methods of foundation treatment is presented in ICOLD (1993; 2005). The uppermost strata of the foundation rock mass is often strengthened with consolidation grouting which increases the rock mass deformation modulus in the area close to the base of the dam and thus contributes to reducing deformation due to subsequent dam loading. Another important objective of consolidation grouting is to seal some of the discontinuities close to the dam/foundation interface, which, as a result of excavation works, is usually a more pervious area than the rock mass at depth. Treatment by both sealing and drainage measures is particularly relevant in hydraulic and hydromechanical analysis of concrete dam foundations and thus this issue is addressed below.

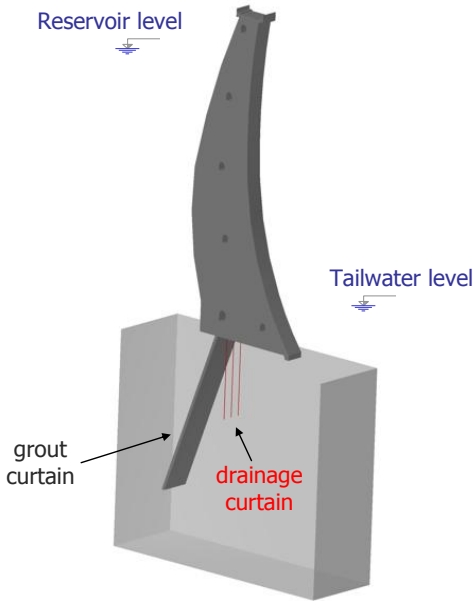
Dam construction and the subsequent filling of the reservoir transmit large loads to the foundation and cause changes in the aperture of the discontinuities through which water flows, both upstream and downstream from the dam, modifying the natural flow pattern. The rock mass in the vicinity of the dam becomes subject to a large difference in hydraulic head between the upstream and downstream areas (large hydraulic gradient). In addition, the cyclic variation in both reservoir level and ambient temperature contribute to continuous change in flow paths (variations in ambient temperature cause changes in the structure's temperature, which may give rise to dam displacements that affect the dam foundation deformation, and

thus the aperture of the discontinuities through which water flows). The flow regime under these conditions has been studied by some researchers, and this issue is also addressed here.

2.5.1 Grout curtains and drainage systems

Seepage through the foundation and abutments is a major concern in concrete dams. Seepage control, necessary to prevent excessive uplift pressures and erosion of material in open joints, is usually made with grout curtains and drainage systems (Figure 2.5). A grout curtain creates a solid mass through which it is more difficult for groundwater to flow, so it reduces seepage under the dam. The drainage curtain is usually a line of boreholes drilled downstream from the grout curtain to collect and control seepage under the dam and so reduce the uplift. Reduction of uplift water pressures increases effective stresses and consequently leads to increased safety.

The most widespread method to reduce the hydraulic conductivity of an area of the rock mass foundation is cement-based injection grouting. A grout curtain underneath a dam is usually constructed by a series of grout holes aligned in a single row, but in some cases it may include two or even more adjacent rows. These are usually drilled from the drainage gallery, close to the upstream face of the dam. In arch dams, special care must be taken in order not to locate these boreholes in the area of tensile stresses that usually develop within the rock mass, below the heel of the dam. The first holes grouted, called primary holes, are commonly spaced 10 to 12 m apart, so the grouting of any of these holes usually does not interfere with the grouting of the adjacent ones. The following series of holes grouted (secondary holes) are located



Drainage boreholes in the gallery of a concrete dam. The grout holes were drilled from the gutter, which is filled with water, as shown in the photo.

Figure 2.5 – Grout curtains and drainage systems in concrete dam foundations.

midway between the primary holes, and the next series (tertiary holes) midway between the secondary and primary holes. Additional grout holes may be necessary if the permeability has not yet been reduced to the desired level. Before grouting, water pressure tests are carried out in each borehole and the decision regarding the necessity of additional grouting is usually based on a permeability criterion. In this way, it is possible to form a continuous curtain or bulb of grouted rock and thus reduce the rock mass permeability in that area. Special care must be taken with grouting pressures, in order not to cause further opening of the discontinuities or enlargement of voids within the foundation. In a generally sound foundation, a typical grout curtain varies in depth from about 0.35 to 0.75 H, where H is the height of the reservoir above the top of the grout curtain.

The drainage curtain is usually drilled from the drainage gallery. In some cases, however, such as in thin arch dams without galleries, it may be drilled either from the downstream face of the dam or from the rock mass surface close to the toe of the dam. Drainage boreholes are drilled after grouting is complete, to minimize the risk of filling the holes with grout. The usual diameter of drainage boreholes is 76 mm, and they are typically located 1.5 to 5 m apart. As a general rule, drainage borehole depths vary from 20 to 40 % of the water head, and from 35 to 70 % of the grout curtain depth (Wyllie 1999). The drain holes may be uncased, when drilled in sound rock, or cased with perforated plastic casing in fractured rock, which will keep the hole open and prevent the rock becoming loose from the borehole walls. Drainage in a concrete dam foundation is always relevant, and is of particular importance in jointed rock masses with discontinuities with a very small aperture where high water pressures may develop over time.

2.5.2 Flow regime in concrete dam foundations

Some of the studies that have been carried out concerning the flow regime in concrete dam foundations are briefly presented below.

The boundaries between different flow regimes (laminar and turbulent) within rock fissures are dependent on the relative roughness and on the Reynolds number (Louis 1969). The relative roughness is given by k/D_h , where k is the absolute roughness of the fissure walls (asperity height) and D_h is the hydraulic diameter of the fissure, equal to four times the hydraulic radius (defined as the area over the perimeter of the conduit), or equal to two times the fissure aperture, if it is assumed that the width of the cross section of the fissure through which the flow occurs is much greater than its aperture. The relative roughness varies between 0 for a smooth fissure and 0.5 when the asperity (roughness) height is equal to the fissure aperture. The Reynolds number is given by:

$$R_e = \frac{D_h \bar{v}}{\nu} \quad (2.26)$$

where D_h = hydraulic diameter of the fissure; \bar{v} = mean flow velocity in the fissure and ν = kinematic viscosity of the water.

Studies carried out by Louis (1969) led to the conclusion that flow in a joint is parallel for relative roughnesses lower than 0.033. In this case, based on test results and on information available from the literature, Louis assumed that the transition from laminar to turbulent flow occurred at the Reynolds number of 2300 (critical Reynolds number). For non-parallel flows, i.e. for relative roughnesses higher than 0.033, the critical Reynolds number depended on the fissure roughness, decreasing with the increase in roughness. The flow laws describe the relation between the Reynolds number and the dimensionless resistance coefficient λ (Louis 1969). Louis compiled the different flow laws and indicated their range of validity, as shown in Figure 2.6. In this figure, the various regions in which different types of flow occur are numbered from I to V. Two different flow laws are shown in Figure 2.6: the first, in region I, is the law of resistance for the isothermic laminar flow of a viscous, incompressible fluid through narrow joints; and the second, in region IV, is the law of resistance proposed by Louis for laminar flow within a rough fissure.

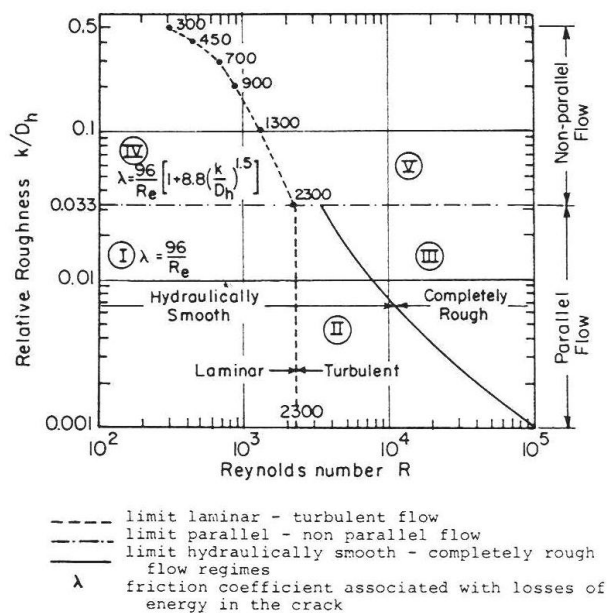


Figure 2.6 – Laws for 1-dimensional flow in a fissure, presented by Louis (1969) (after Goodman et al. 1983).

Louis stated that the relative roughness of natural rock joints is generally greater than 0.033 and highlighted that in nature rock joints are quite often filled with soil materials, such as clay or sand, caused by weathering, tectonic action and sedimentation, and that, in such cases, the flow in the joints can be considered laminar and described with Darcy’s law.

Franciss (1970) studied the hydraulic behaviour of undeformable fissured systems in a linear steady state in order to understand better water movement through jointed rock masses. His research included a theoretical study about the hydraulic conductivity of jointed media, in which he took into account the results that had been presented by Louis (1969), and which led him to the conclusion that flow is predominantly laminar in a rock mass in which the average aperture of the discontinuities is lower than 1 mm and the hydraulic gradient lower than 10 (Figure 2.7). In addition, he statistically analysed the results of 377 Lugeon type tests carried out at various depths in the foundations (mainly granitic) of three different dams in Brazil, and the results of the study indicated that flow was laminar in between 62.9 and 80.4 % of the tests. He therefore concluded that for the hydraulic gradients observed in dam foundations, largely due to the discontinuous nature of seepage paths, seepage velocities are generally low enough for laminar flow to be established, even in fissures with significant hydraulic apertures.

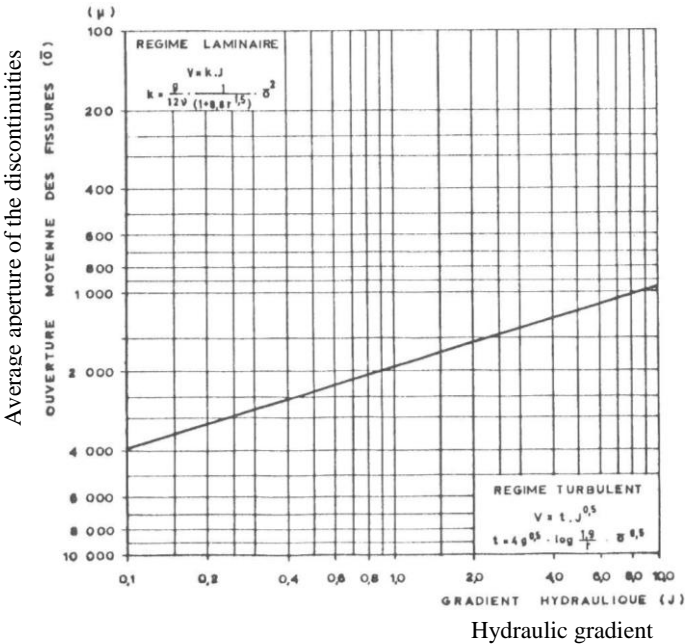


Figure 2.7 – Transition from laminar to turbulent flow (after Franciss 1970).

Wittke (1990) analysed the influence of turbulence on the numerical results in detail. For this, he compared the results of two flow tests carried out with plexiglass models, which simulated jointed rock masses, with the results of discrete models. Devices for measuring the piezometric head were installed at various points within each of the experimental arrangements, to determine the potential distribution. The first model simulated a slope in a rock mass crossed by two sets of discontinuities, in which the height of the water table in one of the discontinuities, located far away from the slope's surface, remained constant. Such a boundary condition could represent, for example, a fault with a large aperture, into which water from remote areas could flow freely. In this model, the discharge from individual discontinuities at the slope face could be measured. The second model simulated the flow into a tunnel in a slope of jointed rock. In both models, the apertures and the discontinuity spacings were relatively large, when compared with the models' other dimensions.

The experimental potential distributions were compared with those obtained with numerical models, in which laminar flow was initially assumed. Taking into account the gradients calculated for individual sections of discontinuity, the flow in various sections was found to be turbulent. Thus, the equations valid for turbulent flow were afterwards considered, and additional numerical results were obtained. Figure 2.8 and Figure 2.9 show the comparison between test and numerical results for both the studied cases.

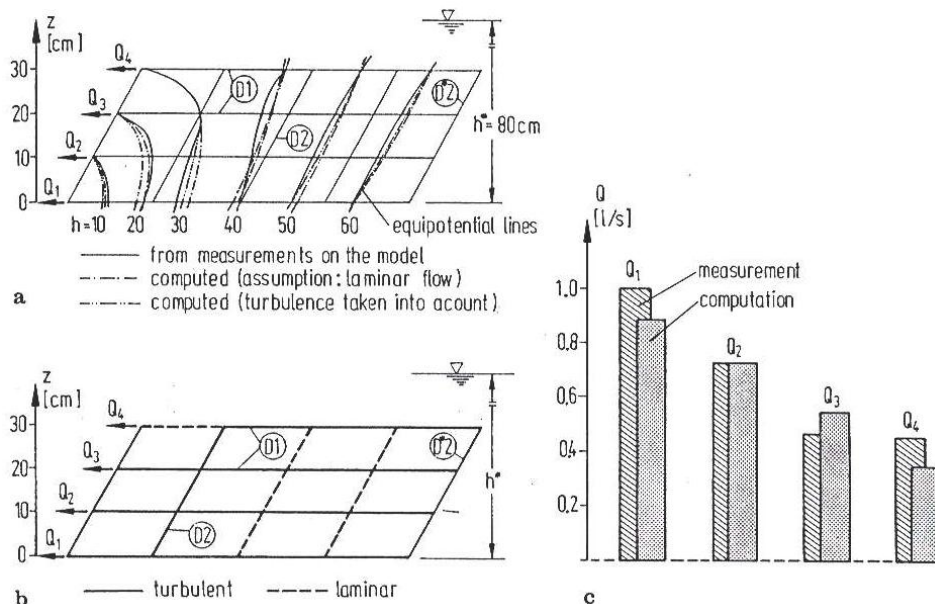


Figure 2.8 – Flow through a slope. Comparison of the results from a model test and from computations: a) distribution of piezometric head; b) flow conditions; and c) seepage water discharges (after Wittke 1990).

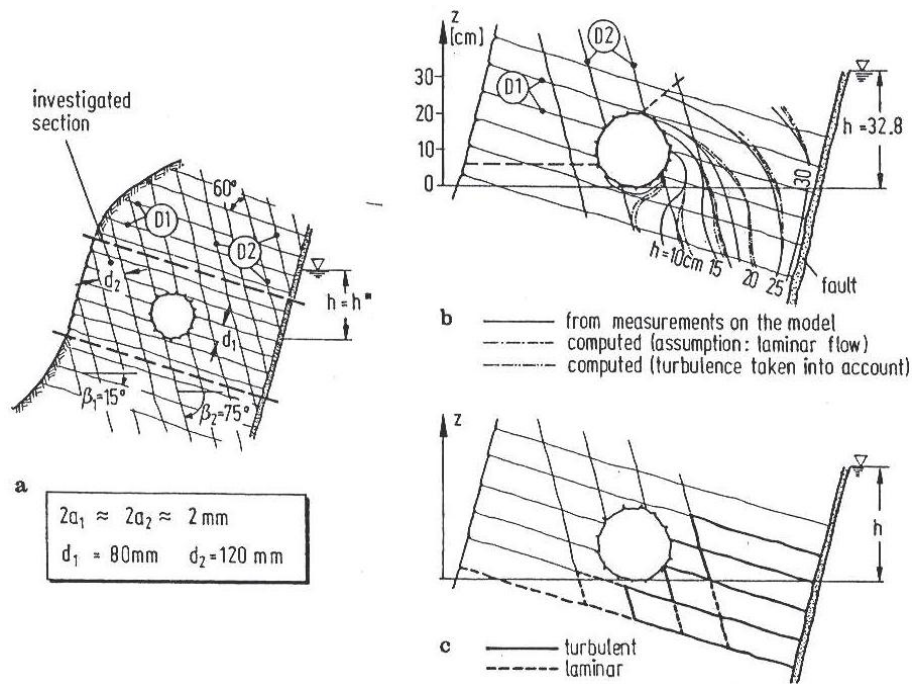


Figure 2.9 – Flow into a tunnel. Comparison of the results from a model test and from computations: a) details of problem; b) distribution of piezometric head; and c) states of flow (after Wittke 1990).

Both figures show that the numerical piezometric heads are very close to those measured and that the consideration of turbulence does not significantly alter the potential distribution. Wittke stated that the deviations between the calculated and measured potentials could be explained by the large aperture of the discontinuities in relation to the length of individual sections of discontinuity. Consequently, the velocity of flow became so large that the energy losses arising at the points of intersection between the two sets of discontinuities could no longer be neglected. Wittke highlighted that the velocities of flow are considerably lower in practical problems, and both the energy losses at intersections and the proportion of discontinuity sections containing turbulent flow are therefore less. In the case of flow through a slope, the difference between the measured discharges and those calculated on the assumption of part turbulent and part laminar flow was 8.6 %.

From these comparative investigations, Wittke concluded that the neglecting of turbulence generally has little influence on the potential distribution, and thus neither on the forces resulting from flow through the rock mass.

From the study carried out general conclusions which also apply to concrete dam foundations can be drawn. Wittke stated that the consideration of turbulence may only become significant if seepage water discharges need to be determined accurately, and highlighted that turbulent flow scarcely arises in problems involving natural rock masses. He added that the statements

concerning the aperture of individual discontinuities are always associated with scatter, which, in practical cases, has a far greater effect on the calculated seepage water discharges than differences due to the state of flow. He also concluded that the seepage flow in a rock mass is steady and approximately laminar in most rock engineering problems, and consequently, problems in which the discontinuities are spaced closely with respect to the structure's dimensions may be solved using the generalized Darcy's law.

Zimmerman and Bodvarsson (1996) show that the laminar solution given by the cubic law is stable when:

$$|\overline{\nabla p}| < \frac{13800 \mu^2}{\rho h^4} \quad (2.27)$$

where $|\overline{\nabla p}|$ = average magnitude of the pressure gradient; μ = dynamic viscosity of the fluid; ρ = fluid density; and h = joint aperture. This expression is obtained from both the average velocity of fluid flow through the fracture and the Reynolds number at which flow changes from laminar to turbulent (critical Reynolds number), and shows that high viscosity, low fluid density and small apertures all tend to stabilize the flow field. The above mentioned researchers state that this stability condition is satisfied in most subsurface flow situations and give the example of water with a dynamic viscosity of 10^{-3} N s/m² (10^{-3} Pa · s) and a density of 10^3 kg/m³, which are the approximate values at 20°C. In this case, even for apertures as large as 10^{-3} m, laminar flow will be stable for pressure gradients as high as about 1.4×10^7 Pa/m. This gradient is equivalent to about 14 MPa/m (140 bars/m), which is much larger than the gradients typically encountered in dam foundations. They add, however, that for a real rough-walled fracture, inertia effects due to tortuous flow paths will lead to deviations from the cubic law long before genuine turbulence occurs, i.e., at lower flow rates. They conclude that, in this case, flow is laminar for pressure gradients lower than 10^4 Pa/m, which is about 0.1 bar/m. This critical gradient is larger than most naturally-occurring groundwater potential gradients.

If there were a continuous rock joint with an aperture of 1 mm close to a dam/foundation interface, developing within the rock mass from the heel to the toe of the dam, the gradient could be higher than 0.1 bar/m. In reality, water usually flows through a network of interconnected discontinuities, whose apertures are smaller than 1 mm, and therefore laminar flow may be assumed. Indeed, according to Barton et al. (1985) numerous tests performed at US dam sites in the depth range 0-60 m indicated that most conducting apertures were in the range of 50-150 μ m at this shallow depth.

2.5.3 Main problems usually found in the behaviour of concrete dam foundations

The role of the foundation in the safety of concrete dams is highlighted in the first chapter. It is mentioned that the majority of recorded failures were due to problems in the foundation rock mass such as those due to weathering processes that lead to a loss of strength, with subsurface erosion and dissolution being the most significant, and lack of shear resistance in rock masses' weak planes of unfavourable direction.

There are a large number of reported cases of dam failure due to the rock mass foundation behaviour or to deficient foundation treatment, of which the most well-known case is the failure of the 61 m high Malpasset dam, in France in 1959, which was the first failure of an arch dam. The failure occurred shortly before the first filling of the reservoir was completed. After many years of research it was concluded that the accident could be satisfactorily explained by the development of full uplift pressures deep in the foundation rock (Londe 1985). These high pressures could have built up due to two simultaneous factors: i) on the left bank the thrust was applied in the direction of the rock schistosity and a crack opening along the schistosity allowed hydrostatic pressure to be installed to a great depth; and ii) rock mass permeability was highly sensitive to stress, and was reduced by a factor of approximately 0.01 due to dam load (Figure 2.10 a). This phenomenon, which was previously unknown, created a hydraulic barrier under the dam which was subjected to high water pressures, and contributed to failure by causing a wedge of rock in the foundation of the left abutment to slide along a fault located under the structure. Investigation carried out after the failure of Malpasset dam led to a consensus among dam engineers that most arch dam foundations should be drained to a deep level and the drainage efficiency checked by an adequate network of piezometers.

Wittke (1990) presented a modified hypothesis for the failure of the Malpasset dam, based on the results of numerical analysis carried out with a three-dimensional finite element (FE) model. The basic failure mechanism was the same as that suggested by Londe, but Wittke assumed an isotropic rock mass permeability, not taking into account the results of laboratory permeability tests carried out after the failure which indicated that the permeability was stress-dependent. Numerical analysis carried out taking into account seepage and uplift showed that due to construction and reservoir filling tensile stresses arose in the left abutment and valley floor in a direction perpendicular to that of the schistosity. The isotropic elastic analysis also indicated shear stresses on the discontinuities downstream from the dam which acted upwards, showing a tendency of the rock mass immediately below the dam to slide downstream. He suggested that the tensile stresses on the schistosity led to the formation of a crack in the left abutment immediately upstream from the dam in which the hydrostatic pressure built up. The great variation in hydraulic head within the rock mass between the

crack and the area downstream from the dam gave rise to high seepage pressures which increased the tendency of the rock mass to slide towards downstream (Figure 2.10 b). This hypothesis was based on the observation of a crack within the rock mass immediately upstream from the heel of the dam, as shown in Alonso (2005).

In Portugal, although a high percentage of concrete dams have been affected by different types of deterioration, both in the dam body and in the foundation, there has never been an accident with this type of dams. The following paragraphs include a brief summary of the main cases of foundation deterioration observed in our country (LNEC 1999a; Mascarenhas 1991; Pedro 1999a; Pedro 2001; Pedro et al. 1989; Ramos 2008). Reported cases concern the foundation of arch dams of different ages, with different geometrical and geotechnical characteristics (Figure 2.11): the cases of Varosa and Vilarinho das Furnas dams, due to grout curtains' lack of resistance to tensile stresses; the cases of Funcho and Odeáxere dams, due to problems related with foundation treatment; the case of Bouçã dam, due to erosion; and the case of Venda Nova dam, due to both erosion and dissolution.

Varosa dam is located on the river Varosa, in the North of Portugal. It is a double curvature arch dam with a maximum height of 76 m, 213 m of development at the crest, and the thickness varies in the central cantilever from 12 m at the base to 3.5 m at the crest. The foundation consists of fresh to moderately weathered granite, crossed by joints with a relatively low resistance. The dam construction ended in the middle of 1976 and the first filling of the reservoir took about a year, from the end of 1976 until the end of 1977. In this dam, shortly after the first filling of the reservoir had been completed, high uplift pressures

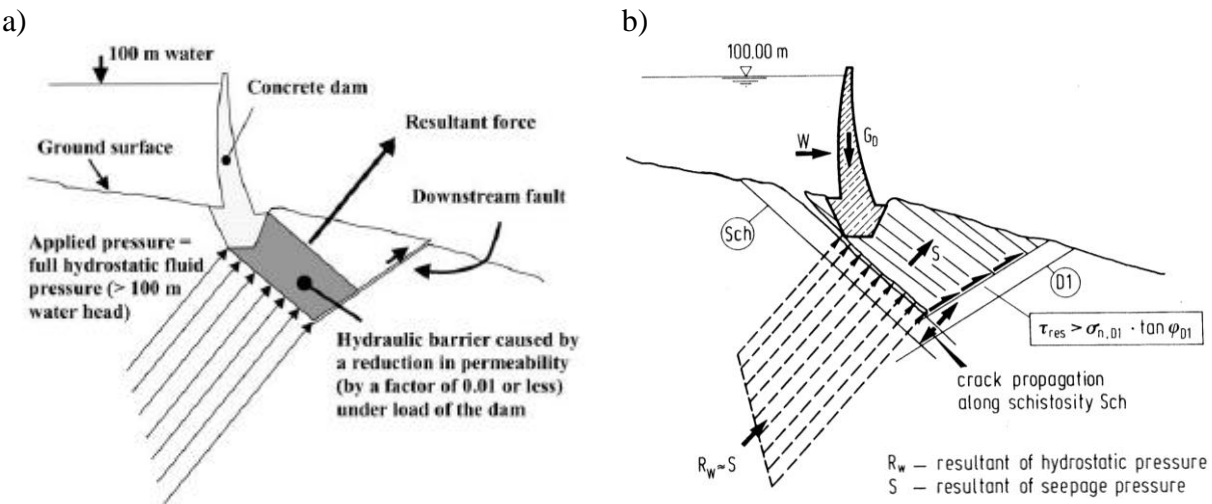


Figure 2.10 - Failure at the Malpasset dam, in France, in 1959: a) Londe's hypothesis (after Rutqvist and Stephansson 2003), and b) Wittke's modified hypothesis (after Wittke 1990).

were observed in the left bank and particularly in the valley bottom, where the percentages of hydraulic head were 100 % close to the heel of the dam and extended towards downstream with values higher than 80 % (percentage of hydraulic head is the ratio of the water head measured at a given level, expressed in metres of height of water, to the height of water in the reservoir above that level). New drains were drilled in the central area, which allowed a decrease in uplift pressures, but around 5 years later, in 1983, an increase in the reservoir level until it was full led to a significant increase in discharges in the bottom of the valley, which tended to increase still further with the water at a stabilized level. In this case it was concluded that the successive loading/unloading cycles due to an operating regime with large daily variations of the water level in the reservoir damaged the grout curtain. Comprehensive analysis showed that the development of high tensile stresses upstream from the dam had led to the opening of the superficial joints and had damaged the grout curtain, in an area less than 1 m deep. Repair work was carried out with both cement grout and acrylic resin.

Vilarinho das Furnas dam, concluded in the end of 1971, is located on the River Homem, in the North of Portugal. It is a double curvature arch with a maximum height of 94 m and a total length between the abutments at the crest elevation of 384.5 m. The foundation consists of granite, crossed by veins of quartz and dolerite. In 1977 excessively high water pressures were recorded in the valley bottom and at the base of the right slope, and this was observed again on several occasions. Some measures have been taken over time, namely the drilling of additional drainage boreholes, in 1977 and 1983, grouting works, in 1980, and cleaning of both drainage and piezometric systems, in 1983. Additional monitoring equipment (piezometers and foundation extensometers) was installed in 1987 so as to better evaluate the hydromechanical behaviour of the dam foundation. Comprehensive analysis of dam behaviour showed that the grout curtain opens when two phenomena occur simultaneously: i) reservoir close to the retention water level and ii) low concrete temperature. The decision was made not to carry out any foundation treatment but to avoid high reservoir levels during the months in which the concrete temperature is low. After this change in the operating regime no more openings of the grout curtain were observed.

Odeóxere dam, located in the South of Portugal, is a double curvature arch concluded in 1958 with a maximum height of 41 m and a total crest length of 150 m. The foundation consists of schist and greywacke and is very deformable, especially in the right bank. In 1967, one of the blocks in the right abutment showed a non-reversible displacement while in the left bank significant seepage was detected under the wing wall of the abutment. Lugeon type tests pointed out the presence of a badly consolidated zone showing high permeability. Grouting was carried out in order to achieve the required consolidation and watertightness.

Funcho dam, located on the River Arade in the South of Portugal, is a 49 m high double curvature arch with 165 m of development at the crest and a width that varies, in the central



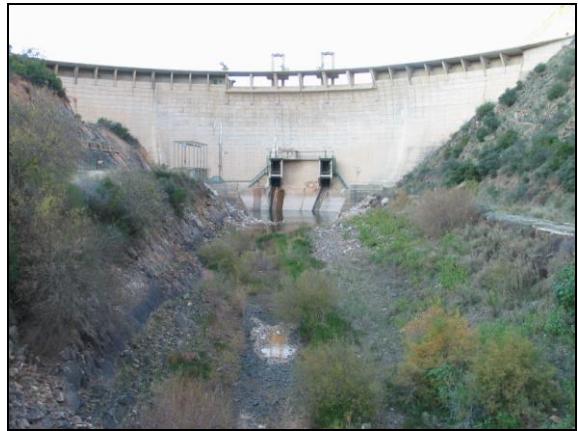
Varosa dam



Vilarinho das Furnas dam



Odeáxere dam



Funcho dam



Bouçã dam



Venda Nova dam

Figure 2.11 – Portuguese dams which had problems due to foundation deterioration.

cantilever, from 6.5 m at the base to 2.25 m at the crest. The foundation rock mass, highly heterogeneous and anisotropic, consists of schist and greywacke (DGRAH 1978). The dam construction ended in 1991 and the first filling of the reservoir, which started at the beginning of November 1992, was only concluded in January 2001. The long period taken for the first filling of the reservoir was due to the need for successive foundation treatments, which made it necessary to hold the filling (LNEC 2005a). Although relatively high permeability values were obtained in Lugeon type tests carried out in the schistose area, it was extremely difficult to seal the discontinuities with cement grout, due to their small aperture and to further weathering of the rock mass when subjected to the induced pressures. In some areas, sealing of the discontinuities could only be achieved with an acrylic resin, whose use is currently forbidden due to its toxicity. This case is mentioned again in chapter 4, as an example of a dam where the use of *in situ* tests similar to those in this study was of major importance in deciding the treatment to be carried out.

Bouça dam, located on the river Zêzere in the central region of Portugal, is a double curvature arch concluded in 1955, 70 m high, with a crest length of 171 m and of which the thickness varies from 7.5 m at the base to 0.9 m at the crest. The foundation consists mainly of granite and of hornfels. In Bouça dam foundation, deterioration was due to progressive clogging of the drainage system during a period of over 30 years. Hydrochemical analysis of the drained water showed mechanical wear of the joint surfaces and of the material inside some faults.

Venda Nova arch-gravity dam, concluded in 1951, is located on the river Rabagão, in the north of Portugal, and has a maximum height of 97 m, and a total length of 345 m between the abutments at the crest elevation. The foundation consists of granite, except in the upper part of the right bank in which there are hornfels. It is crossed by many joints and faults, filled with clay and mylonite. The dam has a peripheral joint in the upstream area of the dam/foundation interface, introduced with the aim of reducing tensile stresses in the rock mass upper area. The rock mass was subjected to cyclic loads and the peripheral joint did not behave properly, and, as in the above-mentioned case of Varosa dam, the grout curtain was damaged due to high tensile stresses in the rock mass. In this case, however, grout curtain deterioration progressed over the years, giving rise to the opening of horizontal joints and leading to a progressive increase in discharges, which went up to around 850 l/min. At the same time, due to the high quantity of water flowing through the foundation, there was a significant increase in erosion and physical-chemical deterioration, which contributed to the increase in permeability in the upstream foundation area. Treatment was carried out with cement grout and acrylic resin.

2.6 Numerical modelling

2.6.1 Continuum equivalent and discontinuum models

There are two different modelling approaches to simulate hydromechanical coupling behaviour of fractured rock masses. The first is based on an equivalent continuum and the second on discrete fracture networks. The choice of continuum or discontinuum approach depends on many case-specific factors, mainly on the size and spacing of the discontinuities when compared to the size of the problem, and on the jointing pattern. The two different types of models may be combined and in this case it is called a hybrid model. This allows some of the disadvantages of each type of model to be avoided. Different numerical models are usually used for each modelling approach.

In equivalent continuum models, materials' properties have to be adjusted in such a way that the major characteristics of the rock mass's physical behaviour are properly represented. Regarding fluid flow, the equivalent permeability of the different rock mass areas may be estimated from the results of Lugeon type tests. The seepage forces induce deformations in the continuous medium, which alters the permeability. This type of analysis requires correlations between stress or strain and permeability to be previously established.

In fracture flow models the discontinuities are explicitly represented, with their individual hydromechanical properties. The flow of water is usually assumed to occur only through the joints. The joint water pressure gives rise to changes in joint apertures and, consequently, changes in flow rates. Discontinuum modelling of the hydromechanical behaviour of jointed rock masses requires field, hydraulic and mechanical characterization data, such as orientation and spacing of discontinuities, joint normal stiffness, joint apertures and residual aperture, which is not readily available.

2.6.2 Models to study the hydraulic and hydromechanical behaviour of dam foundations

2.6.2.1 Analytical solutions and experimental techniques

The first theoretical study about seepage in rock masses with drainage systems was presented by O. Hoffman in 1928. The study was based upon the results presented by Forchheimer about eleven years before, in which the theory of seepage through porous media and a graphical method for the solution of Laplace equation were presented (differential equation which describes the behaviour of fluids in a homogeneous media). In the 1930s and 1940s several studies were published with exact solutions to determine the piezometric surfaces in homogeneous and isotropic foundations, with different cases of grouting and drainage (Terzaghi, Weaver, (Muskat 1946), Dachler, among others).

These models were being developed while an intensive discussion regarding uplift pressures was taking place. The development of the different hypotheses assumed to determine the distribution of water pressures in dam foundations can be found in Serafim (1954), Smith (1971), Andrade (1982), and Schnitter (1994). Until the middle of the 19th century the effect of the uplift pressure was not taken into account neither in the dam body nor in its foundation. The effects of uplift pressures started to receive attention in around 1875 from Belgian engineers, and became a subject of debate after the failure of Bouzey gravity dam in France in 1895, due to seepage through the masonry. Particularly relevant is the study presented in the same year by Lévy (1895) in which he suggested a new design criterion in order to avoid the inflow of water into the dam masonry joints: he stated that the compression at the joint end in the upstream face should be higher than the reservoir water pressure at that point. In addition, he proposed that a vertical drainage system should be installed close to the upstream face of a dam, as a means of minimising problems due to uplift pressures. Lévy's suggestions started an open debate regarding the best way to avoid problems due to seepage. Concerning the dam foundation two different ideas arose: some dam engineers were of the opinion that the effects of uplift pressures could be avoided by intensive grouting, while others argued that it would be preferable to install a line of drains to intercept seepage and thus reduce uplift pressures downstream from the drainage line. This discussion later led to a consensus that the best option would be to combine both solutions, and this is the current practice.

In the 1960s, Arthur Casagrande in the first Rankine Lecture about the control of seepage through foundations and abutments of dams presented an analytical solution, based on Muskat equation, to determine the value of the uplift pressures beneath a dam with a drainage line, assuming the opening of a vertical fissure at the heel of the dam. The results of the solution presented were validated against their comparison with uplift pressures measured in dams with drainage systems (Casagrande 1961).

Serafim and Del Campo (1965) presented a paper with the analytical solution for the distribution of uplift pressures at the base of a dam without drainage systems, in which the importance of the opening and closing of different discontinuities due to the filling of the reservoir was highlighted.

Andrade (1982) presented a solution to determine the hydraulic head in dams with one or more drainage lines, assuming vertical fissures at the heel and at the toe of the dam, and assuming that the dam is impervious and lies on a finite, homogeneous, isotropic and pervious layer. The same author later developed a simplified method where the discontinuities through which water flowed were represented by bars (Andrade 1983; 1984; 1988). It was called "MEPON - Nodal Point Method" and it allowed two and three-dimensional flows to be simulated. The medium was assumed to be deformable and the flow to be dependent on the state of stress within the foundation. It was a mesh method that required the equilibrium

equations to be solved at the nodes, using an iterative procedure. The method was applied to determine the flow rates and the uplift pressures at the base of several concrete dams.

Goodman et al. (1983) proposed a specific analytical solution for flow through a horizontal crack of finite length drained by a series of vertical drains. The solution was used to draw dimensionless diagrams of uplift pressure on the base of a dam and to demonstrate the influence of drains on the distribution and magnitude of uplift forces. This solution was obtained when studying a hypothetical situation of a crack developing under the heel of a dam due to high overturning moment. Such a crack would have a direct hydraulic connection to reservoir and water pressure distribution within the crack and would influence the overall dam stability.

The integration of Laplace equation can be done by analytical or approximated methods, using graphical, experimental or numerical techniques. The use of analytical solutions is restricted as the majority of the solutions available correspond to two dimensional flows in homogeneous and continuum media, with simple boundary conditions. Graphical techniques to draw flow nets were widely used (Forchheimer, Leliavsky, among others), but took a lot of time and were difficult to apply in domains with complex geometric conditions and various boundary conditions. Experimental methods, mainly electric analogs, which associate important features of visual methods with the fact that the flow of electricity through conducting materials is governed by the same differential equations as flow through porous media, were also widely used (Pavlosvsky, Pacher e Yokota, Franciss (1970), Bear, Louis, among others).

2.6.2.2 Hydraulic models

The finite differences method was one of the first numerical methods to provide approximate solutions, and based on this method Serafim (1954) carried out a study with the main objective of contributing to a better understanding of the uplift pressures in dams, a subject under much debate at the time. He drew attention to the fact that these forces are different from the others acting on dams not only because they depend on the internal structure of the concrete and foundations but also because they are influenced by the homogeneity and continuity of their materials. Serafim studied the effect of the water pressure exerted on the internal surfaces of the concrete, and computed stresses due to these pressures in gravity dams, in a horizontal section of the head of a buttress dam and in the arches and cantilevers of an arch dam. He used the iteration method to solve the Laplace equation and presented the study of the two-dimensional flow in radial sections of arch dams and their foundations. Regarding the foundation, he evaluated the influence of the foundation permeability and of both the grout and drainage systems on the uplift forces. Results of further studies carried out by the same researcher are presented in Serafim (1968).

With the occurrence of accidents in large dams, due to seepage in the dam body or in the foundation (Teton, Baldwin Hills, Fontenelle, Voughn Creek and Moyie River in the USA, Malpasset, in France, and Idbar, in the former Yugoslavia), great progress was made from the 1960s onwards in the analysis of foundation problems, together with the development of rock mechanics. With the development of computers, numerical modelling techniques started to be widely used, mainly the FEM, using, when needed, joint elements to simulate discontinuities. Since then, several two and three dimensional studies on seepage in dam foundations have been presented, which assume anisotropic, discontinuous, and/or fractured media, taking into account the influence of the *in situ* stress conditions and the existence of several seepage control measures. The study of the mechanical and hydraulic behaviour of discontinuities, with data collected *in situ* and in laboratory, also played an important role in the development and improvement of some models. Some of these models are briefly presented below.

Mascarenhas (1979) used a series of computer programs developed at the National Laboratory for Civil Engineering (LNEC) to analyse seepage in the foundation of concrete dams. The programs used linear and isoparametric triangular and quadrilateral finite elements and allowed the simulation of two-dimensional flows in both continuum and discontinuum media and of axisymmetric flows in continuum media. The programs developed were structured in such a way that they enabled the implementation of three successive calculating phases: i) the drawing of the FE mesh and validation of data relative to both geometric and hydraulic characteristics; ii) calculation of the seepage factors, namely the hydraulic head, pressure and velocity, and of the mechanical loads due to seepage; and iii) results interpretation. The codes were validated by comparing the numerical results with those obtained in various problems in which the solution was known, or with those that had been previously obtained by other researchers. Parametric studies were carried out to study the influence of grout and drainage systems in the foundation of both gravity and arch dams on the numerical results. The results of the continuum models were compared with those obtained assuming discontinuum media. Seepage through the foundation of two operating concrete dams was also analysed.

Carmo Vaz (1979) developed at LNEC a three-dimensional FE program for analysis of seepage through rock masses in steady-state conditions based on the assumption of continuum medium. Two types of isoparametric FE with linear interpolation functions were used: 8-noded FE of the cubic type, and 6-noded prismatic FE with triangular bases. The computer code, called PERC, included various sub-programs which were structured in a similar way to those mentioned above. The code was validated by comparing the numerical results obtained in two different problems with analytical solutions: the first was the study of a pumping test in a homogeneous medium confined between two impervious boundaries, and the second the study of the hydrodynamic pressures in a reservoir with moving walls. The code was afterwards used in the analysis of the observed behaviour of a multiple arch dam foundation (Mascarenhas et al. 1985; Sousa and Mascarenhas 1984).

Wittke (1990) presented detailed studies carried out with large three-dimensional FE models of the dam-foundation system of both gravity and arch dams. He analysed in detail the interaction between the dam and the rock mass taking into account the seepage flow within the foundation, and presented studies regarding proper boundary conditions and suitable model and mesh sizes both in large models and in detailed analysis. These models have been used to carry out seepage flow and stability analysis of several operating dams (Wittke and Polczyk 2002; Wittke et al. 2003).

Da Silva and Da Gama (2003) developed a FE three-dimensional model for seepage analysis in concrete dam foundations, based on the Darcy's law to represent flow in the continuous permeable rock mass and on the Darcy-Weissbach law for pipes to simulate the flow in smooth or rough drains, both under laminar or turbulent regime. Two different types of finite elements were used to simulate flow in the pervious rock mass, internally divided into tetrahedra. The drain was simulated by one-dimensional finite elements. Non-linear flow in the drains was modelled by means of a "virtual drain" where the Darcy's law for smooth pipes was applied. The model was validated by comparison of numerical results with the results of an analytical solution proposed by Muskat and with the monitoring data of an operating dam. The model has been used in studies of optimization of the design of drainage systems and in studies of the influence of foundation anisotropy on uplift pressures (Da Silva 2005; Da Silva 2006).

2.6.2.3 Hydromechanical models

The first FE numerical models for hydromechanical analysis were presented in the early 70s. These models analysed either linear hydroelastic phenomena in porous media with fully implicit coupling or discrete-fractured media using sequential explicit coupling between the hydraulic and mechanical analysis (Rutqvist and Stephansson 2003).

The first method of fully coupled stress-fluid flow analysis in fractured media was presented by Noorishad et al. (1982). These authors formulated constitutive relationships for the non-linear deformable fractures, based on an extension of Biot's theory of consolidation (Biot's studies provided the constitutive stress-strain relationships on which the analysis of stress and fluid flow in deformable porous elastic media is based) and used the flow line element for modelling fractures, which saved computer storage and reduced run times when compared to modelling with the four-nodal-point element commonly used in FE analysis. The method was capable of solving the two-dimensional quasi-static initial-boundary value problem of coupled stress and fluid flow in saturated deformable fractured porous media. The code was validated by comparison of numerical results with those obtained with the analytical solution of the problem of a single vertical fracture intersecting a well of zero radius. To show the full capability of the method the effect of fracture and matrix deformability in the same problem

was examined in detail, and a second problem of an axisymmetric reservoir with a horizontal fracture at the centre was also investigated.

Asgian (1989) developed a hybrid boundary element-finite difference program for the modelling of fluid flow in deformable, jointed rock. The model was used to simulate reservoir behaviour with variable joint orientations, injection rates, joint dilation angles and variable far-field stress.

Mendonça (1989) developed a three-dimensional FE model for analysis of the hydromechanical behaviour of concrete dam foundations. The foundation rock mass was assumed to be an anisotropic continuum media, with stress-dependent permeability. An iterative technique was used to account for the stress-flow coupling. The code was developed at LNEC and used the same type of elements as the code PERC, which had been developed 10 years before. The model was used to study the behaviour of Bouçã foundation (Figure 2.11), and the results obtained with coupled and uncoupled models were compared. Numerical results were also compared with in situ recorded data, obtained before and after foundation treatment.

Lamas (1993) developed a FE multilaminate model for hydromechanical analysis of pressure tunnels and shafts in fractured rock masses. In addition to the joints belonging to the joint sets, the code allows joint elements to be inserted within a model, so as to simulate main discontinuities, such as faults, or interfaces between different types of material, such as rock and concrete. The program allows both the hydraulic and mechanical models to run independently or in a coupled way. Regarding the hydraulic behaviour, it is possible to model non-confined laminar flow, and fluid flow can take place simultaneously in the equivalent continuum and the discontinuum, and also from each of these media into the other. Regarding the mechanical behaviour, various failure criteria are included. The non-linear hydromechanical analysis is conducted in terms of effective stresses, using an iterative procedure. The model was used to analyse several general problems and was afterwards applied to an operating pressure circuit.

Wei and Hudson (1998) developed a hybrid discrete-continuum model for water flow in the near and far fields of deformable jointed rock masses. In the near field the discontinuum approach was used, with the discrete element method, and water flowed through interconnected fractures only, while in the far field the equivalent continuum model was employed, with the boundary integral equation method. Along the interface of the two domains, both mechanical and hydraulic compatibility conditions were satisfied. Fully coupled hydromechanical analysis could be conducted in the combined near and far fields. The effectiveness of the approach was shown by its application to a conceptual dam foundation problem.

Leitão and Lamas (2006) developed a model of an underground hydroelectric scheme, which included the pressure tunnel, the access tunnels and the underground powerhouse, in order to study the mechanical and hydraulic interaction during the first filling of the pressure tunnel. Analysis was carried out with the code *FLAC^{3D}*, a three-dimensional explicit finite-difference program that uses 8-noded brick elements. The coupled hydromechanical model uses an iterative procedure between two independent hydraulic and mechanical sub-models.

In more recent years, in addition to the use of the FEM, several studies have been carried out using models of flow in discontinuous media (fracture flow models). These models have been applied mainly for gravity dams, namely using discrete element models, with a view to evaluating dam stability, taking into account the water pressures resulting from the flow conditions (e.g. Barla et al. 2004; Gimenes 2000; Gimenes and Fernández 2006; Lemos 1987; Lemos 1999a; Mostyn et al. 1997). A brief summary of the quoted studies is presented in chapter 7, in which dam stability assessment is addressed.

In the case of arch dams 3D models and multiple joint sets are required and it becomes difficult to use fracture flow models. Therefore, the assumption of an equivalent continuum remains the most widely used tool to study the hydraulic behaviour of dam foundations, despite all the investigation carried out regarding flow through discontinuities. Although a wide variety of models suitable for the analysis of rock masses are available, the complexity of jointing patterns and the lack of data on hydraulic properties of the discontinuity sets makes them difficult to apply in most practical cases. Thus, the use of this type of models in the interpretation and operational monitoring of the hydraulic behaviour of dam foundations is not common.

To analyse the hydraulic behaviour of dam foundations it is not only necessary to choose the most suitable model to use but also to take into account that the grout curtain and the drainage system have to be properly simulated, so that the chosen model, which must be realistic and computationally efficient, simulates flow accurately.

2.6.3 Numerical codes used in this study

Analysis presented in this study were carried out with the codes FLAC, UDEC and 3DEC (Itasca 2003; 2004; 2005). These codes were originally developed for application to geotechnical problems, and use explicit step-by-step solution algorithms that obtain static solutions by dynamic relaxation. The three codes allow large displacement analysis and include groundwater models, coupled fluid and thermal modes, and dynamic analysis capability. They offer various constitutive models, which can be altered by the user, using the built-in FISH programming language.

FLAC (Fast Lagrangian Analysis of Continua) is a two-dimensional finite difference program, particularly useful for media that can be modelled as an equivalent continuum with only a few discontinuities. FLAC is primarily used for static analysis of soils and rock masses. The code uses quadrilateral elements or zones, which are made of two pairs of superimposed constant strain triangles, and simulates the performance of materials that behave according to linear or non-linear stress/strain laws in response to the applied forces or boundary conditions. The material can yield and flow, and the grid formed by the different zones can deform and move with the material that is represented. The code includes both interface elements to simulate planes along which slip and/or separation can occur, and structural elements to simulate structural support, which enables its application to a large number of geotechnical problems. Some of the other features are: i) plane-strain, plane-stress and axisymmetric geometry modes; ii) two-phase flow analysis to simulate the flow of two immiscible fluids through a porous medium and iii) determination of the safety factor using the strength reduction method.

In the present study, only the basic groundwater flow model was employed, to analyse steady state seepage flows assuming that the fluid obeys the isotropic form of Darcy's law. FLAC treats steady-flow as an asymptotic case of non-steady-flow. Flow models were run independently from mechanical calculations, and only confined flows were simulated. The option to model axisymmetric geometry, in which cylindrical coordinates are used, was adopted to simulate seepage flow towards a single drain in an equivalent continuum. Two-dimensional analysis of seepage through concrete dam foundations in a horizontal plane and in vertical cross sections of the foundations of both the arch and gravity dams in which *in situ* tests were carried out is presented.

UDEC (Universal Distinct Element Code) is a two-dimensional numerical code that simulates discontinuous media, such as jointed rock masses, subjected to either static or dynamic loading. It is ideally suited to study potential modes of failure directly related to the presence of discontinuous features. The medium is represented as an assemblage of discrete blocks and the discontinuities as boundary conditions between blocks. UDEC enables the modelling of jointed rock masses in which large displacement and opening of the discontinuities occurs. Individual blocks behave as either rigid or deformable material, and in this second case, blocks are subdivided into a mesh of finite-difference elements. These respond according to a prescribed linear or non-linear stress-strain law. The relative motion of the discontinuities is also governed by linear or non-linear force-displacement relations for movement in both the normal and shear directions. This code also allows the simulation of rock reinforcement and surface support.

UDEC is able to perform a fully-coupled hydromechanical analysis, where fracture conductivity is dependent on mechanical deformation and, conversely, joint water pressures

affect the mechanical behaviour (Itasca 2004). In this code, it is assumed that rock blocks are impervious and that flow takes place only through the set of interconnecting discontinuities. Flow is modelled by means of the parallel plate model, and the flow rate per unit width is thus expressed by the cubic law. Total stresses are obtained inside the impervious blocks and effective normal stresses at the mechanical contacts.

In this study, the fluid flow model in UDEC was used to analyse the steady-state seepage flow through the jointed rock foundation beneath the gravity dam studied. Analysis was carried out with a view to evaluating dam stability. A transient analysis was also carried out in order to determine flow times, but was inconclusive because the small timesteps required by UDEC make transient fluid flow analysis impractical in relatively large domains and with very small joint apertures, such as those necessary to analyse flow in dam foundations.

Three-dimensional numerical analysis was carried out with the code 3DEC (Itasca 2003), the three-dimensional version of UDEC. 3DEC simulates the media as a group of convex blocks internally divided into tetrahedra with linear interpolation functions. The code 3DEC is particularly suitable to carry out stability analysis of arch dams, considering some discontinuities in the foundation.

The main interest of the 3DEC code in dam foundation studies is to analyse failure mechanisms involving the rock mass discontinuities and the rock/concrete interface (e.g. Lemos 1999a; Resende et al. 2004). In mechanical modelling, the consideration of a few selected discontinuities is often sufficient to assess the safety conditions. For application to arch dams, special routines are included in 3DEC code (Lemos 1999a) which allow the study of the dam-foundation system, as the dam can be represented as a shell structure, represented by the FEM, and the foundation as a group of blocks. In the present study, 3DEC was used not only in mechanical analysis but also in seepage analysis, as it is useful to study the hydraulic behaviour with the same code which is used to carry out stability analysis.

3DEC is capable of modelling water flow through the discontinuities (Damjanac 1996). In this study, however, an alternative equivalent continuum model was adopted. This new version of the 3DEC code, in addition to fracture flow models, allows the analysis of steady-state flows through the blocks using an equivalent continuum model, including flows bounded above by a phreatic surface. In the equivalent continuum models it is assumed that the hydraulic head is the same at points of adjacent blocks with the same position, which means that it is assumed that from a hydraulic point of view joints between blocks have no influence on the numerical results. In the hydraulic models presented herein, the division into blocks has no physical meaning; it merely makes the mesh design easier.

The choice of 3DEC for equivalent continuum hydraulic models is justified by the fact that the water pressure field thus obtained may be transferred to discontinuum mechanical models for stability analysis.

3 Collection and evaluation of data on the behaviour of dam foundations

3.1 Introduction

Observation is the most reliable means for assessing the safety of the structural system dam-foundation-reservoir. This activity begins at the design stage, with the drawing up of the Monitoring Plan; continues in the construction stage, in which the previously defined instruments are installed and the main material properties are characterized; is of vital importance during the first filling of the reservoir, which is the structure's first loading test; and continues throughout the lifetime of the dam. During construction, the main monitoring activities involve installing the instruments, controlling the effect of construction loads (such as self-weight, thermal loads mainly due to the placement of concrete, injection of contraction joints and foundation treatment), and characterizing material properties. Once the first filling of the reservoir has begun, observation is based on the study of different effects (such as displacements, relative movements of joints, drained water, strains and stresses), trying to establish the relation between each one of these and variations in the main loads. These main loads are also monitored, and for concrete dams under normal operating conditions are hydraulic pressure and variation in ambient (air and reservoir) temperatures. Foundation and dam structure are usually monitored as a whole, and the design of the foundation monitoring system is just part of the overall system (ICOLD 2005).

Monitoring the main loads and structural effects requires installing equipment to measure different factors. The equipment and methodologies used to collect and collate the acquired data is called the monitoring system. This system includes all the sub-systems installed to observe and analyse changes in readings. The factors to be monitored in each dam are defined taking into account the dam type and size, specific project features and the risk factors associated to dam operation. Monitoring systems should be periodically updated according to the stage of the project and foreseen problems.

In Portugal, the systematic observation of concrete dams began in around 1947, when the National Laboratory for Civil Engineering (LNEC) was founded, and followed international trends in dam observation. The Monitoring Plans were designed with a threefold aim: i) for structural safety control; ii) to interpret dam behaviour; and iii) to verify some design criteria and improve knowledge on dam behaviour (Rocha 1964). This philosophy in the development of the Monitoring Plan has been followed since then, which explains the large amount of equipment installed in the majority of large concrete dams (Pedro 1999b). To detect changes in dam behaviour at an early stage, the number of factors to be measured is limited and the

points at which readings are taken are carefully chosen. This is called the “quick observation programme” and usually includes the reading of displacements, movement of some joints and water pressures underneath the dam. In Portugal there are established rules and recommendations regarding the frequency of readings (RSB 2007).

It is widely accepted that over the years a great deal of knowledge about dam behaviour has been obtained. On the other hand, the number of people involved in the safety assessment of dams is not enough to analyse the large quantity of information provided by the monitoring equipment. Therefore, the current trend in dam observation is to focus only on the really key monitoring parameters regarding the safety of each dam (Dunnicliff 1988; Nguyen 2003; Stateler 2006).

Data collection, which is traditionally carried out manually with portable read-out units by on-site personnel, is carried out at intervals defined according to the dam type, stage of the project, and current or foreseen problems. In addition to the measurements taken by instruments installed both in the dam and its foundation, periodic visual inspections in all accessible zones (crest, upstream and downstream faces, foundation, galleries, appurtenant works and reservoir) are essential. In several countries, including Portugal, in addition to the manual readings, part of the monitoring data of some large dams is now also collected by automated data acquisition systems (ADAS). Remote automated readings have several advantages, not least that they enable an almost continuous safety assessment of dams, providing the data obtained is appropriately transmitted, validated, stored, and processed (Farinha et al. 2004). If this is linked to an expert system, warnings can be given when abnormalities are recorded and corrective measures can even be suggested (Portela 2001). However, it should be noted that even with this kind of control visual inspections at dam-sites must be carried out at certain intervals.

The evaluation of dam behaviour, particularly the foundation, and its safety assessment are greatly improved if the monitoring data is compared with predicted values by means of models, which conceptually simulate dam behaviour. These can be either numerical or statistical models. The first require realistic input parameters and the second a large number of monitoring results and substantial experience to support their application to a particular type of structure (Lemos 1999b).

This chapter briefly presents the basis, the methods and the equipment for foundation monitoring, and the methodologies currently used in the analysis of concrete dam foundation monitoring data. Using the traditional simplified methods of quantitative interpretation, a procedure is proposed for the analysis of the recorded discharges, which takes into account the non-linear hydromechanical behaviour of dam foundations.

3.2 Safety control criteria

The safety of a large dam must be ensured during the structure's complete lifetime and therefore a series of measures are usually taken, beginning at the design stage, to fulfil both safety and serviceability requirements. Regarding the dam foundation there are three main scenarios of rock mass foundation deterioration to be concerned with (Pedro et al. 1989):

- i) cracking and movements within the rock mass associated with joint systems and faults,
- ii) absolute displacements of the rock mass surface and relative displacements of adjacent blocks of the dam which may affect the grout curtain or other watertight systems or the operating conditions of the equipment, and
- iii) seepage through the foundation and abutments, because this can lead to high uplift pressures, which destabilize the dam, or to potential high seepage velocities, which cause erosion.

At the design stage, estimates of the hydraulic and mechanical behaviour of the dam foundation are obtained using adequate models and taking into account different scenarios which may occur. The hydromechanical behaviour of a rock mass on which a concrete dam is going to be built is always difficult to know until the first filling of the reservoir, despite all the investigation carried out at previous stages. It is therefore very difficult to establish rules to be followed by the designer. However, based on both design criteria and experience, there are established principals and general criteria that should be followed by the designer with a view to guaranteeing the dam safety.

Particularly relevant is the distribution of water pressures along the base of the dam or along potential sliding surfaces in the foundation. At the design stage, full reservoir head can be assumed at the heel of the dam and zero or tailwater head, if any, at the toe of the dam. It is usually assumed that at the drainage line the head is equal to between one half and one third of the head difference between the heel and toe of the dam. Thus, a bi-linear distribution of the uplift pressure along the base of the dam is assumed. It is normal practice to use the value of one third of the head difference between the head and toe of the dam as this was established from data obtained in piezometric readings taken in the foundations of a number of both Tennessee Valley Authority and US Bureau of Reclamation dams (Casagrande 1961). A more conservative assumption, for an inoperative drainage system, is a linear distribution, i.e. a constant decrease in head between the heel and toe of the dam. The head distribution along the base of the dam depends mainly on the presence and efficiency of the drainage system. Several studies have been carried out by different bodies (Électricité de France (EDF), Swiss Committee on Dams (SCD) and Electric Power and Research Institute (EPRI),

in the USA) regarding analysis of recorded uplift data. All of these studies, which are briefly presented along with the main results in European Club of ICOLD (2004a), were carried out because of the general acknowledgement that design assumptions have never been fully validated. Different criteria have been adopted by different bodies regarding the distribution of uplift pressures along the base of the dam, and great effort has been made in order to analyse the differences in the results (European Club of ICOLD 2004a; USACE 2000).

According to the current Portuguese guidelines for dam design (RSB 2007) the dam safety should be assessed analysing its behaviour for normal operating and failure scenarios. For normal operating conditions it is required that the displacements and stresses in the rock mass close to the surface be relatively small, that the drained water through the foundation be such that it corresponds to an average permeability at the grout curtain area not higher than 1 LU, and that the uplift at the drainage line be lower than the equivalent of $1/3$ of the hydraulic head upstream from the dam. For failure scenarios it is recommended that equilibrium exists in wedges defined by joints and faults for which movement is possible, that out-of-control flow of water through the foundation with high seepage velocity is not likely to occur, and that the drained water through the foundation is such that it corresponds to an average permeability at the grout curtain area not higher than 5 LU.

Two of the above-mentioned requirements merit further comment: the first concerns the desired level of permeability and the second the uplift at the drainage line. Regarding the first, it is worth noting that the attempt to construct a grout curtain with a final water injection rate of 1 LU is considered inappropriate, as this can only be achieved by intensive and often costly grouting schemes and is only necessary in the special cases where the reservoir water is very precious or soluble rock is present in the foundation (ICOLD 2005). Regarding the second, the requirement that the uplift at the drainage line be lower than the equivalent of $1/3$ of the hydraulic head upstream from the dam disregards the head of the toe of the dam, which may be significant, in particular in dams with a reservoir downstream. In this case, and at the design stage, it would be better to require that the pressure at the drainage line be lower than the equivalent of the tailwater head plus $1/3$ of the difference between reservoir and tailwater heads.

At the construction and operation stages, the foundation treatment and proper maintenance of the drainage system are essential to ensure the safety of the dam. Regarding stability, water pressures are the most crucial aspect, but discharge is also a relevant factor as it is correlated with seepage velocity, which should be limited in order to avoid erosion of material in open joints.

For the evaluation of both grout curtain and drainage efficiency, Mascarenhas and Silva (1990) proposed a methodology which takes into account recorded discharges and water

pressures. They mention that the three main aims of grout and drainage systems are: i) to reduce uplift pressures to values close to those foreseen in the design; ii) to restrict seepage velocity so as to keep erosion of material in discontinuities to a minimum, and iii) to restrict seepage through the foundation, taking into account functional and economic factors. To achieve these aims the following criteria are established at the design stage: i) the maximum hydraulic head allowed along the drainage line (Φ_{\max}), expressed in percentage of hydraulic head (percentage of hydraulic head is the ratio of the water head measured at a given level, expressed in metres of height of water, to the height of water in the reservoir above that level, as mentioned in the previous chapter, section 2.5.3); ii) the maximum allowable discharge per metre (q_{\max}); and iii) the maximum global discharge (Q_{\max}). If there is more than one drainage line, these criteria should be established for each of them.

They suggest that a global index I_G (I_P ; I_q ; I_Q) should be used in which:

$$I_P = \frac{\Phi_{0 \max}}{\Phi_{\max}} \quad I_q = \frac{q_{0 \max}}{q_{\max}} \quad I_Q = \frac{Q_0}{Q_{\max}} \quad (3.1)$$

where $\Phi_{0 \max}$ is the maximum percentage of hydraulic head recorded along the drainage line, $q_{0 \max}$ is the maximum recorded discharge per metre along the drainage line and Q_0 the total recorded discharge. The three different sub-indexes, I_P , I_q and I_Q , are called pressure index, unitary discharge index and global discharge index, respectively. Different foundation areas can be analysed using these indexes. Mascarenhas and Silva stress the fact that the global index can only be used if the dam is adequately monitored, if there is confidence in the monitoring data and if detailed knowledge of the seepage pattern has already been obtained.

The global index I_G shows the actual effectiveness of both the grout and the drainage systems, and in the case of an efficient system each of the three sub-indexes I_P , I_q and I_Q should be less than or equal to 1. This methodology was used to analyse the efficiency of additional foundation treatment which had to be carried out in some Portuguese dams, due to excessive recorded discharges or water pressures (Fronhas arch dam, Venda Nova arch-gravity dam and Varosa arch dam), and in every case it was concluded that I_G was significantly lower after treatment (Mascarenhas 1991; Mascarenhas and Silva 1990). It was also used to assess where additional foundation treatment should be carried out in Funcho arch dam (LNEC 1998b), and to assess the efficiency of the grout and drainage systems of the different structures of Alto Rabagão dam. This dam has an arch structure in the main valley and two gravity structures, one on each side.

While the method is very simple and can be effective, the global index does, however, have three main drawbacks. Firstly, it takes both the maximum hydraulic head and discharges prescribed in the design as reference. However, despite all the investigation carried out prior

to dam construction, it is impossible to predict the hydraulic behaviour of the dam foundation in normal operating conditions, and therefore the values established at the design stage should not be considered as “reference”. Secondly, it does not take into account the length of both drainage and piezometric boreholes, nor the depth at which the main seepage paths cross the boreholes. Finally, a high water pressure recorded in a piezometer may be localised and high water pressures are only relevant when acting on a horizontal discontinuity with a large surface, which encompasses the whole base of a dam block. It is worth noting that low water pressures recorded in a piezometer can be misleading in some cases, as is going to be shown in chapter 6.8.

3.3 Foundation monitoring

The first use of instruments in rock foundations of concrete dams was mainly for research purposes (Londe 1993). In fact, after the 2nd World War, with the construction of an increasing number of large dams, the amount of monitoring equipment to control structural behaviour increased significantly but most of the equipment was placed in the superstructure to confirm design hypotheses, and not in the foundation, as rock mass foundation characteristics were not taken into account until the sixties, when it was understood that serious accidents had occurred due to defective foundations.

The mechanical and hydraulic behaviour of rock mass foundations is currently monitored with a group of techniques and equipment which allow the measurement of displacements and strains, uplift pressures, discharges, stresses, and physical and chemical properties of the water. Instruments are systematically installed for the follow-up of the actual behaviour during construction, the first filling of the reservoir and in the longer term.

Regarding the equipment, it is necessary to measure both external loads and responses. The first type includes hydrostatic pressure, meteorological quantities, and seismic events; and the second, which indicate the behaviour of the dam foundation, includes mainly deformations, water pressures, and discharges. Measurable quantities and the different monitoring devices which may be installed are listed and briefly described in Figure 3.1 and Figure 3.2. Additional equipment is often installed in order to evaluate materials' properties.

Displacements are measured using geodetic methods or along lines and the different readings together, some of which are redundant, create a three-dimensional or spatial displacement measuring system. Regarding water pressures, it has to be taken into account that piezometric readings provide much localised information and can vary greatly from point to point, as they depend on the flow paths of water within the rock mass. Piezometers may be installed upstream and downstream from the drainage system, in order to measure the hydraulic head difference and therefore evaluate the efficiency of the seepage control measures. In Portugal,

the majority of the piezometers installed in the foundations of concrete dams have a long single chamber and therefore give only one water pressure value, which is the result of the inflow and outflow of water from different strata or discontinuities which have different hydraulic heads. This type of piezometers, which are accessible to water over their whole length, although not recommended by the ICOLD (2005), remain widely used due to the fact

Quantity	Monitoring device	Remarks
(a) Deformations		
Displacement in vertical boreholes (displacement along vertical lines)	Inverted pendulum (plumbline)	Most accurate monitoring device in rock foundation (Londe, 1982), teletransmission possible, requires "fixed point" and perfectly vertical hole. Accuracy ± 0.2 mm, resp. $\pm 1\%$ of measuring range. Length max. about 50 m.
Displacement along horizontal lines	Wire alignment in galleries with optical sighting of the wire	Equivalent to plumbline
Displacements on ground surface and spatial displacement of individual points (e.g. on abutment)	Various geodetic methods and combinations thereof (leveling, optical alignment, measurement of angle and distance, traverse, triangulation)	Well-trying and simple methods with up-to-date equipment; geodetic network must cover large area; supplementary use of GPS often advantageous
Changes in length (relative displacement of points) and deflection along boreholes (vertical and inclined)	Rod or wire extensometers, single or multiple	Teletransmission possible, accuracy ± 0.5 mm
	Sliding micrometer (differential length variation) Sliding micrometer with inclinometer (differential deflections partly combined with differential length) Deflectometer	Placing and grouting of guiding sleeves is a critical operation; measurements are usually of high accuracy.
Movement of cracks and joints at accessible locations (expansion, shear movement)	Micrometer Deformeter Dilatometer Deflectometer	Measurements in gallery walls or recess may not be representative of the behavior of the entire rock mass. Crack propagation can be monitored by appropriate check marks.
Local rotation in the vertical plane on abutment rock	Clinometer (mechanical or electrical) Clinofor	Near to cavities results are often influenced by stress concentration and transfer effects.

Figure 3.1 – Monitoring deformations in concrete dam rock foundations (after ICOLD 2005).

that multilevel piezometers, which allow measurement of water pressures in isolated sections of the holes, require demanding care in their design and installation. Only a few attempts have been made in Portugal to install multilevel piezometers, which are described in detail in chapter 6, section 6.8.1. Devices like the continuous borehole piezometer (Londe 1973c), the piezofor (Bordes and Debeuille 1987) and the piezodex (Kovari and Köppel 1987), which do not disturb the seepage pattern and allow the complete piezometric profile along a borehole to be logged, were mainly used for research activities.

Part of the water flowing through the foundation is collected by the drainage boreholes, and it is recommended that partial discharges be monitored in addition to the total discharge as this procedure enables the identification of critical areas, if there is a sudden or gradual but consistent change in seepage rates. Physical and chemical analysis of both the reservoir and drained water are carried out in order to detect the occurrence of erosion or dissolution of materials either from the rock mass or the grout curtain.

Quantity	Monitoring device	Remarks
(b) Seepage flow and cleft/pore water pressure in the foundation		
Volume of seepage (by zones and in total)	Volumetric (calibrated container + stopwatch) suitable for drains and springs	Limited to moderate discharges, i.e. up to about 10 liters/s. Filling time of container should be at least 10 s (10 litres/s =600 l/min)
	Rectangular and V-notch weir Parshall flume Sonic gage	Periodic removal of possible deposits, not recommended for discharges <0.05 liter/s. (0.05 litre/s =3 l/min)
	Flow measurement in pipes by venturi meter, sonar or magnet-inductive measurement	Simple means for periodic check of readings necessary (e.g. manometers, weirs, etc)
Presence of water circulating in the foundation rock (uplift on concrete foundations and water pressure in permeable rock and in rock joints)	Observation well (for steady-state water table)	Measures average water table along entire depth of hole
	Standpipe piezometer (Casagrande type)	Measuring section (slotted or perforated, or filter element) sealed watertight from upper part. Slow response time (if pressure is higher than elevation of top of pipe, pressure is measured by a manometer)
	Single or multiple closed piezometer (pressure cell), hydraulic, pneumatic, or electric	Closed system, fast response, installation procedure critical, remote reading, more than one cell per hole possible

Figure 3.2 – Monitoring seepage flow and water pressures in concrete dam rock foundations (after ICOLD 2005).

3.4 Methodologies used in the collecting and evaluation of the monitoring data

3.4.1 Collecting and collating of the monitoring data

The Monitoring Plan establishes the frequency of readings which are usually carried out by expert teams on dam observation. In a first phase, readings are compared with maximum and minimum limits established either by the equipment's measuring range or by previous readings. This allows measurements to be readily repeated and re-checked if there are major changes between subsequent readings, possibly using alternate readout equipment. Data collected should be checked a second time, as soon as it is entered into a computer system, by comparison with performance limits established case by case taking into account previously observed and predicted dam behaviour.

The amount of data concerning each dam is very large and therefore several automatic systems have been developed worldwide for its management and analysis (e.g. Cadei et al. 1990; Gallego et al. 2007; Huai-Zhi and Zhi-Ping 2005). In Portugal, an automatic system called GestBarragens has recently been developed with the aim of supporting the activities concerned with safety control in its various stages (Pina and Portela 2006; Portela et al. 2005). It results from a close partnership between three Portuguese bodies (LNEC; Instituto de Engenharia de Sistemas e Computadores, Investigação e Desenvolvimento (INESC-ID); and Electricidade de Portugal (EDP)) and aims at obtaining, automatically, a diagnosis of the dam's actual performance from analysis of all the information available, particularly that from the monitoring system, with a view to detecting possible changes of safety or functionality conditions. It is hoped that in the future GestBarragens will be linked to an expert system.

3.4.2 Evaluation of the monitoring data

The behaviour of a dam is only properly understood through the careful interpretation of the readings from the most relevant instruments. Analysis of readings over time allows the assessment of the dam behaviour, which is not only the best indication of how the dam is going to behave in the future but also provides a means to detect the occurrence of sudden or gradual changes in dam behaviour, which may require further attention. The current practice in studies of the behaviour of concrete dam foundations is:

- i) to analyse the monitoring data taking into account the variations over time of different measurements (such as total and partial discharges, uplift and corresponding percentage of hydraulic head, and displacements measured in inverted plumb lines and in foundation extensometers);

- ii) to compare measurements taken on different dates in which the main loads have similar values, and
- iii) to analyse the correlation between discharges and water level in the reservoir.

Whenever possible, analysis is carried out in order to correlate readings taken in different instruments. This is the case of discharges and water pressures which are usually analysed together, as their simultaneous analysis provides an indication of the efficiency of both grout and drainage systems. Only in a few cases is the monitoring data compared with the results of numerical or physical models of the dam-foundation system.

In addition to the above-mentioned analyses, it is also usual to perform statistical studies of quantitative interpretation of the recorded displacements. In fact, due to their simplicity, these methods have been extensively used in interpretation of dam behaviour. The next section presents a brief description of these methods and the studies carried out in order to analyse recorded discharges using quantitative interpretation are afterwards presented.

3.4.3 Quantitative interpretation methods

The main loads to take into account in the analysis of concrete dam monitoring results during normal operation are variations in the reservoir level and variations in ambient temperature. As these loads act simultaneously, the most representative structural behaviour effects measured on each date, namely displacements, strains and stresses, are the result of this coupled action. Therefore, to analyse and interpret concrete dam behaviour it is essential to separate and identify each one of the loads contribution to the observed effects. This separation can be easily done when the variation of one of the main loads is predominant, between two dates sufficiently close so that the effects due to variations of material's properties over time or due to ageing process are negligible. In a systematic way, this separation can be done using effect separation methods, also named quantitative interpretation methods which, from the simultaneous consideration of a large number of monitoring results, try to establish a correlation between a given observed structural effect and the variations in each of the main loads.

The first studies on dam behaviour using quantitative interpretation methods were published from 1955 to 1960, most of them in the 6th ICOLD Congress (Ferry and Willm 1958; Rocha 1956; Rocha et al. 1958a; Rocha et al. 1960; Rocha et al. 1958b; Service Construction Aménagements Hydroélectriques du Groupe Edison-Milan 1958; Tremmel 1958; Xerez and Lamas 1958). Most of these studies analysed displacements recorded in concrete dams, and tried to identify the elastic parts of the displacement due both to hydrostatic pressure and to variations in temperature linked to the annual thermal wave. The part of the displacement which could not be explained by the above-mentioned elastic parts was the “time effect”. A

new procedure was later presented by the Italians, in which the correlations between the main loads and the structural effects took into account the results of structural models (Bonaldi et al. 1977; 1980a; 1980b; 1982; Fanelli 1979; Fanelli et al. 1979). Doboz (1982) and Ramos (1985) found a way to separate the part that could be explained by the non-elastic behaviour of the dam concrete from the time effect. Currently, work is focused on the development of models which include thermal corrections to the so called HST models (hydrostatic, seasonal, time models in which it is assumed that the seasonal thermal effects are properly modelled by a cyclical annual wave) by taking into account recorded temperatures. The need for these new models is based on the observation that the HST model is not entirely suitable when there are cyclic water level variations in phase with the seasonal thermal variations, and on the fact that the climate is changing and therefore dams are now subjected to unusual temperature conditions (Léger and Leclerc 2007; Penot et al. 2005).

Quantitative interpretation methods have been widely applied and are the subject of numerous studies (e.g. Bonelli 2004; Breitenstein et al. 1985; Carrère et al. 2000; Crépon and Lino 1999; De Sortis and Paoliani 2007; Florentino et al. 1971; Florentino et al. 1985; Gicot 1964; 1976; Gomes 1981; Gomes and Matos 1985; Guedes and Coelho 1985; Hasegawa and Murakami 1988; Jinping and Zhenzhao 1988; LNEC 1961; Miike and Kobayashi 1989; Pedro et al. 1984; Perner et al. 2001; SCD 2003; Serafim et al. 1962; Silveira 1965; Silveira and Pedro 1964; Silveira et al. 1981; Widmann 1967; Willm and Beaujoint 1967) and, although different assumptions and techniques have been used, the simplicity of the method and the accuracy of the results reported over time have shown that these methods are a powerful tool in the analysis of concrete dam behaviour.

These methods have been classified according to the materials' rheologic behaviour, mainly as elastic and visco-elastic, or according to the structural numerical models on which they rely, as statistical, deterministic, and mixed. In statistical models the main loads' effects are represented by means of functions that are completely independent from one point to another. These methods are purely empirical, therefore requiring chronological series of readings of the different variables over a sufficiently long period of time. The series of cause and effect quantities are then correlated by means of regression techniques. In deterministic models the main loads' effects are represented by functions obtained from the results of numerical models, so they are not totally independent from one point to another. Mixed methods combine the fundamental features of the statistical and deterministic methods, for instance making use of a statistical formulation relative to one of the main loads and a deterministic formulation relative to the other. Detailed description of quantitative interpretation methods and of the above-mentioned models can be found in Gomes (1981), Castro (1997) and SCD (2003) and therefore only the basic formulation of the statistical elastic method is presented here.

Quantitative interpretation studies are carried out during periods when there are no events that may lead to significant structural changes, such as earthquakes or rehabilitation of the foundation or of the dam body. In terms of both concrete and foundation behaviour, of which the properties change over time, this requires the use of mean values of the parameters relative to their behaviour. When an elastic structural behaviour is expected, it is assumed that (Gomes 1981):

- i) the most representative factors of the structural behaviour, in normal operating conditions, can be separated into two parts, one elastic (reversible and instantaneous) mainly due to variations in hydrostatic pressure and temperature, and another non-elastic (irreversible), which is exclusively a function of time;
- ii) the effects due to variations in hydraulic pressures and temperature can be studied separately.

In the first hypothesis, time effects are considered to be independent of changes in the main loads, and therefore the analysis of dam behaviour can first be carried out examining the time effects. In many dams this is a simplification, for example in the case of concrete creep in which a significant part of the time effects depends both on changes in reservoir level and on concrete properties. The second hypothesis is based on the assumption that materials have an elastic behaviour, which is confirmed for the level of stresses that occur in concrete dams in normal operating conditions.

In elastic methods, the different effects associated to an observation date i , on a given point, are related by means of a function of the type:

$$\begin{aligned}
 U_i (h_i, \theta_i, t_i) &= U_h (h_i) + U_\theta(\theta_i) + U_t(t_i) + k + r_i = \\
 &= \sum_i a_i f_i(h) + \sum_j b_j g_j(\theta) + \sum_k c_k p_k(t) + k + r
 \end{aligned}
 \tag{3.2}$$

where $U_i (h_i, \theta_i, t_i)$ is a given observed effect observed on date i , which depends on the hydrostatic pressure, the temperature and the moment when the data is collected, and $U_h(h)$, $U_\theta(\theta)$ and $U_t(t)$ represent, respectively, the parts due to the elastic effect of variations in reservoir water level, due to the elastic effect associated with thermal variations and due to the time effect with the starting point at the beginning of the period under analysis. Each one of these parts can be approximated by pre-established sums of level, temperature and time functions, f_i , g_j , and p_k , and depend on the coefficients a_i , b_j and c_k , which need to be calculated. Separation of effects requires the consideration of the constant k due to the fact that on the observation reference date the calculated value is not zero. The residue r_i represents the deviation between the value observed on date i and the result of the quantitative

interpretation model. Thus r_i represents observation errors and errors due to model's unsuitability.

Coefficients a_i , b_j and c_k are determined through the calculation of a system of n equations, in which n is the number of selected observations. The system of equations can be solved by the Gauss criterion which establishes the parameters that minimize the sum of the squares of the errors r_i (least square method). In a quantitative analysis a reference date has to be given in order to calculate the time effect. This date must be prior to the first date considered in the analysis, but the curves obtained are the same regardless of the given date, as the result is adjusted with the independent term (k).

Quantitative interpretation methods can be used in the analysis of concrete dam measurement data with the following purposes (Florentino 1983):

- i) automated control of future dam behaviour;
- ii) validation of numerical structural models; and
- iii) analysis of evolution in dam behaviour.

Regarding the first above-mentioned purpose, as the results of quantitative interpretation of monitoring data define a structural behaviour model of the dam, the safety assessment of the dam can be made automatically by comparing the observed values on a specific date with the predicted values obtained from the quantitative interpretation of previously measured data. Concerning the second, to validate numerical models, influence lines due to the water pressure and due to thermal loads, determined from the quantitative interpretation of monitoring data and from the numerical model, are compared. The quantitative interpretation covers a range of levels in the reservoir, which should be uniformly distributed. The comparison between influence lines due to the water pressure calculated with the quantitative interpretation and with the numerical model, for the same range of levels in the reservoir, allows the correction of the numerical parameters, which makes the use of the numerical model in the prediction of the dam behaviour possible. Finally, as regards development in dam behaviour, analysis can first be carried out examining the time effect, which is asymptotic and in most cases can be explained by the concrete rheologic behaviour or by ageing processes. However, in this analysis it must be taken into account that the non-elastic effects that may exist can be statistically divided between the different parts negatively affecting the quality of the interpretation.

Quantitative interpretation methods are typically used in the analysis of displacements of concrete dams. Displacements reflect a structural global behaviour and are influenced both by variations in reservoir level, which can be established using quantitative interpretation

methods and compared with the results of a numerical model, and also by variations in ambient temperature. The time effect is in most cases mainly a concrete creep effect which can be analysed and characterised from the results of tests carried out in creep cells, either *in situ* or in laboratory, or can also be an ageing process, such as swelling. Although not often applied in practice, statistical modelling can also be used to analyse strains and stresses. On this subject, Oliveira (2000) presented a new formulation to interpret recorded strains with a view to converting them into histories of stresses, which was later implemented by Moura (2005). In observed factors which do not correspond to linear structural responses, such as joint movements, piezometric levels, uplift and discharges, the use of quantitative interpretation methods is not current, as in these cases the principle of superposition of effects is not valid.

Foundation monitoring results include foundation movement, water pressures and seepage. The use of statistical models of quantitative interpretation to study the behaviour of the foundation, taking into account the monitoring data, has almost been limited to the analysis of displacements recorded with plumb lines and foundation extensometers. The foundation movement close to a dam is treated in a similar manner to dam body movement, which means that the same influence functions and governing variables considered in the prediction of the dam body displacements are generally used (SCD 2003). It is not easy to use these methods to study the hydromechanical behaviour of dam foundations as this behaviour is non linear, due to the influence of stress on permeability and to the possible time gap between the variation in the main loads and the variation in the measurement data. This raises doubts regarding the application of the principle of superposition of effects.

3.5 Quantitative interpretation of recorded discharges

3.5.1 Previous studies

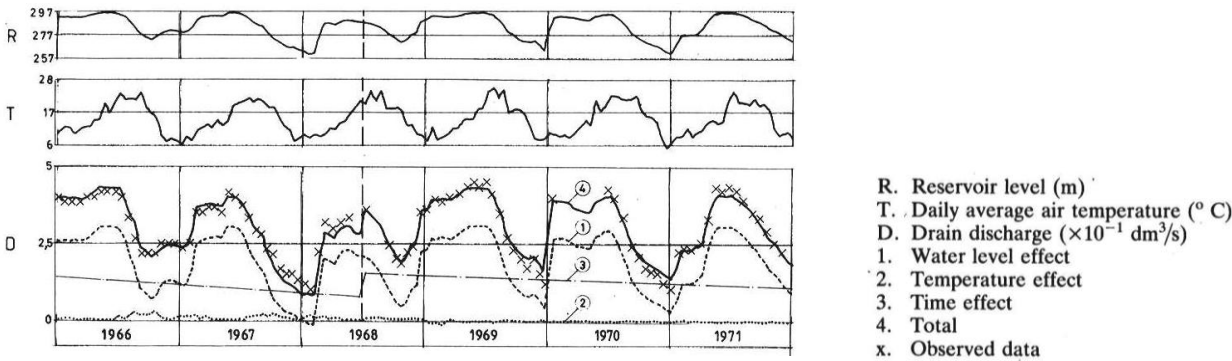
The difficulties regarding the quantitative interpretation of discharges and water pressures were highlighted by Fanelli (1979) who came to the conclusion that the interpretation of seepage and uplift using deterministic models was not always satisfactory because the elastic scheme very often did not work for the foundation rock mass. This was all the more evident when the mechanical properties of the rock were weak. He therefore thought that statistical models should be used after being adjusted to the peculiarity of foundation behaviour. He highlighted that equipment installed within the foundation rock mass often showed long time lags and hystereses in relation to variations in external factors (such as variations in reservoir level) and therefore a simple correlation between synchronous values of causes and effects would generally be inadequate. Memory effects would have to be introduced. Fanelli thought that much development and research work was still necessary in this field. Since this statement, only a few attempts have been made using statistical modelling in the analysis of

piezometric levels and seepage discharges recorded in concrete dam foundations. Some of these studies are briefly referred to in the following paragraphs.

Breitenstein et al. (1985) analysed discharges recorded in five large concrete dams of the same hydro-electric development using a method of quantitative interpretation in which not only the reservoir level and ambient temperature measured on each date are taken into account but also their variation in the preceding weeks.

Drain discharges and water pressures recorded in the foundation of Cabril arch dam were analysed using a procedure in which the influence line of the hydrostatic pressure obtained with a quantitative interpretation was adjusted taking into account results from a numerical model. The same procedure was used in the analysis of discharges and water pressures recorded in the foundation of Venda Nova arch-gravity dam (Gomes and Matos 1985). Figure 3.3 shows that the numerical results obtained in both cases are very close to the recorded data.

(a) Cabril Dam — Drain PE 17



(b) Venda Nova Dam — Drain M1

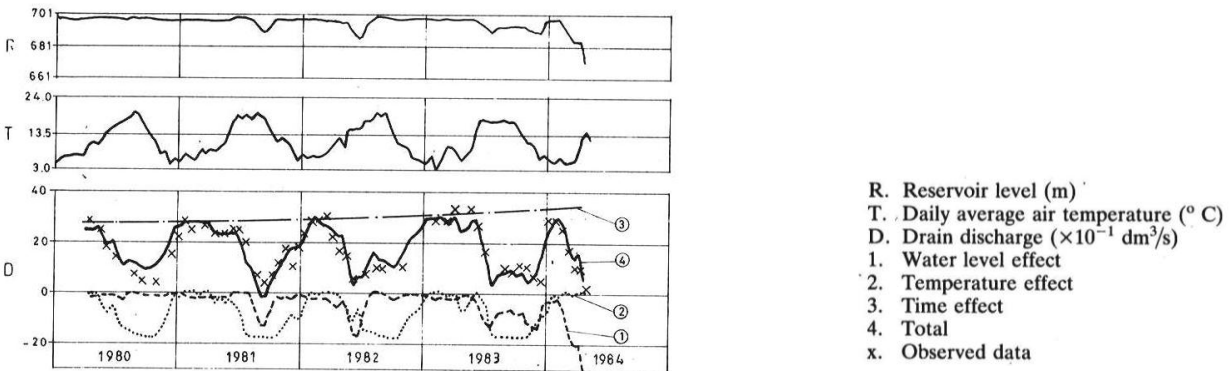


Figure 3.3 - Results of quantitative interpretation of discharges in drains located in a) Cabril dam and b) Venda Nova dam, and comparison with recorded discharges (adapted from Gomes and Matos 1985).

Guedes and Coelho (1985) predicted the piezometric pressure recorded in a piezometer installed in the Funil dam and the seepage discharge close to the Itaipu dam spillway, both in Brazil, using simple methods with only a water height and time. However, to take into account a time lag between the variation in water levels and variations in water pressures and discharges, the water level prevailing 15 days before the date of the prediction was used in pressure analysis and the average water level from days 6 to 11 prior to the day of the measurement was used in analysis of discharges. Results of the quantitative interpretation of discharges are shown in Figure 3.4.

Silva (1988) made quantitative interpretations of discharges recorded in the foundation of Cahora Bassa arch dam, in Mozambique, in which the effect of the hydrostatic pressure was represented by a polynomial curve. This was obtained taking into account the curve which represented the variation in the total discharge due to the variation of the reservoir level during a period in which the latter had increased significantly. Piezometric readings were analysed using the same procedure.

Lombardi et al. (2008) applied an algorithm developed to analyse the functional delays observed in the behaviour of concrete dams, especially those related with the thermal field, in the analysis of discharges recorded in the foundation of an arch dam. A delay of about six days was used for the part of the discharges caused by variations in water level, obtained by an optimisation process.

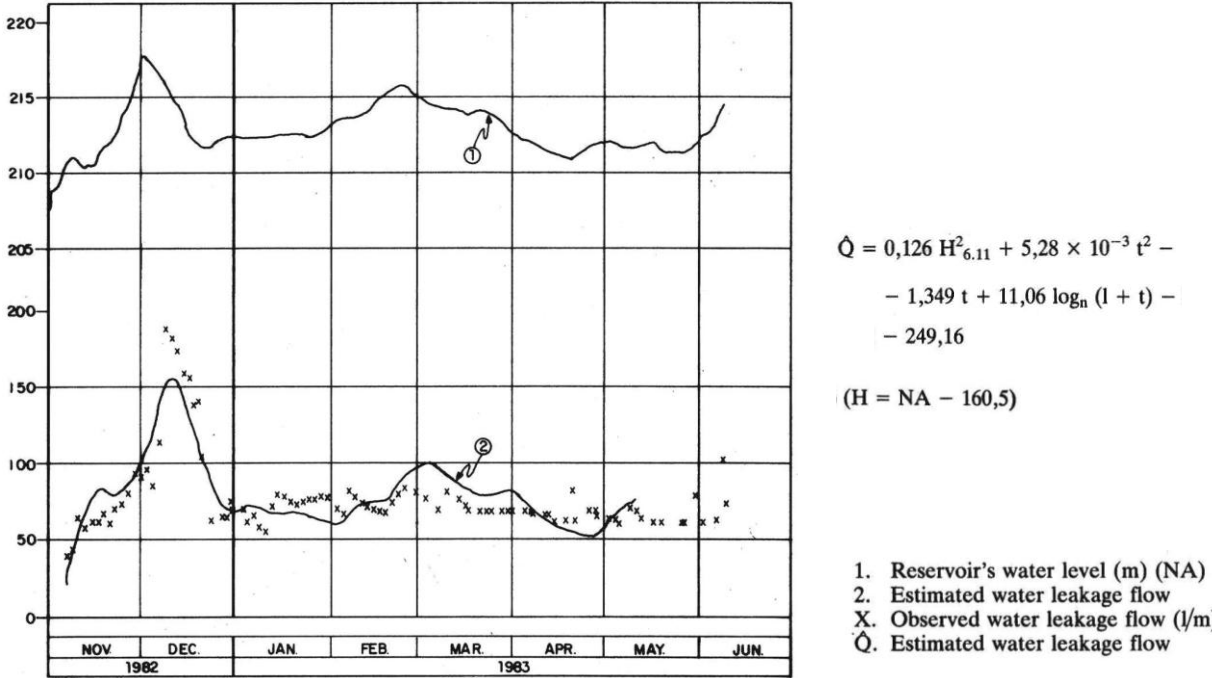


Figure 3.4 - Comparison of the discharges recorded close to the Itaipu dam spillway with the results of a quantitative interpretation (adapted from Guedes and Coelho 1985).

More generally, it is accepted that water pressures depend on the foundation deformations. They are thus, theoretically, influenced by the same variables: reservoir level, concrete temperature and time. Whenever seepage discharge is influenced by precipitation, it is appropriate to include this as a variable (SCD 2003).

3.5.2 This study

An attempt was made to analyse recorded discharges using methods of quantitative interpretation, taking into account the non-linear rock mass hydromechanical behaviour. As with displacements and stresses, it was decided that the main loads to take into account in the analysis of discharges during normal operation are variations in the reservoir level and variations in ambient temperature (variations in ambient temperature cause changes in the structure's temperature, which may give rise to dam displacements that affect the dam foundation deformation, and thus the aperture of the discontinuities through which water flows). The time effect, which when analysing dam displacements can often be explained by the rheologic behaviour of dam concrete or by a swelling process is, in the case of discharges, due to unpredictable effects. These can be changes in seepage paths caused by clearing, erosion or dissolution (as in the case of Venda Nova dam mentioned in the previous chapter), or more commonly, clogging of both seepage paths and drainage boreholes, and can not be correlated with variations in the main loads nor be represented by any curve or law. The cyclic variations in both the water level in the reservoir, due to the dam operating regime, and in annual temperature, add complexity to the dam foundation behaviour as they also contribute to changes in seepage paths.

Clogging of seepage paths over time is a commonly observed phenomenon in concrete dam foundations. In fact, during dam operation very fine materials settle on the reservoir bottom. This fine sediment flows through the foundation discontinuities and when it arrives close to the grout curtain it settles, causing a natural blockage of the discontinuities with very small apertures, which were impossible to fill with cement grout. This phenomenon occurs from the grout curtain towards upstream and is favourable to the dam, as it improves the grouting effect and reduces the quantity of water flowing through the foundation. This natural blockage is enhanced when the discharges are low, with low seepage velocities. However, clogging of the drainage system can be a problem, especially if this leads to an increase in water pressures.

In this chapter, the shape of the influence line of the hydrostatic pressure on discharges in a concrete dam foundation is presented. Using polynomial functions whose graph adequately follows the shape of the above-mentioned line, a series of quantitative interpretation analysis was carried out, taking into account the thermal and time effects in addition to the effect of

hydrostatic pressure. Discharges recorded in both single drains and seepage measuring weirs of two large Portuguese dams were analysed.

A program for quantitative interpretation was purposely developed for this study, with the programming language Visual Basic for Applications (VBA) that can be used within Microsoft Excel. The program was developed in order to analyse all the scalar quantities usually recorded in dam surveillance. Several different functions were considered in order to represent the effect of the hydrostatic load, and of the thermal and time effects. The functions to use in each analysis can be easily and quickly chosen. Program validation was carried out with a comprehensive comparison of results with those of other available codes. The program was developed in such a way that the use of any new functions found useful whilst developing the study could be easily introduced into the code.

3.5.3 Variations in discharges due to variations in the reservoir level

Due to the hydromechanical behaviour of rock masses, the permeability depends on the state of stress and strain within the foundation and, consequently, discharges vary with these changes in rock mass permeability. The permeability of the rock mass in the upstream area, close to and underneath the heel of the dam, is often greater than that at the downstream area, which causes variations in permeability along seepage paths. In order to be able to separate the effect of the hydrostatic pressure on discharges, the shape of the non-linear curve which represents the relation between the water height in the reservoir and the quantity of water collected in a concrete dam drainage system was established using a two-dimensional discontinuous model of a dam foundation, in which the normal stiffness of the foundation discontinuities was varied so as to assume rock mass foundations with different deformability. This model and the numerical simulations carried out are described in detail in chapter 7. Figure 3.5 shows the model of Pedrógão gravity dam used in this analysis. Due to lack of data a much idealised fracture pattern was assumed.

Three different rock mass foundations were considered, with the same geometry but with discontinuities' normal stiffness varying 100 times ($k_n = 1 \text{ GPa/m}$, $k_n = 10 \text{ GPa/m}$ and $k_n = 100 \text{ GPa/m}$). A friction angle (ϕ) of 30° was assumed in the foundation discontinuities, and the joint aperture at nominal zero normal stress (a_0) and residual aperture (a_{res}) were adjusted in such a way that the discharge at the drainage line with a low reservoir level (only 10 m of water height) was the same for the three different models. Numerical simulations were carried out applying successive increments of water head at the reservoir bottom and of hydrostatic pressure in the upstream face of the dam so as to simulate the rising of water in the reservoir. In the three different cases this load path was followed by an unload path, simulating the filling and subsequent emptying of the reservoir.

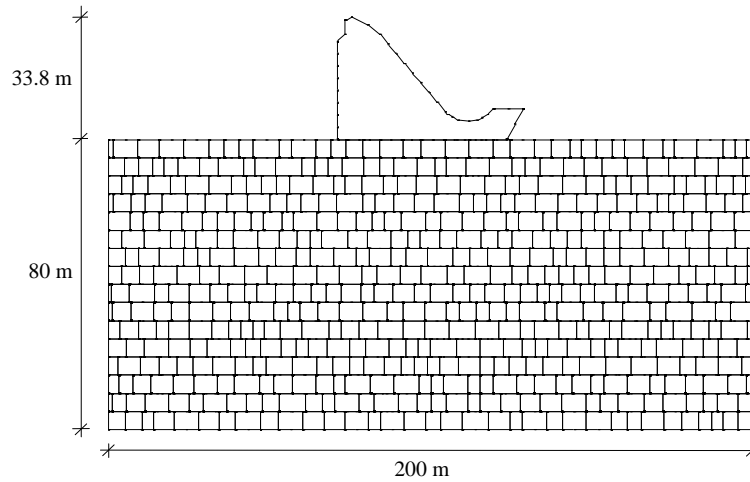


Figure 3.5 – Model of a concrete gravity dam on a jointed rock foundation.

Figure 3.6 a) shows the different curves obtained with the different foundation rock masses. Due to the great difference in drain discharges, only the shape of the curve obtained with the most deformable foundation is clearly identified. Therefore, in order to make the shape of the three different curves visible, discharges calculated with the three different models were divided in each case by the highest discharge. Figure 3.6 b) clearly shows that variations in reservoir level at low levels do not give rise to the same discharge variation when the water level in the reservoir has an equal increase, but is at a higher level. As expected, the curves tend to be linear for the lower reservoir levels as discontinuities' normal stiffness increases. A linear relation between discharge and reservoir level would only be obtained in a 2D numerical simulation in which the flow between the reservoir and the drainage line were confined, in a rock mass with constant permeability and when the hydromechanical effect were not taken into account.

A series of different polynomial curves was adjusted to those shown in Figure 3.6, in order to define the function that better fits the numerical results (Figure 3.7). In the most deformable foundation, in which the discontinuities' normal stiffness is 1 GPa/m, it was found that a function of the type $q = f(h^4)$ would roughly fit the numerical results. Curves defined by polynomials in which the linear or the quadratic terms are considered are not adequate for the lower reservoir levels, as the derivative at the origin is almost zero. However, in this case, these types of curves match the numerical results well for reservoir levels higher than 25 m. Such deformable concrete dam foundations do not actually exist, as concrete dams are built on rock masses which are not easily deformed when subjected to high stresses. In the stiffer foundations, polynomials of the type $h^3 + h$ or $h^4 + h$ are adequate, as their graphs approximately follow the curves which represent the variation in discharges due to variations in reservoir level.

Figure 3.8 shows the variations in discharges during a cycle of filling and emptying of the reservoir. There are slight differences in the discharges calculated in the load and unload cycles, due to the non-linearity of the model. These differences, however, are: i) lower than 1.7 % for the stiffest foundation, ii) lower than 10 % for the rock mass with the normal stiffness of the discontinuities equal to 10 GPa/m, except for a water height of 5 m, in which the difference is around 15 %, and iii) for the most deformable foundation, lower than 10 % for the highest reservoir levels. In this latter case, the difference increases for the lower water levels, but as such foundations are not likely to exist it can be concluded that with the assumed friction angle ($\varphi = 30^\circ$), which is close to friction angles commonly observed in rock masses of average quality (Hoek 2001), the behaviour concerning drain discharges is almost elastic and therefore the use of quantitative interpretation methods is feasible.

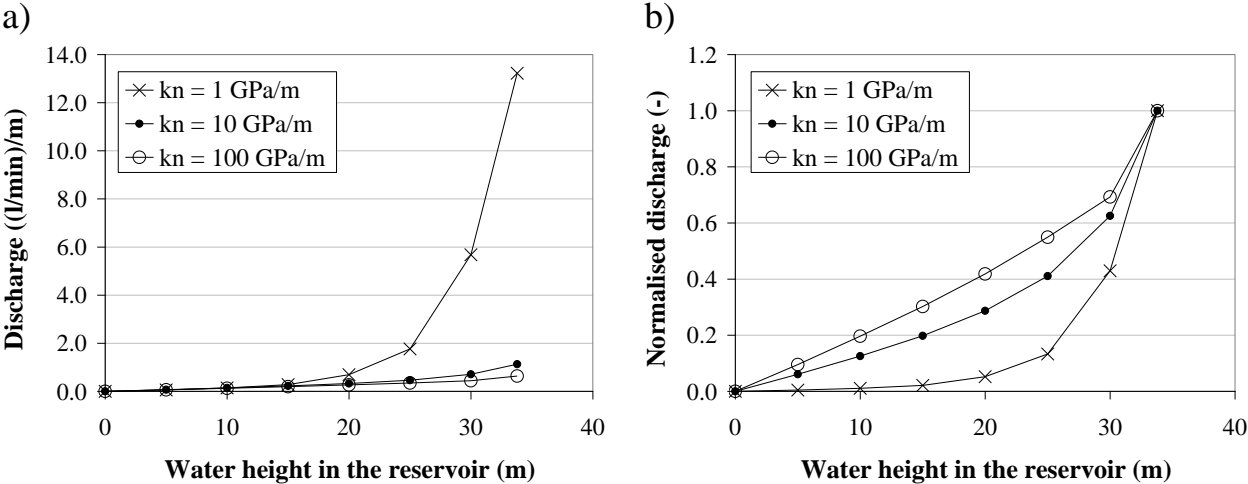


Figure 3.6 – Variations in discharges due to variations in the water level in the reservoir, taking into account the coupled hydromechanical behaviour of foundation rock masses, for different discontinuities’ normal stiffness: a) numerical discharges; b) numerical discharges divided, in each case, by the highest discharge.

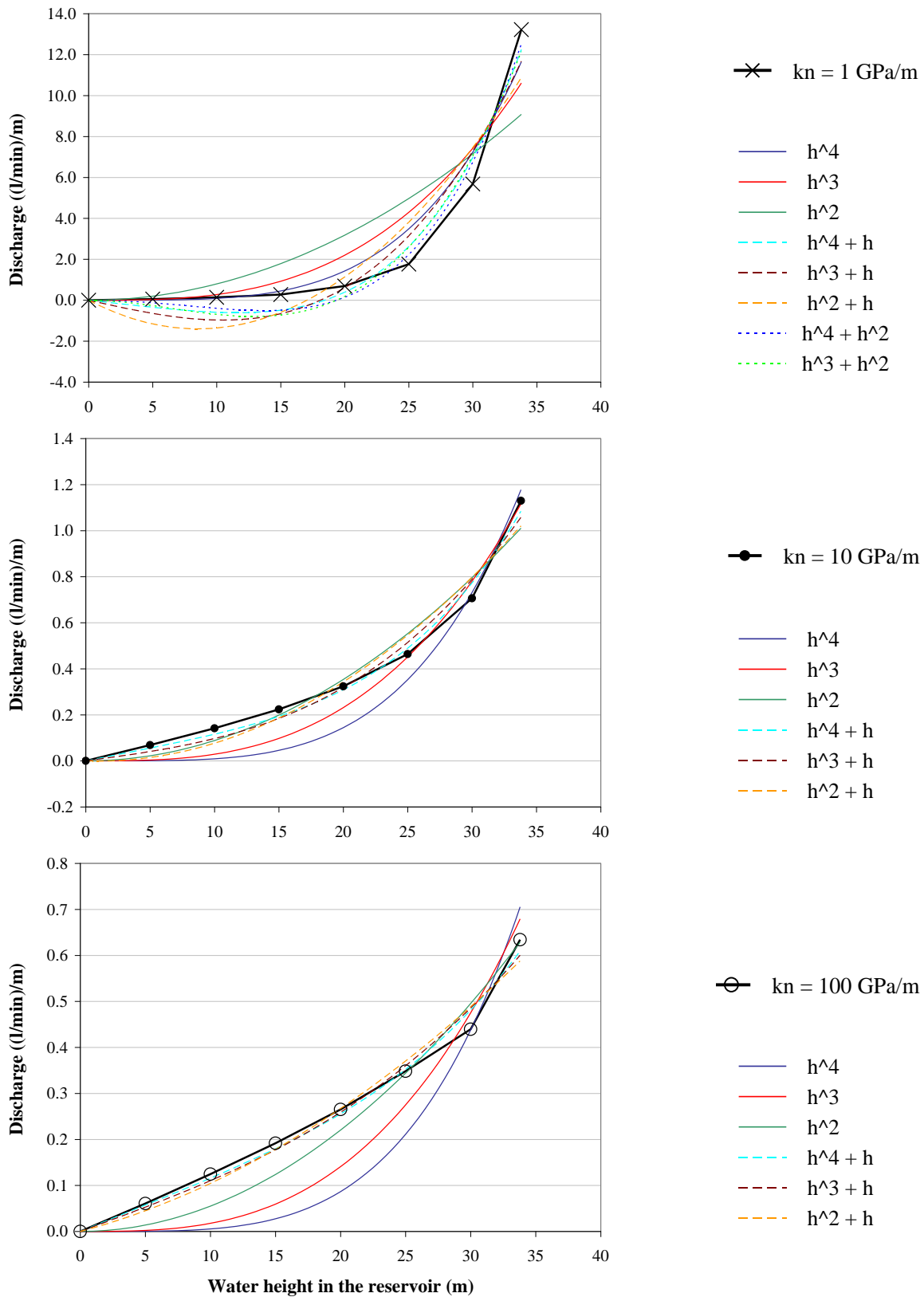


Figure 3.7 – Adjustment of polynomial curves to the numerical results.

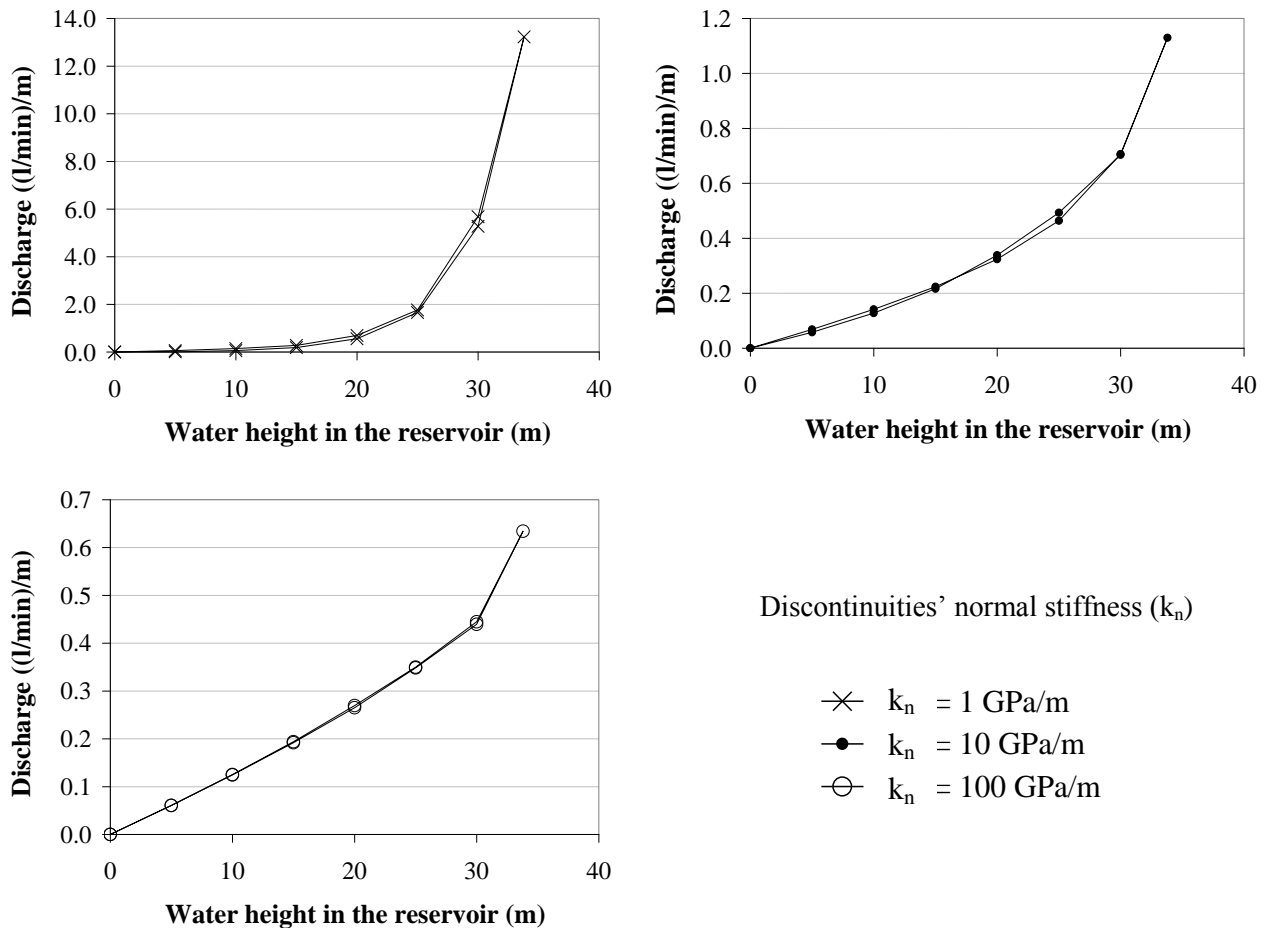


Figure 3.8 - Variations in discharges during a load/unload cycle.

3.5.4 Quantitative interpretation of discharges recorded in Alto Lindoso dam

3.5.4.1 Main characteristics of Alto Lindoso dam

Alto Lindoso dam, designed and owned by EDP, is located on river Lima in the north of Portugal and is part of a hydraulic power system which consists, in addition to the dam, of a hydraulic circuit and an underground powerhouse. It is a double curvature arch dam, almost symmetrical, with a maximum height of 110 m, a total length of 297 m between the abutments at crest elevation and a width that varies at the central cantilever between 4 m at the crest and 21 m at the base. The dam was concluded in 1991 and the first filling of the reservoir took place from 6 January 1992 to 28 April 1994.

The foundation consists of granite with medium to coarse-sized grains and is of good quality, showing, however, some heterogeneity. The main joint sets in the left bank and valley bottom are in the upstream-downstream direction, with average to sub-vertical dips, and in the right bank they are sub-vertical and equally distributed between upstream-downstream and right bank-left bank directions.

Forty four drains were first drilled from the drainage gallery, two per block, with the exception of the foundation of block 14-15, in which four boreholes were drilled. The length of the drainage boreholes is around 38 m in the valley bottom and 20 m in both embankments, which in each case is about 2/3 of the length of the grout curtain. Permeability values of 3.0 to 7.0×10^{-8} m/s were obtained in Lugeon type tests carried out in drains.

3.5.4.2 Monitoring and hydraulic behaviour of the dam foundation

As prescribed in the monitoring plan, 22 piezometers were installed from the downstream area of the drainage gallery, one per block, with the exception of the central cantilever (block 11-12) in which two piezometers were installed, one vertical and the other dipping towards upstream. During the first filling of the reservoir, percentages of hydraulic head of about 30 to 40 % were recorded in the valley bottom in the foundation of blocks 12-13, 13-14 and 14-15. The greatest discharges were recorded in the foundation of blocks 10-11, 11-12, 12-13 and 14-15, in the valley bottom, which make up around 50 % of the total discharge in the drainage gallery.

After the first filling of the reservoir, high percentages of hydraulic head were still recorded in the foundation, in the valley bottom, below dam blocks 11-12, 12-13 and 13-14, and in the right bank, below block 18-19. These percentages of hydraulic head, however, were not accompanied by significant discharges. Between March and May 1998, new drains were drilled in those areas, to reduce water pressures, and a new piezometer was installed in the foundation of block 11-12. Work carried out allowed not only a significant decrease in water pressures in the foundation of the blocks in the bottom of the valley but also an improvement in the drainage of the foundation of block 18-19. More recently, in January 2004, due to an increase in piezometric readings, the drains located in blocks 7-8 and 8-9 were cleaned and unblocked when necessary. Further cleaning was carried out in June 2005 in all drains and piezometers located in blocks 6-7, 7-8, 8-9, 14-15, 15-16, 16-17, 17-18 and 18-19. Figure 3.9 shows the drainage and piezometric systems in the dam foundation.

The drained water, together with that from leakage, is collected in three seepage measuring weirs, which separate the discharges by specific areas (Figure 3.9): the first measures the discharges from the left bank, between blocks 1-2 and 9-10; the second those from the right bank, between blocks 14-15 and 21-22 and the third collects not only the water from the first two, but also that collected in the valley bottom. In this dam, the quantity of water from leakage is very low. Figure 3.10 shows recorded discharges in these three seepage weirs plotted versus time. The same figure shows the variation in the reservoir level. Chart analysis shows that discharges have been decreasing, most probably due to clogging of both the rock mass discontinuities and the drainage system.

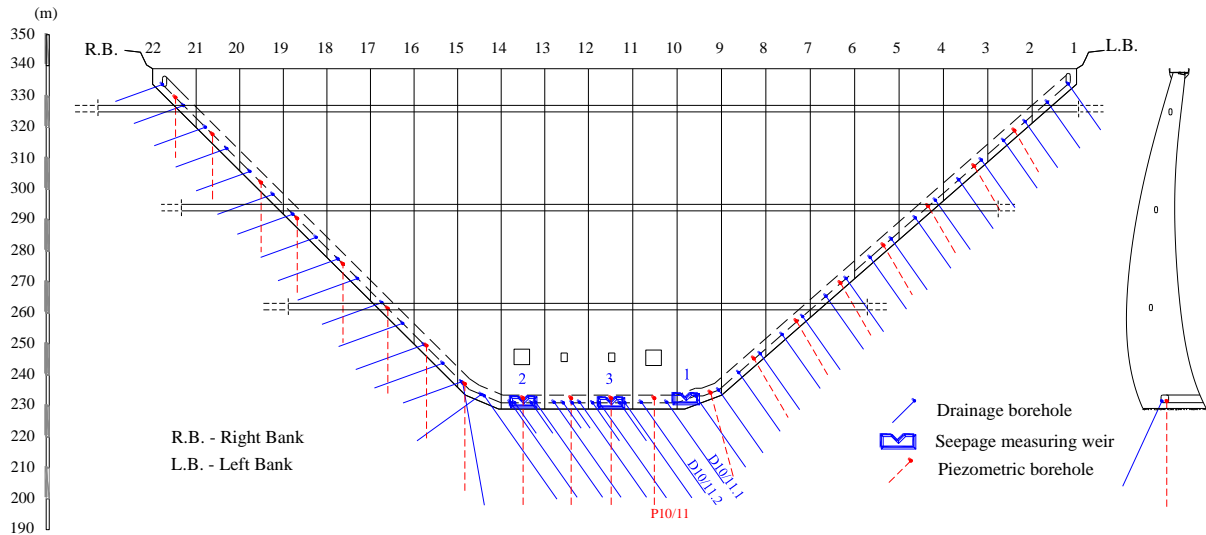


Figure 3.9 – Drainage and piezometric systems in the foundation of Alto Lindoso dam.

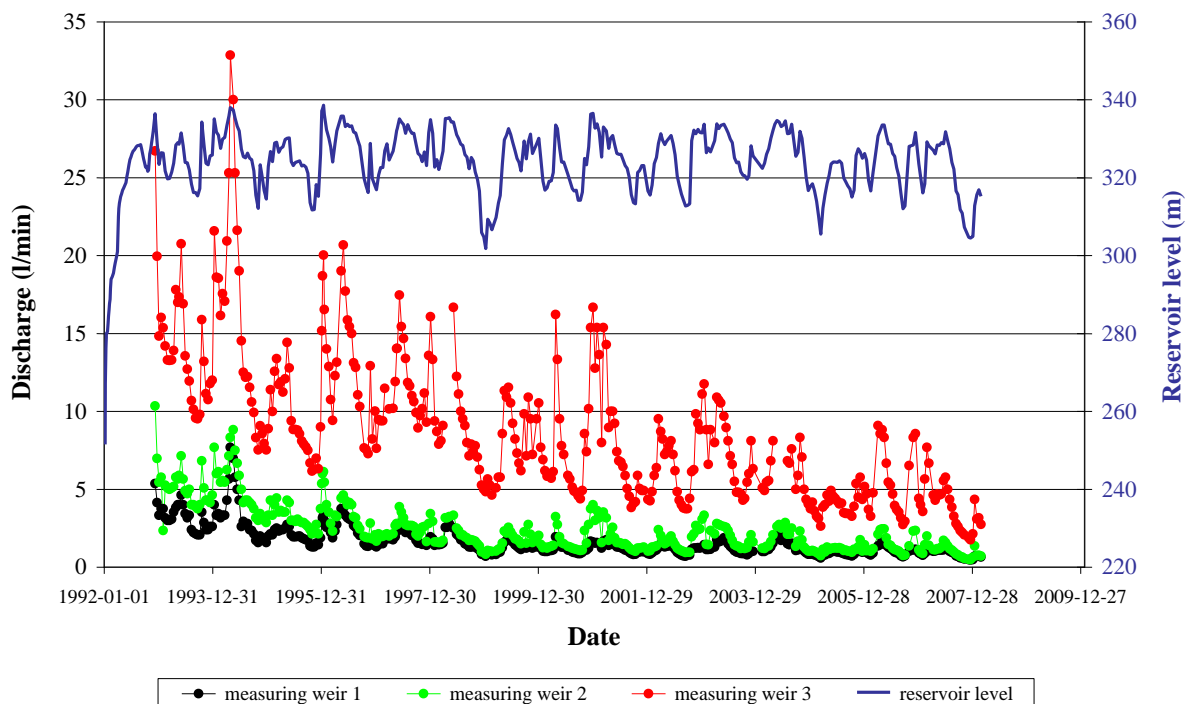


Figure 3.10 – Variation in the reservoir level and recorded discharges in the measuring weirs.

3.5.4.3 Quantitative interpretation of discharges recorded in a single drain

In Alto Lindoso dam, the highest discharges are recorded in the foundation of the blocks located in the valley bottom. The only block in which no drains or piezometric boreholes have been drilled since the beginning of the first filling of the reservoir is block 10-11 and thus the

decision was made to analyse discharges recorded in drain D10/11.1 located in this block (Figure 3.9). Although the opening of new drains can affect the flow pattern in quite a wide foundation area, it was assumed that in the foundation of block 10-11 there had been no significant changes, which allowed quantitative interpretation of recorded discharges to be made taking into account discharges recorded since the beginning of reservoir filling. Figure 3.11 shows the variation of recorded discharges and water pressures in block 10-11 over time. Discharges in both drains have been decreasing (drains D10/11.1 and D10/11.2 shown in Figure 3.9). The water pressure in piezometer P10/11 (Figure 3.9) increased from the end of 1998 until the beginning of 2003, but has apparently been stable since then, varying with the variations in the reservoir level. The percentages of hydraulic head recorded at this piezometer are lower than 16 %, and therefore of no concern.

The study started with a very simple quantitative interpretation with the effect of the hydrostatic pressure represented by a function of $h^3 + h$ and the time effect represented by a cubic polynomial (t^3, t^2, t). A series of quantitative interpretations was afterwards carried out, only changing one function or introducing one new function each time, in order to analyse its influence on the results. Different periods of time were used to calculate the curve that better fits recorded data in each analysis. This curve was used to predict discharges, and these predictions were compared with discharges measured in the subsequent period of time.

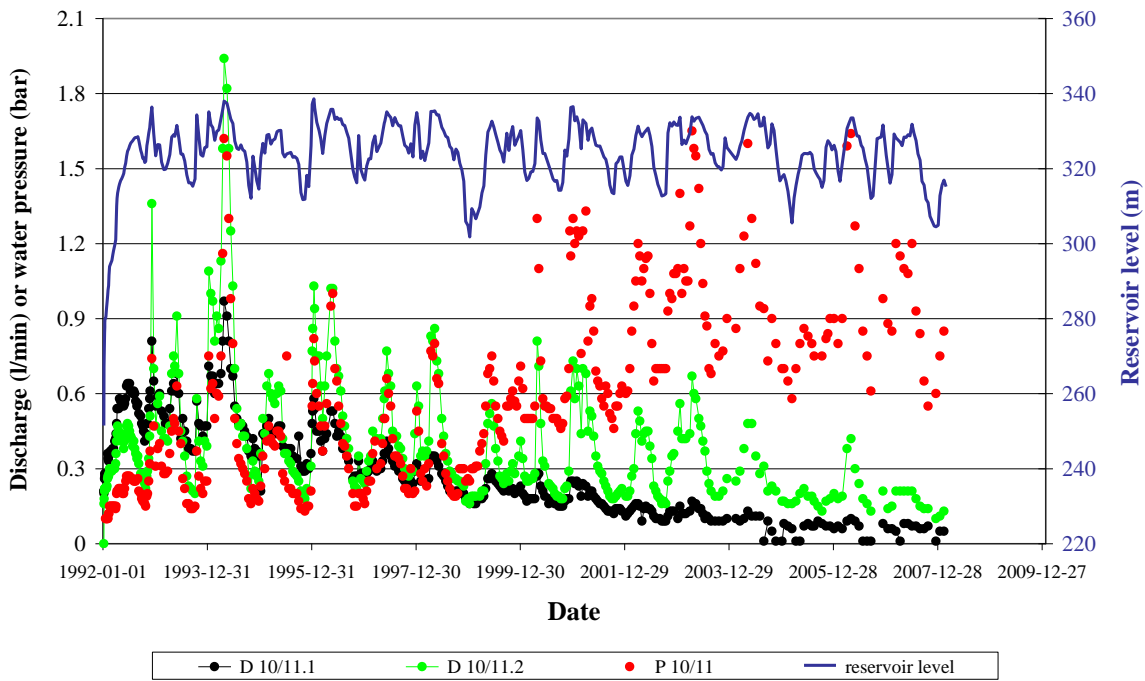


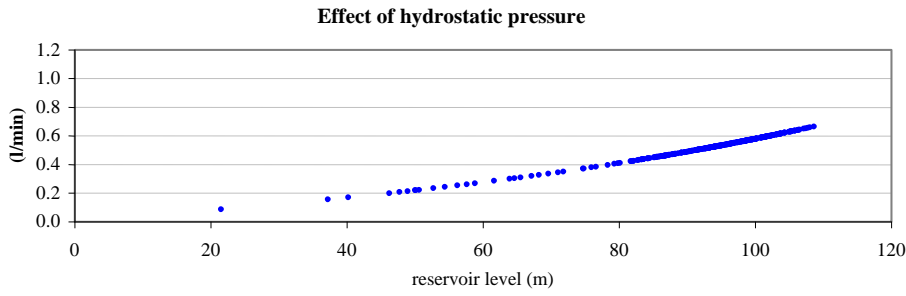
Figure 3.11 – Recorded discharges and water pressures in the foundation of block 10-11.

Figure 3.12 to Figure 3.16 show results of some experiments in which curves calculated with data recorded until the end of 2003 were used to predict discharges from then until mid-February 2008. These figures, in addition to the influence lines of each effect, show the parameters which define the calculated curve, the comparison between recorded and both calculated and predicted discharges, and the errors of the analysis. Similar charts are at the same scale, in order to make comparisons easier. The independent term (k), was added to the time effect.

Results of the first interpretation carried out are shown in Figure 3.12. The effect of the hydrostatic pressure was afterwards represented by a function of $h^4 + h$, instead of $h^3 + h$ (Figure 3.13). A third analysis was carried out in which the thermal effect was included (Figure 3.14). This was simulated with the simplified method developed by Willm and Beaujoint (1967), in which the thermal effect in each point of the structure is assumed to be independent and seasonal, taking into account that in the Portuguese climate the most important wave is that of annual period (Teles 1985). The time effect was then represented by an exponential curve and by a both linear and exponential curve (Figure 3.15 and Figure 3.16). Analysis of the above-mentioned figures together shows that:

1. the effect of hydrostatic pressure is of the same order as the time effect;
2. the hydrostatic pressure effect can be either simulated by a function of $h^3 + h$ or of $h^4 + h$ and, in this case, the linear term is dominant;
3. the thermal effect is very low;
4. the time effect is well approximated by a cubic polynomial.

The general trend in discharge variations is reasonably approximated by the first three interpretations, in which the time effect is represented by a cubic polynomial. However, the calculated curves do not fit recorded discharges well neither in the period of the first filling of the reservoir, in which there are significant differences between recorded and calculated discharges, nor in the subsequent period. None of the curves was considered adequate to predict discharges, as errors increase in the period in which predictions are made. In reality, a quantitative interpretation is an interpolation, only valid in the range of variation of the main loads and over the period of time considered in the analysis. In some cases, like those presented here, quantitative interpretations can not be used as a model to predict future behaviour.

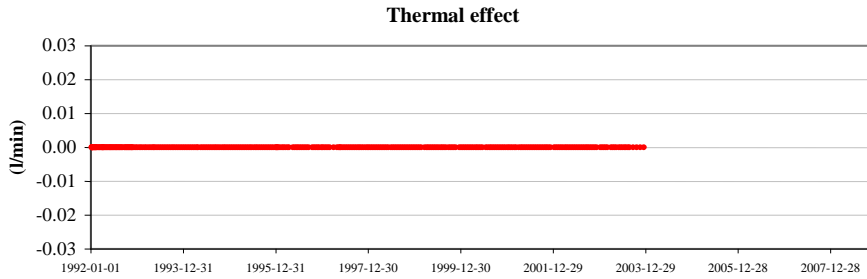


$$h^3$$

$$1.8658 \times 10^{-7}$$

$$h$$

$$3.9278 \times 10^{-3}$$



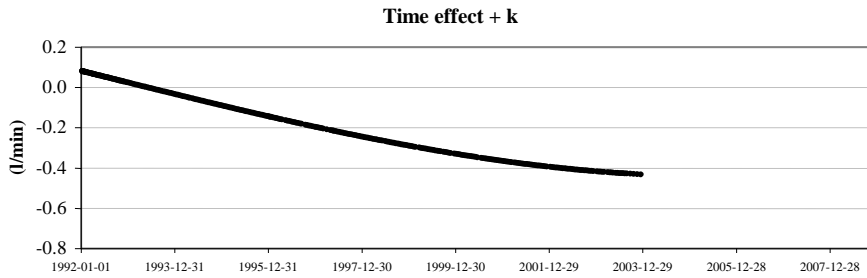
$$\cos(2\pi s / 365)$$

-

$$\sin(2\pi s / 365)$$

-

(s – number of days, starting 1st January)



$$t^3$$

$$2.3121 \times 10^{-12}$$

$$t^2$$

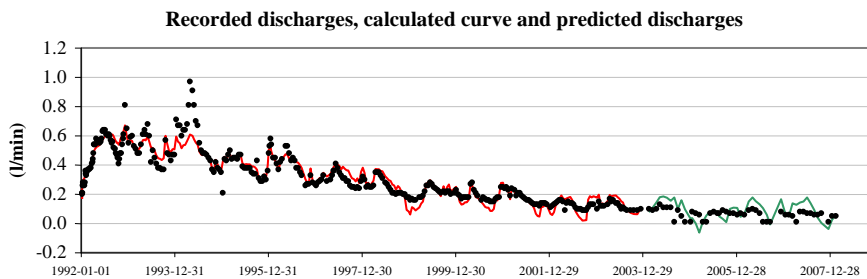
$$-6.5207 \times 10^{-10}$$

$$t$$

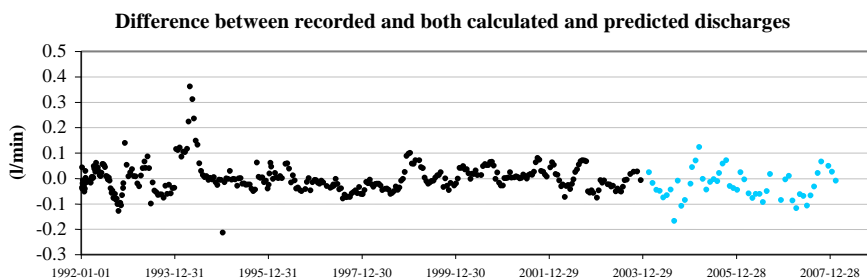
$$-1.5875 \times 10^{-4}$$

$$k$$

$$8.1379 \times 10^{-2}$$

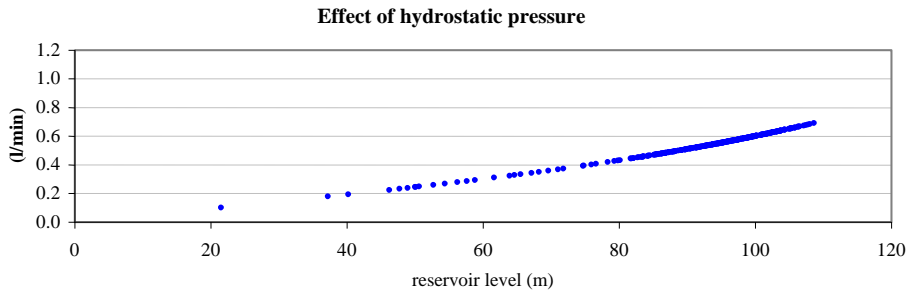


- recorded data
- quantitative interpretation
- predicted discharges



- interpretation
- prediction

Figure 3.12 – Quantitative interpretation of discharges in drain D10/11.1 (first interpretation).

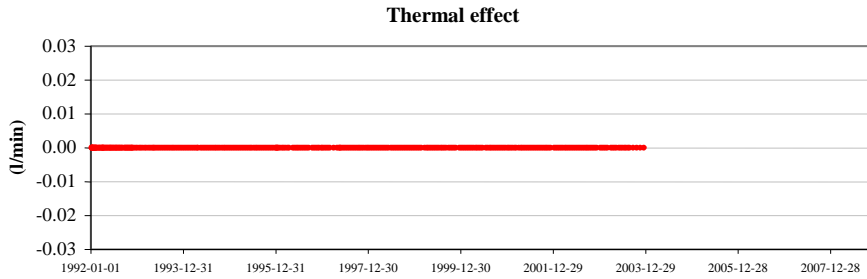


$$h^4$$

$$1.2685 \times 10^{-9}$$

$$h$$

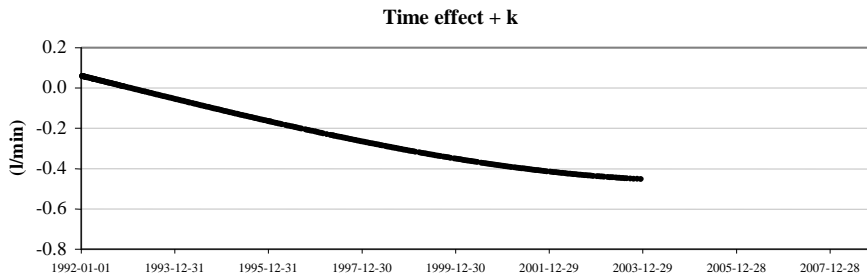
$$4.7398 \times 10^{-3}$$



$$\cos (2 \pi s / 365)$$

$$\sin (2 \pi s / 365)$$

(s – number of days, starting 1st January)



$$t^3$$

$$2.4133 \times 10^{-12}$$

$$t^2$$

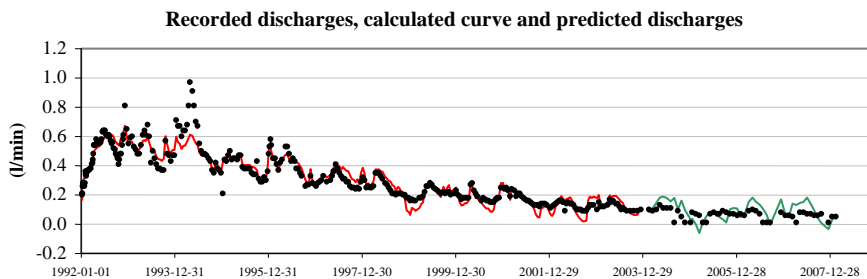
$$-2.8443 \times 10^{-9}$$

$$t$$

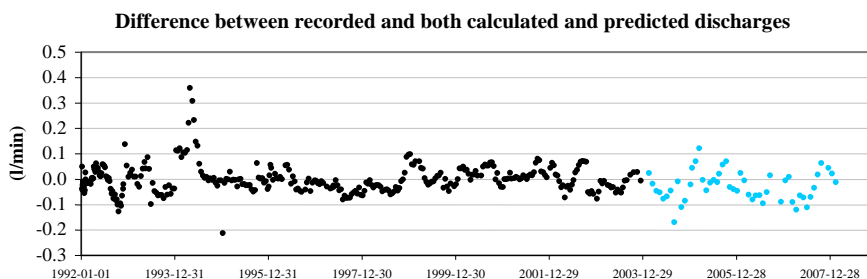
$$-1.5719 \times 10^{-4}$$

$$k$$

$$5.9161 \times 10^{-2}$$

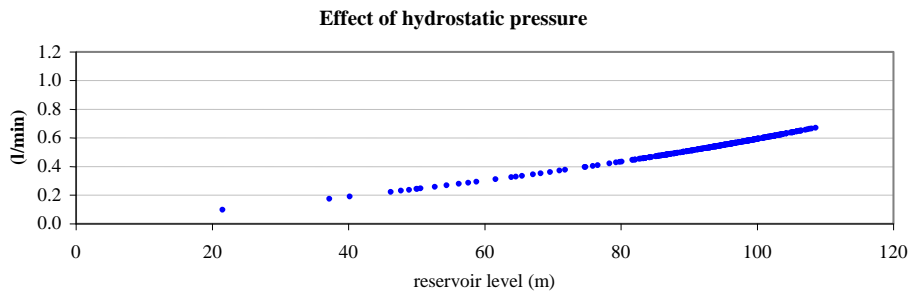


- recorded data
- quantitative interpretation
- predicted discharges



- interpretation
- prediction

Figure 3.13 – Quantitative interpretation of discharges in drain D10/11.1 (second interpretation).

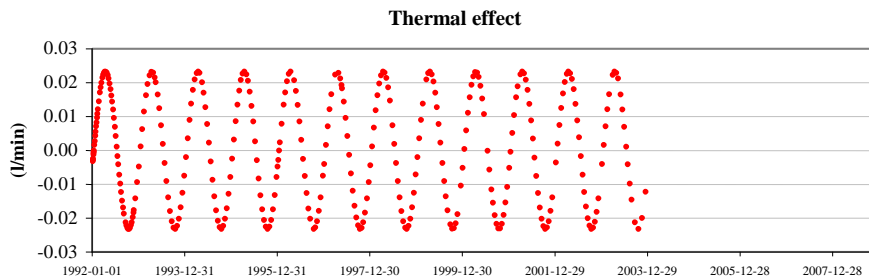


$$h^3$$

$$1.4150 \times 10^{-7}$$

$$h$$

$$4.5075 \times 10^{-3}$$



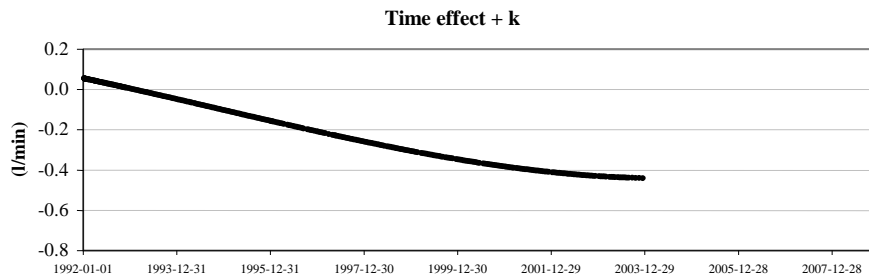
$$\cos(2\pi s / 365)$$

$$-6.3774 \times 10^{-3}$$

$$\sin(2\pi s / 365)$$

$$2.2362 \times 10^{-2}$$

(s – number of days, starting 1st January)



$$t^3$$

$$4.1070 \times 10^{-12}$$

$$t^2$$

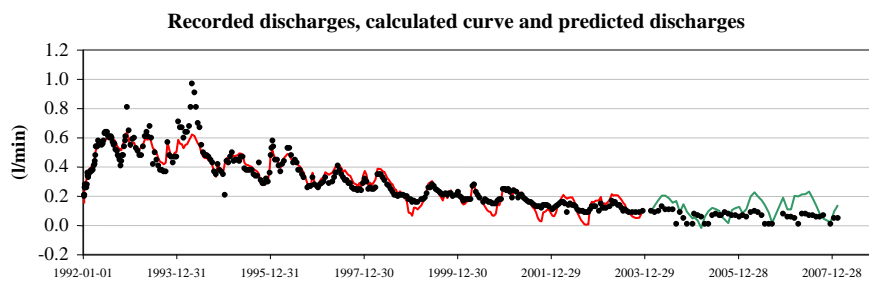
$$-1.3100 \times 10^{-8}$$

$$t$$

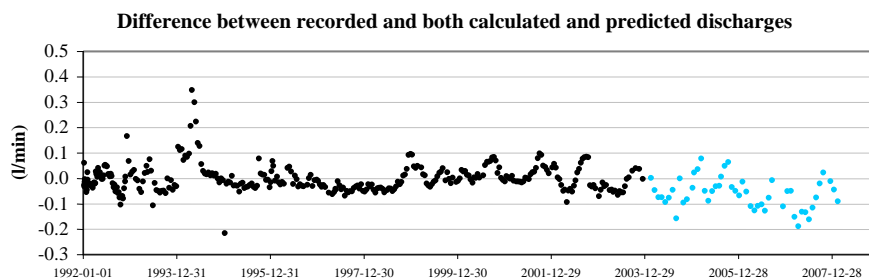
$$-1.3450 \times 10^{-4}$$

$$k$$

$$5.4516 \times 10^{-2}$$

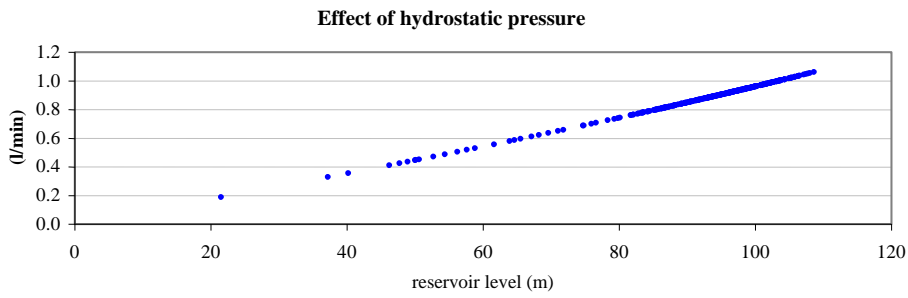


- recorded data
- quantitative interpretation
- predicted discharges



- interpretation
- prediction

Figure 3.14 – Quantitative interpretation of discharges in drain D10/11.1 (third interpretation).

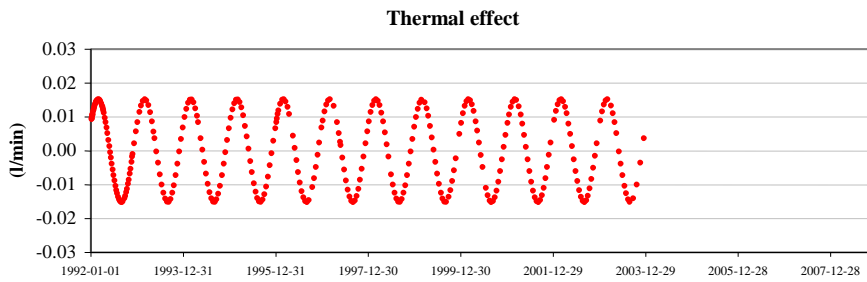


$$h^3$$

$$9.0422 \times 10^{-8}$$

$$h$$

$$8.7004 \times 10^{-3}$$



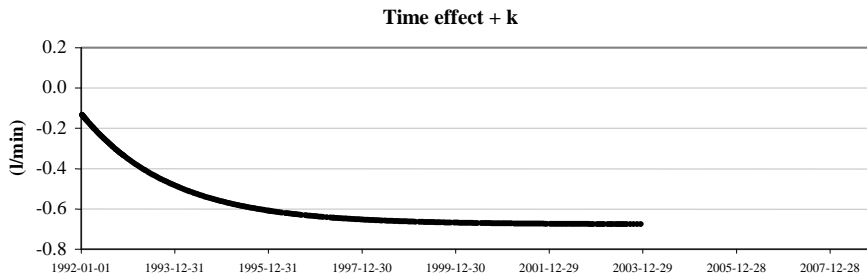
$$\cos(2\pi s / 365)$$

$$7.5596 \times 10^{-3}$$

$$\sin(2\pi s / 365)$$

$$1.3174 \times 10^{-2}$$

(s – number of days, starting 1st January)

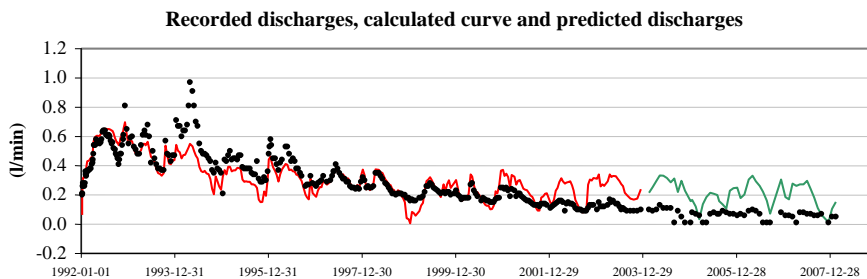


$$1 - e^{(-t/700)}$$

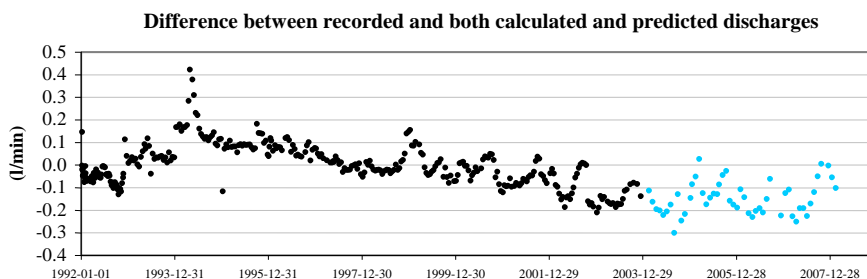
$$-5.4451 \times 10^{-1}$$

$$k$$

$$-1.3288 \times 10^{-1}$$

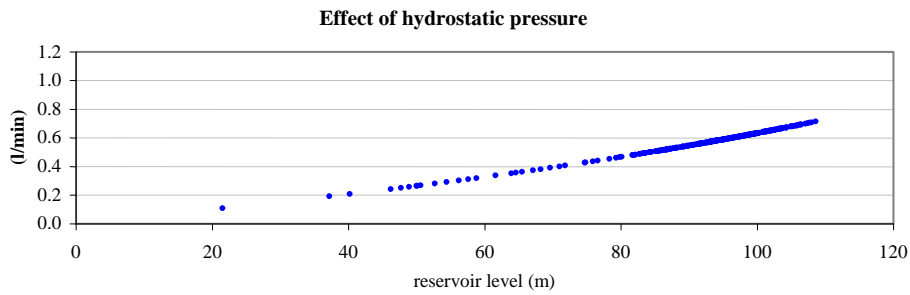


- recorded data
- quantitative interpretation
- predicted discharges



- interpretation
- prediction

Figure 3.15 – Quantitative interpretation of discharges in drain D10/11.1 (fourth interpretation).

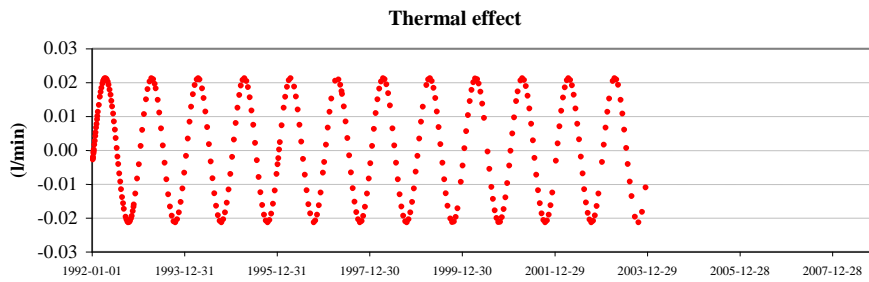


$$h^3$$

$$1.3806 \times 10^{-8}$$

$$h$$

$$4.9476 \times 10^{-3}$$



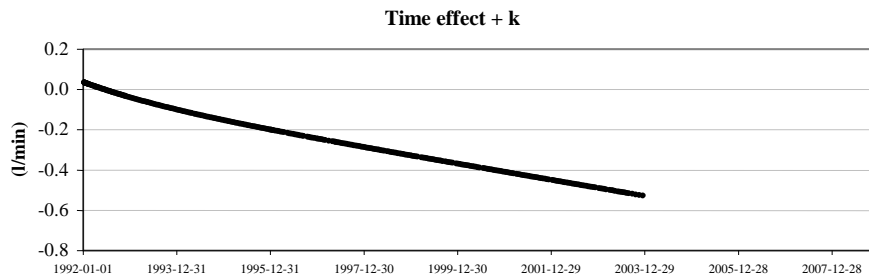
$$\cos(2\pi s / 365)$$

$$-5.5864 \times 10^{-3}$$

$$\sin(2\pi s / 365)$$

$$2.0542 \times 10^{-2}$$

(s – number of days, starting 1st January)



$$t$$

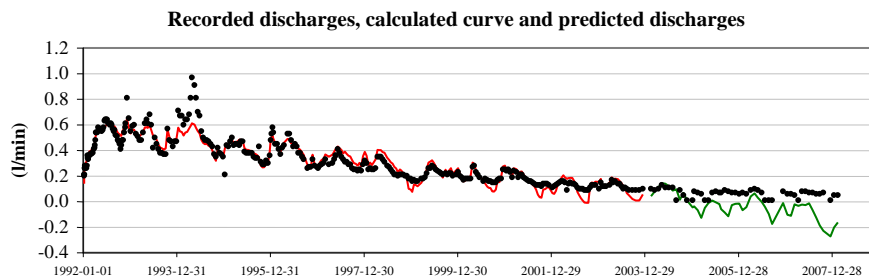
$$-1.0915 \times 10^{-4}$$

$$1 - e^{(-t/700)}$$

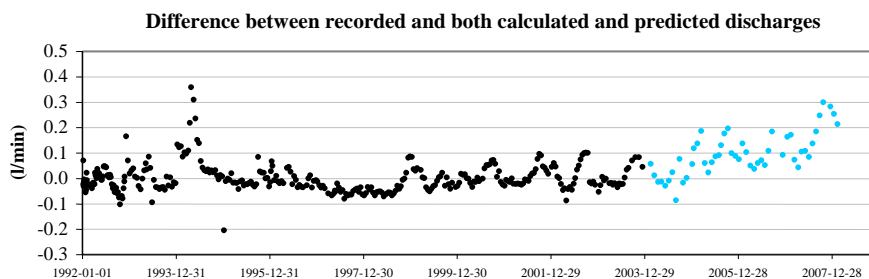
$$-8.6865 \times 10^{-2}$$

$$k$$

$$3.5069 \times 10^{-2}$$



- recorded data
- quantitative interpretation
- predicted discharges



- interpretation
- prediction

Figure 3.16 – Quantitative interpretation of discharges in drain D10/11.1 (fifth interpretation).

3.5.4.4 Quantitative interpretation of discharges recorded in seepage measuring weirs

Results of quantitative interpretations of discharges recorded in single drains were not satisfactory and therefore an attempt was made to interpret the total discharge, recorded in seepage measuring weir 3. In a first interpretation, the effect of the hydrostatic pressure was represented by a function of h^3 and the time effect by a cubic polynomial (Figure 3.17). In this case the effect of hydrostatic pressure becomes significant, unlike what was observed in analysis of discharges in a single drain, in which it was close to the time effect. However, the time effect is not well fitted and predictions are not good. An exponential curve was then used to simulate the time effect and the results were much better, as shown in Figure 3.18. However, for the highest and lowest discharges, the calculated flows are higher than those recorded (the calculated curve exaggerates the peaks), which means that the effect of the hydrostatic pressure is higher than it should be. Taking this second interpretation as reference, another two were carried out by adding a linear term to simulate the time effect and by taking into account the thermal effect (Figure 3.19 and Figure 3.20). Figure 3.19 shows that when a linear term in h is used the curve which represents the effect of the hydrostatic pressure does not make sense, due to the lack of recorded discharges for water heights in the reservoir lower than 72 m. In this case, quantitative interpretations are better carried out with the effect of the hydrostatic pressure represented by a function of h^3 . As in the analysis of seepage in a single drain, the thermal effect is very low (Figure 3.20).

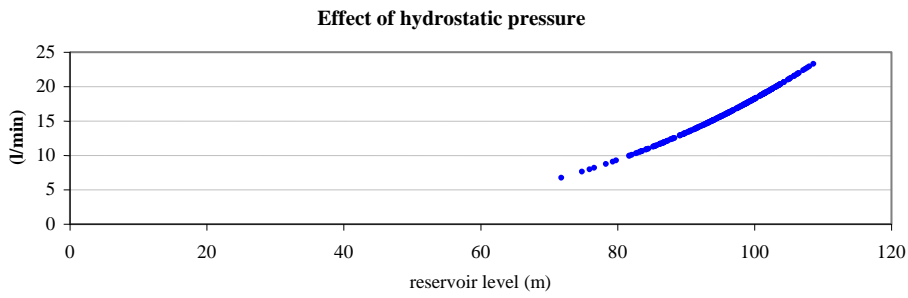
3.5.5 Quantitative interpretation of discharges recorded in Alqueva dam

3.5.5.1 Main characteristics of Alqueva dam

Most of the studies developed in this thesis were carried out with data from Alqueva dam, which is described in detail in the next chapter. Therefore, only the features relevant to the quantitative interpretation of discharges are referred to here. Alqueva dam is a 96 m high double curvature arch dam of which the foundation consists of green schist and phyllite. Dam construction ended in 2003 and the first filling of the reservoir began in February 2002 and is nearly complete. There are five drains per dam block, located 3 m apart. The total discharge is around 100 to 150 l/min, of which around 20 l/min are from the valley bottom.

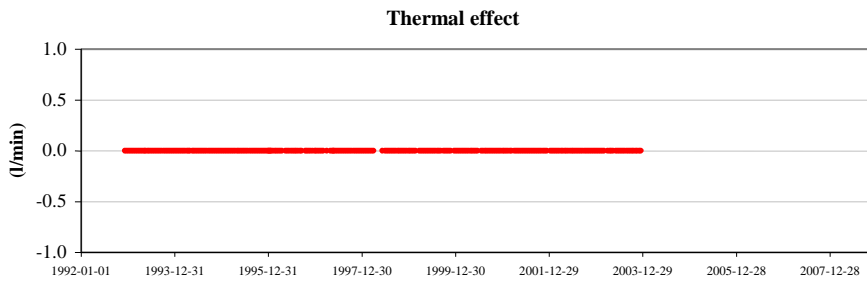
3.5.5.2 Quantitative interpretation of discharges

The study carried out included quantitative interpretations of discharges recorded in the drain of the valley bottom that collects the highest quantity of water (drain D25 D) and of discharges collected in the drainage gallery in an area which encompasses the bottom of the valley. Recorded discharges are shown in Figure 3.21, where it can be seen that there are large variations in discharges which are not justified by variations in the reservoir level. Figure 3.22 to Figure 3.25 show results of some interpretations.



$$h^3$$

$$1.8196 \times 10^{-5}$$



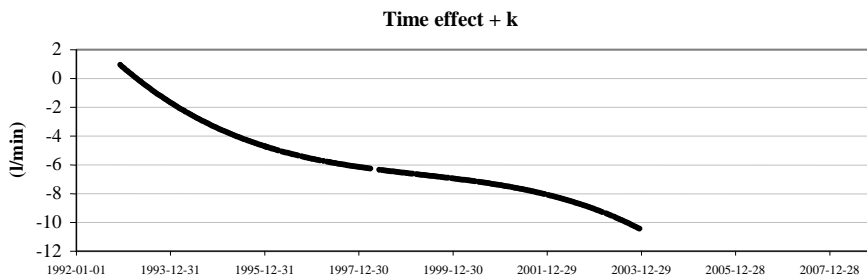
$$\cos(2\pi s / 365)$$

-

$$\sin(2\pi s / 365)$$

-

(s – number of days, starting 1st January)



$$t^3$$

$$-4.1443 \times 10^{-10}$$

$$t^2$$

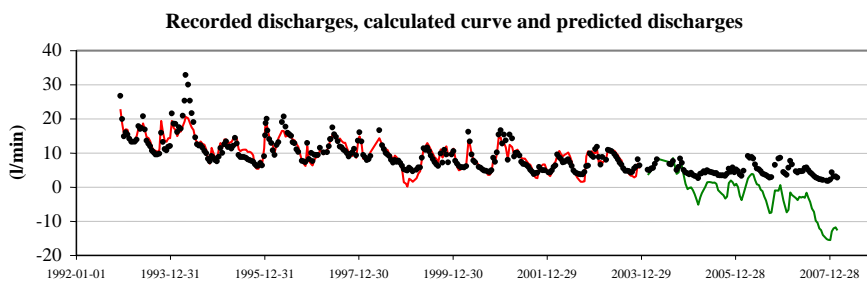
$$3.3142 \times 10^{-6}$$

$$t$$

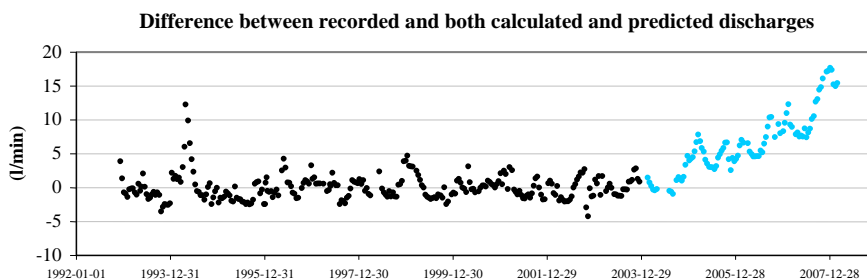
$$-9.8573 \times 10^{-3}$$

$$k$$

$$3.8841$$

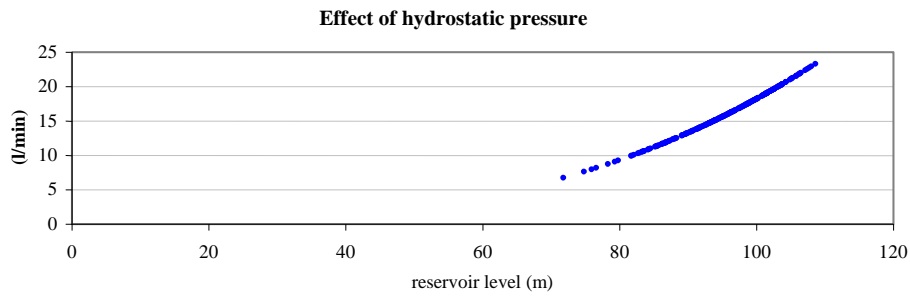


- recorded data
- quantitative interpretation
- predicted discharges



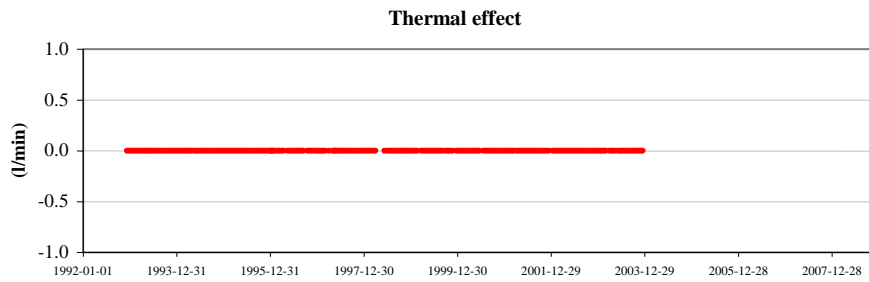
- interpretation
- prediction

Figure 3.17 – Quantitative interpretation of discharges recorded in seepage measuring weir 3 (first interpretation).



$$h^3$$

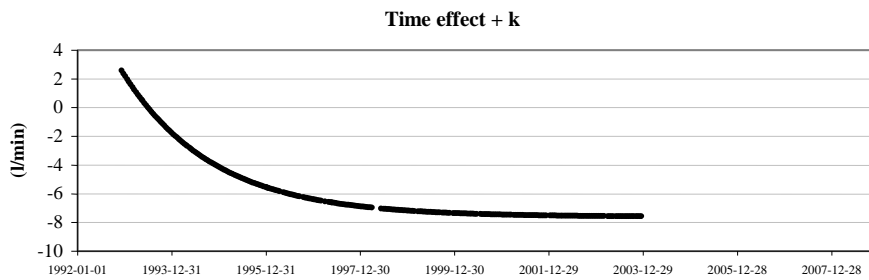
$$1.8201 \times 10^{-5}$$



$$\cos(2\pi s / 365)$$

$$\sin(2\pi s / 365)$$

(s – number of days, starting 1st January)

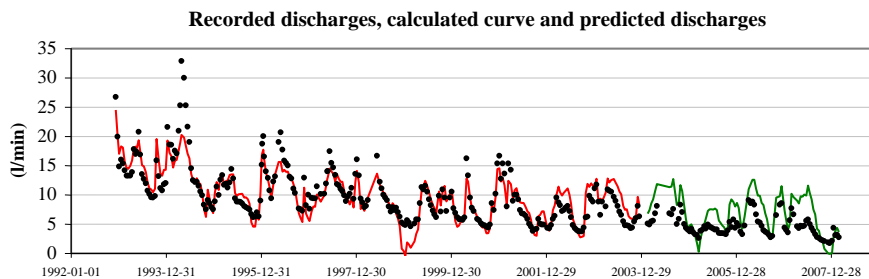


$$1 - e^{(-t/700)}$$

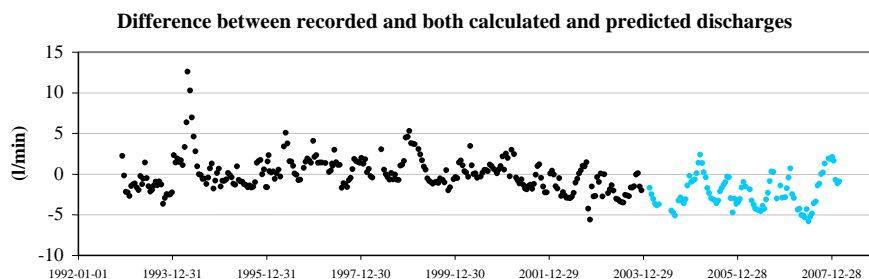
$$-1.6458 \times 10^1$$

$$k$$

$$8.8497$$

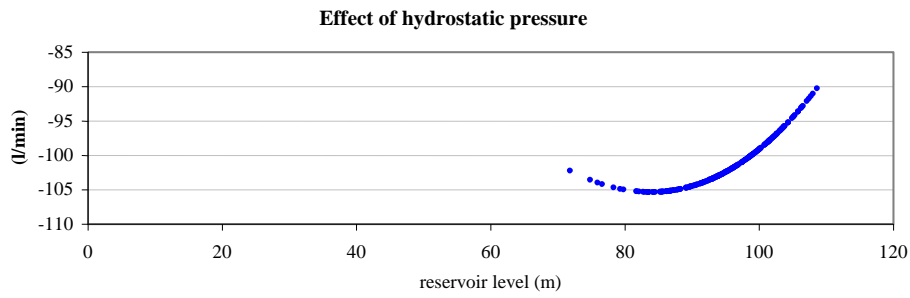


- recorded data
- quantitative interpretation
- predicted discharges



- interpretation
- prediction

Figure 3.18 – Quantitative interpretation of discharges recorded in seepage measuring weir 3 (second interpretation).

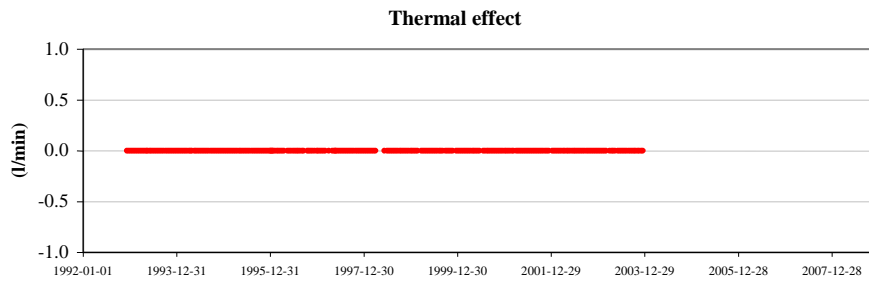


$$h^3$$

$$8.9224 \times 10^{-5}$$

$$h$$

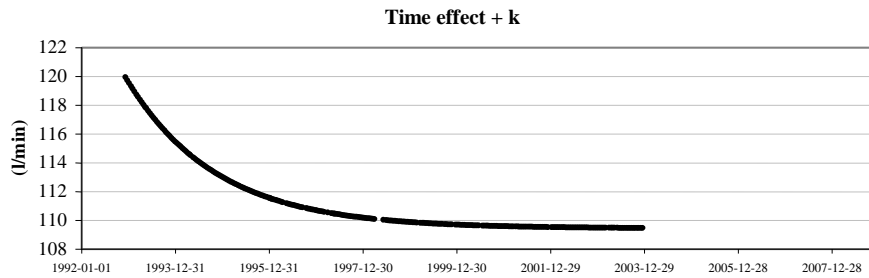
$$-1.8836$$



$$\cos(2\pi s / 365)$$

$$\sin(2\pi s / 365)$$

(s – number of days, starting 1st January)

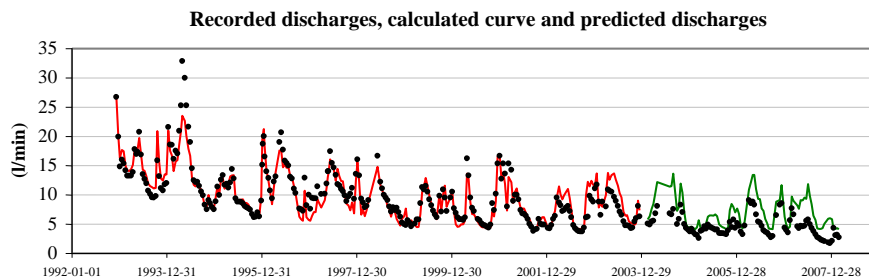


$$1 - e^{(-t/700)}$$

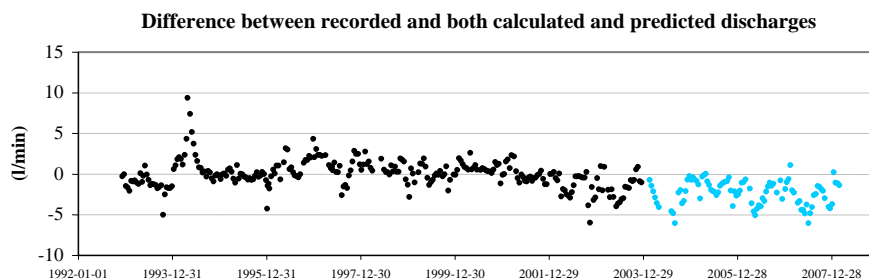
$$-1.6977 \times 10$$

$$k$$

$$1.2641 \times 10^2$$

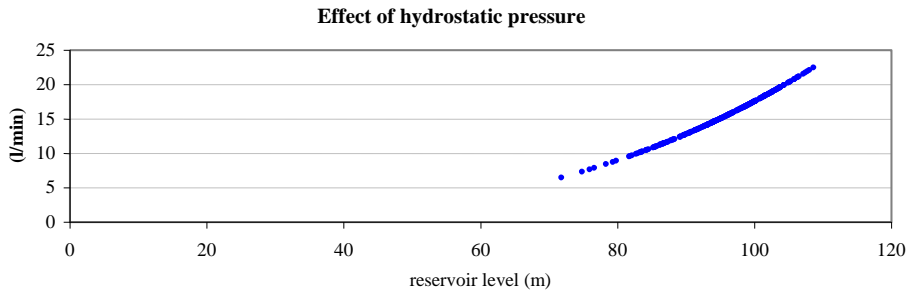


- recorded data
- quantitative interpretation
- predicted discharges



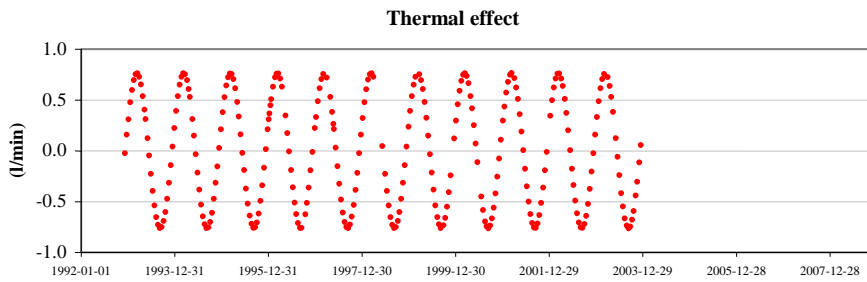
- interpretation
- prediction

Figure 3.19 – Quantitative interpretation of discharges recorded in seepage measuring weir 3 (third interpretation).



$$h^3$$

$$1.7553 \times 10^{-5}$$



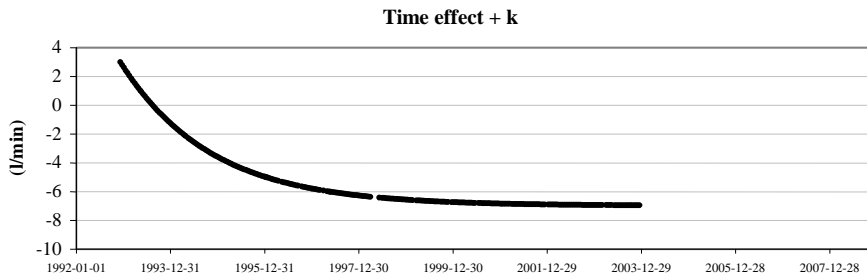
$$\cos(2\pi s / 365)$$

$$2.5940 \times 10^{-1}$$

$$\sin(2\pi s / 365)$$

$$7.1810 \times 10^{-1}$$

(s – number of days, starting 1st January)

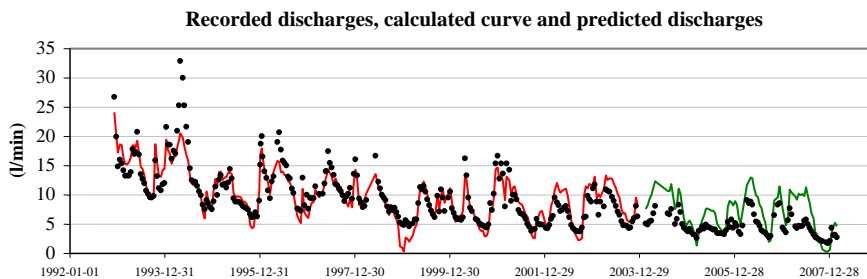


$$1 - e^{(-t/700)}$$

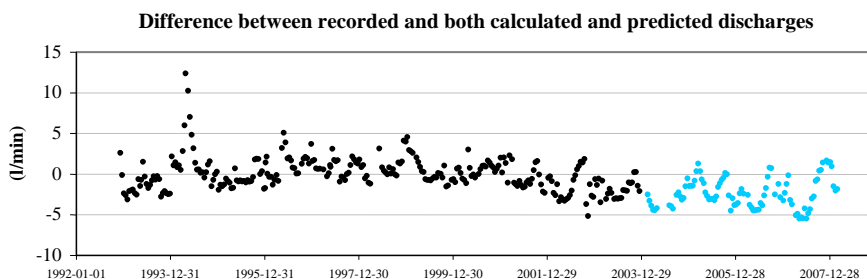
$$-1.6135 \times 10^1$$

$$k$$

$$9.1448$$



- recorded data
- quantitative interpretation
- predicted discharges



- interpretation
- prediction

Figure 3.20 – Quantitative interpretation of discharges recorded in seepage measuring weir 3 (fourth interpretation).

In the case of Alto Lindoso dam the time effect is well approximated by a cubic polynomial because there are no significant variations in recorded discharges. In Alqueva dam, there are large variations in discharges which are not justified by variations in the reservoir level, therefore a simpler function, such as a logarithm or an exponential, is more adequate to simulate the time effect.

The study was carried out in a similar manner to that in Alto Lindoso dam. Due to the large variations in recorded discharges, a simple logarithmic or an exponential function is more adequate to simulate the time effect than a cubic polynomial curve, which tends to adjust to variations. Figure 3.22 shows the results of both interpretation and prediction of discharges in drain D25 D. In this case, the time effect is around half of that due to hydrostatic pressure and, although the calculated curve follows a pattern close to that defined by recorded discharges, the prediction deviates from monitored data. Much more accurate predictions can be obtained with discharges recorded in the valley bottom, as shown in Figure 3.23. Figure 3.24 shows that, as in the case of discharges recorded in seepage measuring weir 3 in Alto Lindoso dam, the linear term in h can not be used. As expected, the thermal effect is very low, as shown in Figure 3.25, but the predictions are better when it is taken into account.

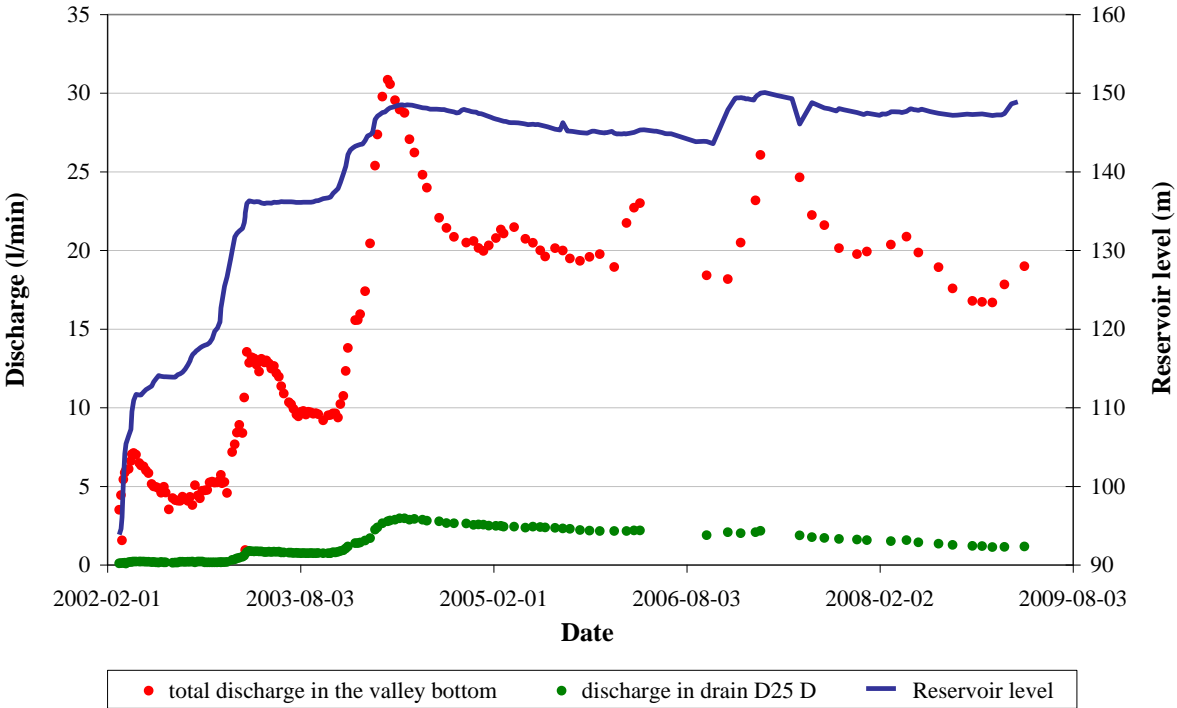
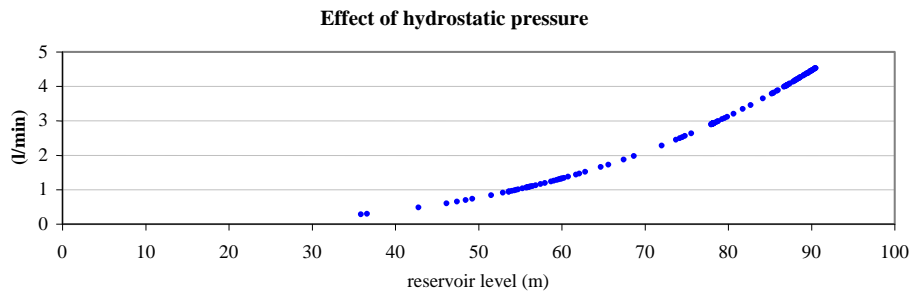
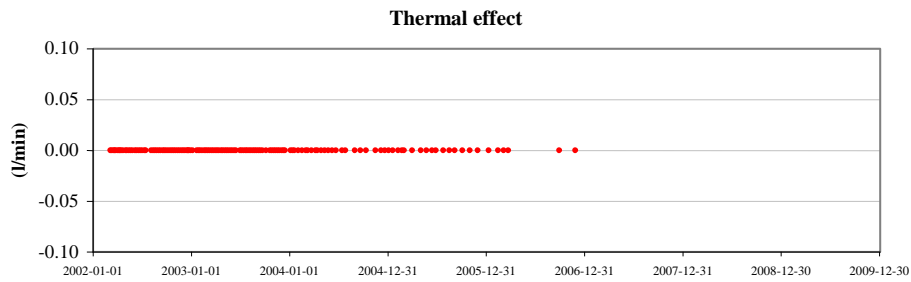


Figure 3.21 – Recorded discharges in the bottom of the valley and in drain D25 D



$$h^3$$

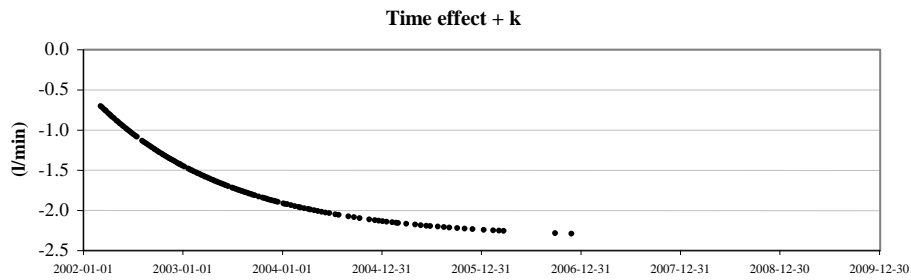
$$6.1107 \times 10^{-6}$$



$$\cos(2\pi s / 365)$$

$$\sin(2\pi s / 365)$$

(s – number of days, starting 1st January)

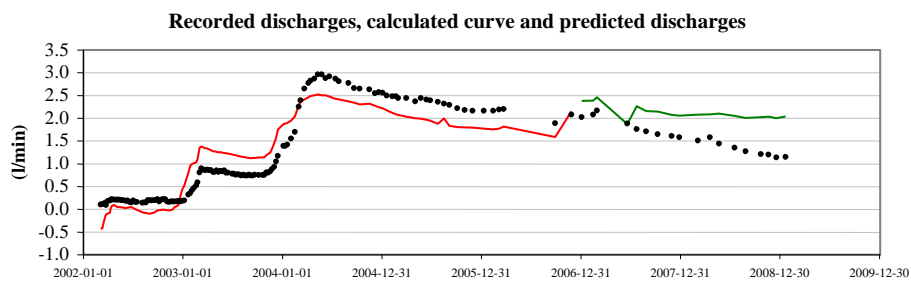


$$1 - e^{(-t/700)}$$

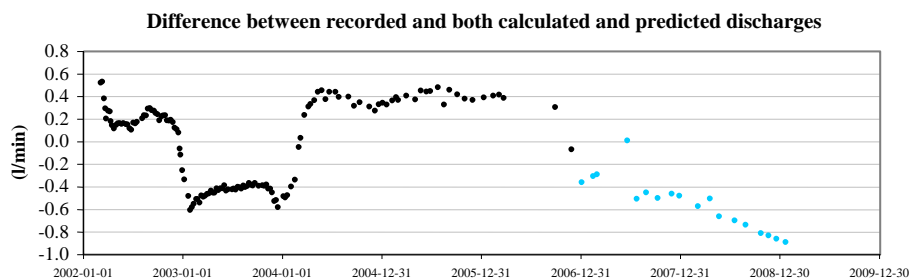
$$-1.6377$$

$$k$$

$$-7.0384 \times 10^{-1}$$

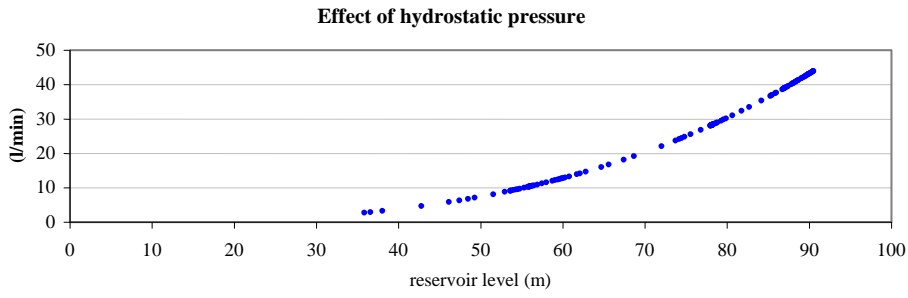


- recorded data
- quantitative interpretation
- predicted discharges



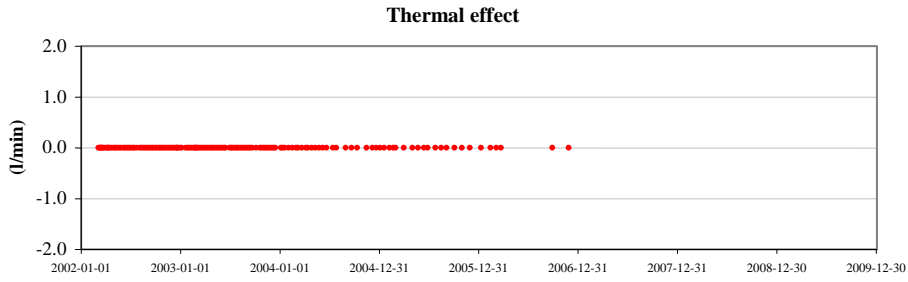
- interpretation
- prediction

Figure 3.22 – Quantitative interpretation of discharges in drain D25 D.



$$h^3$$

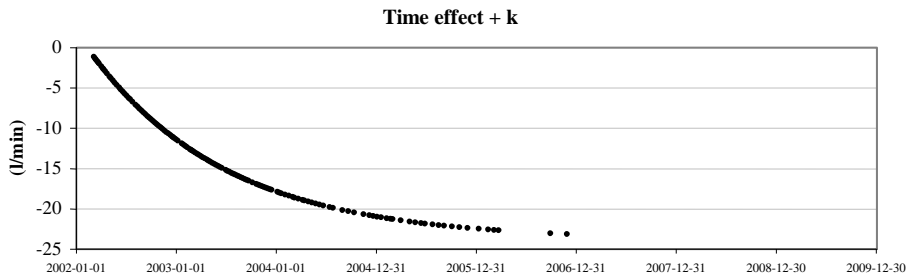
$$5.9212 \times 10^{-5}$$



$$\cos(2\pi s / 365)$$

$$\sin(2\pi s / 365)$$

(s – number of days, starting 1st January)

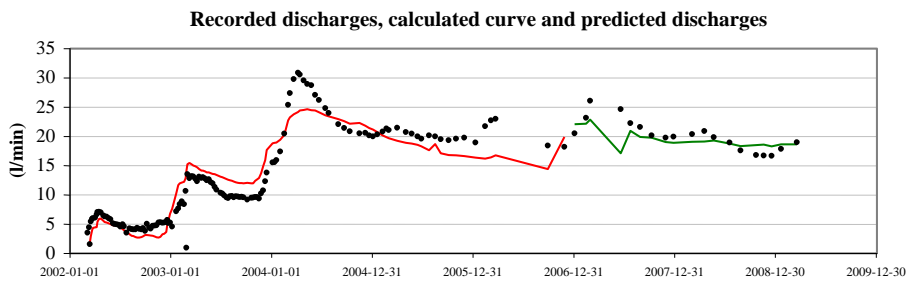


$$1 - e^{(-t/700)}$$

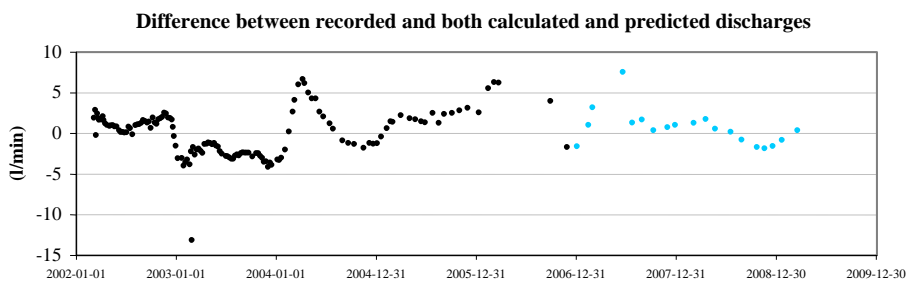
$$-2.2726 \times 10$$

$$k$$

$$-1.1234$$

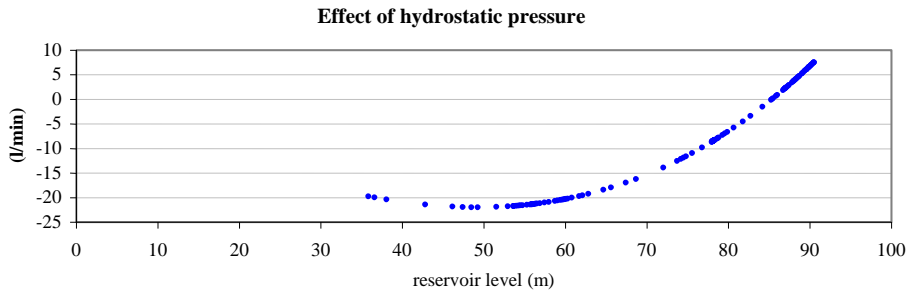


- recorded data
- quantitative interpretation
- predicted discharges



- interpretation
- prediction

Figure 3.23 – Quantitative interpretation of discharges in the valley bottom (first interpretation).

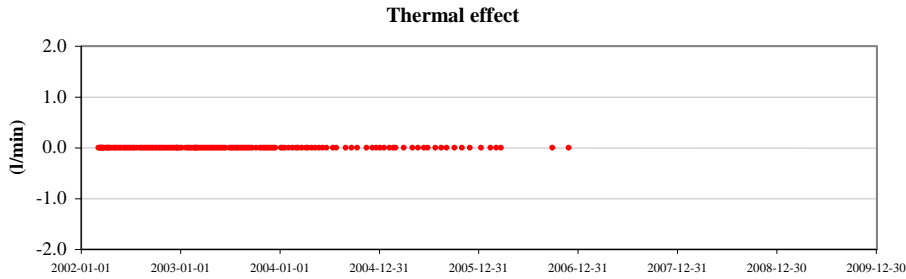


$$h^3$$

$$9.1855 \times 10^{-5}$$

$$h$$

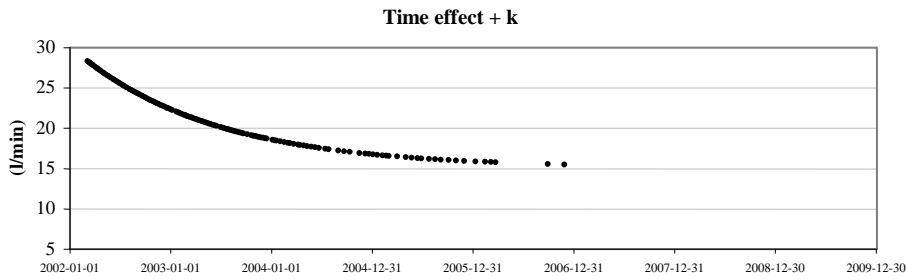
$$-6.6913 \times 10^{-1}$$



$$\cos(2\pi s / 365)$$

$$\sin(2\pi s / 365)$$

(s – number of days, starting 1st January)

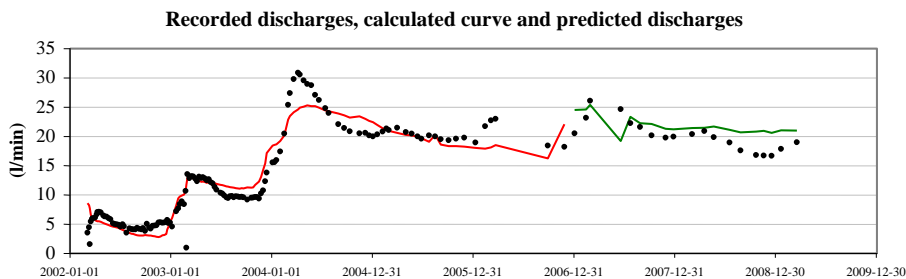


$$1 - e^{-(t/700)}$$

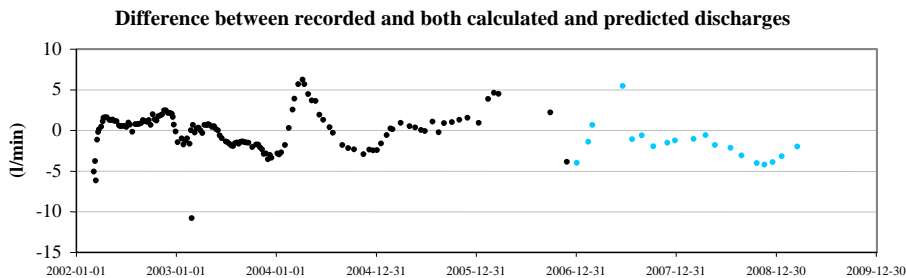
$$-1.3256 \times 10$$

$$k$$

$$2.8337 \times 10$$

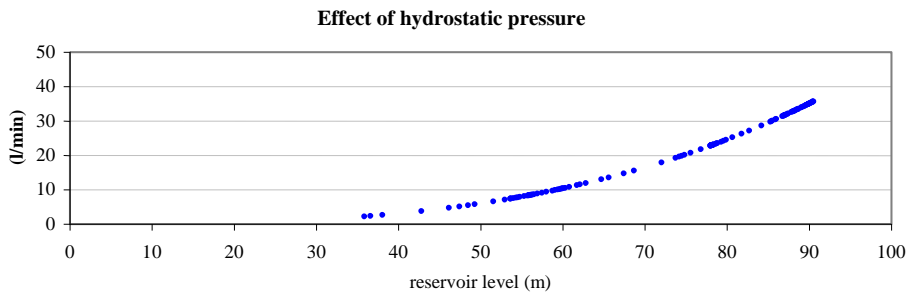


- recorded data
- quantitative interpretation
- predicted discharges



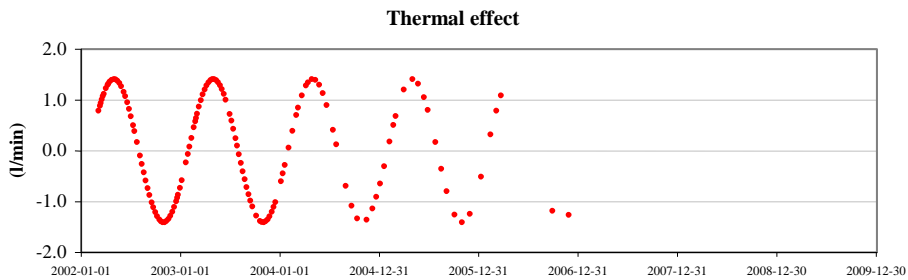
- interpretation
- prediction

Figure 3.24 – Quantitative interpretation of discharges in the valley bottom (second interpretation).



$$h^3$$

$$4.8105 \times 10^{-5}$$



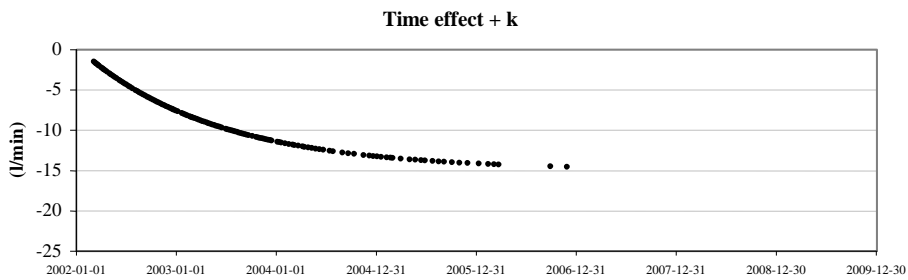
$$\cos(2\pi s / 365)$$

$$-7.0886 \times 10^{-1}$$

$$\sin(2\pi s / 365)$$

$$1.2180$$

(s – number of days, starting 1st January)

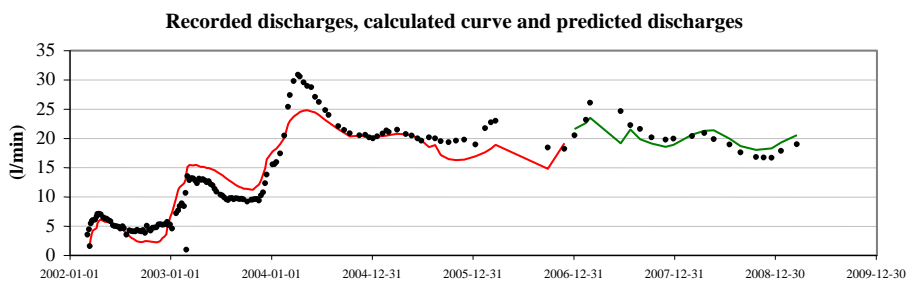


$$1 - e^{(-t/700)}$$

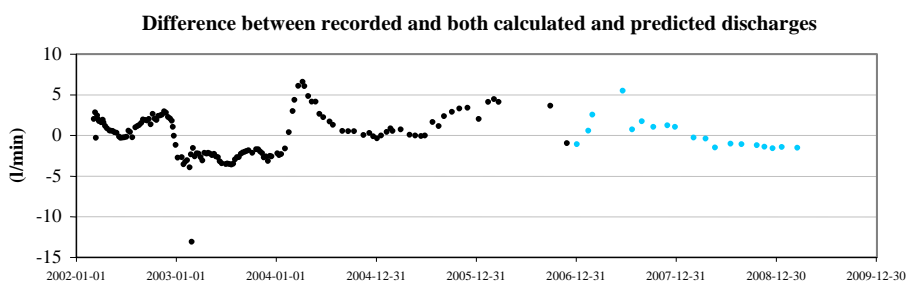
$$-1.3458 \times 10$$

$$k$$

$$-1.4937$$



- recorded data
- quantitative interpretation
- predicted discharges



- interpretation
- prediction

Figure 3.25 – Quantitative interpretation of discharges in the valley bottom (third interpretation).

3.6 Summary and conclusions

Monitoring of dams, including both visual inspections and measurements taken by instruments, helps safety evaluation of dams and their foundations as it enables dam behaviour to be assessed and predictions to be made (ICOLD 2005). Simplified methods traditionally used in the interpretation of the monitoring data, such as quantitative interpretation methods, are relevant not only to evaluate measured behaviour but also to detect changes in dam behaviour at an early stage, so that corrective measures can be taken in due time. The study presented in this chapter focused on quantitative interpretation of discharges, and for this the shape of the influence line of the hydrostatic pressure on discharges in a concrete dam foundation was first established using a numerical model. Using polynomial functions of which the graph adequately follows the shape of the above-mentioned influence line, a series of quantitative interpretation analysis was carried out. Discharges recorded in both single drains and seepage measuring weirs of two different dams were analysed. The study carried out highlighted the difficulties in interpreting recorded discharges, as they are not the sum of a series of structural responses which can be clearly identified, but despite this the following conclusions could be drawn:

- i) the effect that variations in reservoir level have on discharges is adequately simulated by polynomials of the type $h^3 + h$ or $h^4 + h$, except when there is a lack of recorded discharges for lower water levels in the reservoir, in which the effect is better simulated by a function of h^3 ;
- ii) the effect that variations in ambient temperature have on discharges is very small, and can often be neglected;
- iii) discharges recorded in single drains are largely due to localised flow behaviour and, unlike what happens with dam displacements, in which in most cases the time effect can be correlated with a variation in dam concrete deformability over time, the time effect does not necessarily reflect an increase or decrease in the permeability of the discontinuities which cross the drain being studied.

When applied to the analysis of discharges, the method of quantitative interpretation is far more limited than when used in the analysis of dam displacements, due to the great influence that the part given by the time effect plus the independent term has on the results. In fact, when analysing displacements, this part is usually significantly lower than the effect of hydrostatic pressure, while in the analysis of discharges presented here it is about half of that due to hydrostatic pressure. However, results show that this type of analysis can be useful. Indeed, it is concluded that the quantitative interpretations may be used to approximately

predict discharges collected in seepage weirs in a short period of time in which it can be assumed that the trend of the time effect will remain the same.

Quantitative interpretations were carried out for discharges recorded in Alto Lindoso and Alqueva dams and in both dams it is evident that for a given water level, the highest discharges are recorded when that level is reached for the first time. This can be due to the higher rate of variation of the reservoir level, which occurs during the first filling of the reservoir, and which may have an influence on the unblocking of seepage paths.

The analysis was based on the assumption that discharges vary instantaneously with variations in the main loads. In fact, readings of discharges in Alto Lindoso dam, taken with an automated system in a short period of time in which there were significant changes in the reservoir level, were compared with the part due to variations in hydrostatic pressure obtained in a quantitative interpretation (Figure 3.26) and it was concluded that, in this case, there was no time lag. Results shown in Figure 3.26 are from a quantitative interpretation similar to that presented in Figure 3.18, in which the effect of the hydrostatic pressure is represented by a function of h^3 , the thermal effect by a seasonal wave, and the time effect by an exponential curve.

Additionally, an attempt was made to calculate the time necessary to reach steady-state in a hydromechanical analysis, using the code UDEC and the model which was referred to in section 3.5.2. Analysis, of which the results are shown in Figure 3.6 to Figure 3.8, was carried out with a highly efficient special algorithm within UDEC that converges rapidly to the steady state. In transient analysis, the explicit step by step algorithm requires the fluid timestep to be limited, so as to ensure numerical stability. This timestep is given by:

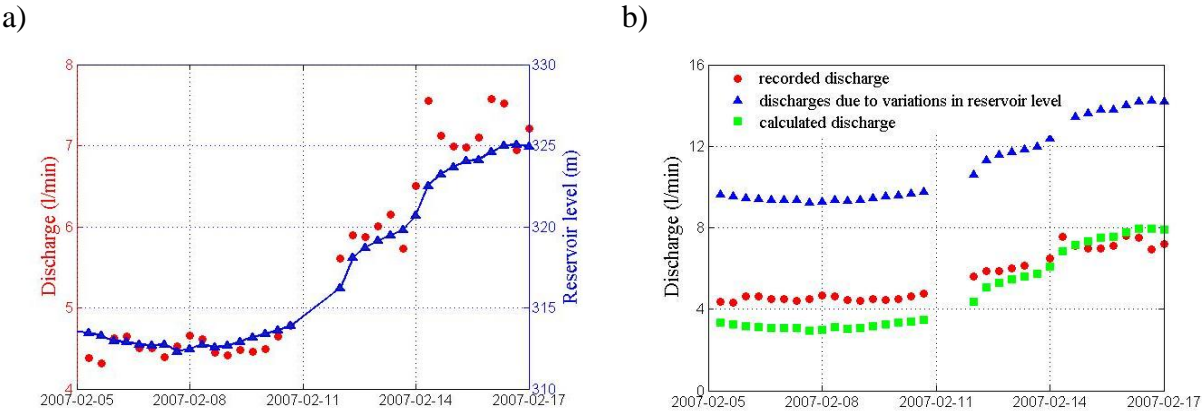


Figure 3.26 – Variations in both reservoir level and total discharges recorded with an automated system (a) and comparison of the total discharges with the part due to variations in hydrostatic pressure obtained in a quantitative interpretation (b).

$$\Delta t_f = \min \left[\frac{V}{K_w \sum_i k_i} \right] \quad (3.3)$$

where V = domain volume; K_w = water bulk modulus; and the summation of the UDEC permeability factors k_i is extended to all contacts surrounding the domain. In UDEC, a “domain” is a segment of a joint (domain volume = joint aperture \times length of joint segment). The minimum value of all the timesteps over all the model’s domains is used in the analysis. In the case studied, the timestep is around 10^{-8} s and the time required to run 1,000,000 cycles is around 2 hours. Flow time is obtained by multiplying the number of cycles by the timestep, and therefore a run time of two hours only simulates 0.02 s of flow. Therefore, transient fluid flow analysis is impractical in relatively large models and with small joint apertures, such as those necessary to analyse flow in dam foundations.

The influence lines due to the hydrostatic effect should represent the permeability of the area being analysed. Additional studies could include quantitative interpretations carried out for different periods of time, gradually longer, but using the same functions to represent the two main effects. This would lead to different influence lines of the hydrostatic effect that should only change slightly from one analysis to another, and could be a way of quantifying phenomena such as clogging of the rock mass. Another issue that requires further attention when analysing discharges collected in measuring weirs is the fact that for different reservoir levels the water may be collected from a different number of drains. Quantitative interpretation should be carried out always using the same drainage system, which means that only water collected in a limited number of drains, probably those from the lower parts of the dam, should be used in the analysis.

This study shows that it is not possible to predict discharges recorded in single drains, as they are largely due to local effects and do not represent the permeability of the rock mass. Therefore, discharges recorded in seepage weirs, collected in relatively large areas, rather than discharges in single drains should be analysed. In fact, leakage measurement is only representative over a certain area, and can be considered an integral factor, reflecting the behaviour of the foundation at more than just one point. In this study quantitative interpretations were only carried out for discharges, as these are more useful for the evaluation of foundation performance than water pressures taken in piezometers, which give only pointwise information (ICOLD 2005).

The study leads to the conclusion that with quantitative interpretation analysis it is difficult to obtain calculated discharges very close to those recorded. However, the general trend in discharge variations is easily obtained and the results of this type of analysis can be used to roughly predict discharges in short periods of time.

Recently, other techniques have been proposed to support the assessment of the field data and results of quantitative interpretation of dam displacements have been compared with those obtained using both the neural network approach, in which the model “learns” from the information contained in a training set of data provided by the user (Mata 2007; Perner et al. 2001), and with algorithms which combine a model selection procedure based on the minimization of the simulation error and a pruning mechanism for the elimination of redundant terms (Piroddi and Spinelli 2003). These methods may be an alternative, or an additional means, to analyse dam behaviour and particularly discharges.

4 Borehole water-inflow tests

4.1 Introduction

The information which is most commonly available regarding the hydraulic performance of dam foundations, namely discharges in the drains and piezometric readings, does not give a clear indication of seepage patterns underneath the dam (ICOLD 2005). Therefore, to obtain detailed information, it is necessary to carry out further tests. Fluid flow in rock masses is usually investigated *in situ* performing hydraulic or tracer tests (Bedmar and Araguás 2002; Committee on Fracture Characterization and Fluid Flow 1996; Ghobadi et al. 2005). In hydraulic tests, which are commonly used to obtain estimates of hydraulic conductivity, some changes are artificially induced into a restricted area of the foundation and the resulting responses are measured. Borehole water-inflow tests are one of the types of test which can be used to study *in situ* hydraulic properties and the way in which flow occurs within dam foundation rock masses. These tests may provide valuable information about seepage patterns within operating dams' foundations and offer the great advantage of not inducing any change in the rock mass.

This chapter starts by describing borehole water-inflow tests, followed by a description of a series of tests carried out in the foundation of two large Portuguese concrete dams: Alqueva arch dam and Pedrógão gravity dam. The main aims of these procedures are presented, along with a reference to the equipment necessary to carry out the tests, the way they should be prepared and conducted, and the key factors to take into account when analysing and interpreting results, in order to obtain the largest quantity of information possible. A reference is made to some studies carried out in three other Portuguese dams where the conclusions drawn from the results of borehole water-inflow tests were of major importance. The main characteristics of both Alqueva and Pedrógão dams are presented, with emphasis on those related with the foundation. This information is essential not only to analyse test results but also to understand studies presented in the three subsequent chapters, which are based on both the dimensions and boundary conditions and/or on data recorded in these dams. Tests were carried out in a series of drainage and piezometric boreholes, and the analysis of results led to a detailed knowledge of seepage patterns in some foundation areas. A brief description of tests and results is presented for each borehole, followed by results analysis. The main difficulties found whilst carrying out tests are referred to and a series of conclusions are drawn from the tests done *in situ*.

4.2 Borehole water-inflow tests

4.2.1 Main aim and brief description of tests

The main aim of borehole water-inflow tests is to understand the flow pattern in a specific area of the foundation. These tests involve only measuring the discharges and water pressures in isolated sections of boreholes and are carried out with the aid of a packer, which consists of an expandable element, usually of stiff, fiber-reinforced synthetic rubber, through which a pipe extends. The packer is inflated inside the borehole at a pre-established level, therefore allowing the isolation of different test intervals within the borehole.

Tests can be carried out with either single or double packers: in the first case the test interval is defined by the bottom of the borehole and the packer and in the second is the area between the two packers. When a single packer is used, tests are usually conducted by raising the equipment and so the length of the test interval is gradually increased. Figure 4.1 shows, as an example, some different stages of water-inflow tests using both single and double packers: steps 1, 2 and n allow the measurement of discharges above the upper packer and at the test interval, defined either by the packer and the bottom of the borehole (step 1) or by the distance between the two packers (steps 2 and n); step n+1 allows the measurement of both water pressure at the test interval and quantity of water flowing into the hole above the packer. The test is conducted in a single borehole, considering and isolating fixed test intervals and testing the hole in consecutive sections along its length. For each test interval, flow rates and water pressures are recorded until steady state conditions are achieved. While testing, discharges and water pressures are also recorded in the nearby drains and piezometers, respectively, which are kept working as normal.

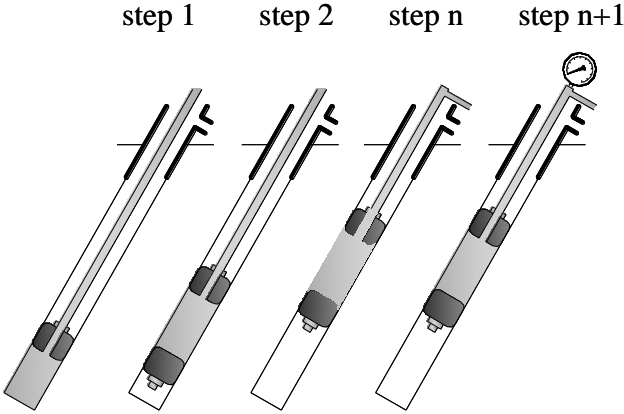


Figure 4.1 – Positioning of packers in the successive steps of borehole water-inflow tests.

4.2.2 Testing equipment

Equipment used to carry out borehole water-inflow tests was initially developed for the oil production industry, but its use has spread to other fields, currently being used in permeability tests, hydraulic fracture tests, grouting for foundation treatment, and in studies of contamination, with the collecting of water samples at various depths (Ask et al. 2009; Giacomel and Rowe 1992; Rowe 2000; Rowe 2001). In addition to the packer, which is the main piece of the equipment used in these tests, it is also necessary to have equipment to i) check the borehole, before carrying out tests; ii) place and keep the packer in position in the borehole; and iii) measure discharges, water pressures and piezometric levels. A detailed list of the equipment required is presented in Appendix 1.

Packers can either be mechanical or hydraulic, depending on the method used to inflate them, but hydraulic packers are easier to handle and allow larger dilations. The inflation medium, which is usually water but can also be oil, air, or nitrogen gas, is introduced between the central pipe that goes through the packer and the expandable rubber. The packer's central pipe is screwed to a series of other pipes, linking the test interval to the borehole head. In this way, either the flow rate into the test interval or water pressures can be measured in borehole water-inflow tests.

The choice of the equipment to carry out tests depends on a series of geometric restrictions and on the rock mass jointing pattern. In concrete dams, tests are usually carried out in drainage galleries, and therefore geometric restrictions include: i) the diameter of the pipe at the borehole's head; ii) the borehole's diameter; iii) the size of the galleries where tests are to be carried out; and iv) the inclination of the axis of the borehole in relation to the gallery floor and sidewalls. In embankment dams, tests are usually carried out in the open air, therefore only the first two above-mentioned restrictions need to be taken into account. The packer, single or double, should have a length which is compatible with the jointing pattern and a suitable diameter, so as to ensure that, when inflated, the test interval is properly isolated. According to Wittke (1990), a common difficulty when carrying out hydraulic tests with packers is leakage between the packer and the borehole wall, due to a lack of inflation, or between the test interval and other test branches, through the surrounding rock mass (Figure 4.2). The use of long packer rubber sleeves and hydraulic packers limits leakages, because their greater ability to expand allows greater pressure against the borehole wall.

In this study, tests were carried out with a double packer with a diameter of 56 mm, and expandable rubbers 0.5 m long. With the aid of a metallic stopper, the equipment is easily assembled as a single packer. The packer was chosen due to its suitability to conduct tests in boreholes with a diameter of 76 mm, which is the usual dimension of the drainage boreholes, with pipes at the head with an interior diameter of 65 mm. The packer has four extension

pipes, which are easily screwed together, and allow test intervals of different lengths (1 m, 3 m, 4 m and 5 m). The water pressure is measured with a pressure transducer, calibrated for readings from 0 to 20 bar, located 0.825 m above the top of the test interval. The scale of the pressure transducer was chosen so as to be suitable for the maximum water pressures expected in Portuguese dams, in which the equipment is going to be used. The water flowing into the test interval can reach the borehole's head through a series of PVC pipes. Figure 4.3 shows the main parts of the equipment and its geometry is shown in Appendix 1.

4.2.3 Preparation of tests and test procedures

Borehole water-inflow tests must be carefully prepared taking into account: i) the specific information required; ii) the particular features of the dam where tests are going to be carried out; and iii) test procedures.

As the main aim of borehole water-inflow tests is to obtain information on how seepage occurs in a certain area of the dam foundation, testing is therefore carried out in a series of boreholes located in that area and the various test results are analysed and interpreted together. At the preparation stage, it is essential to check if there is any impediment to carry out tests in any borehole, such as boreholes filled with coarse sand or with geodrains. Regarding the dam where tests are going to be carried out, it is necessary to ensure the stability of the dam when performing the tests. This is particularly significant in gravity dams, because they are designed to resist the horizontal thrust of the water entirely with their weight. However, uplift forces, which may increase while testing, reduce the stabilizing effect of the structures' weight. Available geotechnical information of the area to be studied should also be carefully analysed, as well as variations in discharges and water pressures, and their relation with the reservoir level. This analysis not only allows better knowledge of the foundation area, but also shows which equipment should be used, namely, pressure gauges with scales and precision suitable for the expected water pressure and sizes of measuring cylinders.

There are no pre-established testing methods, thus the tests were developed within this study to provide information which can be useful in the analysis and safety assessment of any dam foundation. Test procedures, which were continuously corrected and improved while carrying out the tests presented in the next sections, are described in detail in Appendix 1. The test has five main stages:

- i) firstly, it is necessary to measure discharges and water pressures, not only in the borehole which is going to be tested but also in the boreholes located in an area larger than that its expected area of influence, before placing the equipment;

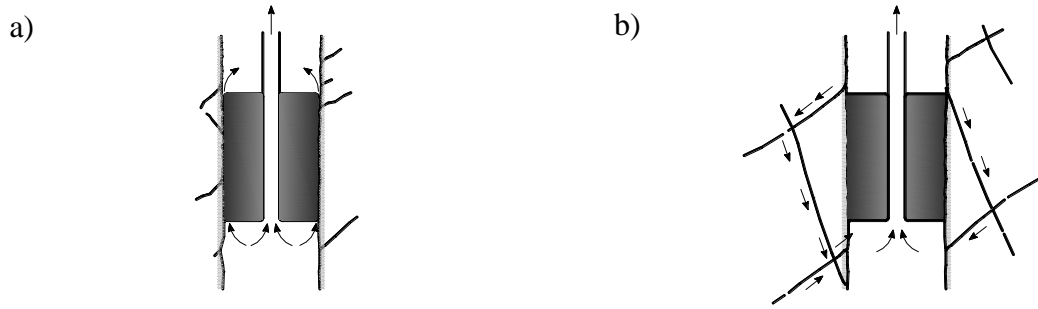


Figure 4.2 – Common difficulties when carrying out hydraulic tests: a) leakage at the packer; b) flow around the packer (adapted from Wittke 1990).



Figure 4.3 – Main parts of the equipment.

- ii) then, a piece of metal with the same diameter as the equipment called “blind device” has to be inserted into the borehole to check for and remove, if possible, any obstructions, to make sure that the equipment will fit;
- iii) thirdly, tests are conducted with a single packer;
- iv) then with a double packer;
- v) and finally it is necessary to repeat all the measurements referred to in i) again to verify if the testing process has altered the seepage pattern.

After tests in a series of adjacent boreholes have been carried out, when some knowledge about seepage in the area in analysis has already been obtained, it may be of interest to conduct new tests in some borehole branches, so as to shed light on or confirm hypotheses concerning seepage paths. In these new tests, some changes may be introduced into test procedures depending on various circumstances which may arise: i) if there is any borehole area which needs to be analysed in depth, the length of the test interval should be decreased; ii) to confirm the existence of seepage paths linking a test interval and adjacent boreholes, it may be necessary to introduce some changes either in the drainage or piezometric systems, by closing or opening boreholes; and iii) when water does not reach the borehole’s head, it is possible to obtain information on seepage velocity within the test interval being studied, increasing the water column and carrying out Lefranc type tests.

It is not easy to estimate the time necessary to carry out tests, as discharges and water pressures should only be taken in steady state conditions. The period of time necessary to achieve this state depends on the rock mass permeability: in areas where it is low, it may take various hours or even days; in more pervious foundation areas, steady-state conditions are quickly achieved. Tests also take longer when the borehole being tested is linked to a large number of other boreholes, as discharges and water pressures must be measured not only in the borehole being tested but also in the boreholes located in its area of influence.

Borehole water-inflow tests can be carried out at any time during the year. However, when planning the tests, it should be taken into account that discharges are higher for higher water levels. In arch dams, tests are better carried out with high reservoir levels and during the winter, when the ambient temperature is low, as, due to arch dams’ behaviour, this is when the aperture of the discontinuities within the rock mass close to the heel of the dam is greater.

4.2.4 Analysis of test results

Analysis of borehole water-inflow test results should be carried out in a qualitative way, examining recorded data, interpreting charts which can be drawn and checking the

consistency between conclusions drawn from tests and other available information, such as geological and geotechnical data of the dam site, boreholes logs, information given by the borehole driller, and results of other complementary tests, including electrical conductivity tests and chemical analysis of water.

Data collected during tests in successive borehole test intervals allows the drawing of the following type of charts: i) discharges and water pressures in the equipment placed in the area of influence of the borehole being tested; ii) discharges and water pressures measured in the borehole; iii) discharge flowing into each of the borehole's test intervals; iv) accumulated discharge from the bottom to the head of the borehole; v) discharge above the test interval; and vi) variations in water pressures along the borehole. Analysis of charts may provide information on:

- i) the depth at which the main seepage paths cross the boreholes;
- ii) the distribution of discharges and water pressures along the boreholes; and
- iii) seepage paths linking different boreholes.

With the simultaneous analysis of water pressures and discharges it is possible to draw conclusions concerning seepage through discontinuities: i) high water pressures and low discharges are due to seepage through discontinuities with a very low aperture; ii) high water pressures and discharges reveal that the grout curtain is probably inefficient and that there are high seepage velocities; on the contrary, low water pressures and discharges may either reveal that there is an efficient grout curtain, that the rock mass is in the process of becoming more impervious due the settlement of sediment within discontinuities, or that the boreholes are clogged; iii) low water pressures and significant discharges show that discontinuities within the foundation are quite open, and that the high quantity of water flows a long way, with high pressure losses. In this case, it can also be concluded that the drainage curtain is in good condition.

Valuable additional data can be obtained with water electrical conductivity tests, which are easily and quickly carried out. Taking into account LNEC's experience, these tests may provide information about the depth at which seepage paths cross each one of the boreholes when discharges are between 0.20 and 3.0 l/min. Discharges lower than 0.20 l/min make seepage paths undetectable and higher than 3.0 l/min lead to similar readings along the borehole, due to the consequent high water velocity.

4.2.5 Previous use of borehole water-inflow tests in Portuguese dams

This section examines some studies carried out in three Portuguese dams (Figure 4.4) where the performance and analysis of a series of tests, among them borehole water-inflow tests, were of major importance. Despite the fact that the first two are embankment dams, they are referred to in this section because when dams have their foundations in rock masses there is no difference between results analysis of tests carried out in either concrete or embankment dams.

4.2.5.1 Beliche dam

Beliche dam is located on River Beliche, in the Algarve, in the south of Portugal. It is a zoned earth-rockfill dam, with a maximum height of 54 m, slightly curved along its length. The foundation rock mass consists of schist and greywacke. The reservoir water is used for irrigation and water supply. The construction of the dam finished in 1986 and the first filling of the reservoir in December 1988.

About five months after the conclusion of the first filling of the reservoir, in May 1989, a leakage was detected in the downstream face of the dam, close to the right bank, at around mid-height of the dam. To understand where the water was coming from and suggest, if necessary, a suitable treatment, the additional monitoring equipment, which had already been studied, was re-analysed and a series of tests was carried out while opening new piezometric boreholes in the vicinity of the leakage. To obtain data about the location and relative aperture of the discontinuities responsible for the water leaking, borehole water-inflow tests with a double packer were carried out. To analyse the seepage paths by trying to detect connections between different discontinuities and between the injection area and other boreholes or between the injection area and the leakage, injection tests with single packers and tracer tests were also carried out. Furthermore, water samples were collected and physical and chemical properties of the water in the foundation and of the leakage were compared (Pinto et al. 1991).

The tests were carried out, mainly to detect the seepage path towards the leakage. If the seepage path was through the dam body it would be necessary to take some measures to avoid piping. The results of the injection and borehole water-inflow tests and of tracer tests led to the conclusion that the seepage path towards the leakage crossed the foundation, which is a schistose rock mass, with a low probability of erosion. As the high uplift pressures recorded were not a danger to the dam stability and safety, no foundation treatment was suggested, and it was decided that it would be sufficient to control the discharges in the leakage over time. In the tracer tests carried out, although different tracers were used, it was only possible to draw some conclusions from the use of sodium chloride. The tests led to the conclusion that the dye tracers were adsorbed onto the foundation rock mass. Some



Beliche dam



Santa Águeda dam



Funcho dam

Figure 4.4 – Portuguese dams where borehole water-inflow tests were carried out.

deficiencies were found during the borehole water-inflow test performance related to the small size of each packer (only 20 cm) and to the difficulty of pumping water from the test interval (Pinto et al. 1991).

4.2.5.2 Santa Águeda dam (Marateca dam)

Santa Águeda dam, also known as Marateca dam is located on the River Ocreza, about 15 km to the north of Castelo Branco, the capital of Beira Baixa. The construction of the dam was concluded in 1991. It is a homogeneous earth-fill dam, with a dipping filter in the downstream slope. The dam has a total length of 1054 m and a maximum height of 25 m. Water is used to supply Castelo Branco and for irrigation. The foundation consists of granite with two micras, mainly biotitic.

In this dam, after about five years of use, some leakages were detected in the downstream area of the dam, close to the right bank. The analysis of the uplift pressures recorded in different piezometers led to the conclusion that there could be significant seepage through the downstream slope of the dam. If the interstitial pressures were high this seepage could lead to hydraulic lifting and progressive erosion of material from the rock mass discontinuities. Thus, to monitor interstitial water pressures, it was decided to install new piezometers in that area of the embankment (LNEC 1997b).

To identify the main seepage paths and to evaluate the way in which seepage occurred along the boreholes, different tests were carried out, namely injection tests and borehole water-inflow tests. The tests were carried out in breaks between drilling. The rotary drilling was done with water and allowed the recovery of rock samples. The identification of the discontinuities and of the areas of highest permeability made it possible to choose the best place for the piezometric chambers in each borehole (LNEC 1997b).

4.2.5.3 Funcho dam

Funcho dam is located on the River Arade, close to the city of Silves, and is part of the Odelouca-Funcho system, of the Algarve Hydraulic Development, which provides water

supply, for irrigation, for a large area of the Algarve. It is a double curvature arch dam with artificial abutments and a thick base. The dam has 49 m of maximum height, 165 m of development at the crest and the thickness varies, in the central cantilever, from 6.5 m at the base, to 2.25 m at the crest. The retention water level is 96.0 m. The dam construction ended in 1991 and the first filling of the reservoir, which started at the beginning of November 1992, was only concluded in January 2001. The foundation rock mass, highly heterogeneous and anisotropic, consists of schist and greywacke (DGRAH 1978).

The long period taken for the first filling of the reservoir was due to the need for successive foundation treatments, which made it necessary to hold the filling (LNEC 2005a). Foundation treatment included injections in the concrete/rock mass interface, consolidation and grouting. The first strengthening of the grout curtain was done in 1992 because, before the beginning of the first filling of the reservoir, with the reservoir at a relatively low elevation, high flow rates were recorded at the drainage curtain (LNEC 1990). At the beginning of 1996, with the reservoir at an elevation of 94.0 m, the filling of the reservoir was halted again, due to some local high flow rates. The design of the second strengthening of the grout curtain was done by the dam owner, Instituto da Água (INAG), who requested that the dam designer, COBA, revise the design and give technical assistance and that LNEC analyse the dam behaviour while the foundation treatment was being carried out (LNEC 1998b).

After carrying out a series of borehole water-inflow and injection water tests in various drainage boreholes, the foundation treatment was slightly altered (LNEC 1998a). The tests carried out gave some information about the probable efficiency of injection with cement grout. This information made it possible to avoid the drilling and injection of some boreholes, which had previously been defined. In one of the areas tested instead of opening and injecting new boreholes it was decided to inject the bottom of two different drains which were too long and extended below the lower part of the grout curtain, thus reducing the total discharge. This injection was done without reducing the drainage efficiency, as the water pressure due to water entering the bottom of the boreholes, was very low. The results of the borehole water-inflow tests led to a detailed knowledge of the main seepage paths which allowed not only the reduction of costs but also the reduction of the time required to conclude the foundation treatment.

4.3 Main characteristics of the dams where tests were carried out

Borehole water-inflow tests were carried out as part of this study in Alqueva and Pedrógão dams, both owned by Empresa de Desenvolvimento e Infra-Estruturas do Alqueva (EDIA) and designed by EDP (EDP 1988; EDP 1994; HIDRORUMO 1999; HIDRORUMO 2001; Miranda and Maia 2004). Both dams are located on the River Guadiana, in the southeast of

Portugal and are part of a multipurpose development designed for irrigation, energy production and water supply.

Alqueva dam is the main structure of the development and creates the largest artificial lake in Western Europe, with storage capacity of 4150 hm³ and a surface area of 250 km² at the retention water level, of which 215 km² are in Portugal and 35 km² in Spain.

Pedrógão dam is located about 23 km downstream from Alqueva dam, and creates a reservoir with storage capacity of 54 hm³ which not only allows the turbines of Alqueva dam to work in a reverse motion, by pumping water from the downstream to the upstream reservoir, but also provides water for irrigation and for energy production. It is the first roller compacted concrete (RCC) dam built in Portugal.

4.3.1 Alqueva dam

4.3.1.1 General description of the dam

Alqueva dam is a double curvature arch dam, with artificial abutments. The structure is extended on the left bank by a group of gravity blocks where a surface spillway is inserted, followed by a structure which closes the valley. The dam has a maximum height of 96 m, a total length of 348 m between the abutments at the crest elevation, and a length of 140 m in the bottom of the valley (Figure 4.5, Figure 4.6 and Figure 4.7). Figure 4.8 shows the dam's central cross section. The dam width is 7 m at the crest, while at the base it varies from 30 m at the central cantilever to 33 m at the abutments. The crest is located at an elevation of 154.0 m and carries a road which links the towns of Moura and Portel. The powerhouse is located at the toe of the dam. Downstream from the dam is a concrete dam-wall, with a maximum height of 55 m, which protects the powerhouse and the substation from the downstream reservoir, created by Pedrógão dam (EDP 1994).

The dam has 35 independent concrete blocks: 24 in the arch, 3 in the right abutment, 4 in the left abutment and 4 in the closing structure of the left bank. It has four main inspection galleries, GV1 to GV4, with floors at elevations of 147.0 m, 126.0 m, 105.0 m, and 84.0 m respectively, and a drainage gallery (GGD) which is aligned with the insertion of the dam in the foundation and has its floor, at the lowest level, at an elevation of 61.0 m. In the abutments, the galleries GV1, GV2 and GGD are split into two galleries, one close to the upstream face of the dam and the other one approximately halfway between the upstream gallery and the downstream face of the dam. In the bottom of the valley the drainage gallery is also split into two galleries, one close to the upstream face and the other one known as the downstream drainage gallery (GDJ). The latter extends towards the right bank in a branch

excavated into the rock mass. The dam-wall has a drainage gallery with the floor in the area downstream from the powerhouse at an elevation of 42.0 m.

In the bottom of the valley the interface concrete/rock mass is at an elevation of 58.0 m, 3 m below the floor of GGD, with the exception of the area at the heel of these blocks, where a foundation plinth 6 m wide was built with its base at an elevation of 55.0 m. At the top of the plinth (58.0 m) there is a peripheral joint (concrete-concrete joint) introduced to avoid vertical stresses in the foundation with the filling of the reservoir. The width of the peripheral joint varies from one block to another, from 7.25 m up to 9.0 m (Figure 4.9).

The construction of the dam began in 1997 and ended in 2003. The first filling of the reservoir began in February 2002 and is still not finished, because, after reaching a water level of 150.0, the dam began operating in normal conditions. Officially the first filling of the reservoir will only finish when water reaches the retention water level, at 152.0 m.

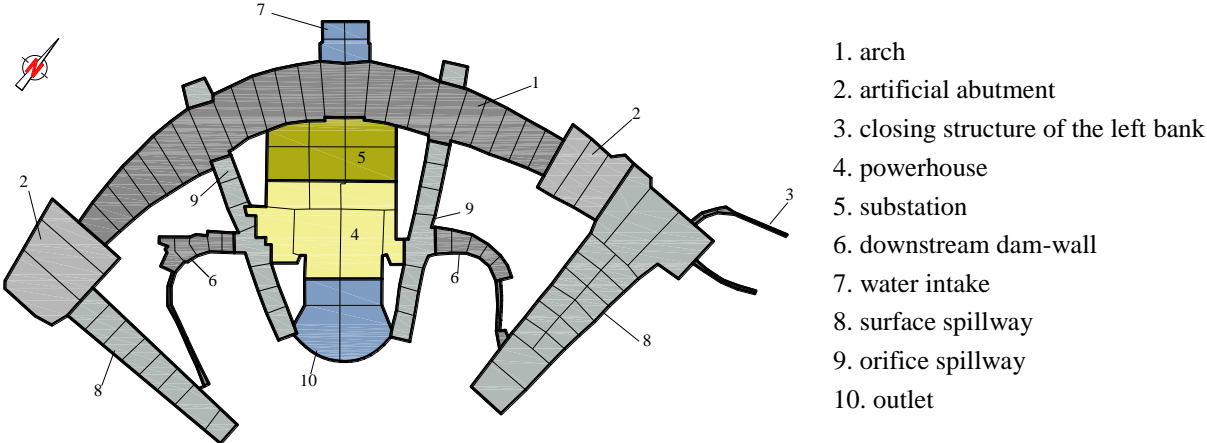


Figure 4.5 – Layout of Alqueva dam.



Figure 4.6 – Alqueva dam. Downstream view from the left abutment.

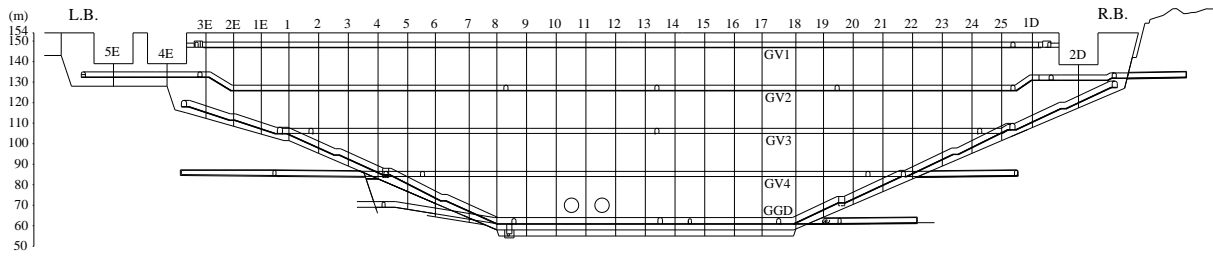


Figure 4.7 – Upstream elevation of Alqueva dam.

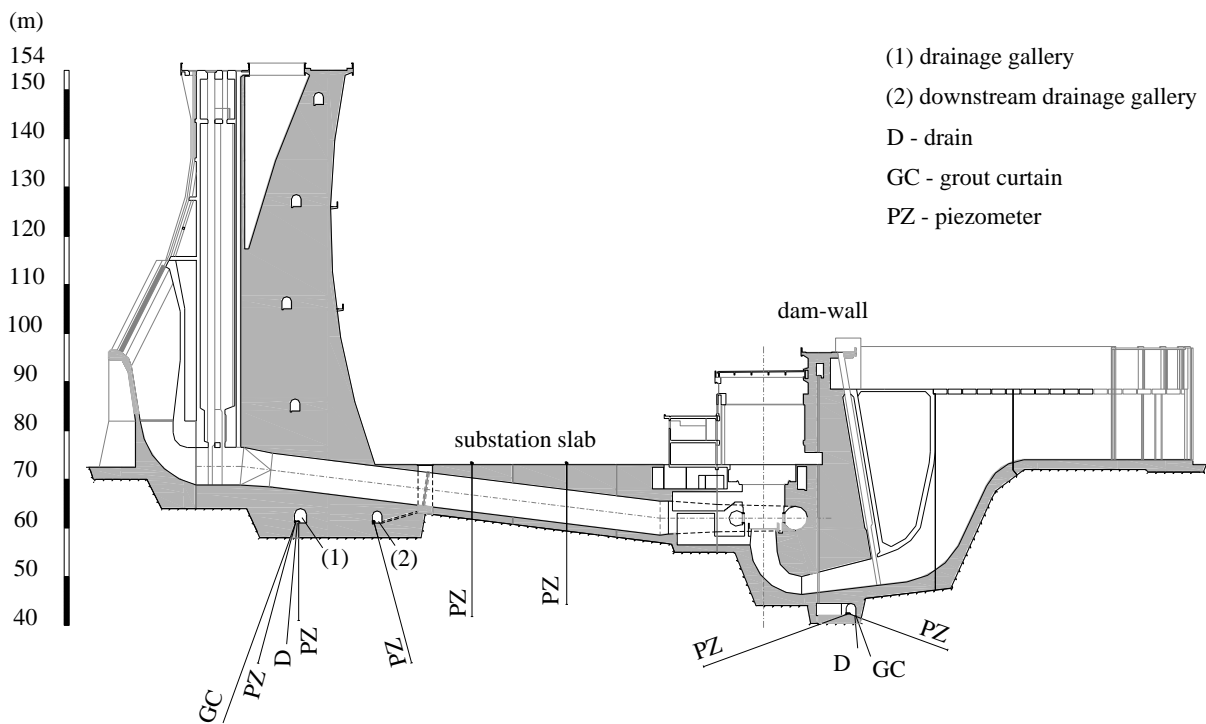
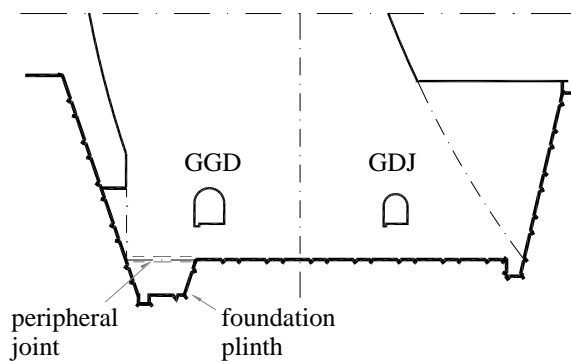


Figure 4.8 – Central cross section of Alqueva dam.



Dam vertical joint	Width of peripheral joint e (m)
8 and 18	7.25 / 7.31
9 and 17	7.96
10 and 16	8.45
11 and 15	8.77
12 and 14	8.95
13	9.00

e – width of peripheral joint

Figure 4.9 – Foundation plinth and peripheral joint at the heel of blocks in the valley bottom.

4.3.1.2 Geological-geotechnical conditions

Detailed geological and geotechnical investigation was carried out at the dam site between 1960 and 1995, when the tender for the dam and powerhouse construction was opened. The studies included site reconnaissance investigation and foundation characterization. Several borehole core drilling surveys were carried out, with a total drilling length of 3750 m, most of them simultaneously doing Lugeon type tests. LNEC conducted a series of *in situ* and laboratory tests. *In situ* tests included geophysical surveys (seismic refraction spreads, seismic tomography and electrical resistivity soundings) and foundation deformability evaluation (plate loading (jacking) tests on exposed rock galleries, flat jacks inserted into exposed rock surfaces, and borehole jacks with dilatometer) (LNEC 1970; LNEC 1973; LNEC 1975; LNEC 1986; LNEC 1995). Laboratory tests were conducted to evaluate anisotropy and to determine shear strength (UCS, ϕ , and c). The shear strength of discontinuities was also studied in the laboratory (LNEC 1984). While excavating and building the dam and the powerhouse, more geological and geotechnical investigation was carried out, mainly in the left bank where the main fault within the project area is located (LNEC 1998a; LNEC 1999b; LNEC 1999c; LNEC 2002; LNEC 2003; Neves and Gonçalves 2002).

The foundation is heterogeneous and consists of good quality green schist in the right bank and the river bottom and of quite good phyllite, with a higher deformability, in the left bank. According to *in situ* tests carried out prior to dam construction the foundation Young's modulus in the left bank varied from 6 to 20 GPa, and the foundation of the right bank and of the bottom of the valley had a Young's modulus greater than 20 GPa (Liberal et al. 2002; LNEC 1973; Neiva et al. 1997). Table 4.1 shows the average cohesion and friction angle of discontinuities in the two different foundation areas. The area of the phyllite is more fractured and is crossed by several faults, the most important being fault 22, which corresponds to the green schist/phyllite interface.

Discontinuities		Cohesion	Friction angle
		c (MPa)	ϕ ($^{\circ}$)
Green schist	discontinuities along schistosity	0.10	24
	discontinuities making an angle $< 15^{\circ}$ with schistosity	0.17	38
	discontinuities making an angle $> 15^{\circ}$ with schistosity	0.18	43
phyllite	discontinuities along schistosity	0.11	22
	sub-vertical and sub-horizontal discontinuities	0.13	29
	discontinuities dipping between sub-vertical and sub-horizontal	0.13	36

Table 4.1 – Average cohesion and friction angle of discontinuities (LNEC 1984).

The phyllite has a very visible schistosity, striking N40°-60°W and dipping 15°-50°NE, although it can go up to 70°NE at specific zones. The green schist looks highly dense and, in general, schistosity is barely evident and subparallel to bedding planes. There are, however, some local zones where these rocks have a very visible schistosity which corresponds in most of the cases to inclusions of chlorite schist (EDP 2006).

Various sets of rock joints were identified, of which the most prevailing are: **A)** N40°-65°W, 12°-65°NE; **B)** N75°W, S75°W; 65°N-90-55°S; **C)** N65°-90°W, 12°-55°NNE; **D)** N20°-42°W, 65°-90°ENE and **E)** N25°-55°W, 65°SE-90° (EDP 2003). Figure 4.10 shows the average position of the main sets of rock joints in relation to the dam. Several faults, aligned with some joint sets, are shown on the surface foundation map, especially in the left bank, but their width is, in general, less than 10 cm, with the exception of fault 22. This latter is, in fact, not a single fault but a geological entity bordered at hanging and foot by two almost parallel faults, with a filling of highly deformable phyllite and with widths lower than a few tenths of centimetres, although locally larger than 1 m. The material between these two faults is fractured and crushed phyllite. The width of this geological entity varies between 3 and 12 m, and the dip angle can be close to 45°. The main faults/fault zones observed, shown in Figure 4.11, and the sets of rock joints to which they belong are (EDP 2006):

- zone of fault 22 (set **C**) in the left bank, below the arch and the abutment;
- fault 66 (set **A**) in the left bank, crossing the foundation of block 1-2;
- fault 29 (set **D**) in the left bank, crossing the foundation of block 1-2;
- zone of faults 17/18 (set **A**) in the central zone of the bottom of the valley, crossing the dam foundation (blocks 12-13 and 13-14) and the powerhouse foundation;
- fault 19 (set **A**) in the bottom of the valley, crossing the powerhouse foundation and the dam foundation, below blocks 10-11 and 11-12.

Most of the joints in phyllite belong to set A, with a short trace length (< 10 m), small gaps (< 0.20 m) and smooth to slightly rough surfaces. In the green schist joints show a very high persistence (> 20 m), with spacing larger than 0.60 m and have rough to very rough surfaces (EDP 2006).

The surface foundation map was prepared using the terminology and symbols suggested in (ISRM 1978; ISRM 1981), and, according to these classifications, the right bank and valley bottom foundation rock mass, where the green schist occurs, is fresh to slightly weathered (W1 to W2) and the mean distance between successive discontinuities measured along an intersecting straight line is wide to moderate (F2 to F3). Close to the main faults the fracture

spacing decreases (F4 to F5). In the left bank foundation, which consists mainly of phyllite, the degree of weathering at the surface is W2 to W3. The fracturing intercept of the phyllite is, in general, F4 to F5 and, less frequently, F3 to F4.

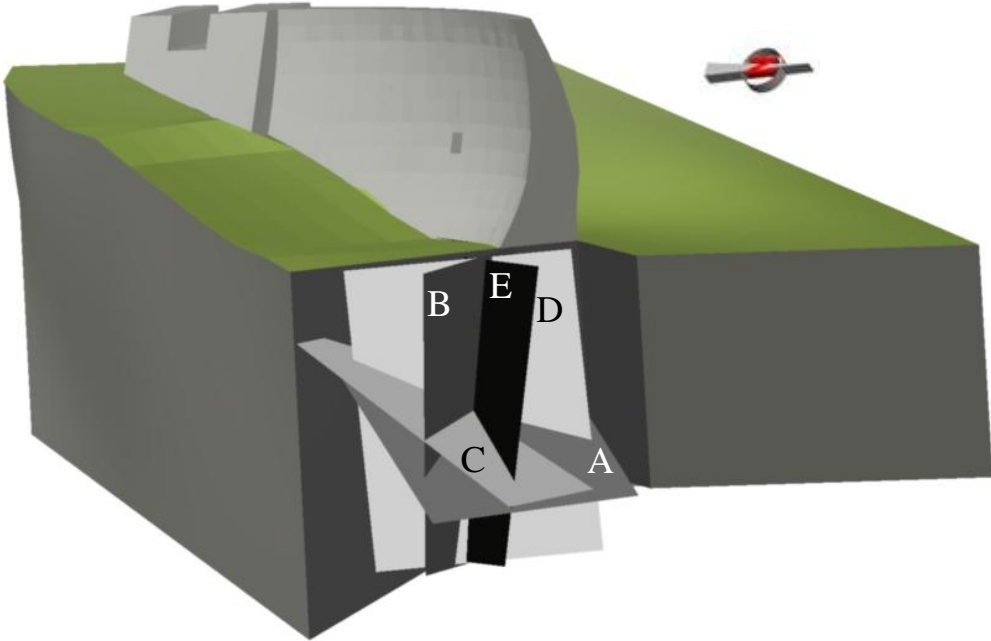


Figure 4.10 – Average position of the main sets of rock joints in relation to the dam.

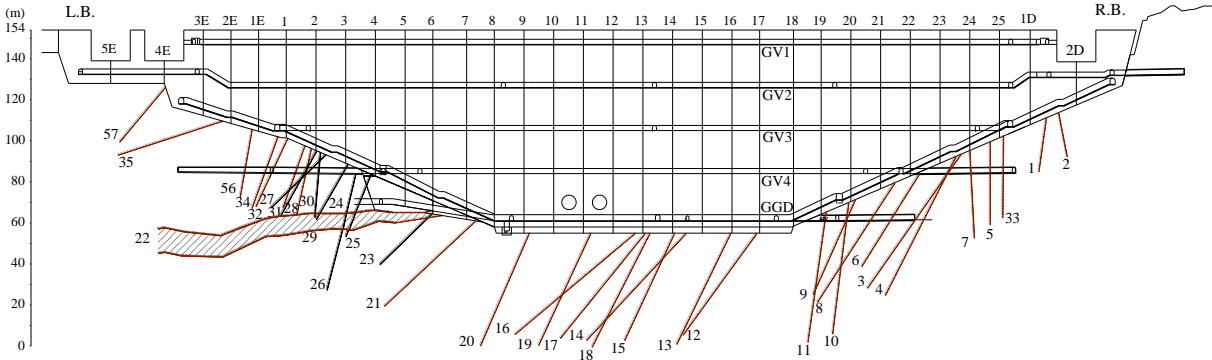


Figure 4.11 – Faults in Alqueva dam foundation.

4.3.1.3 Foundation treatment

Foundation treatment consisted of consolidation of faults, general consolidation of the rock mass in the area of the dam and of the downstream dam-wall, contact grouting, and the installation of a grout curtain and a line of drainage boreholes. Due to the importance of fault 22 in the structural behaviour of the dam, a special treatment was carried out which included the excavation of a set of galleries, the removal of the material inside the fault and its replacement with concrete (LNEC 1995; LNEC 1998a; Muralha et al. 2003). Eight longitudinal galleries were excavated (levels 1 to 7 and 4a shown in Figure 4.12) from which a series of lateral widening areas were excavated, and filled with concrete. The longitudinal galleries were sub-horizontal, in the dam axis direction, and were excavated downwards, from the upper levels to the lower ones. The longitudinal galleries were also filled with concrete while the treatment was being carried out, with the exception of two galleries which were later used for grouting and which remain open for inspection purposes. Figure 4.12 shows design drawings of fault 22 treatment.

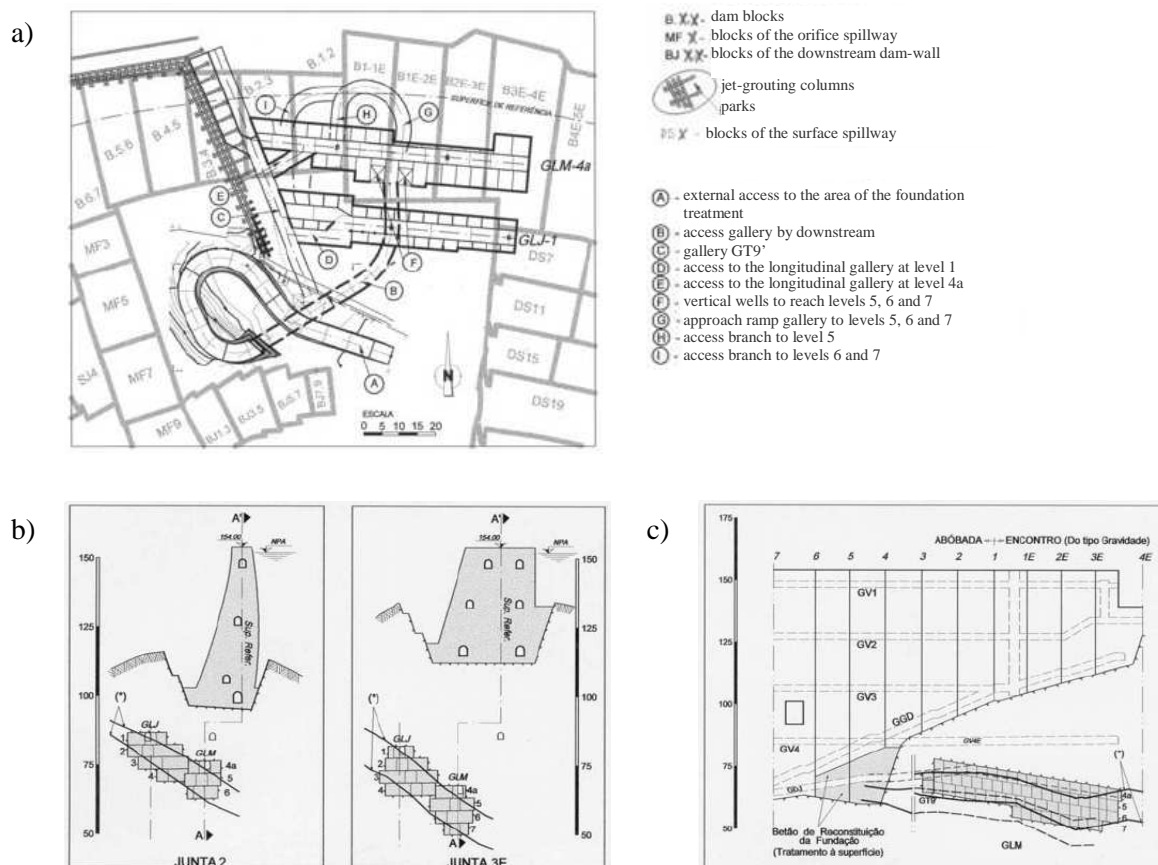


Figure 4.12 – Treatment of fault 22 (design drawings): a) layout of treatment (areas to be treated and access paths); b) cross sections in the upstream-downstream direction; c) cross section along the dam axis (adapted from Liberal et al. 2002).

The treatment of faults 66 and 29 together consisted of placing a concrete block at the base of block 1-2. Treatment of fault 17 consisted of placing concrete blocks in the foundation of the dam and of the powerhouse and in grouting the fault along its dip to a maximum depth of 28.5 m. A small concrete block was also built in the foundation of blocks 10-11 and 11-12, to treat fault 19. The foundation of the downstream dam-wall was also subjected to treatment, which included a grout curtain and a drainage curtain, drilled from the foundation gallery.

To evaluate the effectiveness of the foundation treatment, geophysical tests were carried out before and after the treatment in vertical boreholes drilled at the base of each one of the blocks. The method of crosshole and surface to borehole tomography by seismic waves was used. Results showed that after treatment the field of the velocities of compression waves was more homogeneous and that the lowest velocities had increased. While drilling the above-mentioned boreholes, Lugeon type tests were carried out at several depths (after dam construction but before beginning the grouting injections). The analysis of the results made it possible to identify zones with different permeability: 2.0×10^{-7} m/s down to about 5 m in depth; varying from 2 to 1×10^{-7} m/s between 5 and 10 m in depth; and lower than 1.0×10^{-7} m/s for depths greater than 10 m.

The grout curtain was drilled from the drainage gallery, from gallery GV2 at the base of the blocks which include the surface spillway of the left bank, and from the right bank. The boreholes are located 5 m apart and the average length of the grouting boreholes was 41.0 m, varying from 26 m to 60 m. In the left bank, in the area of fault 22, secondary boreholes were drilled halfway between consecutive primary boreholes, and tertiary boreholes. After grouting, the majority of the permeability values obtained in Lugeon type tests conducted in the vicinity of the treated area, whilst drainage boreholes were being drilled, were lower than 1.0×10^{-8} m/s.

To relieve uplift pressures at the base of the dam, drainage boreholes with a diameter of 76 mm and located 3.0 m apart were drilled from the drainage gallery, the downstream drainage gallery and gallery GV4.

Figure 4.13 shows the drainage system in Alqueva dam foundation. From gallery GV2, at the base of the blocks which include the surface spillway of the left bank, drainage boreholes were drilled 6.0 m apart. Due to some difficulties found while drilling, a geodrain was placed in every borehole of the drainage curtain drilled from the left abutment to the base of block 8-9. From joint 8, in the valley bottom, to the right bank, boreholes were drilled from the GGD with a dip direction of 257° and dipping 85° (dip direction defined clockwise from north, and dip defined as the angle from the horizontal). The average length of the drainage boreholes is 27.2 m, varying from 18 m to 52 m.

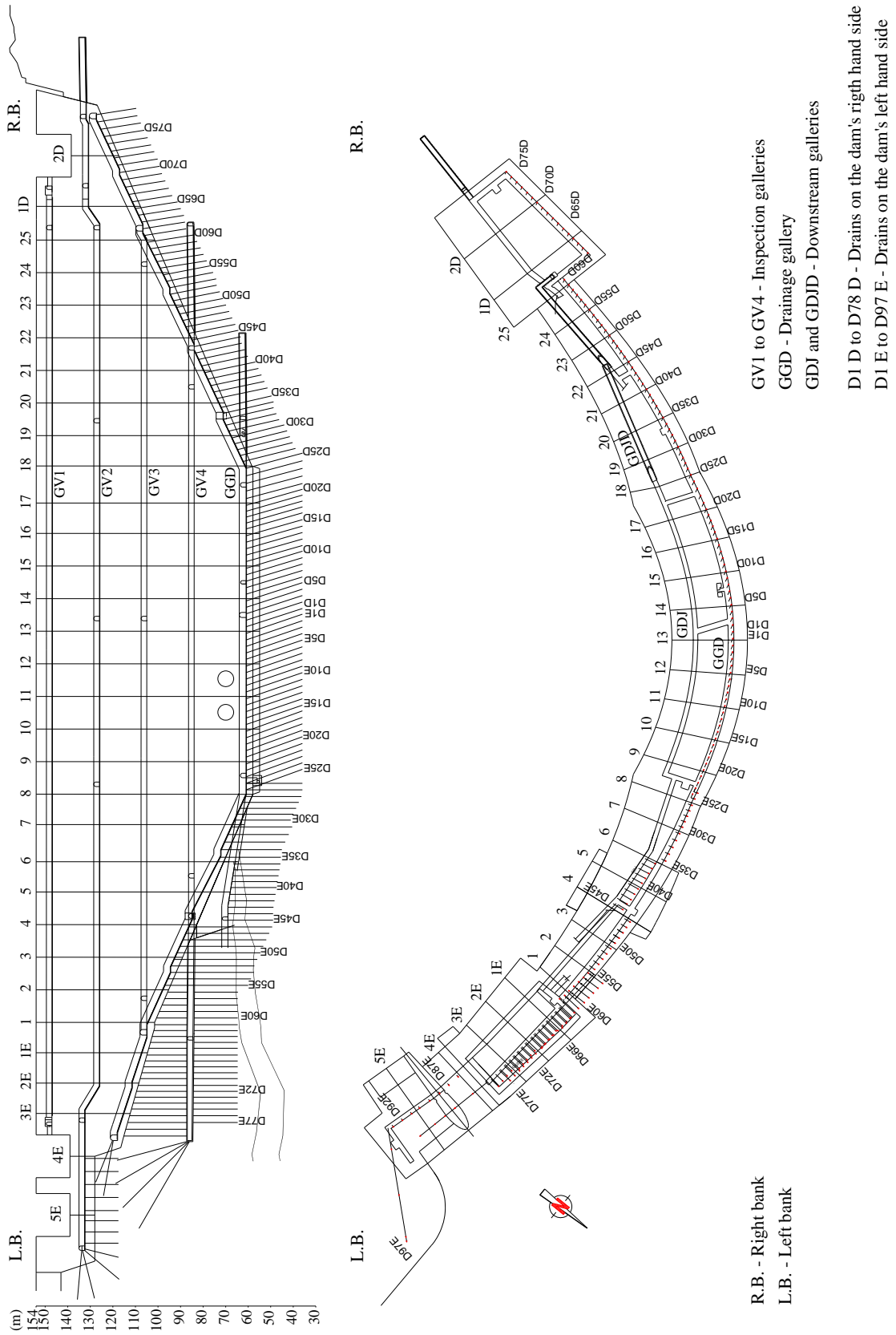


Figure 4.13 – Drainage system in Alqueva dam foundation.

4.3.1.4 Foundation behaviour monitoring

The monitoring system of Alqueva dam includes the measurement of the main loads, namely the reservoir level, both the ambient and reservoir water temperature and the seismic parameters (acceleration time history obtained from three-component strong-motion accelerographs), and of the following hydraulic and structural effects: water pressures, discharges, concrete temperature, displacements, joint movements, strains and stresses. In addition, some creep cells were installed within the dam body in order to evaluate the deformability characteristics of the concrete placed *in situ*. Two specific Monitoring Plans were developed for the follow-up of the actual behaviour during the treatment of fault 22 and during the first filling of the reservoir.

In the dam foundation, displacements are measured with 9 inverted plumb lines (Figure 4.14), 12 borehole (rod) extensometers, and 6 incremental extensometers (Figure 4.15) (LNEC 1997a). The hydraulic behaviour of the dam foundation is analysed measuring the discharges along the drainage system and the water pressures in a network of piezometers. Piezometers were drilled from the drainage gallery, one per dam block, located 15.0 m apart, approximately halfway between joints (Figure 4.16). They were installed immediately downstream from the drainage curtain, and at the same distance from adjacent drains. A further two piezometers were installed in seven of the blocks (25-1D, 21-22, 17-18, 13-14, 8-9, 4-5 e 1E-1) in order to allow measurement of water pressures along the upstream-downstream direction. Sets of piezometers were also installed at the substation slab and at the downstream dam-wall.

The dam's structural behaviour has been as expected based on studies carried out at the design stage and type C1 predictions (Lambe 1973) from recently developed specific models taking into account measurements recorded during construction. Since June 2005, with the water level in the reservoir between 144 m and 150 m, the total discharge has varied from around 100 to 150 l/min, of which 20 l/min is water collected at the drainage gallery, in drains located in the bottom of the valley. Discharges of around 30 l/min are recorded on the right bank, while on the left bank discharges are approximately 10 l/min. Seeps are observed in the drainage gallery, with around 50 l/min in the bottom of the valley and approximately 20 l/min on the right bank. At the dam-wall gallery the total discharge is around 24 l/min. Maximum water pressures are of about 6 bar and maximum percentages of hydraulic head are of about 75 %, and are recorded in piezometers which cross the grout curtain in an upstream direction.

Although there are no evident problems, it was decided to study the foundation behaviour of Alqueva dam during this phase of reservoir filling, in particular in the area of the valley bottom where the highest discharges are recorded, close to the base of the right abutment.

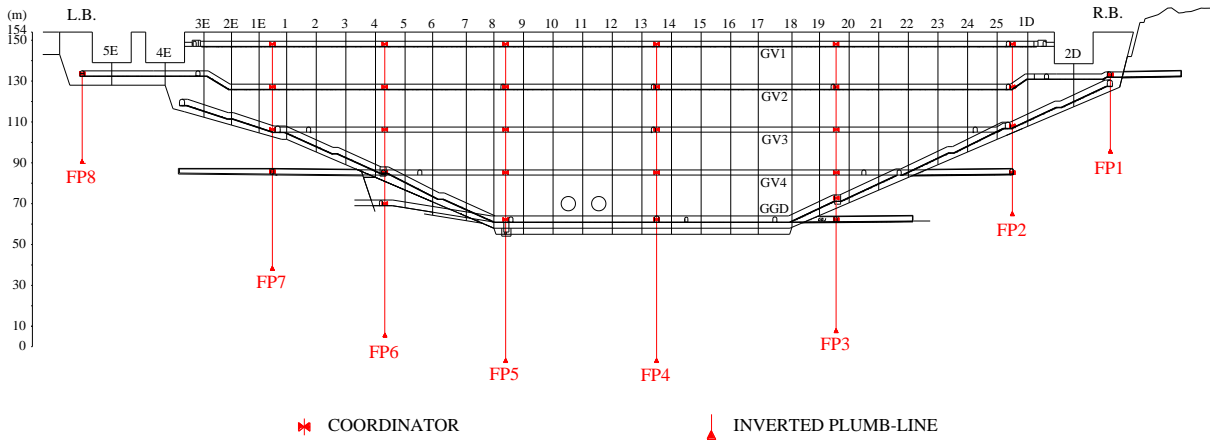


Figure 4.14 – Inverted plumb-lines in Alqueva dam.

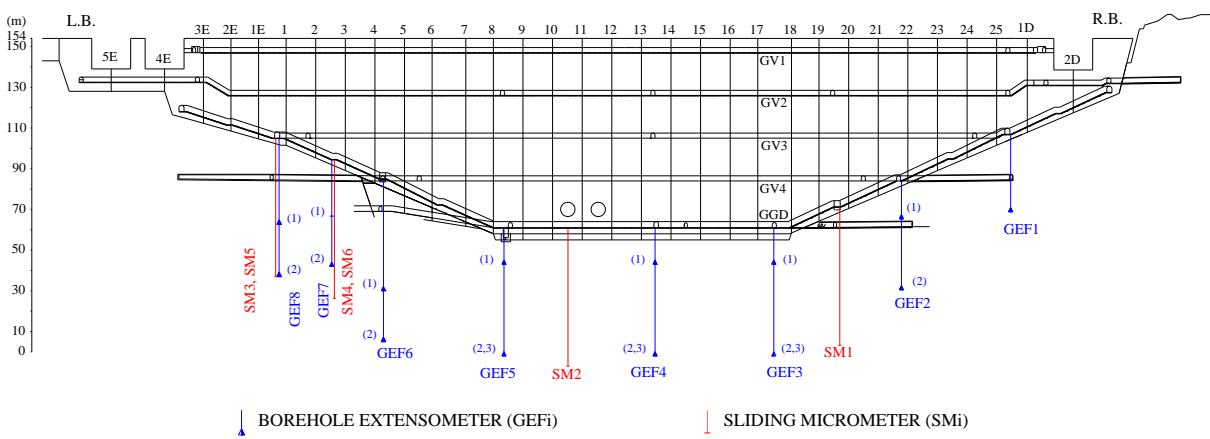


Figure 4.15 – Borehole (rod) and incremental extensometers in Alqueva dam foundation.

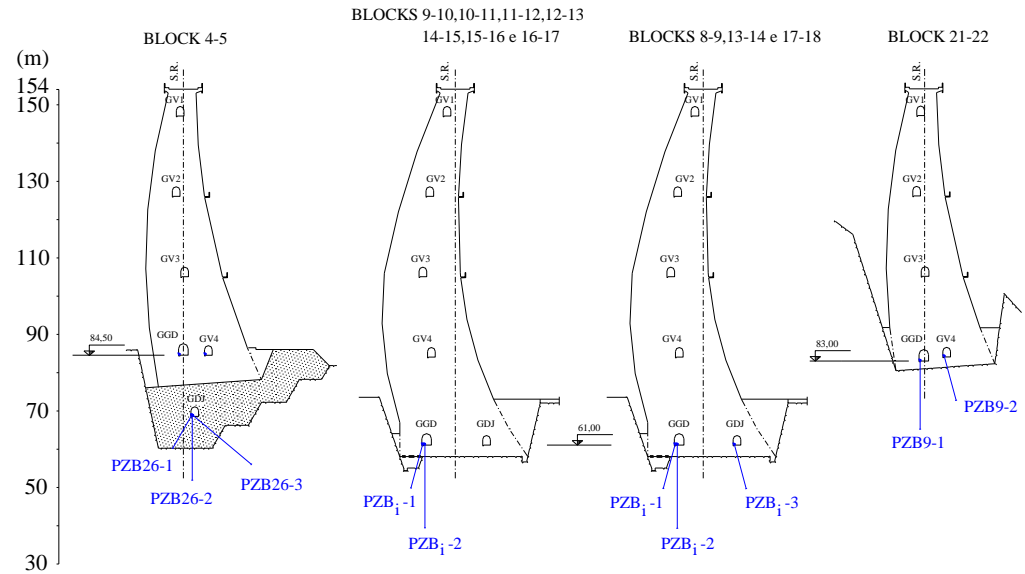


Figure 4.16 – Piezometric network in Alqueva dam foundation.

4.3.2 Pedrógão dam

4.3.2.1 General description of the dam

Pedrógão dam (Figure 4.17 and Figure 4.18) is a straight gravity dam with a maximum height of 43 m and a total length of 448 m, of which 125 m are of conventional concrete and 323 m of RCC. The dam has an uncontrolled spillway with a length of 301 m with the crest at an elevation of 84.8 m. This spillway is divided into ten 28.75 m wide spans separated by nine pillars on which a pre-fabricated pathway was installed. The dam has a drainage gallery with the floor at elevations 54.0 m and 61.0 m. The crest of the spillway is at the retention water level. The maximum water level is 91.8 m (HIDRORUMO 2001).

The construction of the dam began in April 2004, block concreting finished in October 2005 and work was concluded in February 2006, with the first filling of the reservoir already under way. In fact, the first filling of the reservoir of Pedrógão dam had begun four months earlier, on 28 October 2005. The water reached an elevation of 84.71 m, 9 cm below the spillway crest, on 4 April 2006.

4.3.2.2 Geological-geotechnical conditions

Before the construction of the dam, detailed geological and geotechnical investigation was carried out at the dam site which included a surface geological and geotechnical mapping, the opening of trenches and shafts, surface seismic and geoelectric prospecting, and the drilling of boreholes (HIDRORUMO 1999). A detailed logging of samples recovered by drilling was also carried out. *In situ* tests included water pressure permeability tests, dilatometer tests, and geophysical surveys. In laboratory the shear strength of discontinuities was determined and uniaxial compression and ultrasonic tests were carried out on rock samples (LNEC 1999d; LNEC 2004).

The foundation consists of granite with small to medium-sized grains and is of good quality with the exception of the areas located near two faults in the main river channel and on the right bank, where the geomechanical properties in depth are weak (HIDRORUMO 2001). To take into account the existence of these two areas with weaker properties the depth of the excavations in blocks 7-8 and 8-9 was 9.0 m greater than in the adjacent blocks, and blocks are narrower between dam joints 4 and 5. To decrease stresses upon the foundation the bases of blocks 7-8 and 8-9 are wider than the base of the other blocks. According to both *in situ* and laboratory test results, the foundation Young's modulus is greater than 4 GPa. Laboratory tests showed that the normal stiffness of discontinuities (k_n) varies from 4.0 to 68.0 MPa/mm in the loading cycle and from 17.9 to 143 MPa/mm in the unloading cycle. The average shear stiffness, cohesion and friction angle are $k_s = 3.7$ MPa/mm, $c = 0.066$ MPa, and $\phi = 35^\circ$, respectively (LNEC 2004).

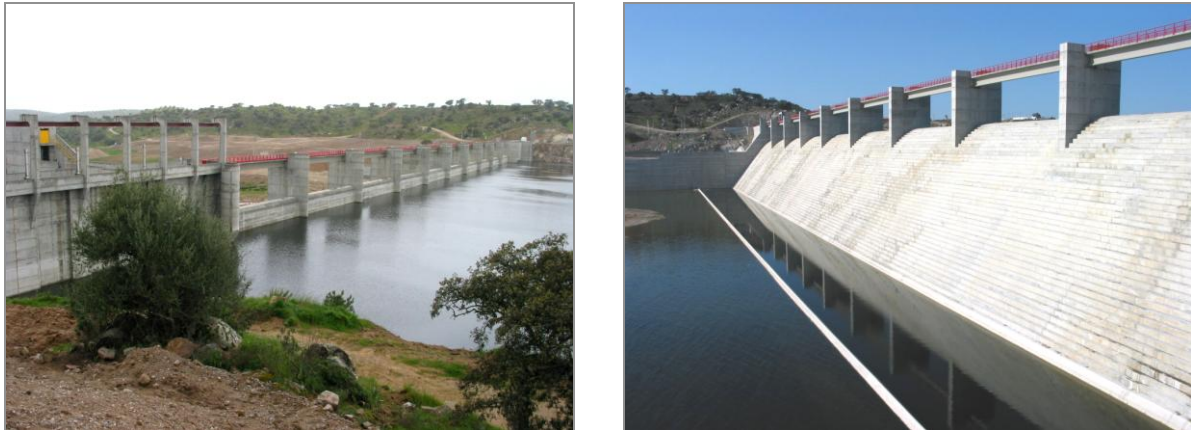


Figure 4.17 – Pedrógão dam. Upstream and downstream view from the left side of the uncontrolled spillway.

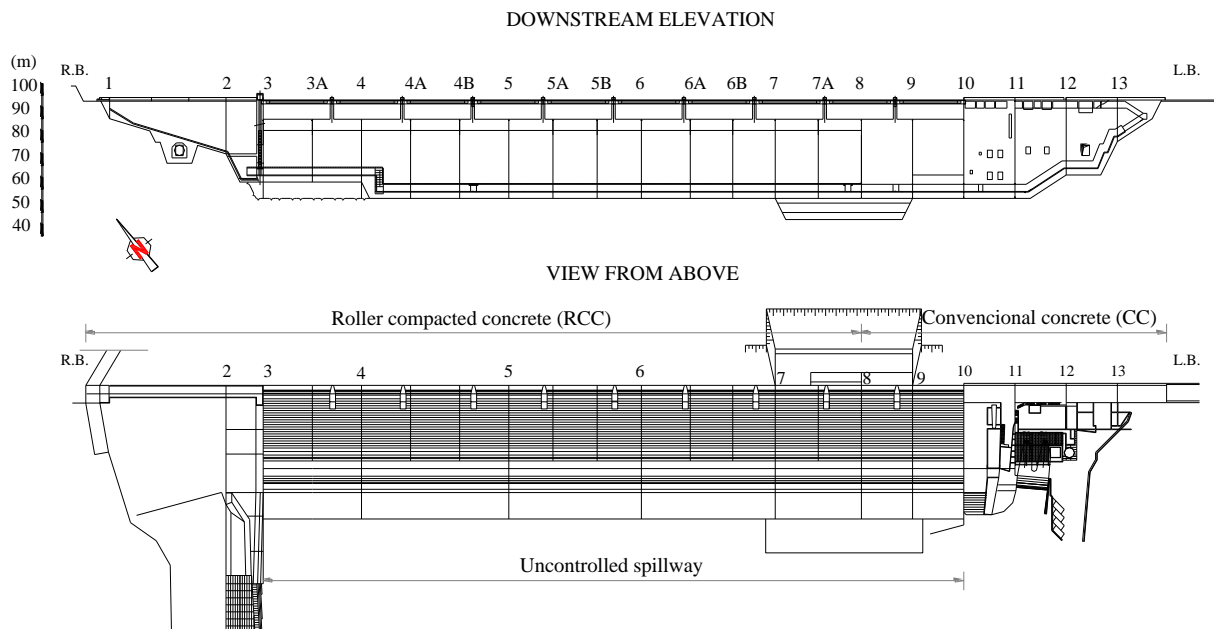


Figure 4.18 – Downstream elevation and plan of Pedrógão dam.

During excavation five sub-vertical and two sub-horizontal joint sets were identified (Neiva et al. 2004; Neves et al. 2000). More detailed analysis of data carried out afterwards made it possible to identify the main joint sets in the different foundation areas (EDP 2004). In the bottom of the valley these are: **a)** N50°E-100°E, 70°SSE-90°-70°NNW; **b)** N30°W-65°W, 70°SW-90°-70°NE; **c)** N20°E-50°E, 70°NW-90°-75°SE; **d)** N15°W-20°E, 70°W-90°-65°E; **g)** N15°E-80°E, 15°-40°SE. Joint set **a)** is predominant, with a spacing between discontinuities from lower than 6 cm to 60 cm, trace lengths of 3 m to more than 20 m, slightly rough to rough, aperture lower than 5 mm and weathered to completely weathered

(W3 to W5, according to ISRM terminology) (EDP 2004). Figure 4.19 shows the average position of the main sets of rock joints in relation to the dam. EDP (2004) drew attention to the fact that the sub-horizontal joints with dip angles lower than 10° may be relevant regarding strength and/or deformability of the dam foundation. In the bottom of the valley only a few sub-horizontal discontinuities were observed, but they were difficult to identify as the conclusions concerning joint discontinuities were drawn from studies in which mainly the 2 horizontal dimensions were observed. The main faults and fracture alignments, which are also the main seepage paths, are aligned in the upstream-downstream direction, occurring mainly in the foundation of blocks 4-5, 7-8 and 8-9, which are the areas where the geomechanical properties in depth are weaker. The different types of granite are adjoined, at the surface, along lines in the upstream-downstream direction. Water pressure permeability tests carried out before the construction of the dam led to the conclusion that the foundations of blocks 1-2 and 9-10, close to the abutments, and 6-7 and 7-8, in the main river channel, were the areas of highest permeability, higher than 2×10^{-7} m/s (Figure 4.20).

4.3.2.3 Foundation treatment

Foundation treatment consisted only of a grout curtain along the alignment of the dam. Prior to this, a group of retaining boreholes was drilled upstream from the grout curtain, to avoid leakage of grout to the area further away from the dam whilst grouting the main curtain. There were several difficulties during grouting due to the fact that cement absorption per metre was very low. Lugeon type tests indicated that the initial high permeabilities recorded at the beginning of the grouting programme had not decreased even after grouting the quaternary holes, and therefore the curtain's desired degree of permeability had not been reached (Tecnasol FGE 2007). The boreholes were drilled from the drainage gallery and their direction was defined taking into account the direction of the main discontinuities. The maximum depth of the grout curtain below concrete/rock mass interface is 49.0 m. No consolidation grouting was performed. A drainage curtain was drilled from the downstream area of the gallery. The drains are located 2.5 m apart and the average length of the holes in the rock mass is about 21 m, varying from 13 up to 31 m. The majority of the boreholes were drilled with a dip direction of 140° and dipping 60° towards downstream.

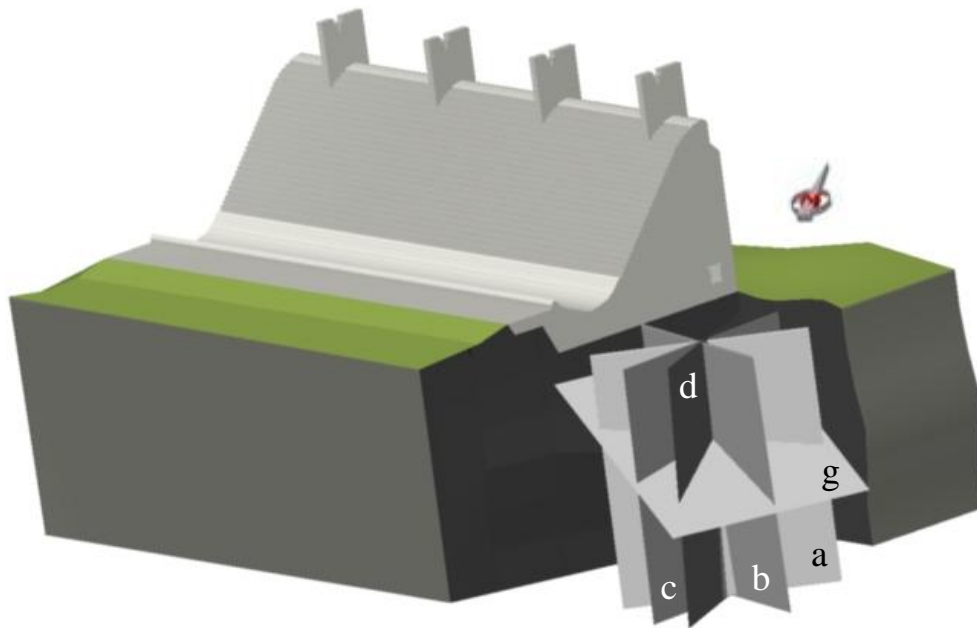


Figure 4.19 – Average position of the main sets of rock joints in relation to the dam.

4.3.2.4 Monitoring of foundation behaviour

The monitoring system of Pedrógão dam includes the measurement of the main loads, namely the reservoir level, both the ambient and reservoir water temperature and the seismic loads, and of the following hydraulic and structural effects: water pressures, discharges, concrete temperature, displacements, joint movements, strains and stresses. A specific Monitoring Plan was developed for the follow-up of the actual behaviour during the first filling of the reservoir.

In the dam foundation, displacements are measured with two inverted plumb lines and with 6 vertical borehole (rod) extensometers and the hydraulic behaviour of the dam foundation is analysed measuring the discharges along the drainage system and the water pressures in a network of piezometers.

The plumb lines were installed in blocks 8-9 and 4B-5. The rod extensometers were installed in the foundations of blocks 2-3, 4-5, 5-6, 7-8, 8-9 and 11-12, and each one has two rods, one fixed at a depth of 10 m below the concrete/rock mass interface, to evaluate rock mass deformations at shallow depths, and the other at a depth greater than 30 m, to evaluate rock mass deformations assuming that the lower point does not move.

In 13 of the dam blocks a piezometer was installed immediately downstream from the drainage curtain dipping 50°, 60° or 70° towards downstream. A second piezometer, vertical and with two piezometric chambers, was installed in four of the blocks (4-5, 5-6, 6-7, and

7-8), in the downstream area, underneath the stilling basin. These are vibrating-wire piezometers which allow readings to be taken in the drainage gallery, as they are located in a non-accessible area. The location and length of each chamber were defined taking into account the boreholes' logs and the results of Lugeon type tests. Figure 4.21 shows two different cross sections of the dam.

Due to the possible collapse of borehole walls, coarse sand or geodrains were placed inside several drains between dam joints 2 and 9, the majority of them at the base of blocks 6-7 and 7-8.

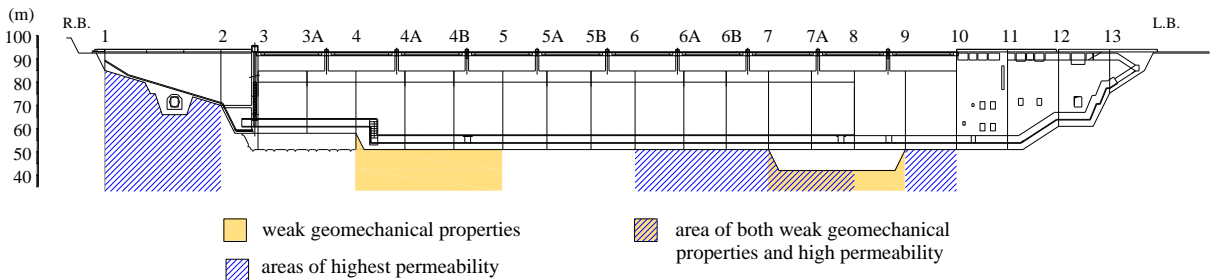


Figure 4.20 – Areas of weak geomechanical properties and of highest permeability in the foundation of Pedrógão dam.

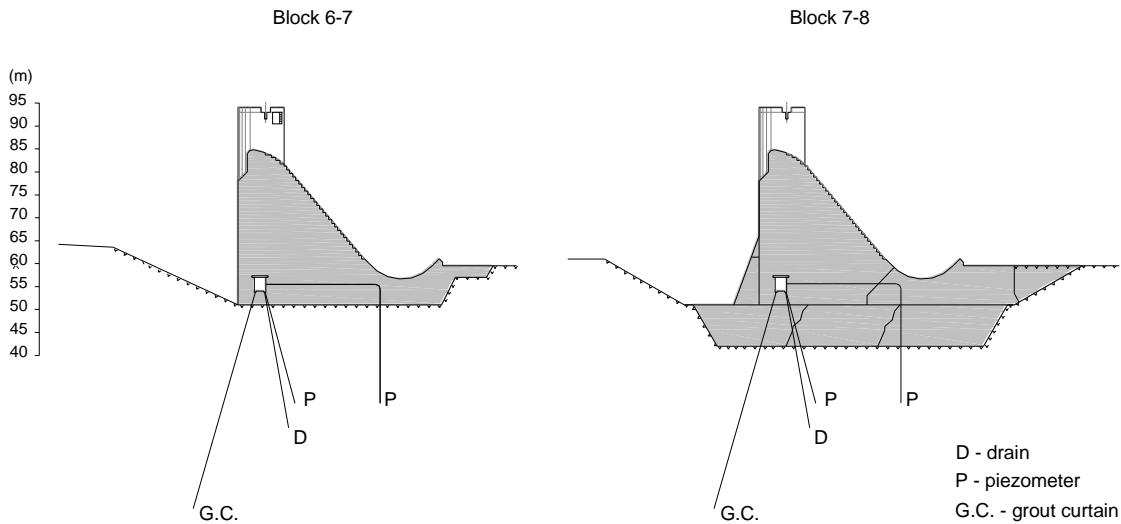


Figure 4.21 – Cross sections of Pedrógão dam.

4.3.2.5 Foundation hydraulic behaviour

When the first filling of the reservoir began, with the water upstream from the dam at an elevation of 61.0 m, 7.0 m above the floor of the drainage gallery in its lower area, the total discharge was already 200 l/min. Since then Pedrógão dam has shown a peculiar seepage pattern, with some local high flow rates. Figure 4.22 shows the variations in the reservoir level since the beginning of its first filling until the end of April 2006, a week before borehole water-inflow tests were carried out. The same figure shows the total and partial recorded discharges plotted versus time. Three areas of the foundation are considered: the left bank includes blocks 9-10, 10-11, 11-12 and 12-13; the right bank includes blocks 2-3, 3-4 and 4-5; and the bottom of the valley includes the remaining blocks.

In the first two months the total discharge reached values of about 650 l/min. The highest discharges were recorded in blocks 6B-7 and 7-7A. Due to the high discharges recorded, some drains were filled with coarse sand. To further reduce the discharges special devices which allow the regulation of uplift/discharge were installed in some of the drains. With these devices, named “piezodrains”, the total discharge can be reduced, at the same time reducing seepage velocity through the foundation and controlling the maximum values of the uplift. Thirty six of the 268 drains were changed into piezodrains. There are piezodrains at the base of all the blocks between dam joints 2 and 9, but they are most concentrated at the base of block 6-7 in which 15 out of 23 drains were working as piezometers or as piezodrains when tests were carried out. These devices were adjusted in the middle of January 2006 in such a way that the maximum values of the water pressures were lower than 50 % of the reservoir head, with the reservoir at 80.4 m. One month later they were adjusted once again and the total discharge was reduced to values not greater than 300 l/min. Since mid-February the reservoir level has ranged between 78.97 m and 84.71 m.

Figure 4.23 shows the average values of the water pressures and of the percentage of hydraulic head along the base of the dam on 4 April 2006, with the reservoir at an elevation of 84.71m. This figure shows that the highest discharges and percentages of hydraulic head were recorded at the base of blocks 6-6B and 6B-7. Figure 4.24 shows the variation in water pressures along the upstream-downstream direction, in the foundation of different dam blocks, recorded on 4 April 2006.

A dam feature which may contribute to the high flow rates recorded is that the floor of the lower area of the drainage gallery is about 8.0 m below the water level downstream from the dam.

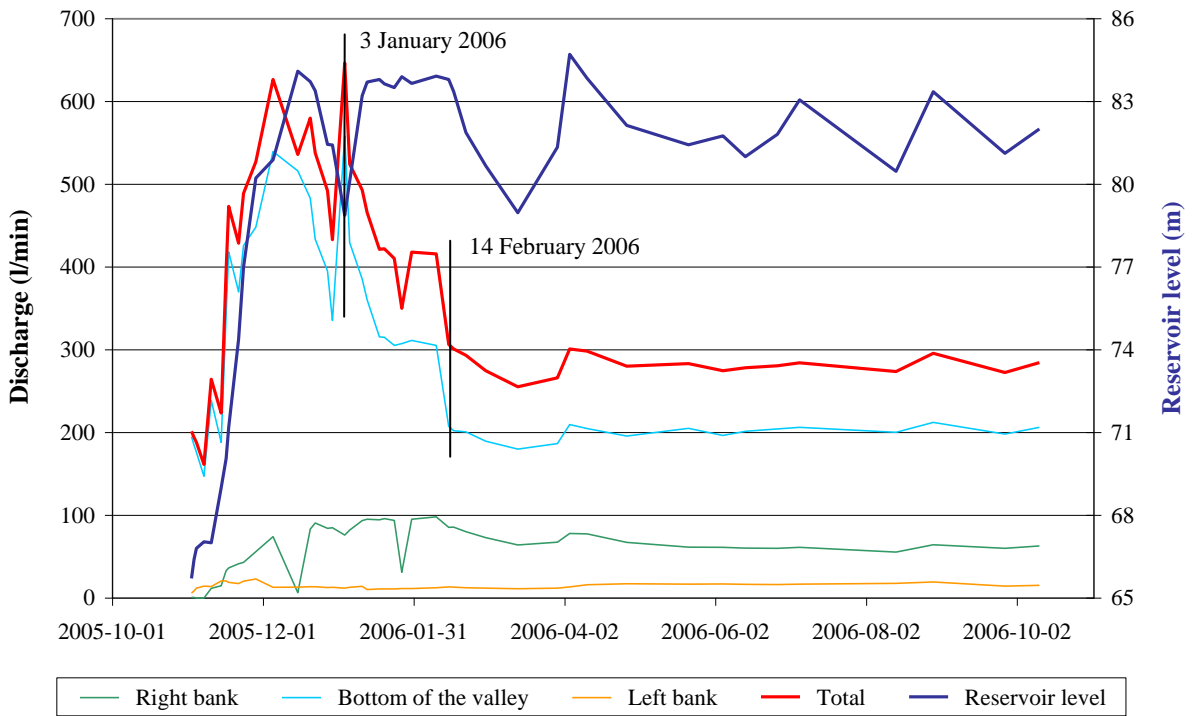


Figure 4.22 – Partial and total flow rates through the foundation.

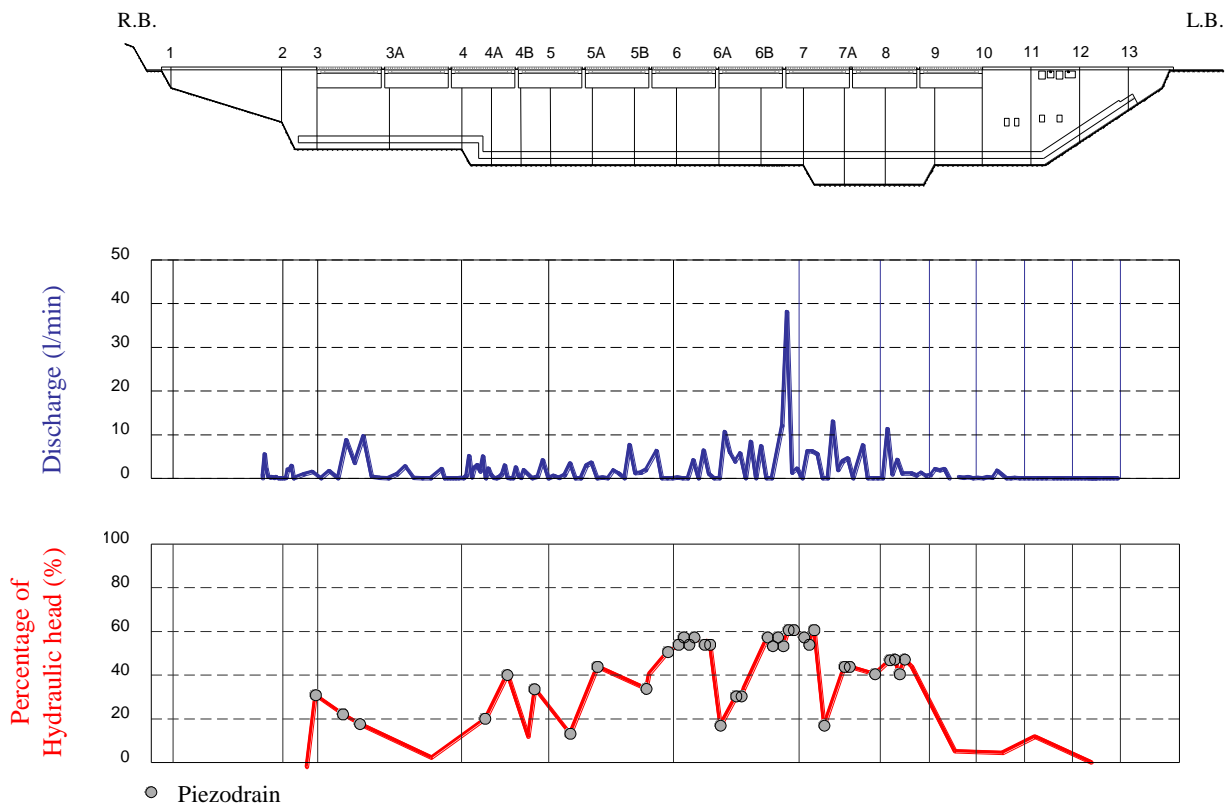


Figure 4.23 – Discharges and average value of the percentage of hydraulic head in the foundation (04.04.2006, $H_{\text{reservoir}} = 84.71\text{m}$).

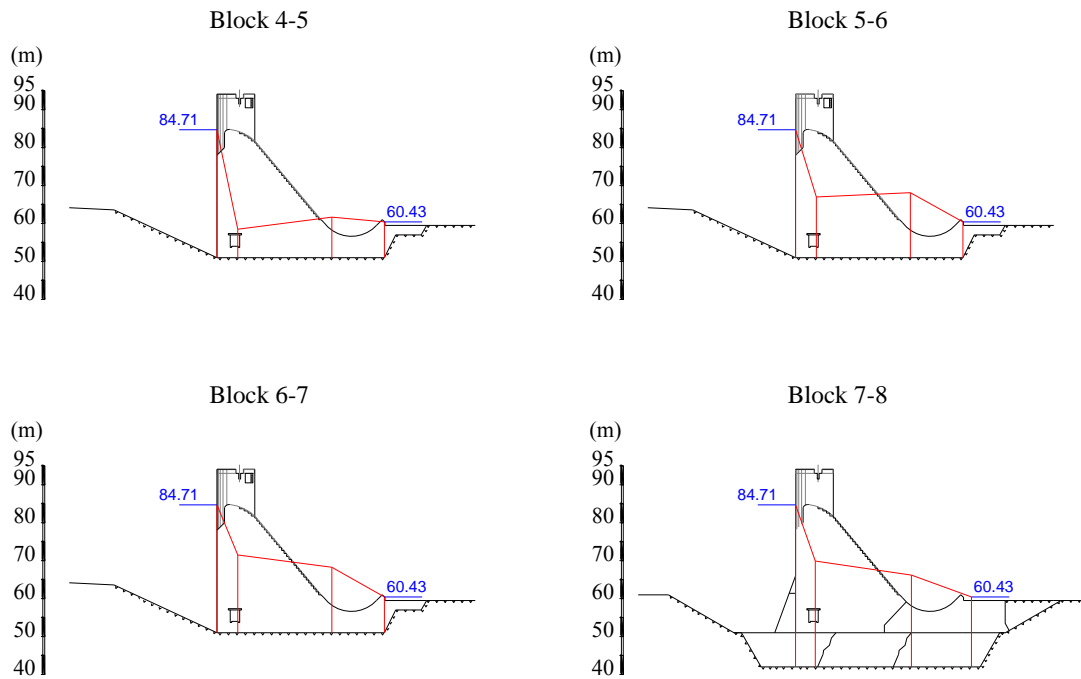


Figure 4.24 – Water pressures along the upstream-downstream direction recorded on 04.04.2006.

4.4 Tests carried out in Pedrógão dam foundation

This section presents the tests carried out in two drainage boreholes in Pedrógão dam foundation in the week from 9-13 May 2006, with the reservoir at around 80.4 m. Tests were first carried out not only with the aim of testing the equipment, which had never been used, and evaluating the previously defined test procedures, but also because the high flow rates recorded in the foundation of this dam were more suitable for testing the equipment and the testing method and for comparing the test results against the results of a numerical model. Moreover, the team responsible for the safety assessment of the dam were also interested in knowing where water was coming from in some foundation areas.

4.4.1 Preparation of tests

4.4.1.1 Area where tests were carried out

It was decided that tests should be carried out in the foundation of block 6-7, where the highest discharges were recorded. In this block, there were only three boreholes which could be tested: D12, D14 and D18. The remaining boreholes were either filled with coarse sand or with geodrains, which prevented the insertion of the equipment. Boreholes D12 and D18 were working as piezometers, and D14 as a drain. According to the design, boreholes were 26.0 m long (HIDRORUMO 2001). Figure 4.25 shows the location of both the drainage and

piezometric boreholes in the foundation of block 6-7 and of block 7-8, close to dam vertical joint 7.

4.4.1.2 Analysis of geological and geotechnical information

The surface foundation map in the area of block 6-7 shows that the foundation was weathered at the surface with close to medium spaced rock joints (W3 and F3-F4, according to ISRM classification). When the surface foundation map was drawn, there were leakages at the base of this block, close to dam joint 6. More detailed information was obtained when the grout curtain boreholes were drilled. Logs show that the foundation is moderately to highly weathered, that the boreholes are crossed by close discontinuities (W3-W4 and F4-F5, according to ISRM classification) and that in several boreholes permeabilities higher than 10 LU were obtained along the majority of the boreholes length, at between 7 to 42 m down from their head. In this block, rotary-percussive drilling was used to open drainage boreholes, which prevented the obtaining of samples.

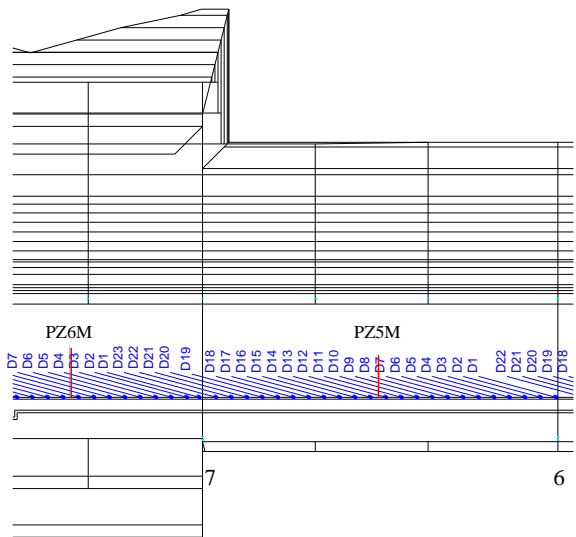
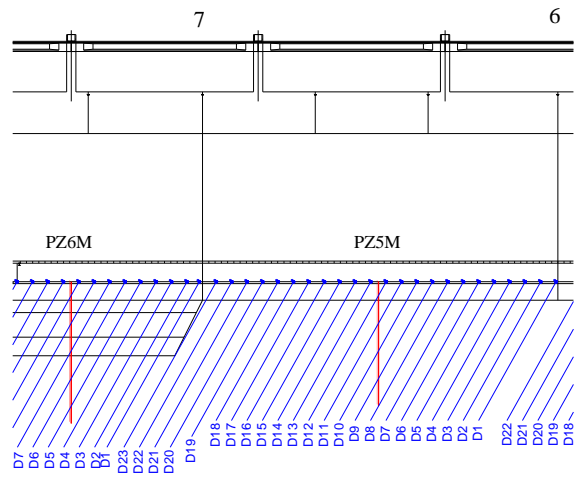
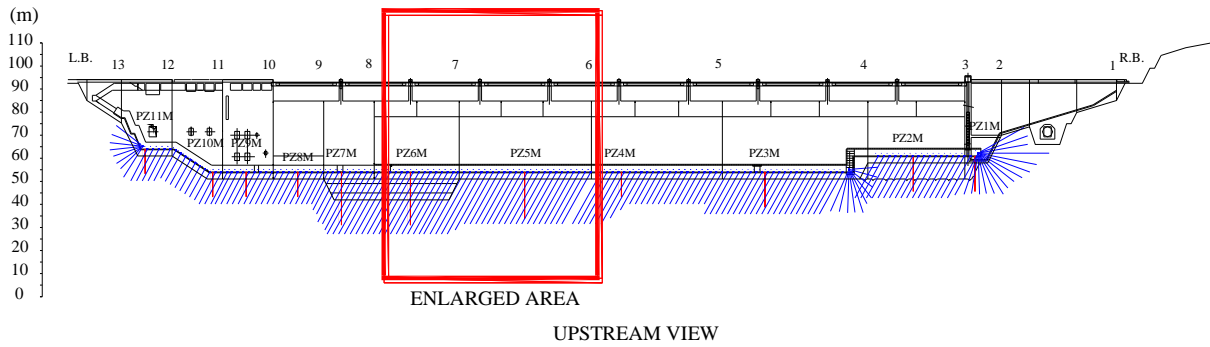
A cross section of the different geomechanical and hydraulic zones established in the foundation of block 6-7 (HIDRORUMO 2001) shows that the area tested was that with weaker geomechanical characteristics and higher permeability.

4.4.1.3 Variation of discharges and water pressures

Variations in discharges and water pressures recorded in drains and piezometers located in the foundation of block 6-7 are shown in Figure 4.26 and Figure 4.27. The first figure shows that in four of the drains (D2, D3, D5 and D6) discharges reached values higher than 60 l/min, before drains were changed into piezodrains. Variations in water pressures followed patterns of variations in reservoir level in the majority of piezometers, with a maximum of 1.8 bar. Higher water pressures were only recorded in piezometer PZ5J-1, located downstream, in the stilling basin, with the 2 m long piezometric chamber located between elevations 38.4 m and 40.0 m.

The available data showed that pressures gauges calibrated from 0 to 2.5 bar and from 0 to 4 bar with reading intervals of 0.1 bar, and measuring cylinders of sizes between 0.125 and 20 l should be used.

When borehole water-inflow tests were carried out, the maximum recorded discharge was around 10 l/min.



KEY:
 — drainage borehole
 — piezometric borehole

Figure 4.25 – Location of drains and piezometric boreholes in the foundation of block 6-7 and of block 7-8, close to dam vertical joint 7.

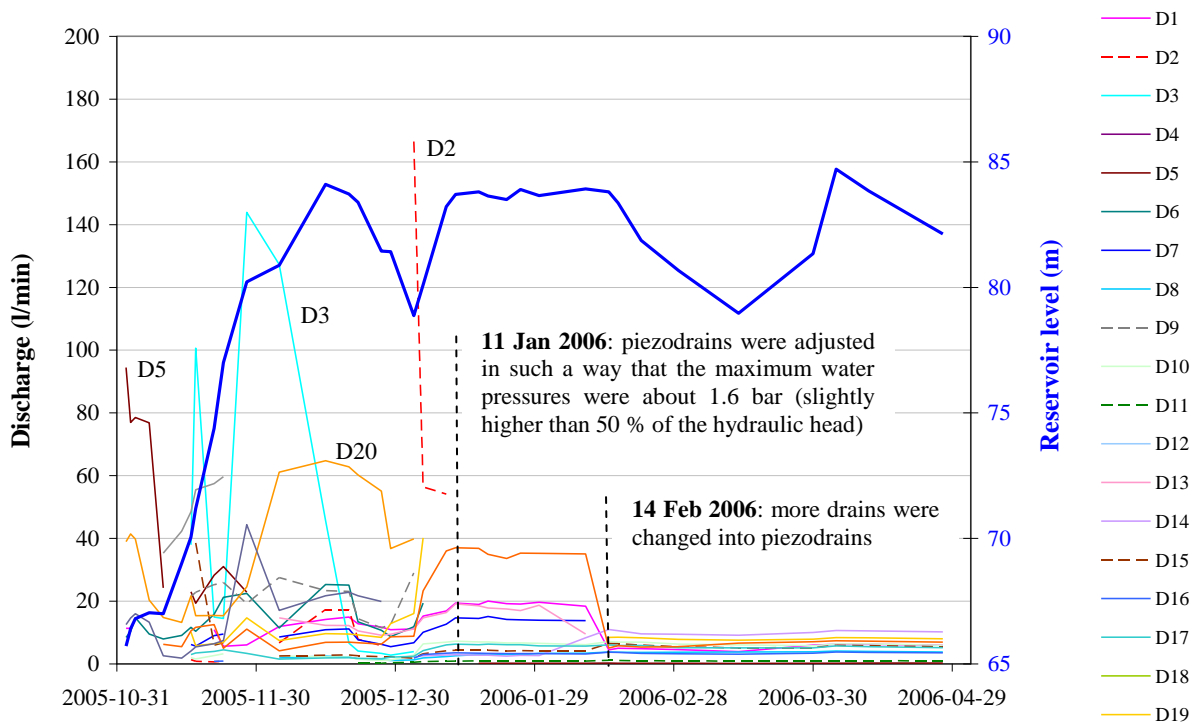


Figure 4.26 – Recorded discharges in the foundation of block 6-7.

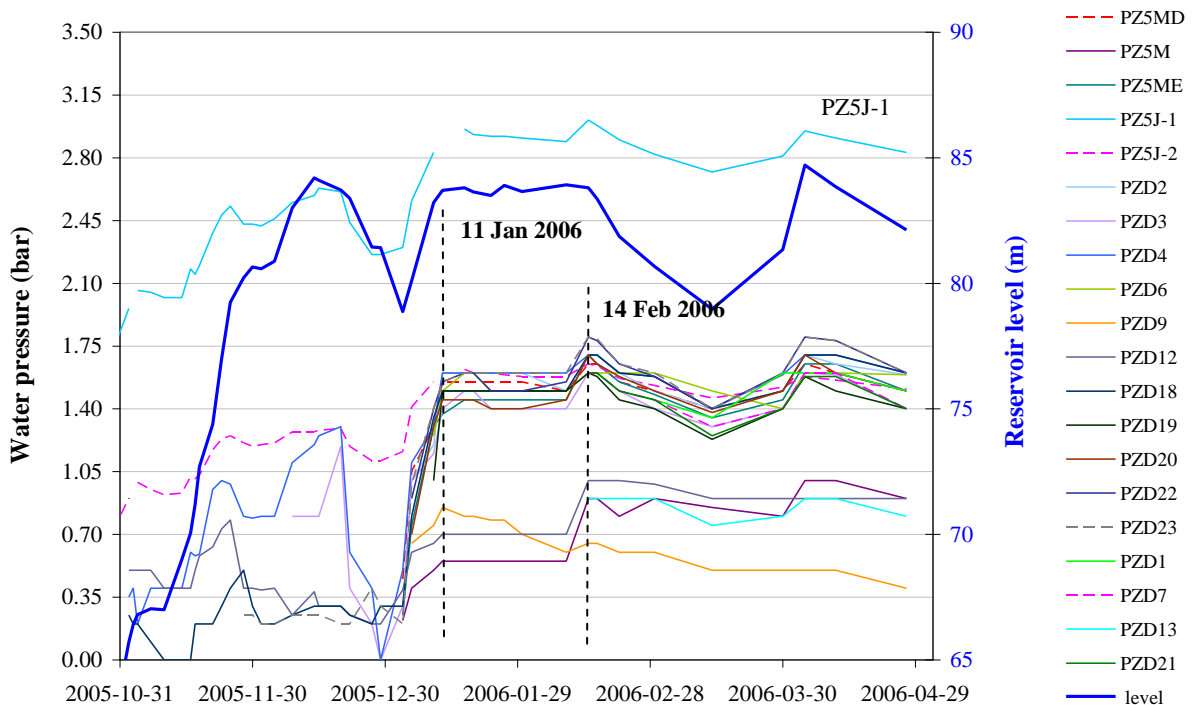


Figure 4.27 – Recorded water pressures in piezometers and piezodrains located in the foundation of block 6-7.

4.4.1.4 Stability analysis

A two-dimensional stability analysis was carried out using the limit equilibrium method and taking into account the weight of the dam, the reservoir and tailwater loads, the uplift water pressures, and seismic loads. To assess safety against dam base sliding, usual and extreme loading combinations were used, prescribed in the Portuguese guidelines for dam design (RSB 2007). This study is presented in chapter 7. Although high flow rates and uplift pressures are recorded, the stability analysis carried out led to the conclusion that the base sliding stability of block 6-7 is ensured for usual load conditions. For extreme load conditions stability is not ensured if drains are inoperable.

4.4.2 Summary of experimental activity

Borehole water-inflow tests were carried out in drain D14 and in piezodrain D18, which was working as a piezometer. Due to time constraints tests were not carried out in drain D12 as had been planned. Just before tests were carried out, discharge in drain D14 was 11.5 l/min and water pressure in piezodrain D18 was 1.45 bar, which was about 50 % of the reservoir head. When this piezodrain was dismantled, in order to carry out tests, discharge was about 60 l/min. Both boreholes were tested in consecutive sections throughout their lengths. Tests should have been carried out with the equipment assembled first as a single and then as a double packer. However, the supplier did not provide, before these first tests were carried out, the part which allows equipment to be assembled as a single packer. Therefore, a PVC stopper had to be made. This stopper could not take the water pressure, which meant that only a single test could be carried out with the single packer.

4.4.3 Tests in drain D14

Before testing began, readings were taken in order to know the reservoir level (80.44 m) and discharges and water pressures in all the drains, piezodrains and piezometers in the foundation of block 6-7. These discharges and water pressures were the “reference values”. The “blind device” was inserted into D14, which made it possible to remove obstructions at 3.75 m, 5.20 m and 9.02 m down from the gallery floor and to measure the borehole length, which was not 26.0 m, as prescribed in the design, but 12.5 m, probably due to wall collapse after drilling. The equipment was assembled first as a single packer and, taking into account the borehole’s length, it was decided that four test intervals would be tested, between the bottom of the borehole and 11.0, 8.0, 5.0 and 2.0 m down from the drain head. In this way, there would be intervals 1.5, 4.5, 7.5 and 10.5 m long. Only the lowest test interval could be tested with the single packer. The rest of the borehole was tested with the double packer.

Results are presented with the test divided into 10 steps, shown in Figure 4.28:

- Step 1:** reference values (recorded before carrying out tests);
- Step 2:** test at the lowest test interval (11.0 m – 12.5 m);
- Step 3:** 8.0 m – 11.0 m test interval;
- Step 4:** confirm that reference values had been reached;
- Step 5:** 5.0 m – 8.0 m test interval;
- Step 6:** 5.0 m – 8.0 m test interval, with the test interval closed;
- Step 7:** confirm that reference values had been reached;
- Step 8:** 2.0 m – 5.0 m test interval, with the test interval working as a drain;
- Step 9:** 2.0 m – 5.0 m test interval, with the test interval closed;
- Step 10:** confirm that reference values had been reached.

Table 4.2 shows all the measurements taken while carrying out tests. Depths are measured along the borehole. Discharges are shown in blue for ease of analysis.

Step 1 concerns reference values. In **step 2**, in which the lowest borehole area was tested, discharges in and above the test interval were measured over time for 25 minutes and it was concluded that discharge stabilization was immediate. In this step, the quantity of water flowing into the test interval was 8.68 l/min, which was around 75 % of the total discharge. The total discharge in the drain being tested was, at this test step, slightly lower than the reference discharge (11.16 l/min < 11.5 l/min), probably due to the fact that the packer was obstructing a seepage path or to a change in water pressure distribution. At this step, there were only changes in drain D11, in which discharge decreased from 0.82 to 0.79 l/min and in piezometer D13, in which water pressure increased by 0.05 bar. Shortly after taking measurements, the PVC stopper which allowed the equipment to be assembled as a single packer failed and the equipment fell into the bottom of the borehole. Therefore, it was impossible both to close the pipes and to test the remaining test intervals with the single packer.

In **step 3**, with the test interval from 8.0 m to 11.0 m down from the drain head, there was no water flowing out of the pipes, and the water level inside the pipes remained 27 cm above the gallery floor. The water pressure at the test interval was that of the water column weight. Taking the test interval's mid-height as reference, the water pressure was:

$$p = \frac{1}{9.8} \times \left(\frac{8.0 + 11.0}{2} + 0.27 \right) \times \cos 60^\circ = 0.49 \text{ bar} \quad (3.1)$$

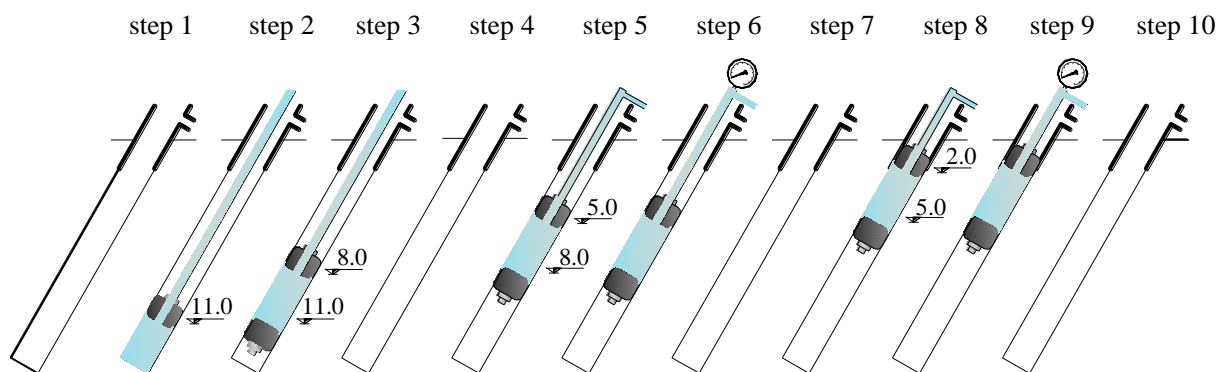


Figure 4.28 – Test steps in borehole D14.

Test step	Time when readings began	D 11	D 12	D 13	PZ5 M	D 14			D 15	D 16	Total discharge	
		(drain)	(piezometer)	(piezometer)		(drain)			(drain)	(drain)		
		discharge (l/min)		water pressure (bar)		total discharge	test interval	above test interval	Water pressure at pipes head (bar)	discharge (l/min)		
1. Reference values.	10h 15 min	0.82	0.80	0.65	0.80	11.5	-	-	-	4.50	3.32	20.14
2. Lowest test interval: 11.0 m – 12.5 m. Single packer.	14h 50min	0.79	0.80	0.70	0.80	11.16	8.68	2.48	-	4.50	3.32	19.77
3. Test interval 8.0 m – 11.0 m.	16h 25min	0.98	1.00	1.20	1.10	3.03	-	3.03	-	5.69	3.48	13.18
	16h 40min	0.98	1.10	1.25	1.175	2.71	-	2.71	-	No measurements were taken		12.86 ⁽¹⁾
4. Check if reference values were re-established.	17h 50min	0.78	0.80	0.625	0.775	12.1	-	-	-	4.73	3.40	21.01
5. Test interval 5.0 m – 8.0 m.	18h 05min	0.78	0.80	0.65	0.775	10.05	9.41	0.65	-	6.29	3.46	20.58
6. Test interval 5.0 m – 8.0 m. Pipes closed.	19h	0.9	1.00	1.00	1.00	1.29	-	1.29	0.65	10.1	3.69	15.98
7. Check if normal reference values were re-established.	19h 20min	0.79	0.80	0.625	0.775	12.1	-	-	-	4.55	3.34	20.78
8. Test interval 2.0 m – 5.0 m.	19h 30min	0.88	0.95	0.90	0.95	2.31	1.93	0.38	-	10.1	3.71	17.00
9. Test interval 2.0 m – 5.0 m. Pipes closed.	19h 55min	0.9	0.975	0.90	1.00	1.44	-	1.44	0.30	10.3	3.69	16.33
10. Check if reference values were re-established.	20h 15min	0.8	0.80	0.625	0.775	12.0	-	-	-	4.61	3.38	20.79

⁽¹⁾ assuming that discharge in drains D15 and D16 did not vary after 16h 25min.

Table 4.2 – Discharges and water pressures in the equipment placed in drain D14's area of influence during the borehole water-inflow test.

The quantity of water flowing in above the test interval was initially of 3.0 l/min but stabilized after around 5 minutes at 2.7 l/min. The change in neighbouring boreholes was almost instantaneous, and it was observed that the area of influence along the drainage line was 12.5 m long, from borehole D11 to D16. In this third step, D14's drainage capacity decreased significantly. The water flowing into the lowest area of the tested borehole or along discontinuities that crossed the areas where packers' rubbers met the borehole's wall was prevented from flowing out, therefore that water found other seepage paths through the rock

mass, increasing discharges and water pressures in all the equipment installed in its area of influence, particularly in borehole D13, in which the water pressure almost doubled. An increase in the quantity of water flowing in above the test interval was also observed at values greater than in the second step.

In **step 4** the packer was deflated and new measurements were taken. Discharge in the drain being tested increased by about 0.6 l/min, which can be explained by the clearing of seepage paths due to the closure of the lowest test interval. With the exception of the water pressure recorded in borehole D12, all the equipment showed a slight difference in relation to reference values: in boreholes D11, D12, D13 and PZ5 M, on the right hand side of the borehole when looking from upstream, discharges and water pressures were slightly lower, and on the left hand side discharges in drains D15 and D16 were a little higher.

In **step 5** the quantity of water flowing into the test interval was 9.40 l/min and above the packers was 0.65 l/min. The only significant change was in D15's discharge, which increased by around 33 %, from 4.73 to 6.29 l/min, due to the closure of borehole D14's lowest area, into which a large quantity of water flowed. In the previous step, prior to the isolation of the 5.0 - 8.0 m test interval, the total discharge was 12.1 l/min. In step 2 about 8.7 l/min flowed into the borehole in the 11.0 – 12.5 m interval. A discharge of 9.40 l/min in the 5.0 – 8.0 m test interval is higher than the total discharge minus the quantity of water flowing into the lowest part of the borehole, therefore seepage paths changed. In a rock mass there are always intersections between discontinuities and therefore one way of explaining this step test's results is that when the borehole branch from 11.0 -12.5 m is working as a drain the easiest flow path is through that branch, i.e. that is the path with the lowest loss of hydraulic head. However, the favoured seepage paths when this branch is closed are those which lead to the area located 5.0 - 8.0 m down from the drain head.

In **step 6** the 5.0 – 8.0 m test interval was closed and the water pressure at the pipes' head stabilized at 0.65 bar after 10 minutes. In the mid-way in the branch being tested the water pressure was 1.045 bar. Discharge flowing in above the packer practically doubled (from 0.65 to 1.29 l/min) and discharges and water pressures increased in all the equipment located in the borehole's area of influence. The most significant increase was in the adjacent drain, D15, in which discharge which had already increased from 4.73 to 6.29 l/min when the test interval was isolated increased to 10.1 l/min when the pipes were closed. The water pressure of 1.0 bar recorded in borehole D13 would be incoherent if discharge in drain D15 had not increased so significantly. If discharges in neighbouring boreholes had not increased, the water pressure at D13 would be equal or greater than that recorded in step 3 (1.25 bar).

After deflating the packers, in **step 7**, measurements were almost the same as those recorded in step 4. In the following step (**step 8**), with the 2.0 – 5.0 m interval, only 1.93 l/min flowed

into the test interval and discharges and water pressures in all the neighbouring boreholes increased. Once again, the most significant discharge increase was in drain D15, from 4.55 to 10.1 l/min. When the pipes were closed, in **step 9**, the water pressure reached steady state conditions in only 45 seconds and was around 0.545 bar at mid-way in the test interval. Only a slight increase in discharges and water pressures was recorded in boreholes located in the vicinity, and the quantity of water flowing in above the packer increased almost four times. In the last test step recorded values were close to those recorded in steps 4 and 7. It would have been interesting to withdraw the borehole from the drainage system, by closing it, and to measure the water pressure at its head so as to assess its influence in the surrounding area. This influence, however, is almost shown in step 9.

Figure 4.29 shows some photos taken whilst carrying out tests.

Figure 4.30 and Figure 4.31 show recorded discharges and water pressures in the equipment in drain's D14's area of influence during the tests. It can be seen that the total discharge decreases significantly in step 3, when the lowest part of the borehole is closed. In step 5, the isolation of the 5.0 – 8.0 m test interval has almost no influence on the total discharge because water flows into this area. In steps 6, 8 and 9, the decrease is lower than in step 3, due to the increase in the quantity of water flowing into drain D15. Discharges in drains D11 and D16 barely change during tests. Whenever the total discharge in D14's area of influence decreases, the water pressures in piezometers located in this area increase proportionally.

Figure 4.32 shows the flow of water entering each water-inflow test interval and the accumulated discharge from the bottom to the borehole head. The drain's recorded discharge in normal operating conditions is shown in both graphs: in the first it allows the assessment of discharges in each test interval in relation to the drain's total discharge; in the second it allows the comparison between accumulated and total discharge. It is clear that the quantity of water that flows into the lowest borehole area also flows into the 5.0 – 8.0 m test interval and thus in Figure 4.32 b) discharge flowing into the lower section of the borehole is included twice. In the same figure it is shown that if this fact is taken into account, by subtracting the quantity of water that flows into the drain's lower section, the accumulated discharge at the drain's head is almost the same as the reference discharge. When comparing discharges it has to be taken into account that the pipes' head varies in the different test steps. In order to accurately compare discharges, pipes' head should be at the same level in every test step. In practice, this would mean that pipes would have to be cut, which is not feasible.

Figure 4.33 a) shows the volume of water entering the borehole section above the packer. The same figure shows the discharge above the test interval when it is closed. Figure 4.33 b) shows the variation of water pressure along the borehole. The highest water pressure is recorded at the 5.0 – 8.0 m test interval and is 1.05 bar.

From tests in drain D14 it is concluded that: i) 75 % of drain discharge flows into the drain in its lowest 1.5 m; ii) the area of influence along the drainage line is around 12.5 m; iii) there are links through rock mass discontinuities, between the test interval from 5.0 m to 8.0 m and the area below; iv) the highest water pressure, of around 1.05 bar, is measured in the 5.0 - 8.0 m test interval. It can also be concluded that this drain is relevant regarding water pressure relief in the foundation of block 6-7 as the exclusion of any borehole branch leads to an increase in water pressures and discharges in boreholes located in its area of influence.



a) equipment assembled as a single packer



b) inserting the packer in the borehole



c) flow of water into the test interval



d) water pressure at the test interval

Figure 4.29 – Borehole water inflow tests.

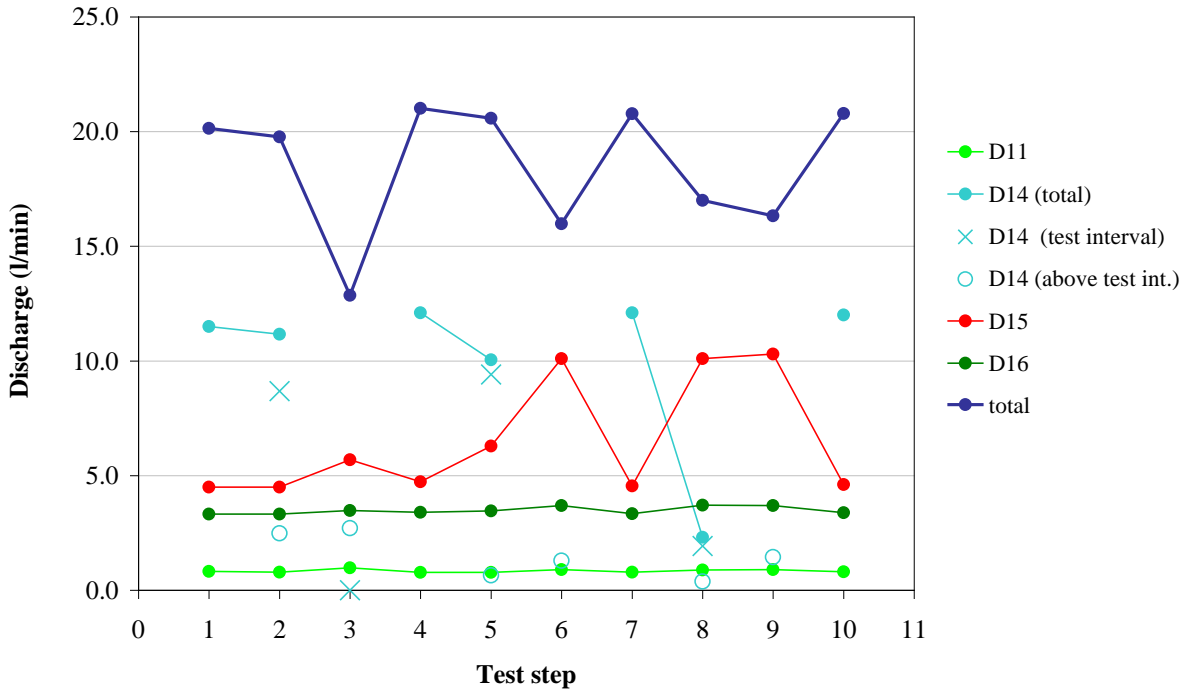


Figure 4.30 – Discharges in the equipment placed in drain D14’s area of influence during the water-inflow tests.

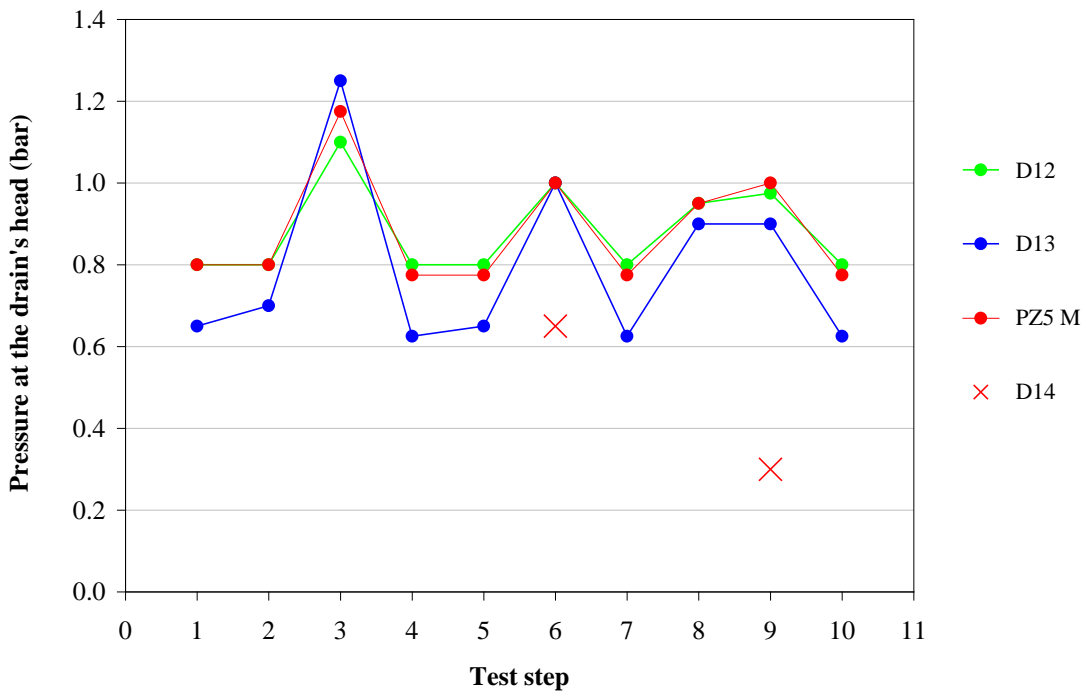


Figure 4.31 – Water pressures in the equipment placed in drain D14’s area of influence during the water-inflow tests.

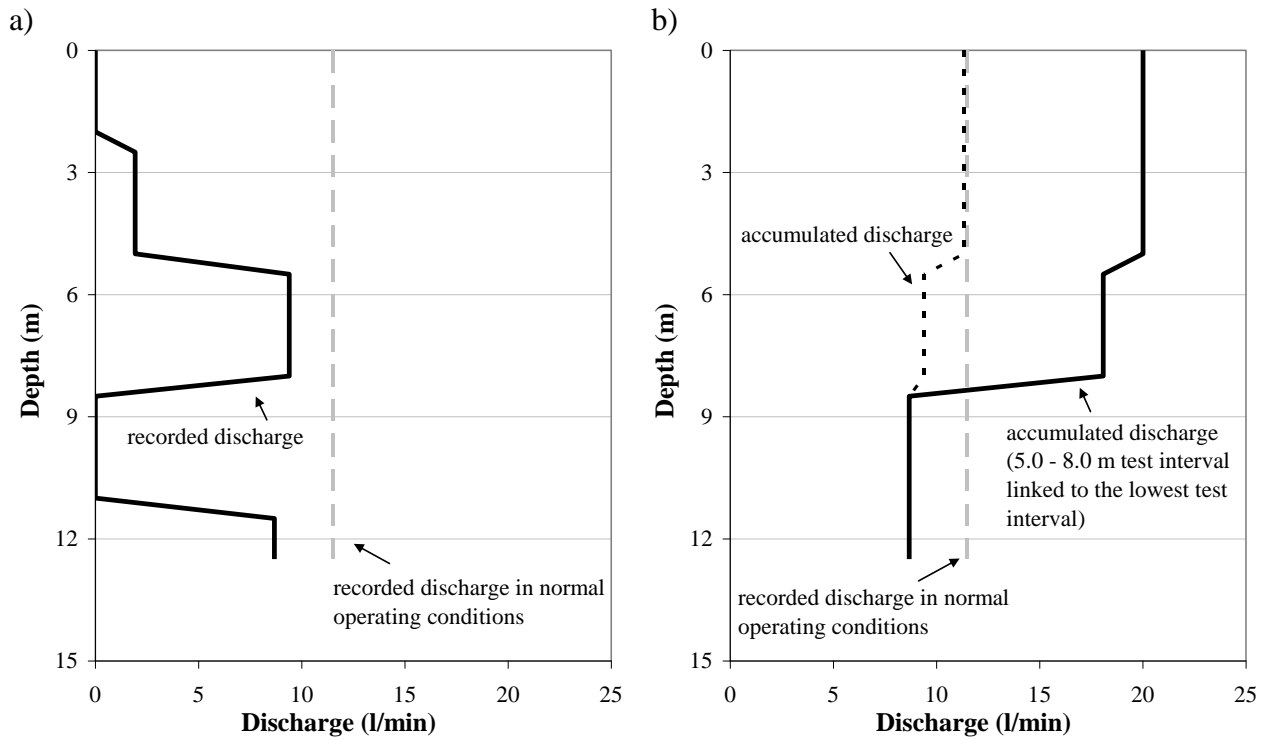


Figure 4.32 – Discharge flowing into each of drain’s D14 test intervals (a) and accumulated discharge from the bottom to the head of the borehole (b), compared with the reference discharge.

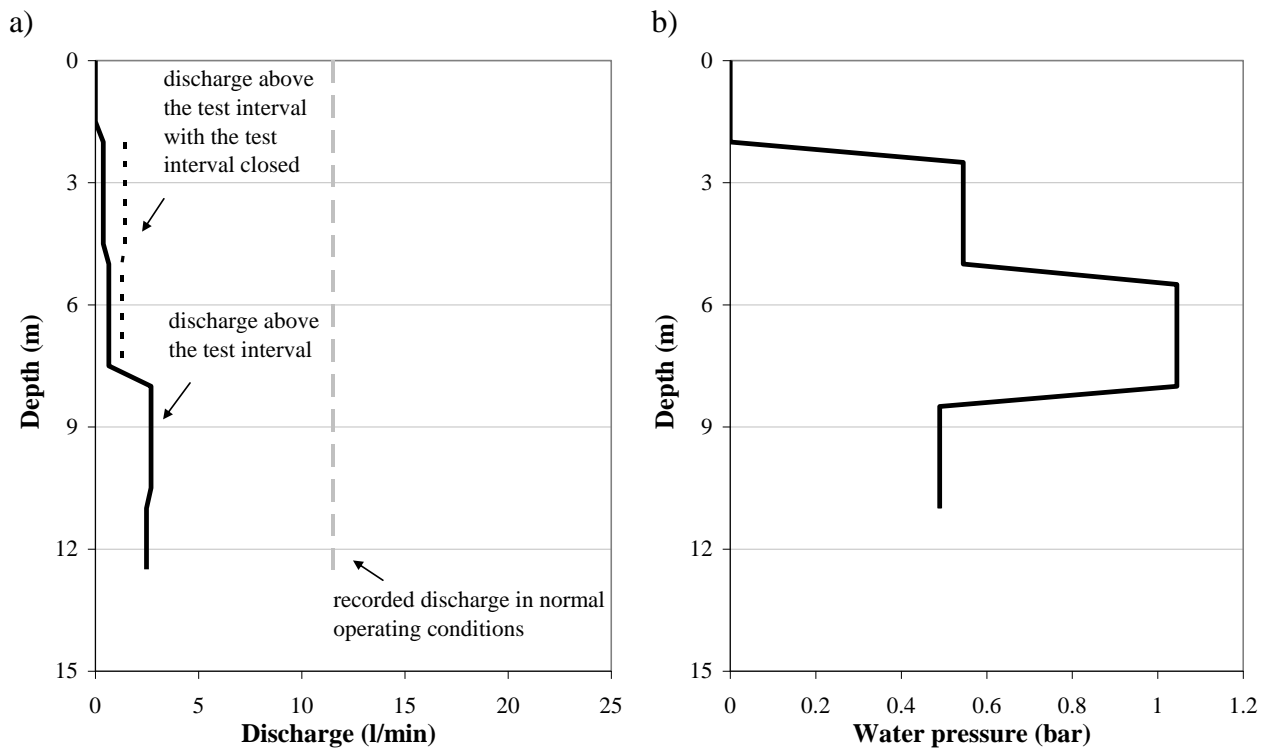


Figure 4.33 – Discharge coming into the borehole section between the packer and the drain head (a) and variation of water pressure along drain D14 (b).

4.4.4 Tests in drain D18

As with tests in drain D14, the reservoir level (80.36 m) was measured before testing began. Borehole D18 was working as a piezometer and therefore, to carry out tests, it was necessary to dismantle it. In order to check its area of influence, discharges and water pressures were recorded in all the drains, piezodrains and piezometers in the foundation of block 6-7 and in part of the foundation of block 7-8, close to joint 7, before and after dismantling the piezometer. Measurements lead to the conclusion that discharges and water pressures decreased in all the equipment located from piezometer PZ5M, in the foundation of block 6-7, to borehole D3, in the foundation of block 7-8 (Figure 4.25). Therefore, the borehole's area of influence is around 30 m along the drainage line. Readings taken with the borehole working as a drain are the "reference values". Reference discharge in borehole D18 is 61.35 l/min.

The "blind device" was inserted into D18. There was an obstruction at 10.5 m, which was easily removed. It was found that from 13.5 to 15 m down from the gallery floor the borehole walls were very irregular, indicating a very fractured area. The borehole length was 25.5 m. The decision was made to start testing with the 20.0 – 23.0 m test interval. The lowest 1.5 m long borehole area was not tested, as it was not possible to assemble the equipment as a single packer. All the measurements taken while carrying out tests are shown in Appendix 1.

In addition to test step 0, which are readings taken before dismantling the piezometer, 13 step tests were considered, shown in Figure 4.34:

- Step 1:** reference values (recorded before carrying out tests, with D18 working as a drain);
- Step 2:** 20.0 m – 23.0 m test interval;
- Step 3:** 17.0 m – 20.0 m test interval;
- Step 4:** 14.0 m – 17.0 m test interval;
- Step 5:** 11.0 m – 14.0 m test interval;
- Step 6:** 8.0 m – 11.0 m test interval;
- Step 7:** 8.0 m – 11.0 m test interval, with the test interval closed;
- Step 8:** 8.0 m – 11.0 m test interval, with both the test interval and piezodrain D19 closed;
- Step 9:** 8.0 m – 11.0 m test interval, after re-adjusting piezodrain D19 to its previous position and with the test interval working as a drain;
- Step 10:** 5.0 m – 8.0 m test interval;
- Step 11:** 5.0 m – 8.0 m test interval, with the test interval closed.
- Step 12:** confirm that reference values had been reached;
- Step 13:** 2.0 m – 5.0 m test interval.

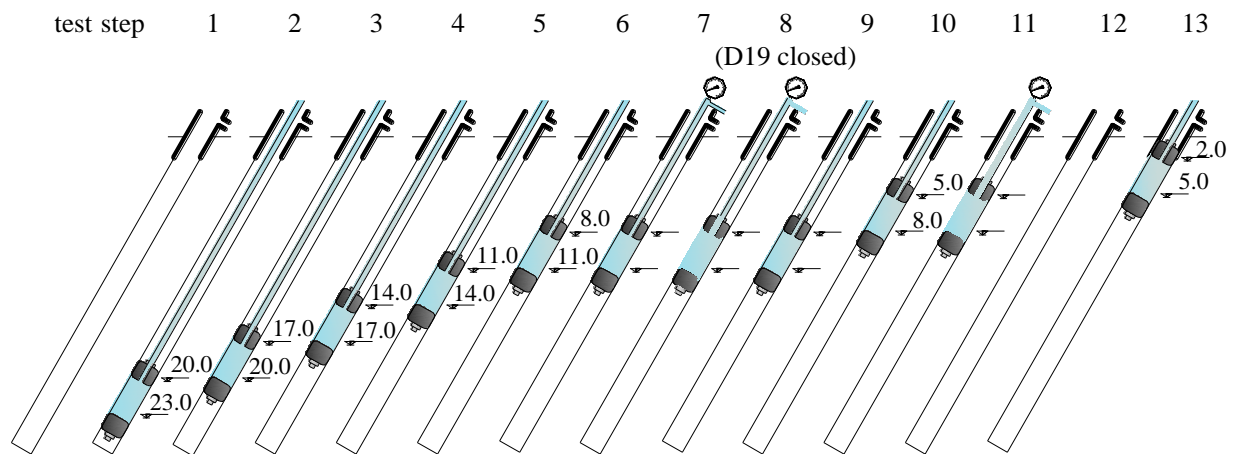


Figure 4.34 – Test steps in borehole D18.

Test results concerning discharges and water pressures in each test interval are shown in Figure 4.35 and Figure 4.36. The following paragraphs describe the various steps in detail.

In the first 5 test steps, water flowing into the areas being tested did not reach the pipes' head, there were only slight changes in the quantity of water flowing in above the test interval and apparently there were no changes in discharges and water pressures in the neighbouring equipment. The water pressure in each test interval was calculated taking into account the length of the water column inside the pipes. In step 2, piezodrain D19, adjacent to the borehole being tested, was closed and no change in borehole D18's discharge was recorded. Piezodrain D19 was re-adjusted to its previous position and it was decided that during tests it should only be closed if there were water flowing out of the pipes. In steps 2 to 5 readings were only taken in drain D18 because it was thought that as there had been no changes in readings in the borehole being tested, there would be no changes in the neighbouring boreholes.

In step 6, when the 8.0 – 11.0 m test interval was closed, there was a sudden change in test results: the total discharge in borehole D18 decreased from 55.0 l/min to 38.9 l/min, and the most significant part of this discharge (around 95 %) flowed into the test interval being tested. This decrease in drain discharge was probably due to the obstruction of one or more discontinuities through which water flowed, as an increase in discharges and water pressures was recorded in almost all the neighbouring equipment. When the pipes were closed (step 7), the water pressure at the pressure gauge increased quickly and reached steady-state conditions in only 7 minutes. Discharges and water pressures increased slightly in equipment located in D18's area of influence. In the following step (step 8), piezodrain D19 was also closed. Discharge flowing into borehole D18 at above the test interval increased, as did the water pressure at the test interval and at the piezodrains located in the neighbouring area. Due to time constraints, discharges were only measured at drain D18.

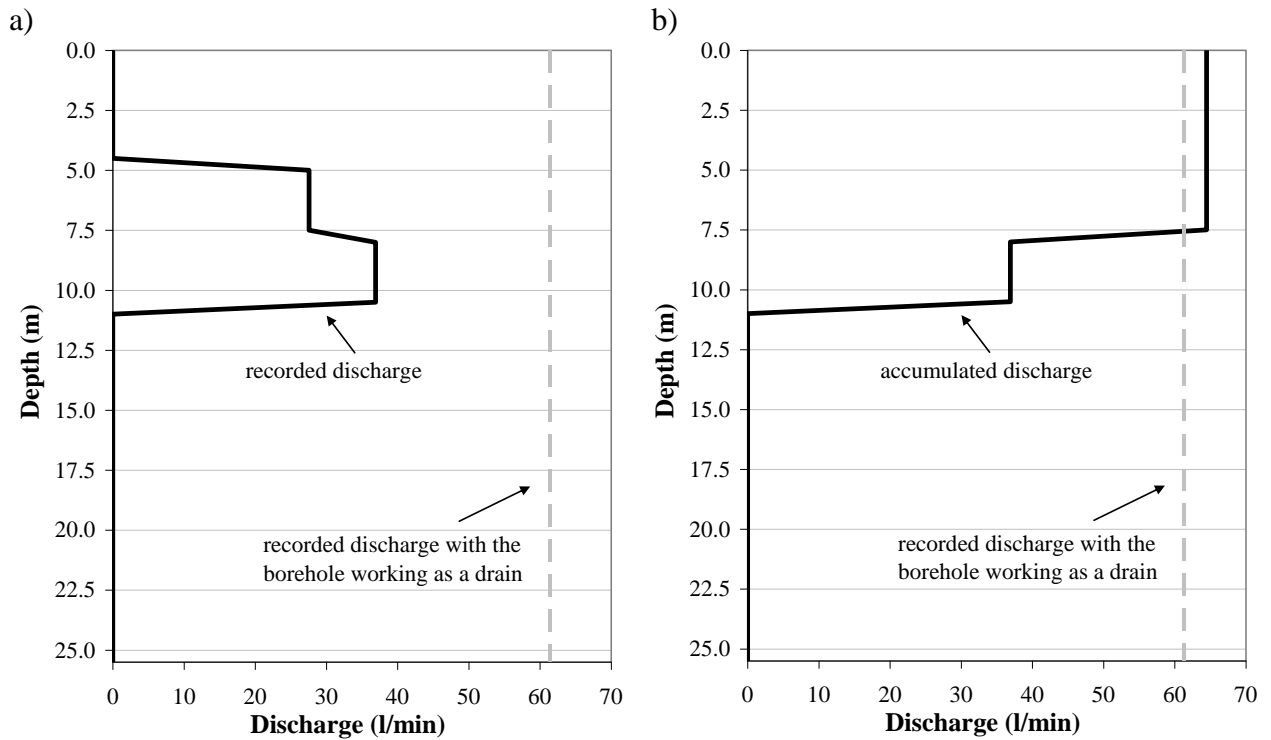


Figure 4.35 – Discharge flowing into each of borehole’s D18 test intervals (a) and accumulated discharge from the bottom to the head of the borehole (b), compared with the reference discharge.

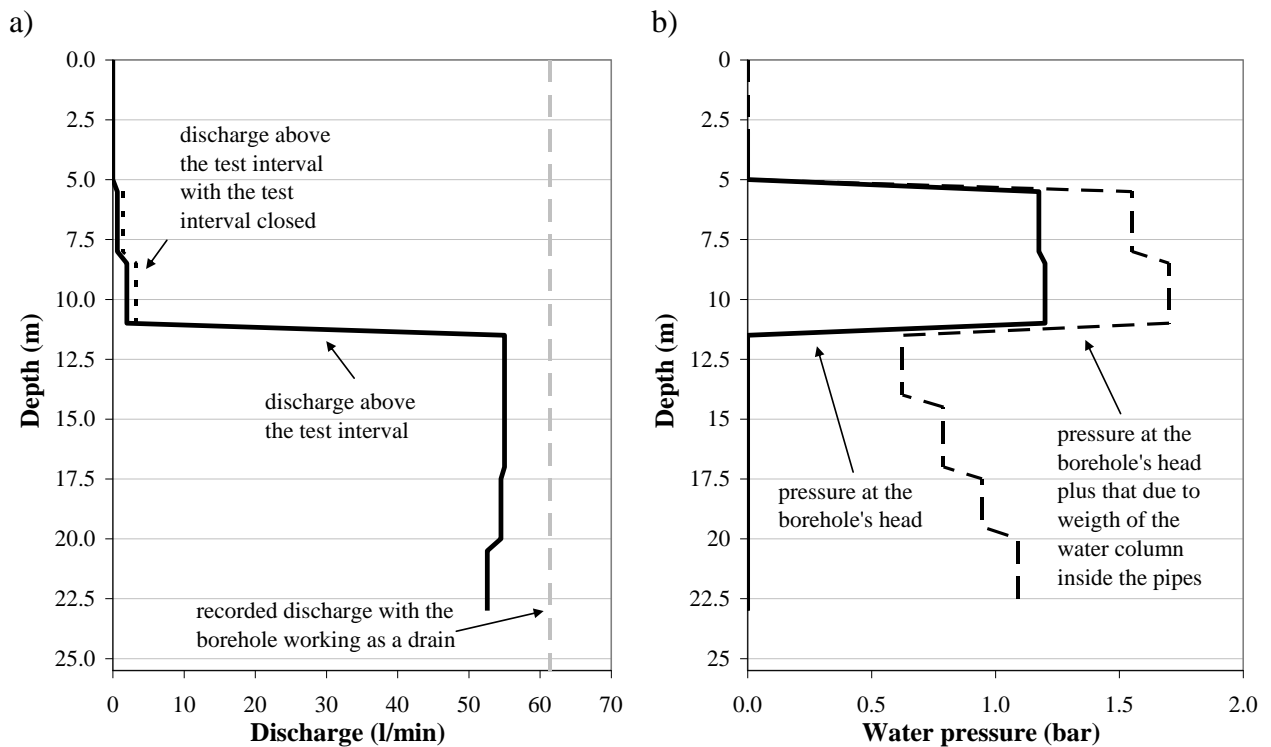


Figure 4.36 – Discharge coming into the borehole section between the packer and the drain head (a) and variation of water pressure along borehole D18 (b).

In step 9, water was allowed to flow out of the pipes and a new attempt was made to re-adjust piezodrain D19 to its previous position. However, this was extremely difficult and, due to the disturbance that any change in adjacent equipment causes, the decision was made not to change anything in neighbouring equipment during borehole water-inflow tests. Discharges in the drain being tested were almost the same as those recorded in step 8 and therefore it was thought that the piezodrain was well positioned. No readings were taken in the neighbouring equipment. The packer was raised 3.0 m and discharges and water pressures in the equipment located in borehole D18's area of influence were taken with the test interval working as a drain and with the pipes closed (step 10). The comparison between readings in steps 6 and 10 showed that there was a significant increase in D19's discharge and a decrease in water pressures. At the same time, discharges recorded in D18 were lower than those recorded in step 6. This could either be due to the clearing of discontinuities, as a result of an increase in seepage velocity, or to the improper re-adjustment of piezodrain D19. Results analysis carried out afterwards showed that piezodrain D19 had not been properly re-adjusted.

Tests carried out in drain D18 lead to the following conclusions:

- i) water flowed into the drain at between 5.0 and 11.0 m down from the drain head;
- ii) the area of influence along the drainage line was around 30 m;
- iii) there was water inflow of around 16.0 l/min at between 7.5 and 8.0 m down from the drain head;
- iv) the test intervals 5.0 – 8.0 m and 8.0-11.0 m were linked through conductive discontinuities around the borehole;

Figure 4.35 clearly shows that both test intervals from 5.0 – 8.0 m and 8.0 - 11.0 m were linked through conductive discontinuities, as the accumulated discharge from the bottom to the borehole head was greater than the reference discharge. As the two test intervals were linked, the water pressure should have been the same in both. The slight difference between recorded water pressures, of 0.025 bar, was probably a measurement error.

Test results show that borehole D18 is highly efficient at lowering water pressures in the neighbouring area. However, this decrease in water pressures is achieved with an excessive increase in discharges in its area of influence, from around 87 l/min to 137 l/min.

4.4.5 Main difficulties found whilst carrying out tests

The double packer used was acquired about a year before these “experimental” tests were carried out and it was necessary to buy and develop a serious of parts without which the tests would not have been possible. Despite the great care taken to check the equipment before tests, some difficulties were still found whilst testing *in situ*. Firstly, the piece of equipment provided by the supplier to hold the steel cable did not fit inside the pipe at the borehole’s head. Therefore, it was necessary to modify it and replace the provided steel cable with another of lower diameter. Secondly, the supplier did not provide, before these first tests were carried out, the part which allows equipment to be assembled as a single packer. Therefore, a PVC stopper had to be made. However, it could not take the water pressure, which meant that only a single test could be carried out. Finally, the recording device for the pressure transducer was not working properly, therefore water pressures could not be taken directly and had to be taken at the boreholes’ head, with pressure gauges. Regarding this latter difficulty, it should be stressed that the recording device is linked to the pressure transducer and it was impossible to check this in the laboratory, as a borehole with water under pressure where the packer could be inflated would be required.

4.4.6 Conclusions drawn from tests carried out in Pedrógão dam foundation

Tests carried out in only two boreholes do not give enough information about seepage in a foundation area. However, in this case they made it possible to identify both the depth at which the main seepage paths cross the boreholes and links between neighbouring boreholes. The following conclusions could be drawn:

- i) the main seepage paths cross the drains at between 5.0 m and 11.0 m down from the drain head;
- ii) steady state seepage is reached relatively quickly, due to the high permeability of the rock mass under blocks 6B-7 and 7-7A.
- iii) the high seepage velocity recorded in the boreholes reveals that the grout curtain is probably inefficient in this area.
- iv) both tested boreholes are relevant regarding water pressure relief in the foundation of block 6-7, but in borehole D18 this decrease in water pressures is achieved with an excessive increase in discharges in its area of influence

These conclusions are consistent with the results of water pressure permeability tests carried out both before the construction of the dam and when the grout curtain boreholes were drilled. The absence of drainage boreholes logs does not allow further analysis.

4.5 Tests carried out in Alqueva dam foundation

4.5.1 Preparation of tests

4.5.1.1 Area where tests were carried out and variation of discharges and water pressures

The decision was made to carry out tests, in block 17-18, where the highest discharges were recorded in the valley bottom. Figure 4.37 shows recorded discharges and water pressures in this block’s foundation. Discharges are very low, with the exception of drain D25 D in which discharges went up to 3.0 l/min. When the water in the reservoir rose from around 120 to 136 m in only 3 months, one or more discontinuities which cross drain D25 D opened, and there was a sudden increase in the drain discharge, from 0.2 to 0.9 l/min. This increase was even higher when the reservoir level increased from 136 to 148 m. In this case, discharge increased almost 4 times.

Tests were to be carried out in drain D25 D, PZB 13-2 and PZB 13-3, in order to obtain information along the upstream-downstream direction. Analysis of discharges recorded in the neighbouring blocks showed that it would also be interesting to carry out tests in drain D26 D, located in block 18-19, and D20 D, in block 16-17. Figure 4.38 shows the location of drains and piezometric boreholes in blocks 16-17, 17-18 and 18-19.

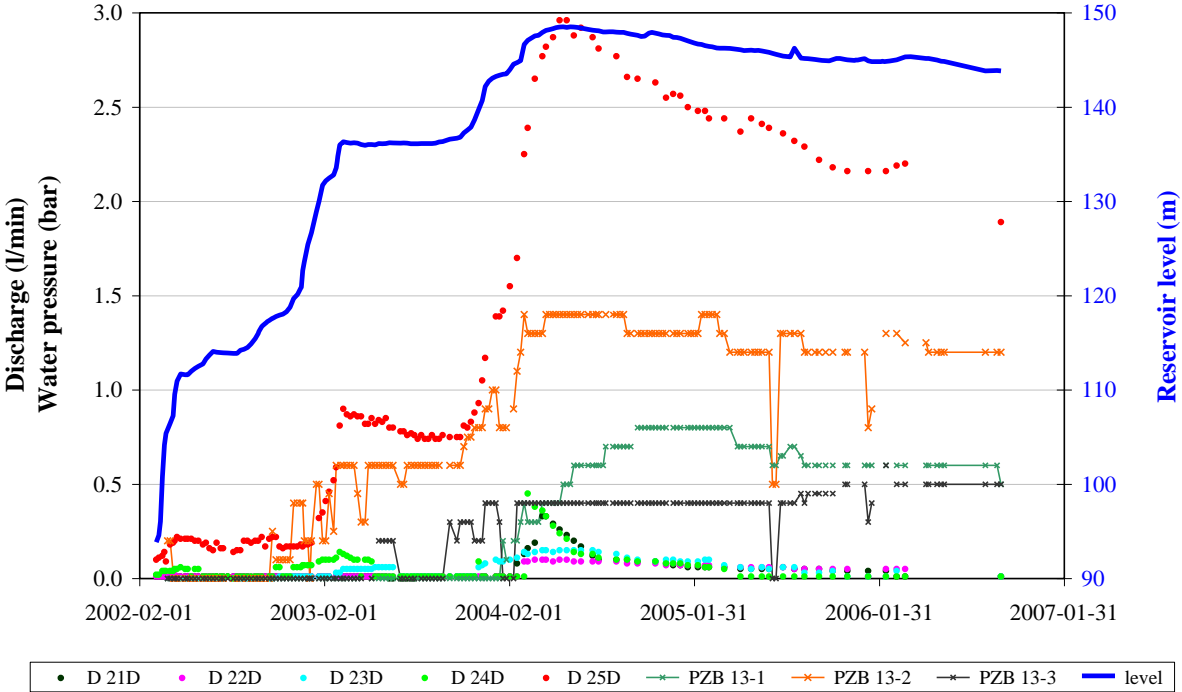


Figure 4.37 – Recorded discharges and water pressures in the foundation of block 17-18.

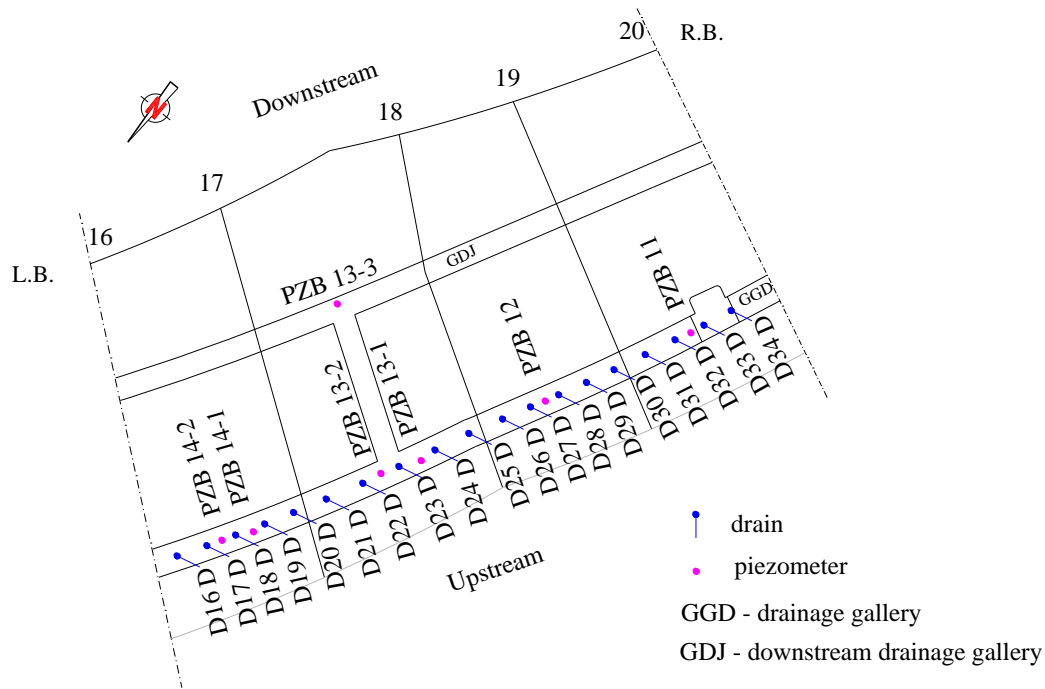


Figure 4.38 – Location of drains and piezometric boreholes in the foundation of blocks 16-17, 17-18 and 18-19.

4.5.1.2 Analysis of geological and geotechnical information

The surface foundation map shows that the foundation of blocks 16-17, 17-18 and 18-19 was fresh to slightly weathered at surface with wide to medium spaced rock joints (W1-W2 and F2-F3, according to ISRM classification).

Available drainage borehole logs show that, in this area, the foundation was fresh to slightly weathered, with moderate to close rock joints (W1-2 and F3-4, according to ISRM terminology), crossed by numerous thin layers and veins of quartz and carbonates and, in block 16-17, by discontinuities at different depths, some of them filled with cement grout. The rock mass was almost impervious, with permeabilities of around 0.1 LU.

Lugeon type tests were carried out with the reservoir empty but with the structure's weight acting on the foundation. The reservoir filling causes the dam to rotate towards downstream, with the consequent opening of sub-vertical discontinuities upstream from the dam and increase in the aperture of the sub-horizontal discontinuities located below the heel of the dam. As a consequence, the foundation permeability in the area upstream from the dam increases.

4.5.2 Summary of experimental activity

Borehole water-inflow tests in six drain and piezometric boreholes were carried out in three different weeks with the reservoir at various elevations: the first tests were done from 16-20 October 2006, with the water level around 143.6 m; the second from 19-23 March 2007, with the water level around 150.0 m; and the third from 3-7 September 2007, with the water at an elevation of about 148.0 m. Both the electrical conductivity of water and temperature were measured every 0.5 m along the tested boreholes prior to water-inflow testing, using a portable conductivity meter with automatic temperature compensation.

In the first week, tests were conducted in drain D25 D and in piezometer PZB13-2. In order to obtain information about seepage in the upstream-downstream direction, an attempt was made to do borehole water-inflow tests in piezometer PZB13-3, installed at the downstream drainage gallery, where an uplift water pressure of 0.5 bar was recorded, which was 6.1 % of the hydraulic head. However, the low discharge drained by the borehole (0.02 l/min) would make borehole water-inflow tests useless.

New tests were carried out in March 2007, with the reservoir at an elevation 6.4 m higher than when the first tests were performed. The main aim of these new tests was to study seepage in the base of blocks 17-18 and 18-19 in more detail and to detect possible seepage changes due to the raising of the water level in the reservoir. In order to detect these changes, tests should have been repeated in drain D25 D. However, the monitoring data led to the conclusion that between the tests carried out in October 2006 and March 2007, the discharge in drain D25 D and the water pressure recorded with the drain closed were only about 8 % higher (from 2.0 l/min up to 2.18 l/min and from 4.825 bar up to 5.25 bar), thus it was decided not to repeat the tests in that drain. In the week before this second group of tests was done, drains D25 D, D26 D and D27 D, located in the area being studied, were successively closed, recording discharges and water pressures before and after closing the drains, in steady state conditions, in an area assumed to be larger than the boreholes' area of influence. Tests were conducted in boreholes D26 D and D27 D, in block 18-19, and D20 D, in block 16-17. Due to time constraints, readings during testing in drain D20 D were taken in transient conditions. In order to obtain more accurate results, new borehole water-inflow tests were carried out in this drain in September 2007.

Additional information to that provided from the borehole water-inflow tests was obtained by gradually closing drainage boreholes and doing water electrical conductivity and temperature analyses:

- On 21 March 2007, during the second round of water-inflow tests, the electrical conductivity of water was measured along the two boreholes of the GDJD floor

where the highest discharges are recorded and in the following week, from 26-29 March both drains were closed, in turn, with a pressure gauge at their heads. These tests aimed to obtaining an indication of the seepage pattern downstream from the grout and drainage curtains.

- From 21-25 May 2007, with the reservoir at around 149.30 m, water electrical conductivity and temperature analysis tests were done in the majority of the drainage boreholes located in the bottom of the valley and in blocks 18-19 and 19-20, on the right bank, in order to obtain information about where each one of the boreholes was crossed by seepage paths. From 20-21 November 2007, with the reservoir at 147.56 m, new tests were carried out in some boreholes.
- From 5-8 May 2008, with the reservoir at around 148.0 m, all the drains located in block 17-18 were gradually closed, so as to identify seepage links between boreholes, to assess the way in which water pressures varied in the foundation of the dam block, and to obtain the average water pressure in the block foundation.

Some information about tested boreholes is given in Table 3.1: borehole reference, block where it is installed, length, type of test, date when tests were carried out, water level in the reservoir at the time of each test, water pressure at the borehole head when the hole is closed and corresponding percentage of hydraulic head.

As tests in Pedrógão dam foundation have been presented in great detail in the previous sections, covering different situations, the following sections include a much simpler description of the similar tests done in Alqueva dam foundation followed by presentation and discussion of the results. The situations which are referred to and analysed are those which stood out as being unusual or different. Measurements taken during testing and both water electrical conductivity and temperature profiles are shown in Appendix 1.

4.5.3 Tests in drain D25 D

In the electrical conductivity and temperature profiles along drain D25 D obtained prior to water-inflow testing (Figure 4.39) there is a sudden variation in the electrical conductivity at between 6.0 and 8.5 m down from the drain head and in temperature at between 6.5 and 8.0 m, therefore it was concluded that this was probably the area where water was flowing into the borehole. Flow rates and water pressures in each drain and piezometric boreholes installed at the base of blocks 16-17, 17-18 and 18-19 were first recorded. After the readings, drain D25 D was closed with a pressure gauge at its head, which allowed the measurement of the hydraulic water pressure being released by the drain and the assessment of the drain's length of influence along the drainage line (18 m) comparing discharges and water pressures

measured in the nearby boreholes before and after closing the drain, in steady state conditions. The later opening of the drain and the measurement, over time, of the discharges and water pressures in the boreholes placed in the drain's area of influence provided information about the period of time necessary to reach steady state conditions (around 90 minutes).

Borehole reference	Block	Borehole length (m)	Tests	Test date	Water level in the reservoir (m)	Water pressure with the drain closed (bar)	Percentage of hydraulic head (%)	
D25 D	GGD 17-18	23.57	Drain closed	16 Oct. 06	143.58	4.825	58.6 %	
				20 Oct. 06	143.66	4.450	54.0 %	
				13 Mar. 07	150.08	5.250	59.1 %	
			Electr. cond.	13 Oct. 06	143.65	-	-	
				Water-inflow	16 Oct. 06	143.58	-	-
					17 Oct. 06	143.60	-	-
18 Oct. 06	143.60	-	-					
	PZB 13-2	GGD 17-18	23.43	Water-inflow	18 Oct. 06	143.60	1.3	15.9 %
				19 Oct. 06	143.64	-	-	
PZB 13-3	GDJ 17-18	-	-	19 Oct. 06	143.64	0.5	6.1 %	
D26 D	GGD 18-19	26.0	Drain closed	14 Mar. 07	150.07	4.650	53.6 %	
				Electr. cond.	19 Mar. 07	149.99	-	-
				Water-inflow	21 Mar. 07	149.95	-	-
D27 D	GGD 18-19	23.0	Drain closed	19 Mar. 07	149.99	0.4	4.7 %	
				Electr. cond.	20 Mar. 07	150.01	-	-
				Water-inflow	21 Mar. 07	149.95	-	-
D20 D	GGD 17-18	22.5	Drain closed	21 Mar. 07	149.95	1.20	13.6 %	
				Electr. cond.	22 Mar. 07	149.93	-	-
				Water-inflow	23 Mar. 07	149.93	-	-
					3-7 Sep. 07	148.04	0.75	8.6 %
DGDJM-5D	GDJ floor upstr.	2.75	Electr. cond.	21 Mar. 07	149.95	-	-	
				Drain closed	27 Mar. 07	149.86	0.125	1.4 %
DGDJI-2D	GDJ halfway	4.6	Electr. cond.	21 Mar. 07	149.95	-	-	
				Drain closed	29 Mar. 07	149.87	0.275	3.1 %
D25 E to D32 D	Blocks in the valley bottom and at the base of the slope on the right bank	Varied from	Electr. cond.	21-25 May 07	149.30	-	-	
				20-21 Nov. 07	147.56	-	-	
D21 D to D26 D	17-18 and 18-19		Drains closed	5-8 May 08	≈ 148.0	Varied from 0.275 to 5.6	Varied from 3.2 to 64.7 %	

Table 4.3 – Information about the boreholes where tests were carried out.

Tests were carried out from the borehole bottom upwards, first with a single and then with a double packer. The latter was only used in test intervals where water was coming in. Figure 4.40 shows the water pressure variation after closing different test intervals. The time necessary to reach a constant pressure varied from around 40 to 90 minutes.

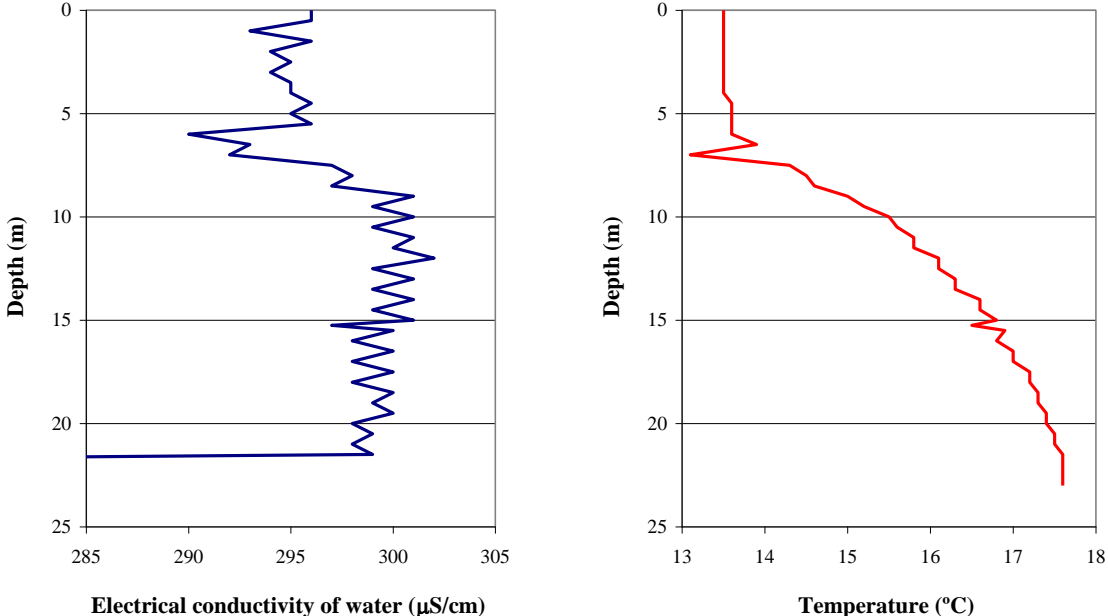


Figure 4.39 – Electrical conductivity of water and temperature profiles along drain D25 D.

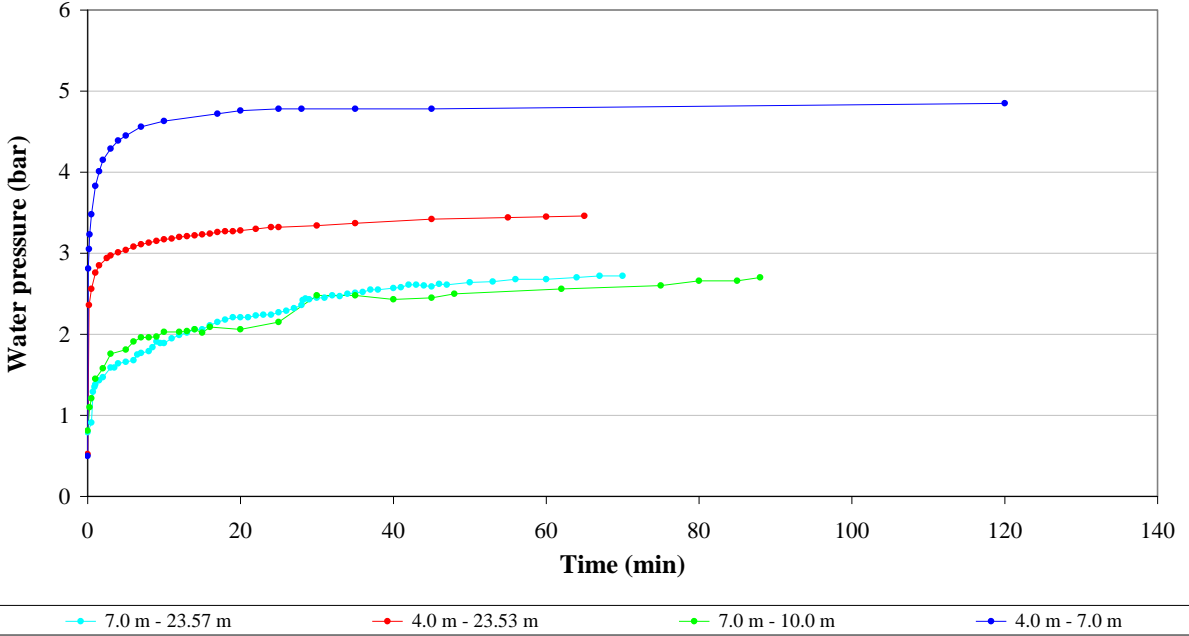


Figure 4.40 – Water pressure variation at the different test intervals after being closed.

Analysis of discharge and water pressure variations in the equipment placed in drain D25 D's area of influence led to the following main conclusions: i) the discharge in most of the drains located less than 6.0 m away from D25 D increased when either the drain or the test intervals were closed; this discharge increase was more significant in drain D26 D, adjacent to the drain being tested; ii) the closure of drain D25 D had no influence on the discharges recorded in drains D24 D and D28 D; iii) after closing drain D25 D, the total discharge coming into the drain increased; iv) the sum of the discharges in the borehole's area of influence varied slightly during the test; however, a significant decrease was noticed when drain D25 D was closed and when test intervals from 4.0 m to the bottom of the borehole and from 4.0 – 7.0 m were closed; v) in the four piezometers located in the drain's area of influence, including that located in the downstream drainage gallery, water pressure increased when the drain was totally or partially closed, PZB13-1 being the most sensitive to test interval closure.

Analysis of discharges and water pressures in each test interval compared with the reference discharge showed that the water flowing out of the drain head entered the borehole at between 1.0 and 10.0 m down from the drain head, and that 90 % of the water entered the borehole at between 4.0 m and 7.0 m down from the drain head. It was also concluded that there were no seepage paths between the three 3.0 m long test intervals into each water flowed. Results of water conductivity analysis along the borehole, which led to the conclusion that water flowed into the borehole at between 6.0 m and 8.5 m down from the drain head, are consistent with the results of water-inflow tests.

The water pressure at the various test intervals obtained with both the single and double packer was compared with the water pressure when the drain was closed and it was concluded that, in this case, the highest water pressure, recorded when the 4.0 – 7.0 m test interval was closed, extended along the entire length of the borehole. In the single packer test, with the test interval at between 4.0 m and the bottom of the borehole, the water pressure was around 3.4 bar, lower than that recorded when the double packer was used at the test interval 4.0-7.0 m. It has been concluded that in both tests the equipment was not in exactly the same position and that in the single packer test a seepage path was plugged by the packer.

At the end of the week in which these first tests were carried out, drain D25 D was closed again and a water pressure of 4.45 bar was achieved, which was 54 % of the hydraulic head. From the beginning to the end of the week, the water pressure and corresponding percentage of hydraulic head decreased in drain D25 D and increased in piezometers PZB 12 and PZB 14-2. Differences in the recorded pressures were probably due to changes in seepage conditions induced by closing consecutive sections along drain D25 D.

Rotary-percussive drilling was used to open drain D25 D and therefore no borehole log is available to analyse in conjunction with water-inflow tests results.

4.5.4 Tests in piezometer PZB 13-2

In piezometer PZB 13-2, after obtaining “reference values”, the purge valve was opened and closed which showed that water pressure was recovered in only about 5 minutes. The pressure gauge was then removed from the top of the borehole and it was kept working as a drain. The comparison of discharges and water pressures observed before and after removing the pressure gauge led to the conclusion that the borehole’s length of influence along the drainage line was about 27 m, and that piezometer PZB 13-3, located in the downstream drainage gallery was also in the borehole’s area of influence. It was curious to observe that the removal of the pressure gauge had no influence on the recorded discharges, except in drain D22 D, adjacent to the borehole being tested, in which a slight discharge reduction was observed.

The test was carried out with the single packer in successive ascending test intervals, raising the packer 3 m each time. It was observed that around 64 % of the reference discharge flowed into the 19.0 m – bottom of the borehole interval. The water pressure recorded when this test interval was closed was 2.5 times greater than the reference pressure. While testing the next interval, from 16.0 m to the bottom of the borehole, no water was flowing into the test interval and it was observed that the water which was entering was flowing into the borehole from above the packer. It was concluded that the test interval from 16.0 m to 19.0 m was connected with the area above 16.0 m, by seepage paths in the surrounding rock mass. To find out the elevation at which the connection took place, the remaining test intervals were successively isolated. In all these test steps the water was flowing into the borehole from above the packer. While examining the test results, it was observed that one of the vertical boreholes where geophysical tests had been carried out was drilled only about 0.5 m away from the borehole being tested. It was concluded that there were seepage paths linking both boreholes, not only in the 16.0 m - 19.0 m test interval but also in depths not greater than 0.75 m, probably in the block/pavement concrete interface.

In this case, the existence of seepage paths linking the piezometric borehole and the borehole drilled to perform geophysical tests, which allows water leaks, releases water pressures; therefore, contrary to what is observed in D25 D’s test, the maximum water pressure is not recorded at the borehole’s head.

It may be concluded that PZB 13-2 is a useless borehole due to the fact that, regarding the safety evaluation of the dam, the information provided by this piezometer is misleading.

4.5.5 Tests in drain D26 D

Tests in drain D26 D were carried out straightforwardly in only 7 steps using the single packer and raising the equipment 1.0 m each time. As the water electrical conductivity and

temperature profiles had shown that water probably entered the borehole at between 3.5 and 5.0 m down from the drain head, the packer was first placed at the depth of 7.0 m, which significantly decreased the time spent doing the test. It was concluded that the borehole's length of influence along the drainage line was about 30 m and that the total discharge flowed into the borehole at between 4.0 and 5.0 m down from the drain head.

4.5.6 Tests in drain D27 D

In this drain, the results of water electrical and temperature analysis were not conclusive and therefore the borehole was tested along its whole length. Tests led to the conclusion that the water flowing from the drain head entered the borehole at between 1.0 and 7.0 m down from the drain head, equally distributed between the two 3.0 m long test intervals (4.0 – 7.0 m and 1.0 – 4.0 m). Whenever the test interval was closed, a water-spout from the gallery floor was observed, which shows that water pressures in the borehole being tested were being relieved, and that this is therefore an effective drain.

4.5.7 Tests in drain D20 D

The first tests carried out in drain D20 D, in March 2007, were limited by time constraints which meant that readings were taken in transient conditions. Despite this, the tests showed that the drain's length of influence along the drainage line was about 27 m and, as with drain D25 D and piezometer PZB 13-2, its area of influence extended towards downstream, at least as far as piezometer PZB 13-3. It was possible to conclude that water flowed into the borehole at between 4.0 m and 10.0 m down from the drain head and that about half of the quantity of water flowed into the borehole at between 4.0 m and 7.0 m. Differences in discharges recorded when the single and the double packers were used were probably due to the equipment not being at exactly the same position.

New borehole water-inflow tests were carried out in September 2007, which were carefully conducted allowing the time necessary to reach steady state conditions. Great care was also taken with the positioning of the packers inside the borehole. In order to obtain more detailed results, a test interval of only 1 m was used. As the first tests had led to the conclusion that the water first entered the borehole at between 7.0 m and 10.0 m down from the drain head, the single packer was first placed at a depth of 10.0 m, and it was observed, as expected, that there was no water flowing into the test interval. This was also observed in the following test interval, when the packer was raised by 1 m.

Tests carried out led to the following conclusions:

- i) water first entered the borehole at between 8.0 m and 9.0 m down from the drain head and there was no change in readings taken in adjacent drains when this test interval was closed;
- ii) the second place where water entered the borehole was at between 5.0 m and 6.0 m down from the drain head, and the third at between 4.0 m and 5.0 m; these seepage paths were linked, but only the discontinuity located at between 4.0 m and 5.0 m down from the drain head influenced readings on the downstream piezometer.
- iii) tests in drain D20 D only induced changes in readings in the adjacent drains (D19 D and D21 D), in piezometer PZB 14-1, and in piezometer PZB 13-3, located in the downstream drainage gallery.

At the end of the tests, as it was observed that discontinuities located at between 4.0 m and 6.0 m down from the drain head were linked, it was decided to isolate a test interval which included all these discontinuities. With the equipment available it was not possible to isolate a test interval of 2.0 m, therefore, keeping in mind that there was no water flowing into the borehole at between 6.0 m and 7.0 m down from the drain head, an interval of 3.0 m was considered, from 4.0 m to 7.0 m.

4.5.8 Additional tests

4.5.8.1 Water electrical conductivity analyses

In May 2007, with the reservoir at around 149.3 m, water electrical conductivity and temperature analysis tests were carried out in the majority of the drainage boreholes located in the bottom of the valley and in the first two blocks at the base of the slope, on the right bank.

Analysis along the boreholes was carried out with readings every 0.5 m. The electrical conductivity and temperature profiles are shown in Appendix 1. From the simultaneous analysis of both graphs it was possible to identify the depth at which seepage paths cross the drains, as this occurs at the depths in which there is a sudden variation in either one or both parameters. In some cases, however, changes in the electrical conductivity profile can be due to changes in rock mass lithology, and therefore the profiles should be analysed alongside each borehole log. In most of the electrical conductivity profiles results obtained close to the drain bottom are not shown, as, due to the presence of sediments, they are much lower than the data obtained at lower depths. The depth at which the concrete/rock mass interface occurs is shown in gray or green in each graph presented in Appendix 1 (section A1.5), with the

exception of those regarding boreholes where rotary-percussive drilling was used because no information is available about the section of the borehole which goes through concrete.

During tests it was observed that in the area of the valley bottom close to the left bank there are a great number of completely or partially clogged boreholes. Analysis of the matter which obstructs the boreholes showed that it consists mainly of calcite, which almost certainly comes from the cement grout, which was placed in greater quantities in the left bank. The slow seepage velocities increase the time period for which the water is close to cement and the right conditions for precipitation are probably found when the water reaches the borehole. Figure 4.41 shows water electrical conductivity analysis being carried out and the head of one of the clogged boreholes.

Figure 4.42 shows where water flows into each borehole in the area tested, detected by both water-inflow tests and water electrical conductivity analysis. The accuracy of the latter tests can be verified, as in the boreholes where both tests were carried out inflows of water in the same areas were identified. Tests led to the conclusion that water flows into the majority of the boreholes mostly at shallow depths, in an area close to the concrete/rock mass interface. Most of the detected inflows of water below the boreholes' mid-depth are apparently in areas where the boreholes are crossed by faults. These could be due to a vein of different matter crossing the borehole. Some of the holes in which this occurs were drilled using rotary-percussive methods and therefore no log is available, and even from those available, no further information could be obtained. Figure 4.42 also shows that the bottom of almost every borehole is obstructed, due to the presence of sediment.



Figure 4.41 – Inserting the conductivity probe inside the borehole and a clogged borehole.

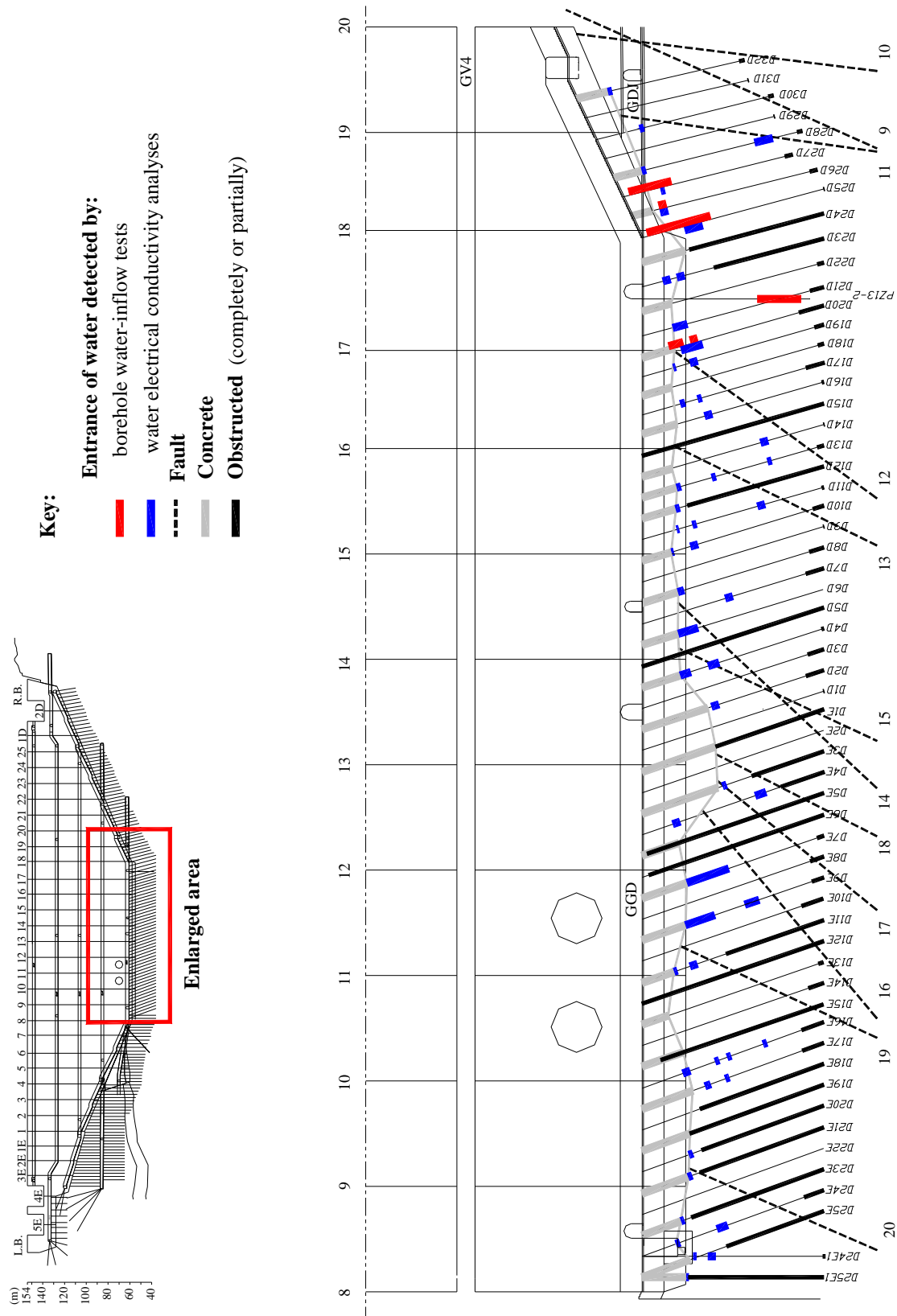


Figure 4.42 – Inflow of water into each borehole in the bottom of the valley and in the first two blocks at the base of the slope, on the right bank.

4.5.8.2 Tests in drains located in the floor of the downstream drainage gallery branch excavated in the rock mass (GDJD)

The downstream drainage gallery has a branch which extends towards the right bank and is excavated into the rock mass. In this area, called GDJD, the gallery has a concrete covering and is drained with fans of boreholes drilled in the floor, the sidewalls and gallery ceiling, in sections located 2.5 m apart. A pipe was installed at the heads of the drains which collect the greater quantity of water, to allow measurement of discharges and to conduct the water into gutter pipes (Figure 4.43).

According to the geological-geotechnical surface foundation map (EDP 2006) the whole gallery was excavated in green schist of good geotechnical quality: the rock mass is fresh to slightly weathered (W1 to W2) and the mean distance between successive rock joints measured along an intersecting straight line varies between moderate to close (F3 to F4) and wide to moderate (F2 to F3). The rock mass crossed by this gallery shows some thin faults (in the order of 2 to 10 cm) and some faults, mainly at the top of the gallery area, where some leakages were observed (Figure 4.44).

In order to have an indication of the rock mass seepage pattern downstream from the grout and drainage curtains, the electrical conductivity of water was measured along the two boreholes of GDJD floor where the highest discharges were recorded, whose approximate location is shown in Figure 4.44: i) drain DGDJM-5D, with a discharge of 0.41 l/min, and ii) drain DGDJI-2D, with a discharge 0.05 l/min. Both drains are located around 14.0 m downstream from the drainage curtain. Test results are shown in Appendix 1.



Figure 4.43 – Top of the extension of the downstream drainage gallery towards the right bank.

The first drain tested, dipping towards upstream, is only 2.75 m long and, according to test results, water flows into the borehole at its bottom or about 1.0 m down from the floor elevation. The second drain tested is vertical, 4.75 m long, and located halfway between gallery sidewalls. Water probably enters this drain at a depth of 2.3 m. The diameter of these boreholes is 55 mm, therefore it was not possible to carry out borehole water-inflow tests with the available equipment.

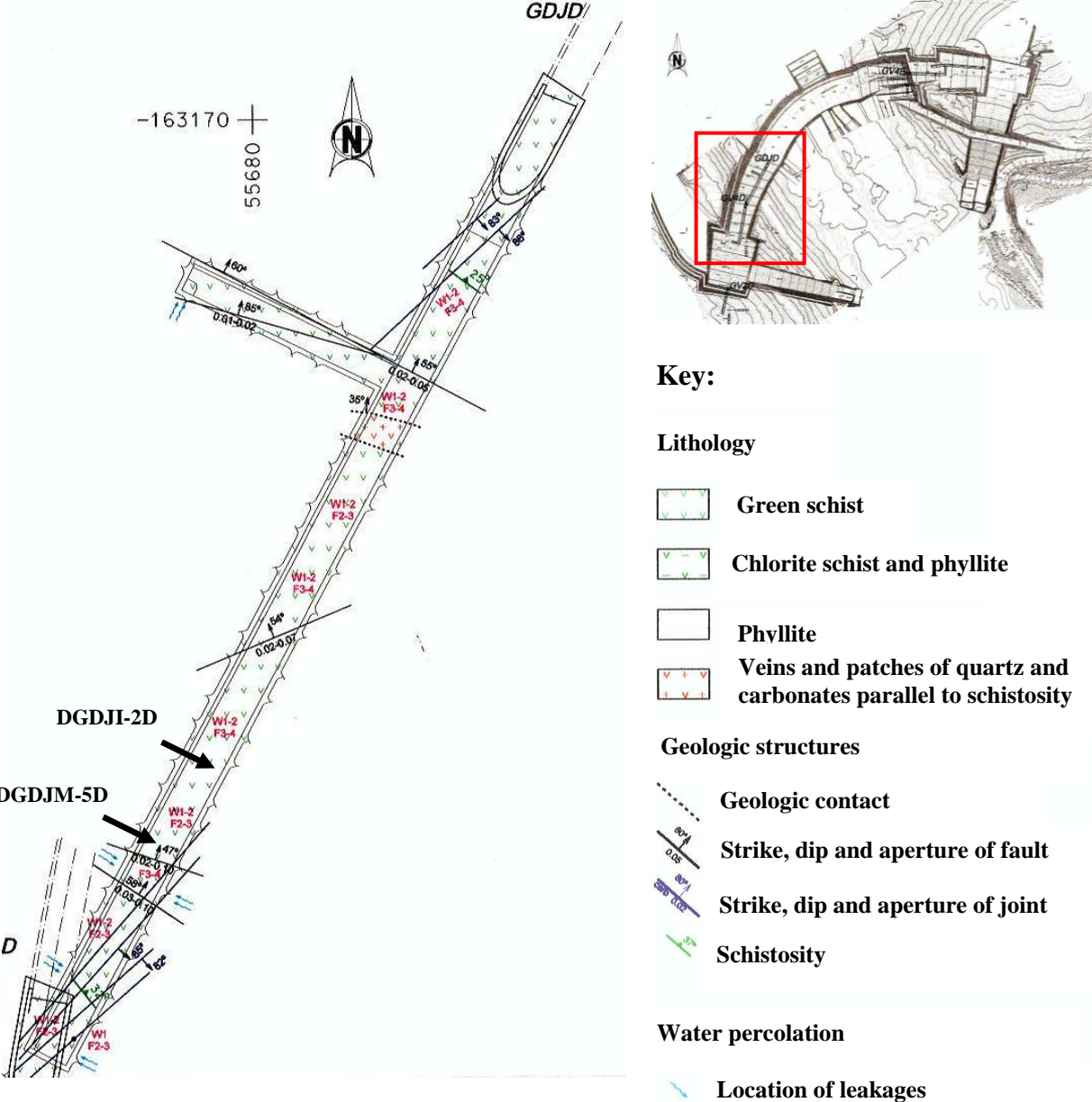


Figure 4.44 – Geological-geotechnical characterization of GDJD’s floor (adapted from EDP 2006), with an approximate location of tested boreholes.

In the following week both drains were closed, in turn, with a pressure gauge at their heads. Water pressures of 0.15 bar and 0.275 bar were observed, which were 1.4 % and 3.1 % of the hydraulic head, respectively. Drain DGDJM-5D was kept closed for seventeen hours and forty five minutes and drain DGDJI-2D was closed during the next day, for about seven and a half hours. In this period of time the reservoir remained at an elevation of 149.9 m.

Closing drain DGDJM-5D led to an increase in discharges recorded in six drains located in the vicinity of the borehole, and an increase of 0.05 bar in uplift pressures recorded in piezometers PZB 12 and PZB13-1. Thus, it can be concluded that the water pressure is low and that the drain is linked to the adjacent drains and to the mentioned piezometers through rock mass discontinuities. Information about changes in discharges recorded in the drainage gallery is not available, as discharges were only recorded before the drain was closed. Closing drain DGDJI-2D led to a discharge increase in four of the drains located in its vicinity and to an increase of 0.05 bar in piezometer PZB13-1. Flow rates in drains located in the drainage gallery before and after closing the drain were not recorded.

4.5.8.3 Closure of all the drains and piezometers located in block 17-18

During the development of a global hydraulic model of the dam foundation, presented in chapter 6.6, it was found useful to obtain the average water pressure in the foundation of block 17-18 and to know how water pressures vary at the base of the dam block. These tests were carried out from 5-8 May 2008 with the reservoir level around 148.0 m, as shown in Table 4.3. Discharges and water pressures were recorded in normal operating conditions and then drains D25 D and D26 D were simultaneously closed. Readings were taken about 21 hours later, in steady state conditions. Drains D21 D to D24 D were closed afterwards and readings were taken again after 21 hours. Measurements are shown in Appendix 1. When both drains D25 D and D26 D were closed simultaneously, water pressures of 5.6 and 5.05 bar were recorded respectively. Water pressures increased in the surrounding piezometers and discharges increased not only in the surrounding drains but also through the leakage from the floor of the downstream drainage gallery. The additional closure of drains D21 D to D24 D, caused, as expected, further increase in discharges and water pressures in some of the boreholes. However, the water pressure at drain D25 D remained 5.6 bar, which was 61 % of the hydraulic head, and in drains D21 D to D24 D when closed varied from 0.275 to 2.7 bar, which was 3.17 % to 31 % of the hydraulic head. The average percentage of hydraulic head at the dam block was around 27 %, but it could be concluded that the high percentage of hydraulic head recorded at drain D25 D while carrying out borehole water-inflow tests was localised, and therefore of no concern to the stability of the dam.

4.5.8.4 Survey of piezometers

A careful survey of piezometers installed in the arch's central block (block 13-14) and in block 8-9, in the valley bottom close to the left bank, was carried out. In piezometers PZB 17-2 and PZB 17-3, in which a zero pressure had been observed, the pressure gauges for a range of 0 to 10 bar were installed. However, when the purge valve was opened, a small amount of discharge was observed, therefore there must be a water pressure, which is less than 0.2 bar, as accuracy of measurement is 0.2 bar in pressure gauges for a range of 0 to 10 bar. In order to make dam monitoring more accurate, these pressure gauges should be replaced by others with a range of 0 to 2 bar and accuracy of 0.05 bar.

Block	Piezometer	Water pressure (bar)	Approximate discharge (l/min)	Water pressure recovery after closing the purge valve
8-9 (valley bottom, close to the left bank)	PZB 22-1	4.4	0.25	fast
	PZB 22-2	0.75	0.10	slow
	PZB 22-3	0.75	0.20	slow
13-14 (central cantilever)	PZB 17-1	0.65	0.15	fast
	PZB 17-2	0	Very low	slow
	PZB 17-3	0	Very low	slow

Table 4.4 – Water pressure and discharges measured by piezometers installed in blocks 8-9 and 13-14.

4.5.9 Conclusions drawn from tests carried out in Alqueva dam foundation

Tests carried out in Alqueva dam foundation led to the conclusion that water flows into the majority of the boreholes mostly at shallow depths, in an area close to the concrete/rock mass interface. From the water-inflow tests carried out in drains and piezometric boreholes located in blocks 17-18 and 18-19 it was also possible to conclude that, in this area of the rock mass, discontinuities through which water flows link the various boreholes in a relatively large area which extends towards downstream, as could be concluded from tests carried out in the gallery branch excavated in the rock mass. Conductive discontinuities have a very small aperture, as recorded discharges and water pressures in the borehole's area of influence only stabilize after about an hour and a half.

The plans for the foundation monitoring system usually advise installing piezometers half way between drains, in order to observe maximum water pressures. In Alqueva dam, a piezometer was installed in each block, halfway between joints. Boreholes to carry out geophysical tests were also drilled approximately in the middle of each block. Borehole water-inflow tests allowed the detection of seepage paths linking piezometric borehole PZB 13-2 and one of the boreholes where geophysical tests were carried out. The latter borehole works as an extra drain, located around 0.5 m from the piezometric borehole.

Therefore, water pressure measured in piezometer PZB 13-2 is lower than it would be if the borehole where geophysical tests were carried out had not been drilled. It can be concluded that greater care should be taken in the design of the foundation monitoring system.

Following these tests EDIA was requested to close the boreholes where geophysical tests had been carried out. It was suggested that a PVC pipe should be installed at each borehole head, closed with a screw-cap. Closing the geophysical borehole located close to piezometer PZB 13-2 with a pressure gauge at its head would allow confirmation that there is a seepage path linking the two holes, as the water pressure in both boreholes would be the same. After confirming the existence of this seepage path, it would only be necessary to measure water pressures in the piezometers. EDIA closed the boreholes with wooden plugs.

Both the position and direction of the main discontinuities can be analysed taking a 3D imprint, with the aid of a thin sheet of soft rubber wrapped around the inflatable element of the packer, fitted with special rubber cement. Once the packer is inflated inside the hole, this soft rubber cover is able to take 360° imprints of the inside wall, which can be examined at the surface. Although a roll of rubber sheet was available, it was not used in the tests carried out within this study as experiments carried out in LNEC's laboratory led to the conclusion that it would be impossible to identify discontinuities with very small apertures, such as those in the foundation area being studied.

4.6 Summary and conclusions drawn from tests carried out *in situ*

The testing programme was undertaken to obtain knowledge of seepage patterns underneath concrete dams. From the tests carried out in both Pedrógão and Alqueva dam it was not only possible to draw some conclusions about the depth at which the seepage paths cross each one of the tested boreholes, about the distribution of discharges and water pressures along the boreholes, and about seepage paths linking various boreholes, but also to verify previously defined test procedures and detect some faults in the monitoring plan definition. Results analysis showed that tests are better carried out with both single and double packers, as the two sets of results provide different and additional information. Test results, analysed in conjunction with other available information, such as site geological and geotechnical data and results of water electrical conductivity analyses, are very useful to better define the complex flow system in specific zones of the foundations of operating dams. The simultaneous analysis of water pressures and discharges at each test interval can give information about the aperture of the discontinuities through which water flows.

Tests carried out in Pedrógão dam foundation showed that seepage velocities are very high and that both boreholes tested were crossed by seepage paths in an area close to the concrete/rock mass interface. Both boreholes tested are relevant regarding water pressure

relief but this decrease in water pressures is achieved with a high increase in discharges. On the contrary, in Alqueva dam foundation seepage velocity is very low, which leads to clogging of drilled boreholes and, possibly of the foundation discontinuities. Tests provided an indication of the seepage pattern, showing that water flows into the majority of the boreholes in an area close to the concrete/rock mass interface and that the drainage boreholes are linked through conductive discontinuities in a relatively large area. The high percentage of hydraulic head recorded in one of the tested drains was localised and therefore not significant regarding the safety of the dam even if it were closed or clogged.

As noted throughout this chapter, there are situations in which borehole water-inflow tests cannot be carried out, for example in boreholes filled with coarse sand or where geodrains have been installed.

Great attention was paid to detect any test feature which could be improved and slight but effective changes were gradually introduced. A further improvement would be to introduce an automatic data collection system as in fact, during tests, water pressures displayed at the recording device were written by hand on test data sheets at pre-established time intervals. More detailed and accurate information on variations in water pressures during tests could be easily obtained via a data logger linked to a laptop.

Water-inflow test procedures were defined so as to obtain as much information as possible. However, these procedures can be simplified, depending on the information required. In the tests presented here, time was allowed in each test step to reach steady state conditions. If only approximate water pressures and discharges in each test interval were sufficient, readings could have been taken in transient conditions, which would significantly decrease the time taken to carry out tests. In this way, a large area of the foundation could be analysed in a relatively short period of time. Water electrical conductivity analysis proved to be a quick and accurate way to obtain information about the depth at which seepage paths cross the boreholes and therefore it can be used to identify these areas in the majority of the Portuguese concrete dams, in which discharges are usually low.

Although some recent methods have shown increasing possibilities to assist with assessment of seepage conditions, such as infrared imaging and methods which correlate seepage with magnetic fields or with subsurface temperature, they are not yet routinely used. The tests presented in this chapter supplement the usual seepage information available from drains and piezometers and could in future be used in other dams, as they allow the assessment of seepage patterns underneath the dam. At a given dam, the use of borehole water-inflow tests and water electrical conductivity analysis with the reservoir at different levels, will probably allow the detection of changes in seepage paths due to changes in loads. The knowledge obtained is relevant regarding the identification of possible failure modes and therefore helps

in the development of an appropriate monitoring programme, which indirectly contributes to a greater safety assessment of the dam.

5 Numerical modelling of seepage in concrete dam foundations

5.1 Introduction

The performance and safety assessment of concrete dams, which have their foundations on rock masses, are based on the analysis of monitoring data and their comparison with numerical results. To study the dam foundation hydraulic behaviour and ensure reliable predictions of total discharges and hydraulic heads it is not only necessary to take into account the complexity of the rock mass, but also to model both the grout curtain and the drainage system properly. The grout curtain is usually modelled assuming an area of lower hydraulic conductivity. The drain can be modelled by its axis, but the choice of mesh size in the vicinity of the drain must be carefully analysed. Modelling each one of the drains in 3D models of dam foundations leads to excessively fine meshes, which are very difficult to use. Whenever possible, 2D models of dam foundation vertical sections are used. In these models, the modelling of the drainage curtain is equivalent to a hypothetical trench in the perpendicular direction of the section being studied.

Analysis presented in this chapter is based on the assumption of an equivalent continuum. The performance of the FLAC model in hydraulic analysis was first assessed. For this, two simple flow cases were studied: i) steady state seepage flow towards a single drain through a confined aquifer; and ii) steady state seepage flow through a horizontal plane in a dam foundation (2D horizontal plane model). For both cases, analysed with FLAC 4.0 (Itasca 2002), the numerical results were compared with analytical solutions, in terms of discharges and heads. Two-dimensional numerical simulations were performed with various grids, so as to study the influence of the mesh size. The representation of the drain by its actual geometry or, in a simplified manner, by its axis was also examined. Three-dimensional analysis of seepage was afterwards carried out with 3DEC (Itasca 2003). The performance of both FLAC and 3DEC codes was compared using the second above-mentioned flow case. Finally, to assess and check the performance of the code 3DEC in unconfined steady state flow analysis, i.e. flows bounded above by a phreatic surface, the steady state flow in a homogeneous, isotropic and continuum media between two reservoirs was numerically analysed.

The dimensions of Alqueva dam were taken as reference and a 3D numerical model of a vertical slice of the foundation below the central cantilever was developed. This model was used to study the influence of drainage, of boundary conditions, of grout curtain permeability, of model size and of mesh size. The same model was used to compare the results of a 3D model with those obtained both with an equivalent 2D vertical model and with the 2D horizontal plane model.

5.2 Validation tests of the codes FLAC and 3DEC

5.2.1 Radial flow to a single well

The analysis of flow to a single well can often be solved by analytical methods. This analysis is particularly important as the study to multiple wells and many problems involving complicated boundary conditions can be solved by superposition of solutions for single well problems (USACE 1993), using a linear combination of basic solutions, in order to satisfy boundary conditions.

5.2.1.1 Analytical solution

The solution of the steady state seepage flow towards a single well through a confined aquifer, in a homogeneous and isotropic media (Figure 5.1), can be obtained by integrating Darcy's law or the one-dimensional Laplace equation (Bear 1988; Muskat 1946) and is written as:

$$H - h = \frac{Q}{2 \pi T} \ln \left(\frac{R}{r} \right) \quad (5.1)$$

In the previous equation:

$$T = k_H D = k g \rho_w D \quad (5.2)$$

where T = transmissivity of aquifer (m^2/s); k_H = hydraulic conductivity (m/s); k = permeability ($(\text{m}^3 \text{ s})/\text{kg}$); g = acceleration due to gravity (m/s^2); ρ_w = water density (kg/m^3); and D = aquifer thickness (m). In Equation 5.1, H = total head at the outer boundary (m); h = total head at well (m); Q = constant discharge from well (m^3/s); R = radius of influence, or radius beyond which the well has no influence (m); and r = radius of the well (m).

5.2.1.2 Geometry and boundary conditions

The steady state seepage flow towards a cylindrical drain was numerically analysed. A drain diameter of 0.076 m was assumed, which is the usual dimension of the drainage boreholes. The radius of influence is 10 m (model boundary is at 10 m from the hole centre), and a layer of 0.5 m is considered. The hydraulic conductivity is 2.0×10^{-7} m/s, the total head at the outer boundary is 100 m and at the drain is 50 m. The initial hydraulic head of the domain is 50 m. Taking into account Equation 5.1, the discharge from the drain is 5.6374×10^{-6} m^3/s .

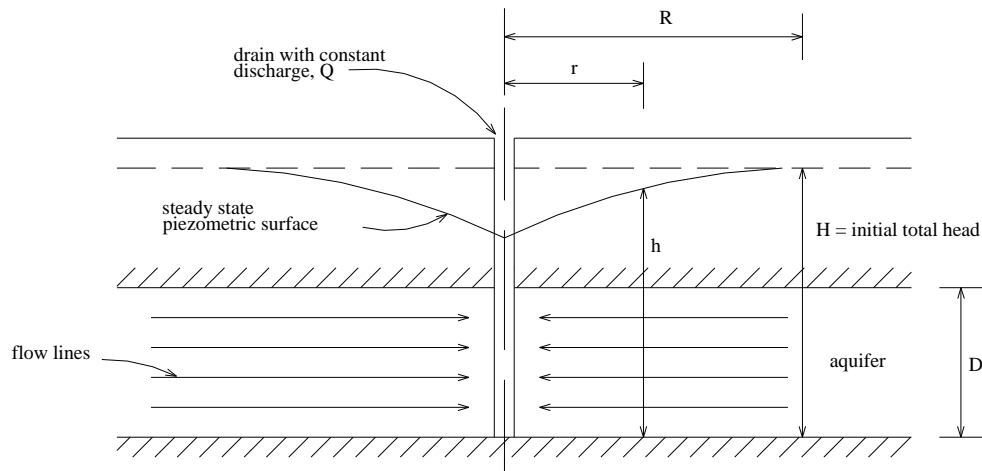


Figure 5.1 – Radial flow in a horizontal aquifer confined between impervious strata (artesian flow) (adapted from USACE 1993).

5.2.1.3 Axisymmetric model

Analysis was carried out with an axisymmetric model with the axis of symmetry along the axis of the hole. To study the differences in the results when the diameter of the hole is and is not considered, numerical analysis was carried out taking into account the diameter of the hole (left boundary at $x = 0.038$ m) or modelling the drain by its axis (diameter null and left boundary aligned with the hole axis). The model is 10 m wide by 0.5 m high. The axis of the hole is aligned with the left boundary of the domain, where $x = 0$ m.

To evaluate the effect of mesh size in the vicinity of the drain on solution accuracy different grids were considered: in the direction of the hole axis (y) grids contain just one row of elements, with a width of 0.5 m; in the radial direction (x) grids with 10, 31, 50, 75 and 100 elements are considered, spaced uniformly within the domain or spaced in a way that the element size increases according to a geometric ratio between successive element sizes (FLAC optional *ratio* keyword).

Figure 5.2 shows some of the meshes used. The numerical values of the discharges in some numerical analyses and their difference, in percentage, to the analytical solution are shown in Table 5.1. For eight of the cases studied, Figure 5.3 shows the piezometric heads in the radial direction, obtained by the numerical and analytical approaches. Figure 5.4 shows the difference between numerical discharge and the analytical solution with an increase in the number of mesh elements when the drain is modelled by its diameter.

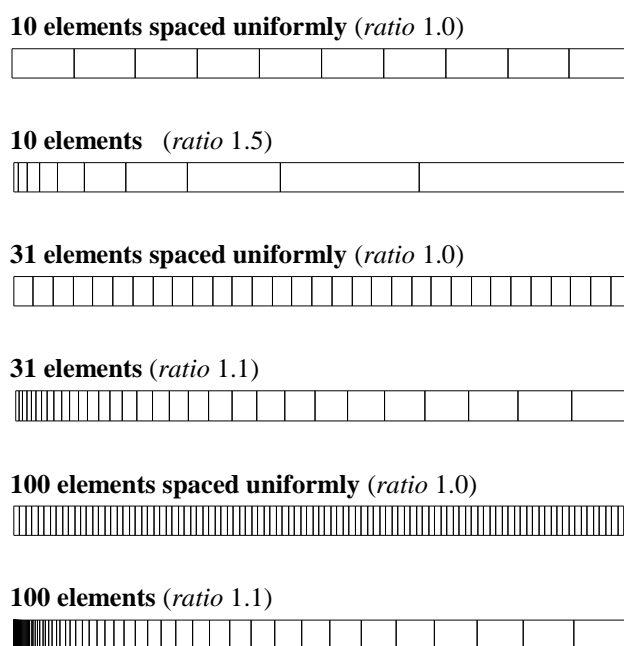


Figure 5.2 – Meshes adopted for numerical analysis with FLAC (axisymmetric model).

	Number of elements	Geometric ratio between successive element sizes in the x direction	Dimension of the first element in the x direction (m)	Discharge in the drain ($\times 10^{-6} \text{ m}^3/\text{s}$)		Difference to the analytical solution (%) ($5.6374 \times 10^{-6} \text{ m}^3/\text{s}$)	
				Precision		Precision	
				single	double	single	double
Drain modelled with diameter	10	1.0	0.996	7.6745	7.6746	36.1	36.1
		1.2	0.384	6.5716	6.5718	16.6	16.6
		1.5	0.088	5.8679	5.8682	4.1	4.1
	31	1.0	0.321	6.3932	6.3935	13.4	13.4
		1.1	0.055	5.7161	5.7166	1.4	1.4
		1.2	0.007	5.6513	5.6526	0.25	0.27
100	1.0	0.100	5.8156	5.8176	3.16	3.20	
	1.1	0.0001	5.5882	5.6406	-0.87	0.06	
	1.2	2.4×10^{-8}	*	5.6488	-	0.20	
Drain modelled by its axis	10	1.0	1.0		7.3634		30.6
		1.2	0.385		6.0493		7.3
		1.5	0.088		4.7632		-15.5
	31	1.0	0.323		5.8204		3.25
		1.1	0.060		4.3921		-22.1
	100	1.0	0.1		2.2802		-40.4

* it is not possible to calculate drain discharge with the single precision version of FLAC.

Table 5.1 – Axisymmetric model. Numerical discharges and comparison with the analytical solution.

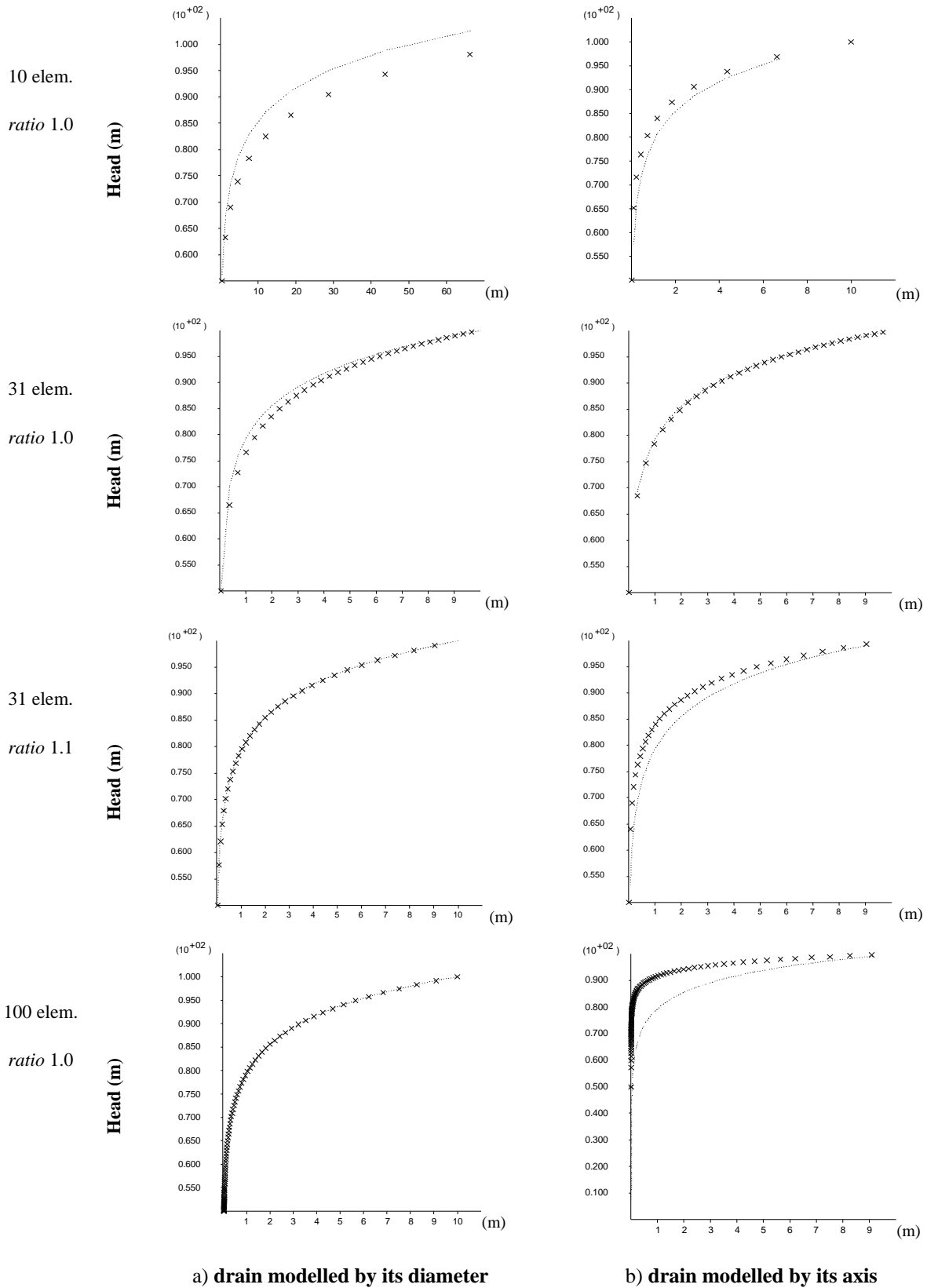


Figure 5.3 – Piezometric heads in the radial direction. Numerical values (×) compared to the analytical solution (.....).

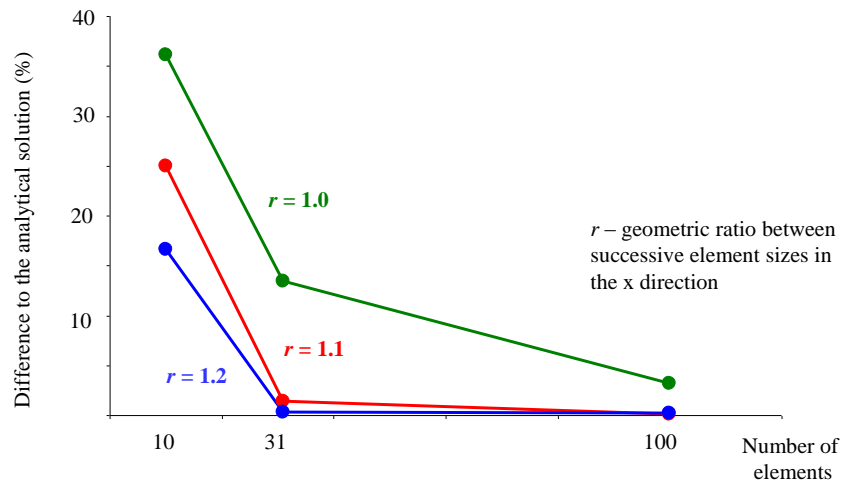


Figure 5.4 – Drain modelled by its diameter. Difference between numerical discharge and the analytical solution with an increase in the number of mesh elements.

5.2.1.4 Results analysis

The results presented show that:

1. If the diameter of the hole is taken into account, the finer the mesh in the vicinity of the drain the better the comparison between FLAC results and the analytical solution (both in drain discharges and in hydraulic heads). However, accurate results are obtained if the dimension of the first element near the hole is close to the drain radius (for example, grid with 31 elements and ratio 1.1).
2. In some of the cases studied the error when the drain is modelled by its axis is smaller than when the drain hole is considered (10 elements and ratio 1.2 or 31 elements spaced uniformly). This difference in the error is due to the fact that, in this model, the numerical result converges to the analytical solution by superior values, which means that the permeability of the numerical model is greater than the real one. When the drain is modelled by its axis and the hole is not considered, the permeability of the domain is reduced, so the error of modelling the drain by its axis compensates the error of considering a permeability value greater than the real one.
3. If the drain is modelled by its axis, finer meshes in the vicinity of the drain lead to the solution of flow towards a drain with an infinitesimal diameter. Figure 5.3 shows that when a grid with 31 elements is considered, the numerical values of piezometric heads are closer to the analytical values when the elements are spaced uniformly than when a finer mesh in the vicinity of the drain is considered (ratio 1.1). In order to determine the most suitable dimension of the element close to the drain, a series of numerical experiments was carried out that lead to the conclusion that it must be greater than 0.27 m (slightly greater than three times the diameter of the hole).

From the study carried out the conclusion was drawn that numerical errors occur when the dimension of the first element close to the drain is less than 0.0001 mm and the analyses are run with the single-precision version of FLAC. The double-precision version solves this problem.

5.2.1.5 Influence of the radius beyond which the drain has no influence

To check if a different radius of influence would alter the most suitable dimension of the element close to the drain, new numerical analysis was carried out modelling the drain by its axis and using $R = 100$ m. In this case, with the same permeability and boundary conditions as used previously, drain discharge is 3.9892×10^{-6} m³/s. Table 5.2 shows the numerical discharges and the difference, in percentage, to the analytical solution. Table 5.3 summarizes the results obtained with the domain divided into 10 and into 31 elements, in which it can be verified that the most suitable dimension of the first element close to the drain is independent of the radius of influence.

5.2.1.6 Influence of the drain diameter

Finally, to check the influence of the drain diameter, new numerical analysis was carried out modelling the drain by its axis and using drain diameters 2 and 10 times greater than the usual dimension of the drainage boreholes ($\phi_1 = 0.152$ m and $\phi_2 = 0.76$ m). In these cases, with $R = 100$ m and the permeability and boundary conditions previously used, drain discharge is 4.3741×10^{-6} m³/s and 5.6374×10^{-6} m³/s, respectively. Table 5.4 and Table 5.5 show, for each diameter and for meshes with 10 and 31 elements, calculated discharges and their difference, in percentage, to the analytical solutions, and Table 5.6 shows the ratio between the most suitable dimension of the element close to the drain and the drain diameter. Results show that whatever the drain diameter the most suitable dimension is equal to around 3.5 times the drain diameter. In coarser meshes ($R = 100$ m and $\phi = 0.152$ m) the ratio is slightly lower, around 3.1.

	Number of elements	Geometric ratio between successive element sizes in the x direction	Dimension of the first element in the x direction (m)	Discharge in the drain ($\times 10^{-6} \text{ m}^3/\text{s}$)	Difference to the analytical solution (%)
					($3.98915 \times 10^{-6} \text{ m}^3/\text{s}$)
Drain modelled by its axis	10	1.2	3.852	6.0493	51.6
		1.28	2.591	5.6353	41.3
		1.6	0.551	4.4666	12.0
		1.8	0.225	4.0025	0.33
		1.8065	0.2185	3.9897	0.01
	31	1.0	3.226	5.8204	45.9
		1.1	0.55	4.3921	10.1
		1.136	0.2662	3.9916	0.06
		1.13624	0.2649	3.9891	0.00
	100	1.0	1.0	4.7827	19.9
		1.02	0.3203	4.0774	2.2
		1.02265	0.2699	3.9891	0.00
	300	1.0	0.333	4.0974	2.71
		1.0013	0.2728	3.9930	0.1
1.00135		0.2706	3.9890	0.0	

Table 5.2 – Drain modelled by its axis ($R = 100 \text{ m}$). Numerical discharges and comparison to the analytical solution.

Radius of influence (m)	Mesh			
	10 elements		31 elements	
	Geometric ratio between successive element sizes in the x direction	Dimension of the first element in the x direction (m)	Geometric ratio between successive element sizes in the x direction	Dimension of the first element in the x direction (m)
10	1.2795	0.2598	1.0115	0.270
100	1.8065	0.2185	1.1362	0.2649

Table 5.3 – Drain modelled by its axis. Most suitable dimension of the element close to the drain, in order to obtain a drain discharge as close as possible to the analytical solution.

	Number of elements	Geometric ratio between successive element sizes in the x direction	Dimension of the first element in the x direction (m)	Discharge in the drain ($\times 10^{-6} \text{ m}^3/\text{s}$)	Difference to the analytical solution (%)
					($4.37414 \times 10^{-6} \text{ m}^3/\text{s}$)
Drain modelled by its axis	10	1.2	3.852	6.0493	38.3
		1.6	0.551	4.4666	2.1
		1.63	0.4795	4.3870	0.3
		1.635	0.4686	4.3742	0.001
		1.63502	0.4685	4.3741	\approx 0.00
	31	1.1	0.55	4.3920	0.41
		1.101	0.5389	4.3801	0.14
		1.1015	0.5336	4.3741	\approx 0.00

Table 5.4 – Drain modelled by its axis ($R = 100 \text{ m}$). Numerical discharges and comparison to the analytical solution (drain diameter $\phi_1 = 2 \times 0.076 = 0.152 \text{ m}$).

	Number of elements	Geometric ratio between successive element sizes in the x direction	Dimension of the first element in the x direction (m)	Discharge in the drain ($\times 10^{-6} \text{ m}^3/\text{s}$)	Difference to the analytical solution (%) ($4.37414 \times 10^{-6} \text{ m}^3/\text{s}$)
Drain modelled by its axis	10	1.2	3.852	6.0493	7.31
		1.27	2.723	5.6838	0.82
		1.279	2.604	5.6401	0.05
		1.2795	2.598	5.6377	0.005
		1.27956	2.597	5.6374	≈ 0.00
	31	1.0	3.226	5.8204	3.25
		1.01	2.768	5.6609	0.42
		1.011	2.725	5.6451	0.14
		1.01146	2.705	5.6378	0.007
		1.01149	2.704	5.6374	≈ 0.00

Table 5.5 – Drain modelled by its axis ($R = 100 \text{ m}$). Numerical discharges and comparison to the analytical solution (drain diameter $\phi_2 = 10 \times 0.076 = 0.76 \text{ m}$).

	Borehole diameter ϕ (m)	Number of elements	Dimension of the first element in the x direction (m)	Ratio between the size of the first element close to the drain and the drain diameter
Drain modelled by its axis	$2 \times 0.076 = 0.152$	10	0.4685	3.1
		31	0.5336	3.5
	$10 \times 0.076 = 0.76$	10	2.597	3.4
		31	2.704	3.6

Table 5.6 – Drain modelled by its axis ($R = 100 \text{ m}$). Ratio between the most suitable dimension of the element close to the drain and the drain diameter.

5.2.2 Two-dimensional horizontal model of seepage in a concrete dam foundation

The two-dimensional horizontal model of seepage flow through a concrete dam foundation consists of a horizontal section in any plane of the foundation (concrete/rock mass interface or any other plane below the contact) in which the drainage curtain is represented and where the fluid boundary conditions are the heights of water above the considered plane, upstream and downstream of the dam, respectively.

In this model, in which the existence of the grout curtain is neglected, it is assumed that the flow takes place in a homogeneous and isotropic medium. To study the seepage flow through a horizontal plane in a dam foundation, the dimensions of Alqueva dam were taken into account. FLAC results were compared to the analytical solution (Andrade 1982).

5.2.2.1 Analytical solution

To study the seepage flow through the dam foundation a simplified numerical model was used in which it is assumed that an impervious dam rests on a finite, homogeneous, isotropic and pervious layer (Andrade 1982). In this model the fluid flow is horizontal and takes place from a vertical fissure that comes from the heel of the dam, where the reservoir pressure is assumed, towards a vertical fissure that comes from the toe of the dam, where the tailwater pressure is applied. It is assumed that both the vertical fissures and the drains reach the rock foundation's impervious base. Water flow obeys Darcy's law. Figure 5.5 shows the numerical model.

In this model a portion of the total discharge that flows into the domain from upstream (q_u) flows to the drains (q_{drain}) and the rest flows towards downstream (q_d):

$$q_u = q_{drain} + q_d \quad (5.3)$$

where,

$$q_u = k \frac{H_u - S_d}{d} y a \quad (5.4)$$

$$q_{drain} = k \lambda (S_d - P_d) y a \quad (5.5)$$

$$q_d = k \frac{S_d - H_d}{b} y a \quad (5.6)$$

The average value of the hydraulic head at the line of the drains is given by:

$$S_d = \frac{b d \lambda P_d + H_u b + H_d d}{b d \lambda + c} \quad (5.7)$$

In Figure 5.5 and in Equations 5.3-5.7, a = spacing between drains (m); b = distance from the drainage curtain to the toe of the dam (m); d = distance between the upstream face and the drainage curtain (m); P_d = pressure at the drain given by the distance from the drain head to the considered plane (m); λ = coefficient to correct the permeability in the line of drains; H_u and H_d = heights of the reservoir and of the tailwater above the considered plane, respectively; y = thickness of the pervious layer (m); and c = base width of the dam (m).

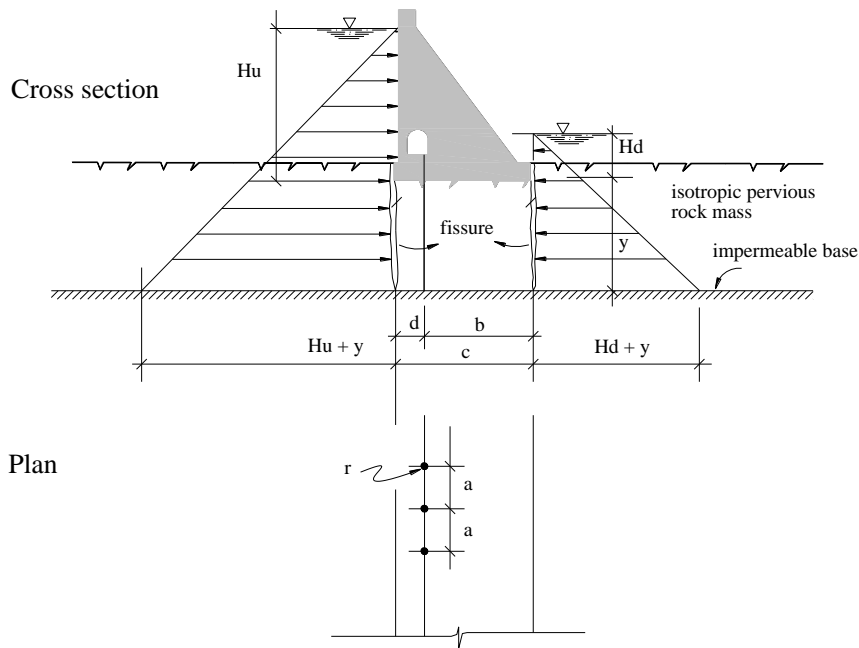


Figure 5.5 – Seepage in a dam foundation: numerical model (after Andrade 1982).

In a homogeneous and isotropic media, the value of λ , which represents the effect of the drainage curtain in the foundation, is a function of the spacing between drains (a) and of the drain perimeter (p) and is given by:

$$\lambda = \frac{2 \pi}{a \ln \frac{a}{p}} \quad (5.8)$$

In Equations 5.5 and 5.7, P_d is the pressure at the drain, usually assumed to be a function of the distance from the drain head to the plane in which seepage is being studied. In this case, it is assumed that the water pressure at the drain head is zero, which is suitable in the majority of cases as seepage velocity inside the drains is normally low. However, in rock masses with high permeability and dams in which the drains are inappropriate, the water pressure may be higher than that given by the drain head. On the contrary, it is also possible that the water inside the drain does not reach the drain head. Thus, when modelling seepage in the foundation of operating dams, the water pressure at the drainage line must be as close as possible to that monitored.

This model also enables the study of seepage in an anisotropic media, with different permeability in the plane of flow and in the perpendicular plane where the drainage system is located, using a different coefficient to correct the permeability in the line of drains. Seepage velocity close to and inside the drains, and water pressures, may also be calculated, taking into account discharges at the drainage line.

5.2.2.2 Geometry and boundary conditions

The steady state seepage flow through a horizontal plane in Alqueva dam foundation was analysed, at a plane 9.5 m below the dam/foundation interface, which is at level 58.0 m (Figure 5.6). The drains are assumed to be vertical and, as mentioned in the previous chapter, have 25.0 m of length, 0.076 m of diameter and are located 3.0 m apart. The reservoir level is 143.0 m and the tailwater level is 75.0 m. The drain head is at an elevation of 61.0 m. The hydraulic conductivity is assumed to be 2.0×10^{-7} m/s. The base width of the dam is 33.4 m and the distance between the upstream face and the drainage curtain is 7.5 m. Due to symmetry, the numerical model extends from drain centre to a distance half way between drains. Given the dimensions listed above, the model is 33.4 m wide by 1.5 m high .

For this particular problem, taking Figure 5.5 and Equations 5.3 to 5.8 into account, the value for S_d is 23.975 m and the values for the discharges, per metre of width of the model, are $q_u = 5.642 \times 10^{-6}$ m³/s; $q_{drain} = 5.7 \times 10^{-6}$ m³/s; and $q_d = -0.058 \times 10^{-6}$ m³/s (the negative value means that water flows from downstream towards the drain).

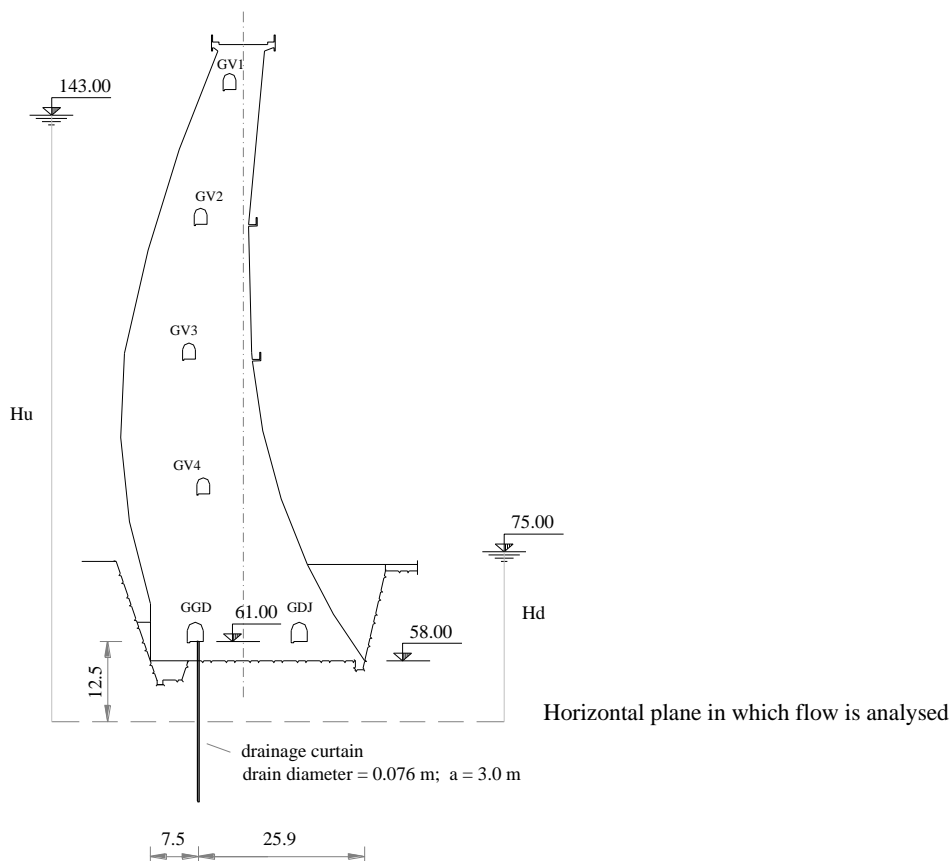


Figure 5.6 – Cross section of Alqueva dam central cantilever (assuming a vertical drainage curtain). Horizontal plane in which flow is analysed.

5.2.2.3 Results analysis

To assess the influence of modelling the drain by its axis, numerical analysis was also carried out taking into account the diameter of the hole. The complete mesh has 1500 (100×15) elements. In the first two mesh details shown in Figure 5.7 the dimension of the elements in the vicinity of the drain is, in both directions, about 0.05 m, i.e. slightly greater than the drain radius. A third mesh was considered in which the x-dimension of the elements close to the drain is about 0.027 m. As Figure 5.7 indicates, the meshes have increasing zone size away from the drain. The numerical values of the discharges and their difference, in percentage, to the analytical solution are shown in Table 5.7. Figure 5.8 shows, for the meshes that lead to more accurate results, the variations in hydraulic head along five lines.

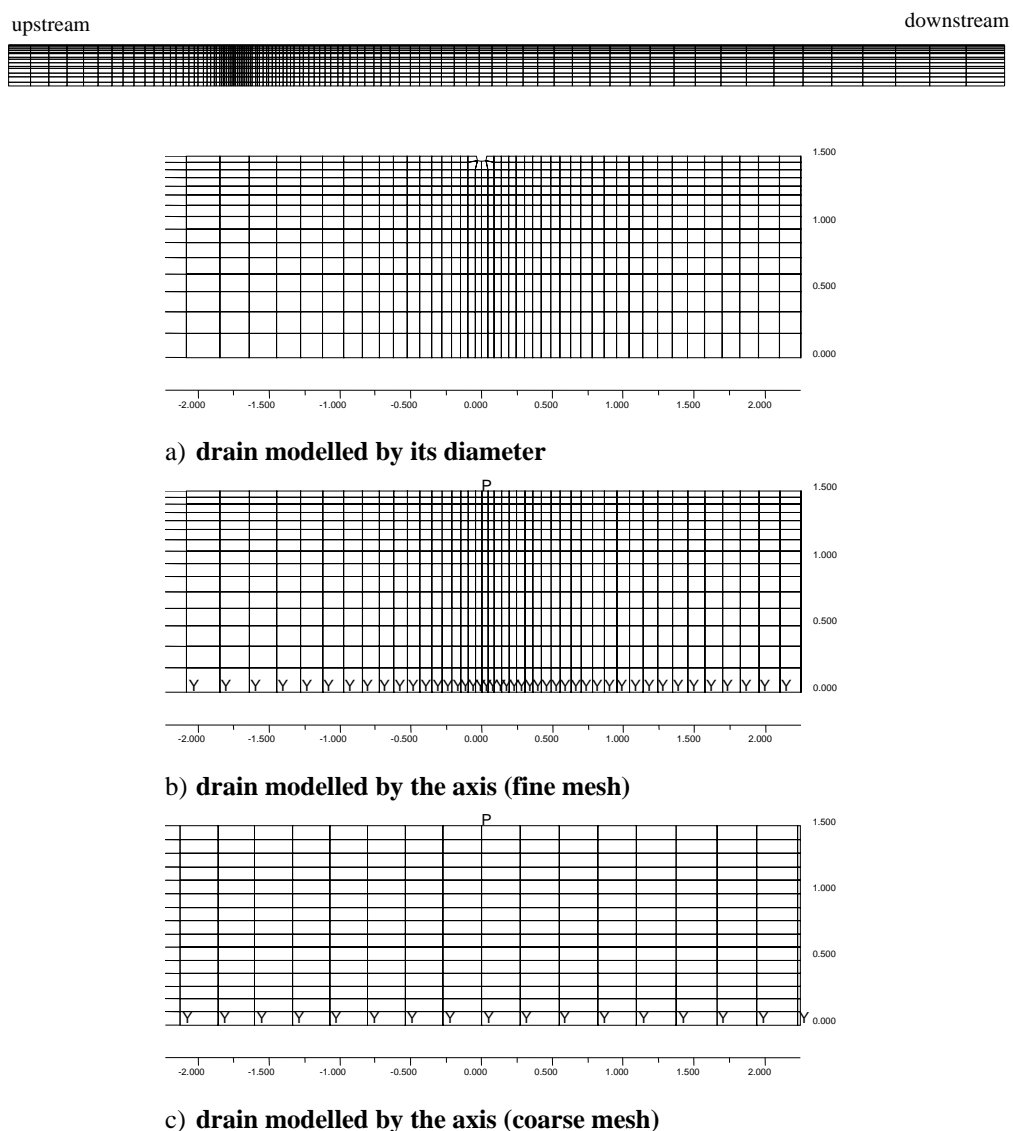


Figure 5.7 – Complete mesh and detail of meshes in the vicinity of the drain for numerical analysis of the horizontal plane flow problem.

Model	Average value of the hydraulic head in the line of drains (m)	Discharge ($\times 10^{-6}$ (m ³ /s)/m)		
		upstream	drain	downstream
a) Drain modelled by its diameter	23.33 (- 2.7%)	5.68 (0.6%)	5.74 (0.7%)	- 0.071 (22.2%)
b) Drain modelled by its axis	28.26 (17.9%)	5.26 (- 6.8)	5.19 (- 9.1%)	+ 0.047 *
c) Drain modelled by its axis (coarse mesh)	22.73 (- 5.2%)	5.66 (0.3%)	5.72 (0.4%)	- 0.064 (10.3%)
Analytical solution	23.98	5.64	5.70	- 0.058

* Water flows out of the model through the downstream boundary, in contrast to what happens with the analytical solution.

Table 5.7 – Two-dimensional horizontal model. *FLAC* results and comparison to analytical solution (error in brackets).

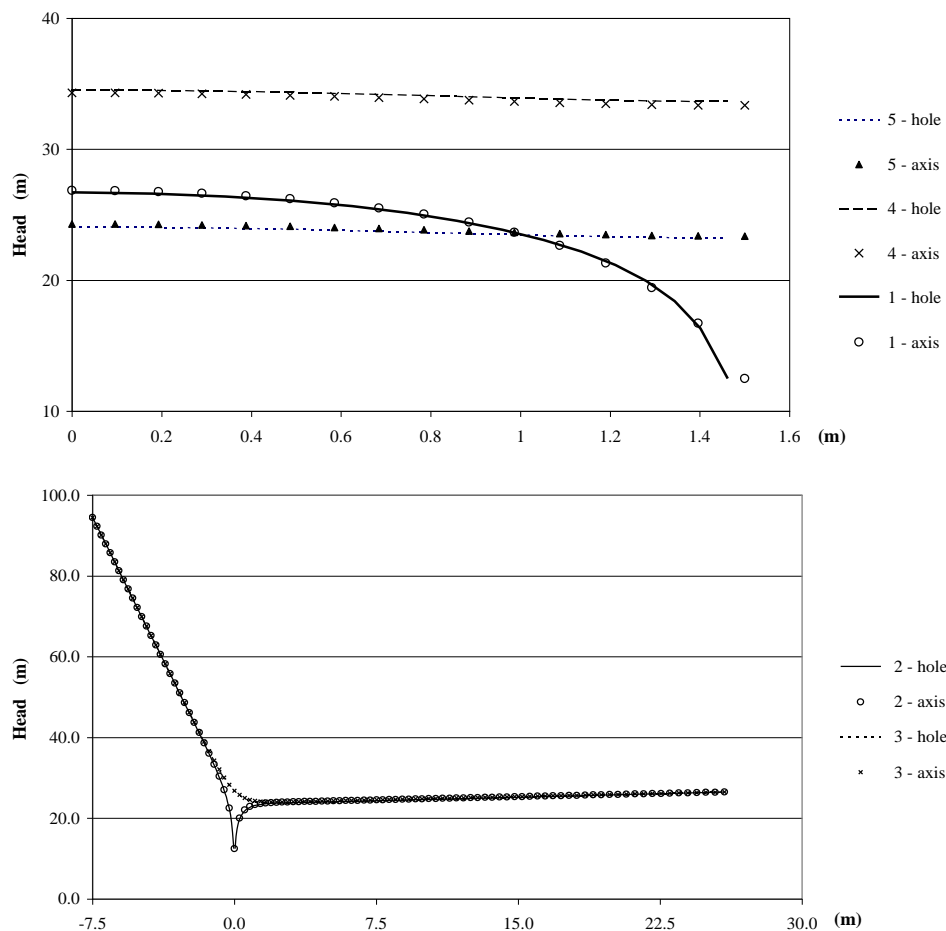


Figure 5.8 – Variations in the hydraulic head along five lines (meshes a) and c)): 1 – line of drains; 2 – line perpendicular to line of drains, that crosses one drain; 3 – line perpendicular to line of drains, midway between drains; 4 – line parallel to line of drains, about 1 m upstream; 5 – line parallel to line of drains, about 1 m downstream.

Comparison of discharges calculated with the first two meshes (Table 5.7) shows that when the drain is modelled by its axis the flow into the drain is 10 % lower than when the drain is modelled by its diameter. The third mesh, in which the drain is modelled by its axis and the dimension of the elements in the vicinity of the drain is around 0.27 m, leads to the discharges closest to the analytical solution. In comparison with the results obtained with the mesh in which the drain is modelled by its diameter, discharges obtained with this third mesh are closer to the analytical solution, but the average value of the hydraulic head in the line of drains is less accurate. As in the case of seepage flow towards a single drain, modelling the drain by its axis is feasible, but the mesh can not be too fine close to the drain. Elements close to the drain in the mesh shown in Figure 5.7 b) are too small, and therefore results are not accurate.

Numerical analysis was carried out with a fourth mesh in which the dimension of the elements in the vicinity of the drain is, in both directions, about 3.5 times the drain diameter and it was concluded that the size of the elements in the direction of the drainage line has almost no influence on numerical results.

Figure 5.8 shows that hydraulic heads obtained with the mesh shown in Figure 5.7 c) are very close to those obtained with the mesh in which the drain is modelled by its diameter (shown in Figure 5.7 a)).

If instead of a drainage curtain with drains with 0.076 m of diameter located 3.0 m apart, there is a hypothetical continuous trench with the same depth of the drains, the flow into this trench can be calculated using Equation 5.4, taking for S_d the value of the hydraulic head at the drain. For this problem the value of the discharge at the trench would be $6.56 \times 10^{-6} \text{ (m}^3\text{/s)/m}$, which is around 15 % higher than the flow into the drainage line. Therefore, when there is a drainage curtain with drains with a diameter of 0.076 m located 3.0 m apart, the quantity of water that flows into the drains is 87 % ($q_{\text{drain}}/q_{\text{trench}} = 0.87$) of that which would flow into a trench. If the drains are located 6.0 m apart, the total discharge at the drainage line is $9.005 \times 10^{-6} \text{ (m}^3\text{/s)/m}$. The total discharge at the trench would be twice that calculated with drains 3.0 m apart. Therefore, when the drains are located 6.0 m apart, the quantity of water that flows into the drains is 69 % of that which would flow into a trench.

Results here presented show that:

1. If the diameter of the hole is taken into account accurate results are obtained if the dimensions of the elements adjacent to the drain are close to the drain diameter.
2. For meshes of the same order, the flow into the drain when it is modelled by its axis is 10 % smaller than when the drain is modelled by its diameter.

3. Sensitivity studies determined that if the drain is modelled by its axis the dimension of the elements in the vicinity of the drain should not be lower than 0.27 m (confirms one of the conclusions drawn in section 5.2.1).
4. The total discharge at a drainage curtain, with drains with a diameter of 0.076 m located 3.0 m apart, is 87 % of the total discharge at a hypothetical trench with the same depth as the drains. This result is particularly important both in three-dimensional models, where it is not possible to model each one of the drains, and in 2D models of vertical cross sections of the dam foundation.

5.2.3 Seepage in a horizontal layer

The performance of 3DEC and FLAC was compared studying the steady state seepage flow in a horizontal layer of a dam foundation, using the 2D horizontal model of seepage presented in the previous section (section 5.2.2). With this model, a series of studies was carried out in which 2D and 3D numerical results, obtained with various meshes, were compared with the analytical solution (Andrade 1982). The 3D model is the same size as the 2D model previously presented, except for the width, and the same hydraulic properties and loads are assumed.

5.2.3.1 Influence of mesh size

In the 3D meshes analysed, with a width of 0.1 m, the domain is divided into three blocks and the drain is modelled by its axis. The influence of mesh size was studied with four different meshes, successively larger, called $m1$, $m2$, $m3$ and $m4$. In these meshes, the size of the edges of the tetrahedral zones increases gradually from the drain and in the radial direction from ec to ed , in a distance of 7.5 m to both the right and left hand side of the drain. In the remaining domain the average size of the tetrahedral edges is fixed, and is assumed to be, in each mesh, equal to ed . Figure 5.9 shows one of the meshes used in the 2D analysis and the division into blocks used in the 3D models, along with an internal mesh.

Table 5.8 shows the geometric characteristics of each mesh and the numerical discharges at the drain and in both the upstream and downstream boundaries. The same table shows the comparison with the analytical solution (as a percentage). Discharges are more accurate when mesh $m2$ is used, in which element edges close to the drain are around 20 cm. As meshes $m1$ and $m2$ lead to discharges lower than those obtained with the analytical solution and mesh $m3$ to higher discharges, the use of a mesh with $ed = 0.4$ and ec between 20 and 30 cm allows better results to be obtained. Results presented in Table 5.8 are consistent with the conclusions drawn so far regarding the representation of the drain: i) as the drain is being

modelled by its axis, the mesh must not be too fine close to the drain (as in mesh *m1*); and ii) for finer meshes it would be necessary to model the drain by its diameter.

a) 2D model



b) 3D model

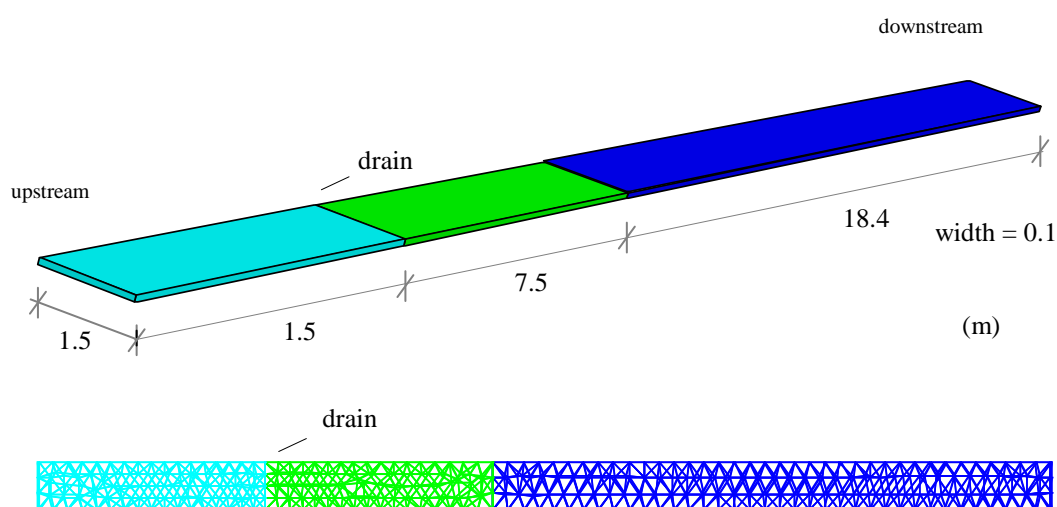


Figure 5.9 – Horizontal seepage flow: a) mesh used in the 2D model and b) schematic view of the domain in the 3D model (division into blocks and internal mesh).

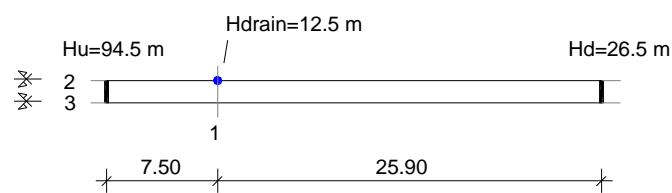
Mesh	Mesh geometric characteristics		Discharge ($\times 10^{-6}$ (m ³ /s))					
	<i>ec</i> (m)	<i>ed</i> (m)	upstream		drain		downstream	
<i>m1</i>	0.1	0.4	-5.3772	(-4.69%)	5.3452	(-6.22%)	0.0141	(75%)
<i>m2</i>	0.2	0.4	-5.6044	(-0.67%)	5.6314	(-1.22%)	-0.0567	(-2.29%)
<i>m3</i>	0.3	0.4	-5.7586	(2.07%)	5.8408	(2.47%)	-0.0965	(66%)
<i>m4</i>	0.4	0.5	-5.8834	(4.28%)	6.0038	(5.33%)	-0.1313	(126%)
Analytical solution			5.642		5.7		-0.058	

Table 5.8 – Geometric characteristics of the different 3D meshes. Calculated discharges and comparison with the analytical solution (in brackets).

5.2.3.2 Comparison between the results of 2D and 3D models

The simultaneous analysis of results from the 2D horizontal plane model (Table 5.7) and from the 3D model of flow through a horizontal layer (Table 5.8) shows that the 3DEC's mesh *m2* leads to the closest results both to the analytical solution and to the best results obtained with the FLAC's plane model, in the case in which the drain is modelled by its diameter.

The variation of the hydraulic head along 3 different lines is shown from Figure 5.10 to Figure 5.12.



- 1 – line of drains;
- 2 – line perpendicular to line of drains, that crosses one drain;
- 3 – line perpendicular to line of drains, midway between drains;

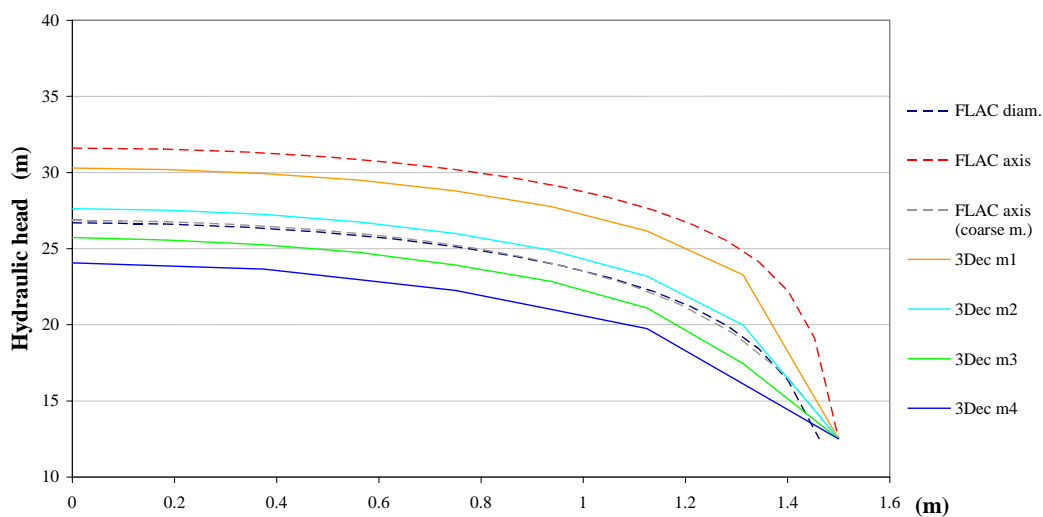


Figure 5.10 – Comparison between variations in the hydraulic head along the line of drains in the 2D and 3D models.

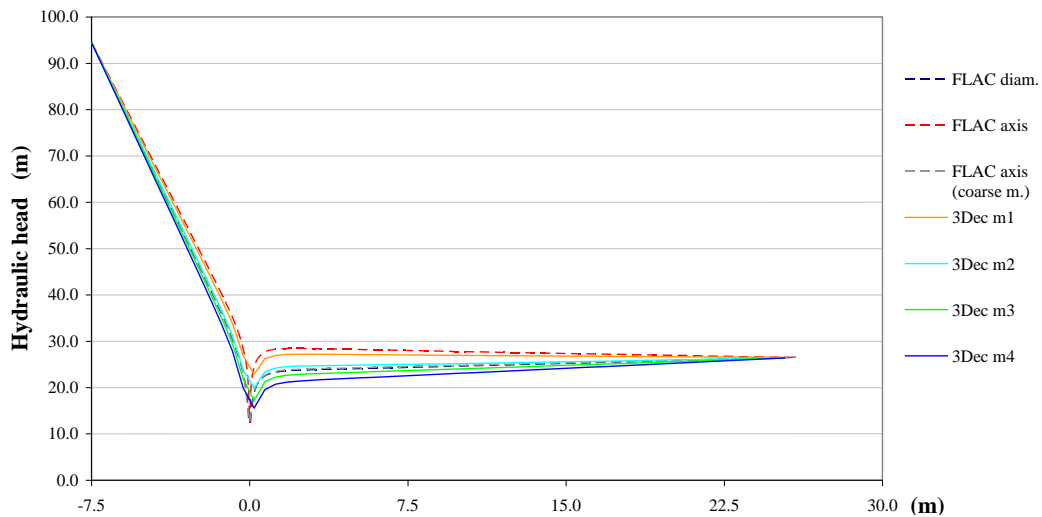


Figure 5.11 – Comparison between variations in the hydraulic head along the line perpendicular to the line of drains, which crosses one drain, in the 2D and 3D models.

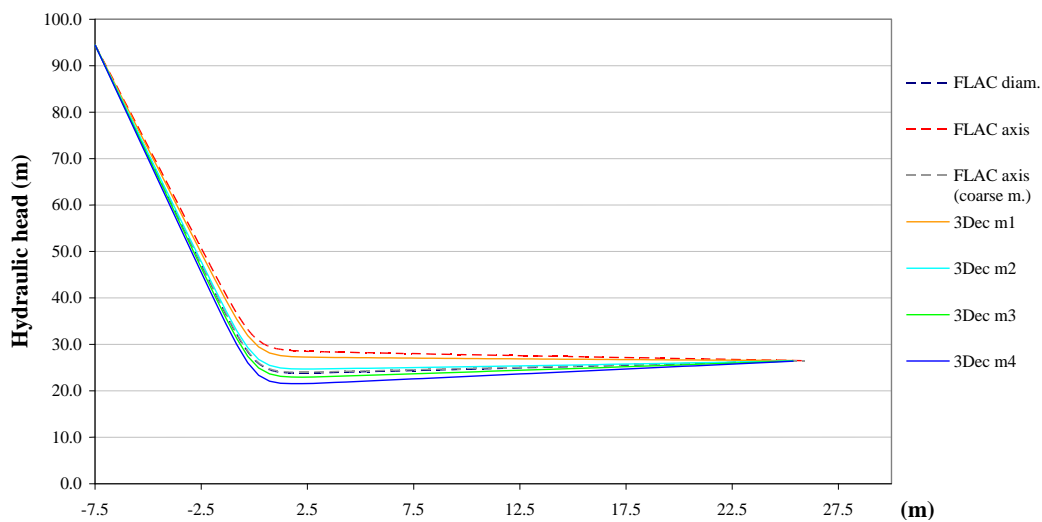


Figure 5.12 – Comparison between variations in the hydraulic head along the line perpendicular to the line of drains, midway between drains, in the 2D and 3D models.

The results presented in Table 5.7, in Table 5.8 and in Figure 5.10 to Figure 5.12 show that:

1. Discharges obtained with the 3D fine mesh *m1* are close to those obtained with the fine plane mesh in which the drain is modelled by its axis. However, both meshes are too fine and give results that are not close to the solution.
2. In the 3D model, if the mesh is enlarged and mesh *m2* instead of mesh *m1* is used, the discharge increases, which compensates for the error of not representing the drain by its diameter.

3. As the mesh is further enlarged (meshes $m3$ and $m4$) discharges increase and the hydraulic head along the different lines decreases. It is worth noting, however, that with mesh $m4$ the error is still small (around 5 %).
4. The solutions that lead to discharges closer to the analytical solution and to closer lines of variation in hydraulic head are obtained with the plane model in which the drain is represented by its diameter and with the 3D mesh $m2$.
5. Along the different lines it is observed that the model in which the hydraulic heads are further away from the analytical solution, by superior values, is the plane model with the drain modelled by its axis. The 3D model with the finer mesh $m1$, also leads to hydraulic heads higher than those obtained with the best solutions. It is worth noting that the drain is modelled by its axis to allow the use of a coarser mesh, in order to reduce run times, and therefore the problem of excessive mesh refinement is not likely to occur.

The study of steady state flow through a horizontal layer with 3D models leads to basically the same conclusions as those obtained in 2D analysis: in 3D models, as in 2D models, the most suitable size of the elements in the vicinity of the drain is about three times the drain diameter.

5.2.4 Unconfined steady state flow

To test 3DEC's formulation for unconfined groundwater steady state flows, i.e. flows bounded above by a phreatic surface, the problem of flow between two reservoirs through a continuous, homogeneous and isotropic medium was numerically analysed. Water enters and leaves the pervious medium through vertical boundaries.

It is very difficult to study flows in which one of the boundary conditions is the phreatic surface, not only because it is a nonlinear boundary condition, but also because the position of this boundary is, a priori, unknown (Bear 1988). However, to study unconfined flows Dupuit developed, and published in 1863, a theory based on a number of simplifying assumptions resulting from the observation that in most groundwater flows the slope of the phreatic surface is not very steep. Therefore, Dupuit assumed that in flows in phreatic aquifers: i) the hydraulic gradient is equal to the slope of the phreatic surface; ii) the flow is essentially horizontal; and iii) equipotential surfaces are vertical (Figure 5.13).

With the simplified assumptions established by Dupuit, it is possible to integrate the differential equation obtained from Darcy's law. Thus the Dupuit simplification leads to the specific discharge expressed by (known as the Dupuit-Forchheimer discharge formula):

$$Q = \frac{k_H}{2L} (H_1^2 - H_2^2) \quad (5.9)$$

where Q = discharge per model unit width ((m³/s)/m); k_H = hydraulic conductivity (m/s); L = distance between the two reservoirs (m); H_1 = highest hydraulic head (m); H_2 = lowest hydraulic head (m).

Although the shape of the phreatic surface is approximate, the discharge is the exact value (Bear 1988).

Analysis done with 3DEC allows the logic for flow inside a block divided into tetrahedral zones with free surface to be tested. A media with a permeability of 1×10^{-3} m/s was assumed, of which the boundaries are defined by a brick shape 4 m long (x), 2 m high (y) and 0.2 m wide (z), between two reservoirs with hydraulic heads of 2 m and 1 m, respectively. In this case, the total discharge is 7.5×10^{-5} m³/s. Meshes were automatically generated in two different ways: first, irregular meshes, from the average edge length of the tetrahedral-shaped zones, in which average edge lengths of 0.9 m, 0.4 m and 0.2 m were used; second, regular meshes only possible for brick elements, from the number of divisions along each axis, where 1 zone along z axis, 4 zones along y and 8 zones along x or 1 zone along z axis, 8 zones along y and 16 zones along x were used. In this second case the divisions create brick shape volumes which are internally divided into tetrahedra. For both cases numerical discharges were compared with the analytical solution. Analysis of Table 5.9 leads to the conclusion that the results are quite accurate. The slight difference between numerical discharges and the analytical solution are due to approximations involved in the simulation of the free surface.

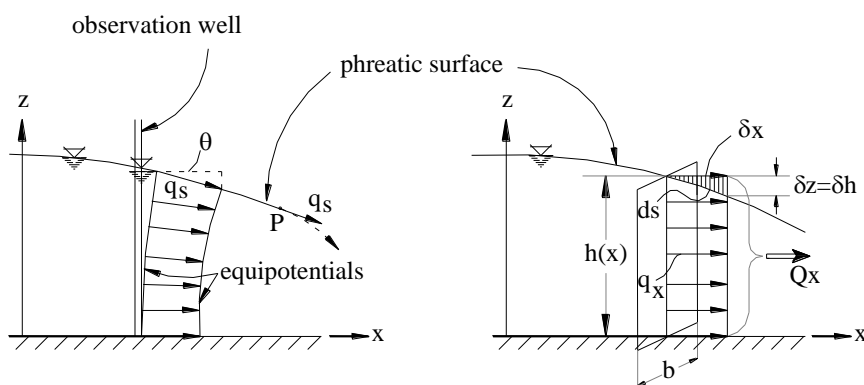


Figure 5.13 – The Dupuit assumptions. Unconfined steady state flow between two reservoirs (after Bear 1988).

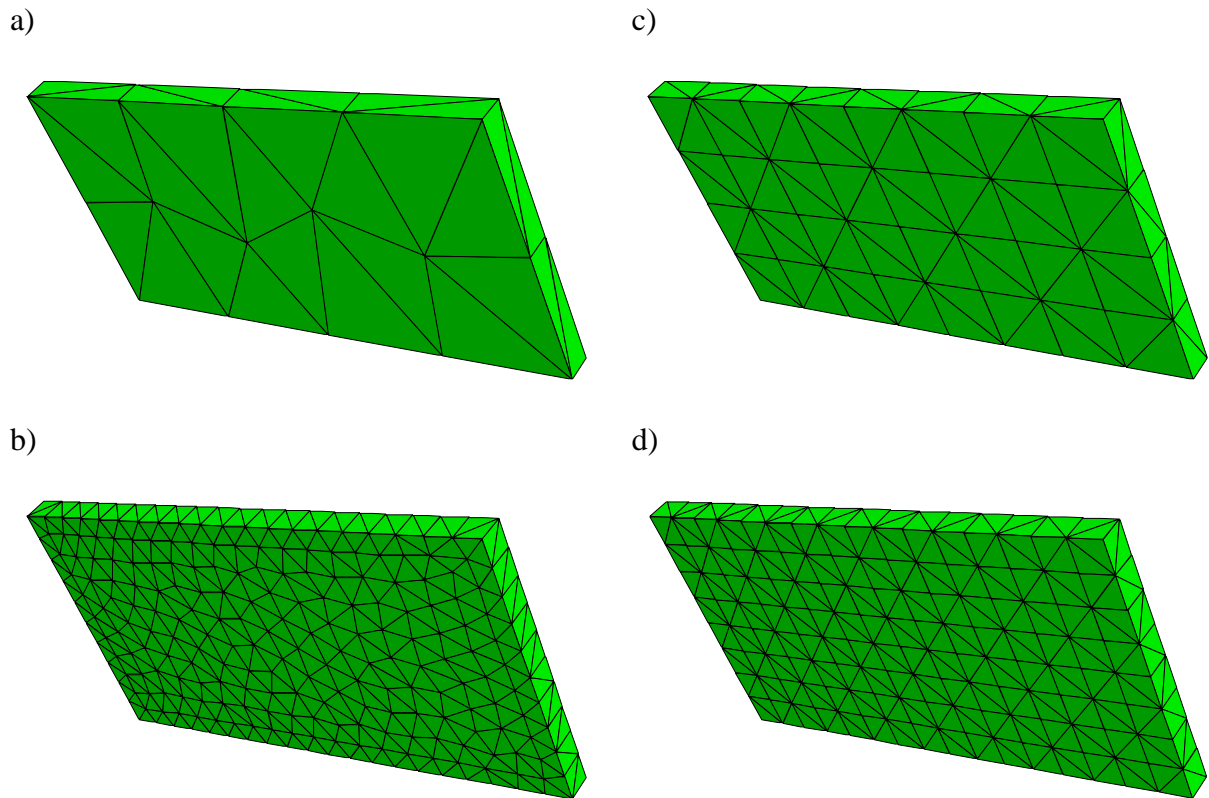


Figure 5.14 – Different meshes used in the analysis of unconfined steady state flow: a) and b) standard meshes generated from the average edge length of the tetrahedral-shaped zones; c) and d) regular meshes, generated from the number of divisions along each axis.

Model		Discharge ($\times 10^{-5} \text{ m}^3/\text{s}$)	Difference to the analytical solution (%)
Irregular mesh Average edge length of the tetrahedral zones	0.9 (Figure 5.14 a) (32 grid points, 59 zones)	7.57	0.933
	0.5 (90 grid points, 198 zones)	7.55	0.667
	0.2 (Figure 5.14 b) (462 grid points, 1245 zones)	7.49	-0.134
Regular mesh Number of zones along directions z, y and x	$1 \times 4 \times 8$ (Figure 5.14 c) (90 grid points, 160 zones)	7.62	1.6
	$1 \times 8 \times 16$ (Figure 5.14 d) (306 grid points, 640 zones)	7.55	0.667
Analytical solution		7.5	

Table 5.9 – Steady state unconfined flow between two reservoirs. Comparison between numerical discharges and analytical solution.

5.3 Three-dimensional hydraulic models of concrete dam foundations

5.3.1 Introduction

The 2D horizontal seepage model presented in section 5.2.2 does not take into account the effect of the grout curtain. Therefore, to study seepage flow in a concrete dam foundation, a 3D model is used in this section, in which both the grout and drainage curtains are simulated. In this first phase of analysis, flow is modelled in a foundation slice that extends from upstream from the dam towards downstream but whose width is only 1.5 m, which is half of the distance between drains. The influence of different factors such as drainage, boundary conditions, grout curtain permeability, model size and mesh size are analysed, and the results of a 3D model are compared with those obtained with a 2D model, using the same mesh and the same numerical code.

5.3.2 Model characteristics

The dimensions of Alqueva dam were used as reference and two 3D numerical models of part of the area of the foundation below the central cantilever were developed. A first model, called *small model*, has a width of around 60 m, a height of 50 m and, taking advantage of symmetry, a thickness of 1.5 m. The upper boundary of the model is at the same elevation as the dam/foundation interface (58.0 m). It was assumed that the grout curtain, which crosses the whole model width, is 1 m thick. The drain is modelled by its axis (diameter zero) and the drain is at the model boundary ($z = 1.5$ m). The model was divided into 8 blocks, internally divided into 68019 tetrahedra, with a total of 19330 grid points (Figure 5.15). The mesh is finer close to the drain and the relative position of the grout and drainage curtains is respected. The mesh was defined by the average edge length of the tetrahedral zones, which increases, radially and gradually, from 0.4 m to 0.8 m, from the upper point of the drain to the external boundary. The number of zones across the model's thickness decreases gradually from 4 to 1 from the drain area to the lower boundary. Figure 5.15 shows the position of the grout curtain and the drain, of which the depth is about half of the grout curtain's length and, in the mesh, ends at the horizontal joint. The same figure shows the blocks around the grout and drainage curtains, and the mesh which is automatically generated.

The above-mentioned model was used to develop a second, called *large model*, adding blocks upstream, downstream and downwards. This new domain, with $150.0 \times 78.0 \times 1.5$ m³ was divided into thirteen blocks, internally divided into 189076 tetrahedra, with a total of 49910 grid points (Figure 5.16). In these new blocks the average edge length of the tetrahedral zones is 1.0 m.

It is assumed that the rock mass foundation is homogeneous and isotropic with a permeability of 1.0×10^{-7} m/s. The grout curtain dips 20° towards upstream, is located about 7.0 m downstream from the upstream face and is 41 m long. The drainage curtain is located about 0.5 m downstream from the grout curtain and dips 5° towards upstream but it was assumed to be vertical, in order to simplify the model. The numerical analyses were carried out assuming the reservoir at an elevation of 143.0 m and the water downstream from the dam at an elevation of 75.0 m. A zero pressure was assumed at the drain head.

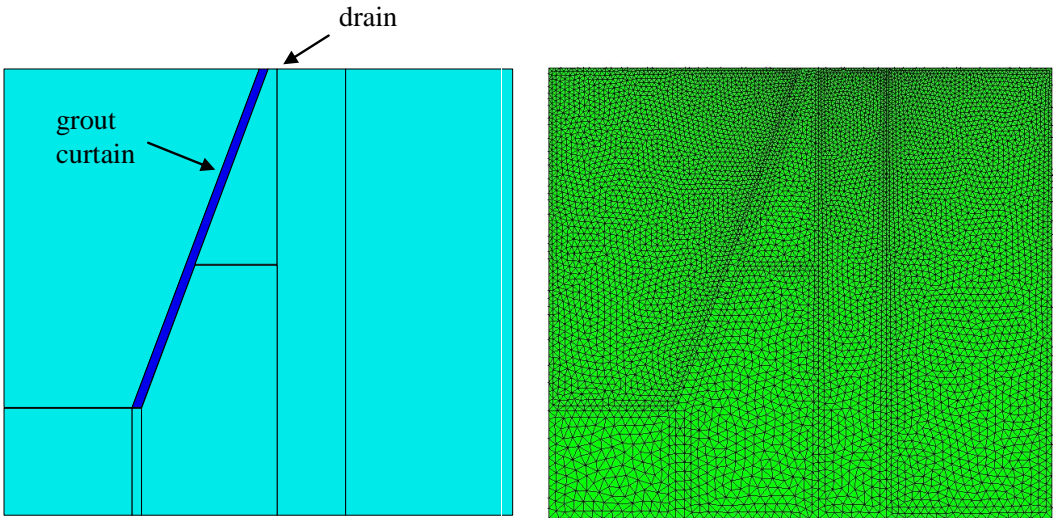


Figure 5.15 – 3D *small model*. Division into blocks and internal mesh.

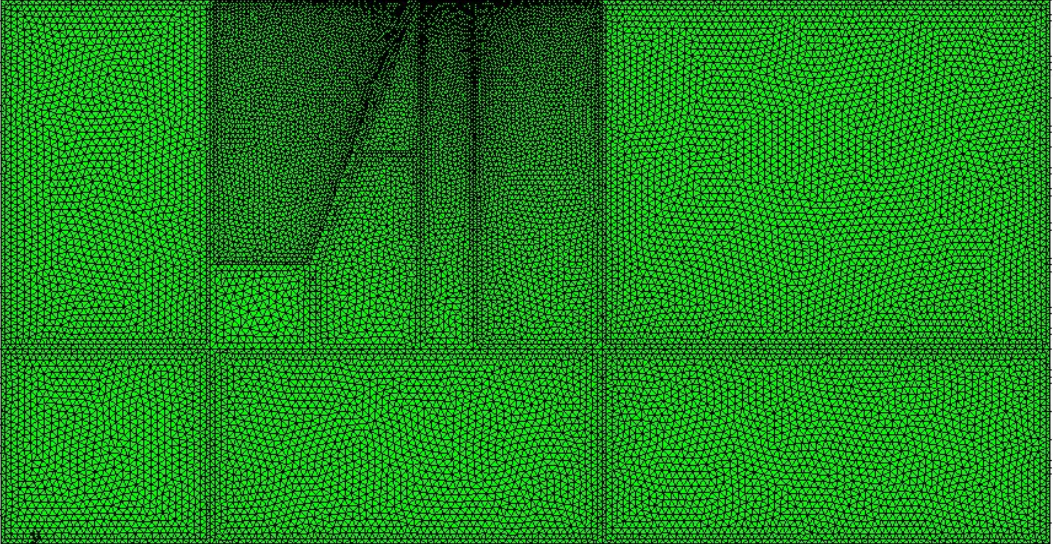


Figure 5.16 – 3D *large model*. Division into blocks and internal mesh.

5.3.3 Influence of grout curtain permeability in a foundation with no drainage system

The *small model* was used to carry out seepage analysis assuming the hydraulic head on the upstream and downstream lateral boundaries and considering that a grout curtain was installed in the dam foundation, but no drainage boreholes were drilled. Therefore, the water entering the model from the upstream boundary flows directly towards downstream. Table 5.10 shows the numerical discharges for different values of $k_{\text{grout curtain}}/k_{\text{rock mass}}$: i) the grout curtain with the same permeability as the rock mass (it simulates seepage in a foundation with no grout curtain); ii) grout curtain 10 times less pervious than the rock mass; iii) grout curtain 100 times less pervious than the rock mass; and iv) grout curtain 1000 times more impervious than the rock mass. The results of a run in which the grout curtain permeability was assumed to be zero and of another run in which the zones corresponding to the grout curtain were deleted are also shown.

The main aim of grouting is to reduce discharges and seepage velocity. Results in Table 5.10 show that, taking the situation without grout curtain as reference, the quantity of water that flows through the model decreases by about:

- 9 % if the grout curtain permeability is 1/10 of that of the rock mass;
- 36 % if the grout curtain permeability is 1/100 of that of the rock mass;
- 50 % if the grout curtain permeability is 1/1000 of that of the rock mass;
- 53 % if it is assumed that $k_{\text{grout curtain}} = 0.0$ or if the zones simulating the grout curtain are deleted.

$\frac{k_{\text{groutcurtain}}}{k_{\text{rock mass}}}$	Discharge ($\times 10^{-6} \text{ m}^3/\text{s}$)
1	9.1307
0.1	8.3203
0.01	5.8394
0.001	4.5093
0	4.2914
Without zones in the grout curtain's area	4.2923

Table 5.10 – Foundation with grout curtain but without drainage. Numerical discharges for different $k_{\text{grout curtain}}/k_{\text{rock mass}}$.

Results also show that to assume an impervious grout curtain it is sufficient to assume that the grout curtain is 1000 times less pervious than the surrounding rock mass. Numerical analysis shows that with 3DEC it is possible to simulate an impervious grout curtain, without computational problems, not only deleting the zones simulating the grout curtain but also assuming that its permeability is zero. The small difference between the results obtained in these two situations is due to a slight difference in a scaling parameter used by the 3DEC algorithm for steady state solutions.

In the 3DEC explicit algorithm, run time increases when the differences in the permeability of the different groups of elements are large, therefore it is not advisable to assume very low numbers for the grout curtain permeability. In practice, as it was concluded, a ratio of 1:1000 is enough. If a more impervious grout curtain is to be assumed, zero permeability should be considered, which avoids the zones simulating the grout curtain being included in seepage analysis.

5.3.4 Influence of drainage

The *small model* was used to carry out numerical analysis identical to that presented in the previous sub-chapter, assuming that the dam foundation not only has a grout curtain but also a drainage curtain. The drain is modelled by its axis, and the hydraulic head of the drain's head is assumed along the axis. Table 5.11 shows the numerical discharges for different $k_{\text{grout curtain}}/k_{\text{rock mass}}$.

Taking as reference the situation without drainage, the results of which are presented in the previous section, it can be seen that the quantity of water flowing into the model increases by around:

- 76 % if the grout curtain permeability is the same as the rock mass permeability;
- 64 % if the grout curtain permeability is 1/10 of that of the rock mass;
- 34 % if the grout curtain permeability is 1/100 of that of the rock mass;
- 22 % if the grout curtain permeability is 1/1000 of that of the rock mass;
- 20 % if it is assumed that the grout curtain is impervious.

Taking as reference the situation in which no grout curtain is considered, it can be seen that drain discharge decreases:

- by around 14.5 % if the grout curtain is 10 times less pervious than the surrounding rock mass;
- to about half (decreases 48.3 %) if the grout curtain is 100 times less pervious than the rock mass;

- by around 62 % to 64 % in the situations where an impervious grout curtain is assumed, namely, when it is assumed that the grout curtain is 1000 times less pervious than the rock mass, $k_{\text{grout curtain}} = 0.0$, or without zones in the grout curtain area.

Analysis of discharges flowing into or out of each gridpoint in the upstream and downstream boundaries and along the drain show that, in this model with both grout and drainage curtains, the water enters the domain from the upstream boundary, flows out of the model from the drain and, in the downstream boundary, enters the domain above a certain level, and flows out of the domain below that level. This level varies with $k_{\text{grout curtain}}/k_{\text{rock mass}}$: when the grout curtain permeability is the same as that of the rock mass, the above-mentioned elevation is 37.0 m; if $k_{\text{grout curtain}}/k_{\text{rock mass}} = 0.1$, the elevation is 36.0 m; if $k_{\text{grout curtain}}/k_{\text{rock mass}} = 0.01$, the elevation is 32.5 m; and in the remaining situations, it is 31.0 m.

The main aim of drainage is to reduce the hydraulic head. Figure 5.17 shows a comparison between the numerical hydraulic heads in a foundation with and without drainage, for different $k_{\text{grout curtain}}/k_{\text{rock mass}}$. The results without drainage correspond to those presented in the previous section. Figure analysis shows the significant reduction of the hydraulic head in the area below the concrete/rock mass interface.

$\frac{k_{\text{groutcurtain}}}{k_{\text{rockmass}}}$	Discharge ($\times 10^{-6} \text{ m}^3/\text{s}$)		
	upstream	drain	downstream
1	-16.123	15.044	1.0320
0.1	-13.659	12.870	0.7417
0.01	-7.8960	7.7783	0.0158
0.001	-5.5328	5.7445	-0.2685
0	-5.1940	5.4463	-0.3102
With no zones in the grout curtain's area	-5.1932	5.4465	-0.3102

Table 5.11 – Foundation with both grout and drainage curtains. Numerical discharges for different $k_{\text{grout curtain}}/k_{\text{rock mass}}$.

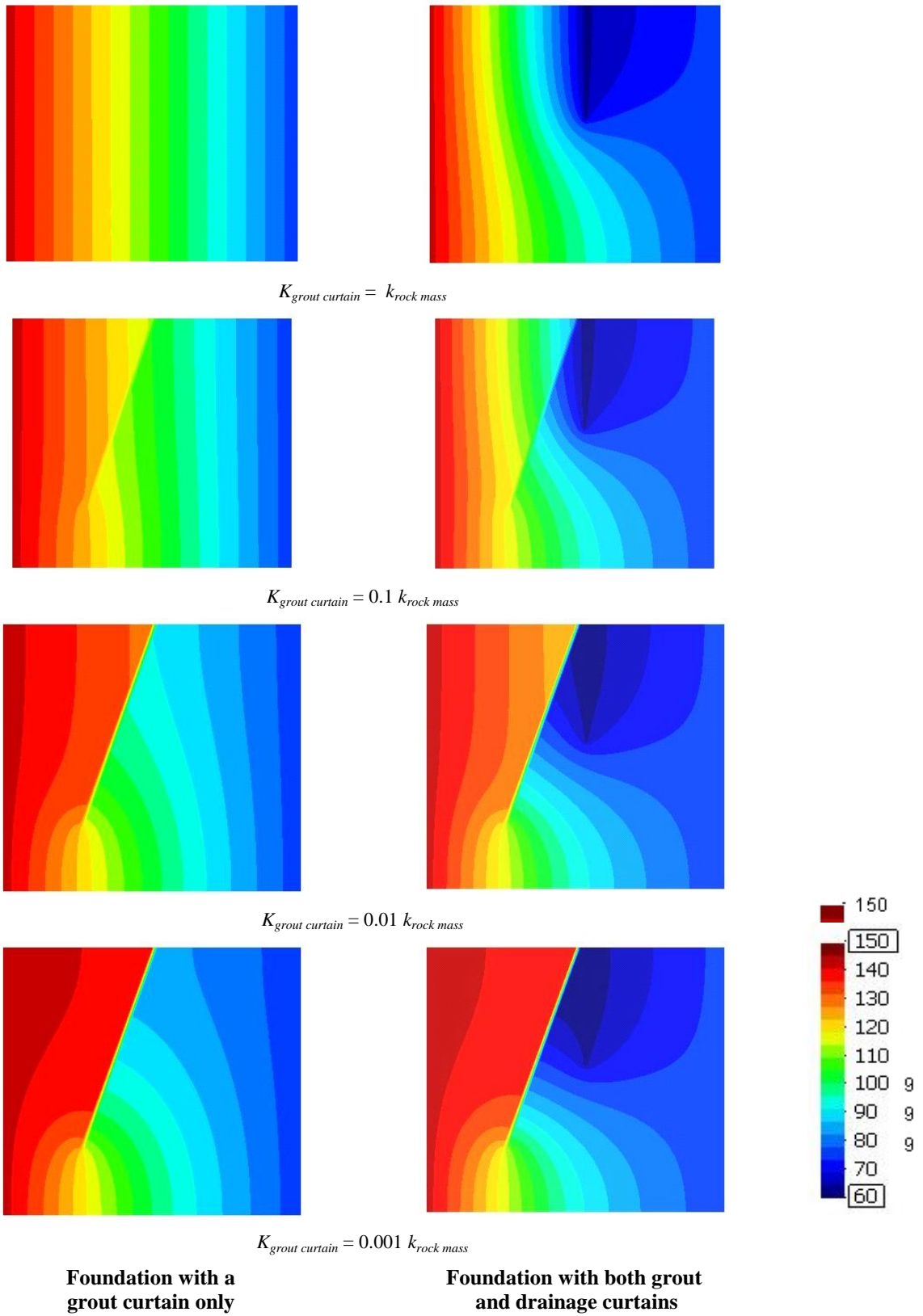


Figure 5.17 – *Small model*. Comparison of hydraulic head contours with & drainage.

5.3.5 Influence of boundary conditions

Small model

In the numerical analysis presented in the previous sub-chapters, the upstream and downstream hydraulic heads were assumed in the lateral boundaries, therefore it is assumed that water flows out of the model through the drain and flows into or out of the model through vertical boundaries that go down through the rock mass. To study the influence of boundary conditions, a different situation was analysed, still with the *small model*, in which it is assumed that the lateral and bottom boundaries are impervious, as well as the dam concrete/rock mass interface. In this case, water flows into and out of the domain, with the exception of the drain, through the rock mass surface, upstream and downstream from the dam, where the upstream and downstream hydraulic heads are assumed. Seepage close to an impervious boundary is parallel to that boundary. Figure 5.18 shows the two above-mentioned boundary conditions. Table 5.12 shows the numerical discharges in each situation, assuming different relationships between the grout curtain and rock mass permeability.

Table 5.12 shows that when the lateral and bottom boundaries and the dam/rock mass interface are assumed to be impervious (case b) in Figure 5.18), discharges flowing out of the drain, when $k_{\text{grout curtain}}/k_{\text{rock mass}}$ is 0.1, 0.01, and 0.001, are 87 %, 72 % and 66 %, respectively, of discharges determined when the hydraulic heads are assumed in the vertical boundaries upstream and downstream from the domain. Percentages of water flowing into the model from upstream, for each the above-mentioned situations are 80 %, 67 % and 59 %, respectively. Figure 5.19 shows the hydraulic head contours in each situation.

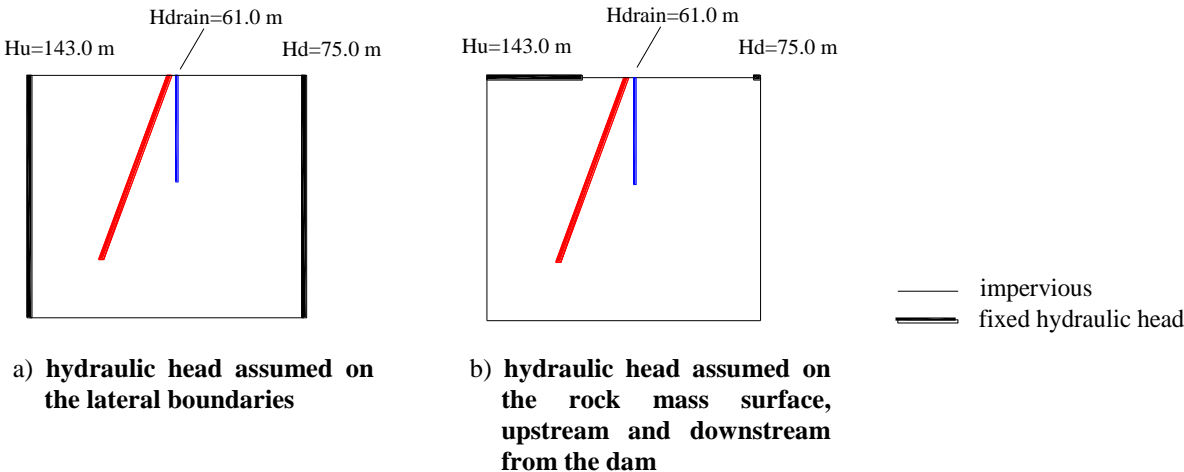


Figure 5.18 – *Small model*. Different boundary conditions.

Boundary condition: Assumed hydraulic head	$k_{groutcurtain}$	Discharge ($\times 10^{-6} \text{ m}^3/\text{s}$)		
	$k_{rockmass}$	upstream	drain	downstream
on the lateral boundaries, upstream and downstream	0.1	-13.659	12.870	0.7417
	0.01	-7.8960	7.7783	0.0158
	0.001	-5.5328	5.7445	-0.2685
on the rock surface, upstream and downstream	0.1	-10.928	11.201	-0.4663
	0.01	-5.3130	5.5840	-0.5505
	0.001	-3.2629	3.7868	-0.5710

Table 5.12 – *Small model*. Discharges for different boundary conditions and different relationships between the grout curtain and rock mass permeability.

Figure 5.20 shows the variations in the hydraulic head along nine 50 m long vertical lines, for each of the above-mentioned boundary conditions, when the grout curtain permeability is 10 times lower than that of the rock mass. The location of the vertical lines is shown underneath.

From the analysis of Figure 5.19 and Figure 5.20 it can be concluded that, when the hydraulic head is assumed on the upstream and downstream lateral boundaries, the variation of the hydraulic head along the vertical lines close to the drain (lines 1, 2, 3, 4 and 5) is about 30 m. This variation is independent of the grout curtain permeability. Indeed, if it is assumed that the grout curtain is 100 or 1000 times less pervious than the rock mass, the hydraulic head along the vertical lines is slightly less but the difference between the maximum and minimum does not change.

When the lateral and bottom boundaries and the dam/foundation interface are assumed to be impervious, the head loss on the upstream boundary is about 54 m and the variation in the hydraulic head along the vertical lines close to the drain is about 14 m.

With this *small model*, the hypothesis of assuming the hydraulic head on the upstream and downstream vertical boundaries, as it neglects the head loss in vertical seepage, mainly in the upstream area, leads to greater discharges at the drains. However, to draw conclusions about the vertical seepage, the model should be larger in the upstream area. Moreover, it is not realistic to assume that the upper boundary is impervious, as the rock mass surface is pervious. Therefore, to analyse seepage in concrete dam foundations it is adequate to consider the hydraulic head on the rock mass surface, upstream and downstream from the dam, and assume the lateral surfaces, the bottom surface and the dam/foundation interface to be impervious.

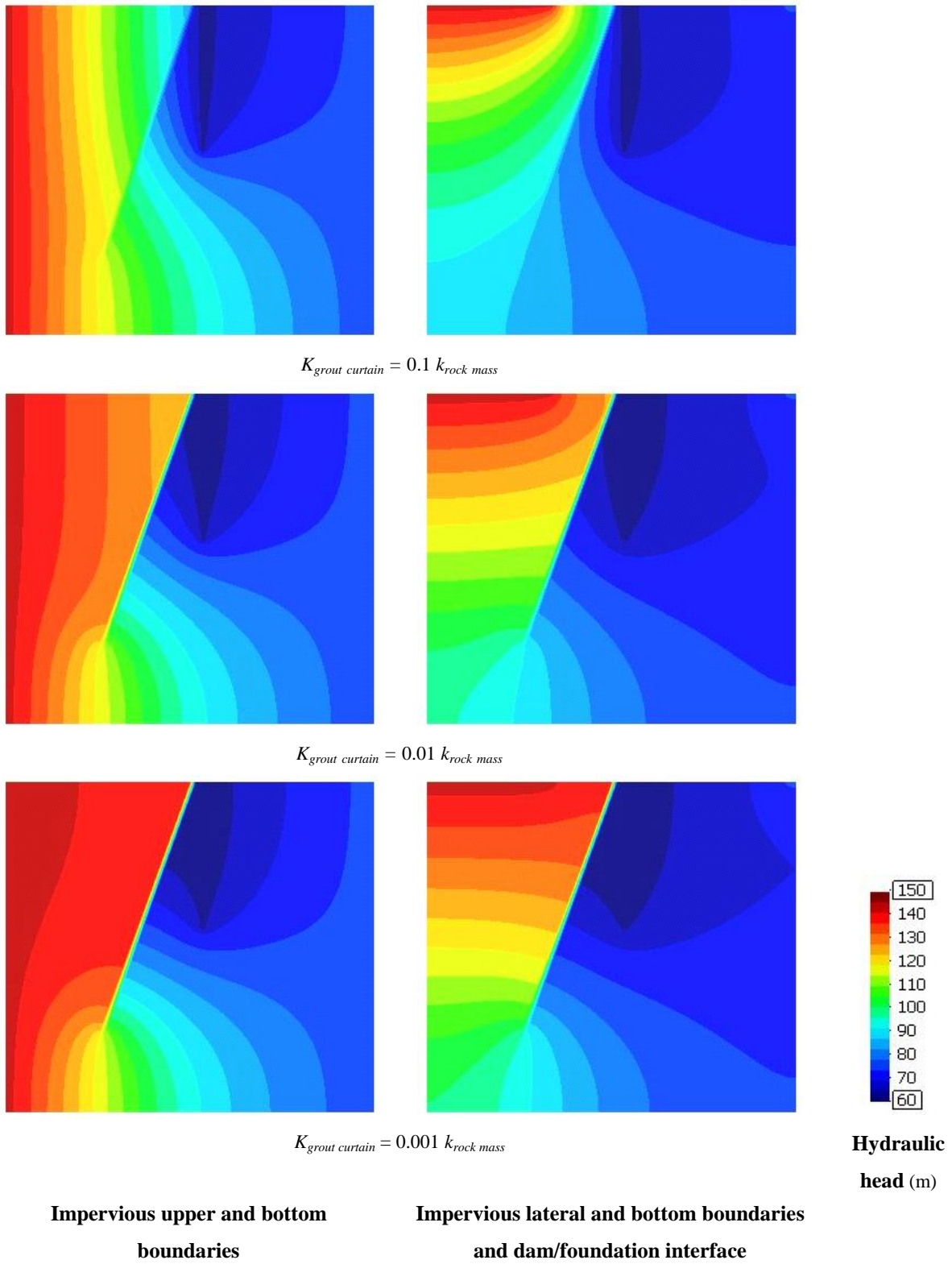


Figure 5.19 – Hydraulic head contours with two different boundary conditions and different $k_{grout\ curtain}/k_{rock\ mass}$.

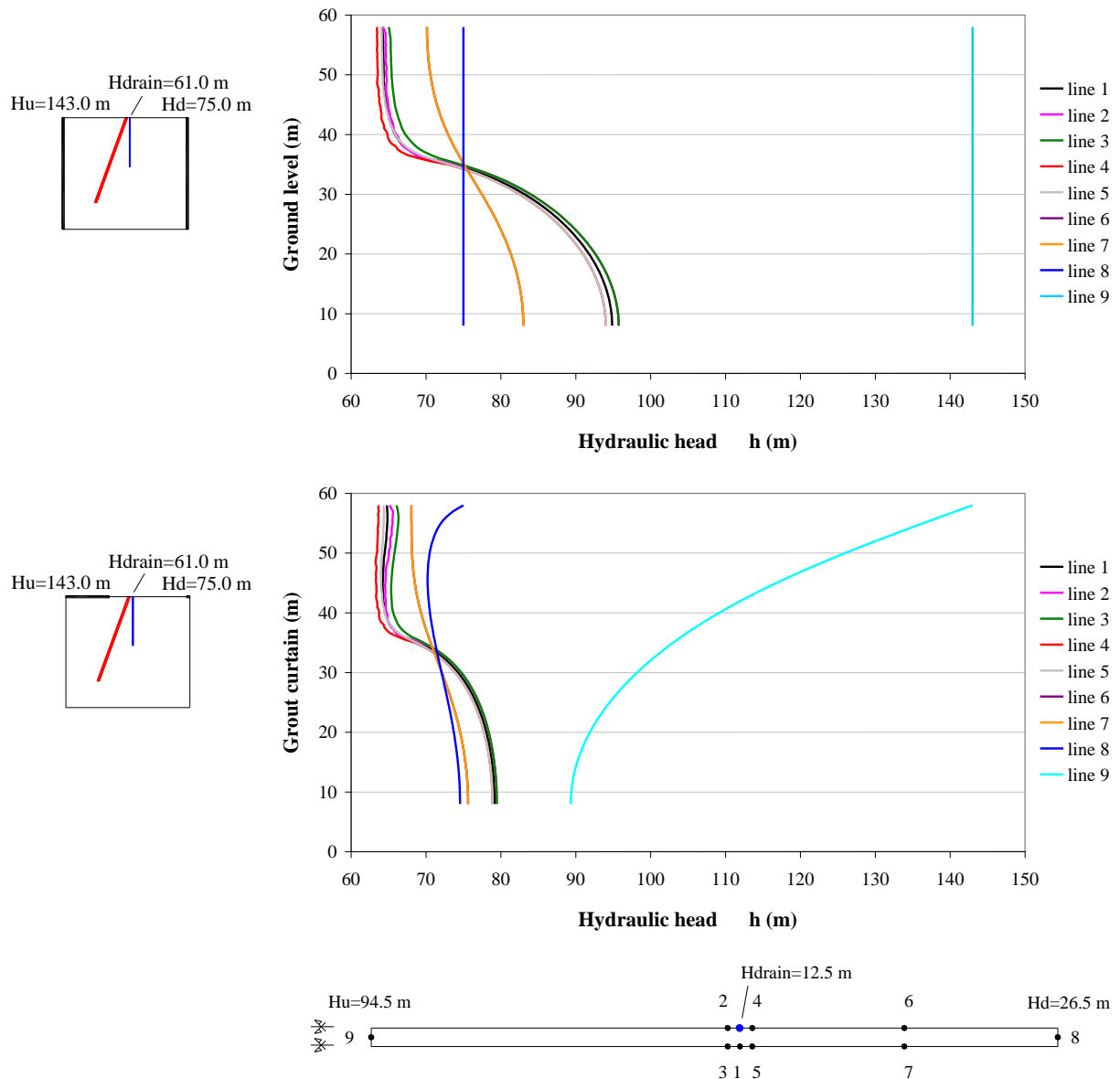


Figure 5.20 – *Small model*. Variation in hydraulic head along 50 m long vertical lines for the two different boundary conditions (assuming that the grout curtain permeability is 10 times lower than that of the rock mass).

Large model

In the *small model* the boundaries are too close to the area of interest, namely the bottom boundary in relation to the grout curtain. In the *large model*, boundaries are further away from the seepage area of interest. To study the influence of the boundary conditions five cases were compared, assuming in all of them that the grout curtain permeability is 100 times lower than

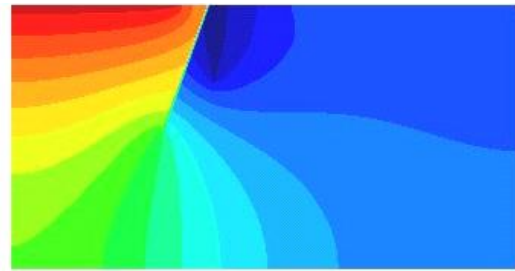
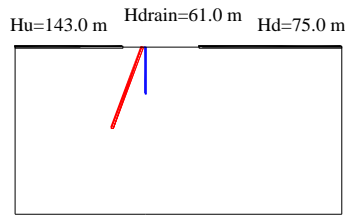
that of the rock mass. The considered boundary conditions are described and represented in Figure 5.21, together with the hydraulic head contours. The numerical discharges in each of the cases studied can be found in Table 5.13.

The analysis of Figure 5.21 and of the values presented in Table 5.13 allows the comparison between the different cases:

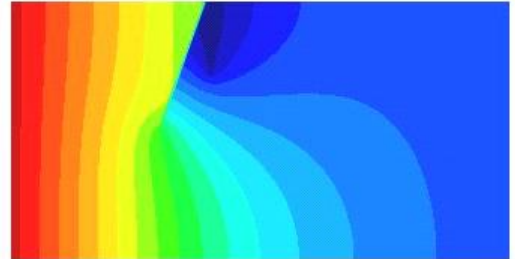
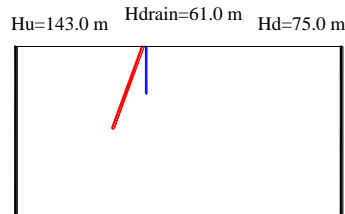
- From i) and iii) it is possible to conclude that, when it is assumed that water can get into and out of the model not only by the rock mass surface but also by the model vertical boundaries, the discharge coming from the upstream boundary increases by about 26 %, the discharge into the drain increases by about 13 % and the discharge which flows out of the model by the downstream boundary is 6 times greater. It is also evident that the discharge coming out from the downstream boundary is almost the same in both cases, thus it can be concluded that part of the discharge coming in from the area upstream from the dam flows, in case iii), directly to the vertical boundary downstream from the dam.
- From i) e iv) it is possible to conclude that, in the case being studied, the dimension of the downstream pervious boundary has almost no influence on the recorded discharges. In both cases, the discharge flowing into the drain is about 95 % of the discharge coming into the model from the upstream area.
- Cases ii) and iii) lead to the conclusion that when the hydraulic head is assumed on the vertical boundaries, neglecting the vertical hydraulic loss in those areas, the numerical discharges are in excess. However, in case ii), in which the entrance of water by the upper boundary is not allowed, that error is masked and the value of the discharge in the drain is close to the value obtained in case i).
- In case v), in which the hydraulic head is assumed only at the drain head and not along its length, the drainage has almost no influence.

The study carried out leads to the conclusion that the boundary conditions considered in case i), in which the lateral and bottom boundaries as well as the dam/foundation interface are assumed to be impervious, are the most suitable boundary conditions to study seepage in concrete dam foundations. Figure 5.22 shows, for this case, the variation of the hydraulic head along 50 m long vertical lines, in three sections of the plane perpendicular to the line of drains that crosses the drain.

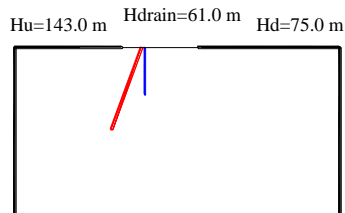
i) hydraulic head assumed on the rock mass surface upstream and downstream from the dam



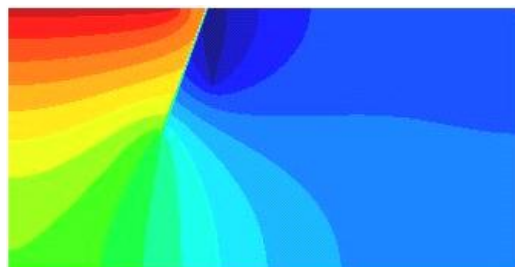
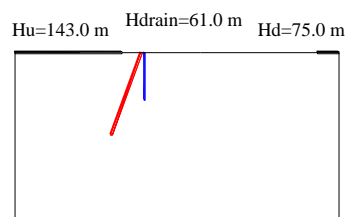
ii) hydraulic head assumed on the lateral boundaries



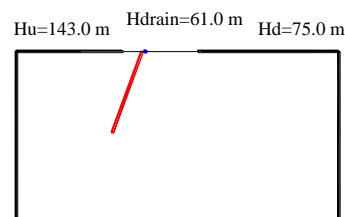
iii) hydraulic head assumed on the lateral boundaries and on the rock mass surface, upstream and downstream from the dam



iv) hydraulic head assumed on the rock mass surface, upstream and downstream from the dam, considering the existence of an impervious slab downstream from the dam/foundation interface



v) hydraulic head assumed on the lateral boundaries and on the rock mass surface, upstream and downstream from the dam; drain modelled by a point (at the upper end)



Boundary conditions

Hydraulic head contours



Figure 5.21 – Schematic representation of boundary conditions and hydraulic head contours for $H_u = 143.0$ m and $H_d = 75.0$ m, with $k_{\text{grout curtain}} = 0.01 k_{\text{rock mass}}$.

Boundary condition	Discharge ($\times 10^{-6} \text{ m}^3/\text{s}$)		
	upstream	drain	downstream
i)	-7.560	7.257	0.191
ii)	-8.325	7.180	1.034
iii)	-9.514	8.162	1.226
	(-4.176-5.338) *		(0.210+1.017) *
iv)	-7.559	7.180	0.267
v)	-6.806	1.082	5.591
	(-2.822-3.984) *		(3.535+2.057) *

* The first and second values presented are the discharges crossing the upper horizontal boundary and vertical boundary respectively (upstream or downstream from the dam).

Table 5.13 – Numerical discharges for different boundary conditions (see Figure 5.21).

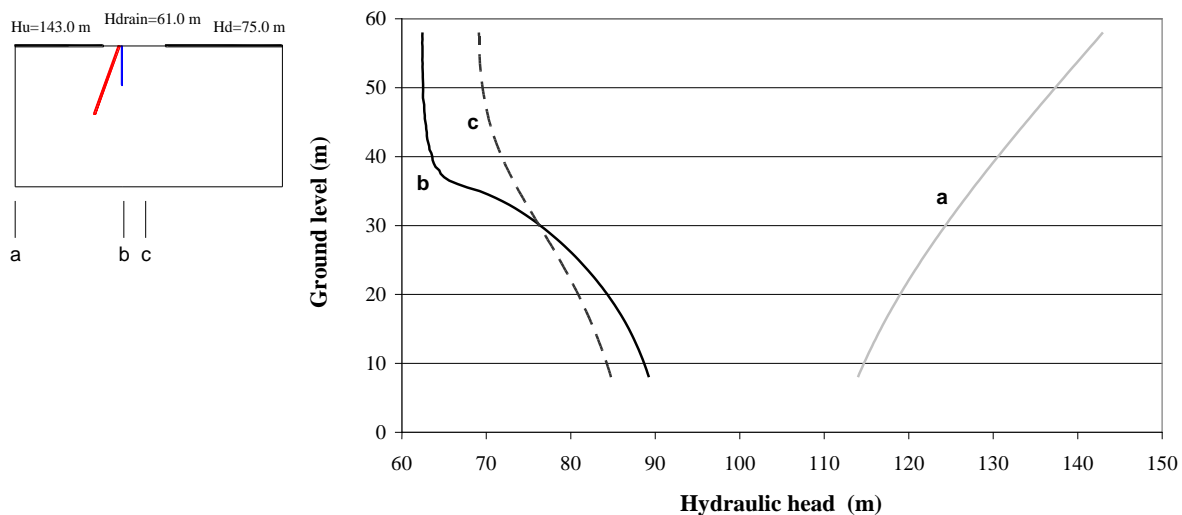


Figure 5.22 – Variation of the hydraulic head along 50 m long vertical lines assuming that the lateral and bottom boundaries and the dam/foundation interface are impervious.

5.3.6 Influence of grout curtain permeability

To assess the influence of grout curtain permeability, the discharges and foundation hydraulic head contours with the grout curtain 10, 100, and 1000 times less pervious than the rock mass were compared. In practice, the latter is equivalent to simulating an impervious grout curtain. Table 5.14 shows the numerical values of the discharges and Figure 5.23 shows the hydraulic head contours for a grout curtain 10 and 100 times less pervious than the rock mass.

Analysis of the values presented in Table 5.14 leads to the conclusion that, when comparing to the case of an impervious grout curtain, the discharges coming into the model from the upstream area and into the drain increase by about 37 % and 150 % when the grout curtain is 100 times or just 10 times less pervious than the rock mass. Decreasing grout curtain permeability leads to a significant reduction in the discharges but, as can be seen in Figure 5.23, has little influence on the hydraulic head contours downstream from the grout curtain.

5.3.7 Influence of model size

Methods based on a domain subdivided into a mesh of zones, such as the distinct element method used in 3DEC, require the model size to be specifically defined, introducing artificial boundaries. These boundaries should be sufficiently far away from the area being studied, so that their location does not have an influence on numerical results. To study the influence of model size, situations b) and a) of the *small model* were compared with situations i) and ii) of the *large model*, respectively. Table 5.15 shows the numerical discharges in each case.

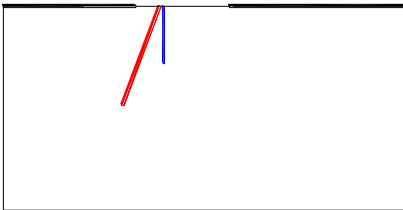
Boundary conditions	$\frac{k_{grout\ curtain}}{k_{rock\ mass}}$	Discharge ($\times 10^{-6} \text{ m}^3/\text{s}$)		
		upstream	drain	downstream
<div style="display: flex; justify-content: space-around; font-size: small;"> $H_u=143.0 \text{ m}$ $H_{drain}=61.0 \text{ m}$ $H_d=75.0 \text{ m}$ </div> 	0.1	-13.792	13.303	0.3821
	0.01	-7.5598	7.2569	0.1910
	0.001	-5.5124	5.2863	0.1111

Table 5.14 – Numerical discharges for $k_{grout\ curtain}/k_{rock\ mass} = 0.1; 0.01$ and 0.001 .

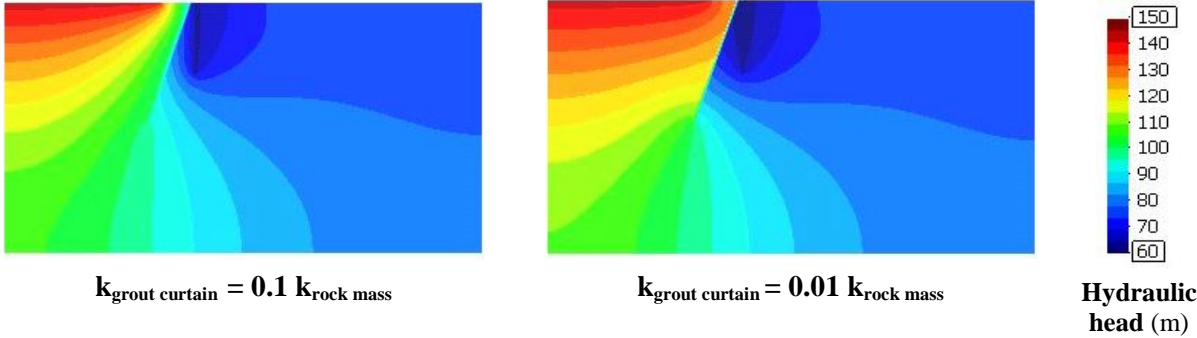


Figure 5.23 – 3D model. Hydraulic head contours ($H_{upstream} = 143.0 \text{ m}$; $H_{downstream} = 75.0 \text{ m}$).

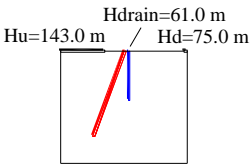
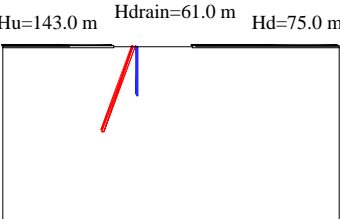
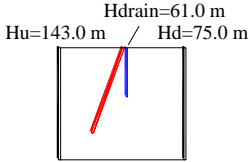
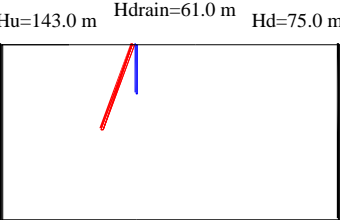
Boundary condition	Discharge ($\times 10^{-6} \text{ m}^3/\text{s}$)		
	upstream	drain	downstream
	-5.3130	5.5840	-0.5505
	-7.5598	7.2569	0.1910
	-7.8960	7.7783	0.0158
	-8.3246	7.1804	1.0343

Table 5.15 – Influence of model size. Numerical discharges when the hydraulic head is assumed either on the foundation surface upstream and downstream from the dam or on the lateral boundaries ($k_{\text{grout curtain}}/k_{\text{rock mass}} = 0.01$).

When the hydraulic head is assumed on the foundation surface, upstream and downstream from the dam, the quantity of water that flows into the model through the upstream boundary is 42 % greater in the *large model* than in the *small model*, and the drain discharge is 30 % greater. The *small model* results are justified not only because they are affected by the small size of the upstream pervious boundary but also because the upstream lateral vertical boundary, which is impervious, is located very close to the grout curtain. The large difference between discharges obtained with the two models reveals that, with these boundary conditions, the size of the *large model* is more appropriate.

In the second situation studied, in which the hydraulic head is assumed on the lateral model boundaries, upstream and downstream, both the drain discharge and the quantity of water flowing through the model between the upstream and downstream boundaries at the lower elevations are higher than they should be (Table 5.15). In the *small model*, vertical boundaries upstream and downstream are very close to the dam's area of influence. Boundary conditions

assumed in this second situation are less realistic than assuming the hydraulic head on the foundation surface. Analysis of results obtained with both models leads to the conclusion that the quantity of water that flows into the model from upstream is only 5 % greater in the *large model* than that obtained with the *small model*, and the drain discharge about 8 % lower. However, whilst in the downstream boundary of the *small model* water flows out of the domain for elevations lower than 32.5 m and enters the domain for elevations higher than this, in the *large model* water flows out of the model from all the grid points located at the downstream boundary. In this situation the size of the *large model* is also more appropriate.

It should be mentioned that in analysis carried out with the *small model*, convergence in steady state conditions is achieved in about 10×10^5 steps, which takes, in this model, two and a half hours. In the *large model* convergence is achieved, in both cases referred to in this sub-chapter, in about 3×10^5 steps, which takes about fifteen hours.

5.3.8 Influence of mesh size

To assess the influence of the mesh size a second mesh was defined which is similar to the mesh shown in Figure 5.16 but coarser. In this mesh, the average edge length of the tetrahedral zones increases, radially and gradually, from 0.75 m to the model width (1.5 m), from the upper point of the drain to the external boundary of the eight central blocks. In the remaining blocks the zones average edge length is 1.5 m. This mesh has 37422 tetrahedra with 13107 grid points, which are about 20 % of the total elements and 26 % of the grid points of the initial model. This second mesh has two tetrahedra across the model thickness in the vicinity of the drain and only one in the remaining domain.

In both meshes referred to in the previous paragraph, the average dimension of the tetrahedron edges increases radially and gradually, from the upper point of the drain to the external boundary of the eight central blocks. The finer mesh has, in the upper area of the drain, four elements along its width, thus the average dimension of the tetrahedron edges closer to the drain is 0.375 m. However, at the elevation of the drain's lower end, in the area where the majority of the flow comes into the drain, the mesh has just two elements along its width. Therefore, a third mesh was defined, based on the first, which is finer in the vicinity of the drain and along the drain whole length. In this third mesh, the average length of the tetrahedron edges is 30 cm, which is slightly greater than 3.5 times the diameter of the hole. This mesh has 20 blocks, 241303 tetrahedra and 61949 grid points.

The numerical discharges obtained with each model are presented in Table 5.16, assuming that the grout curtain permeability is 100 times lower than the rock mass permeability. It is possible to conclude that the coarse mesh leads to discharges into the drain just 5.7 % higher than the very fine mesh. About 42 % of the drain discharge flows into the drain in its lower

5.0 m. The hydraulic head contours obtained with each one of the meshes are almost coincident. The differences are due to the fact that the number of elements across the model thickness is different, at each elevation, in each one of the models. In the very fine mesh, convergence in steady state conditions is achieved in about 4.6×10^5 steps, which takes about 27.5 hours. With the coarse mesh, convergence is achieved in about 1.32×10^5 steps, which takes just one hour and a half.

From the study carried out it is possible to conclude that when the coarse mesh is used errors in discharges and in hydraulic heads are within acceptable limits. The mesh size is not a constraint in the present model, which encompasses only a slice of the foundation, but is particularly important in a complete foundation model. It may be concluded that in a large 3D model a coarse mesh may be used away from the zone of interest. This is the case in chapter 6, in which a coarse mesh is used away from the drainage area, as shown in Figure 6.19.

5.3.9 Comparison between the results of 2D and 3D models

To compare the results of 2D and 3D models, but removing the influence of different meshes or different codes, a 2D model was simulated with 3DEC, assuming at the line of the drains the same hydraulic head across the model thickness (it simulates a hypothetical continuous trench at the line of the drains, as in a 2D model). As the same mesh is used in both models, the effect of the mesh size is eliminated.

The study carried out led to the conclusion that the discharge into the drains in the 3D model is about 94 % of the total discharge at the trench. Therefore, if drains with a diameter of 0.076 m are located 3.0 m apart, and a zero pressure is assumed at the drain heads in a 2D model, the discharge into the drain is just 6 % greater than the discharge in a 3D model. But if the spacing between drains is 6.0 m, the total discharge at the drainage curtain in the 3D model is about 84 % of the total discharge at the trench.

Model	Discharge ($\times 10^{-6} \text{ m}^3/\text{s}$)		
	upstream	drain	downstream
Very fine mesh (finer in the vicinity of the drain, along its whole length)	7.5522	7.1602	0.2417
Fine mesh	7.5598	7.2569	0.1910
Coarse mesh	7.6421	7.5667	0.0377

Table 5.16 – Influence of mesh size. Numerical discharges with different meshes.

The 2D simulation was repeated assuming at the trench the average value of the hydraulic head at the line of the drains (63.03m). This value was determined taking into account the variation of the average value of the hydraulic head in depth and the area of influence at different elevations. Table 5.17 shows the numerical values of the discharges with the 3D and 2D models. In the 2D model, two different hypotheses were considered for the value of the hydraulic head at the line of the drains:

- i) the same as the hydraulic head at the drain head;
- ii) the average value of the hydraulic head at the line of the drains.

It is concluded that if the average value of the hydraulic head at the line of the drains is assumed at the trench, which is slightly greater than the hydraulic head at the drain head (Figure 5.24), the total discharge at the trench decreases, approaching values closer to the discharges at the drains in a 3D model (only 0.5 % greater). The lines of variation of the hydraulic head along horizontal lines at different elevations allow the conclusion that 5.0 m away from the line of the drains the differences in the piezometric heads are less than 1 %. Therefore, 5.0 m away from the line of the drains the numerical values of the 2D and 3D models are almost the same. It can be concluded that instead of representing each drain, a continuous trench provides good results if the head is properly set.

5.3.10 Comparison between the average hydraulic head at the line of the drains calculated with the 3D model and with the 2D horizontal model

Table 5.18 shows the average hydraulic heads at the drainage line, at various elevations, obtained with the 3D model and with the 2D horizontal model, using the analytical solution suggested by Andrade (1982). The results presented were obtained with the assumed most suitable boundary conditions, i.e., with the hydraulic head assumed on the rock mass surface upstream and downstream from the dam, and with the models with the boundary conditions closer to the hypothesis of vertical fissures coming from the heel and toe of the dam.

Model		Discharge ($\times 10^{-6}$) (m ³ /s)		
		upstream	drain	downstream
3 D	$H_{\text{drain}} = 61.0$ m (elevation of the drain head)	-7.560	7.257	0.191
	$H_{\text{drain}} = 61.0$ m (elevation of the drain head)	-7.728	7.712	-0.095
2 D	$H_{\text{drain}} = 63.03$ m (average value of the hydraulic head at the line of the drains)	-7.584	7.294	0.177

Table 5.17 – Numerical discharges with 3D and 2D models.

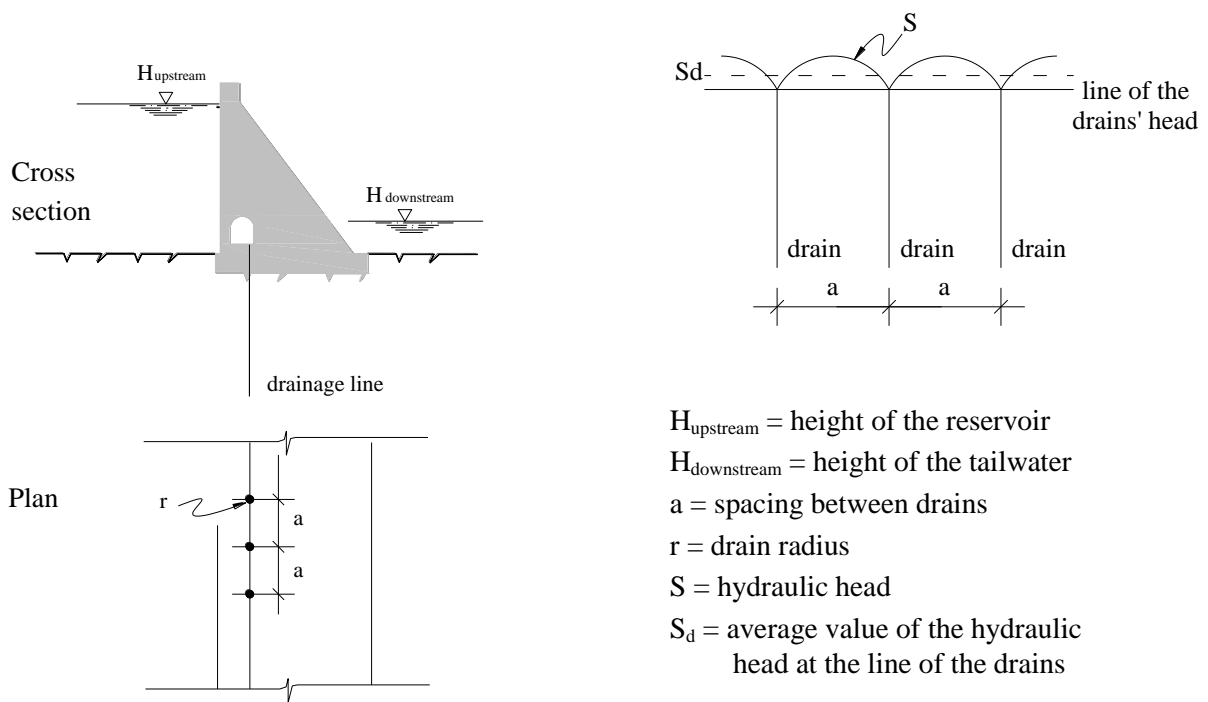


Figure 5.24 – Hydraulic head at the drainage line.

Average hydraulic head at the drainage line (m)				
Elevation (m)	3D Model			Analytical solution suggested by Andrade
	$H_u=143.0$ m	$H_{\text{drain}}=61.0$ m	$H_d=75.0$ m	
58.0		62.13	62.12	61.98
48.5		62.24	62.28	62.15
47.0		62.28	62.34	62.22
40.0		63.06	63.28	63.14
36.0		65.13	65.66	65.45
				72.47

Table 5.18 – Comparison between the average hydraulic head at the line of the drains calculated with the 3D model and with the 2D horizontal model.

The 2D horizontal model of seepage through a concrete dam foundation neglects the existence of the grout curtain, therefore the average hydraulic head at the drainage line is overestimated. As in a horizontal section in any plane of the foundation there is a decrease in the hydraulic head at the grout curtain area, the upstream hydraulic head assumed in Equation 5.7 must not be defined by the reservoir level but by the hydraulic head downstream from the grout curtain. To confirm this hypothesis it is not only necessary to have the results of a 2D model of seepage in a vertical cross section of the foundation, but also to remember that, when using Equation 5.7, the distance from the drainage line to the grout curtain and not the distance from the drainage line to the upstream face of the dam must be considered.

Results obtained with the model which is presented in the next chapter, in section 6.2, lead to the conclusion that:

- 1) at elevation 48.5 m the hydraulic head downstream from the grout curtain is 62.5 m;
- 2) with $H_u = 62.5$ m and a distance from the drainage line to the grout curtain of 3.5 m (distance in the model at elevation 48.5 m), S_d is 13.3, therefore the average hydraulic head at the drainage line 61.8 m ($13.3 + 48.5$);
- 3) the difference between numerical results is 0.6 % of the difference of hydraulic head between upstream and downstream.

Table 5.19 shows the results obtained for the remaining considered elevations. The difference between numerical results and those obtained with the analytical solution suggested by Andrade assuming the hydraulic head downstream from the grout curtain is, with the exception of elevation 36.0 m, around 1 % of the difference in hydraulic head between upstream and downstream. At elevation 36.0 m the difference is 3.3 %.

Results obtained confirm the theory that the hydraulic head downstream from the grout curtain must be used when determining the average hydraulic head at the line of the drains with Andrade's analytical solution.

The 3D model in which the hydraulic head is assumed on the rock mass surface upstream and downstream from the dam was run again with a distance between drains of 6.0 m. Results in Table 5.20 show that at elevation 48.5 m the difference between the hydraulic head determined with the numerical model and with the expression suggested by Andrade is 3.5 % of the difference in hydraulic head between upstream and downstream. The highest difference, of around 8.5 %, is at elevation 36.0 m.

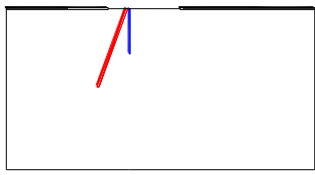
Average hydraulic head at the drainage line (m)			
Elevation (m)	3D Model	Andrade's solution assuming H_u equal to the reservoir level	Andrade's solution assuming the numerical hydraulic head downstream from the grout curtain and taking into account the distance from the grout curtain to the drain, at each elevation
	$H_u=143.0$ m $H_{drain}=61.0$ m $H_d=75.0$ m 		
58.0	62.13		61.40
48.5	62.24		61.84
47.0	62.28	72.47	61.98
40.0	63.06		62.39
36.0	65.13		62.87

Table 5.19 – Comparison between the average hydraulic head at the drainage line obtained with the 3D model and with the 2D horizontal model (Andrade 1982), with the drains located 3.0 m apart.

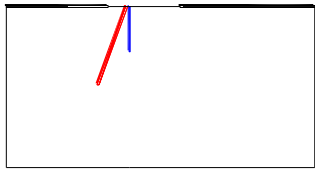
Average hydraulic head at the drainage line (m)			
Elevation (m)	3D Model	Andrade's solution assuming H_u equal to the reservoir level	Andrade's solution assuming the numerical hydraulic head downstream from the grout curtain and taking into account the distance from the grout curtain to the drain, at each elevation
	$H_u=143.0$ m $H_{drain}=61.0$ m $H_d=75.0$ m 		
58.0	64.28		61.51
48.5	64.89		62.49
47.0	65.09	84.09	62.75
40.0	67.08		63.68
36.0	70.52		64.71

Table 5.20 – Comparison between the average hydraulic head at the drainage line obtained with the 3D model and with the 2D horizontal model (Andrade 1982), with the drains located 6.0 m apart.

When the drains are located 3.0 m apart, the variation in hydraulic head along the line of the drains is small and the results of the 3D model are very close to those obtained with Andrade's solution, assuming, as previously mentioned, the hydraulic head downstream from the grout curtain. When the drains are located 6.0 m apart, the hydraulic head downstream from the grout curtain obtained with the 2D model of a vertical cross section of the dam foundation no longer corresponds to the average hydraulic head at the perpendicular direction, therefore there is a considerable difference between the results obtained with the 3D model and with the analytical solution.

Results obtained lead to the conclusion that Andrade's analytical solution, which can be quickly and easily applied, is very useful to estimate, at the planning stage, the variation in discharges at the drainage line when the spacing between drains is changed.

5.4 Conclusions

The study of dam hydraulic behaviour requires the use of relatively large meshes, where the modelling of drainage systems is simplified. From the numerical simulation of two simple flow cases, the influence of the mesh size and of different ways of modelling the drains was assessed. Comparisons with analytical solutions showed the good performance of both the FLAC and 3DEC models.

The study carried out led to the conclusion that if a drain with a diameter of 0.076 m is modelled by its axis the dimension of the elements in the vicinity of the drain should not be lower than 0.27 m. It is worth noting that the drain is modelled by its axis to allow the use of a coarser mesh, in order to reduce run times.

The study of the hydraulic behaviour of a concrete dam foundation with 3D models led to the following main conclusions:

1. In 3D models, as in 2D models, when the drain is modelled by its axis the mesh in the vicinity of the drain must not be too fine. The most suitable size of the elements in the vicinity of the drain is about 3.5 times the drain diameter.
2. In the study of the hydraulic behaviour of dam foundations it is adequate to consider the hydraulic head on the rock mass surface, upstream and downstream from the dam, and assume to be impervious the lateral surfaces, the bottom surface and the dam/foundation interface.
3. Decreasing grout curtain permeability leads to a considerable decrease in the water flow through the model and in the discharges coming to the drain, but has little influence on the hydraulic head values.

4. The artificial boundaries that define the model limits must be far away from the area of interest, so that its definition has no influence on the results. However it should be noted that in 3D models the increase in the model dimensions leads to a great increase in the number of the system degrees of freedom and, consequently, an increase in run times.
5. In the studied case, the widening of the mesh to another with about 20 % of the number of elements and 26 % of the number of grid points of the initial mesh, has little influence on the value of the discharges into the drains, and reduces run times by about 90 %.
6. In a three dimensional model, when there is a drainage curtain with drains with a diameter of 76 mm located 3.0 m apart, the total discharge at the drainage curtain is 94 % of the total discharge at the equivalent trench. If the spacing between drains is 6.0 m, the total discharge at the drainage curtain is 84 % of the total discharge.
7. If the drainage curtain is modelled by an hypothetical continuous trench with the same depth as the drains where the average value of the hydraulic head at the line of the drains is assumed, the total discharge at the trench is almost the same as the total discharge in a 3D model, and 5.0 m away from the line of the drains the difference in the piezometric heads is less than 1 %.

This last conclusion is particularly significant in global 3D models of the foundation where it is not possible to model each one of the drains.

Conclusions drawn from the study presented in this chapter were taken into account whilst developing each one of the different models presented in the following two chapters. In both, the study of dam foundation hydraulic behaviour starts with two-dimensional models, which are especially useful as they are very simple and can be employed if the dam geometry does not vary in the perpendicular direction and if it can be assumed that the flow takes place at the plane of the model. However, the flow in fractured rock masses is mainly three-dimensional and in site-specific studies 3D models provide a more realistic approach to the flow simulations.

6 Analysis of seepage in Alqueva dam foundation

6.1 Introduction

Comprehensive numerical analysis of seepage in Alqueva dam foundation is presented in this chapter. The study consisted in the development of a series of numerical models, which were progressively validated and calibrated against field data. The first to be developed was a simplified two-dimensional model of a vertical cross section, based on the hypothesis of an equivalent continuum medium. Although Alqueva dam is an arch dam, both structural and valley shapes and dimensions allow, as an initial approach, the analysis of seepage along a cross section at the bottom of the valley using a two dimensional model. This model was developed before carrying out experimental activities and therefore conclusions drawn from *in situ* tests reported in chapter 4.5 were not taken into account.

In the analysis of the hydraulic behaviour of concrete dam foundations, 2D models of vertical cross sections are useful, as they are very simple and can be used if the dam geometry is consistent along its length and if it is assumed that the flow takes place at the plane of the model. However, to study seepage in more detail three-dimensional models must be used. Taking into account the conclusions of the previous chapter, two different 3D models of the foundation of Alqueva dam were developed: the first was a detailed 3D model of a part of the foundation, in which each one of the drains is modelled; the second, a global model, in which the drainage system is simulated in a simplified way. The detailed model was developed for the analysis of the tests data. Modelling each one of the drains in 3D models of dam foundations leads to excessively fine meshes, which are very difficult to use. However, they are extremely useful in the analysis of seepage in specific areas, which involves relatively small foundation volumes and a low number of drains are modelled. The development of detailed models for seepage analysis in two site-specific areas of the foundation is described and the results are presented and analysed. A parameter study was carried out to identify which of the parameters have the greatest influence on the numerical discharges and hydraulic heads.

Test results and the knowledge gained with the detailed models were used to develop a much more simplified global hydraulic model of the dam foundation, a scale of representation which is significant for safety assessment studies. In this model, the drainage system is simulated in a simplified way, by a hypothetical continuous trench with the same depth as the drains. Comparisons between numerical discharges, calculated with this global model, and recorded discharges led to the conclusion that the apertures of the discontinuities through which water flows vary with changes in reservoir level. Therefore, based on the results of

borehole water-inflow tests, presented in chapter 4.5, and on available field data, an attempt was made to estimate the correlation between stress and permeability in some areas of the dam foundation.

In the last part of the chapter, a numerical study on the significance of readings taken in piezometers is presented. In a chapter on numerical modelling of seepage in Alqueva dam foundation, this section may seem out of place. However, the study was carried out using the dimensions of Alqueva dam as reference, with a 3D model based on the detailed 3D models developed for the analysis of the test results.

6.2 Two-dimensional model of a vertical cross section at the bottom of the valley

6.2.1 Model description

The 2D model presented in this section was developed prior to water-inflow testing, only as a preliminary approach to the analysis of seepage in the dam foundation at the bottom of the valley (Farinha and Lemos 2006). The analysis was carried out with FLAC 4.0 (Itasca 2002). In two-dimensional models, the modelling of the drainage curtain is equivalent to a hypothetical trench in the perpendicular direction of the section being studied. Therefore, the numerical value of the discharges in the drains is greater than in reality.

The model is about $1000 \times 500 \text{ m}^2$ and the boundaries are quite a way from the dam's area of influence, encompassing about 480 m of foundation upstream from the dam, the areas below the dam's central block, the powerhouse slab and the downstream dam-wall, and about 390 m downstream from this wall. The model is 500 m deep (Figure 6.1). Although the majority of the flow takes place through the foundation discontinuities it is assumed that joint spacing is small compared to the size of the rock mass being studied and that joint orientation is fairly random. Thus, the hydraulic properties of an equivalent continuum are considered. It is assumed that water flows according to Darcy's law, in a homogeneous and isotropic media.

The mesh was designed to be finer close to the drains and for no zone to have a length more than 10 times its width. The mesh is composed of 3596 zones. Both grout curtains, below the central cantilever and below the downstream dam-wall, which are about 44.0 m and 9.0 m deep, respectively, are simulated by a band of elements 1 m wide. The drains and piezometers are modelled at the same position and with the same length as the holes drilled in the foundation (Figure 6.2).

The mesh has three areas with different hydraulic conductivities. Taking into account the results of water pressure permeability tests performed in vertical boreholes where geophysical tests were also carried out, it was first assumed that the hydraulic conductivity was

2.0×10^{-7} m/s above elevation 48.0 m and 1.0×10^{-7} m/s below (Farinha and Lemos 2006; LNEC 2005b). After more detailed analysis of the test results, which are shown in Table 6.1, it was assumed that in the foundation of the dam's central block (block 13-14), the hydraulic conductivity was 1.0×10^{-7} m/s above elevation 48.0 m and 0.5×10^{-7} m/s below (Farinha et al. 2006). It was assumed that the grout curtains' hydraulic conductivity was 200 times lower than the hydraulic conductivity of the foundation's most pervious area.

6.2.2 Hydraulic boundary conditions and numerical results

For boundary conditions the following water pressures were assumed: i) corresponding to the water heights in the areas in contact with the Alqueva and Pedrógão reservoirs, including the upstream slope of the insertion of the dam in the foundation; ii) zero at drain heads; iii) corresponding to the distance from the drain head to the considered level, along the drainage boreholes. The remaining boundaries are assumed to be impervious. Figure 6.2 shows a detail of the numerical model below the dam, powerhouse slab and downstream dam wall.

The monitoring results on different dates were compared with numerical results (Farinha et al. 2006). Table 6.2 shows the average values of the recorded discharges in the foundation of the dam's central blocks and the corresponding numerical results on the date of the second stage of the water level during the controlled first filling of the reservoir, at elevation 143.0 m (in which the water pressure was 82 % of the water pressure that is going to be reached at the retention water level) and on the two dates when, up to the end of 2005, the highest levels upstream and downstream from the dam were reached.

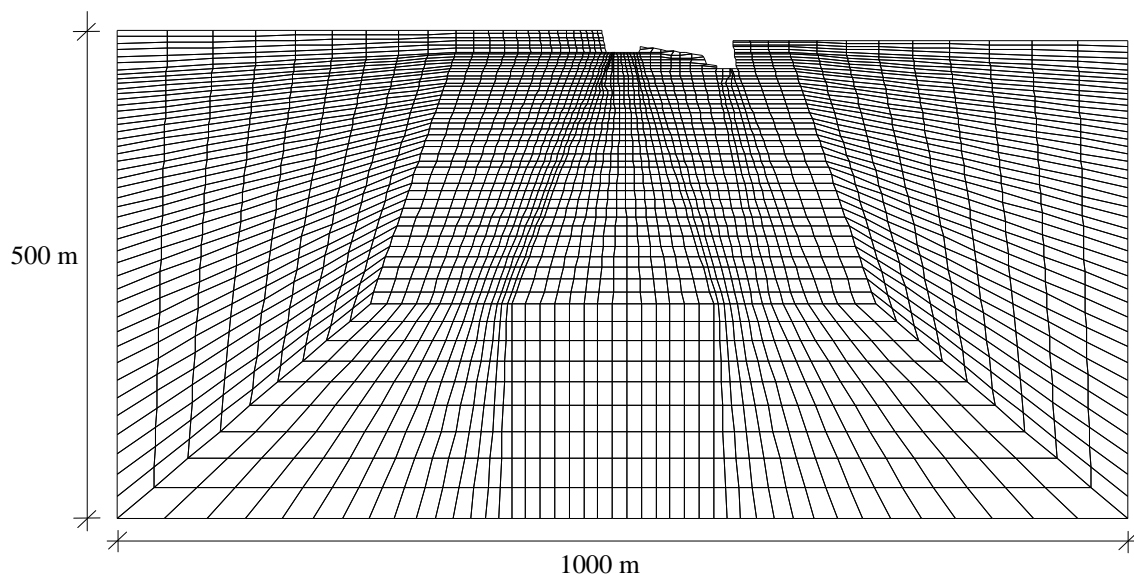


Figure 6.1 – Foundation numerical model.

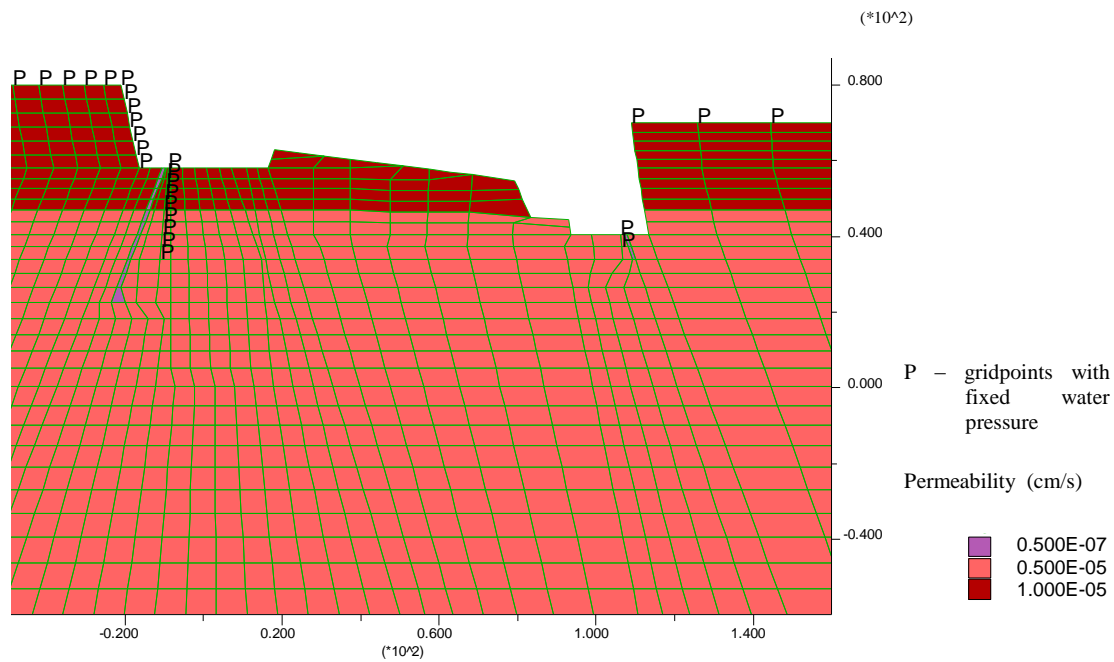


Figure 6.2 – Detail of the foundation numerical model. Geometry, materials and gridpoints with fixed water pressure (boundary conditions).

Depth (m)	BLOCK										Average value of permeability (LU)
	8-9	9-10	10-11	11-12	12-13	13-14	14-15	15-16	16-17	17-18	
5	2.9	2.03	2.1	2.45	0.24	1.1	2.1	0.96	1.0	0.73	1.561
10	2.77	0.52	1.2	1.62	0.46	0.7	2.7	0.9	0.0	0.15	1.102
15	0.48	0.19	0.5	0.7	0.3	0.5	0.3	0.55	0.5	0.15	0.417
20	3.79	0.4	0.5	1.08	0.07	0.3	0.1	0.37	0.5	0.55	0.766
25		0.23						0.92	0.2	0.14	0.373

Table 6.1 – Results of hydraulic conductivity tests (in Lugeon Units) carried out in the foundation of Alqueva dam, after dam construction but before grouting.

Date	H_{upstream} (m)	$H_{\text{downstream}}$ (m)	Average value of the discharges ($\times 10^{-6} \text{ (m}^3/\text{s)/m}$)			
			Recorded values		Numerical results	
			dam	dam-wall	dam	dam-wall
2004.01.07	143.0	75.00	1.80	1.58	3.17	1.66
2004.05.11	148.53	74.83	3.36	1.49	3.38	1.69
2005.11.29	145.01	80.60	2.29	1.38	3.33	1.83

Table 6.2 – Average value of the recorded discharges and comparison to numerical results.

The analysis of the values shown in Table 6.2 led to the conclusion that the numerical discharges were of the same order as the recorded discharges, although in the dam the differences were greater than 45 % for the reservoir lower levels. These differences were assumed to be due to the fact that the same values of permeability were used in the different numerical experiments, not taking into account variations in permeability with the state of stress in the foundation.

Figure 6.3 shows the hydraulic head contours in the foundation considering the water levels recorded on 2005.11.29 and Figure 6.4 shows, for the same date, seepage velocity in the foundation. The variations in the hydraulic head along the line where the piezometers are positioned, with the length defined at the design stage at the base of the central cantilever are presented in Figure 6.5 (PZB 17-1, 2 and 3). It should be noted that piezometric boreholes are shorter than defined in the design stage, as shown in Figure 4.16. On the date in question, the hydraulic heads recorded in the foundation of the dam's central area, in piezometer PZB-2, varied from 62.0 m to 74.0 m, with an average value of 67.2 m. The piezometers installed in Alqueva dam foundation are boreholes closed with a pressure gauge at their heads, and thus the hydraulic head is the same along these boreholes. In the 2D model presented, however, in contrast to what was done in the 3D models that are presented in the following sections, the hydraulic head was not constrained to be an unknown constant along each borehole's length and so the lines in Figure 6.5 show the variations in piezometric head along the line where the boreholes are positioned, as if they had not been drilled.

It was decided that the grout curtains' assumed hydraulic conductivity of 200 times lower than that of the foundation most pervious area was not appropriate and so new numerical analysis was carried out with a hydraulic conductivity 10 and 20 times lower. In the former case, to match the observed discharges at the dam for the reservoir higher levels, maintaining the ratio between permeability values of the two foundation zones, a rock mass hydraulic conductivity of 3.7×10^{-8} m/s above elevation 48.0 m and 1.85×10^{-8} m/s below would be needed. In the latter case, a rock mass hydraulic conductivity of 4.5×10^{-8} m/s above elevation 48.0 m and 2.25×10^{-8} m/s below would be needed. However, in both cases the numerical discharges at the dam-wall are about half of the recorded values. Table 6.3 shows a comparison of recorded and numerical discharges on the same dates as in Table 6.2. Figures 6.6 to 6.8 and 6.9 to 6.11 are similar to Figure 6.3, 6.4 and 6.5 but with the new numerical results.

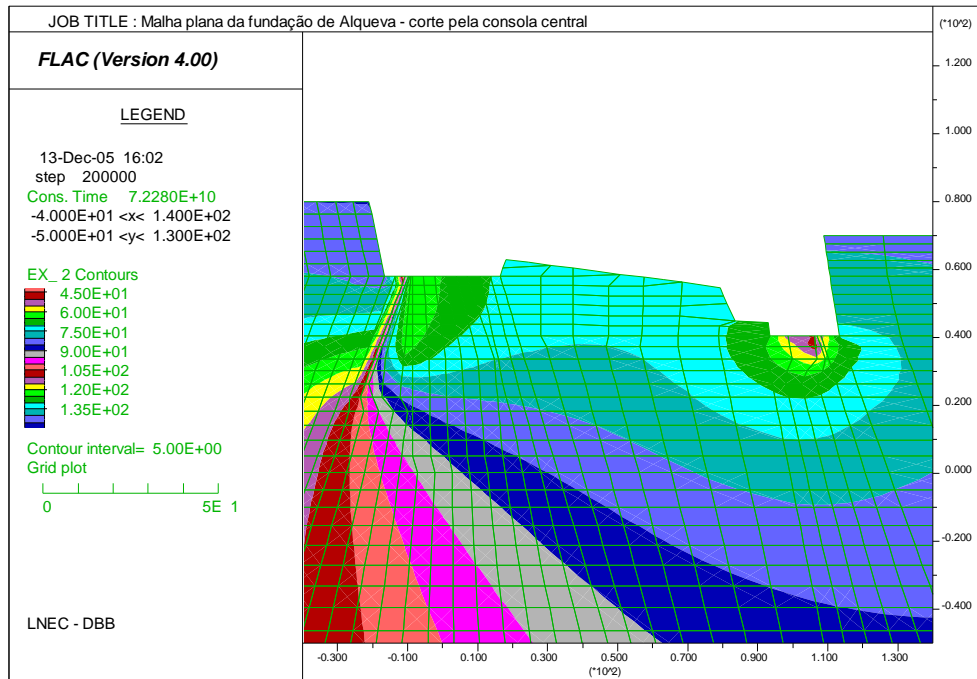


Figure 6.3 – Hydraulic head contours ((m) for $H_{\text{upstream}} = 145.01$ m and $H_{\text{downstream}} = 80.60$ m).

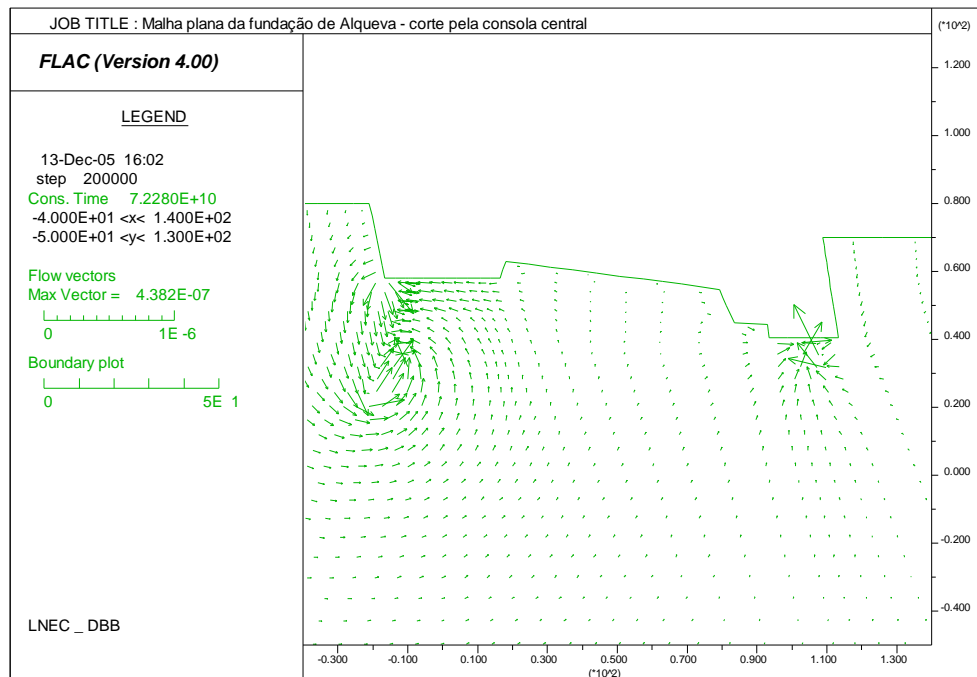


Figure 6.4 – Seepage velocity in the foundation ((m/s) for $H_{\text{upstream}} = 145.01$ m and $H_{\text{downstream}} = 80.60$ m).

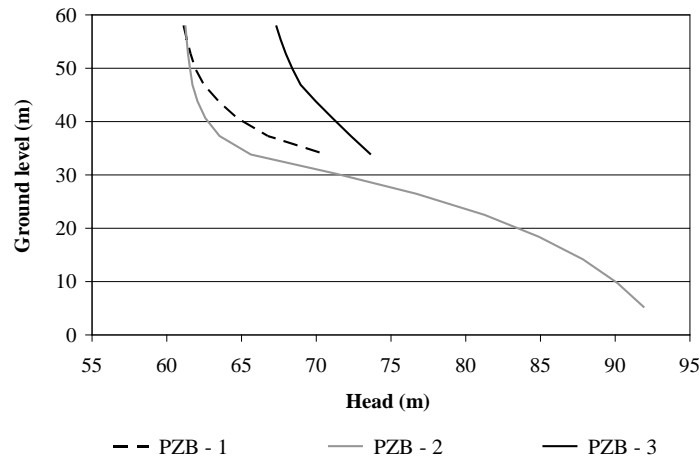


Figure 6.5 – Variations of piezometric head along the line where the piezometers are positioned at the base of the central cantilever.

Date	H upstream (m)	H downstream (m)	Average value of the discharges ($\times 10^{-6}$ (m ³ /s)/m)					
			Recorded values		Numerical results (1)		Numerical results (2)	
			dam	dam-wall	dam	dam-wall	dam	dam-wall
2004.01.07	143.0	75.00	1.80	1.58	3.17	0.72	3.14	0.83
2004.05.11	148.53	74.83	3.36	1.49	3.39	0.73	3.35	0.84
2005.11.29	145.01	80.60	2.29	1.38	3.28	0.79	3.26	0.92

- (1) $k_{\text{rock mass}} = 3.7 \times 10^{-8}$ m/s above elevation 48.0 m
 $k_{\text{rock mass}} = 1.85 \times 10^{-8}$ m/s below elevation 48.0 m
 $k_{\text{grout curtain}} = 3.7 \times 10^{-9}$ m/s
- (2) $k_{\text{rock mass}} = 4.5 \times 10^{-8}$ m/s above elevation 48.0 m
 $k_{\text{rock mass}} = 2.25 \times 10^{-8}$ m/s below elevation 48.0 m
 $k_{\text{grout curtain}} = 2.25 \times 10^{-9}$ m/s

Table 6.3 - Average value of the recorded discharges and comparison to numerical results (grout curtains' hydraulic conductivity 10 and 20 times lower than the hydraulic conductivity of the foundation's most pervious area).

The 2D model presented here was developed at a preliminary stage of the study so as to approximately simulate seepage flow in the valley bottom, and therefore no further model improvement was attempted in order to obtain numerical discharges closer to those recorded. In a 3D model it would be necessary to simulate the variation in discharges and water pressures from each dam block to another. A 2D “average” model, like that presented here, can only give a rough idea of flow.

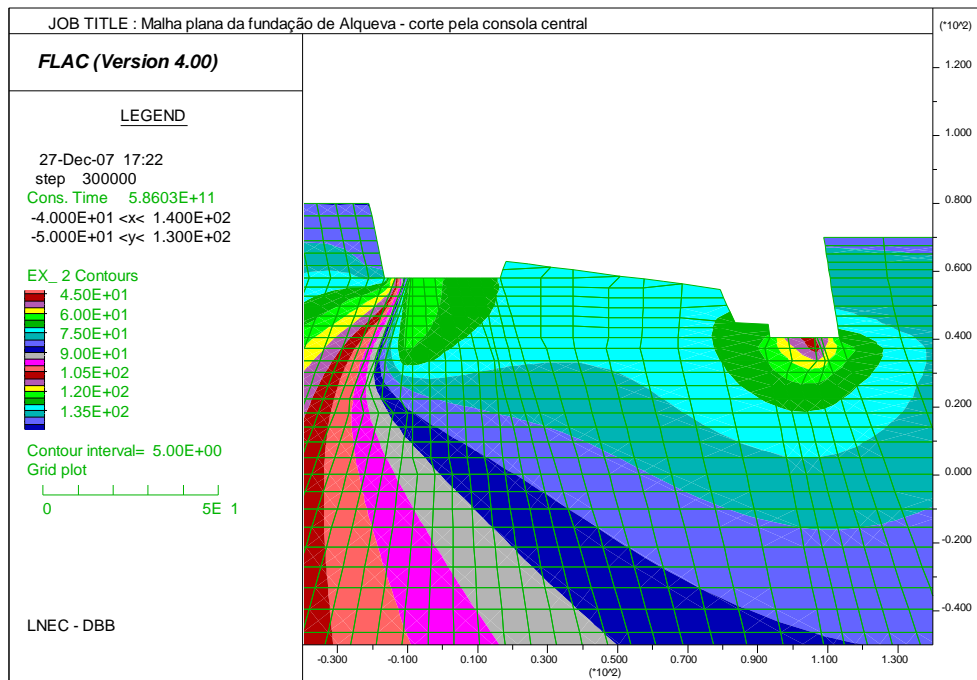


Figure 6.6 – Hydraulic head contours ((m) for $H_{\text{upstream}} = 145.01$ m and $H_{\text{downstream}} = 80.60$ m and with the grout curtains' hydraulic conductivity 10 times lower than the hydraulic conductivity of the foundation's most pervious area).

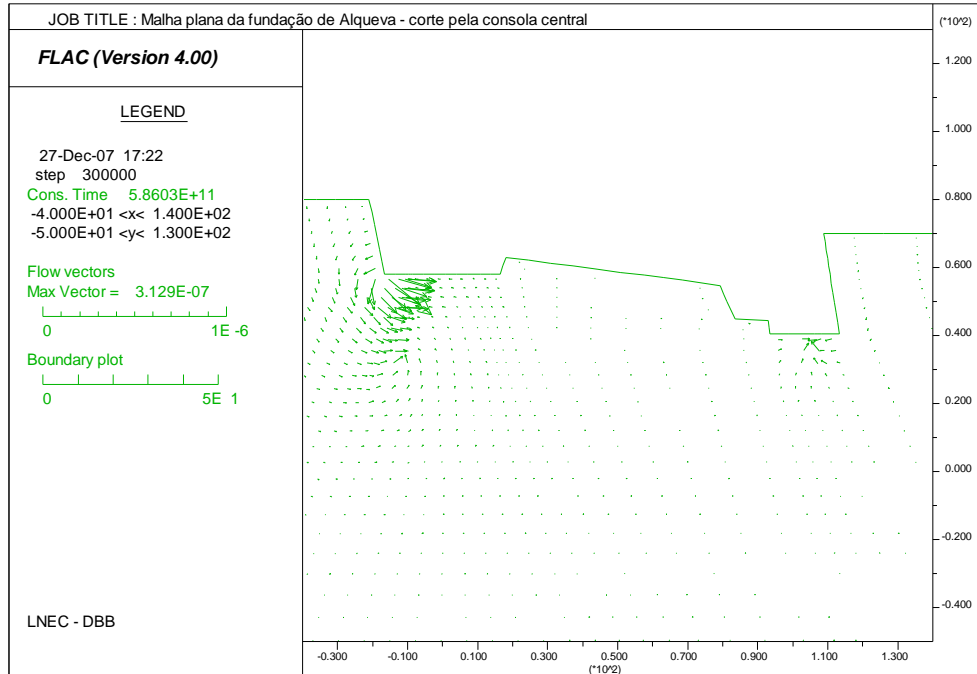


Figure 6.7 – Seepage velocity in the foundation ((m/s) for $H_{\text{upstream}} = 145.01$ m and $H_{\text{downstream}} = 80.60$ m and with the grout curtains' hydraulic conductivity 10 times lower than the hydraulic conductivity of the foundation's most pervious area).

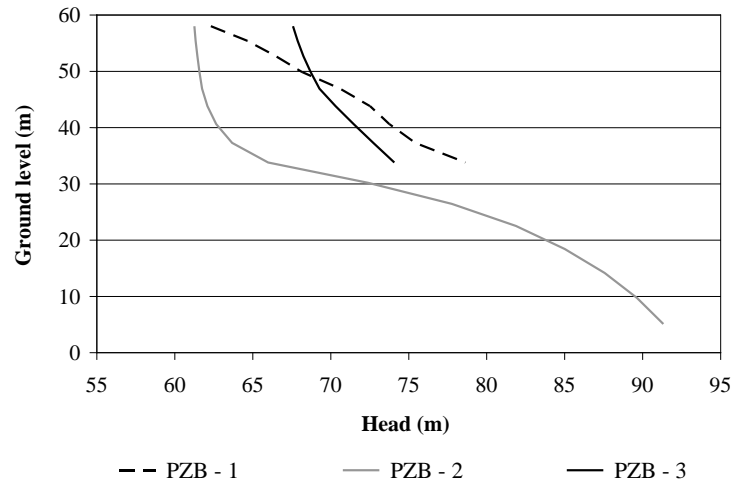


Figure 6.8 – Variations of piezometric head along the line where the piezometers are positioned at the base of the central cantilever (grout curtains’ hydraulic conductivity 10 times lower than the hydraulic conductivity of the foundation’s most pervious area).

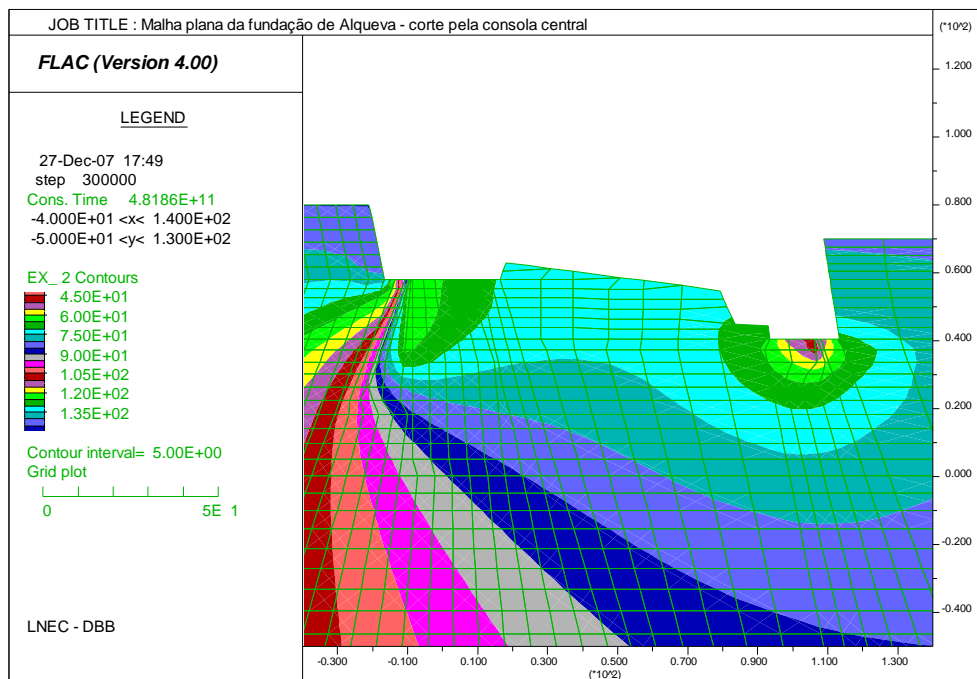


Figure 6.9 – Hydraulic head contours ((m) for $H_{upstream} = 145.01$ m and $H_{downstream} = 80.60$ m and with the grout curtains’ hydraulic conductivity 20 times lower than the hydraulic conductivity of the foundation’s most pervious area).

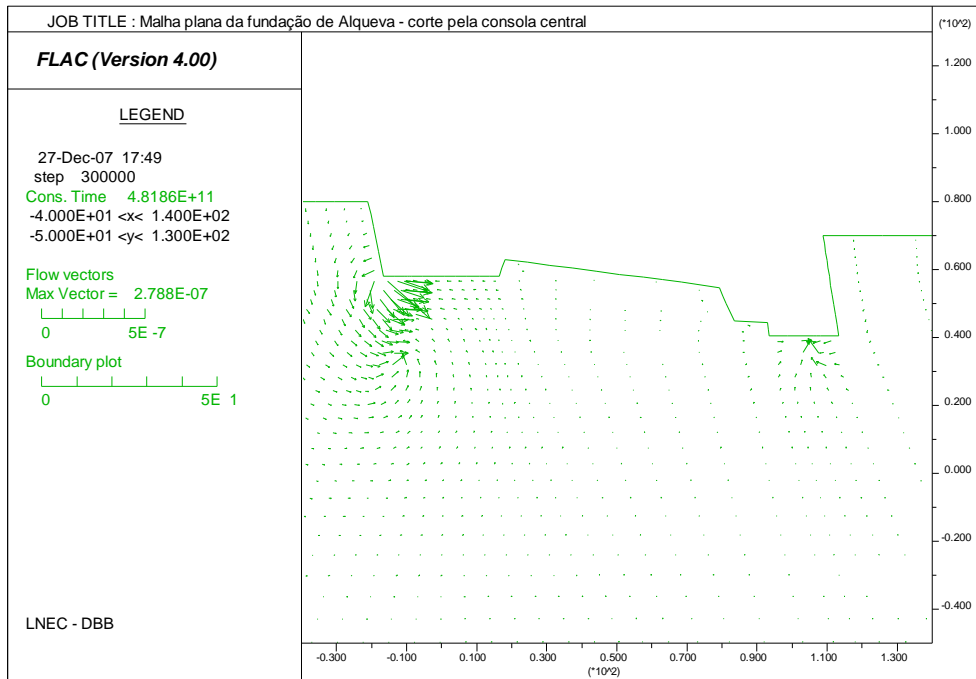


Figure 6.10 – Seepage velocity in the foundation ((m/s) for $H_{\text{upstream}} = 145.01$ m and $H_{\text{downstream}} = 80.60$ m and with the grout curtains' hydraulic conductivity 20 times lower than the hydraulic conductivity of the foundation's most pervious area).

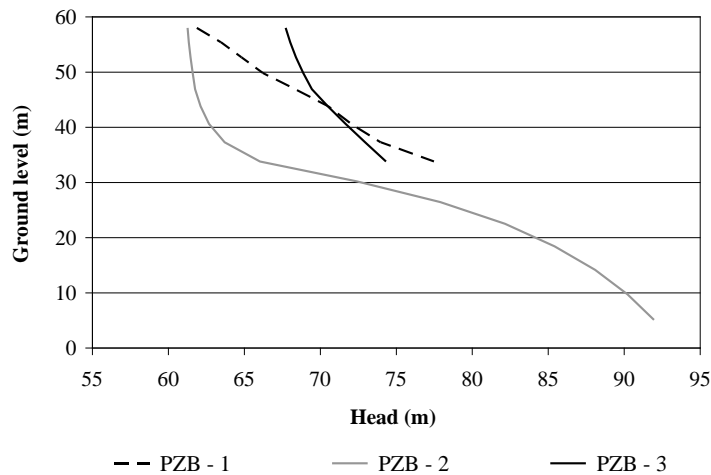


Figure 6.11 – Variations of piezometric head along the line where the piezometers are positioned at the base of the central cantilever (grout curtains' hydraulic conductivity 20 times lower than the hydraulic conductivity of the foundation's most pervious area).

6.2.3 Influence of the boundary distances used in the numerical model

The distance at which boundaries should be placed from the area being studied when analysing the hydraulic behaviour of vertical cross sections of dam foundations was assessed using the model previously presented, with two simplifying assumptions: i) the downstream dam wall was not considered, in order to carry out the study assuming only one grout curtain and one drainage curtain; and ii) the same hydraulic conductivity was assumed in the whole foundation rock mass (2.0×10^{-7} m/s).

The study was carried out with five different meshes (*m1* to *m5*) with the boundaries successively further away from the dam. As the dam is 96.0 m high and the system dam/powerhouse creates an impervious boundary of about 140 m at the concrete/rock mass interface in the upstream-downstream direction, a reference distance L of 140.0 m is assumed. Figure 6.12 shows the different meshes used.

Tables 3.6 and 3.7 show the numerical results with the water level in the reservoir at an elevation of 152.0 m and the water downstream from the dam at an elevation of 80.0 m, assuming the foundation to be drained and not drained, respectively. Results analysis leads to the following conclusions:

- i) when drained foundations are considered, meshes larger than four times the reference distance in the horizontal direction and two times in the vertical direction give very close results (differences in drain discharges less than 2.5 %);
- ii) when the foundation is not drained, the quantity of water flowing through the model when the mesh is about 4 and 3 times the reference distance (in the horizontal and vertical directions, respectively), is 55 % of that obtained with a model with a size of about 14 and 7 times the reference distance.

Therefore, when most of the water flows between the reservoir and the drainage curtain it is enough to consider distances from the dam area to boundaries of about those considered in model *m2*. When there is a significant quantity of water reaching the downstream boundaries, the model boundaries should be further away from the dam's area.

Model	Length in relation to the reference distance L	Mesh
<i>m1</i>	horizontal direction $\approx 3 L$ vertical direction $\approx 0,9 L$	
<i>m2</i>	horizontal direction $\approx 3,6 L$ vertical direction $\approx 1,8 L$	
<i>m3</i>	horizontal direction $\approx 7,1 L$ vertical direction $\approx 3,6 L$	
<i>m4</i>	horizontal direction $\approx 10,7 L$ vertical direction $\approx 5,4 L$	
<i>m5</i>	horizontal direction $\approx 14,3 L$ vertical direction $\approx 7,1 L$	

Figure 6.12 – Meshes used to study the distance from the dam area at which boundaries should be located.

Mesh	Mesh size	Drain discharge ($\times 10^{-5}$ (m ³ /s)/m)	Difference to the discharge obtained with the model which has the furthest boundaries (%)
<i>m1</i>	300 × 124	1.1147	0.911
<i>m2</i>	500 × 250	1.1941	0.976
<i>m3</i>	1000 × 500	1.2176	0.995
<i>m4</i>	1500 × 750	1.2221	0.999
<i>m5</i>	2000 × 1000	1.2238	1.000

Table 6.4 – Drained foundation. Numerical discharges and comparison with the discharge obtained with the model which has the furthest boundaries.

Mesh	Mesh size	Discharge ($\times 10^{-5}$ (m ³ /s)/m)	Difference to the discharge obtained with the model which has the furthest boundaries (%)
<i>m1</i>	300 × 124	0.5034	0.35
<i>m2</i>	500 × 250	0.7989	0.55
<i>m3</i>	1000 × 500	1.1221	0.78
<i>m4</i>	1500 × 750	1.3096	0.91
<i>m5</i>	2000 × 1000	1.4427	1.00

Table 6.5 - Foundation with no drainage curtain. Numerical discharges and comparison with the discharge obtained with the model which has the furthest boundaries

6.3 Detailed three-dimensional model of a local area

6.3.1 Model description

A detailed three-dimensional model was developed to carry out more in-depth analysis in specific areas of the foundation. The model is formed by a series of adjacent vertical strips, which extend from about 50.0 m upstream from the upstream face of the dam to 50.0 m downstream from the downstream dam-wall. The model, which can be limited to a specific area, is formed by a group of strips with two different widths: the inner strips are 3.0 m wide, the distance between drains, and, due to symmetry, the outer strips are 1.5 m wide, corresponding to half the distance between drains. Each strip has a vertical length of 78.0 m, which is around two times the projection of the grout curtain in the vertical direction. The cross section of the dam in the valley bottom, from the upstream face of the dam to the downstream face of the downstream dam-wall, measures from around 115 m, in the lateral areas, to around 140 m, in the central cross section, thus the average value of 130.0 m was

assumed. The model of a single strip has a volume of $230.0 \times 78.0 \times 3.0 \text{ m}^3$ or $230.0 \times 78.0 \times 1.5 \text{ m}^3$. The modelling of each strip takes into account both the horizontal and vertical curvatures of the dam where it meets the foundation. Each one of these strips is divided into blocks, which are internally divided into tetrahedra.

Figure 6.13 shows the position of the foundation model in the area where the bottom of the valley meets the right hand side abutment. This model includes three drains and is formed by two inner strips 3.0 m wide and two outer strips 1.5 m wide, thus being only 9.0 m wide.

It is assumed that the grout curtain, which crosses the whole model width, is 1 m thick. The drain is modelled by its axis (diameter zero) and is positioned at the inner strip boundary, in strips 1.5 m wide, and at both strip boundaries, in strips 3.0 m wide. Each one of the 1.5 m wide strips is divided into 25 blocks, and each of the 3.0 m wide strips into 27 blocks, the difference being in the number of blocks in the vicinity of the drains, in the drainage curtain direction.

The relative position of the grout and drainage curtains is respected. The grout curtain dips 20° towards upstream, is located about 7.0 m downstream from the upstream face and is 41 m long. The drainage curtain is located about 0.5 m downstream from the grout curtain and dips 5° towards upstream but it was assumed to be vertical, in order to simplify the model.

The mesh is finer close to the drains and along the drains' whole length and was defined by the average edge length of the tetrahedral zones. For the 1.5 m wide strips a different number of zones was assumed in different locations: 4 zones across strips' width in the vicinity of the drains; 2 zones in the blocks surrounding the area in the vicinity of the drains; and only 1 zone in the remaining domain. The average dimension of the tetrahedron edges closer to the drain is 0.30 m. Each strip has 127386 tetrahedra and 37695 grid points. In the 3.0 m wide strips the number of zones across the width doubles. Figure 6.14 shows the division into blocks and internal mesh of a 1.5 m wide strip, as well as the position of the grout curtain and the drain, of which the depth is about half of the grout curtain's length and, in the mesh, ends 3 m above the horizontal joint.

The main weakness of this model is the assumption that, in the area being studied, water flow takes place in the upstream-downstream direction, parallel to the main river channel.

In order to simplify the definition of different areas' material properties, rock mass and grout curtain were defined as separate regions. The blocks adjacent to the reservoir and to the downstream area, where the tailwater pressure is assumed, were also defined as different regions, to make it easier to define hydraulic boundary conditions. Figure 6.15 shows the model's four different regions.

In the analysis presented in this section it is assumed that the rock mass foundation is homogeneous and isotropic with a permeability of 1.0×10^{-7} m/s and that the grout curtain is 100 times less pervious. As noted before, such a low ratio between the permeability of the grout curtain and that of the rock mass is not considered appropriate. This is modified in the following section.

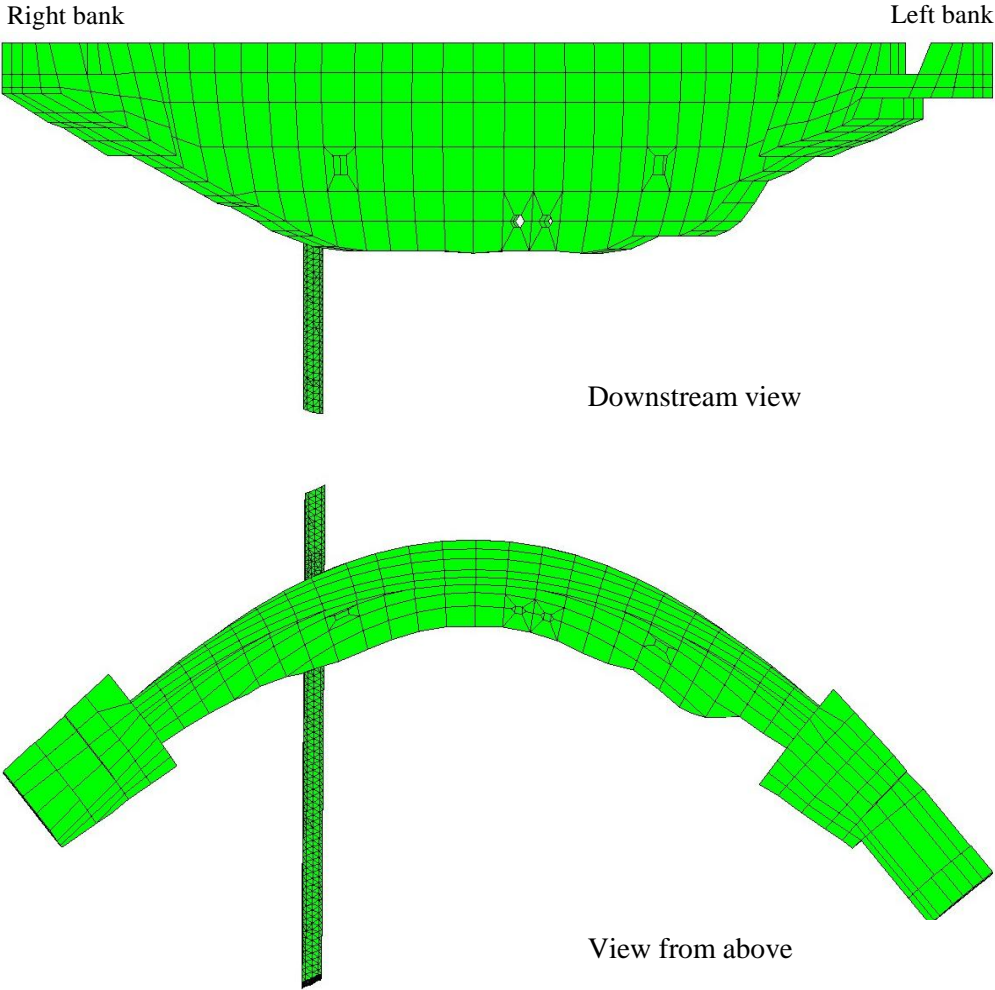


Figure 6.13 – Position of the foundation model 9.0 m wide in the area where the bottom of the valley meets the right hand side abutment.

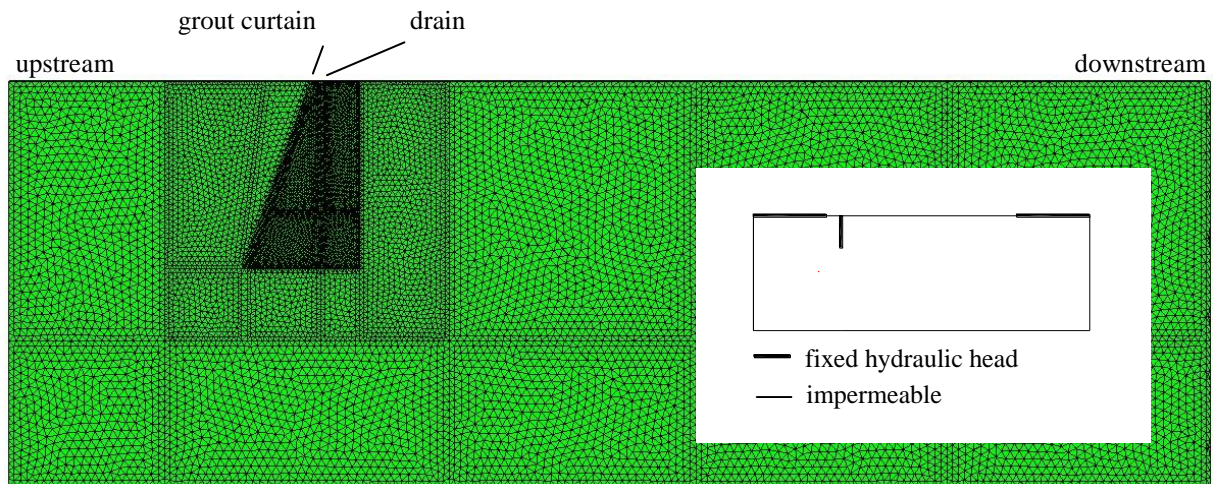


Figure 6.14 – Face in the upstream-downstream direction of the three-dimensional model of the foundation. Division into blocks and internal mesh, and hydraulic boundary conditions.

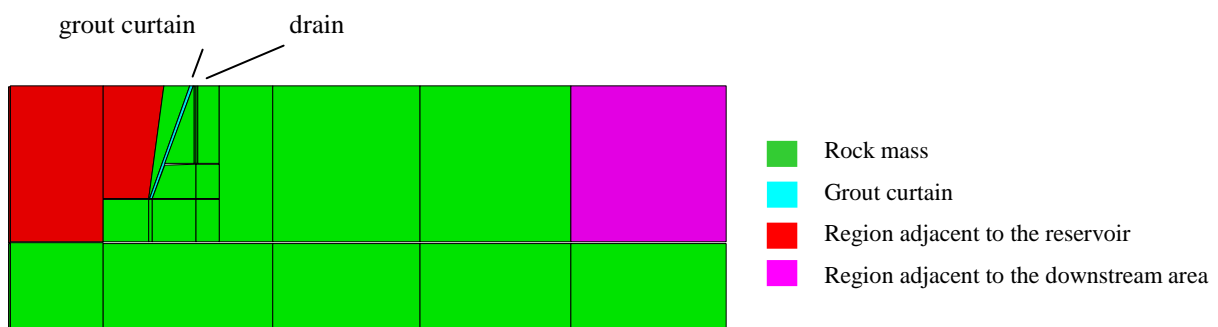


Figure 6.15 – Regions defined in the 3D model of the foundation of Alqueva dam.

6.3.2 Hydraulic boundary conditions and numerical results

Numerical analysis was carried out assuming the reservoir at an elevation of 143.0 m and the water downstream from the dam-wall at an elevation of 75.0 m. The concrete/rock mass interface and the bottom and lateral boundaries were assumed to be impervious. A zero pressure was assumed at the drains' head.

Seepage analysis was first carried out using a single strip 1.5 m wide, in an area of the foundation with a width corresponding to half the distance between drains. With this model, the numerical discharges are (the negative value means that water flows into the model):

$$Q_{\text{upstream}} = - 8.0149 \times 10^{-6} \text{ m}^3/\text{s};$$

$$Q_{\text{drain}} = 7.7368 \times 10^{-6} \text{ m}^3/\text{s};$$

$$Q_{\text{downstream}} = 0.2380 \times 10^{-6} \text{ m}^3/\text{s}.$$

The quantity of water flowing into and out of the model is respectively:

$$Q_{\text{into the model}} = 8.0928 \times 10^{-6} \text{ m}^3/\text{s};$$

$$Q_{\text{out of the model}} = 8.0183 \times 10^{-6} \text{ m}^3/\text{s};$$

and the maximum unbalanced nodal flux, at the block nodes, is $1.6058 \times 10^{-11} \text{ m}^3/\text{s}$. The reason why the quantity of water flowing into and out of the model does not sum up is explained in section 6.3.4.

The hydraulic head contours are presented in Figure 6.16 .

6.3.3 Influence of mesh size

In order to reduce run times, two other meshes were defined which are similar to the fine mesh shown in Figure 6.14 but with larger elements. In the second mesh, called coarse mesh, the average edge length of the tetrahedral zones close to the drain remains 0.30 m but it doubles in the other blocks. The third mesh, called very coarse mesh, differs in the average edge length of the zones close to the drain, which is 0.60 m. The second mesh has 27012 tetrahedra with 10297 grid points, which are about 21 % of the total elements and 27 % of the grid points of the initial model and the third mesh has 21947 tetrahedra with 8394 grid points, which are about 17 % of the total elements and 22 % of the grid points of the initial model. Figure 6.17 shows mesh details at the drain's upper and lower areas for both fine and very coarse meshes.

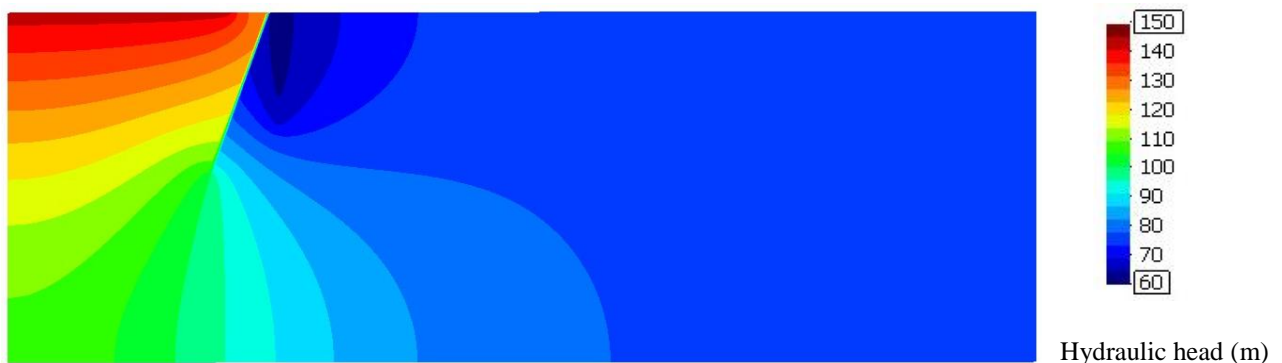


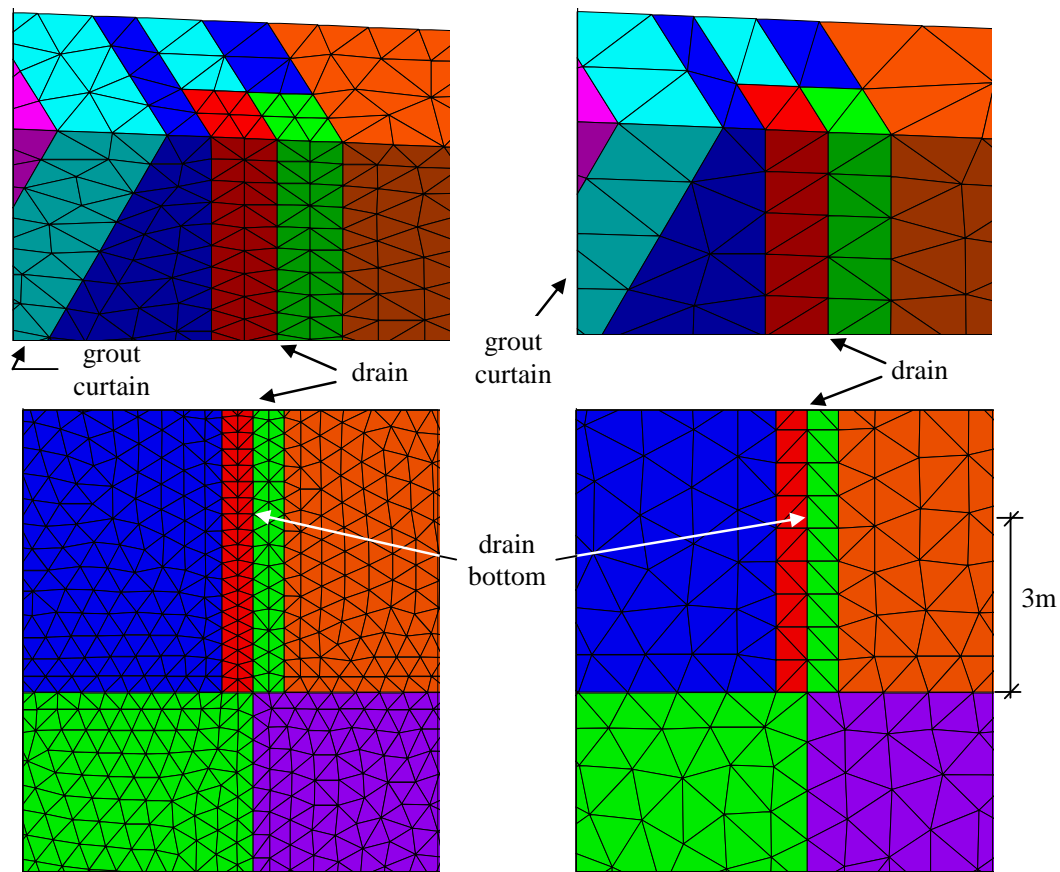
Figure 6.16 – Hydraulic head contours for $H_u = 143.0 \text{ m}$ and $H_d = 75.0 \text{ m}$, with $k_{\text{grout curtain}} = 0.01 k_{\text{rock mass}}$.

The numerical discharges obtained with each model are presented in Table 6.6. It is possible to conclude that drain discharges using the coarse and very coarse mesh are just 1.8 % and 3.4 % respectively greater than those obtained with the fine mesh.

In the fine mesh, convergence in steady state conditions is achieved in about 3.0×10^5 steps, which takes about 8 and a quarter hours. With the coarse mesh, convergence is achieved in about 1.5×10^5 steps, which takes 54 minutes and with the very coarse mesh in about 1.0×10^5 steps, which takes just 30 minutes. Run times presented (Table 6.7) were obtained in numerical analyses conducted with a single strip 1.5 m wide. If the model includes more strips, run times increase accordingly.

Variations in hydraulic head along horizontal lines 40 m long in various sections of two planes perpendicular to the line of drains were compared. The first plane crosses the drain and the other is 1.5 m away from the drain, midway between drains. Five horizontal lines were considered in each plane, positioned at the top, the middle and the bottom of the drain, and 1 m and 5 m below the bottom of the drain. Comparison of results obtained with the fine and the very coarse mesh (Figure 6.18) led to the conclusion that with the exception of the areas inside the grout curtain and around the drain, differences in hydraulic head along the lines are less than 2.6 %. Inside the grout curtain, differences reach about 17 % (because the very coarse mesh has only one element across the grout curtain's thickness, while the fine mesh has two), but in the vicinity of the drain, differences in the hydraulic head are less than 4 %.

In the case studied, the widening of initial mesh elements to create another with about 17 % of the number of elements and 22 % of the number of grid points, has little influence on the value of the discharges and on the hydraulic heads, and reduces run times by about 90 %. Therefore, the very coarse mesh, shown in Figure 6.17 and in Figure 6.19, was used in the subsequent analyses.



Fine mesh

Very coarse mesh

Figure 6.17 – Fine mesh and very coarse mesh: details at the drain’s upper and lower areas.

Model	Discharge ($\times 10^{-6}$) (m ³ /s)			Water flowing into the model ($\times 10^{-6}$ m ³ /s)	Water flowing out of the model ($\times 10^{-6}$ m ³ /s)	Unbalanced flow ($\times 10^{-11}$ m ³ /s)
	upstream	drain	downstream			
Fine mesh	- 8.0149	7.7368	0.2380	8.0928	8.0183	1.6058
Coarse mesh	- 8.0382	7.8760	0.2271	8.1948	8.1658	2.1721
Very coarse mesh	- 8.1177	8.0025	0.1929	8.2760	8.2479	2.2151

Table 6.6 – Influence of mesh size. Numerical discharges with different meshes.

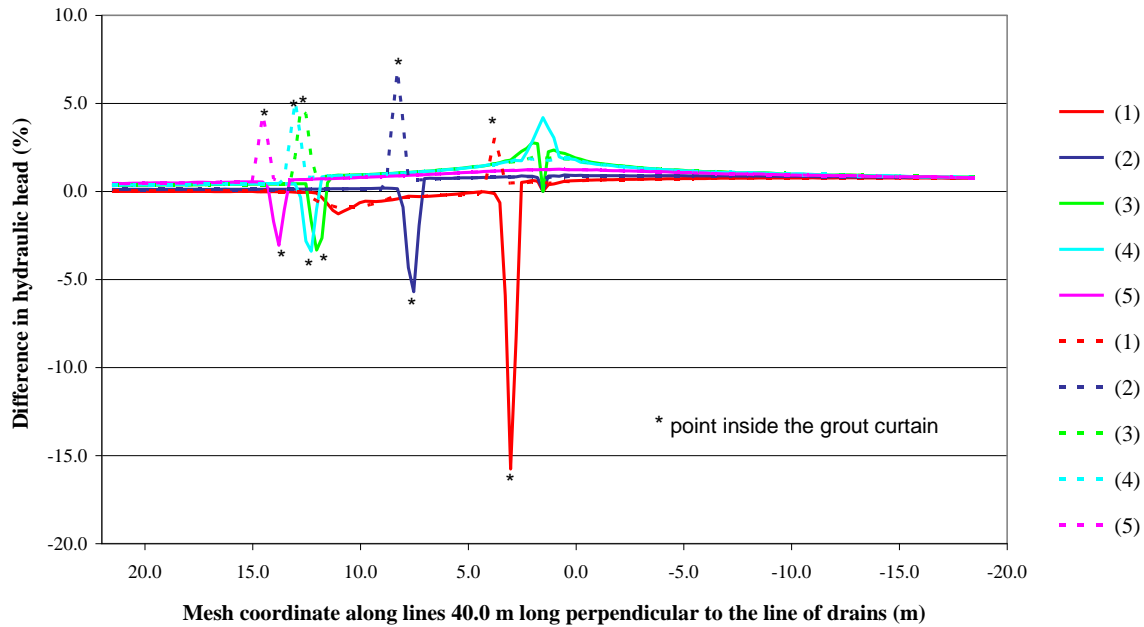
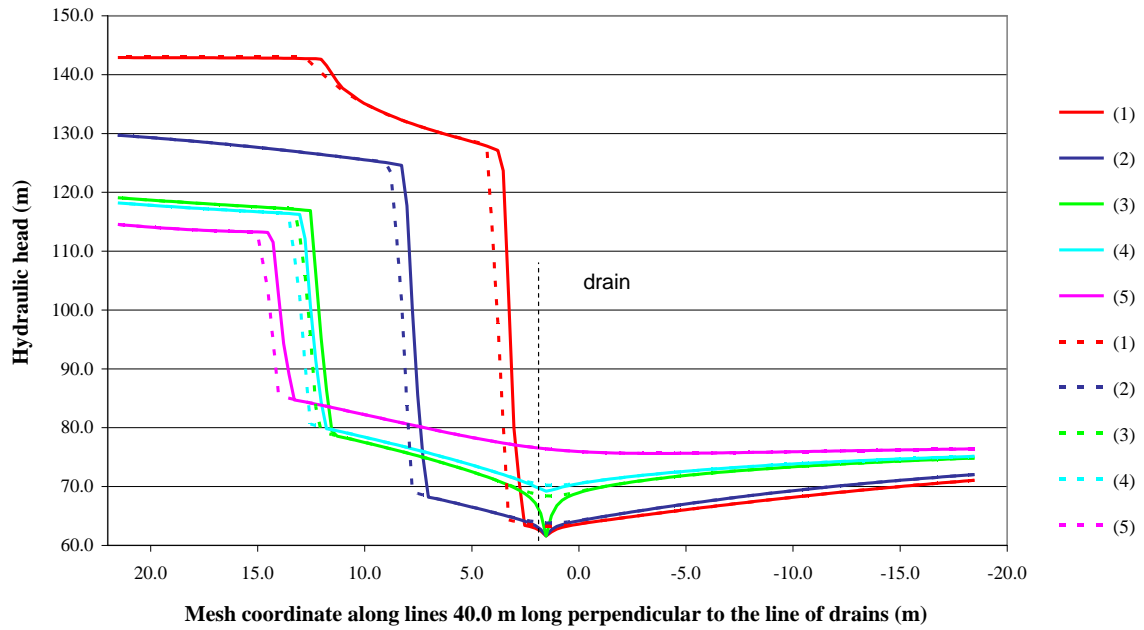
Model	Number of steps to reach steady state conditions	Run time
Fine mesh	3×10^5	8 hours 15 minutes
Coarse mesh	1.5×10^5	54 minutes
Very coarse mesh	1×10^5	30 minutes

Table 6.7 – Influence of mesh size. Number of steps to reach steady state conditions and run times.

6.3.4 Use of single/double precision version

The numerical results presented in the previous sub-chapter show that there is a difference of between $0.04 \text{ m}^3/\text{s}$ and $0.08 \text{ m}^3/\text{s}$ in the quantity of water flowing into and out of the model. Numerical analysis was carried out with the single-precision version, but 3DEC includes a separate executable code written entirely in double-precision. This version is useful in models where critical information is lost because of the dimension of the models, such as fluid flow models where more than 1,000,000 cycles may be executed, but requires three times the amount of memory required by the single-precision version (Itasca 2003). To confirm that the difference between inflow and outflow values was due to the use of the single-precision version, numerical experiments were carried out with the double-precision version. Table 6.8 shows a comparison of the numerical value of the discharges with both versions.

Analysis of results shows that when the double-precision version is used the quantity of flow into and out of the blocks is almost the same. The single-precision code is rounded off to six decimal places. The value of the unbalanced flow is around 10^{-11} , therefore, in practice, the numerical value of the discharge is not altered in each step (it is like adding zero). In the double-precision version, rounded off to 20 decimal places, the solution converges and the value of the out-of-balance flow is around 10^{-19} . Differences in numerical discharges obtained with single and double-precision versions are less than 0.4 % and run times are significantly less when single-precision is used (Table 6.9), because of the smaller number of steps necessary to reach convergence. Therefore single-precision was used in subsequent numerical analysis.



—	Plane perpendicular to the line of drains, crossing the drain
- - - -	Plane perpendicular to the line of drains midway between drains
(1)	Top of the drain
(2)	Middle of the drain
(3)	Bottom of the drain
(4)	1 m below the bottom of the drain
(5)	5 m below the bottom of the drain

Figure 6.18 – Hydraulic head (fine mesh) and differences in percentage in hydraulic head (fine mesh and very coarse mesh) along horizontal lines 40 m long at various elevations.

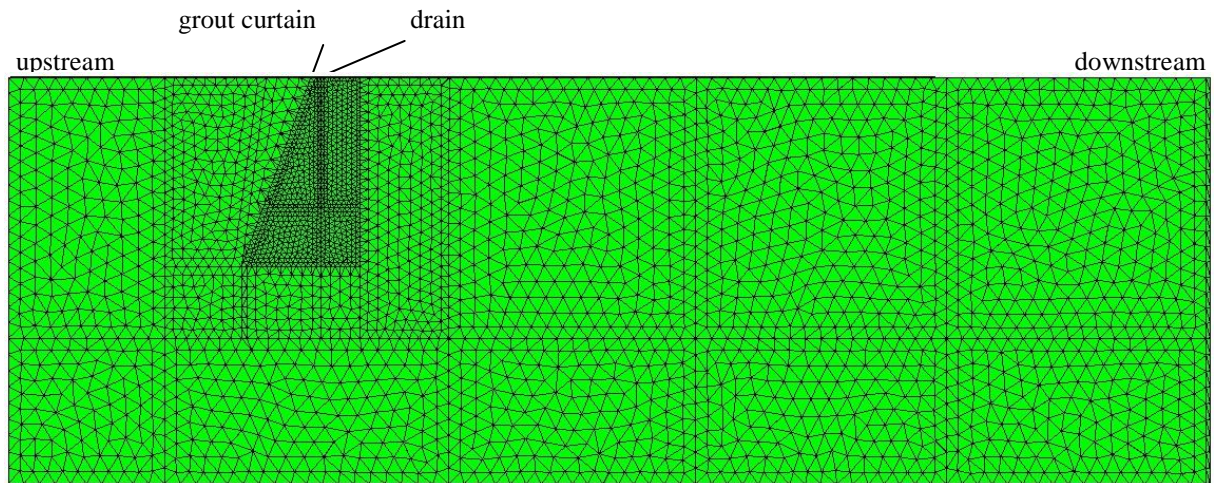


Figure 6.19 - 3D model of the foundation of Alqueva dam. Division into blocks and internal mesh of a 1.5 m wide vertical strip. Very coarse mesh.

Model	3DEC version	Discharge ($\times 10^{-6} \text{ m}^3/\text{s}$)			Water flowing into the model ($\times 10^{-6} \text{ m}^3/\text{s}$)	Water flowing out of the model ($\times 10^{-6} \text{ m}^3/\text{s}$)	Unbalanced flow (m^3/s)
		upstream	drain	downstream			
Fine mesh	single	- 8.0149	7.7368	0.2380	8.0928	8.0183	1.6058×10^{-11}
	double	- 7.9957	7.7693	0.2568	8.0728	8.0728	3.6227×10^{-16}
Coarse mesh	single	- 8.0382	7.8760	0.2271	8.1948	8.1658	2.1721×10^{-11}
	double	- 8.0308	7.8876	0.2351	8.1872	8.1872	3.9599×10^{-20}
Very coarse mesh	single	- 8.1177	8.0025	0.1929	8.2760	8.2479	2.2151×10^{-11}
	double	- 8.1108	8.0138	0.2008	8.2688	8.2688	4.0785×10^{-19}

Table 6.8 – Numerical value of the discharges with single and double-precision versions.

Model	3DEC version	Number of steps to reach steady state conditions	Run time
Fine mesh	single	3×10^5	8 hours 15 minutes
	double	4.5×10^5	15 hours
Coarse mesh	single	1.5×10^5	54 minutes
	double	2×10^5	1 hour 42 minutes
Very coarse mesh	single	1×10^5	30 minutes
	double	2×10^5	1 hour 15 minutes

Table 6.9 – Number of steps to reach steady state conditions and run times with single and double-precision versions.

6.4 Numerical modelling of borehole water-inflow tests

6.4.1 Introduction

In this section, the development of detailed 3D numerical models for seepage analysis in two site-specific areas of the foundation is described and the results are presented and analysed. Borehole water-inflow tests carried out in drains D20 D and D25 D are simulated using models 9 m wide which include the drain tested and the two adjacent drains.

As mentioned in Chapter 4 (section 4.5), borehole water-inflow tests were carried out in the area of the valley bottom where the highest discharges are recorded, where the bottom of the valley meets the right hand side abutment. Figure 6.20 shows where water flows into each borehole located in the vicinity of drains D20 D and D25 D, identified with both water electrical conductivity analysis and borehole water-inflow tests.

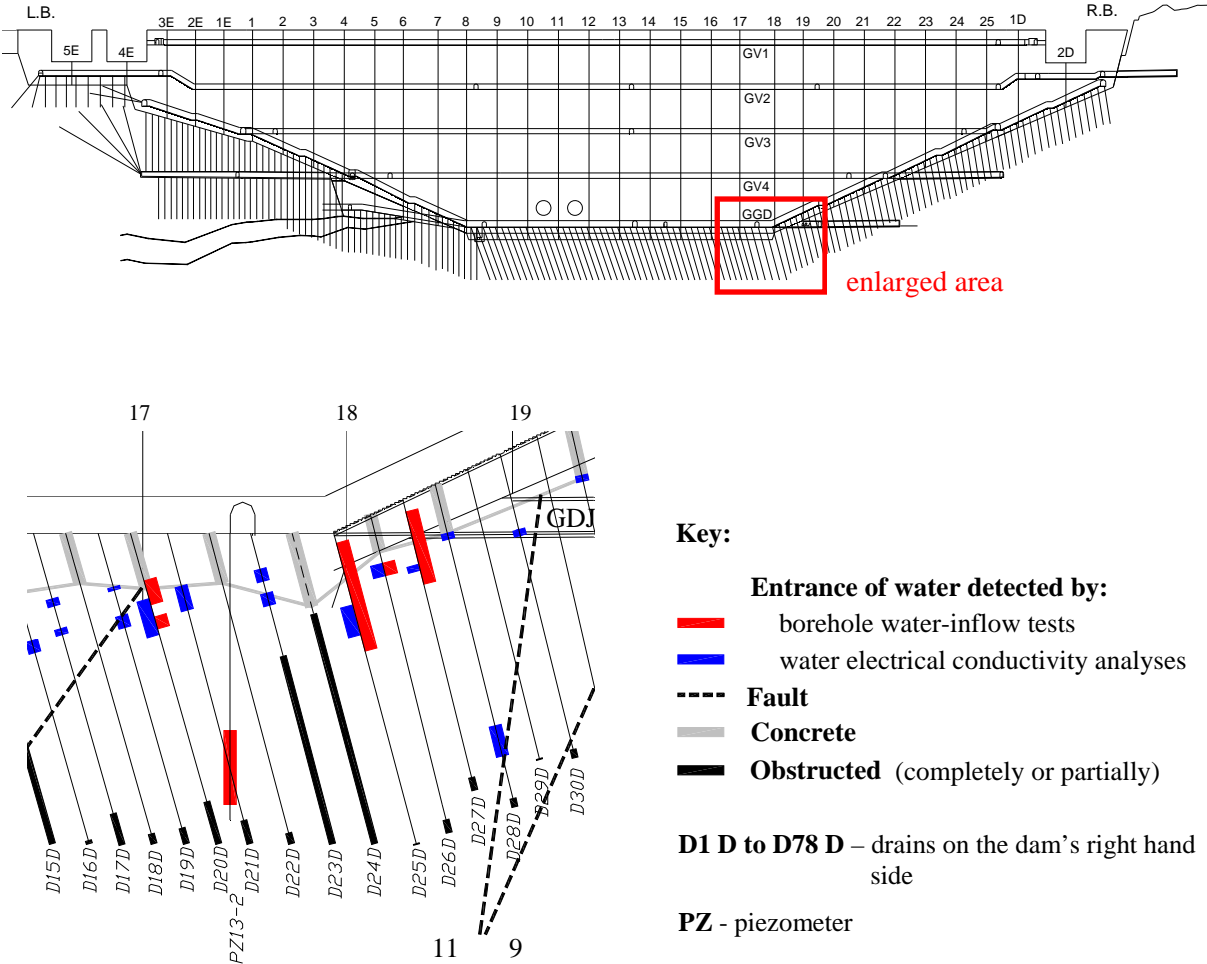


Figure 6.20 – Inflow of water into each borehole in the area where the bottom of the valley meets the right hand side abutment.

As previously mentioned, in borehole water-inflow tests, fixed test intervals are considered and isolated and the boreholes are tested in consecutive sections throughout their lengths. For each test interval, flow rates and water pressures in the hole being tested and in the nearby boreholes are recorded until steady state conditions are achieved. In this study closed boreholes are simulated by constraining the hydraulic head to be an unknown constant along each borehole's length, at the same time not allowing water to flow out of the hole. Closed borehole intervals, either with single or double packers, are simulated in the same way, this time allowing discharges above the single packer, or above the upper packer whenever a double packer is used. Areas where flow paths cross the drains are modelled by bands of elements of higher permeability. With the current 3DEC code it is not possible to display neither these bands of elements, nor areas inside one or more than one model block with a different permeability, therefore three-dimensional AUTOCAD drawings were made which allow the presentation of the various models' assumed hypotheses. Figure 6.21 shows a 3D perspective of a part of the 9 m wide foundation model in relation to the dam, in which the three drains included in the model are shown in red and the grout curtain, located upstream from the drains, is shown in dark gray.

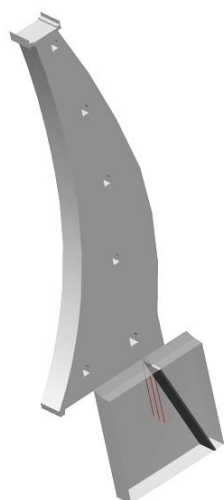
6.4.2 Numerical modelling of tests carried out in drain D25 D

6.4.2.1 Introduction

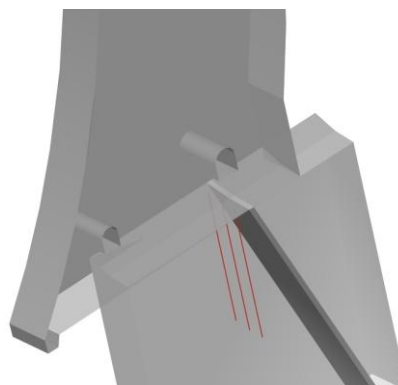
Tests carried out in drain D25 D led to the conclusion that water flowed into the borehole in the top 10 m and that 90 % of the water flowed into the borehole at between 4.0 to 7.0 m down from the drain head. As shown in Figure 6.20 water inflow in drain D26 D was only observed at between 4.0 and 5.0 m down from the drain head, and drain D24 D was obstructed 0.65 m below concrete/rock mass interface. To simulate tests carried out in drain D25 D, where only a single area where water flowed into the borehole was observed, it was necessary to develop a model which could simulate two different situations (Figure 6.22):

- normal operating conditions;
- drain D25 D closed.

In situ results on two different dates had been recorded with differences in the water level in the reservoir of 6.5 m. Table 6.10 shows the observed discharges and water pressures of both situations on the two different dates. Results presented reveal that the raising of the reservoir from elevation 143.6 m up to elevation 150.0 m leads to a slight increase in flow rates (8.5 % up to 19 %). On both dates, when drain D25 D is closed water pressures of about 5.0 bar are reached, which correspond to almost 60 % of the hydraulic head.

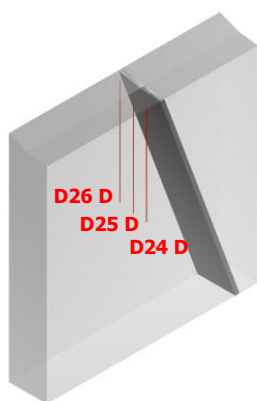


9m wide foundation model in relation to the dam

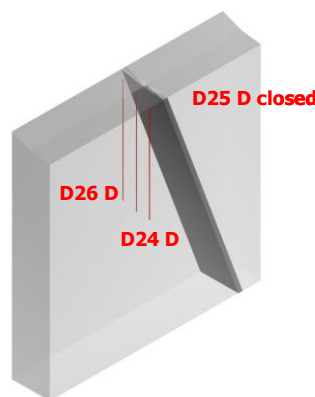


Model detail in the vicinity of the drains

Figure 6.21 – Perspective of the three-dimensional AUTOCAD drawing developed to represent the various models' assumed hypotheses.



Normal operating conditions



Drain D25 D closed

Figure 6.22 – Situations to be considered to simulate tests carried out in drain D25 D.

Date	H reservoir (m)	Normal operating conditions			Drain D25 D closed				
		Discharge (l/min)			Discharge (l/min)			Water pressure (bar)	Percentage of hydraulic head (%)
		D24 D	D25 D	D26 D	D24 D	D25 D	D26 D		
Oct. 2006	143.6	0.04	2.01	1.03	0.04	-	1.29	4.825	58.6 %
Mar. 2007	150.0	drops	2.18	1.23	drops	-	1.53	5.250	59.1 %

Table 6.10 – Discharges and water pressures measured in drains D24 D, D25 D and D26 D both in normal operating conditions and with drain D25 D closed.

6.4.2.2 Hydraulic boundary conditions

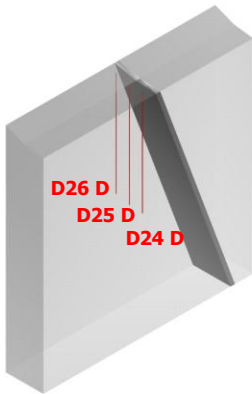
The first numerical analysis, presented in section 6.2, was carried out assuming the reservoir at an elevation of 143.0 m and the water downstream from the dam-wall at an elevation of 75.0 m. A zero pressure was assumed at the drains' head. These boundary conditions are adequate in a global seepage model of the foundation. However, for a detailed analysis of seepage in a restricted area, the downstream boundary condition is not appropriate, as the grout and drainage curtains drilled from the downstream dam-wall change seepage flow in the upstream-downstream direction. Therefore, the following numerical analysis was carried out assuming the hydraulic head recorded at the piezometers installed at the substation slab, at the toe of the dam. From 16-20 October 2006, with the reservoir at an elevation around 143.6 m, and from 19-23 March 2007, with the water level around 150.0 m, average hydraulic heads of 69.9 m and 70.3 m were recorded at the mentioned piezometers. A hydraulic head of 70.0 m was assumed on both dates. With these boundary conditions, the model could have been shortened downstream from the dam, in order to reduce run times, but it was decided to maintain it.

6.4.2.3 Numerical experiments

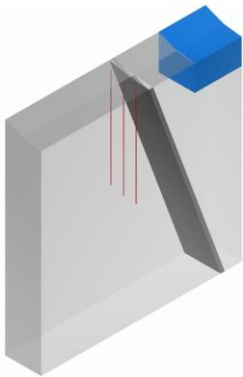
The detailed 3D model to simulate tests carried out in drain D25 D was developed in various steps with progressive enhancements, shown in Figure 6.23. In each one of these steps the two situations to be simulated were taken into account and the different parameters were adjusted in order to make the numerical results correspond more closely to the observed discharges and water pressures, shown in Table 6.11. It is assumed that the rock mass foundation is homogeneous and isotropic and that the grout curtain is 10 times less pervious than the rock mass.

Firstly, a homogeneous and isotropic media was assumed and the rock mass permeability necessary to obtain the average value of the discharges in drain D25 D's area of influence was determined (Figure 6.23 - Step 1). Secondly, a near-surface area of higher permeability upstream from the dam was considered, in order to simulate the assumed existence of vertical fissures within the rock mass close to the heel of the dam (Figure 6.23 - Step 2). These fissures are opened by the development of tensile stresses in this area, due to the filling of the reservoir. Thirdly, a horizontal layer of higher permeability between the upstream area and the drains was considered. This layer crosses the grout curtain, simulating a probable area of the foundation where the total sealing of discontinuities with very small apertures was not achieved (gap in the grout curtain). It was first assumed that this layer of higher permeability was 3.0 m deep and crossed the whole model's width (Figure 6.23 – Step 3) but the layer width was then gradually changed, in order for numerical values to correspond to recorded discharges and water pressures (Figure 6.23 – Steps 4 and 5). Finally two different layers

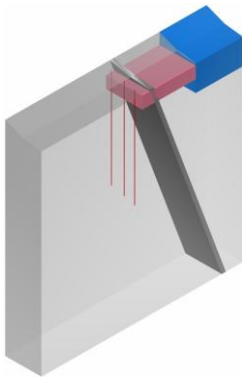
were modelled upstream from drains D25 D and D26 D; both layers are 3.0 m deep but the layer at D26 D is 2.0 m higher to take into account the point at which discontinuities cross each one of the drains (Figure 6.23 – Step 6). With this final change numerical results were closer to observed values.



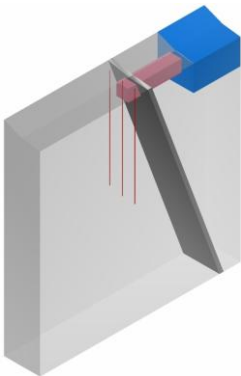
Step 1 - Homogeneous and isotropic rock mass.



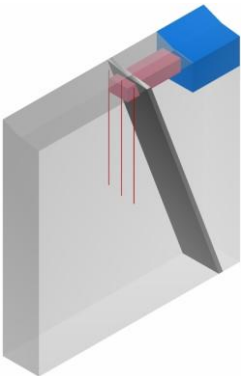
Step 2 - Near-surface area of higher permeability upstream from the dam.



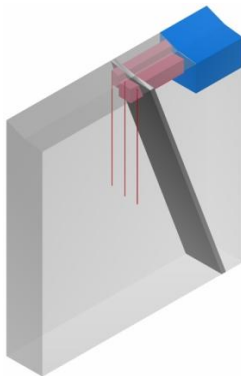
Step 3 - Horizontal layer of higher permeability between the upstream area and the drains, crossing the whole model's width.



Step 4 - Horizontal layer of higher permeability between the upstream area and the drains, upstream from drain D25 D.



Step 5 - Horizontal layer of higher permeability between the upstream area and the drains, upstream from drain D25 D and with a width equal to half the distance between drains, close to drain D25 D, upstream from drain D26 D.



Step 6 - Horizontal layers of higher permeability between the upstream area and drains D25 D and D26 D:
 i - with a width equal to the distance between drains, upstream from drain D25 D; and
 ii - with a width equal to half the distance between drains, close to drain D25 D, upstream from drain D26 D.
 The layer at drain D26 D is 2.0 m higher.

Figure 6.23 – Steps of model elaboration.

Date	H	H	H	Discharge in drain D25 D (l/min)	Average discharge in drain D25 D's area of influence (l/min)/m		Water pressure with drain D25 D closed (bar)
	reservoir	downstream	substation		including D25 D	not including D25 D	
	(m)	(m)	slab (m)				
Oct. 2006	143.6	81.95	69.9	2.01	0.23	0.12	4.825
Mar. 2007	150.0	81.60	70.3	2.18	0.27	0.15	5.25

Table 6.11 – Observed discharges in both drain D25 D and its area of influence, and water pressure at the drain head when it is closed.

During the model's development the first numerical experiments were carried out with a single strip 1.5 m wide and with a drain 25 m long. In order to avoid errors, an auxiliary model was also used, similar to that described in the previous section (section 6.3) but in which the parallel vertical foundation strips are positioned in such a way as to build a brick shape 9 m wide. Each drain is 25 m long and the same hydraulic head is assumed in the model's three drains. The model described in section 6.3, which takes into account both the horizontal and vertical curvatures of the dam where it meets the foundation, was used as a basis for the development of the seepage model in the vicinity of drain D25 D. In this latter model, the hydraulic head in each drain is the same as the drain head's elevation. The drains were first assumed to be 25 m long, in order to compare numerical results with those obtained with the auxiliary model. The drains' real length was used once the model had been developed.

Numerical experiments were carried out comparing the numerical results to the monitoring data collected in October 2006. A detailed description of results obtained in each modelling step is presented in the following paragraphs. In order to make the comparison of observed and numerical discharges easier, results are shown in (l/min) or ((l/min)/m).

First modelling step (Figure 6.23 - Step 1): a homogeneous and isotropic media was assumed. In a rock mass of uniform permeability k , the leakage varies linearly with k . Numerical analysis was carried out for two different hydraulic conductivity values: 1.5×10^{-8} m/s and 5.0×10^{-8} m/s (Table 6.12). Taking into account these results and the linear relationship between discharges and hydraulic conductivity values, a rock mass hydraulic conductivity of 4.0×10^{-8} m/s was first assumed in order to match the average discharge observed in drain D25 D's area of influence (0.23 (l/min)/m). As it had been observed that there is a seepage path crossing drain D25 D in its upper area, and the highest discharge is that observed in drain D25 D, it was later realised that rock mass permeability should be less than 4.0×10^{-8} m/s. The average discharge recorded in drain D25 D's area of influence, not including discharge in drain D25 D (0.12 (l/min)/m) would be achieved with a rock mass permeability of 2.0×10^{-8} m/s. However, the results of Lugeon type tests carried out while

drilling boreholes D24 D and D26 D led to the conclusion that, in the boreholes' vicinity the rock mass hydraulic conductivity was about 1.0×10^{-8} m/s (in drain D25 D rotary-percussive drilling was used; therefore no borehole log is available). A rock mass of 1.0×10^{-8} m/s was afterwards assumed. The average discharge is 0.17 l/min, or 0.06 (l/min)/m, which is 26 % of the observed discharge. This homogeneous model does not take into account either the usual existence of vertical or sub-vertical fissures within the rock mass close to the heel of the dam or the seepage paths detected while carrying out the borehole water-inflow tests.

Second modelling step (Figure 6.23 - Step 2): In a second modelling step, the existence of a near-surface area of higher permeability upstream from the dam was considered. It was assumed that this area's hydraulic conductivity was 10.0×10^{-7} m/s and that it was 7.0 m deep and 5.0 m long in the upstream-downstream direction. Table 6.13 shows the numerical results obtained with the three different models described on the previous page. It can be seen that the three models lead to the same average discharge. The model that takes into account curvatures of the dam where it meets the foundation leads to different discharges in the three drains, because each drain head is at a different elevation. In this case, about 40 % of the total discharge flows out of the model through drain D24 D, about 36 % through drain D25 D and about 24 % through drain D26 D. With this area of higher permeability, the average discharge increases about 24 % (from 0.17 l/min up to 0.21 l/min).

In a homogeneous and isotropic media the discharge per metre through a layer of height h is given by:

$$q = k i h \quad (6.1)$$

Flow in planar rock fractures can be modelled by means of the parallel plate model and the flow rate per unit width is thus expressed by the cubic law:

$$q = \nu a = \frac{a^3 g}{12 \nu} i \quad (6.2)$$

In the previous equations: k = hydraulic conductivity (m/s); i = hydraulic gradient (m/m); a = fracture hydraulic aperture (m); ν = kinematic viscosity of the fluid (m^2/s); and g = acceleration of gravity (m/s^2).

Model	Rock mass permeability ($\times 10^{-8}$ m/s)	Discharge (l/min)					Average discharge (l/min/m)
		upstream	drain			downstream	
			D24 D	D25 D	D26 D		
Homogeneous and isotropic rock mass	1.0	-0.17	-	0.17	-	0.00	0.06
	1.5	-0.26	-	0.26	-	0.00	0.09
	5.0	-0.85	-	0.85	-	0.00	0.28

Table 6.12 – Numerical discharges for different rock mass hydraulic conductivity values (model shown in Figure 6.23 - Step 1 (with a single strip 1.5 m wide)).

Model	Discharge (l/min)					Average discharge (l/min/m)
	upstream	drain			downstream	
		D24 D	D25 D	D26 D		
Single strip 1.5 m wide	-0.11	-	0.207	-	0.00	0.07
Auxiliary model	-0.63	0.207	0.208	0.207	0.01	0.07
Model that takes into account curvatures of the dam where it meets the foundation	-0.60	0.255	0.226	0.151	-0.01	0.07

Table 6.13 – Numerical discharges in models where a small area of higher permeability upstream from the dam is considered ($k_{\text{near surface area upstream from the dam}} = 10.0 \times 10^{-7}$ m/s) (Figure 6.23 - Step 2).

The average value of the fracture hydraulic aperture is determined equalling Equations 6.1 and 6.2. In the case being studied, $k = 10.0 \times 10^{-7}$ m/s; $h = 5.0$ m; $\nu = 1.01 \times 10^{-6}$ m²/s (water at 20 °C); and $g = 9.8$ m/s². Taking Equation 6.2 into account, the near-surface area of higher permeability upstream from the dam simulates a vertical discontinuity with a hydraulic aperture of 0.18 mm.

Third modelling step (Figure 6.23 - Step 3): As previously mentioned, 90 % of the water flowed into drain D25 D at between 4.0 to 7.0 m down from the drain head. To take into account this observed seepage path, a horizontal layer of higher permeability between the upstream area and the drains was considered. This layer is 3.0 m deep, and crosses drain D25 D at between 4.0 to 7.0 m down from the drain head. Numerical experiments were carried out with different permeability values (Table 6.14). Taking into account these results, a horizontal layer's hydraulic conductivity of 5.0×10^{-7} m/s was assumed, in order for the numerical discharge to correspond to that recorded in drain D25 D.

Model	horizontal layer's permeability ($\times 10^{-7}$ m/s)	Discharge (l/min)					Average discharge ((l/min)/m)
		upstream	drain			downstream	
			D24 D	D25 D	D26 D		
Single strip 1.5 m wide	1.0	- 0.57	-	0.57	-	0.00	0.19
	2.5	- 1.11	-	1.11	-	0.00	0.37
	4.0	- 1.64	-	1.63	-	0.00	0.54
	5.0	- 1.98	-	1.98	-	0.00	0.66

Table 6.14 - Numerical discharges for different hydraulic conductivity values of the horizontal layer upstream from the drains (model shown in Figure 6.23- Step 3 (with a single strip 1.5 m wide)).

When the above-mentioned parameters are considered in the model that takes into account curvatures of the dam where it meets the foundation, the numerical discharges are:

$$Q_{\text{upstream}} = - 5.21 \text{ l/min}$$

$$Q_{\text{drain D24 D}} = 2.61 \text{ l/min}$$

$$Q_{\text{drain D25 D}} = 1.89 \text{ l/min}$$

$$Q_{\text{downstream}} = 0.01 \text{ l/min}$$

$$Q_{\text{drain D26 D}} = 1.33 \text{ l/min}$$

Modelling steps 4 and 5 (Figure 6.23 - Steps 4 and 5): Numerical experiments were carried out with different layer widths, in order to make numerical results correspond to recorded discharges and water pressures. Two layer widths were considered: i) layer 3.0 m wide, upstream from drain D25 D; and ii) layer 4.5 m wide upstream from drain D25 D and with a width equal to half the distance between drains, close to drain D25 D, upstream from drain D26 D. In these modelling steps, numerical analysis was carried out not only with the three drains' assumed length of 25.0 m but also considering their real length. Results are shown in Table 6.15. With these models, both discharges and water pressures at drains D25 D and D26 D are not significantly different from those recorded. However, this model does not simulate properly the depth at which water inflow to drain D26 D was observed.

Horizontal layer's width (m)	Drains' length (m)	Discharge (l/min)					Average discharge ((l/min)/m)	Water pressure at drain D25 D's head (bar)
		upstream	drain			downstream		
			D24 D	D25 D	D26 D			
3.0 (*)	25.0	- 2.16	0.29	1.82	0.17	0.01	0.25	-
(1)	real	- 2.11	0.07	1.92	0.22	0.02	0.25	-
(2)	real	- 0.88	0.19	-	0.68	0.05	0.10	5.6
4.5 (**)								
(1)	real	- 2.73	0.07	2.23	0.77	0.02	0.34	-
(2)	real	- 1.81	0.14	-	1.85	0.05	0.22	4.0

(*) Upstream from drain D25 D.

(**) Upstream from drain D25 D and with a width equal to half the distance between drains, close to drain D25 D, upstream from drain D26 D.

(1) Normal operating conditions.

(2) Drain D25 D closed.

Table 6.15 – Numerical discharges for different widths of the horizontal layer upstream from the drains (model shown in Figure 6.23 - Steps 4 and 5 (that takes into account curvatures of the dam where it meets the foundation)).

Modelling step 6 (Figure 6.23 - Step 6): Finally, as previously mentioned, two different layers were modelled, upstream from drains D25 D and D26 D; both layers are 3.0 m deep but the layer at D26 D is 2.0 m higher to take into account the point at which discontinuities cross each one of the drains. These layers simulate horizontal discontinuities with a hydraulic aperture of 0.12 mm. New numerical analysis was carried out assuming the water level in the reservoir and the hydraulic head recorded at the piezometers installed at the substation slab in March 2007.

Figure 6.24 shows the parameter values used in the final model. Table 6.16 shows a comparison of recorded and numerical discharges and water pressures of both simulated situations on the two different dates (numerical results are shown in red). With this model, numerical discharges are about 8 % to 10 % higher than the recorded discharges and water pressures are about 6 % to 13 % lower, which can be considered sufficiently accurate. It can also be concluded that there is no change in the layers' hydraulic aperture due to increase in the water level in the reservoir from elevation 143.6 m up to 150.0 m.

Figure 6.25 shows the flow of water (l/min) entering each borehole water-inflow test interval, compared with the numerical results. The same figure shows a comparison of the recorded and the numerical accumulated discharge from the bottom to the borehole head. The drain's recorded discharge in normal operating conditions (reference discharge) is shown in both

graphs: in the first it allows the assessment of discharges in each test interval in relation to the drain's total discharge; in the second it allows the comparison between accumulated and total discharge.

Figure 6.26 shows the hydraulic head contours around the drains for a homogeneous rock mass, with a permeability of 1.0×10^{-8} m/s, and for the heterogeneous model.

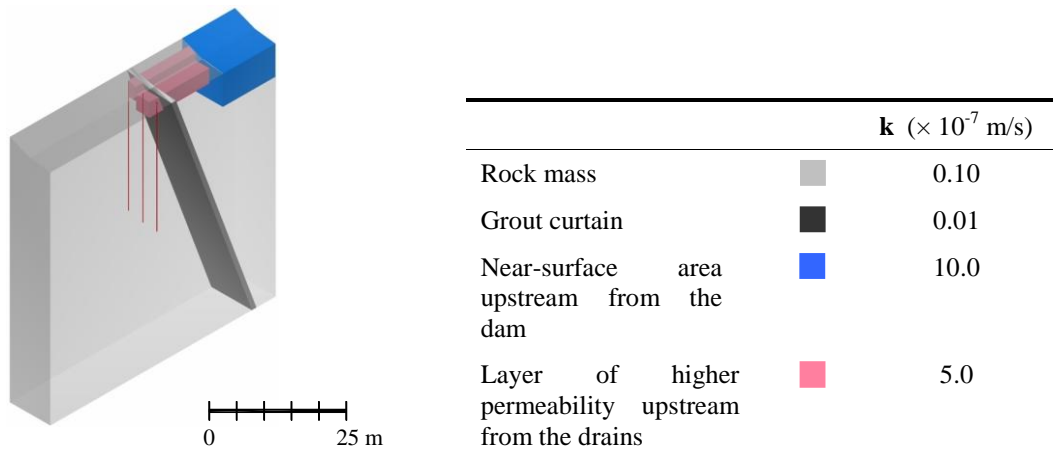


Figure 6.24 – Seepage model in the vicinity of drain D25 D (Figure 6.23 - Step 6). Model parameters.

Date	H reservoir (m)	Normal operating conditions			Drain D25 D closed				
		Discharge (l/min)			Discharge (l/min)			Water pressure (bar)	Percentage of hydraulic head (%)
		D24 D	D25 D	D26 D	D24 D	D25 D	D26 D		
Oct. 2006	143.6	0.04	2.01	1.03	0.04	-	1.29	4.825	58.6 %
		0.07	2.18	0.82	0.15	-	1.81	4.18	50.7 %
Mar. 2007	150.0	drops	2.18	1.23	drops	-	1.53	5.250	59.1 %
		0.07	2.35	0.88	0.16	-	1.96	4.50	50.6 %

Table 6.16 – Recorded discharges and water pressures and comparison to numerical results (shown in red).

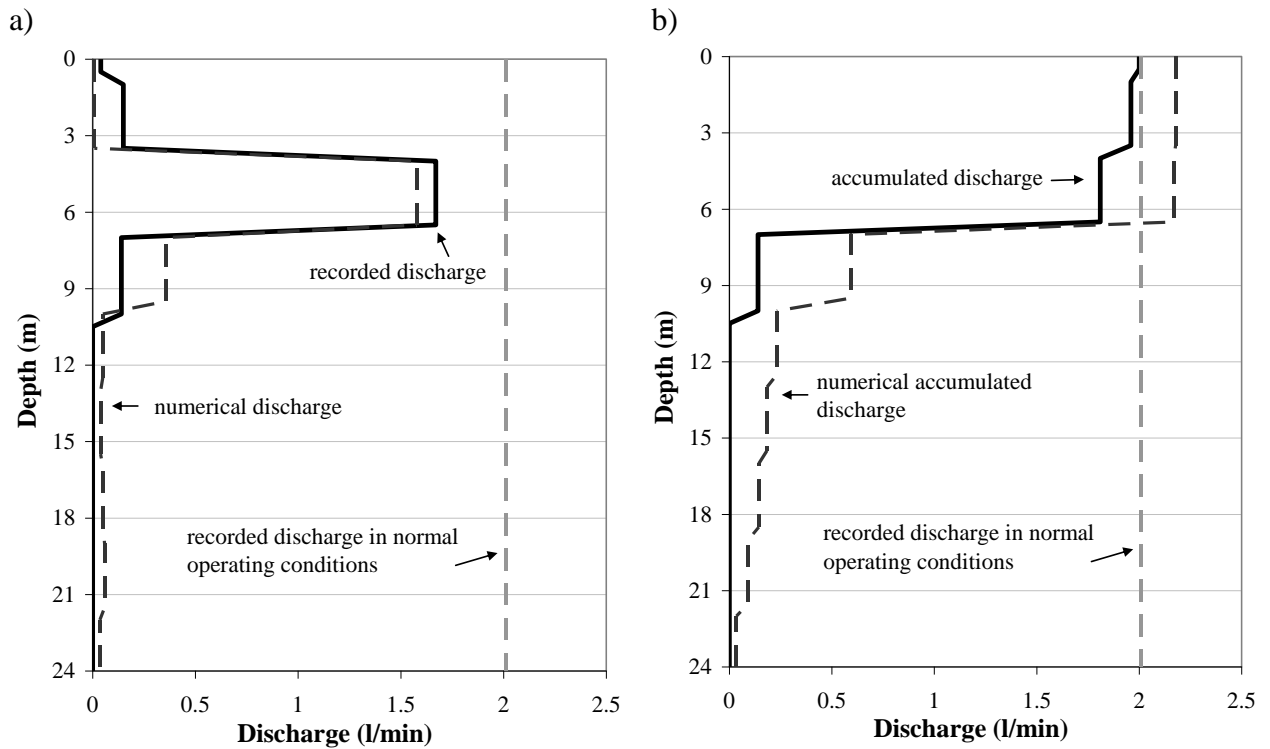


Figure 6.25 – Recorded and numerical discharge flowing into each of drain’s D25 D water-inflow test intervals (a) and accumulated discharge from the bottom to the head of the borehole (b).

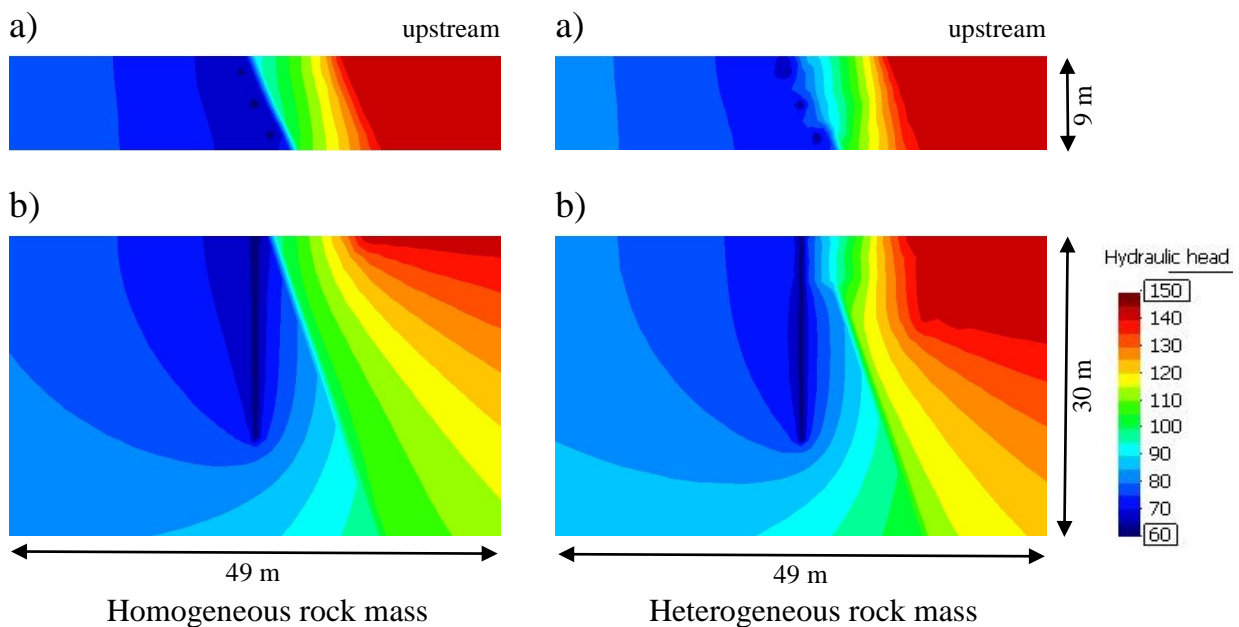


Figure 6.26 – Hydraulic head contours around the drains for a homogeneous rock mass and for the heterogeneous model: a) view from above; b) cut through drain D25 D, in the upstream-downstream direction.

6.4.2.4 Effect of local surface topography

The final model presented in the previous section takes into account the valley shape and the curvature of the dam where it meets the foundation. Drain D25 D is located in a particular area, where the bottom of the valley meets the right hand side abutment. In order to assess the effect of surface topography on water flow in the area between drain D25 D and the other two drains which are included in the model (D24 D on the valley floor and D26 D at the base of the slope), and study the distribution of discharges between the drains due to model geometry, a numerical experiment was carried out assuming that the hydraulic head in each one of the drains is the same as the drain’s head elevation, and neglecting the existence of water in the reservoir and in the area downstream from the dam. The medium was assumed to be homogeneous with a hydraulic conductivity of 1.0×10^{-8} m/s. The numerical experiments were carried out (Figure 6.27): i) assuming the three drains with a length of 25.0 m; and ii) considering the drains’ real length, assuming that drain D24 D is clogged from 6.75 m downwards. Numerical discharges are shown in Table 6.17. Results analysis reveals that:

- i) water flows into the model through drain D26 D and out of the model through the other two drains;
- ii) as expected, numerical discharges through the upstream and downstream areas are in practice zero, as they are four orders of magnitude smaller than drains’ numerical discharges;
- iii) when it is assumed that the three drains are 25.0 m long, about 42 % of the water flows out of the model through drain D24 D and about 58 % through drain D25 D;
- iv) when the drains’ real length is used, only about 10 % of the water flows out of the model through drain D24 D and about 90 % through drain D25 D.

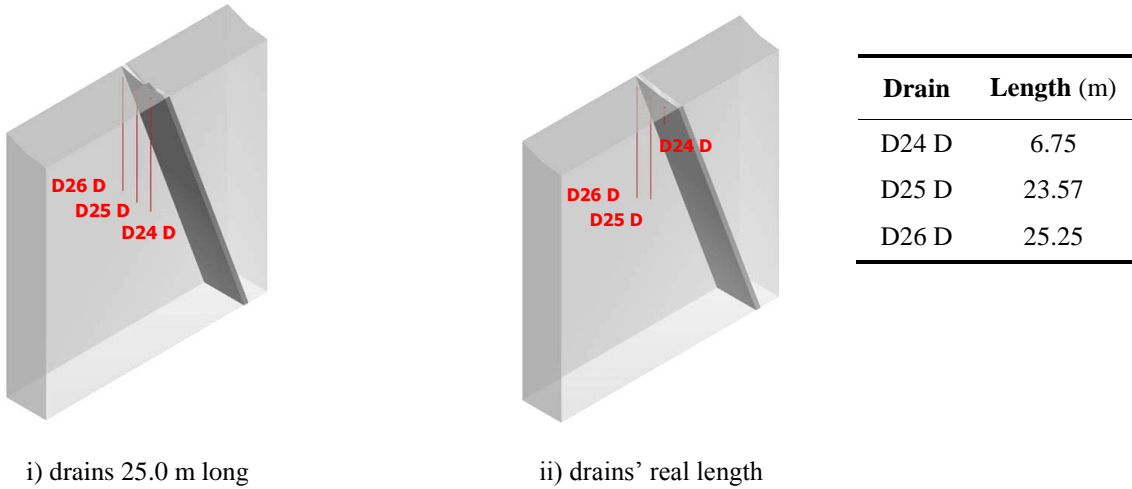


Figure 6.27 – Seepage model to study the effect of local surface topography.

Drains' length (m)	Discharge (m ³ /s)					Water flowing into the model (× 10 ⁻⁷ m ³ /s)	Water flowing out of the model (× 10 ⁻⁷ m ³ /s)	Out-of-balance flow (× 10 ⁻⁷ m ³ /s)
	upstream (× 10 ⁻⁷)	drain (× 10 ⁻⁷)			downstream (× 10 ⁻⁷)			
		D24 D	D25 D	D26 D				
25.0	0.00044	1.5256	2.1124	- 3.8998	0.00029	3.6998	3.6380	9.6 × 10 ⁻⁵
Real	0.00046	3.0815	2.8052	- 3.1834	0.00039	3.1834	3.1133	1.1 × 10 ⁻⁵

Table 6.17 – Distribution of discharges between the drains due to model geometry.

6.4.3 Numerical modelling of tests carried out in drain D20 D

6.4.3.1 Introduction

Tests carried out in drain D20 D led to the conclusion that water flowed into the borehole in two distinct areas: at between 8.0 to 9.0 m and at between 4.0 to 6.0 m down from the drain head. As shown in Figure 6.20 water inflow in the adjacent drains, D19 D and D21 D, also occurred in an area very close to the concrete/rock mass interface: in drain D19 D both at the concrete/rock mass interface and at 6.5 to 7.5 down from the drain head, and in drain D21 D in the first 2.0 m down from the concrete/foundation interface. Test results led to the conclusion that, unlike the lower flow path crossing drain D20 D, the upper was linked to both the adjacent drains. The model developed for the analysis of the tests in drain D20 D, should be able to simulate four different situations (Figure 6.28):

- normal operating conditions;
- drain D20 D closed;
- the single packer placed 7.0 m down from the drain head; and
- the double packer placed in such a way that the test interval extended from 4.0 to 7.0 m down from the drain head.

Table 6.18 shows the observed discharges and water pressures in the four different situations recorded in the tests carried out in September 2007. The average discharges in drain D20 D's area of influence, including and not including discharge in drain D20 D, were 0.07 and 0.02 (l/min)/m, respectively. In March 2007, with the water level in the reservoir around 150.0 m, the discharge in drain D20 D was 0.93 l/min and the water pressure when the drain was closed 1.20 bar, which corresponded to 13.6 % of the hydraulic head.

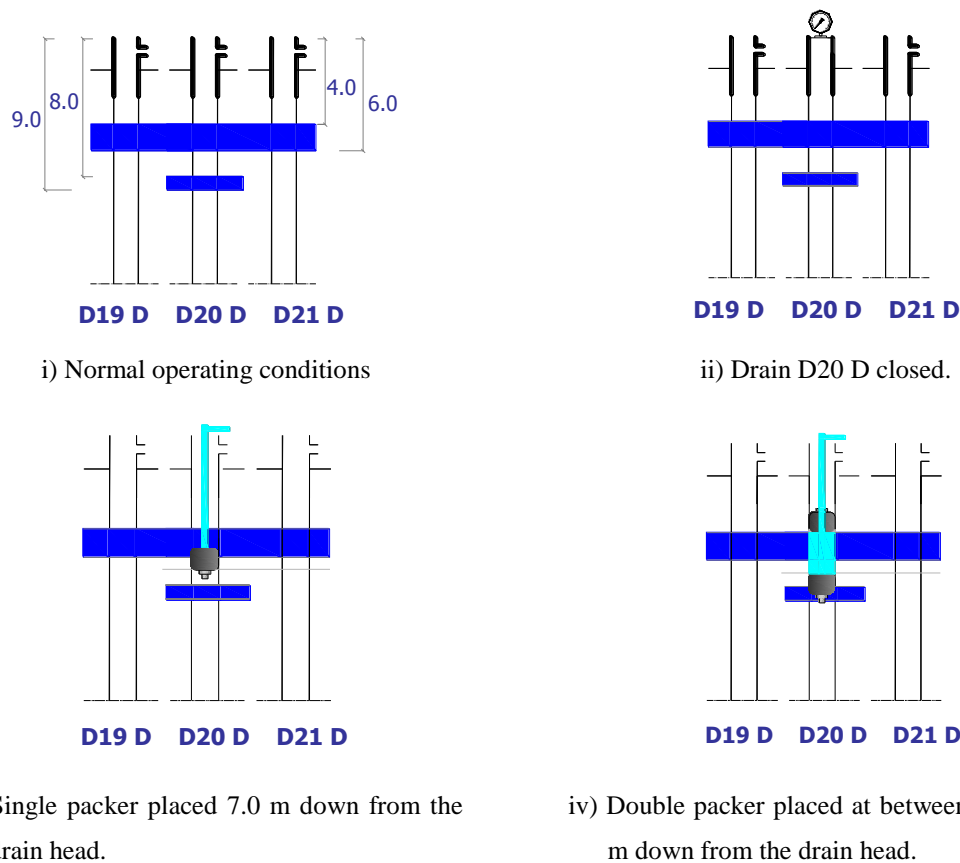


Figure 6.28 – Situations to be considered to simulate tests carried out in drain D20 D.

	Discharge (l/min)			Water pressure (bar)	Hydraulic head (m)	Percentage of hydraulic head (%)
	D19 D	D20 D	D21 D			
1. Normal operating conditions	0.14	0.58	0.04	-	-	-
2. Drain D20 D closed	0.31	-	0.24	0.75	68.70	8.6 %
3. Single packer placed 7.0 m down from drain head	0.13	0.54	0.04	1.50	76.92	17.5 %
4. Double packer placed at between 4.0 to 7.0 m down from drain head	0.30	-	0.24	0.625	62.55	7.3 %

Table 6.18 – Discharges and water pressures measured in drains D19 D, D20 D and D21 D in four different situations (September 2007, $H_{\text{reservoir}} = 148.0$ m; $H_{\text{downstream}} = 84.2$ m).

6.4.3.2 Hydraulic boundary conditions

As in the numerical modelling of tests carried out in drain D25 D, the water level in the reservoir and the hydraulic head recorded at the piezometers installed at the substation slab were assumed as boundary conditions. From 3-7 September 2007, with the reservoir at an elevation around 148.0 m, an average hydraulic head of 72.7 m was recorded at the piezometers.

6.4.3.3 Numerical experiments

The detailed 3D model to simulate tests carried out in drain D20 D was developed in a similar way to that for drain D25 D. However, a greater number of numerical experiments had to be carried out, due to difficulties found during the model's development. As previously, it is assumed that the rock mass foundation is homogeneous and isotropic and that the grout curtain is 10 times less pervious.

Firstly, a homogeneous and isotropic media was assumed and the rock mass hydraulic conductivity necessary to obtain the average value of the discharges in drain D20 D's area of influence, not including discharge in drain D20 D, was determined. In drain D20 D's area of influence, discharges are very low, therefore a hydraulic conductivity of 1.5×10^{-9} m/s was first assumed. Lugeon type tests carried out while drilling drains D18 D and D20 D led to the conclusion that the hydraulic conductivity was almost zero in most of the test intervals. At drain D18 D's upper section, in a length of 5.0 m down from concrete/rock mass interface and at drain D20 D's lower area, permeability values of 1.0×10^{-8} m/s were recorded.

Secondly, a near-surface area of higher permeability upstream from the dam was considered. This area is identical to the one considered in the model presented in the previous chapter, both in dimension and hydraulic conductivity. With this area of higher permeability, discharge increases about 22 % (from 0.027 l/min to 0.033 l/min).

In the above-mentioned steps only the first test stage, simulating normal operating conditions, was modelled.

Thirdly, a horizontal layer of higher permeability between the upstream area and drain D20 D was considered. This layer was located 8.0 to 9.0 m down from the drain head, in order to simulate the lower seepage path. Several numerical experiments were carried out in order to make results correspond to the observed discharges and water pressures, in normal operating conditions, with drain D20 D closed, and with the single packer placed 7.0 m down from the drain head. It was observed that with the hydraulic conductivity necessary to achieve the recorded discharge in drain D20 D, the water pressure below the packer was much higher than that recorded. Numerical discharges in adjacent drains were lower than those recorded.

To reduce water pressures, it was assumed that the top 5.0 m of the foundation rock mass were more pervious than the remaining domain. This upper area of higher hydraulic conductivity tried to simulate a more disturbed area, due to foundation excavation. The existence of this area would lead to greater discharges and, consequently, lower water pressures. Results were only slightly altered when the existence of this area was taken into account, thus it was decided not to make this change.

In order to reduce water pressures, at the same time maintaining the numerical discharge in drain D20 D, the horizontal layer of higher permeability upstream from the drain was extended 35.0 m downstream to reach the substation. It was later realised that in the model this layer should be at least 2.0 m deep, to include all the zones. Due to great difficulties in making numerical discharges in drains D19 D and D21 D correspond to recorded discharges, it was decided to consider the average value of the discharges recorded in these two drains. In this case, advantage was taken of symmetry and therefore only one half of the domain width was taken into account in subsequent analysis.

Another attempt was made to reduce water pressures, increasing the rock mass hydraulic conductivity at its lower depths. This would also lead to a greater discharge in adjacent drains. Numerical experiments were carried out with rock mass hydraulic conductivity values varying from 1.5×10^{-9} m/s up to 7.5×10^{-9} m/s. In each numerical experiment, the horizontal layer's hydraulic conductivity had to be adjusted.

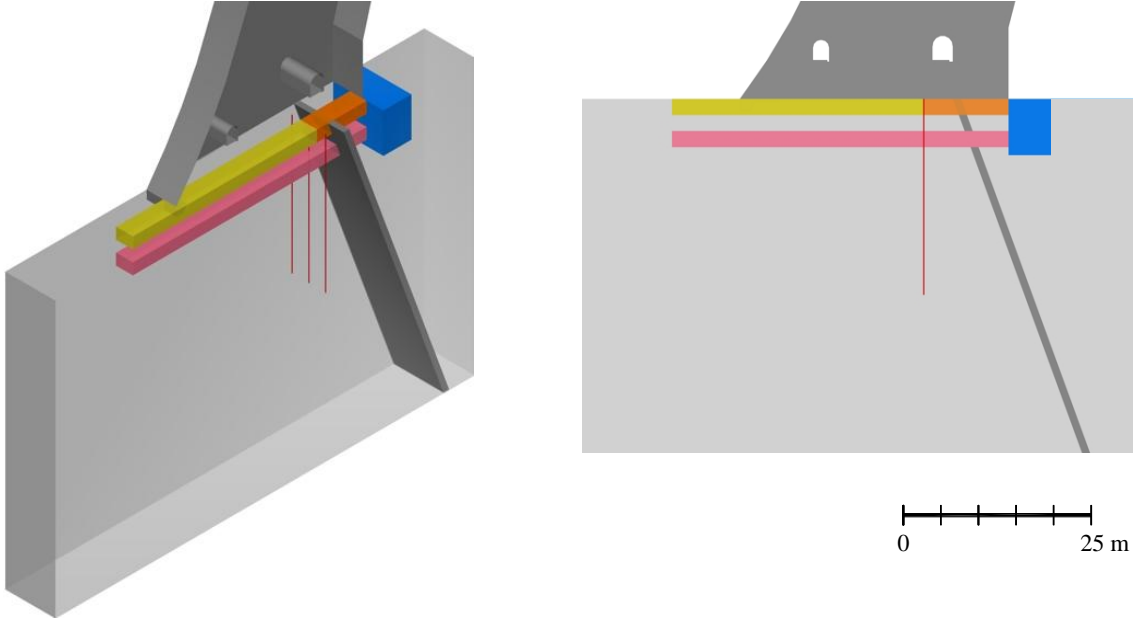
The existence of the upper seepage path was afterwards simulated with a layer of higher permeability which extended from the upstream area to the substation. Once again, with the hydraulic conductivity values necessary to achieve the discharge distribution along drain D20 D, the numerical water pressures were much higher than those recorded.

While carrying out borehole water-inflow tests in drain D20 D it was observed that there was a small quantity of water leaking from the floor of the downstream drainage gallery. When the borehole was closed the amount of water increased. The lower recorded water pressures could be due to this loss of water; therefore to simulate this leakage, an additional hydraulic boundary condition was considered: it was assumed that 14.0 m downstream from the drain, in a square with sides 4.0 m long, the hydraulic head on the model's upper horizontal boundary was the same as the gallery floor elevation.

Finally, the upper layer's hydraulic conductivity downstream from the drain was increased. This change led to almost the same numerical discharges in drains and to lower water pressures. The layer's lower hydraulic conductivity upstream from the drain simulates the presence of the grout curtain, which is probably partially inefficient in this area.

Figure 6.29 shows the parameter values used in the final model. Table 6.19 shows a comparison of recorded and numerical discharges and water pressures in the four different situations (numerical results are shown in red). With this model, numerical discharges in drain D20 D are about 3 % to 15 % lower than the recorded discharges and the differences in hydraulic head are less than 8 %, which, as in the case of drain D25 D, can be considered sufficiently accurate. However, the model does not simulate properly the increase in discharges in the adjacent drains when drain D20 D is closed (modelling situations 2 and 4).

Analysis of numerical discharges, shown in Table 6.20, reveals that in the four different situations about 68 % of the quantity of water that flows into the model comes from the reservoir and the remaining water from downstream. The leakage from the floor of the downstream drainage gallery plays a significant role in the model, as:



	k ($\times 10^{-7}$ m/s)			k ($\times 10^{-7}$ m/s)	
Rock mass	■	0.03	Upper layer of higher permeability upstream from the drains	■	1.5
Grout curtain	■	0.003	Upper layer of higher permeability downstream from the drains	■	30.0
Near-surface area upstream from the dam	■	10.0	Lower layer of higher permeability	■	0.43

Figure 6.29 – Seepage model in the vicinity of drain D20 D. Model parameters.

- in modelling situations 1 and 3, discharge in drain D20 D is very close to that lost through the leak; and
- in modelling situations 2 and 4, the quantity of water flowing out of the model from the leakage is more than 80 % of the discharge coming into the model.

However, these results do not correspond to what was observed, as, although there was no way of measuring, it was evident that the amount of discharge was very small, apparently less than 0.05 l/min. In this final model, the lower layer, with a hydraulic conductivity of 4.3×10^{-8} m/s, simulates a horizontal discontinuity with a hydraulic aperture of only 0.05 mm. The upper layer, with an equivalent hydraulic conductivity of 5.41×10^{-7} m/s, simulates a layer with a hydraulic aperture of 0.11 mm.

Figure 6.30 shows the discharge (l/min) entering each borehole water-inflow test interval, compared with the numerical results. The same figure shows a comparison of the recorded and the numerical accumulated discharge from the bottom to the borehole head. The drain's recorded discharge in normal operating conditions (reference discharge) is also shown. Figure 6.31 shows the parameter values of an alternative model, in which it is assumed that the grout curtain is partially inefficient in the area where it is crossed by the upper layer of higher hydraulic conductivity. Analysis of discharges and water pressures obtained with this model (Table 6.21) leads to the conclusion that results are only slightly different from those obtained with the model shown in Figure 6.29.

	Discharge (l/min)			Water pressure (bar)	Hydraulic head (m)	Percentage of hydraulic head (%)
	D19 D	D20 D	D21 D	D20 D	D20 D	
1. Normal operating conditions	0.14 0.06	0.58 0.56	0.04 0.06	-	-	-
2. Drain D20 D closed	0.31 0.08	-	0.24 0.08	0.75 -	68.70 68.33	8.6 % 8.2 %
3. Single packer placed 7.0 m down from drain head	0.13 0.09	0.54 0.46	0.04 0.09	1.50 -	76.92 76.99	17.4 % 17.5 %
4. Double packer placed at between 4.0 to 7.0 m down from drain head	0.30 0.10	-	0.24 0.10	0.625 -	62.55 67.35	7.3 % 6.3 %

Table 6.19 – Recorded discharges and water pressures and comparison to numerical results (shown in red).

	upstream	Discharge (l/min)			leakage from the floor of GDJ	downstream
		drain				
		D19 D	D20 D	D21 D		
1. Normal operating conditions	- 0.80	0.06 ($\approx 5\%$)	0.56 ($\approx 48\%$)	0.06 ($\approx 5\%$)	0.48 ($\approx 41\%$)	- 0.36
2. Drain D20 D closed	- 0.75	0.08 ($\approx 7\%$)	-	0.08 ($\approx 7\%$)	0.94 ($\approx 85\%$)	- 0.36
3. Single packer placed 7.0 m down from drain head	- 0.77	0.09 ($\approx 8\%$)	0.46 ($\approx 41\%$)	0.09 ($\approx 8\%$)	0.48 ($\approx 43\%$)	- 0.36
4. Double packer placed at between 4.0 to 7.0 m down from drain head	- 0.74	0.10 ($\approx 9\%$)	-	0.10 ($\approx 9\%$)	0.89 ($\approx 81\%$)	- 0.36

Table 6.20 – Numerical discharges. Percentage of the quantity of water that flows into the model (in brackets).

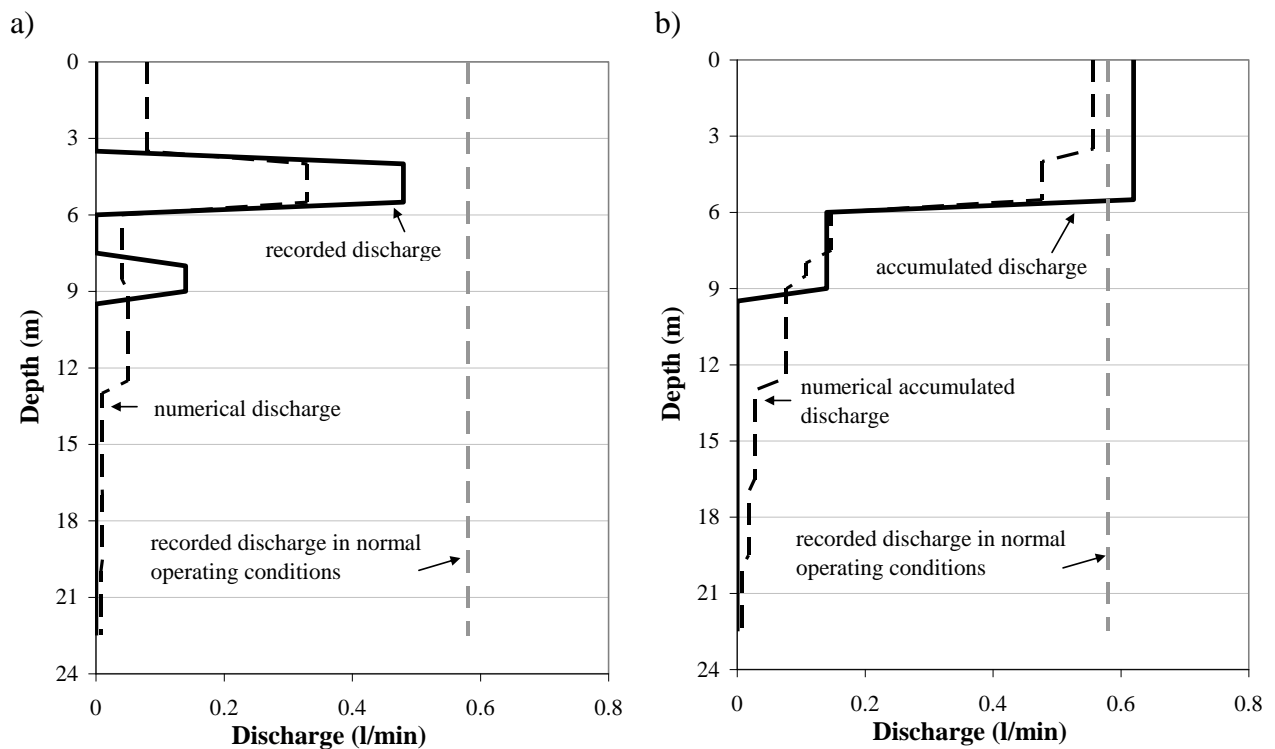
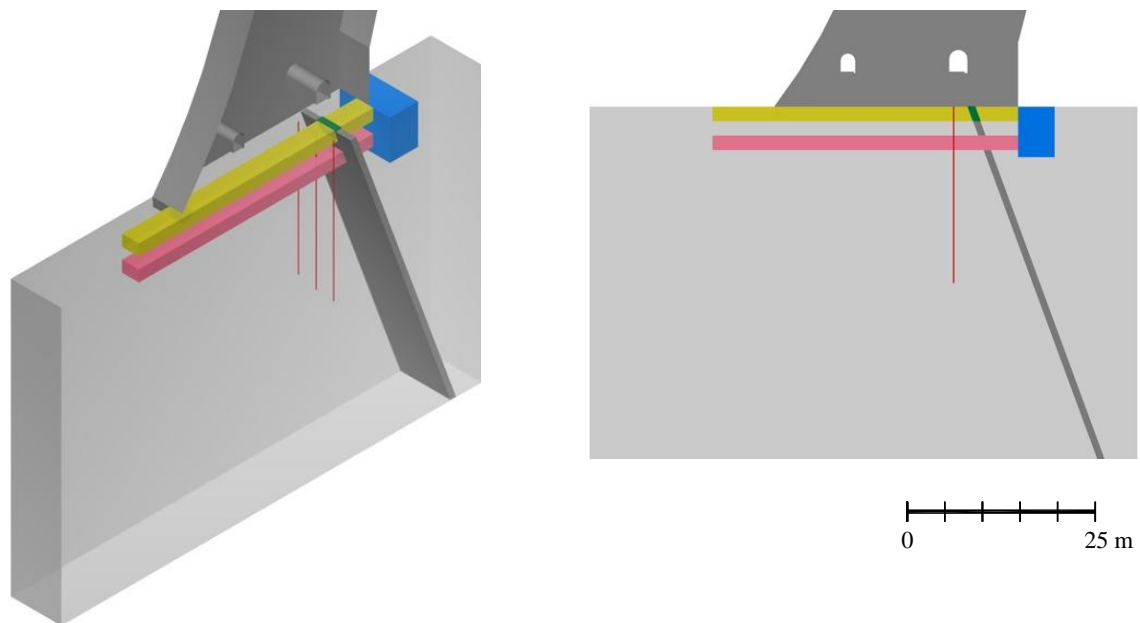


Figure 6.30 – Recorded and numerical discharge flowing into each of drain's D20 D water-inflow test intervals (a) and accumulated discharge from the bottom to the head of the borehole (b).









	k ($\times 10^{-7}$ m/s)			k ($\times 10^{-7}$ m/s)	
Rock mass		0.03	Near-surface area upstream from the dam		10.0
Grout curtain		0.003	Upper layer of higher permeability		30.0
Grout curtain partially inefficient		0.143	Lower layer of higher permeability		0.43

Figure 6.31 – Alternative model. Seepage model in the vicinity of drain D20 D (assuming that the grout curtain is partially inefficient in the area where it is crossed by the upper layer of higher permeability). Model parameters.

	Discharge (l/min)			Water pressure (bar)	Hydraulic head (m)	Percentage of hydraulic head (%)
	D19 D	D20 D	D21 D	D20 D	D20 D	
1. Normal operating conditions	0.14	0.58	0.04	-	-	-
	0.06	0.64	0.06			
2. Drain D20 D closed	0.31	-	0.24	0.75	68.70	8.6 %
	0.09	-	0.09	-	68.91	8.6 %
3. Single packer placed 7.0 m down from drain head	0.13	0.54	0.04	1.50	76.92	17.4 %
	0.10	0.52	0.10	-	79.73	18.0 %
4. Double packer placed at between 4.0 to 7.0 m down from drain head	0.30	-	0.24	0.625	62.55	7.3 %
	0.11	-	0.11	-	67.74	7.9 %

Table 6.21 – Alternative model. Recorded discharges and water pressures and comparison to numerical results (shown in red).

As noted during analysis of results obtained, this model does not properly simulate the increase in discharges in the adjacent drains when drain D20 D is closed (modelling situations 2 and 4). In reality there are discontinuities linking the different drains which lead to flow between drains, not just through the rock mass.

An additional weakness of this model is the excessive floor leakage, which in reality is only a very small amount, probably no greater than 0.05 l/min. This excess in the model can be explained by the larger quantity of water flowing from downstream.

6.4.4 Conclusions

A numerical simulation of borehole water-inflow tests carried out in two restricted foundation areas was carried out. Results of rock mass *in situ* permeability tests and areas where seepage paths cross each drain, identified with both borehole water-inflow tests and water electrical conductivity analysis, were taken into account. The analysis described in this section indicates that equivalent continuum models can be used successfully to model the hydraulic behaviour of specific areas of the foundation. The validity of the numerical models was assessed by comparing the numerical results to the readings taken while carrying out borehole water-inflow tests (discharges and water pressures).

Tests carried out in drain D25 D were easily simulated as there was only one area where water flowed into the borehole and therefore there were only two different situations to be taken into account. Tests carried out in drain D20 D led to the conclusion that seepage paths crossed the drain at two different elevations, which led to a far more complex model, as the number of parameters increased and there were more situations to be simulated with the same model.

Models were validated against data collected *in situ*. During model development, parameters were continually adjusted as necessary. Back-analysis techniques are sometimes used to determine unknown or ill-known physical parameters (e.g. Castro 1997); however, in this case, even with the low number of parameters considered in each model, this would have presented significant difficulties, namely due to the excessive run-times required. Therefore, during the model's development, a trial-and-error estimating procedure was carried out to continually adjust parameters.

In the following section the influence of the different parameters on numerical results is analysed. As will be shown in section 6.6, parameters determined using detailed numerical models can not be used directly in a global 3D model of the dam foundation. In fact, in this type of models, only average measurements can be simulated.

6.5 Parameter studies

6.5.1 Introduction

This section describes the parametric studies carried out to identify which of the parameters in the model developed to simulate seepage in drain D25 D's vicinity, presented in section 6.4.2, have the greatest influence on the numerical discharges and hydraulic heads. A series of numerical experiments was performed by varying the value of one parameter while the other parameters were kept constant. Analysis was carried out to investigate the effect of:

- i) rock mass permeability;
- ii) grout curtain permeability;
- iii) higher rock mass permeability upstream from the dam;
- iv) permeability of horizontal layers upstream from the drains; and
- v) width of higher permeability layers upstream from the drains.

The influence of total or partial clogging of drain D24 D was also investigated.

6.5.2 Influence of rock mass permeability

To assess the influence of rock mass permeability, a comparison was made between the numerical discharges and the numerical water pressure at drain D25 D when closed, with the rock mass permeability varying from 1.0×10^{-9} m/s up to 10×10^{-7} m/s. Results in each of the cases studied can be found in Table 6.22 and Figure 6.32, in which numerical results obtained with the model for drain D25 D ("reference values") are highlighted.

Analysis of Figure 6.32 leads to the conclusion that discharges in drains increase approximately in a linear way with an increase in rock mass permeability. In normal operating conditions the greatest discharge increase occurs in drain D25 D. Drain D24 D is clogged 0.65 m below concrete/rock mass interface, therefore the rate of increase is smaller.

In the model for drain D25 D it is assumed that there is a near-surface area of higher permeability upstream from the dam and two horizontal layers of higher permeability between the upstream area and drains D25 D and D26 D. Having this model in mind, if the rock mass were impervious and drain D25 D were closed, the hydraulic head at drain D25 D would be the same as that of the reservoir. As rock mass permeability increases, there is a simultaneous increase in discharges and decrease in the hydraulic head at drain D25 D.

	Rock mass hydraulic conductivity ($\times 10^{-7}$ m/s)	Discharge (l/min)				Average discharge ((l/min)/m)	Water pressure at drain D25 D's head (bar)	
		upstream	drain					
			D24 D	D25 D	D26 D			
Normal operating conditions	0.01	- 1.85	0.01	1.93	0.62	0.00	0.28	-
	0.05	- 2.08	0.04	2.05	0.72	0.01	0.31	-
	0.1	- 2.33	0.07	2.18	0.82	0.02	0.34	-
	0.5	- 3.86	0.28	2.95	1.43	0.08	0.52	-
	1.0	- 5.44	0.50	3.78	2.06	0.13	0.70	-
	5.0	15.59	1.68	9.42	6.14	0.38	1.92	-
	10.0	25.98	2.64	15.58	10.39	0.52	3.72	-
Drain D25 D closed	0.01	1.03	0.02	-	1.41	0.00	0.16	4.91
	0.05	1.27	0.08	-	1.60	0.03	0.19	4.55
	0.1	1.53	0.15	-	1.82	0.05	0.22	4.18
	0.5	3.10	0.52	-	3.10	0.18	0.40	2.83
	1.0	4.67	0.85	-	4.38	0.30	0.58	2.26
	5.0	14.40	2.68	-	12.64	0.94	1.70	1.46
	10.0	24.34	4.34	-	21.44	1.49	2.86	1.26

Table 6.22 – Numerical discharges and water pressures for different rock mass permeability values in normal operating conditions and with drain D25 D closed.

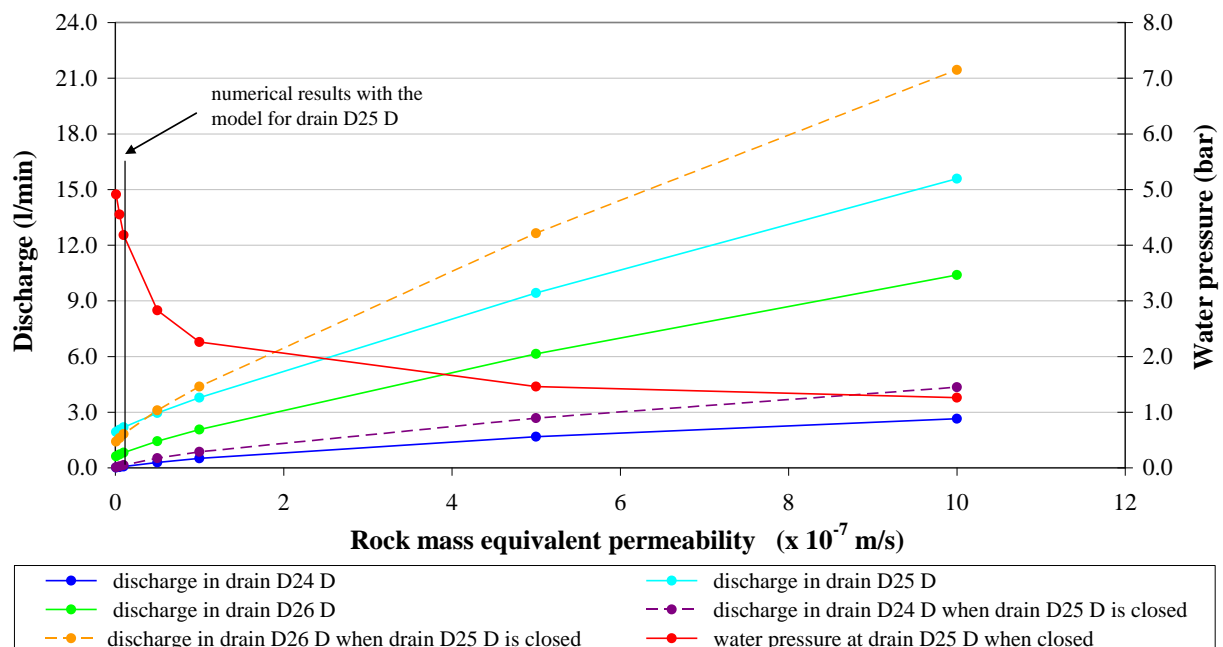


Figure 6.32 – Variation of discharges in each drain and in the water pressure at drain D25 D when closed, with different rock mass permeability values.

Results presented show that lowering rock mass equivalent permeability does not significantly alter either discharges or water pressures; but an increase has much more influence, leading to greater discharges and to a sudden loss of water pressure. It also leads to larger quantities of water flowing into the drains at their lower areas, which is not realistic.

6.5.3 Influence of grout curtain permeability

To assess the influence of grout curtain permeability, calculations were carried with the grout curtain 1000, 100, 10 and 2 times less pervious than the rock mass and with the grout curtain as pervious as the rock mass. In practice, the former is equivalent to simulating an impervious grout curtain; therefore these values encompass the range from an impervious to a non-existent grout curtain. Results are shown in Table 6.23 and Figure 6.33.

Analysis of Figure 6.33 leads to the conclusion that changing grout curtain permeability has little influence on both discharges and water pressure at drain D25 D's head, when the drain is closed. Preliminary studies of three-dimensional hydraulic foundation models, presented in chapter 5.3, led to the conclusion that decreasing grout curtain permeability leads to a considerable decrease in the water flow through the model and in the discharges coming to the drain, but has little influence on the hydraulic head values. In the model being studied, both horizontal layers of higher permeability upstream from drains D25 D and D26 D cross the grout curtain, therefore the amount of leakage and hydraulic heads are only slightly affected by the grout curtain permeability.

	$\frac{k_{groutcurtain}}{k_{rockmass}}$	Discharge (l/min)					Average discharge ((l/min)/m)	Water pressure at drain's D25 D head (bar)
		upstream	drain			downstream		
			D24 D	D25 D	D26 D			
Normal operating conditions	0.001	- 2.13	0.06	2.07	0.73	0.01	0.32	-
	0.01	- 2.18	0.06	2.09	0.75	0.01	0.32	-
	0.1	- 2.33	0.07	2.18	0.82	0.02	0.34	-
	0.5	-2.42	0.08	2.23	0.86	0.03	0.35	-
	1.0	- 2.45	0.09	2.24	0.87	0.03	0.35	-
Drain D25 D closed	0.001	- 1.41	0.13	-	1.72	0.04	0.21	4.03
	0.01	- 1.44	0.14	-	1.74	0.05	0.21	4.07
	0.1	- 1.53	0.15	-	1.82	0.05	0.22	4.18
	0.5	1.58	0.16	-	1.86	0.06	0.23	4.24
	1.0	1.60	0.17	-	1.86	0.06	0.23	4.25

Table 6.23 - Numerical discharges and water pressures for different grout curtain permeability values in normal operating conditions and with drain D25 D closed.

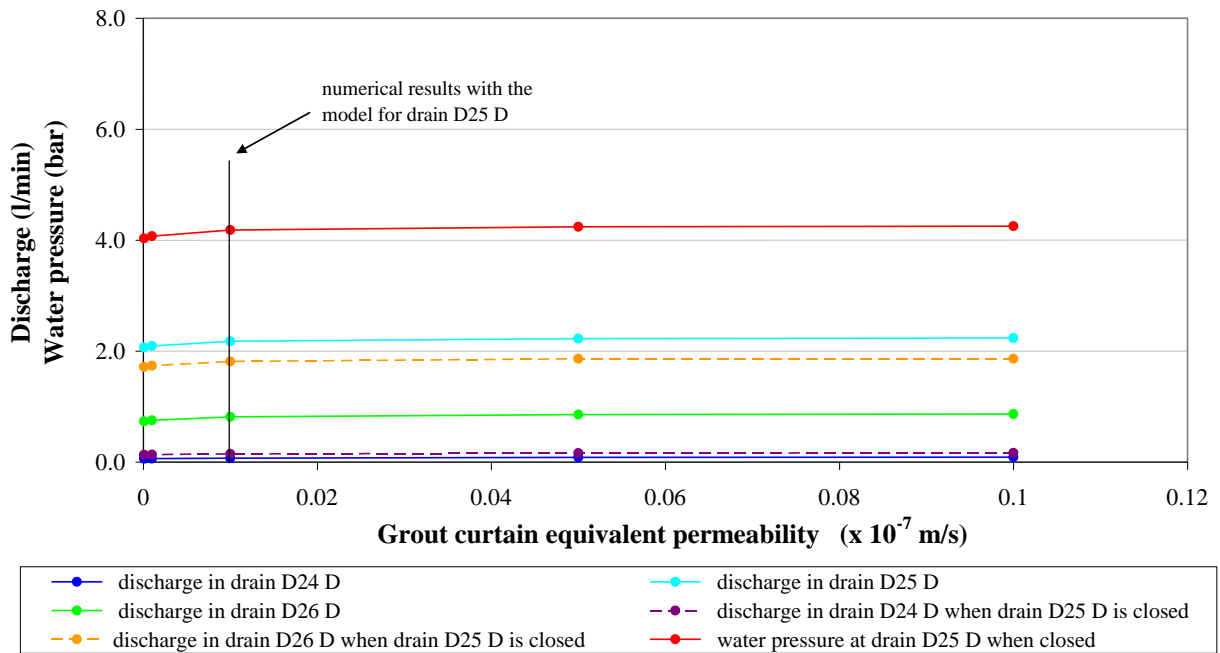


Figure 6.33 – Variation of discharges in each drain and in the water pressure at drain D25 D when closed, with different grout curtain permeability values.

6.5.4 Influence of higher rock mass permeability upstream from the dam

To study the influence of higher rock mass permeability upstream from the dam numerical analysis was carried out by varying permeability in that area from 0.1×10^{-7} m/s (actual rock mass permeability) up to 20×10^{-7} m/s. Results are shown in Table 6.24 and Figure 6.34.

Results show that when the hydraulic conductivity of the area of higher permeability increases (doubles from 10×10^{-7} m/s to 20×10^{-7} m/s) there is only a slight increase both in drain discharges and water pressure when drain D25 D is closed. In the model being studied, it has been concluded that the majority of the water flows towards the drains first through the area of higher permeability upstream from the dam and then through the layers of higher permeability upstream from the drains. Therefore, flow is governed by an equivalent hydraulic conductivity.

In estimating an equivalent vertical hydraulic conductivity of a layered aquifer L m deep it is assumed that the vertical velocity remains constant, thus the head loss across each layer is inversely proportional to the hydraulic conductivity (the layers are horizontal and water flows in a vertical downwards direction). The equivalent hydraulic conductivity is given by:

$$\frac{1}{k_e} = \frac{1}{L} \left(\sum \frac{l_i}{k_i} \right) \quad (6.3)$$

	Rock mass permeability upstream from the dam ($\times 10^{-7}$ m/s)	upstream	Discharge (l/min)			Average discharge ((l/min)/m)	Water pressure at drain's D25 D head (bar)	
			drain		downstream			
			D24 D	D25 D	D26 D			
Normal operating conditions	0.10	- 1.25	0.06	1.77	0.65	0.01	0.27	-
	1.0	- 1.70	0.06	1.95	0.73	0.02	0.31	-
	2.5	- 1.98	0.07	2.06	0.77	0.02	0.32	-
	5.0	- 2.18	0.07	2.13	0.80	0.02	0.33	-
	7.5	- 2.27	0.07	2.16	0.81	0.02	0.34	-
	10.0	- 2.33	0.07	2.18	0.82	0.02	0.34	-
	20.0	- 2.43	0.07	2.21	0.83	0.02	0.35	-
Drain D25 D closed	0.10	- 0.88	0.13	-	1.57	0.04	0.19	3.65
	1.0	- 1.16	0.14	-	1.69	0.05	0.20	3.90
	2.5	- 1.33	0.14	-	1.75	0.05	0.21	4.03
	5.0	- 1.44	0.14	-	1.79	0.05	0.21	4.12
	7.5	- 1.49	0.15	-	1.80	0.05	0.22	4.16
	10.0	- 1.53	0.15	-	1.82	0.05	0.22	4.18
	20.0	- 1.59	0.15	-	1.83	0.05	0.22	4.23

Table 6.24 - Numerical discharges and water pressures for different rock mass permeability values upstream from the dam in normal operating conditions and with drain D25 D closed.

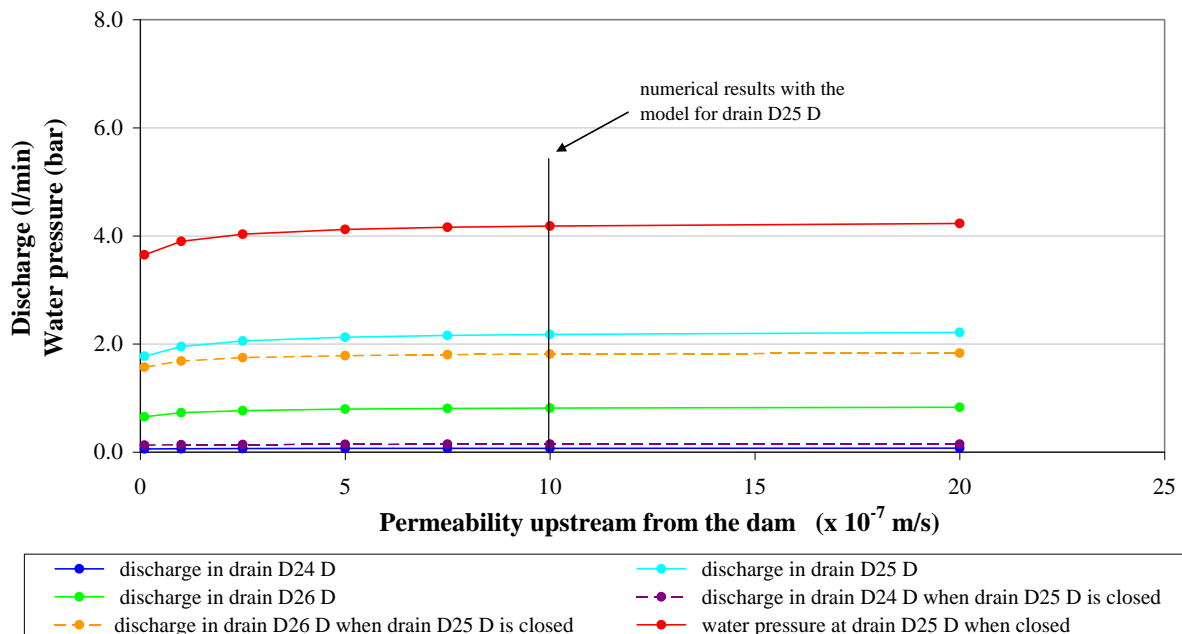


Figure 6.34 – Variation of discharges in each drain and in the water pressure at drain D25 D when closed, with different permeability values of the rock mass upstream from the dam.

Where l_i is the vertical length of each layer and k_i is the hydraulic conductivity of each layer. Analysis of Equation 6.3 leads to the conclusion that if the hydraulic conductivity of one of the layers is greatly increased, there may be almost no change in the equivalent hydraulic conductivity, as on the equation's right hand side, depending on the relative values of the various k_i , it may be like adding zero. Therefore, increasing a k_i beyond some value has limited effect.

When the permeability of the near-surface area of higher permeability upstream from the dam decreases, there is a decrease in both discharges in drains D25 D and D26 D and in the water pressure at drain D25 D when closed. The decrease in discharges was expected, as in a rock mass of uniform permeability k , discharges are proportional to k . It is known that in a rock mass of non-uniform permeability with zones k_1, k_2, k_3 , etc., the seepage pressure at a given point depends on the relative values of k_1, k_2, k_3 , etc. (Londe 1973c). To analyse water pressures in more detail, variations in hydraulic head along a horizontal line that crosses drain D25 D in the upstream-downstream direction were studied. The line crosses the horizontal layer of higher permeability upstream from the drain at half its depth. Results of the main model were compared with the results of a model in which the near-surface area upstream from the dam is as pervious as the rock mass (model in which it is assumed that there is no area of higher permeability upstream from the dam) (Figure 6.35).

The area of higher permeability is located between mesh coordinates 10.0 m and 15.0 m in the upstream-downstream direction. Analysis of Figure 6.35 allows the comparison of the different cases:

- In normal operating conditions, the decrease in the permeability of the area of higher permeability from 10×10^{-7} m/s to 0.1×10^{-7} m/s leads to a greater loss of hydraulic head in that area;
- When drain D25 D is closed, the greater loss of hydraulic head in the area being studied leads to a smaller hydraulic head at the point where the horizontal line meets the layer of higher permeability upstream from the drain (line a). As the permeability is lower, discharges are smaller; therefore the loss of hydraulic head in the horizontal layer of higher permeability upstream from the drain is smaller. This is the reason why the slope of the blue line is less steep than that of the red one.

Results show that changing the assumed hydraulic conductivity of the near-surface area of higher permeability upstream from the dam has limited effect; therefore the existence of vertical fissures in that area can be simulated by any k value as long as it is much greater than that of the rock mass.

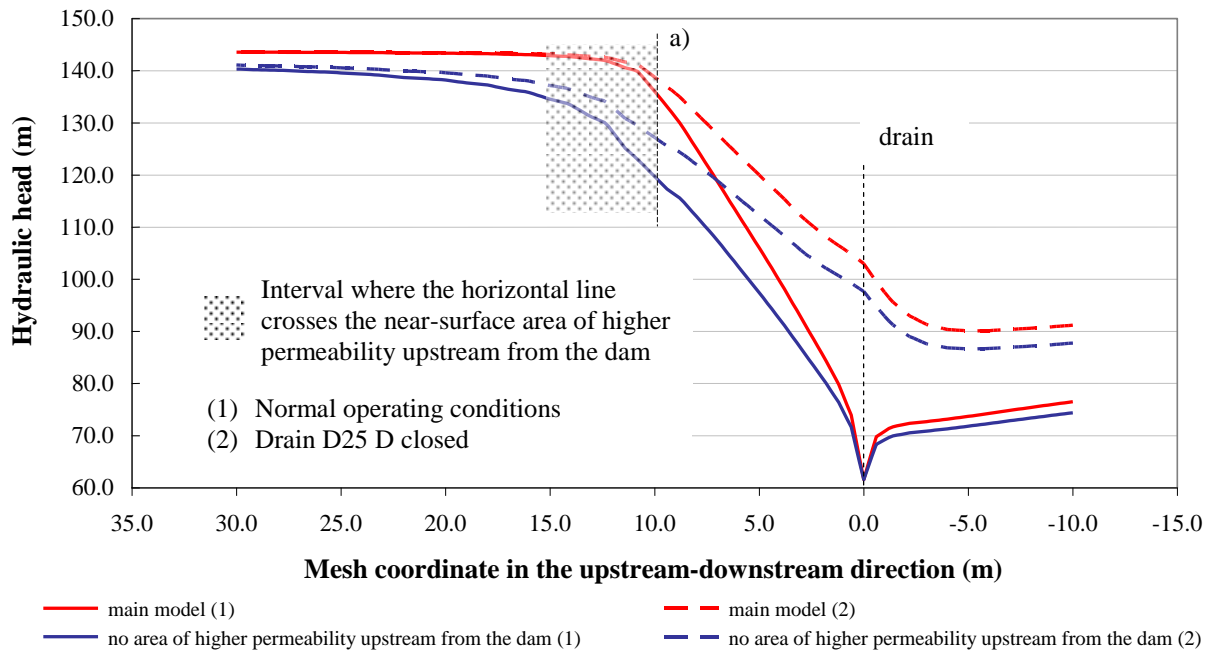


Figure 6.35 – Variations in hydraulic head along a horizontal line 40 m long that crosses drain D25 D in the upstream-downstream direction in the main model (reference values) and in a model where there is no area of higher permeability upstream from the dam.

6.5.5 Influence of the permeability of the horizontal layers upstream from the drains

To study the influence of the permeability of the horizontal layers between the upstream area and the drains, numerical analysis was carried out by varying permeability in those layers from 2.0×10^{-7} m/s up to 20×10^{-7} m/s. Results are shown in Table 6.25 and Figure 6.36.

Results show that discharges are proportional to the permeability of the horizontal layers upstream from the drains. As in the case presented in the previous sub-chapter, water pressures decrease with a decrease in the horizontal layers' permeability. As previously, to analyse water pressures in more detail, variations in hydraulic head along a horizontal line that crosses drain D25 D and is in the upstream-downstream direction were studied and the results of the main model, in which the permeability of the layers upstream from the drains is 5.0×10^{-7} m/s, were compared with the results of a model in which the permeability of the layers upstream from the drains is 2.0×10^{-7} m/s (Figure 6.37).

The area of higher permeability is located between mesh coordinates 10.0 m and 15.0 m and layers of higher permeability between coordinates 0.0 m and 10.0 m, in the upstream-downstream direction. Analysis of Figure 6.37 leads to the following conclusions:

- in normal operating conditions, the decrease in the layers' permeability leads to a greater loss of hydraulic head where the area of higher permeability upstream from the dam meets the layer upstream of the drains (line a);
- when drain D25 D is closed, a decrease in the layers permeability leads to a greater loss of hydraulic head and, consequently, to a lower hydraulic head at the drain.

Results lead to the conclusion that changing the permeability of the horizontal layers upstream from the drains has a large effect on drain discharges and a lesser effect on pressures when the drain is closed.

	Horizontal layers upstream from the drains permeability ($\times 10^{-7}$ m/s)	Discharge (l/min)				Average discharge ((l/min)/m)	Water pressure at drain's D25 D head (bar)	
		upstream	drain					downstream
			D24 D	D25 D	D26 D			
Water flowing in a regular way in the foundation	2.0	- 1.32	0.07	1.06	0.47	0.02	0.18	-
	4.0	- 2.01	0.07	1.81	0.70	0.02	0.29	-
	5.0	- 2.33	0.07	2.18	0.82	0.02	0.34	-
	6.0	- 2.65	0.07	2.54	0.93	0.02	0.39	-
	8.0	- 3.25	0.07	3.27	1.15	0.02	0.50	-
	10.0	- 3.82	0.07	3.98	1.37	0.02	0.60	-
	15.0	- 5.15	0.07	5.72	1.91	0.02	0.86	-
	20.0	- 6.38	0.07	7.42	2.44	0.02	1.10	-
Drain D25 D closed	2.0	- 0.96	0.13	-	0.99	0.05	0.13	3.61
	4.0	- 1.35	0.14	-	1.55	0.05	0.18	4.06
	5.0	- 1.53	0.15	-	1.82	0.05	0.22	4.18
	6.0	- 1.70	0.15	-	2.08	0.05	0.25	4.27
	8.0	- 2.03	0.15	-	2.61	0.05	0.31	4.39
	10.0	- 2.35	0.15	-	3.13	0.05	0.37	4.46
	15.0	- 3.10	0.16	-	4.42	0.06	0.50	4.55
	20.0	- 3.79	0.16	-	5.69	0.06	0.65	4.59

Table 6.25 - Numerical discharges and water pressures for different permeability values of the horizontal layers upstream from the drains, in normal operating conditions and with drain D25 D closed.

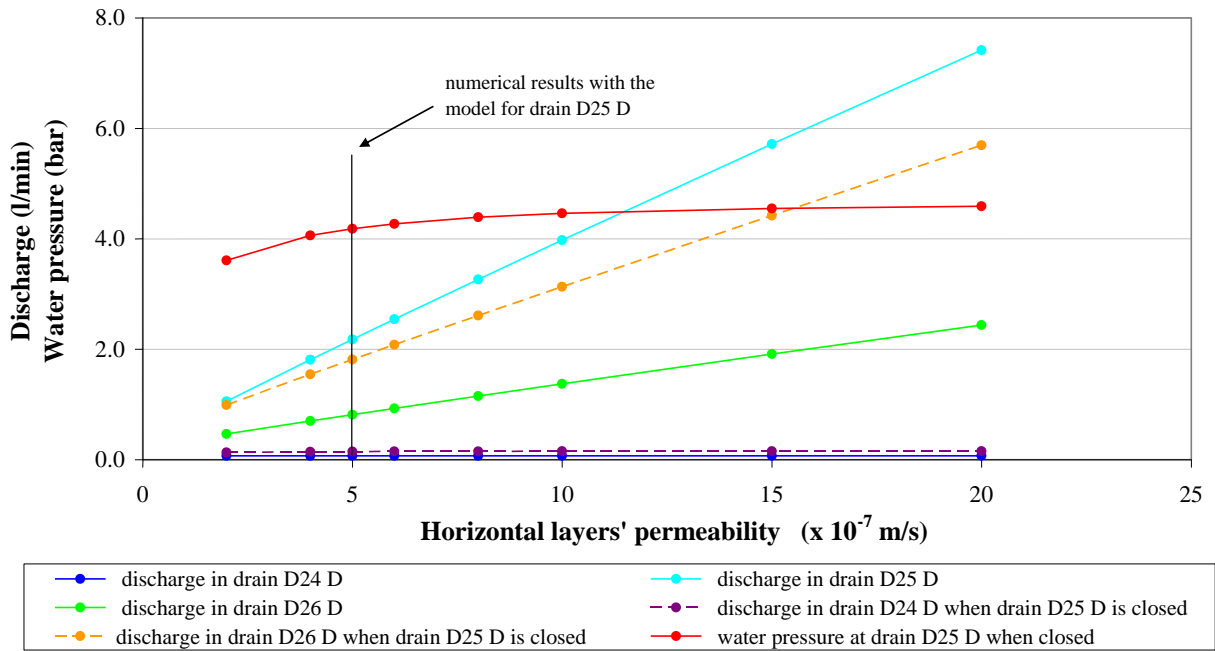


Figure 6.36 – Variation of discharges in each drain and in the water pressure at drain D25 D when closed, with the different permeability values for the horizontal layers upstream from the drains.

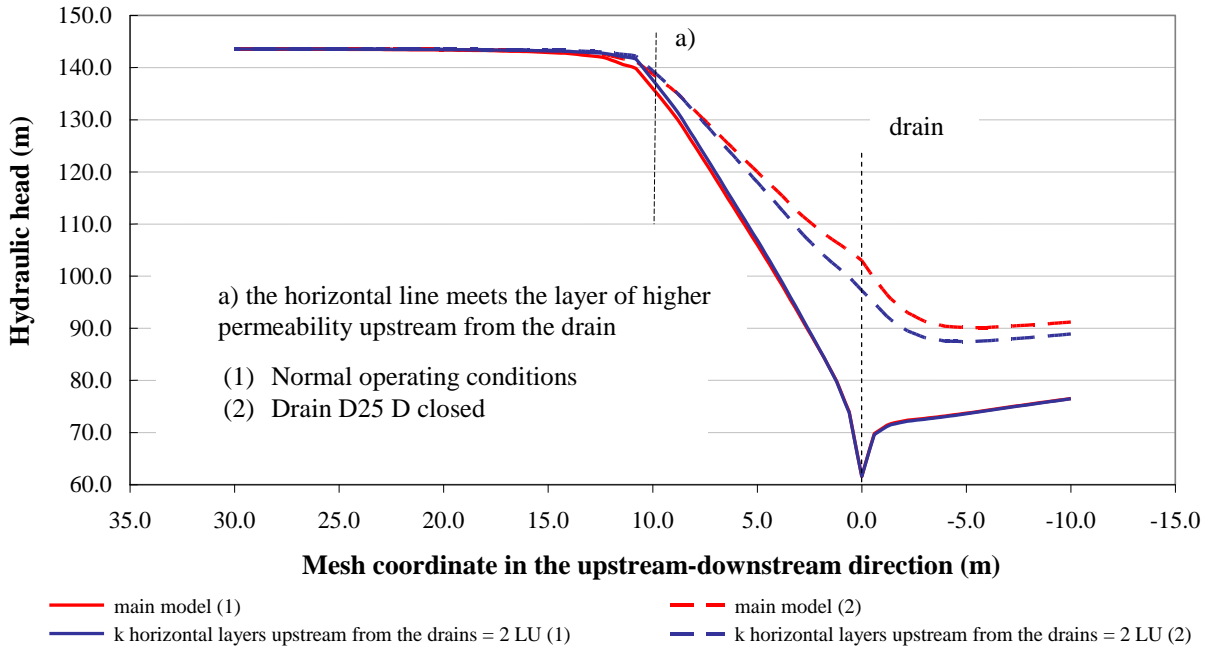


Figure 6.37 - Variations in hydraulic head along a horizontal line 40 m long that crosses drain D25 D in the upstream-downstream direction in the main model and in a model where the permeability of the horizontal layers upstream from the drains is 2.0×10^{-7} m/s.

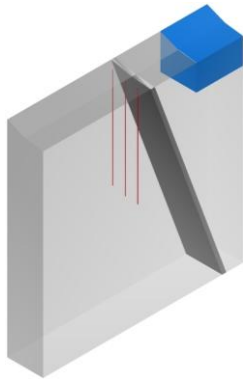
6.5.6 Influence of the width of higher permeability layers upstream from the drains

The influence of the width of the higher permeability layers upstream from the drains was assessed carrying out a numerical analysis in which layers' width was gradually increased (Figure 6.38):

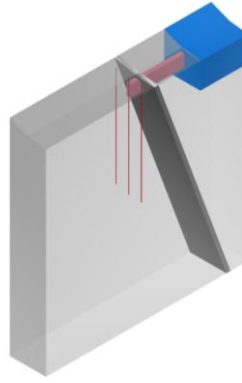
- firstly, it was assumed that there was no layer of higher permeability (Figure 6.38 a);
- secondly, the layer's width upstream from drain D25 D was increased by 1.0 m for three times, until the distance between drains was reached (Figure 6.38 b, c and d);
- thirdly, the layer width upstream from drain D26 D (the layer at drain D26 D is 2.0 m higher than the layer at drain D25 D) was increased by 0.5 m for three times, until half-distance between drains was reached (main model) (Figure 6.38 e, f and g);
- Finally, it was assumed that the layer at drain D26 D was 3.0 m wide, the distance between drains, and that there was also a layer upstream from drain D24 D.

Results are shown in Table 6.26 and Figure 6.39. Results analysis show that discharges and water pressure in drain D25 D when closed increase gradually as the layer upstream from drain D25 D becomes larger. Discharge increase is greater in drain D25 D, which is crossed by the layer. Increases in both discharges and water pressure also occur as the width of the layer upstream from drain D26 D increases, until the seepage path crosses drain D26 D. When the latter is crossed by the layer: i) there is an increase in the quantity of water in drain D26 D, both in normal operating conditions and with drain D25 D closed; ii) a slight decrease in the quantity of water in drain D25 D; and iii) a great loss of water pressure in drain D25 D when closed. Therefore, the widths of the higher permeability layers upstream from the drains used in the final model allow a good match of the distribution of discharges to the drains in the two simulated situations. Even small variations in widths lead to results that do not correspond to readings taken while carrying out the tests.

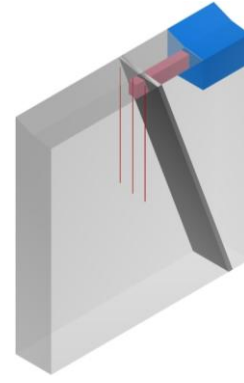
The study carried out leads to the conclusion that in this area of Alqueva dam foundation, which is an area of low permeability, drainage is crucial for controlling water pressures as discontinuities with a very small aperture are never grouted.



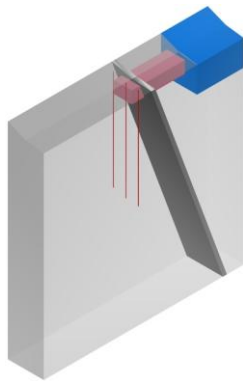
a) no layer of higher permeability upstream from the drains.



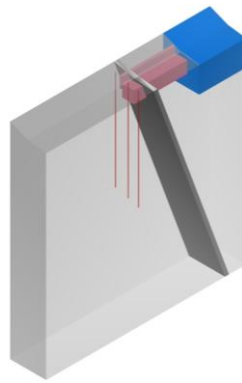
b) 1 m wide layer upstream from drain D25 D.



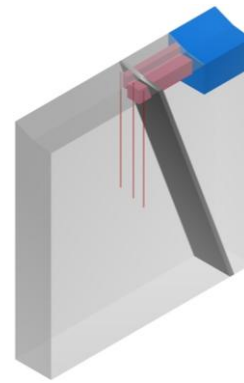
c) 2 m wide layer upstream from drain D25 D.



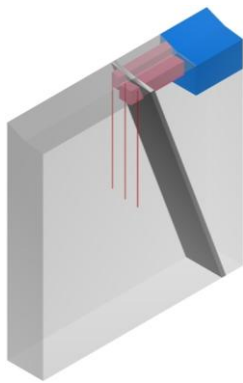
d) 3 m wide layer upstream from drain D25 D.



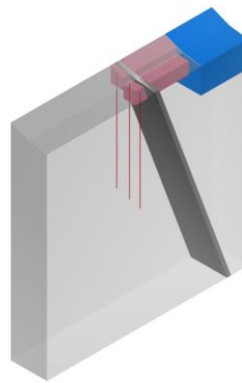
e) 3 m wide layer upstream from drain D25 D and 0.5 m wide layer upstream from drain D26 D.



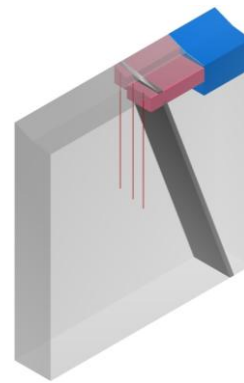
f) 3 m wide layer upstream from drain D25 D and 1.0 m wide layer upstream from drain D26 D.



g) 3 m wide layer upstream from drain D25 D and 1.5 m wide layer upstream from drain D26 D (**main model**).



h) 3 m wide layers upstream from drains D25 D and D26 D.



i) 3 m wide layers upstream from drains D24 D, D25 D and D26 D (total width = 9 m).

Figure 6.38 – Models with different widths of the horizontal layers upstream from the drains.

	Layers' width (m)	Discharge (l/min)				Average discharge ((l/min)/m)	Water pressure at drain D25 D's head (bar)	
		upstream	drain					downstream
			D24 D	D25 D	D26 D			
Normal operating conditions	0.0	- 0.55	0.05	0.31	0.21	0.02	0.06	-
	1.0	- 1.12	0.04	0.94	0.20	0.02	0.13	-
	2.0	- 1.51	0.05	1.34	0.20	0.02	0.18	-
	3.0	- 2.11	0.07	1.92	0.22	0.02	0.25	-
	3.5	- 2.19	0.07	2.17	0.26	0.02	0.28	-
	4.0	- 2.22	0.07	2.34	0.29	0.02	0.30	-
	4.5	- 2.33	0.07	2.18	0.82	0.02	0.34	-
	6.0	- 2.60	0.07	2.23	1.68	0.02	0.44	-
	9.0	- 4.24	2.13	2.06	1.58	0.02	0.64	-
Drain D25 D closed	0.0	- 0.48	0.08	-	0.40	0.04	0.05	2.22
	1.0	- 0.71	0.12	-	0.59	0.05	0.08	4.03
	2.0	- 0.83	0.15	-	0.73	0.06	0.10	4.62
	3.0	- 0.96	0.18	-	0.77	0.06	0.11	5.34
	3.5	- 0.97	0.18	-	0.86	0.06	0.12	5.48
	4.0	- 0.97	0.19	-	0.91	0.07	0.12	5.59
	4.5	- 1.53	0.15	-	1.82	0.05	0.22	4.18
	6.0	- 1.93	0.14	-	2.82	0.05	0.33	3.84
	9.0	- 3.72	2.71	-	2.33	0.04	0.56	2.94

Table 6.26 - Numerical discharges and water pressures for different widths of the horizontal layers upstream from the drains, in normal operating conditions and with drain D25 D closed.

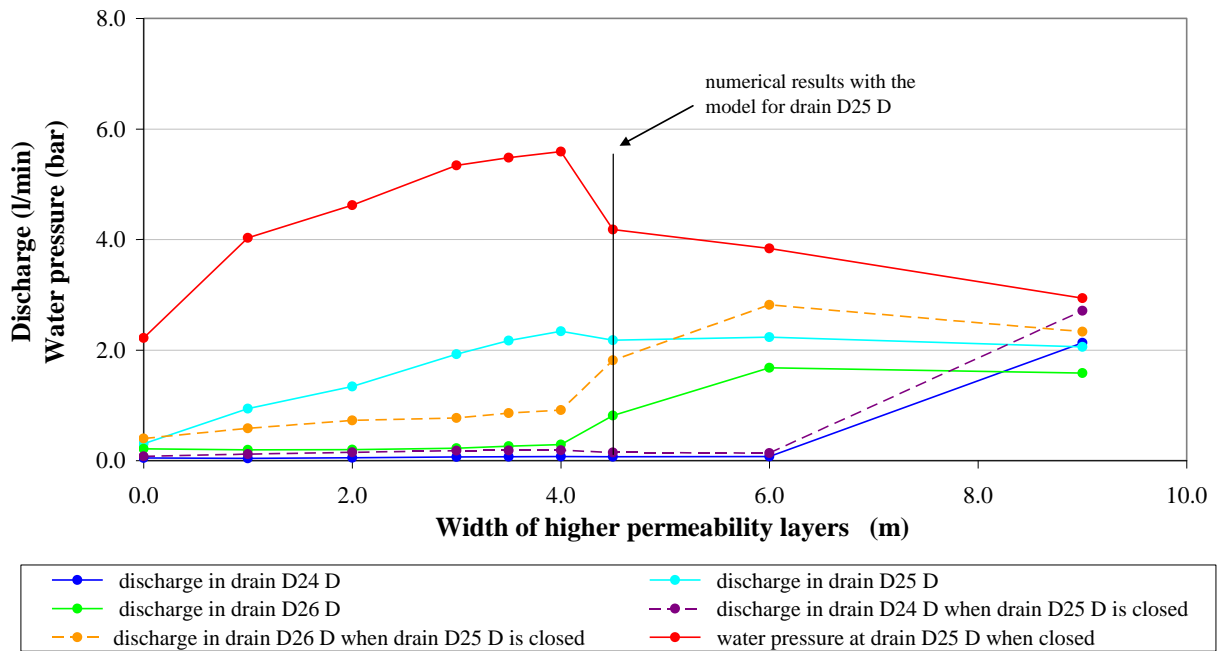


Figure 6.39 – Variation of discharges in each drain and in the water pressure at drain D25 D when closed, with different widths of the higher permeability layers upstream from the drains.

6.5.7 Influence of total or partial clogging of drain D24 D

Field results showed that drain D24 D was obstructed at elevation 54.67 m but there is no way of knowing how far the blockage extends. It was assumed in the main model that the drain was completely blocked from that point but it was also decided to simulate a partial blockage. Modelling drain D24 D as only partially clogged for 0.5 m, from elevation 54.17 m to 54.67 m, instead of being completely clogged from elevation 54.67 m downwards, leads to very slight changes in discharges (Table 6.27):

- an increase of 1.4 % in the quantity of water in drain D24 D;
- an increase of 0.06 % in the quantity of water in drain D25 D; and
- a decrease of 0.09 % in the in the quantity of water in drain D26 D.

From the numerical results it was also possible to conclude that the hydraulic head in drain D25 D when closed is, in both cases, 4.18 bar.

	Drain D24 D blockage	upstream	Discharge (l/min)			downstream	Average discharge ((l/min)/m)	Water pressure at drain's D25 D head (bar)
			drain					
			D24 D	D25 D	D26 D			
Normal operating conditions	complete	- 2.33	0.07	2.18	0.82	0.02	0.34	-
	partial	- 2.33	0.07	2.18	0.82	0.02	0.34	-
Drain D25 D closed	complete	- 1.53	0.15	-	1.82	0.05	0.22	4.18
	partial	- 1.53	0.15	-	1.81	0.05	0.22	4.18

Table 6.27 – Discharges with drain D24 D completely blocked from 6.75 m downwards and partially clogged for 0.5 m, both in normal operating conditions and with drain D25 D closed.

6.5.8 Conclusions

Parametric studies are important whenever there are ill-known or unknown parameters, for which values have to be attributed. Parameter analysis carried out led to the conclusion that the model for drain D25 D is only slightly affected by variations in both the grout curtain permeability and in the hydraulic conductivity of the more pervious area upstream from the dam, as long as it is much greater than that of the rock mass. It was also concluded that knowing whether drain D24 D was totally or only partially obstructed was not relevant. However, the model is highly sensitive to increase in rock mass equivalent permeability, which leads to a non-realistic situation, with larger quantities of water flowing into the drains at their lower areas. Drain discharges are also highly affected by changes in the permeability of the horizontal layers upstream from the drains. The widths of these layers are also essential parameters, as recorded water pressures and discharges could only be obtained with the widths adopted.

6.6 Global three-dimensional hydraulic model

Results of tests carried out *in situ*, presented in chapter 4.5, and conclusions drawn from the detailed 3D models, presented in the previous sections, were used to develop a global hydraulic model of the foundation. In this type of model, due to the size of the area being studied, the average edge length of the tetrahedral zones is much greater than the ones employed in the previous section, and it is often necessary to simulate the drainage system in a simplified way. As mentioned in chapter 5, the drainage system can be simulated by a hypothetical continuous trench with the same depth as the drains.

For application to arch dams, special routines for concrete arch dam analysis are included in 3DEC code (Lemos 1996; 1998; 1999a) which allow the adequate geometric fitting of the concrete structure, represented by finite element blocks, and the rock mass in the foundation, represented by regular polyhedral deformable blocks. The FE mesh of the dam arch is first created, usually using suitable pre-processing software, and is represented by one or more blocks and formed by 20-noded isoparametric brick elements. These finite elements, of an order higher than the foundation tetrahedra, allow the modelling of the curved arch geometry and provide a good approximation of the bending behaviour of concrete arches, even with only one element across the thickness. When the dam is represented by a group of blocks, the movement of the contraction joints can be taken into account. When only one element across the dam's thickness is used, there are only three grid contact points across the shell thickness, and the stress distribution is not very accurate. Meshes with more than one element across the thickness allow a better simulation not only of contact stresses but also of uplift distribution in the concrete/rock mass interface. Therefore, a dam-foundation system can be analysed in a more accurate and efficient way than would be possible with the uniform stress tetrahedral elements employed in the standard deformable blocks available in 3DEC (Lemos 1998; Resende et al. 2004).

6.6.1 Model description

The hydraulic foundation rock mass model was developed in various steps taking into account the mesh of Alqueva dam, shown in Figure 6.40, and the existence of both the grout and drainage curtains. The methodology used in model development is presented. Although 3DEC code was used, the methodology could easily be applied with other computer codes. The FE mesh of Alqueva dam arch, with two elements across the thickness, was created outside 3DEC by a code developed at LNEC (Batista 1998). Figure 6.41 shows the modelling steps. In this figure, the curved finite element faces that compose the dam are divided into triangular faces, in order to simplify the graphical representation.

In the first modelling step, the blocks under the dam are created with one of their faces adjacent to the foundation surface of the FE mesh (Figure 6.41 a). As the faces of the foundation surface may be curved, it is first necessary to set the nodes along the edges of contact faces exactly at the midpoint of the edges, so that they can fit the polyhedral foundation blocks (Itasca 2003). Each element's foundation surface is divided into eight triangles, by including an extra grid-point at the centre of the element face. Five blocks are created under each foundation surface, as shown in Figure 6.42. Blocks under the dam go down to elevation 0.0. Then these blocks are cut in order to define the drainage length. Different colours represent different region numbers. After cutting the foundation, the same region number is given to blocks below the cut. The drainage curtain is simulated by a hypothetical continuous trench and was defined cutting the upstream upper blocks mid-way along vertical planes. In this way, the drainage curtain is defined about 10 m downstream from the upstream edge.

In the second and third modelling steps, blocks upstream and downstream from the dam are created taking into account the upstream and downstream edges (Figure 6.41 b and c). To apply boundary conditions at an appropriate distance from the dam, the model was extended to a length of 475 m in the upstream-downstream direction. Figure 6.41 c) shows the different blocks created upstream from the dam, where the grout curtain is represented in red. In order to simplify the model, the grout curtain is modelled adjacent to the upstream edge, not underneath the dam itself. Foundation blocks are afterwards cut at a distance of about 35 m upstream and downstream from the dam in order to define finer meshes in the areas close to the dam.

Finally, the model is extended laterally and downwards, with brick shape blocks, in order to create a model large enough for the boundaries not to have an influence on numerical results. As previously mentioned, the foundation mesh is automatically created by 3DEC, given the average dimension of the tetrahedral zones. In the model shown in Figure 6.41 d) the dam is represented by a mesh of 30 blocks and the rock mass by 1443 blocks. The new version of the 3DEC code used in this study allows the analysis of steady-state flow using an equivalent continuum model in tetrahedral zoned blocks, but not in FE blocks. Therefore, the dam, which was essential to create the foundation model, had to be deleted in the global hydraulic model.

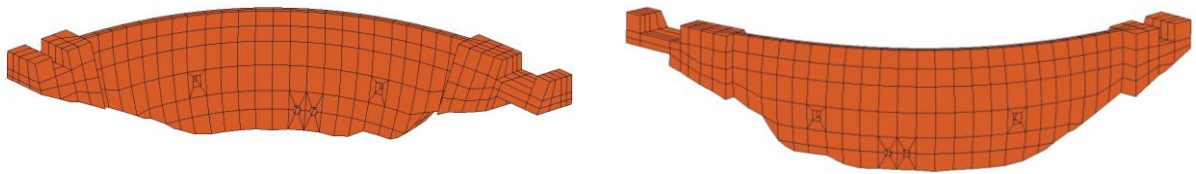
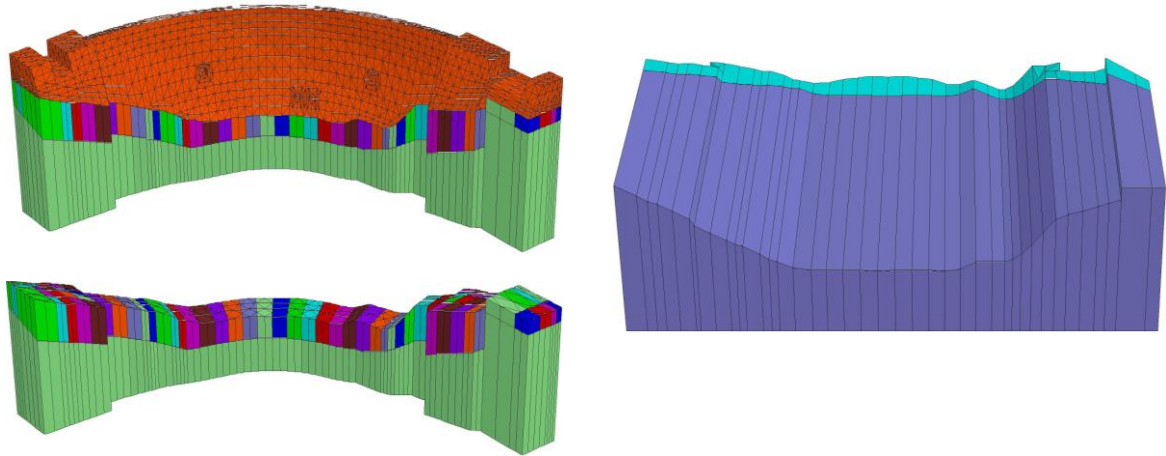
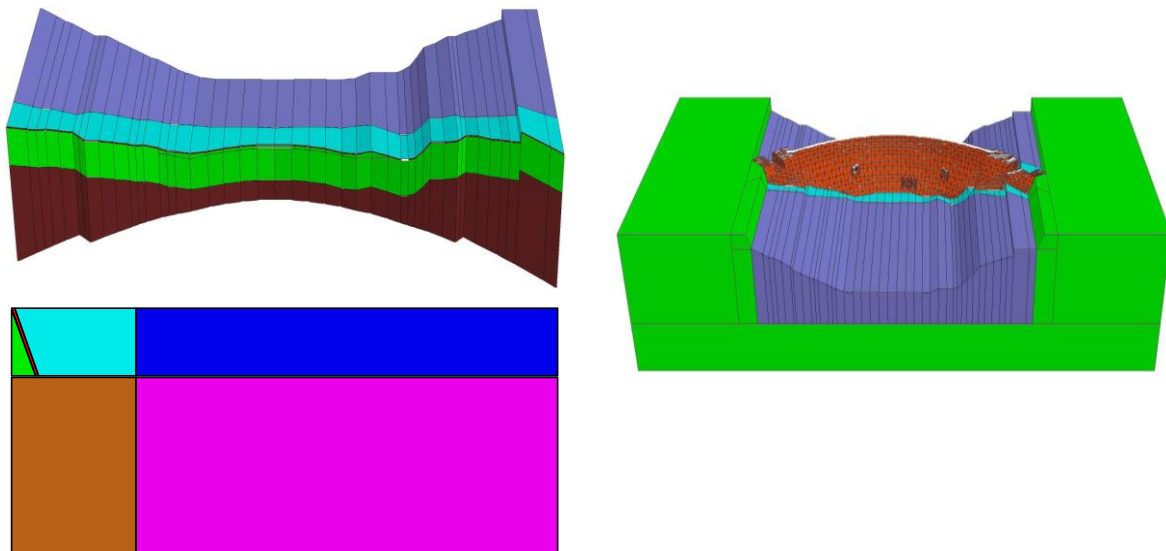


Figure 6.40 – Downstream and upstream views of the 20-node finite element mesh of Alqueva dam.



a) Rock blocks below concrete/foundation interface

b) Foundation blocks downstream from the dam.



c) Foundation blocks upstream from the dam

d) Perspective of the hydraulic foundation model (view and cross section).

Figure 6.41 – Modelling steps, using 3DEC's Arch Dam Module.

A very coarse mesh was first created, in which the average edge lengths of the tetrahedral zones were: i) 6.0 m in the blocks surrounding the drainage curtain; ii) 10.0 m in the vicinity of the above-mentioned blocks, including the grout curtain area; iii) 15.0 m in areas close to the dam in the upstream and downstream direction (shown in light blue in Figure 6.41 b and c; and iv) 30.0 m in the remaining rock mass. The mesh, with 40595 grid-points and divided into 64277 tetrahedra, is shown in Figure 6.43 a). Because the edges of the tetrahedral zones in the model's outer blocks are so long, the phreatic surface is not clearly identified in the results' graphical representation, thus a finer mesh was created in which the average lengths of the tetrahedral zones are about two thirds of those assumed in the very large mesh (4.0 m, 8.0 m, 12.0 m and 20.0 m instead of 6.0 m, 10.0 m, 15.0 m and 30.0 m, respectively). This second mesh, which was used in subsequent analysis, has 67413 grid-points and is divided into 139397 zones (Figure 6.43 b).

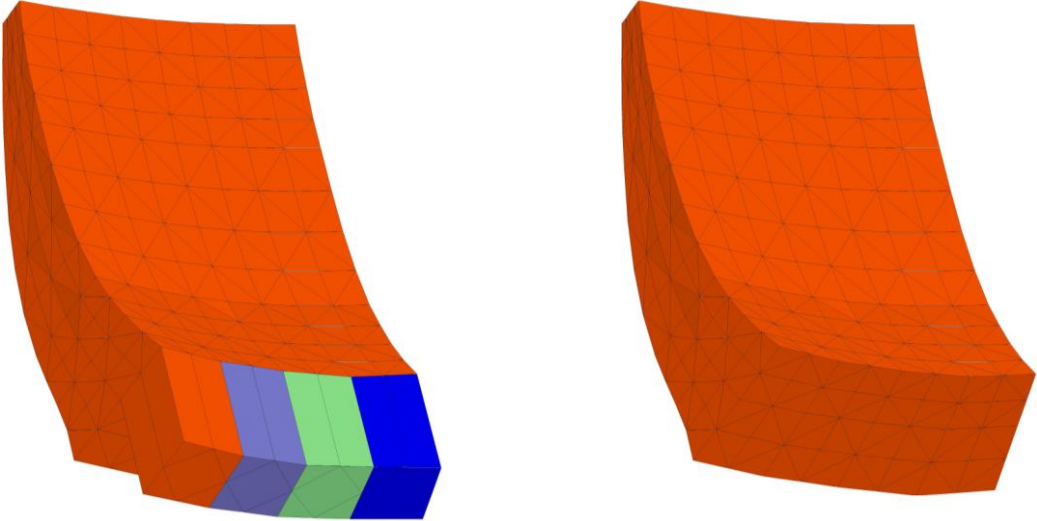


Figure 6.42 – Generation of polyhedral blocks (left) matching FE block faces (right).

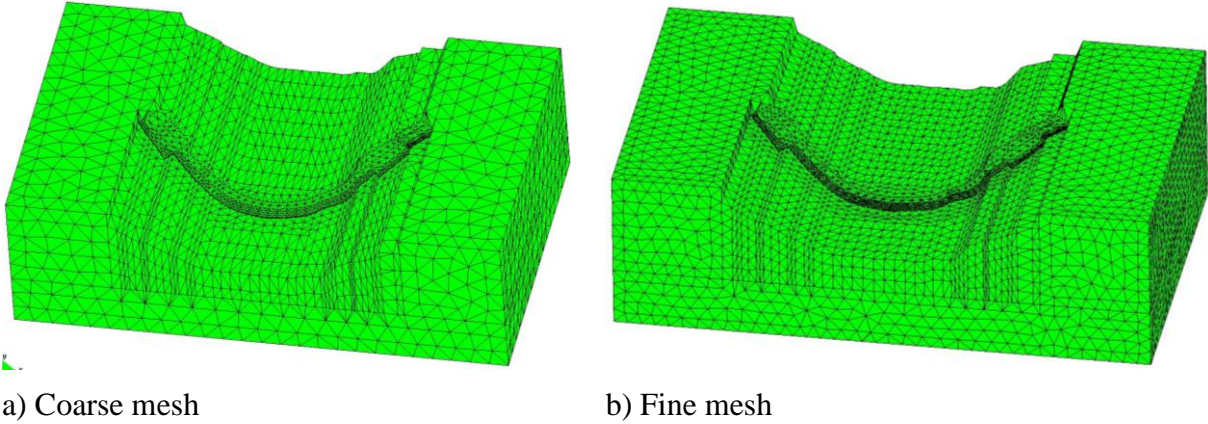


Figure 6.43 – Internal mesh of the global foundation model.

6.6.2 Hydraulic boundary conditions

Numerical analysis was carried out using the water levels recorded in October 2006, while carrying out the first borehole water-inflow tests, with the reservoir at an elevation of 143.6 m and water downstream from the dam-wall at an elevation of 81.95 m. At the drainage curtain, the hydraulic head in each block was assumed to be equal to the average elevation of the drains' head.

In the 3DEC models presented thus far hydraulic boundary conditions were easily applied, in areas defined by coordinate ranges in the x, y and z directions. In this global model, however, it is not as easy to apply neither the upstream and downstream heads, due to surface topography, nor the hydraulic head at the drainage curtain, due to its horizontal and vertical curvature. A procedure was devised, using the concept of the unit normal vector to a plane, by which only the surfaces in contact with a) the reservoir, b) tailwater, and c) drainage curtain, were identified. This allowed hydraulic heads to be properly applied, by allocating a different surface region number, as allowed by 3DEC, to each set a), b), and c).

Unlike the detailed analysis of seepage presented in the previous sections where flow took place in the upstream-downstream direction through a confined medium, here seepage flow is not confined as there is a water table in each abutment, due to the natural side-hill seepage.

6.6.3 Results analysis

A series of numerical experiments was carried out, with the model of which the mesh is shown in Figure 6.43 b), in order to obtain numerical discharges in the foundation of each dam block close to those observed. These experiments led to the conclusion that parameters determined using the detailed numerical models described in section 6.4 can not be used directly in a global 3D model of the foundation as, due to the difference in the elements' size and scale, local permeable layers and individual drains can not be represented. However, the different areas identified in the detailed models can be simulated, taking into account the average value of discharges and water pressures recorded in each block. It was assumed that the rock mass equivalent permeability was 1.0×10^{-8} m/s. A near-surface area of higher permeability (10×10^{-7} m/s) was simulated upstream from the grout curtain, which encompasses the valley bottom and the base of each slope (Figure 6.44). As in the detailed models, horizontal layers of higher permeability between the above-mentioned near-surface area and the drainage curtain were considered in some of the dam blocks, to take into account areas where flow paths cross the drains, identified with the tests carried out *in situ*.

The model was first run assuming that the rock mass equivalent permeability was 1.0×10^{-8} m/s, and that the grout curtain was 10 times less pervious. In order to represent the near-surface area and the horizontal layers of higher permeability the model had to be cut again. This new model has 1534 blocks, 68333 gridpoints, and is divided into 140131 tetrahedra (Figure 6.45). The new model's mesh is slightly finer than that shown in Figure 6.43 b), in the areas where cuts were made. With the above-mentioned hydraulic boundary conditions, the numerical discharge at the valley bottom is 12.47 l/min, which is about 68 % of the total discharge recorded in that area (18.42 l/min). Numerical analysis was carried out in steps, changing a parameter at a time. Table 6.28 shows, as an example, the increase in the quantity of water flowing through the model and in the foundation of block 17-18 when the permeability of different foundation areas was changed.

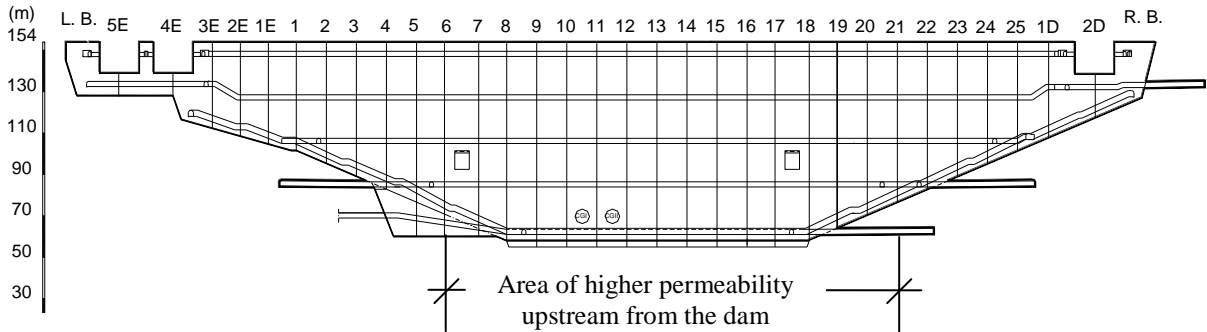
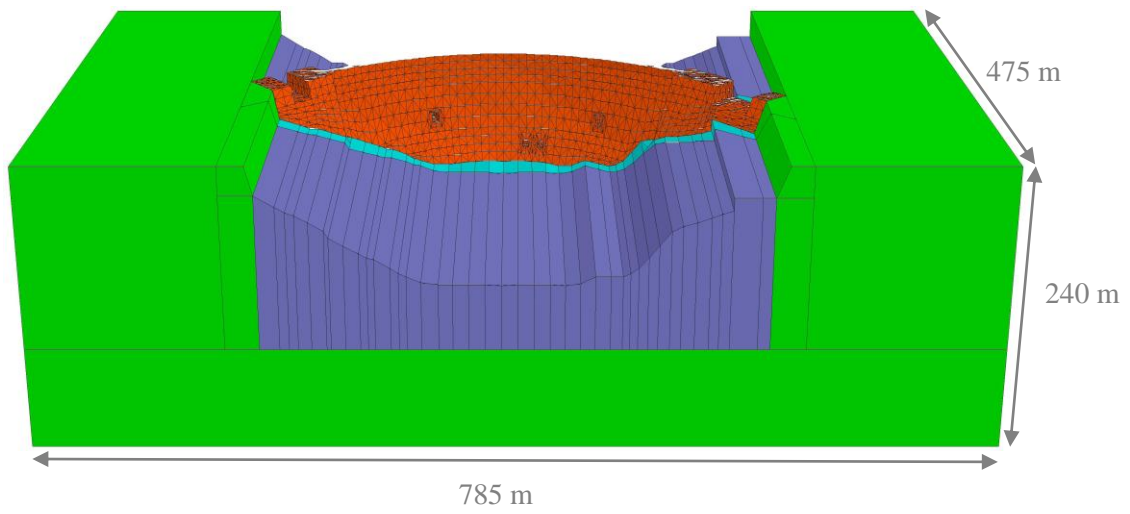


Figure 6.44 - Upstream elevation of Alqueva dam. Location of the area of higher permeability upstream from the dam assumed in the hydraulic model of the dam foundation.

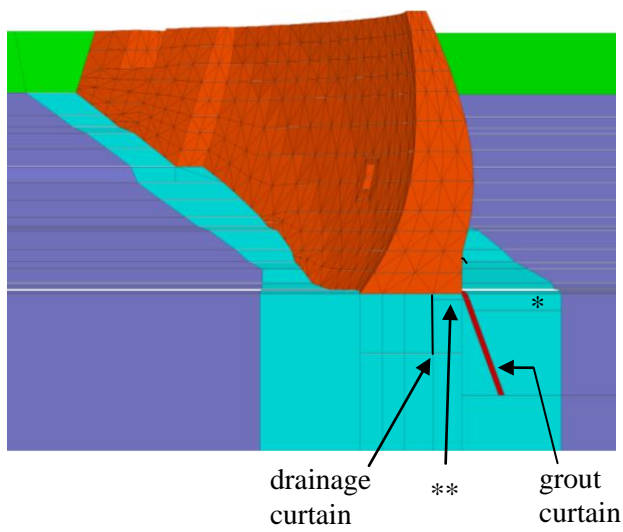
Model	Increase in the quantity of water flowing through the model (in percentage) (reference value = 12.47 l/min)	Increase in the discharge in the foundation of block 17-18 (in percentage) (reference discharge = 1.51 l/min)
a) Near-surface area of higher permeability assumed only upstream from block 17-18	0.07 %	1.3 %
b) Near-surface area of higher permeability upstream from the dam in the valley bottom and at the base of each slope (between dam vertical joints 6 to 21)	0.5 %	1.3 %
c) A more pervious horizontal layer, with a permeability of 5.0×10^{-8} m/s, between the upstream area and the drainage curtain, upstream from and underneath the dam block 17-18, in addition to the near-surface area of higher permeability simulated in model b).	8.6 %	199 %

Table 6.28 – Sensitivity to higher permeabilities.

a)



b)



- * near-surface area of higher permeability upstream from the dam
- ** horizontal layers of higher permeability

c)

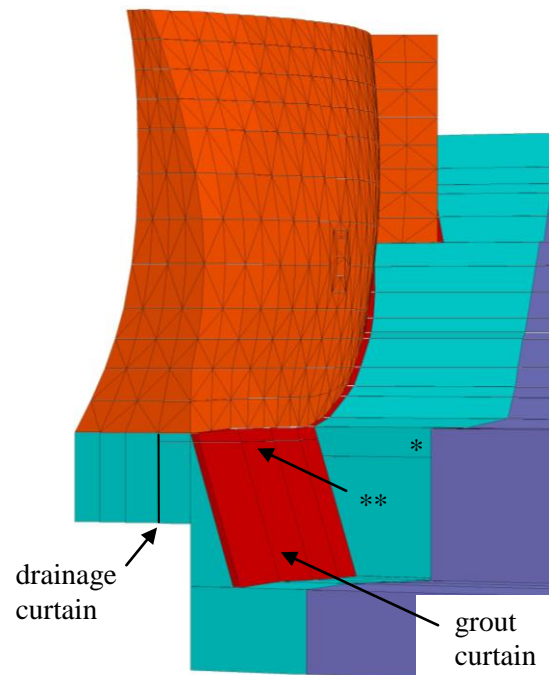


Figure 6.45 – Global foundation model: perspective (a), cross section with simulated grout and drainage curtains (b) and detail showing the grout curtain representation (c).

The procedure explained in the previous paragraphs was then applied to the remaining blocks: in the foundation of some of the dam blocks located in the valley bottom, the permeability of the horizontal layers between the near-surface area of higher permeability and the drainage curtain was gradually adjusted in order to obtain numerical discharges close to average recorded discharges. Table 6.29 shows three sets of permeability values which were assumed while carrying out numerical analysis. Numerical errors obtained were analysed using three different parameters, which provide complementary information:

- iii) mean error, \bar{x} , which gives an idea of the trend, showing whether the numerical results are higher or lower than those recorded, given by:

$$\bar{x} = \frac{\sum_{i=1}^n error}{n} \quad (6.4)$$

- iv) mean absolute error, $|\bar{x}|$, which measures how close numerical results are to recorded data, giving an idea of the error's magnitude:

$$|\bar{x}| = \frac{\sum_{i=1}^n |error|}{n} \quad (6.5)$$

- v) mean squared error, which measures the average of the square of the error:

$$s_n^2 = \frac{\sum_{i=1}^n (error)^2}{n} \quad (6.6)$$

The lower the mean absolute error and the mean squared error, the better the model. Analysis of Table 6.30 shows that the set of permeability values with which numerical results are closer to those recorded is set 3.

In the final model (Set 3), in addition to rock mass equivalent permeability, only four different permeability values were used: 0.4, 0.5, 1.0 and 3.5×10^{-7} m/s. Figure 6.46 shows how close the total discharges recorded in each arch block are to the numerical results obtained with the heterogeneous foundation model described above. The same figure shows the results of a model with a homogeneous rock mass with a permeability of 1.0×10^{-8} m/s.

Dam block	Permeability of the horizontal layers between the near-surface area of higher permeability upstream from the dam and the drainage curtain ($\times 10^{-7}$ m/s)		
	Set 1	Set 2	Set 3
	6-7	-	-
7-8	-	-	-
8-9	0.5	0.5	1.0
9-10	0.5	0.5	0.5
10-11	-	-	-
11-12	0.5	0.5	0.4
12-13	0.5	0.5	0.4
13-14	-	-	-
14-15	-	-	-
15-16	0.5	0.5	0.5
16-17	0.5	0.5	0.5
17-18	0.5	0.5	0.4
18-19	0.5	0.5	0.4
19-20	3.5	3.0	3.5
20-21	-	-	-

Table 6.29 – Assumed permeability of the horizontal layers between the near-surface area of higher permeability upstream from the dam and the drainage curtain.

Model	Parameter used to compare models		
	Mean error	Mean absolute error	Mean squared error
Homogeneous rock mass	-0.18 (min = -3.93; max = 1.85)	0.67	78.73
Set 1	0.16 (min = -0.95; max = 0.92)	0.37	78.15
Set 2	0.14 (min = -0.95; max = 0.92)	0.39	78.15
Set 3	0.165 (min = -0.87; max = 0.92)	0.30	78.11

Table 6.30 – Error analysis: mean error, mean absolute error and mean squared error.

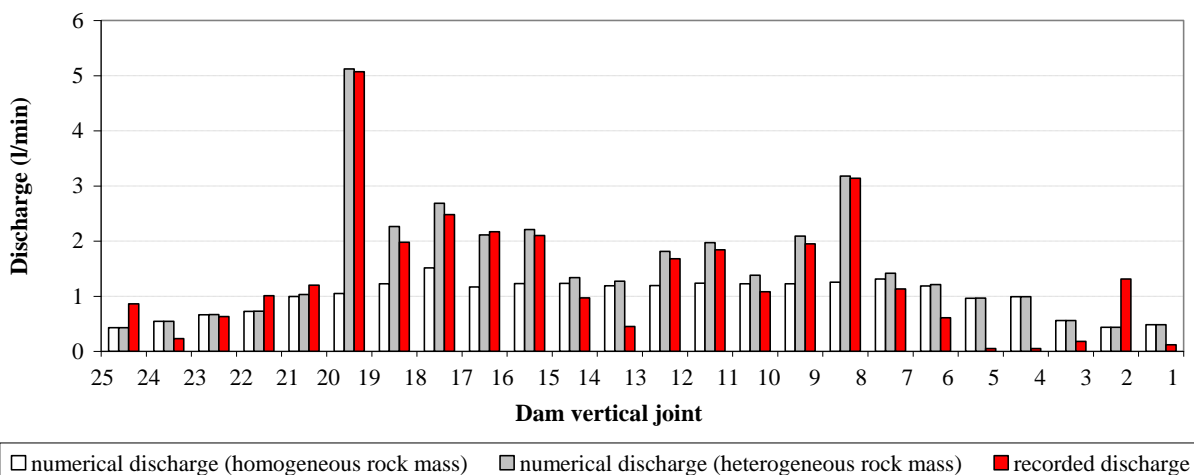


Figure 6.46 – Recorded discharges in the foundation of each dam block and comparison with numerical results.

Figure 6.47 shows the hydraulic head contours. The graphical interface used to show the results (GID) (CIMNE 2006) only shows the hydraulic head contours on block surfaces, therefore when the phreatic surface is below the top of the block, that block appears as a hollow space. In order to represent the hydraulic head more accurately it is necessary to show cuts, as in Figure 6.48. In this figure part of the drainage curtain is visible in the cut perpendicular to the main river channel.

With the aim of comparing numerical water pressures with those recorded in the foundation of block 17-18, when drains D21 D to D26 D were closed simultaneously, presented in section 4.5.8.3, the model was run once more, this time assuming the same hydraulic head on the surfaces which simulate the drainage curtain in the foundation of the above-mentioned block, as if there were a hypothetical continuous piezometric trench, and preventing water from flowing out of this trench. The hydraulic head on these surfaces is the average drain head's elevation in block 17-18. In the 3DEC code, this is simulated by linking all the gridpoints located on the surfaces which define the "piezometric trench", for all the gridpoints on those surfaces to have the same hydraulic head.

The *in situ* tests were carried out with the reservoir at around 148.0 m and the tailwater at 81.6 m. When drains D21 D to D26 D were closed simultaneously, water pressures of 0.275 to 5.6 bar were recorded in drains and piezometers located in the foundation of block 17-18, with an average of 2.30 bar. This average water pressure was around 27 % of the hydraulic head. With the global 3D hydraulic model and with the previously mentioned water levels, the head at the drainage curtain in the foundation of block 17-18 is 88.10 m, which is 32 % of the hydraulic head. The numerical hydraulic head is very close to that recorded, and therefore it can be concluded that the simplified global hydraulic model here presented can provide mean water pressures and flow rates for each dam foundation block.

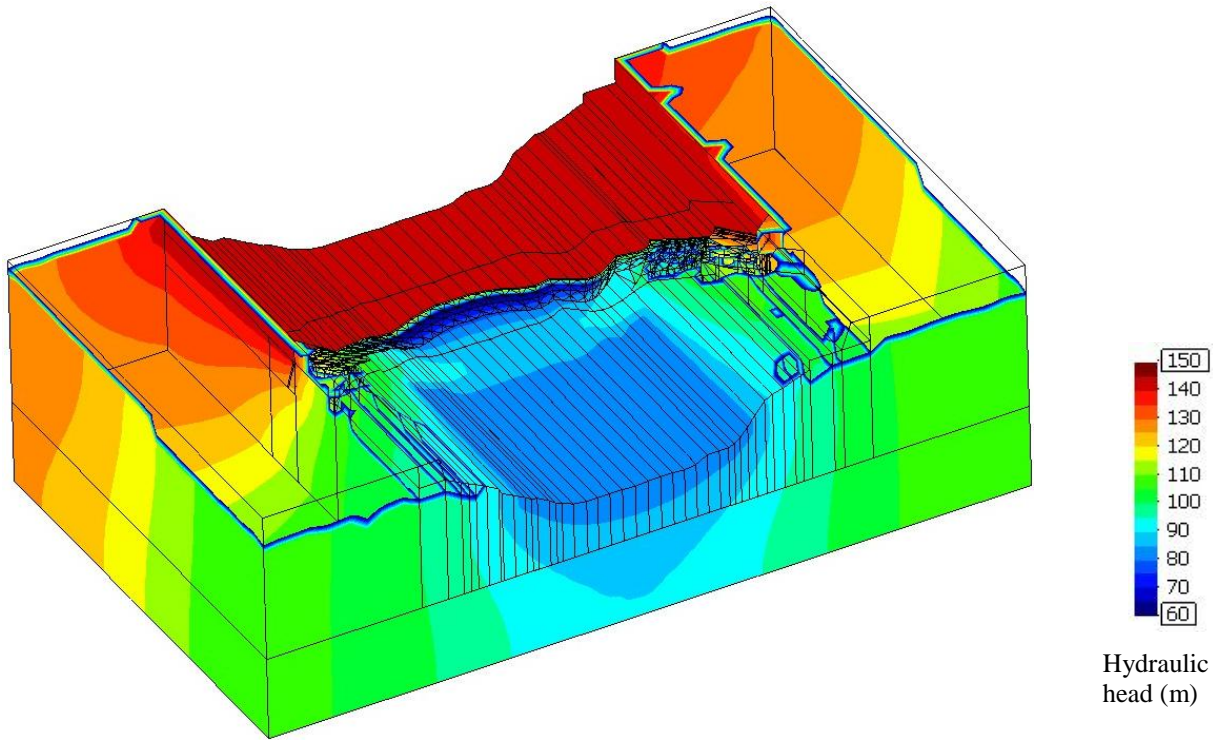


Figure 6.47 – Hydraulic head contours (m) in the global hydraulic model of Alqueva dam foundation (for $H_u = 143.6$ m; $H_d = 81.95$ m).

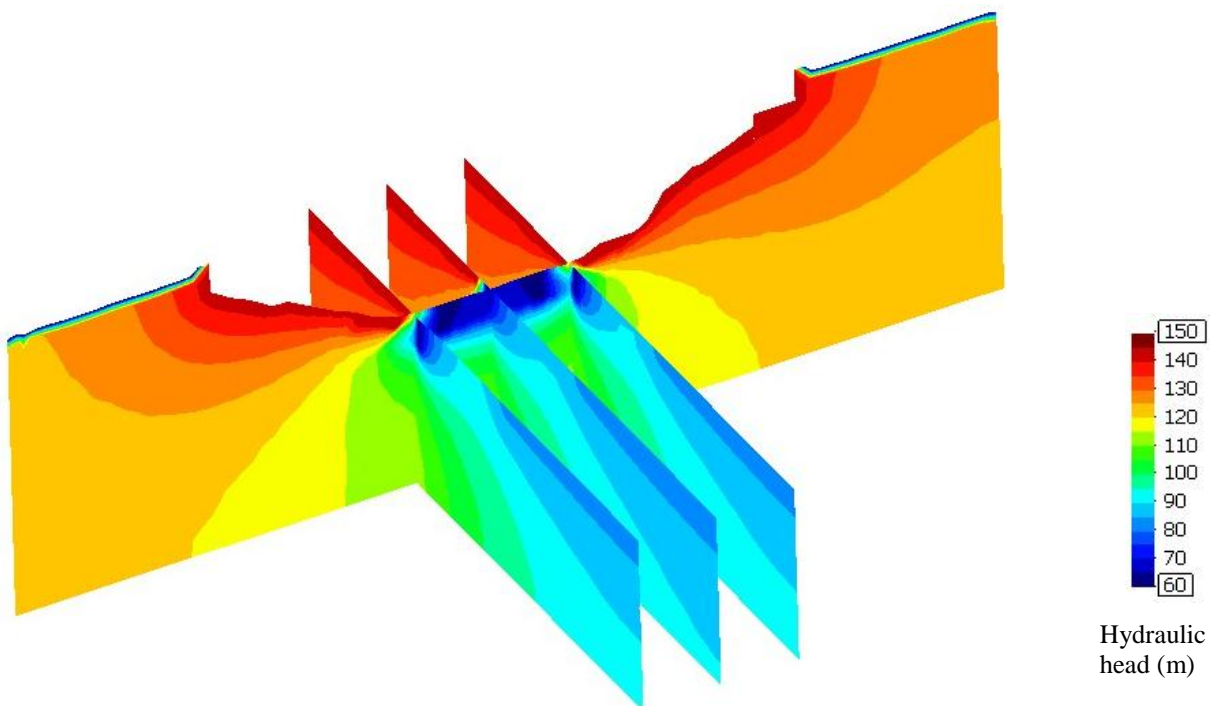


Figure 6.48 – Hydraulic head contours (m) in three cuts parallel and in one cut perpendicular to the main river channel, shown in their relative positions (for $H_u = 143.6$ m; $H_d = 81.95$ m).

6.7 Hydromechanical interaction in the foundation of Alqueva dam

6.7.1 Introduction

In the previous section, seepage was analysed using a global 3D model of the dam foundation. In this model it was assumed that there is an area of higher permeability upstream from the dam, in the valley bottom and at the base of each slope (between dam vertical joints 6 to 21 as shown in Figure 6.44), and horizontal layers of higher permeability between the upstream area and the drainage curtain, upstream from, and underneath, some of the dam blocks located in the mentioned area. Numerical analysis was carried out assuming water levels recorded in October 2006, in the week in which the first borehole water-inflow tests were done. Comparisons made afterwards between numerical and recorded discharges led to the conclusion that the apertures of the discontinuities through which water flows vary with changes in reservoir level. Therefore, based on the results of borehole water-inflow tests, presented in chapter 4, and on available field data, an attempt was made to estimate the relation between stress and permeability.

The hydromechanical interaction in the foundation of Alqueva dam was studied taking into account the results of the hydraulic model described in the previous section and of a mechanical model developed afterwards, which is going to be presented in section 6.7.3. Uncoupled hydraulic and mechanical analyses were carried out independently, and curves between stress and permeability were established taking into account recorded discharges in the foundation of each dam block and total stresses obtained with the mechanical model.

The main aim of the study is to develop a methodology which can be used to establish rules which, from a hydraulic model calibrated for specific reservoir and tailwater levels, allow the calculation of discharges for other reservoir levels. These rules, that directly relate the permeability with the state of stress, can be established taking into account either effective or total stresses. In the study presented here mechanical analysis was carried out without taking into account water pressures and therefore total stresses were obtained. If the effective stress had been considered, different curves would be obtained, which, however, should lead to results equivalent to those obtained. From a theoretical point of view, because water flows through the foundation, it would be more correct to consider the mechanical actions of the water, and the effective stress rather than the total stress. However, in this case of Alqueva dam, as is going to be confirmed, vertical fissures open in the foundation close to the heel of the dam and flow through the conductive discontinuities is mainly horizontal. Therefore, in this case, it can be assumed that vertical stresses are not affected by seepage forces. Effective stresses are relevant for the safety assessment, in which what really matters is the water pressure at the base of the dam or in sub-horizontal discontinuities close to the base. This issue is going to be addressed in the following chapter.

This section describes the study carried out in order to establish a relation between stress and permeability in some areas of Alqueva dam foundation. Firstly, the results of the comparisons which led to this study are presented, followed by a description of the numerical mechanical model developed in order to estimate the aperture of vertical discontinuities within the rock mass close to the heel of the dam and to assess stresses in the foundation rock mass. The results of this model are analysed and compared with field data. The section then goes on to show how relationships between the permeability of the horizontal layers, which simulate water conductive joints, and the average vertical stresses in the same areas can be established. In addition, an attempt is made to establish a relation between local rock mass deformability and permeability. In the last part of this section, assumptions and simplifications made during analysis are discussed. Finally, a brief summary and the main conclusions of the study are presented.

6.7.2 Comparison of numerical and recorded discharges with the reservoir at different elevations

The global model of the dam foundation referred to in the previous section was calibrated for the reservoir at an elevation of 143.6 m and water downstream from the dam-wall at an elevation of 81.95 m. The same model was used to determine the total discharges in each arch block with the reservoir at different elevations, corresponding to the various water level stages during the controlled first filling of the reservoir:

- around 115.0 m, recorded on 18 September 2002 (stabilizing level 1 (NE1));
- around 130.0 m, recorded on 6 February 2003 (P1);
- around 143.5 m, recorded on 21 January 2004 (P2); and
- around 150.0 m, recorded on 28 February 2007 (stabilizing level 2 (NE2)).

On the first three mentioned dates, tailwater level was around 74.8 m. From 28 October 2005, the first filling of Pedrógão reservoir increased Alqueva's tailwater level, which was 81.95 m on 16 October 2006, in the week when the first water-inflow tests were carried out, and 81.2 m on 28 February 2007.

Comparisons between recorded and numerical discharges for the different water levels, shown in Figure 6.49, lead to the conclusion that, in the area being studied, the model overestimates discharges for water levels lower than 143.6 m and underestimates discharges for water levels higher than that. In fact, this is observed in every block with only a few exceptions: numerical discharges are lower than those recorded on 6 February 2003 in dam block 14-15 and on 21 January 2004 in dam blocks 8-9, 9-10 and 14-15; and are higher than those recorded on 28 February 2007 in dam blocks 13-14 and 17-18.

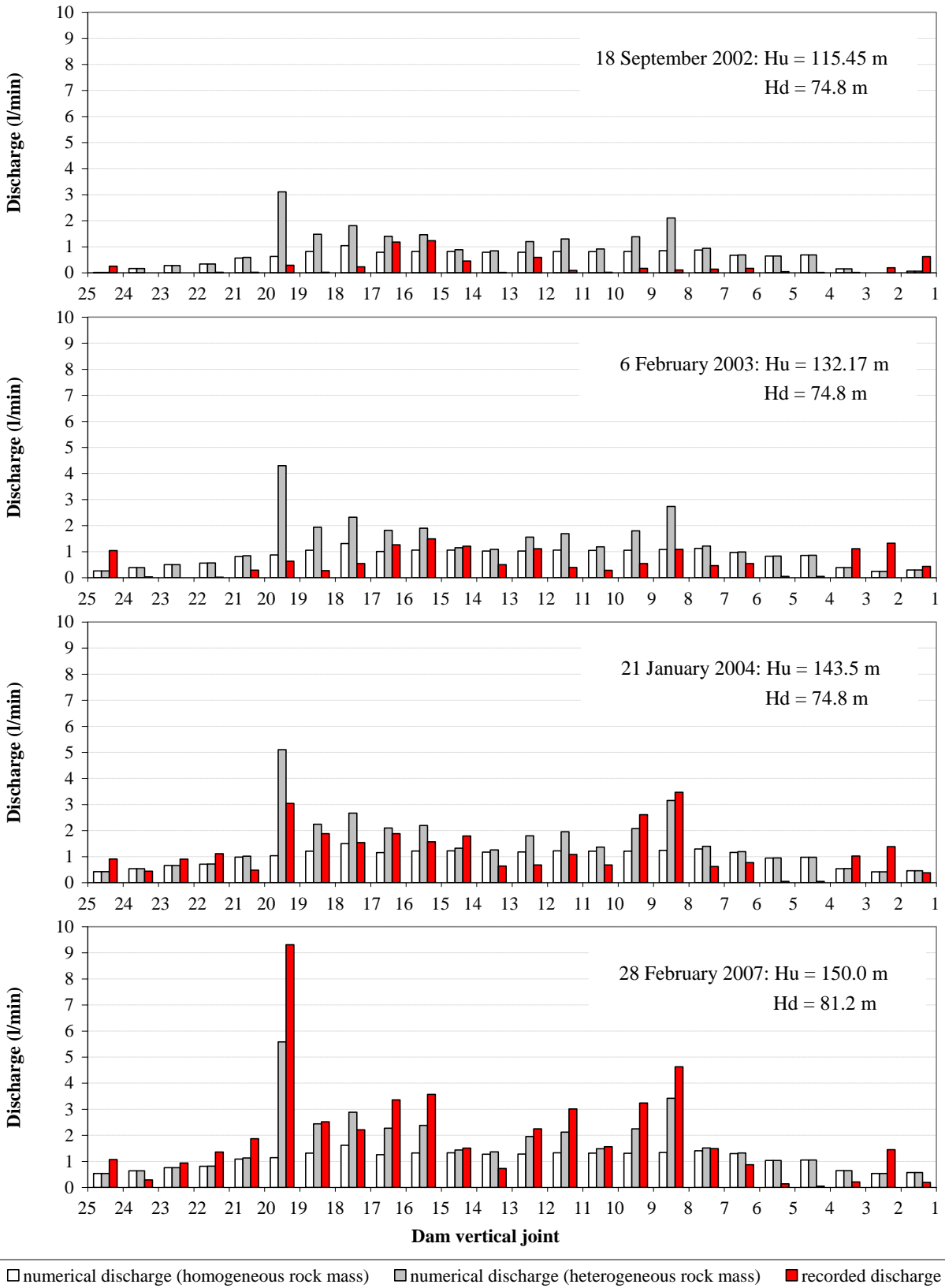


Figure 6.49 – Recorded discharges in the foundation of each dam block and comparison with numerical results for different water levels (numerical model calibrated for the reservoir at 143.6 m and tailwater at 81.95 m; H_u – reservoir level; H_d – tailwater level).

Results of numerical analysis carried out for the water levels recorded on 18 September 2002 show that discharges obtained with the homogeneous foundation model are higher than recorded discharges in every dam block, therefore the model can not be employed for the lower water levels in the reservoir.

Figure 6.50 shows numerical discharges in the foundation of each dam block for the various reservoir levels. Figure analysis shows that in block 19-20, where the highest total discharges are recorded, numerical flow increases about 81 %, from 3.1 to 5.6 l/min, when the water level in the reservoir increases 35 m, from about 115 m up to about 150 m. Figure analysis also shows that almost the same results are obtained for the water levels recorded in January 2004 and October 2006, which leads to the conclusion that the tailwater level has very little influence.

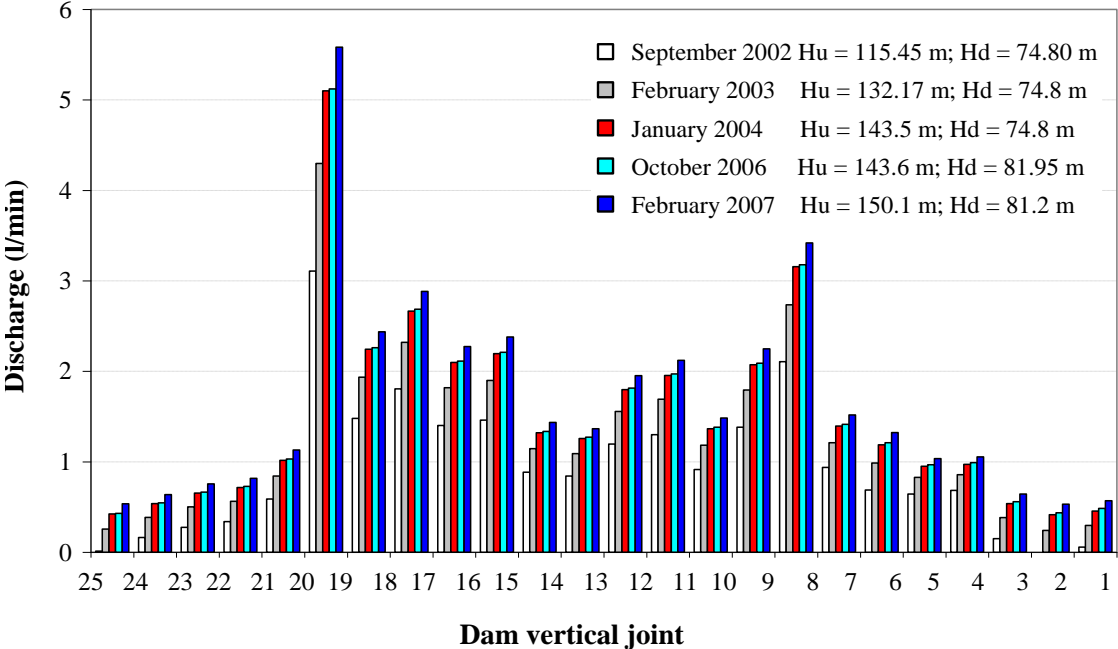


Figure 6.50 – Numerical discharges in the foundation of each dam block for different reservoir levels (Hu – reservoir level; Hd – tailwater level).

6.7.3 Numerical mechanical model

6.7.3.1 Model description

The model used to carry out mechanical analysis is geometrically similar to the hydraulic model presented in the previous chapter. However, unlike the above mentioned model, which only includes the foundation, the mechanical model of the dam-foundation system requires that not only the dam be represented but also the location of fault 22, in order to simulate the area of lower modulus of elasticity, where the phyllite occurs. Phyllite deformability is assumed above the lower wall of the fault and green schist deformability in the remaining rock mass. Fault 22 is assumed to be 10 m wide. The model is shown in Figure 6.51.

The dam is simulated by a group of finite element elastic blocks separated by joints, which represent vertical contraction joints. In the foundation a joint is assumed at the dam/rock mass interface (“foundation joint”), and, as the grout curtain is simulated adjacent to the upstream edge, two hypothetical joints were assumed between the grout curtain and the rock mass, at the upstream and downstream faces of the grout curtain, respectively (“grout curtain/rock interface”), so as to estimate the aperture of discontinuities in the uppermost strata of the foundation. The grout curtain/rock interface is considered only between dam joints 6 to 21, corresponding to the location of the area of higher permeability upstream from the dam assumed in the global hydraulic model of the dam foundation (Figure 6.44).

The rock mass, assumed to be isotropic, is represented by 2178 deformable blocks, internally divided into 143881 zones. The average edge lengths of the tetrahedral zones are the same as those used in the hydraulic model (4.0 m in the blocks surrounding the drainage curtain, 8.0 m in the vicinity of the above mentioned blocks, including the grout curtain area, 12.0 m in the areas close to the dam in the upstream and downstream direction, and 20.0 m in the remaining rock mass).

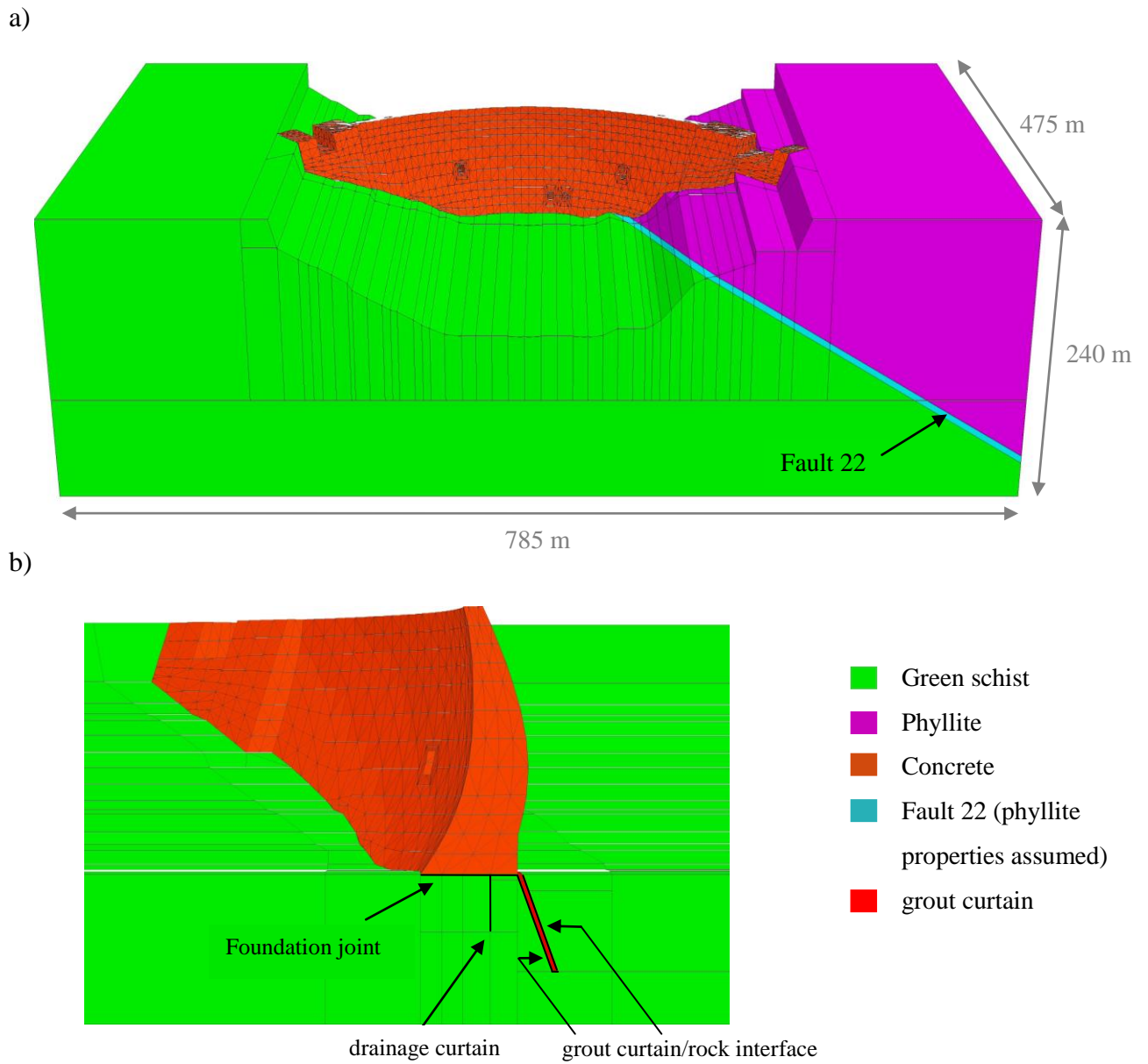


Figure 6.51 - Global mechanical model: perspective (a) and cross section (b).

6.7.3.2 Material properties

Material and joint properties are shown in Table 6.31 and Table 6.32. Both dam concrete and foundation rock mass, as well as the dam contraction joints, are assumed to follow elastic linear behaviour. Foundation joint and grout curtain/rock interface are assigned a Mohr-Coulomb constitutive model.

Dam Young's modulus is assumed to be 20 GPa. The existence of contraction joints leads to an increase in the dam's deformability which, in practice, is difficult to quantify. When modelling, if the dam is simulated as a single block, dam Young's modulus is usually adjusted in such a way that numerical results already include the effect of joint deformability. When the dam is simulated as a group of blocks separated by joints, deformability properties of both concrete and joints have to be adjusted to match the whole structure's deformability. In order to have a measure of the effect of these joint stiffnesses it is possible to define a fictitious equivalent width of concrete which has the same deformability of the joint. This equivalent width (e) is given by:

$$e = \frac{E}{k_n} \quad (6.7)$$

Therefore, in this case, a joint normal stiffness (k_n) of 10 GPa/m corresponds to the assumption that vertical contraction joints have a width of 2 m of material identical to dam concrete. Joint widths of 0.5 to 2 m of material identical to dam concrete are normally used in 3D analysis of dams behaviour (Lemos et al. 2006; Pina et al. 2006). A ratio of 0.5 is assumed between normal and shear stiffnesses ($k_n = 10$ GPa/m and $k_s = 5$ GPa/m).

Contraction joints were injected with the dam concrete at temperatures lower than 10°C, with the joints quite wide open, in order to ensure that, once injection was concluded, the dam would behave as a monolithic block. Analysis of recorded joint movements with the reservoir at different levels higher than 112 m shows that the opening and closure of joints is lower than 0.5 mm, which is within jointmeter's accuracy (LNEC 2008), therefore the joints can be considered closed. The only exceptions are the joints which link the arch to both gravity structures, in the right and left banks (joints 1 and 25), in which apertures up to 1.5 mm were recorded in jointmeters located close to the downstream face of the dam, on dates when the temperature was very low. As the dam joints are closed, the assumption of joint elastic behaviour is justified.

It is assumed that rock mass Young's modulus is 10 GPa where schist occurs and that the phyllite area is two times more deformable. Grout curtain properties are the same as those in the rock mass foundation, either schist or phyllite.

Foundation joint and grout curtain/rock interface properties were changed during numerical analysis, as shown in Table 6.32. Firstly, the model was run until equilibrium, assuming elastic behaviour (Model 1). Two non-linear analyses were afterwards carried out: in Model 2, non-linear behaviour of grout curtain/rock interface was assumed, with a friction angle of 35° and zero cohesion and tensile strength at this interface; in Model 3, the above-mentioned joint properties were assumed not only at the grout curtain/rock interface but also at the upstream area of the foundation joint (in the valley bottom, between dam joints 8 to 18, the upstream area of the foundation joint simulates the peripheral joint at the heel of the blocks, introduced to avoid stresses with the filling of the reservoir, as shown in Figure 4.9).

In 3DEC, the way to simulate elastic continuity at the interfaces, shear and tensile strength being prevented, is to assign very high cohesion and tensile strength to the interfaces. Therefore, in Model 1, cohesion and tensile strength were assigned 10²⁰ GPa at both interfaces. In Model 2 this value was only assigned to the foundation joint.

As shown in Table 6.32, in Models 2 and 3, joints assumed to have non-linear behaviour were assigned zero tensile strength and zero cohesion. Assigning a zero tensile strength allows the interfaces to open in areas where tensile stresses occur. With a shear strength defined by cohesion zero and an assumed friction angle, only friction prevents interfaces from sliding.

Material	Density (kg/m ³)	Young's modulus (<i>E</i>) (GPa)	Poisson's ratio -
Dam	2400	20	0.2
Rock mass			
green schist	2650	10	0.2
phyllite	2650	5	0.2
Grout curtain			
in the green schist area	2650	10	0.2
in the phyllite area	2650	5	0.2

Table 6.31 – Material properties.

Model	Normal stiffness <i>k_n</i> (GPa/m)	Shear stiffness <i>k_s</i> (GPa/m)	Friction angle <i>φ</i> (°)	Cohesion <i>c</i> (MPa)
Model 1: elastic	10	5	all joints with elastic behaviour	
Model 2: non-linear behaviour of grout curtain/rock interface	10	5	35°	0
Model 3: non-linear behaviour of both upstream area of the foundation joint and grout curtain/rock interface	10	5	35°	0

Table 6.32 – Joint mechanical properties in each of the three different models.

6.7.3.3 Sequence of analysis

Dam and foundation displacements and stresses were obtained in a simplified way considering three successive loading stages:

- i) *in situ* stresses due to the weight of the rock mass, before dam construction;
- ii) dam weight; and
- iii) hydrostatic load at various reservoir elevations.

In the first stage, the usual procedure is to assume an approximate initial state of stress, and to obtain the *in situ* stresses by running the model until equilibrium, so that the determined *in situ* stresses take the valley geometry into account. At this stage of the analysis, the dam and the grout curtain have not yet been constructed, thus they should not be considered in the numerical analysis. However, in 3DEC, all the blocks must be created before zoning them and running the model. In this code, the procedure to ensure that dam weight and stiffness do not influence *in situ* stresses is to assign zero gravity load to FE blocks and to assume a very low dam Young's modulus, to make the dam follow the valley deformation. Stresses due to dam deformation are set to zero once equilibrium is reached, in order not to include these stresses in subsequent analysis. Therefore, at this stage of analysis, dam Young's modulus, which is about 20 GPa, was assumed to be 100 times lower.

Numerical analysis started from a given hydrostatic state of stress, close to the *in situ* state of stress due to rock mass weight. An estimate of the initial vertical stress component was obtained, as usual, assuming that it increases with depth, due to the weight of the upper rock mass. This relationship is valid, as shown by Hoek and Brown (1980), who collated worldwide *in situ* stress data. There is, however, a significant amount of scatter in the measurements (Figure 6.52). In an elastic homogeneous media, assuming that the two horizontal stresses are equal, this simplified hypothesis of *in situ* stresses due only to rock mass weight, leads to:

$$\sigma_y = -\gamma_r \cdot y \quad (6.8)$$

$$\sigma_x = \sigma_z = k \sigma_y \quad (6.9)$$

with:

$$k = \frac{\nu}{1 - \nu} \quad (6.10)$$

where γ_r is the rock mass unit weight, y is the depth below the surface of the rock mass (in the 3DEC model presented here, x-axis towards the left bank; y-axis vertical; and z-axis towards upstream); and ν is the Poisson's ratio. Assuming elastic behaviour, a Poisson's ratio of 0.2

(Table 6.31) corresponds to a ratio of horizontal to vertical stresses of 0.25. In practice, higher k values are observed, as shown in Figure 6.53. The same figure shows that close to the surface readings are extremely widely scattered, but with increasing depth, the k values decrease.

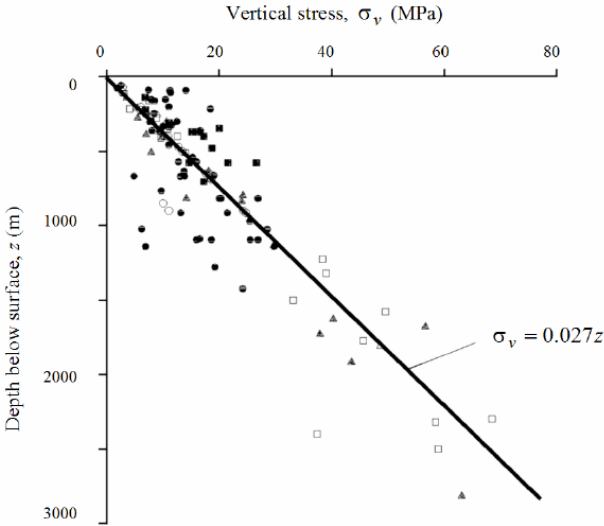


Figure 6.52 – Collated worldwide in situ stress data: vertical stress components (after Hoek and Brown 1980).

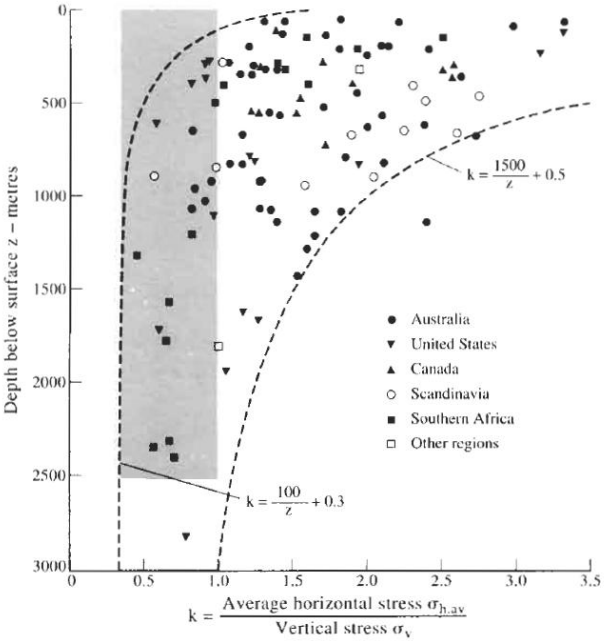


Figure 6.53 – Collated worldwide in situ stress data: mean horizontal stress component (after Hoek and Brown 1980).

Prior to dam construction, direct measurements of horizontal stresses were taken using small flatjacks inserted into exposed rock surfaces, in excavated galleries (LNEC 1973). Two measurements were taken on the left bank, 13 and 20 m below rock mass surface and one on the right bank, 12 m below surface, from which ratios of horizontal to vertical stresses of 0.87, 0.94, and 1.26 were determined, respectively. The small amount of available data is not enough to provide useful information; therefore it was assumed that the ratio of horizontal to vertical stresses was 0.5, which is more realistic than the k value given by the elasticity theory.

In situ stresses were determined assuming a homogeneous rock mass, with a unit weight of 26.5 kN/m^3 and a Young's modulus of 10 GPa, assumed to be uniform in the whole foundation. The simplest hypothesis of a homogeneous foundation was considered, and the more deformable area where the phyllite occurs was assigned the same properties as the schistous area. It was assumed that the hydrostatic state of stress varied linearly in each valley slope, from the valley bottom to the top of both right and left banks.

Regarding boundary conditions, vertical displacements at the base of the model and horizontal displacements perpendicular to each of the four lateral model boundaries were prevented.

The simplifications made at this stage of analysis have little effect on numerical results, as in near surface structures, such as dams, the effect of *in situ* stresses is low.

In the second stage, additional loading corresponds to dam weight, therefore real dam Young's modulus and stiffness were assumed. Dam construction sequence was not taken into account, and the dam weight was applied as a whole. Joints and interfaces were assumed to have elastic behaviour. In this phase, the foundation was assumed to be more deformable above the lower wall of fault 22, in the phyllite area. Boundary conditions were the same as those assumed in the previous phase. As the dam weight is a vertical load, the same results are obtained with these boundary conditions as with displacements prevented at the base of the model and at the lateral boundaries.

In the third stage, hydrostatic loading corresponding to various reservoir levels was applied to the upstream face of the dam. Boundary conditions were changed, preventing any displacement at the base of the model and at the lateral boundaries. The model was first brought to equilibrium assuming elastic behaviour. From this state of equilibrium, Models 2 and 3 were run for more steps, until convergence was achieved, as in this way interfaces were allowed to open. Once they open, stresses become zero.

6.7.3.4 Results analysis

First loading stage (in situ stresses)

At the beginning of the numerical analysis, *in situ* stresses due to the weight of the rock mass are obtained. Figure 6.54 shows principal stresses in tetrahedra belonging to each foundation block, in a vertical cross section perpendicular to the valley axis (compressive stresses are negative). Results show a realistic stress pattern, with vertical stresses increasing with depth and horizontal stresses decreasing close to the surface of the rock mass and valley slopes.

Second loading stage (dam weight)

In the second phase of analysis, influence of dam weight is assessed. Gridpoint displacements were set to zero before cycling the system until equilibrium. Horizontal arch displacements at crest elevation (154 m), shown in Figure 6.55, are towards upstream and are higher in the left bank because phyllite is more deformable than the green schist. Figure 6.56 shows displacements and principal stresses at, and underneath, the central cross section. The crest of the central cantilever moves towards upstream, with a horizontal displacement of 9.8 mm and vertical displacement of 13.3 mm downwards. In the dam concrete, maximum compressive stresses were determined in directions close to the vertical, at the heel of the dam, and at this stage went up to 4.7 MPa. Tensile stresses in the arches were barely obtained.

In the rock mass, maximum vertical displacements were determined underneath the dam and were higher in the left bank, because phyllite is more deformable than green schist. Maximum vertical displacements of 9.4 mm were determined. In foundation blocks below the heel of the central cantilever average compressive stresses of around 2.2 MPa were determined, which approximately corresponds to vertical stresses due to dam weight ($2400 \text{ kg/m}^3 \times 10 \text{ m/s}^2 \times 96 \text{ m} = 2.3 \text{ MPa}$).

Third loading stage (hydrostatic loading)

The mechanical response of the dam/foundation system under hydrostatic loading, for different reservoir levels, is obtained in the third phase of analysis. The following paragraphs present the radial displacements at the crest of the central cantilever, normal joint displacements, and average vertical stresses in the foundation blocks below the dam arch which simulate conductive joints in the global hydraulic model of the dam foundation. Gridpoint displacements were reset at the beginning of this loading stage, so the displacements presented are only due to hydrostatic loading. Results for the three different models considered in this phase of analysis are presented:

Model 1 – elastic;

Model 2 – non-linear behaviour of grout curtain/rock mass interface;

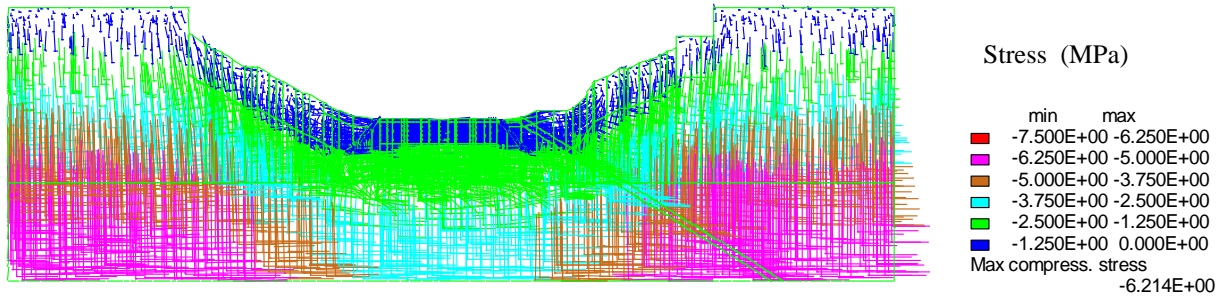


Figure 6.54 - *In situ* principal stresses. Vertical cross section ($z = 3$ m).

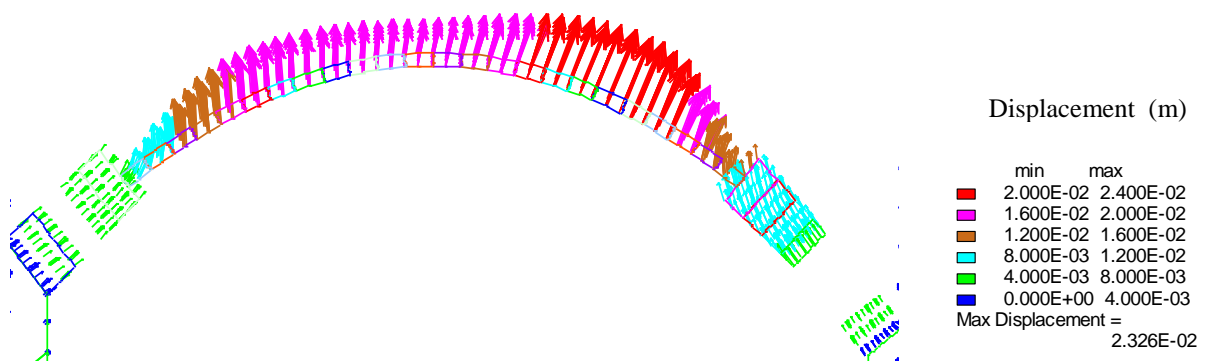


Figure 6.55 – Displacements at crest elevation ($y = 154$ m) due to dam weight.

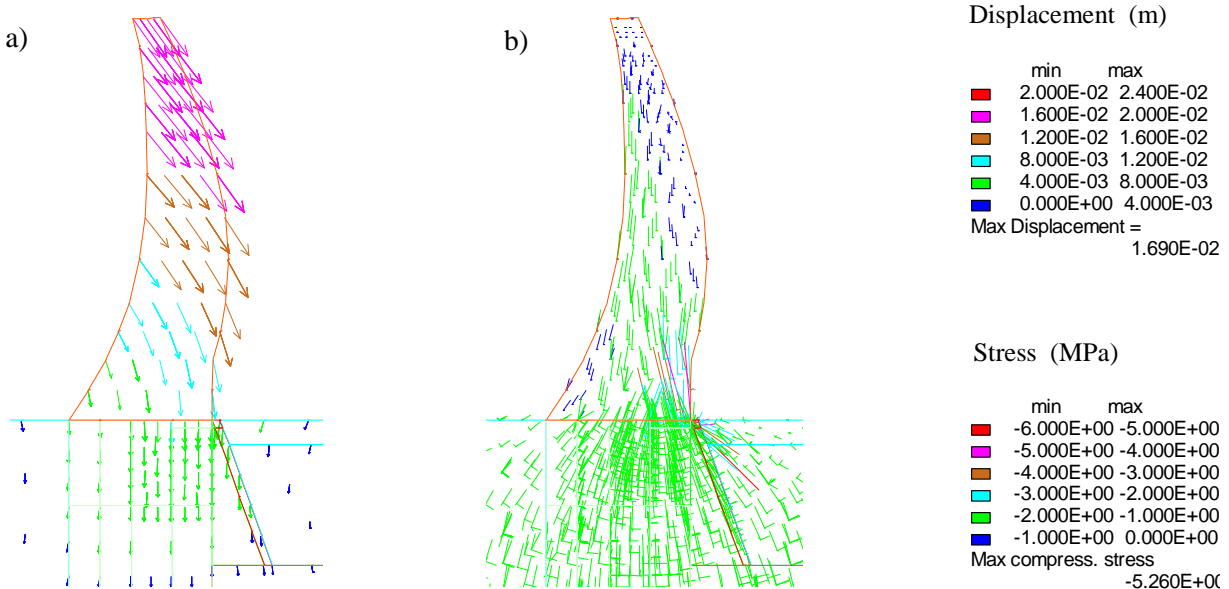


Figure 6.56 – Central cross section. Displacements (a) and principal stresses (b) due to dam weight.

Model 3 – non-linear behaviour of both grout curtain/rock mass interface and foundation joint.

As in the previous loading stage, two figures showing the horizontal arch displacements at crest elevation (154 m), and displacements and principal stresses at, and underneath, the central cross section are presented (Figure 6.57 and Figure 6.58). Both figures show results of Model 1, for the highest reservoir level. Naturally, displacements are towards downstream and are slightly higher in the left bank, due to the existence of the phyllite area. The crest of the central cantilever moves towards downstream, with a horizontal displacement of 60.47 mm and vertical displacement of 7.32 mm downwards. In the dam concrete, maximum compressive stresses of around 10 MPa were determined in the lower area of block 21-22, close to the downstream face of the dam. In the central cantilever, maximum compressive stresses of around 4.5 MPa were determined not only in the lower arch area, close to the downstream face of the dam, but also in the arch upper area.

Numerical analysis with the dam simulated as a single block, without vertical joints, was carried out and the results were compared to those obtained with the elastic model presented here (Model 1), in which dam joints behave elastically. Displacements at the crest of the central cantilever for the highest reservoir level and for the various reservoir levels referred to in section 1.2, determined with both models are shown in Table 6.33. The percentage of displacement increase when the existence of joints is assumed is shown in brackets. It can be seen that, for the highest reservoir level, contraction joints 2 m wide of material identical to dam concrete lead to an increase of around 15 % in the numerical horizontal displacement at the crest of the central cantilever, and of around 5 % in the vertical displacement.

Table 6.34 shows numerical radial displacements at the crest of the central cantilever for the different reservoir levels, determined with the three different models (Models 1, 2 and 3). Horizontal radial displacements and vertical displacements for the various reservoir levels are shown in Figure 6.59. The non-linear behaviour of the grout curtain/rock interface and of both the grout curtain/rock interface and foundation joint has only a slight effect on displacements, and only for the higher reservoir levels. For the highest reservoir level, a horizontal radial displacement at the crest of the central cantilever of around 60 mm is determined. In this case, the horizontal radial displacement obtained with Model 1 is 98 % of that obtained with Model 3, which corresponds to a difference of 1.2 mm, and the vertical displacement is 36 % higher, which corresponds to a difference of 1.9 mm.

Displacement histories in both y- and z-directions monitored at different points in the rock mass upstream and downstream from the grout curtain, in a section that crosses the dam central cantilever in the upstream/downstream direction led to the conclusion that the grout curtain/rock interface opens at the downstream face of the grout curtain, as shown in Figure

6.60. Tensile stresses below the heel of the central cantilever, due to the filling of the reservoir, lead to the opening of the interfaces, with maximum normal and shear displacements shown in Table 6.35 and Figure 6.36, respectively. Analysis of the results of Model 3 shows that for the highest water level grout curtain/rock interface normal displacement is about 1.5 up to 2.1 mm in the upper 3 m. For the same reservoir level, the foundation joint opens about 3.4 mm close to the area where the upstream face of the dam meets the foundation (Figure 6.60), and slides about 1.4 mm. In both models, the maximum shear displacement at the grout curtain/rock interface decreases when the reservoir level increases from 115.5 m to 132.2 m, and gradually increases for higher reservoir levels. As shown in Figure 6.61, this is due to a change in the relative direction of movement between the grout curtain and the surrounding rock mass, when the reservoir goes up from 132.2 m to 143.6 m.

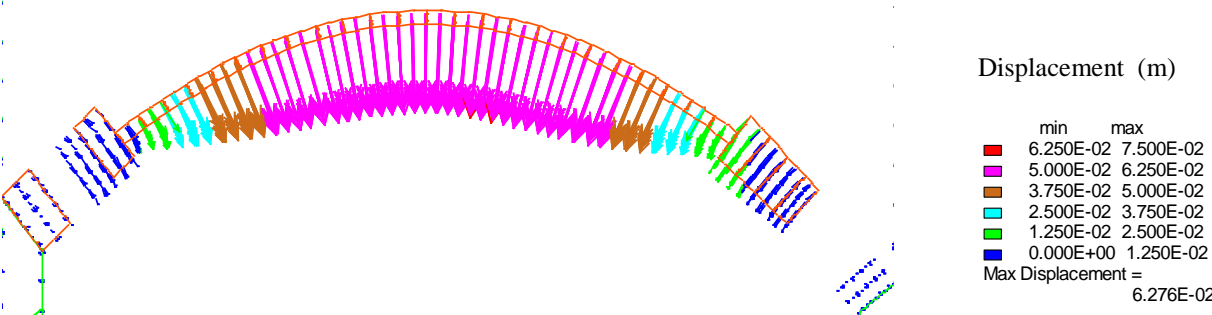


Figure 6.57 – Displacements at crest elevation (y = 154 m) due to hydrostatic loading for the reservoir at 154.0 m (highest reservoir level).

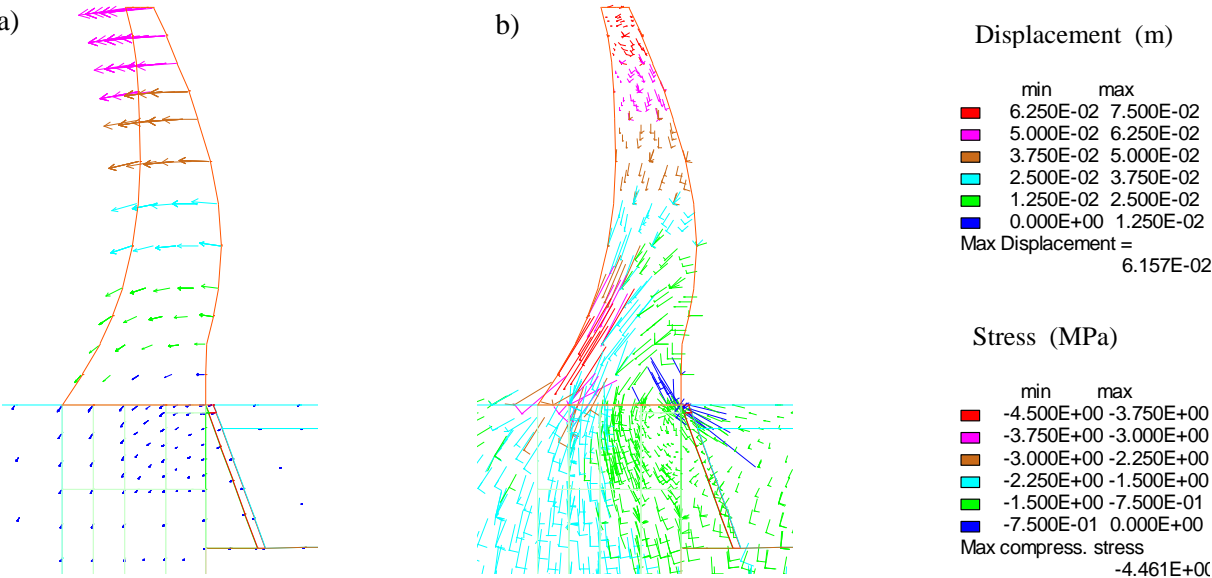


Figure 6.58 – Central cross section. Displacements (a) and principal stresses (b) due to hydrostatic loading for the reservoir at 154.0 m (highest reservoir level).

Water level in the reservoir (m)	Radial displacements at the crest of the central cantilever (mm)			
	Dam simulated as a single block		Model 1: dam simulated as blocks separated by joints	
	y (mm)	z (mm)	y (mm)	z (mm)
154.0	-6.96	-52.46	-7.32 (+5%)	-60.47 (+15%)
150.1	-6.85	-38.69	-7.08 (+3%)	-45.07 (+16%)
143.6	-7.55	-30.19	-7.73 (+2%)	-35.47 (+17%)
132.2	-9.08	-14.30	-9.12 (+0.4%)	-17.46 (+22%)
115.5	-10.91	-3.38	-10.93 (+0.2%)	-4.54 (+34%)

Table 6.33 – Comparison of radial displacements at the crest of the central cantilever due to increase in reservoir level obtained with the dam simulated as a single block and with the dam simulated as a group of FE elastic blocks separated by joints (y-axis vertical; z-axis towards upstream).

Water level in the reservoir (m)	Radial displacements at the crest of the central cantilever (mm)					
	Model 1		Model 2		Model 3	
	y (mm)	z (mm)	y (mm)	z (mm)	y (mm)	z (mm)
154.0	-7.32	-60.47	-6.37	-61.14	-5.38	-61.70
150.1	-7.08	-45.07	-6.44	-44.81	-6.02	-45.41
143.6	-7.73	-35.47	-7.28	-35.24	-7.21	-35.43
132.2	-9.12	-17.46	-9.15	-17.26	-9.14	-17.20
115.5	-10.93	-4.54	-11.31	-3.82	-11.32	-3.84

Table 6.34 – Radial displacements at the crest of the central cantilever due to increase in reservoir level (y-axis vertical; z-axis towards upstream).

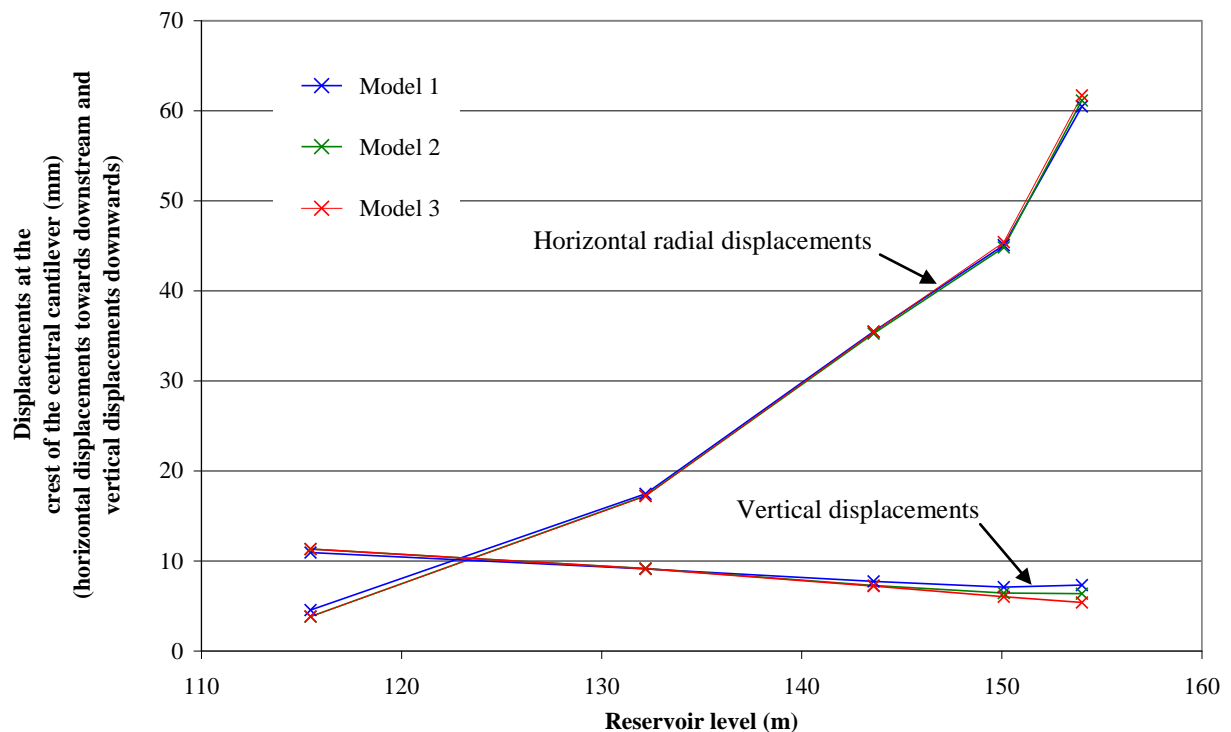


Figure 6.59 – Horizontal radial displacements and vertical displacements at the crest of the central cantilever due to increase in reservoir level.

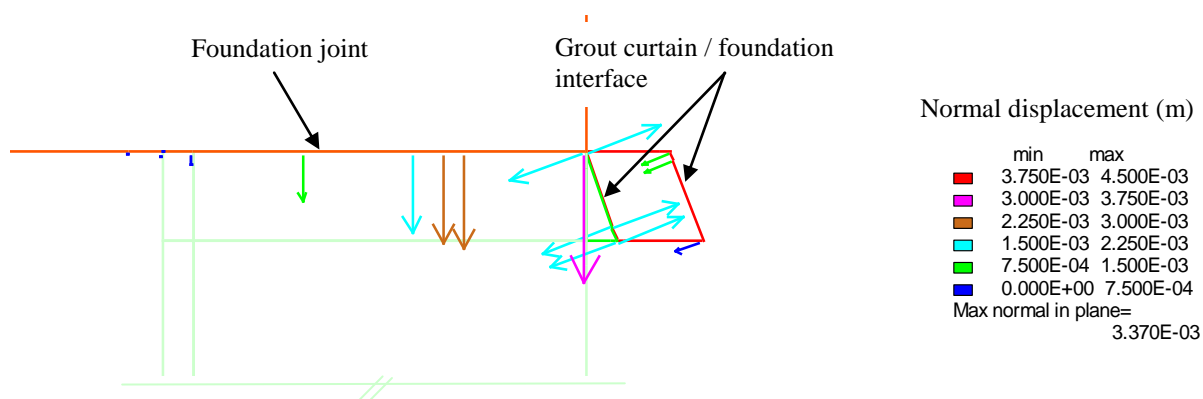


Figure 6.60 – Normal joint displacement vectors for the reservoir at 154.0 m.

Water level in the reservoir (m)	Maximum joint apertures (mm)			
	Model 2		Model 3	
	Foundation joint	Grout curtain/rock interface	Foundation joint	Grout curtain/rock interface
154.0	0.12	3.13	3.37	2.14
150.1	0.06	2.75	1.54	2.00
143.6	0.06	2.17	0.27	1.66
132.2	0.14	1.19	0.14	1.15
115.5	0.24	0.24	0.24	0.21

Table 6.35 – Maximum joint aperture for different reservoir levels.

Water level in the reservoir (m)	Maximum joint shear displacement (mm)			
	Model 2		Model 3	
	Foundation joint	Grout curtain/rock interface	Foundation joint	Grout curtain/rock interface
154.0	0.16	4.22	1.41	2.43
150.1	0.14	2.88	1.43	1.83
143.6	0.13	1.75	1.18	1.28
132.2	0.08	0.15	0.15	0.17
115.5	0.05	1.86	0.05	1.85

Table 6.36 – Maximum shear joint displacement for different reservoir levels.

As previously mentioned, the main purpose of this chapter is to establish relationships between the permeability of the horizontal layers considered in the hydraulic global model of the dam foundation, which simulate water conductive joints, and the average vertical stresses in the same areas. In 3DEC, each block is internally divided into tetrahedra with uniform stress; therefore vertical stresses in the foundation blocks below the heel of the dam which, in the hydraulic model, simulate conductive joints were obtained by averaging the vertical tetrahedral stresses. With the exception of blocks below dam blocks 7-8 and 8-9, which are crossed by fault 22, all elements are of about the same volume, therefore a simple average is adequate. If there were very narrow zones, weighted averages would have to be determined, taking into account each zone's volume.

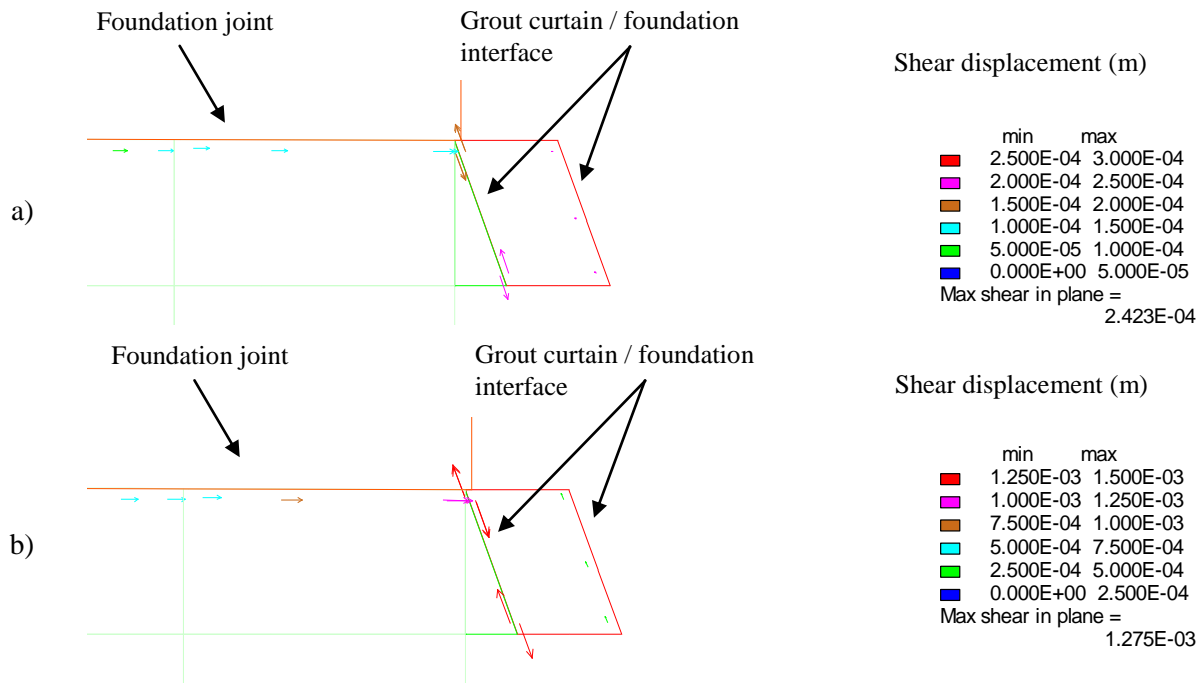


Figure 6.61 - Shear joint displacement vectors for the reservoir at a) 132.2 m, and b) 143.6 m.

Naturally, as water rises in the reservoir vertical compressive stresses decrease. In the valley bottom, unlike close to both abutments, tensile stresses are calculated below the heel of the dam for the highest reservoir levels (Figure 6.62). Here, stresses increase gradually from the base of each slope towards the valley axis and Model 1 leads to lower compressive stresses and higher tensile stresses. Figure 6.62 analysis shows that the decrease in vertical tensile stresses in the foundation blocks below the heel of the dam is affected much more by the non-linear behaviour of the foundation joint than by that of the grout curtain/rock interface. Variations in average total vertical stresses in the foundation of the central cantilever and of block 20-21 with changes in reservoir level are shown in Figure 6.63. For the highest water level, the tensile stress of 0.5 MPa determined with Model 1 below the heel of the central cantilever is almost three times that determined with Model 3. At the base of the central cantilever, vertical stresses determined with both models 2 and 3 are almost the same with the reservoir up to 143.6 m; but for reservoir levels higher than that, tensile stresses determined with Model 3 are lower, due to the opening of the foundation joint. At the base of block 20-21, however, differences in vertical stresses determined with the three different models only occur for reservoir levels higher than 150.1 m.

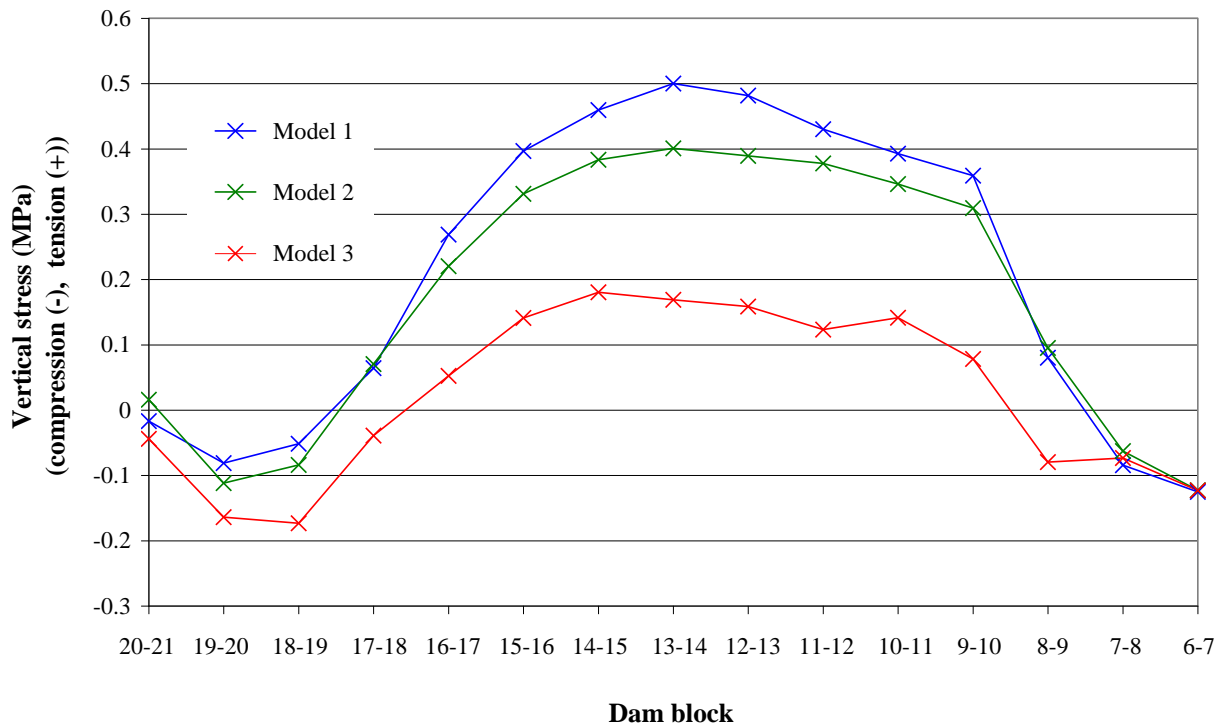


Figure 6.62 - Average total vertical stresses in the foundation blocks below the heel of the dam which, in the hydraulic model, simulate conductive joints, with the reservoir at 154.0 m.

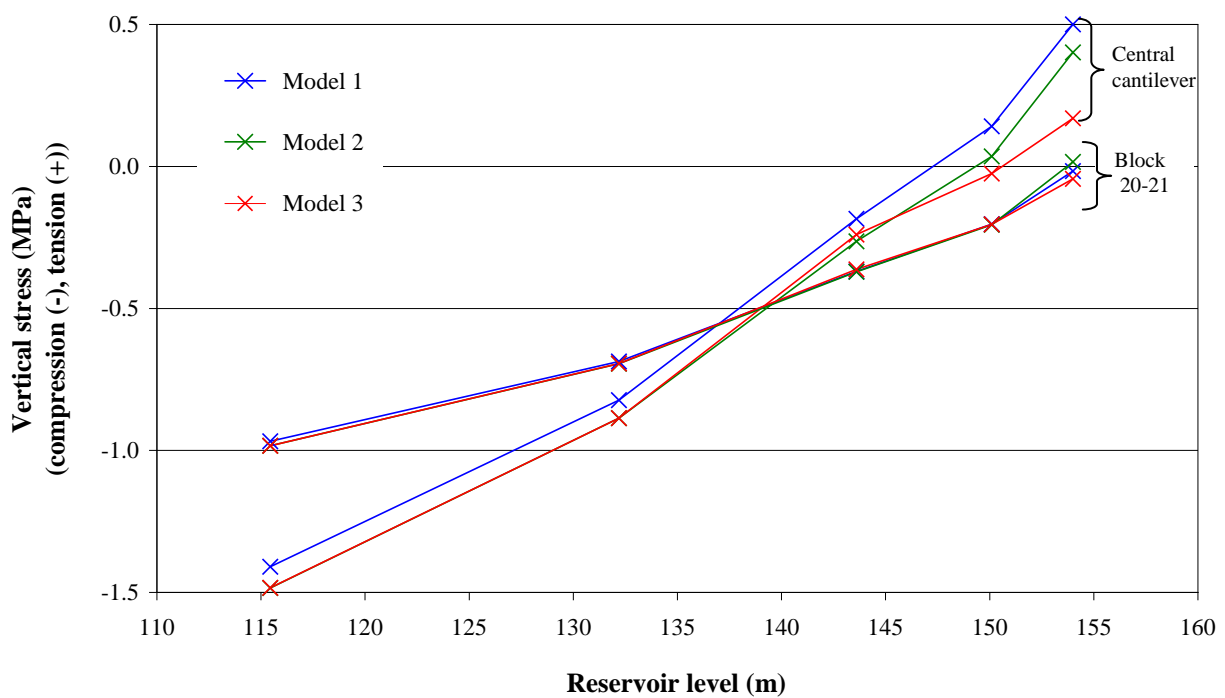


Figure 6.63 – Variations in average total vertical stresses in the foundation blocks below the heel of the central cantilever and of block 20-21 which, in the hydraulic model, simulate conductive joints, with changes in reservoir level.

6.7.3.5 Comparison of monitored and numerical results

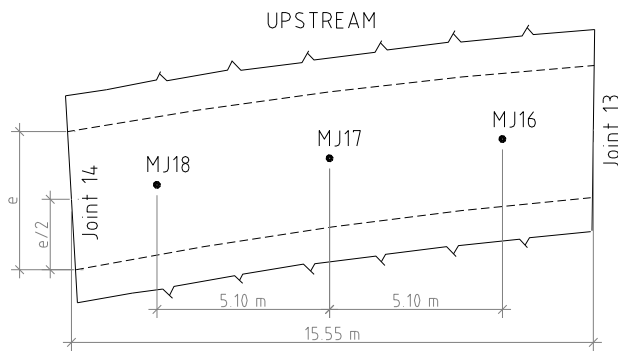
Horizontal displacement at the crest of the central cantilever

Studies of quantitative interpretation based on recorded displacements in the inverted plumb-lines, led to the conclusion that horizontal displacements at the crest of the central cantilever due to hydrostatic loading are about 50 mm with the reservoir at around 150.0 m (LNEC 2009). Numerical horizontal displacements for the same reservoir level, presented in Table 6.34, are about 90 % of that recorded.

Vertical displacement at foundation joint

The peripheral joint is monitored with joint gauges, located around 5 metres apart along its length, positioned in such a way that each block has three gauges, one of which is located approximately halfway between dam vertical joints, as shown in Figure 6.64 for the case of the central cantilever. Figure 6.65 shows vertical displacements in the joint gauges located at the base of the central cantilever plotted versus time. Joint apertures were assumed to be zero on 2002.02.05, when the first filling of the reservoir began, therefore, from that date, recorded displacements would be mainly due to variations in hydrostatic load and to variations in ambient and reservoir temperatures (because variations in ambient and reservoir temperatures cause changes in the structure's temperature which, in turn, give rise to arch displacements towards upstream if the temperature increases, or towards downstream otherwise). However, during the first four months of reservoir filling, not only was foundation treatment still in progress, but also, following artificial dam cooling, contraction joints were injected. In addition, construction of gravity blocks close to the left bank had been concluded only about one month before the beginning of reservoir filling, therefore the thermal field in dam concrete was significantly asymmetric. This is probably the reason why the first readings shown in Figure 6.65 are so widely scattered.

For the highest reservoir levels recorded until the end of June 2008, of about 150 m, displacements of 0.6 up to 0.92 mm were recorded in joint gauge MJ18, the readings of which always showed a coherent pattern. As shown in Table 6.35, a numerical maximum foundation joint aperture of 1.5 mm is determined for the reservoir at an elevation of 150.1 m. At a distance of around 4.5 m from the upstream face of the dam, foundation joint aperture is about 0.8 mm (half of the maximum), which is within the range of recorded displacements.



e – width of peripheral joint

Dam vertical joint	Width of peripheral joint e (m)
8 and 18	7.25 / 7.31
9 and 17	7.96
10 and 16	8.45
11 and 15	8.77
12 and 14	8.95
13	9.00

Figure 6.64 – Location of joint gauges in the peripheral joint at the base of the central cantilever.

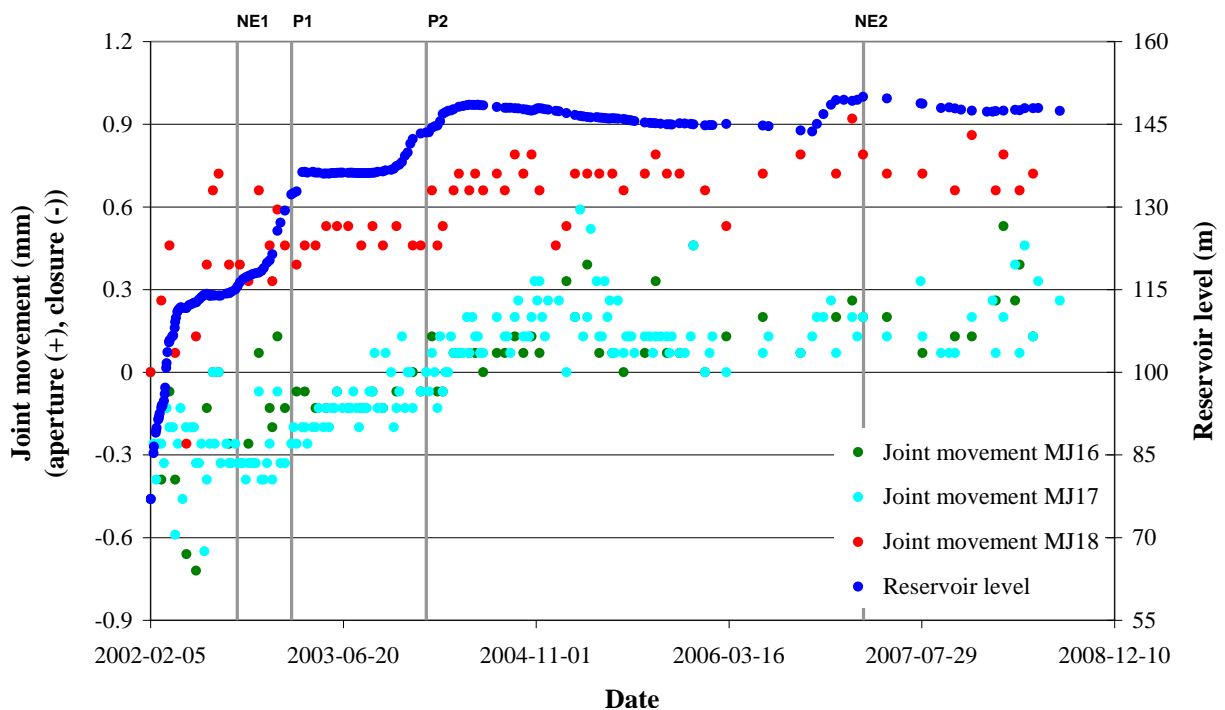


Figure 6.65 – Recorded vertical displacements at three points located in the peripheral joint at the base of the central cantilever.

Stresses in the foundation rock mass due to increase in reservoir level

Foundation strains in the vertical direction calculated from readings taken in rod extensometers GEF4 installed below the central cantilever were analysed and a rough comparison with average numerical strains was afterwards carried out. GEF4 includes both double and single extensometers in the upstream and downstream drainage galleries, respectively (Figure 6.66). Figure 6.67 shows strains plotted versus time. As with joint gauges located in the peripheral joint, readings were assumed to be zero at the beginning of the first

filling of the reservoir. It is observed that the length of rod extensometers (1) and (2), located in the upstream area, increases as the reservoir rises, whereas the length of extensometer (3), located at the downstream area, decreases (in vertical extensometers located in dam foundations, an increase in the relative displacement of the rod's top and bottom is related to rock mass decompression, while a decrease is related to rock mass compression). Strains recorded in extensometer (1) are higher than those in extensometer (2) therefore the majority of the heave in that area occurs in the upper 15.0 m of the foundation rock mass. Extensometers located in the upstream area are more influenced by variations in ambient temperature than the one located downstream. With the reservoir level approximately constant, an increase in ambient temperature leads to settlement of both extensometers located at the upstream area, while a decrease leads to their heave, which is explained by arch dams' behaviour.

Table 6.37 shows recorded strains for different reservoir levels. In an attempt to determine variations in strains due merely to variations in reservoir level, only readings taken in February/beginning of March were considered. Even though, there is a difference of around 11°C (from 7.8° up to 18.5°) in average ambient temperatures recorded in those selected dates. Variations in vertical strains are shown in Table 6.38, taking readings recorded on 2004.02.03 as reference.

Due to the size of the blocks below the central cantilever, shown in Figure 6.68, only a rough comparison of recorded and numerical strains could be carried out. Numerical average vertical stresses for the different reservoir levels and variations in strains are shown in Table 6.39 and Table 6.40. Strains were calculated taking into account the rock mass deformability modulus assumed in the mechanical model, and variations in strains were determined taking the previously mentioned date as reference. In Table 6.40, percentages of recorded strains are shown in brackets. For the highest reservoir level, differences are of about 33 %.

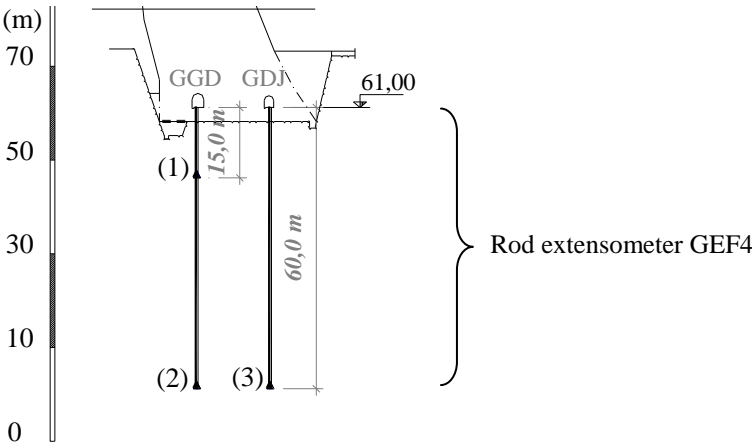


Figure 6.66 – Rod extensometers below the central cantilever.

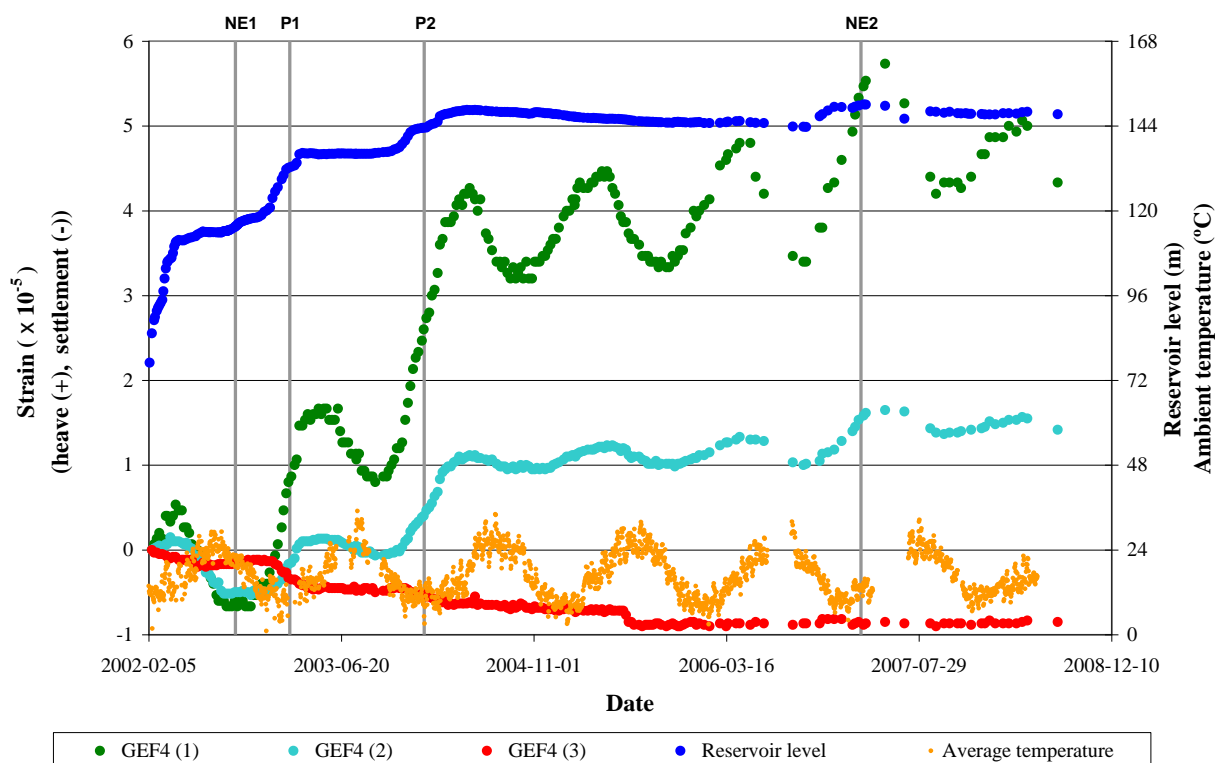


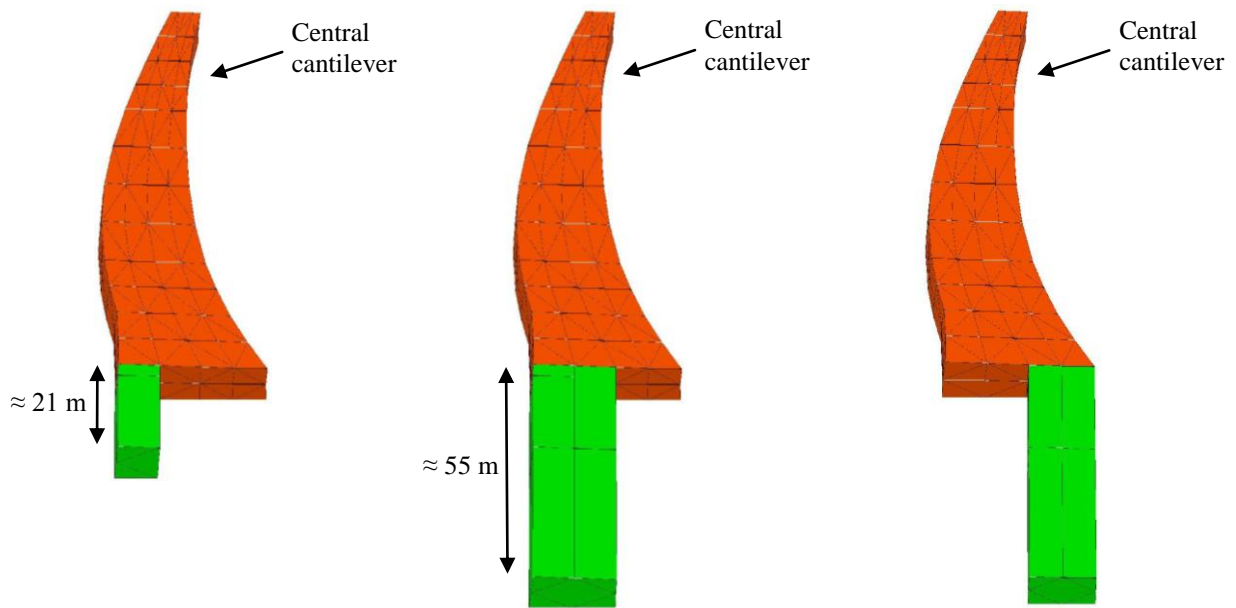
Figure 6.67 – Recorded strains in rod extensometer GEF4.

Date	Reservoir level (m)	Average ambient temperature (°C)	Strain ($\times 10^{-5}$)		
			GEF4(1)	GEF4(2)	GEF4(3)
2007.02.22	149.8	13.7	5.33	1.53	-0.85
2008.03.03	147.6	16.1	4.87	1.50	-0.87
2006.02.27	144.9	7.8	4.53	1.23	-0.87
2004.02.03	144.1	14.4	2.80	0.50	-0.55
2003.03.11	136.4	18.5	1.47	0.10	-0.42

Table 6.37 – Recorded strains in rod extensometer GEF4 for different reservoir levels.

Date	Reservoir level (m)	Strain variation ($\times 10^{-5}$)		
		$\Delta \epsilon_{yy} = \epsilon_{yy}(H) - \epsilon_{yy}(144.1 \text{ m})$		
		GEF4(1)	GEF4(2)	GEF4(3)
2007.02.22	149.8	2.53	1.03	-0.30
2008.03.03	147.6	2.07	1.00	-0.32
2006.02.27	144.9	1.73	0.73	-0.32
2004.02.03	144.1	-	-	-
2003.03.11	136.4	-	-	-

Table 6.38 – Variations in strains recorded in rod extensometer GEF4, using readings recorded on 2004.02.03 as reference.



Foundation blocks used to compare readings from GEF4(1)

Foundation blocks used to compare readings from GEF4(2)

Foundation blocks used to compare readings from GEF4(3)

Figure 6.68 – Foundation blocks below the central cantilever used to determine average vertical strains to compare with those determined from readings taken in rod extensometer GEF4.

Date	Reservoir level (m)	Average vertical stress ($\times 10^{-1}$ MPa)		
		GEF4(1)	GEF4(2)	GEF4(3)
2007.02.22	149.8	-2.42	-7.27	-16.02
2008.03.03	147.6	-3.06	-7.84	-15.97
2006.02.27	144.9	-3.86	-8.44	-15.84
2004.02.03	144.1	-4.11	-8.62	-15.80
2003.03.11	136.4	-7.28	-1.05	-15.32

Table 6.39 – Average vertical stresses in foundation blocks below the central cantilever for different reservoir levels.

Date	Reservoir level (m)	Stress variation (MPa)			Strain variation ($\times 10^{-5}$)		
		$\Delta\sigma_{yy} = \sigma_{yy}(H) - \sigma_{yy}(144.1\text{ m})$			$\Delta\varepsilon_{yy} = \Delta\sigma_{yy} / E$		
		GEF4(1)	GEF4(2)	GEF4(3)	GEF4(1)	GEF4(2)	GEF4(3)
2007.02.22	149.8	0.169	0.135	-0.02	1.69 (-34%)	1.35 (+31%)	-0.20 (-33%)
2008.03.03	147.6	0.105	0.078	-0.02	1.05 (-49%)	0.78 (-22%)	-0.20 (-33%)
2006.02.27	144.9	0.03	0.017	-0.004	0.30 (-83%)	0.17 (-77%)	-0.04 (-87%)
2004.02.03	144.1	-	-	-	-	-	-
2003.03.11	136.4	-	-	-	-	-	-

Table 6.40 – Variations in numerical stresses and estimated variations in rock mass vertical strains (percentages of recorded strains shown in brackets).

Aperture of horizontal discontinuities through which water flows

In dam block 17-18, recorded discharge increased around 8 times when the water in the reservoir increased from 115.45 m, recorded on 18 September 2002, to 143.6 m, recorded when the first borehole water-inflow tests were carried out in drain D25 D (from 0.23 l/min up to 1.93 l/min). Taking into account the cubic law and assuming that water flows through a single discontinuity, variation in a discontinuity's aperture is equal to the cubic root of discharge increase; therefore, due to the above-mentioned increase in reservoir level, discontinuity aperture doubles.

Numerical modelling of tests carried out in drain D25 D led to the conclusion that the horizontal layers of higher permeability upstream from the drain simulated horizontal discontinuities with a hydraulic aperture of 0.12 mm. In the global hydraulic foundation model, a similar layer in dam block 17-18 simulated a horizontal discontinuity with a hydraulic aperture of 0.06 mm. Taking these results into account and assuming that the discontinuity aperture doubles, a rough estimate is that aperture probably increases 0.10 mm, from 0.05 mm to 0.15 mm. In Model 3, differences in average vertical stresses for the various reservoir levels were used to determine variations in apertures of horizontal water conductive discontinuities below the heel of the dam. The following equations were used:

$$\Delta u_{yy} = \Delta \varepsilon_{yy} \cdot L \quad (6.11)$$

$$\Delta \varepsilon_{yy} = \frac{\Delta \sigma_{yy}}{E} \quad (6.12)$$

where Δu_{yy} is the variation in the discontinuity aperture due to increase in reservoir level, $\Delta \varepsilon_{yy}$ and $\Delta \sigma_{yy}$ are variations in vertical strains and stresses, respectively, L is the height of the blocks which simulate seepage paths and E is rock mass deformability modulus. Table 6.41 shows determined variations in the aperture of a horizontal water conductive discontinuity below dam block 17-18. Results obtained with the reservoir at an elevation of 115.45 m were used as reference.

Dam block	Reservoir level (m)	Average vertical stress σ_{yy} (MPa)	Stress variation $\Delta \sigma_{yy} = \sigma_{yy} (H) - \sigma_{yy} (115.45 \text{ m})$ (MPa)	Strain variation $\Delta \varepsilon_{yy} = \Delta \sigma_{yy} / E$	Variation in discontinuity aperture $\Delta u = \Delta \varepsilon_{yy} \times L$ (mm)
17-18	154.0	-0.0389	1.3569	1.3569×10^{-4}	0.41
	150.1	-0.1987	1.1971	1.1971×10^{-4}	0.36
	143.6	-0.4299	0.9659	0.9659×10^{-4}	0.29
	130.2	-0.9372	0.4586	0.4586×10^{-4}	0.14
	115.45	-1.3958	-	-	-

Table 6.41 – Variations in apertures of horizontal water conductive discontinuities below dam block 17-18 due to variations in average vertical stresses (numerical values).

Results presented in Table 6.41 are probably excessively high, as the variation in discontinuity aperture of 0.29 mm for the reservoir level of 143.6 m is greater than that expected taking recorded discharges into account. This may be due either to an excessive estimate of variations in vertical stresses, or to an inadequate rock mass deformability modulus. Concerning the latter, an average rock mass deformability modulus of 10 GPa was assumed in the green schist area, but the Young's modulus varies from one foundation area to another. Results presented in Table 6.41 for the reservoir at 143.6 m would lead to a variation of 0.10 mm in the discontinuity aperture if it were assumed that the area below the heel of block 17-18 was less deformable than the average, and a Young's modulus of 29 GPa were considered.

6.7.4 Hydromechanical interaction

6.7.4.1 Introduction

The hydromechanical interaction in the foundation of Alqueva dam was studied taking into account the results of both the hydraulic and mechanical models developed and carrying out independently uncoupled hydraulic and mechanical analyses. Firstly, the numerical hydraulic model was run for different reservoir levels and, for each level, the permeability of the horizontal layers which simulate water conductive joints was adjusted so that numerical discharges in the foundation of each dam block were close to recorded discharges. Secondly, the mechanical model was run assuming the same water levels, and average vertical stresses in the foundation blocks were obtained (blocks below the heel of the dam which, in the hydraulic model, simulate conductive joints). Finally, the above-mentioned results of both models allowed the plotting of graphs of stress versus permeability, from which a different correlation for some dam blocks could be established.

6.7.4.2 Correlation between stress and permeability

The mechanical model described in the previous section allows the calculation of stresses for different reservoir and tailwater levels and, as previously mentioned, does not take into account variations in ambient and reservoir temperature. Therefore, to establish the relation between stress and permeability, ensuring that discharges are mainly due to the effect of the hydrostatic loading, with small changes due to variations in dam temperature, only discharges recorded in February/beginning of March were taken into account in the subsequent analysis. Recorded discharges with the reservoir at low elevations were neglected, as it had been concluded that the hydraulic model could not be employed for the lower reservoir levels. Discharges monitored on six different dates were considered, with the reservoir level varying around 18 m, from 132.2 m up to 150.1 m.

Recorded discharges in the foundation of the dam blocks located in the valley bottom and at the base of each slope on the above-mentioned dates, shown in Figure 6.69, reveal that field data is not always consistent, as discharges do not always increase with the reservoir level. That is the case, for example, with discharges recorded on 2008.03.04, with the reservoir at 147.6 m, which, in dam blocks between joints 6 to 12, 13 to 15 and in block 17-18 were lower than those recorded on 13.02.2006, with the water 2.8 m lower. Around 20 % of the readings shown in Figure 6.69 were discarded due to inconsistency (21 readings out of 90). Discharges recorded in the foundation of the central cantilever (block 13-14) and those recorded with the three lower reservoir levels in blocks 10-11 and 20-21 also had to be neglected because numerical discharges obtained with the homogeneous model were higher than those recorded (in the homogeneous model an equivalent permeability of 1.0×10^{-8} m/s is assumed in the whole foundation and the grout curtain is assumed to be 10 times less pervious than the rock mass).

After running the numerical hydraulic model for the various reservoir levels, the permeability of the horizontal layers which simulate water conductive joints was adjusted so that numerical discharges in the foundation of each dam block were close to recorded discharges (Table 6.42). This adjustment was carried out taking into account that in a homogeneous rock mass discharges vary linearly with permeability.

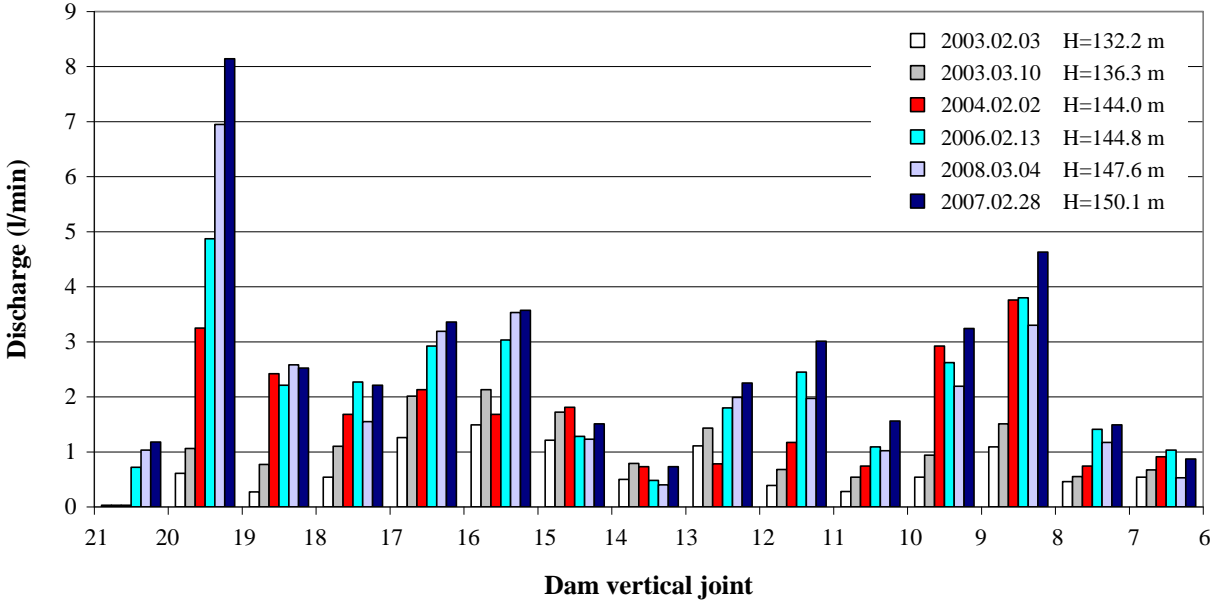


Figure 6.69 – Recorded discharges in the foundation of each dam block with the reservoir at different elevations.

Results presented in Table 6.42 reveal that in the foundation of one of the blocks, the permeability of a horizontal layer for a lower reservoir level can be higher than that for a higher level (e.g. block 8-9 and reservoir levels 144.8 m and 147.6 m). This is due to the fact that although the same model is used, boundary conditions vary. In some cases, an equivalent permeability lower than that of the rock mass (1.0×10^{-8} m/s) was calculated, which would mean that the horizontal layer which simulates water conductive joints was less pervious than the surrounding media. These results are not logical, and therefore were not taken into account. Figure 6.70 shows the variation in the permeability of the horizontal layers which simulate water conductive joints with the reservoir level of the blocks in which the number of points is equal or greater than 5. Exponential curves were adjusted to the values obtained, using regression analysis, and the R-squared values also displayed on the chart, varying from around 0.82 to 0.98, show that this type of curve fits the available data well.

The average vertical stresses at the heel of the five above-mentioned blocks obtained with the mechanical model are shown in Figure 6.71. Analysis of the results began with an attempt to establish a correlation between stress and permeability assuming that, in each block, the permeability of the horizontal layer was a function of the vertical stress only. However, the results obtained were not coherent and it was later understood that permeability depends not only on average vertical stresses but also on local geological features, which vary from one dam foundation block to another:

$$k = f(\sigma_{yy}, \text{geology of the foundation of each dam block})$$

Dam block	Equivalent permeability ($\times 10^{-7}$ m/s) for different reservoir levels					
	132.2 m	136.3 m	144.0 m	144.8 m	147.6 m	150.1 m
6-7	-	-	-	-	-	-
7-8	-	-	-	-	-	-
8-9	-	0.247	0.980	1.283	0.987	1.568
9-10	-	-	0.969	0.778	0.502	1.029
10-11	-	-	-	-	-	-
11-12	-	-	-	0.626	0.355	0.828
12-13	0.138	0.254	-	0.376	0.454	0.563
13-14	-	-	-	-	-	-
14-15	-	-	-	-	-	-
15-16	0.258	0.566	0.243	0.880	1.067	1.041
16-17	0.219	0.551	0.510	0.896	0.983	1.058
17-18	-	-	0.100	0.255	-	0.192
18-19	-	-	0.463	0.368	0.477	0.424
19-20	0.196	0.580	2.362	3.704	5.262	5.993
20-21	-	-	-	-	-	-

Table 6.42 – Equivalent permeability of the horizontal layers which simulate water conductive joints for different reservoir levels.

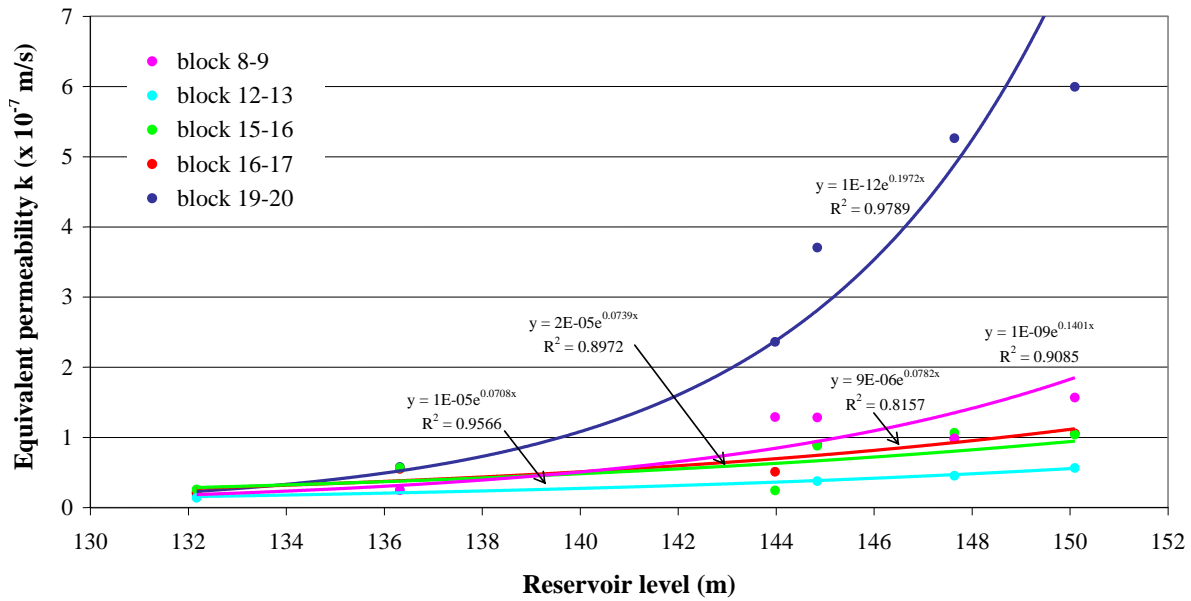


Figure 6.70 – Variation in the permeability of the horizontal layers which simulate water conductive joints with the reservoir level.

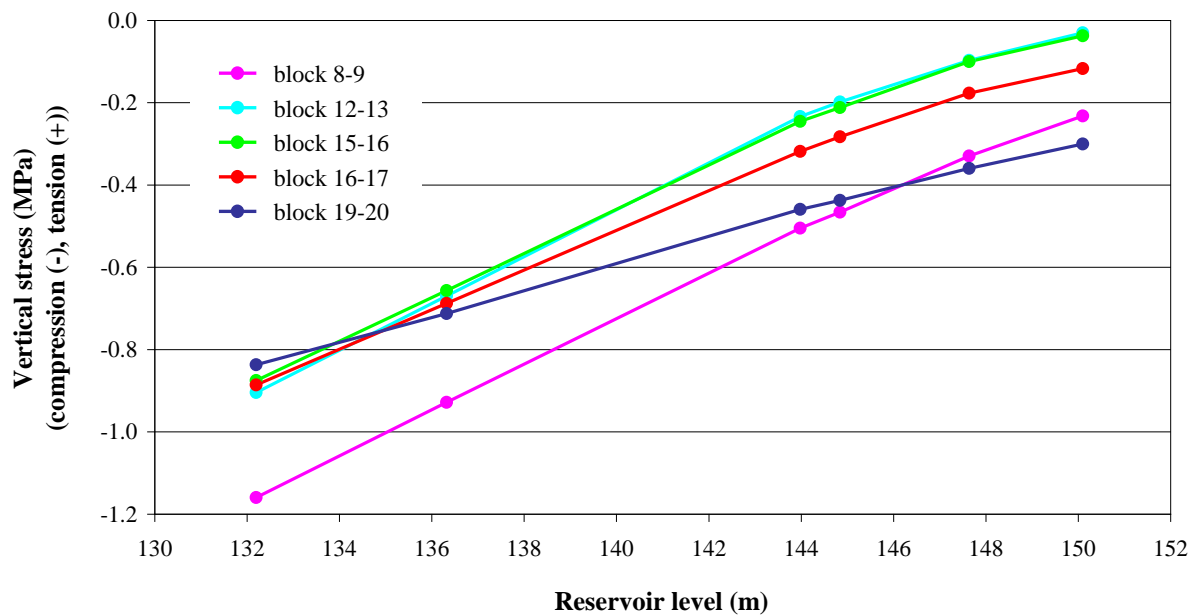


Figure 6.71 - Variations in average vertical stresses in the foundation blocks below the heel of the dam with changes in reservoir level.

Therefore, to establish a correlation between stress and permeability taking into account the influence of local geology it was necessary to choose a reservoir level as a reference and to plot graphs, for each dam block, of $(\sigma_{yy} / \sigma_{yy \text{ ref}})$ versus (k / k_{ref}) . When a water level is chosen as a reference and regression analysis is used to adjust curves to the values obtained, more weight is given to the permeability and stress obtained with that level. In order not to give more weight neither for the higher levels nor for the lower, monitored discharges on

2006.02.13 and stresses obtained with the reservoir at 144.8 m were used as reference. Figure 6.72 shows the variation of the permeability of the horizontal layers which simulate conductive joints below the heel of different dam blocks with vertical stress. Both exponential and logarithmic curves were adjusted to each block's set of data. In order to improve the adjustment of the curves, two pairs of values were neglected: block 8-9, with the reservoir at 147.6 m, and block 15-16, with the reservoir at 144.0 m. Figure analysis leads to the conclusion that, although there is not a significant difference between the curves, exponential laws fit data better.

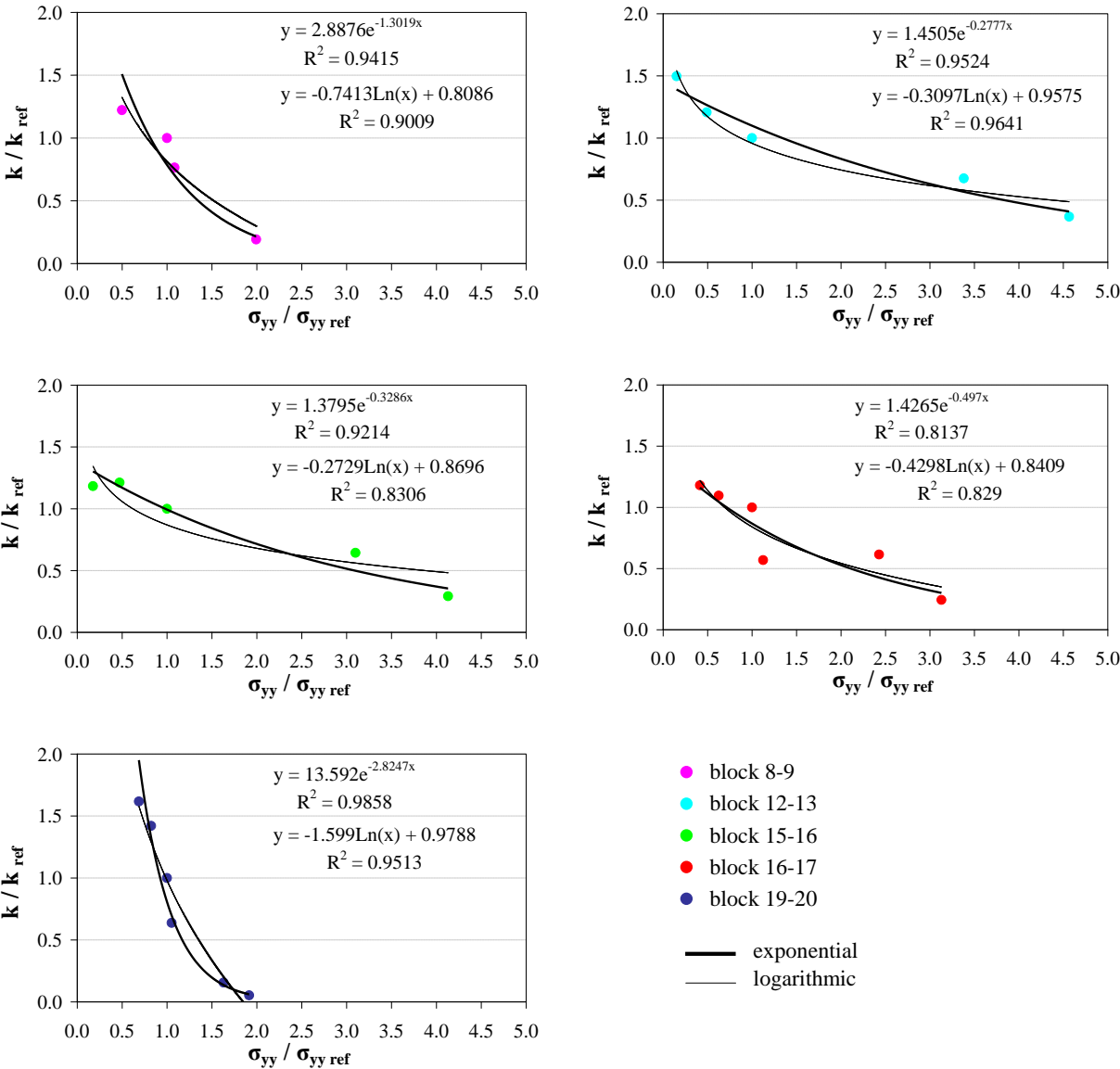


Figure 6.72 – Variation of the permeability of the horizontal layers which simulate conductive joints below the heel of different dam blocks with vertical stress. Adjustment of exponential and logarithmic curves.

Figure 6.73 shows the data obtained and the exponential curves for the five dam blocks together. The conclusion was drawn that variations in vertical stresses have less influence on permeability in the more pervious layers in the foundation of blocks 12-13, 16-17 and 17-18, and a large effect in blocks 8-9 and 19-20. For the highest water levels, compression stresses are very low, as shown in Figure 6.71, therefore the points obtained for the lower values of $(\sigma_{yy} / \sigma_{yy \text{ ref}})$ are more scattered.

The number of recorded discharges analysed, on six different dates with the reservoir at different elevations, only made it possible to establish the dependence of permeability on stress for the foundation of five dam blocks. If a greater amount of data had been analysed, more and perhaps better relationships could have been established.

The equivalent permeability values shown in Table 6.42 for the reservoir at 144.8 m, assumed as the reference level, were used to estimate the aperture of a hypothetical single discontinuity through which water flowed in the foundation of each block. These apertures are shown in Table 6.43 and were determined taking into account Darcy's law and the cubic law, according to which discharge varies with the cube of the aperture:

$$q = k_H i h \quad (6.13)$$

$$q = \frac{a^3 g}{12 \nu} i \quad (6.14)$$

where q = discharge per metre through a layer of height h ; k_H = hydraulic conductivity [$L T^{-1}$]; i = hydraulic gradient (head loss/length over which head loss occurs); a = fracture hydraulic aperture [L]; ν = kinematic viscosity of the fluid [$L^2 T^{-1}$]; and g = acceleration due to gravity [$L T^{-2}$]. Assuming that the variation in the aperture of a horizontal discontinuity with the average vertical stress is approximately linear, variations in the aperture of a single horizontal discontinuity were compared with the curves established for blocks 8-9 and 19-20 and are shown in Figure 6.74. It can be seen that for block 19-20 the discharges match quite well when it is assumed that water flows through a single discontinuity, whereas for block 8-9 there is a considerable difference indicating that water flows through more than one discontinuity.

Discharges in each dam block were afterwards determined using the established curves shown in Figure 6.73, and the numerical results were compared with recorded discharges. The charts in Figure 6.75 and Figure 6.76 show recorded discharges alongside both the results of the model calibrated for water levels on different dates, using the equivalent permeability values shown in Table 6.42, and those of the model in which the different curves σ - k established were used. Results obtained with both the above-mentioned models are accurate, but the latter has the advantage of using a generic law which is valid for the different water levels. In these

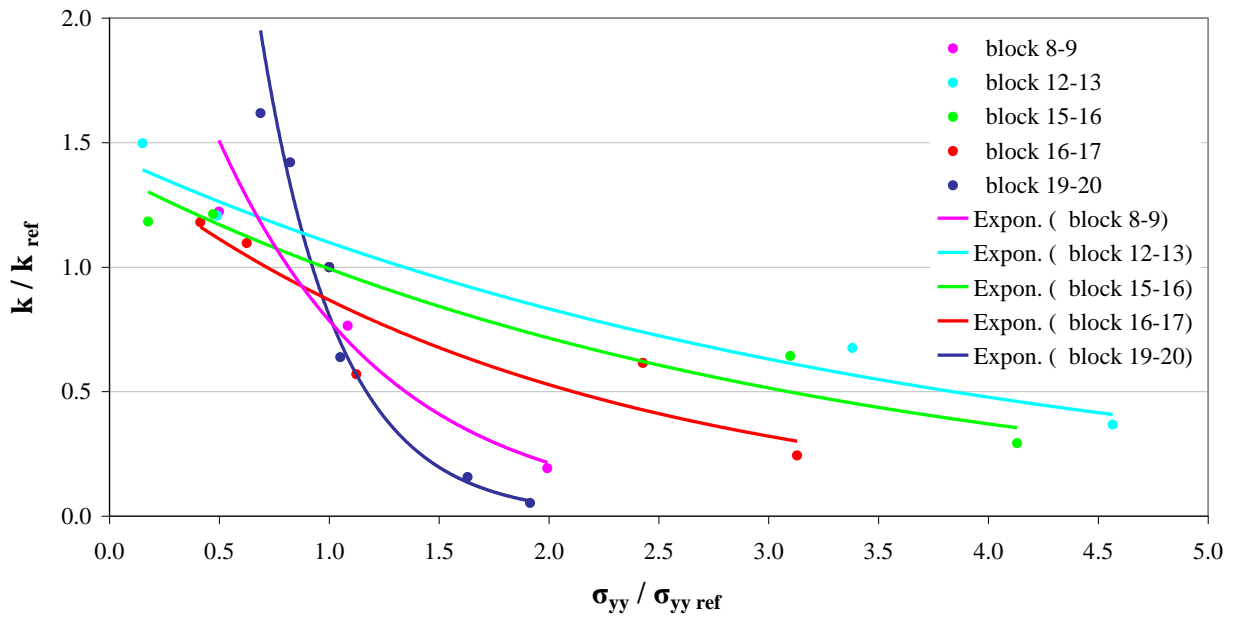


Figure 6.73 – Variation of the permeability of the horizontal layers which simulate conductive joints below the heel of different dam blocks with vertical stress.

Dam block	Area of the block in a direction perpendicular to that of the flow (m × m)	k_{ref} ($\times 10^{-7}$ m/s)	e^3 ($\times 10^{-13}$ mm ³)	e (mm)
8-9	$\approx 13.0 \times 3.0$	1.283	4.758	0.08
12-13	$\approx 15.0 \times 3.0$	0.376	1.395	0.05
15-16	$\approx 14.4 \times 3.0$	0.880	3.265	0.07
16-17	$\approx 12.7 \times 3.0$	0.896	3.326	0.07
19-20	$\approx 6.5 \times 3.7$	3.704	16.951	0.12

Table 6.43 – Hydraulic aperture of a single discontinuity which simulates the horizontal layers of higher permeability below the heel of different dam blocks with the reservoir at 144.8 m.

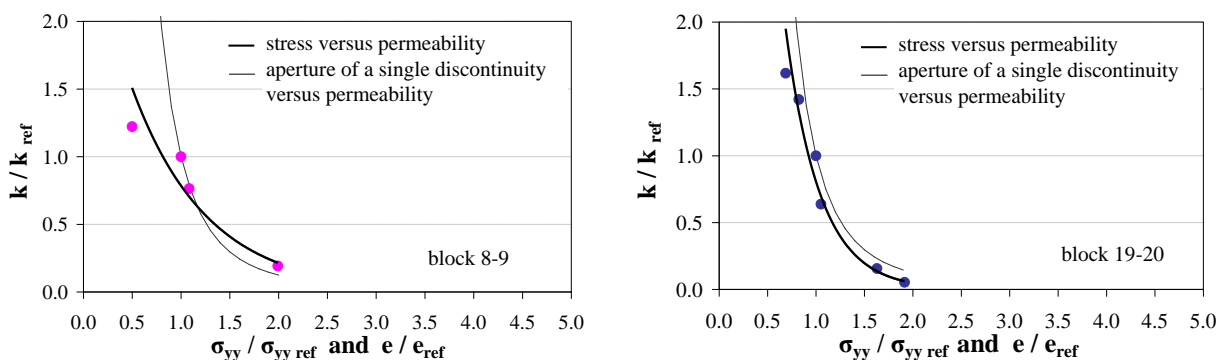


Figure 6.74 - Variation of the permeability of the horizontal layers which simulate conductive joints below the heel of block 8-9 and 19-20 with vertical stress and with the aperture of a single discontinuity.

figures, dam blocks in which the hydromechanical effect was considered are highlighted with an arrow. It must be noted that in each graph the white column shows model results which were forced to be as close as possible to the recorded discharges on each date.

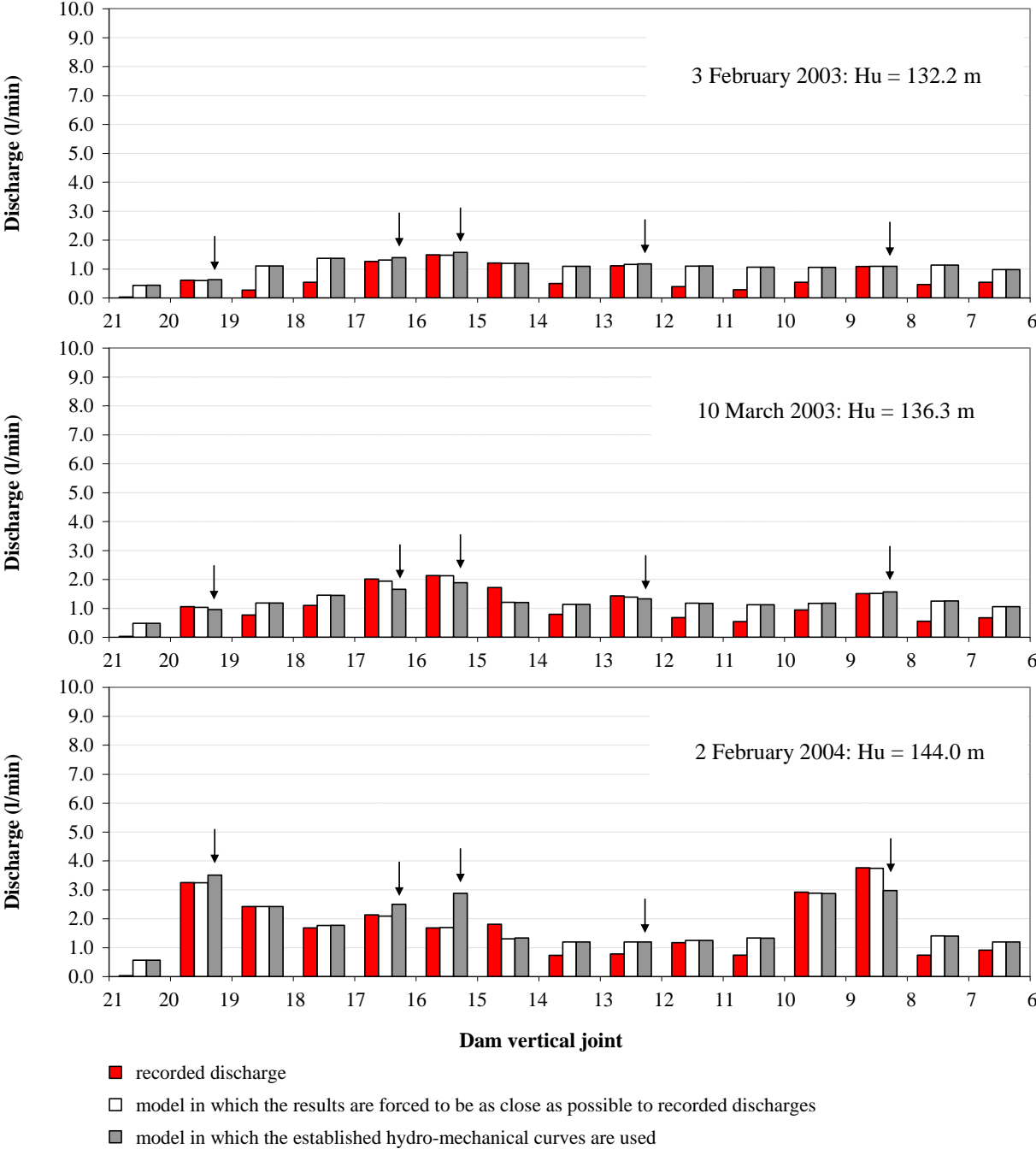


Figure 6.75 – Recorded discharges in the foundation of each dam block with different reservoir levels and comparison with the results of a model calibrated for water levels on the different dates and with those of the uncoupled hydromechanical model (arrows indicate dam blocks in which the hydromechanical effect was considered).

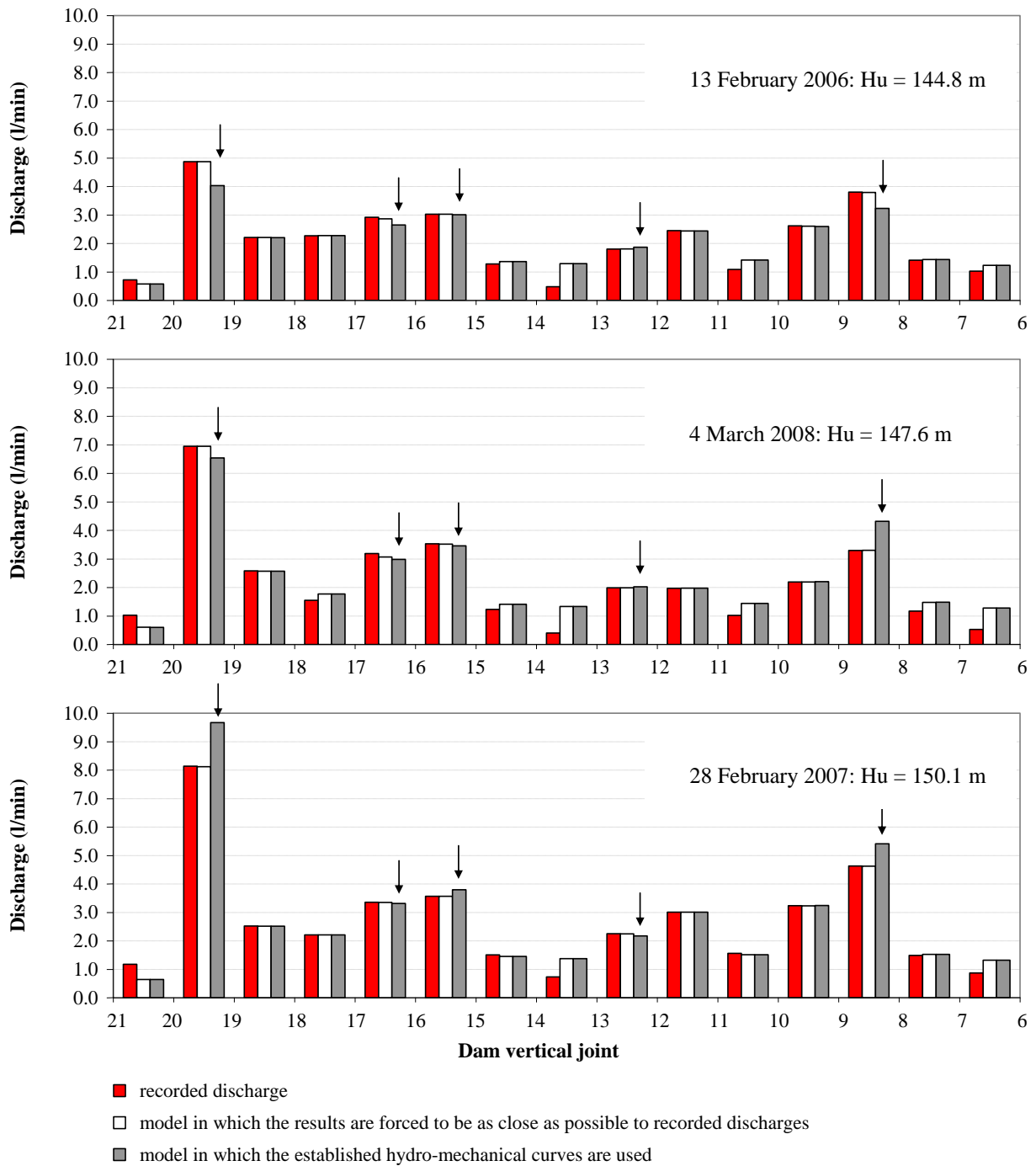


Figure 6.76 – Recorded discharges in the foundation of each dam block with different reservoir levels and comparison with the results of a model calibrated for water levels on the different dates and with those of the uncoupled hydromechanical model (arrows indicate dam blocks in which the hydromechanical effect was considered).

6.7.4.3 Correlation between permeability and local rock mass deformability

According to most authors it is more correct to relate permeability with strain than with stress, in an equivalent continuum, as the aperture of discontinuities with a very high normal stiffness barely changes with variations in stresses (Brown and Bray 1982; Chen et al. 2007; Wei and Hudson 1990).

In the previous section, curves which represent the dependence of permeability on stress were established. These curves follow the pattern:

$$k_{horizontal} = k_0 e^{-\alpha \sigma_{vertical}} \quad (6.15)$$

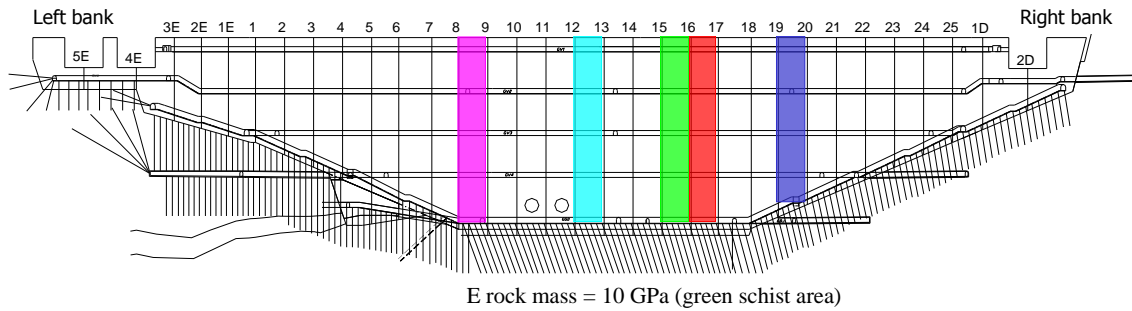
Taking into account that stresses in the vertical direction are given by $\sigma_{vertical} = E \varepsilon_{vertical}$, the stress can be replaced by the strain, and Equation 6.15 can be written in the following way:

$$k_{horizontal} = k_0 e^{-\alpha E \varepsilon_{vertical}} = k_0 e^{-\beta \varepsilon_{vertical}} \quad (6.16)$$

In the previous equation, $\beta = \alpha E$. Assuming that the average value of β , $\bar{\beta}$, is given by $\bar{\beta} = \bar{\alpha} \bar{E}$ and that the rock mass is the same in every foundation block, with an average Young's modulus of 10 GPa (assumed in the mechanical model in the green schist area), the different curves shown in Figure 6.73 can be due to differences in the horizontal layer's deformability. In dam blocks 8-9 and 19-20, the curves are steeper, therefore the horizontal layers of higher permeability are probably in more deformable rock mass areas, with a Young's modulus lower than that assumed. On the contrary, the curves established for dam blocks 12-13, 15-16 and 16-17, which are less steep, probably correspond to rock mass areas with a higher Young's modulus. The foundation of dam block 8-9 is probably more deformable because it is located close to the area where the green schist meets the phyllite. The greater deformability of the foundation of block 19-20 may be explained by the fact that it is crossed by 4 faults, as shown in Figure 4.11, which were not treated (faults 8, 9, 10 and 11).

The arithmetic mean of the different α determined in the curves established for the five different dam blocks is 1.05, therefore $\bar{\beta} = 10.5$. Figure 6.77 shows the estimated Young's modulus of each layer, determined by:

$$E_i = \frac{\bar{\beta}}{\alpha_i} \quad i = 1 \text{ to } 5$$



Dam block	α	Estimated Young's modulus of the rock mass in the foundation of each dam block (GPa)
8-9	1.302	8.03
12-13	0.278	37.67
15-16	0.329	31.83
16-17	0.497	21.05
19-20	2.825	3.70

Figure 6.77 – Estimated Young's modulus in the foundation of different dam blocks based on the stress-permeability curves.

Taking the highest Young's modulus as a reference (block 12-13), analysis of Figure 6.77 leads to the conclusion that the layer in the foundation of block 15-16 is 1.2 times more deformable, that in block 16-17 is 1.8 times more deformable, that in block 8-9 is 4.7 times more deformable, and that in block 19-20 is 10.2 times more deformable. These results are consistent with what is known about the local geology.

The modulus of deformation of the rock mass is given by:

$$\frac{1}{E_{RM}} = \frac{1}{E_R} + \frac{1}{k_n s} \quad (6.17)$$

where E_R is the modulus of deformation of the rock matrix, k_n is the fracture normal stiffness, and s is fracture spacing. Therefore, when the normal stiffness is very high, the dominant term is $1/E_R$, and when normal stiffness is low, the dominant term is $1/(k_n s)$. It is concluded that, in a discontinuum model high normal stiffness values should be considered in discontinuities located in the area of the more pervious layers in blocks 12-13, 15-16 and 16-17, and low values in blocks 8-9 and 19-20.

6.7.4.4 Discussion

The study presented in this section was carried out assuming various hypotheses and simplifications which are justified in the following paragraphs.

Numerical analysis was carried out assuming that both dam concrete and rock mass behave in an elastic linear manner. This constitutive model can be used for dam concrete as the study is carried out for moderate loads, corresponding to normal dam operation, which do not lead to non-elastic behaviour. In the rock mass, the behaviour is not linear whenever joints open. The rock mass was assumed to be isotropic, both from a mechanical and hydraulic point of view. However, schist is anisotropic, but there is no data available to characterize the anisotropy.

Numerical mechanical analysis led to the conclusion that, for the highest reservoir level, the normal displacement of the grout curtain/rock mass interface is about 1.5 to 2.5 mm in the upper 3 m. In hydraulic analysis carried out in previous chapters, using both detailed and global models, permeability of the area of higher permeability upstream from the dam simulates a vertical discontinuity with a hydraulic aperture of only 0.18 mm. However, as parameter studies have led to the conclusion that changing the assumed hydraulic conductivity of this area has limited effect, as long as it is much greater than that of the rock mass, no change in the hydraulic model is required.

Comparison of recorded and numerical results here presented aims to show that the geomechanical model developed is quite realistic, simulating the actual dam/foundation behaviour reasonably well. A comprehensive study, however, would have to include comparison of results obtained at a larger number of points.

The horizontal displacement at the crest of the central cantilever due to hydrostatic loading was compared against results of quantitative interpretation studies. However, numerical foundation joint apertures and strains in the foundation rock mass were compared taking into account dam monitoring results, which are dependent not only on variations in reservoir level but also on variations in ambient temperature, acting simultaneously. More accurate comparisons could have been achieved if quantitative interpretation studies had been carried out in order to separate and identify each one of the loads' contributions to the observed effects. Due to the large size of foundation blocks below the dam arch, only a rough comparison of recorded and numerical strains in the foundation could be made. However, strains of the same order as those recorded were determined.

In the mechanical model, hydrostatic loading was only applied to the upstream face of the dam. In order to obtain total stresses, it should have been applied not only to the upstream face of the dam but also to the base of the reservoir and on the open area of the grout curtain/foundation interface (it should not be applied on the open area of the foundation joint because the foundation joint is sealed). These two simplifications have little effect on vertical stresses close to the base of the dam, which is what really controls seepage. An alternative model, probably more correct, would be to use effective stresses, and in this case the water pressures would have to be taken into account in the mechanical analysis. In this study,

conclusions were drawn from relative values and therefore are not affected by the above-mentioned simplification.

Study of the hydromechanical interaction required a careful selection of recorded discharges, in order to use only coherent data. Incoherent field data is due to the fact that discharges depend not only on discontinuities' aperture but also on seepage paths, which may vary with changes in the reservoir level or ambient temperature. When these changes occur, a portion of the water that flows into the foundation of one of the dam blocks can change its path and flow into the foundation of adjacent blocks, as a result of the opening and closure of discontinuities.

The dependency of permeability on local geological features, in addition to dependency on stress level, makes it very difficult or even impossible, to have a single σ -k law.

6.7.4.5 Summary and conclusions

This section presents a methodology which can be used to establish rules which, from a hydraulic model calibrated for a specific water level in the reservoir, allow the calculation of discharges for both higher and lower reservoir levels, taking into account that permeability depends not only on the stress level but also on local geological features. This simple methodology, which uses an uncoupled mechanical-hydraulic analysis, has been applied successfully in the analysis of recorded discharges in the foundation of some blocks of Alqueva dam.

Equivalent continuum models were used to carry out both hydraulic and mechanical analysis. The simplified global hydraulic model of the dam foundation takes into account the results of borehole water-inflow tests and conclusions drawn from detailed 3D models of the area around the tests. The main seepage paths were simulated by regions of different permeability. The mechanical model here presented allows taking into account the non-linear behaviour of both dam joints and interfaces (in this case, foundation joint and grout curtain/rock interface). Two areas of different deformability were considered, simulating both the green schist and the phyllite regions.

Due to the influence of local geology, different rules relating stress and permeability were established for different foundation areas. There is not a single law representative of the whole foundation. Exponential laws were found to fit the considered data well, and these laws allow the calculation of discharges for both higher and lower reservoir levels. However, it must be borne in mind that this is only valid within the range of the considered water levels. In the foundation of one of the dam blocks it could be concluded that flow is mainly controlled by a single discontinuity. More accurate relations could have been obtained if a

larger amount of reliable data was available. The simplicity of the method presented here makes it very useful in the safety assessment of concrete dams.

The main advantage of carrying out uncoupled hydromechanical analysis is that model calibration is easier. Coupled analysis is much more complex and it requires different laws to be attributed to the foundation of each dam block. The study was carried out with equivalent continuum models, an alternative to which would be to use discontinuum models. This, however, would present significant difficulties due to lack of data. In fact, both the position and aperture of discontinuities are unknown and, in addition, water flows only through some of the discontinuities. The 3D nature of the analysis makes it even more difficult. The issue of hydromechanical analysis using discontinuum models with a view to evaluating dam stability will be addressed in the following chapter.

6.8 Piezometric measurements in concrete dam foundations

6.8.1 Introduction

Piezometers in concrete dam foundations have a twofold aim: the first is to evaluate the drainage efficiency in the reduction of uplift pressures, and the second is to measure water pressures close to the dam/rock mass interface or in discontinuities within the foundation along which sliding may occur. Drainage efficiency is evaluated by using piezometers installed upstream and downstream from the drainage curtain, to monitor the head difference. Uplift pressures and pressures in discontinuities, which have a destabilizing effect, should be measured using small intake areas (Post 1985). However, the majority of the piezometers installed in the foundations of Portuguese concrete dams are boreholes drilled in the rock mass, with a pipe at the head, fitted with a pressure gauge, and have a long single chamber. In fact, there are only six Portuguese concrete dams where multilevel piezometers or piezometers with a small intake area were installed:

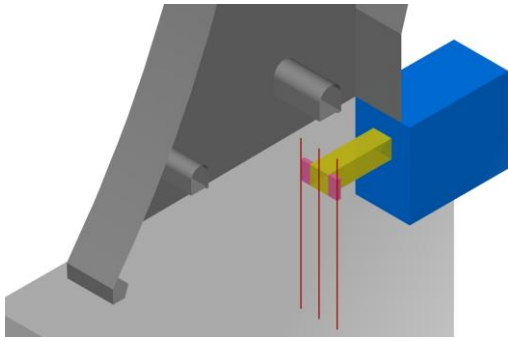
- In Funcho dam, a 49 m high arch dam (of which the main characteristics are briefly described in sections 2.5.3 and 4.2.5.3), two multilevel piezometers were installed, one with two and the other with three different chambers. The foundation consists of schist and greywacke. The results of borehole water-inflow tests, which led to a detailed knowledge of the main seepage paths, were used to decide where to locate the chambers (LNEC 1998b).
- In Penha Garcia dam, a 25 m high gravity dam located on the River Ponsul, in the Castelo Branco district, with a foundation of quartzite, piezometers were installed in 8 boreholes at two levels. However, the work was not properly done and chambers were not isolated from each other, the same water head being recorded in both chambers in each of the boreholes.
- In the stilling basins of both Coimbra and Crestuma dams, several multilevel piezometers were installed. These are barrages (gate-structure dams) located on the River Mondego, in the city of Coimbra, and on the River Douro, 13 km upstream from Porto, respectively. In Coimbra dam there are 20 piezometers in two cross sections, which allow measurement of hydraulic heads at different levels, in the upstream-downstream direction. The gates and the stilling basins transmit the water load to flanking piers, which go as deep as 25 to 40 m, to bedrock of marl, crossing nearly 35 m of alluvium. In Crestuma dam foundation there are 20 boreholes, each of them equipped with three porous ceramic tubes 0.15 m long. Piezometric readings are taken in three cross sections. The piers cross 40 m of alluvium to a bedrock of schist. In both dams, piezometers are located within the alluvial strata (Pinto and Maranhã das Neves 1987).

- In Pedrógão dam stilling basin, as mentioned in chapter 4.3.2, there are four multilevel piezometers, each with two chambers, whose length varies from 1.5 m to 2.55 m. The location and length of each chamber was defined taking into account the boreholes' logs and the results of Lugeon type tests.
- In Alqueva dam, two piezometric chambers were installed in two boreholes in the downstream dam wall. Logs and hydraulic test results, as well as the results of the 2D model of a vertical cross section at the bottom of the valley presented in chapter 6.2 were used to decide the location and length of each chamber (LNEC 2005b).

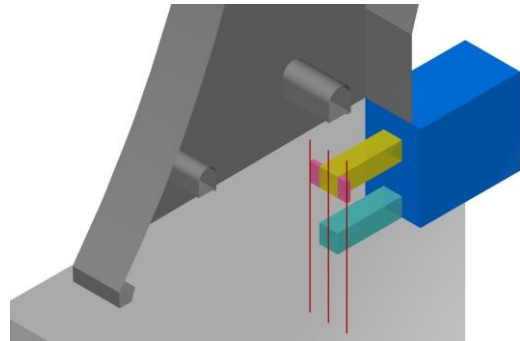
As previously mentioned, in chapter 3.3, piezometers accessible to water over their whole length take very rough measurements and give only general data which is of limited use (Londe 1973b) and are not recommended by the ICOLD (2005), as the water pressure measured at the pressure gauge is the result of the inflow and outflow of water from different strata or discontinuities which have different hydraulic heads. A numerical study was carried out to evaluate the extent to which the water pressures that have been recorded in the numerous piezometers located in the foundation of our large concrete dams can be misleading.

The study was carried out using the dimensions of Alqueva dam as reference, with a three-dimensional model based on the model referred to in chapter 6.3, and includes only three boreholes: a piezometer, to which water flows not only through horizontal layers of higher permeability between the upstream area and the piezometer, but also through the rock mass, and two adjacent drains. It was first thought that the study could be carried out with an axisymmetric model with the axis of symmetry along the axis of the piezometer. However, this idea was abandoned, as an axisymmetric model would not take into account the fact that seepage takes place in the upstream-downstream direction. The study was progressively developed using very simple models and comparing the hydraulic head at the piezometer with a long single chamber to the hydraulic heads calculated in more than one chamber. Five different possible situations were analysed, sketched in Figure 6.78:

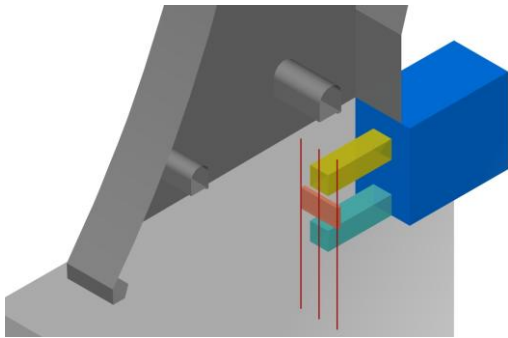
1. impervious rock mass and a single layer of higher permeability upstream from the piezometer, linked to the adjacent drains;
2. either impervious or pervious rock mass and two independent layers of higher permeability upstream from the piezometer, with the upper one linked to the adjacent drains;
3. impervious rock mass, two horizontal layers of higher permeability upstream from the piezometer and a link between the piezometer and the adjacent drains at an elevation different from those of the horizontal layers;



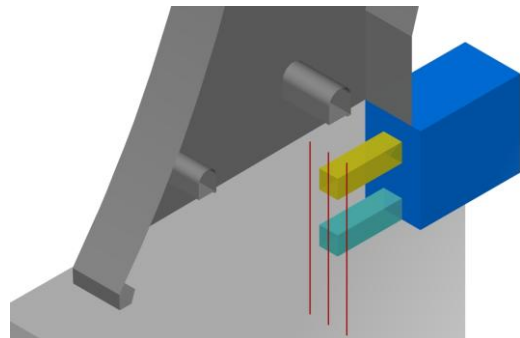
Situation 1



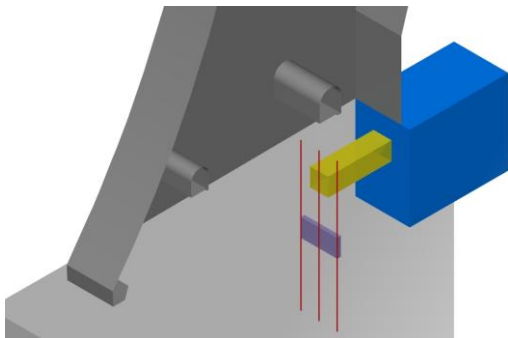
Situation 2



Situation 3



Situation 4



Situation 5

		k ($\times 10^{-7}$ m/s)	Link between the piezometer and the drains:	k ($\times 10^{-7}$ m/s)
Rock mass	■	0.0, 0.1 to 3.0		
Near-surface area upstream from the dam where the reservoir head is assumed	■	-	- at the same level as the upper layer	■ varied
Upper layer of higher permeability	■	varied	- at the same level as the lower layer	■ varied
Lower layer of higher permeability	■	varied	- midway between the lower and upper layers	■ varied

Figure 6.78 – Seepage models in the five different situations.

4. two layers of higher permeability upstream from the piezometer linked by a pervious rock mass;
5. rock mass with a low permeability, a single layer of higher permeability upstream from the piezometer and a link between the piezometer and the adjacent drains at a lower elevation.

In this study, an impervious rock mass simulates a medium with a very low permeability, when compared to that of the pervious layers. The horizontal layers of higher permeability and the links between the piezometer and the adjacent drains simulate discontinuities through which water flows. To obtain a quantitative understanding of the effect of different relative permeability values on the readings at the pressure gauge, numerical water pressures along the borehole and at the borehole head were determined and compared, for different permeability values in each situation. Discharges were also quantified and analysed.

6.8.2 Model description

The model used in this study is, as previously mentioned, based on the model referred to in chapter 6.3.1, formed by a series of adjacent vertical strips. However, the existence of the grout curtain was neglected, and therefore a simpler block division was used below the upstream area of the dam base, between the heel of the dam and the drainage curtain. As in the numerical analysis of borehole water-inflow tests, presented in chapter 6.4, the model includes only three boreholes, the one in the middle being the piezometer. Due to symmetry, seepage needs only to be analysed in an area of the foundation with a width corresponding to one and a half times the distance between boreholes, thus being only 4.5 m thick. Both the piezometer and the adjacent drain are modelled by their axis (diameter zero). The piezometer and the drain, both vertical, are assumed to be 25 m long, and are located 10.5 m downstream from the upstream face of the dam. It is assumed that the piezometer and the drain are aligned in a direction perpendicular to the valley axis. Although piezometers are usually located downstream from the drainage curtain with a length of about two thirds of that of the drains, this assumption does not affect the validity of the study.

Horizontal cuts were made upstream from the piezometer and drain, in order to assume the existence of horizontal layers of higher permeability, which simulate discontinuities through which water flows. These layers are 3.0 m high and are located 3.0 to 6.0 m and 11.0 to 14.0 m below the upper edge of the model. Vertical cuts in the upstream-downstream direction in the above-mentioned horizontal layers were afterwards made, halfway between boreholes, so as to assume that the main layers of higher permeability are only upstream from the piezometer.

Blocks located upstream from the heel of the dam, down to a depth of 14 m were deleted, so that the same hydraulic head could be assumed at the upstream face of the horizontal layers. This simulates the existence of vertical fissures that come from the heel of the dam, where the reservoir head is applied. The model, with about $230.0 \times 78.0 \times 4.5 \text{ m}^3$ is divided into 76 blocks, internally divided into 58085 tetrahedra, with a total of 19773 grid points (Figure 6.79). The mesh is finer close to both the drain and the piezometer and defined by the average edge length of the tetrahedral zones: 0.60 m in blocks adjacent to the piezometer and drain; 0.90 m in blocks in the vicinity of the above-mentioned blocks; 2.0 m in blocks located around the area of interest and 3.0 m in the remaining blocks.

Figure 6.80 shows the position of the horizontal layers of higher permeability through which water flows from the upstream area towards the piezometer, as well as the links between these layers and the adjacent drain. The cross section of the more pervious layers upstream from the piezometer in a direction perpendicular to that of the flow is $3.0 \times 3.0 \text{ m}^2$, and that of the layers linking the piezometer to the adjacent drains is $0.6 \times 3.0 \text{ m}^2$. Each of the following areas were considered as a different model region: rock mass, upper layer of higher permeability, lower layer, the blocks linking the upper layer to the adjacent drain, and the blocks linking the piezometer to the adjacent drain, considered in situations 3 and 5. In this way, the permeability of each area could be easily changed. The pervious rock mass foundation considered in situations 2, 3 and 5 was assumed to be homogeneous and isotropic with a permeability that varied from $0.1 \times 10^{-7} \text{ m/s}$ to $3.0 \times 10^{-7} \text{ m/s}$.

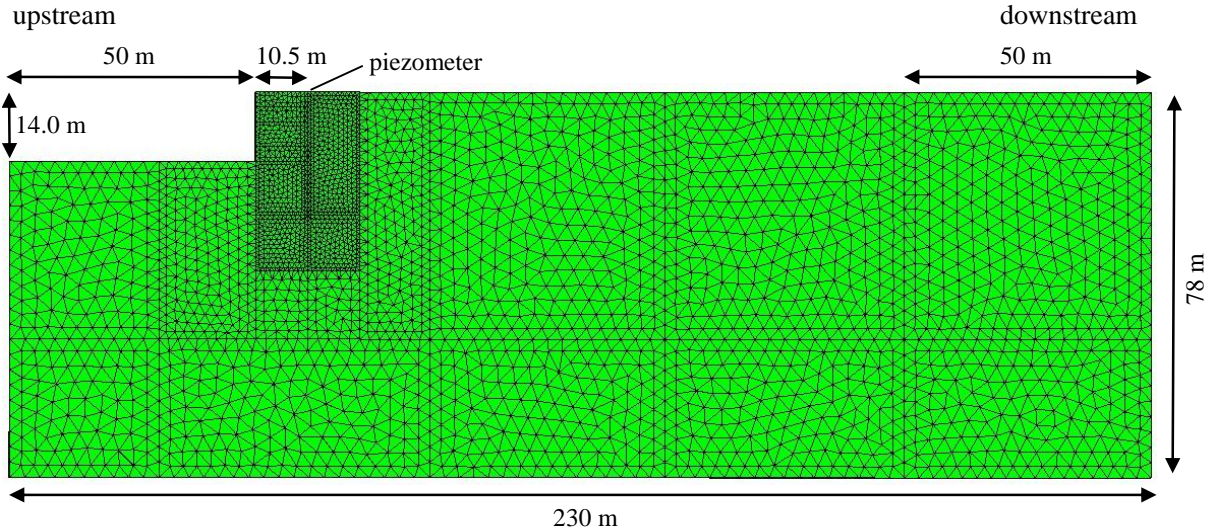


Figure 6.79 – Lateral face of the simplified 3D model of the foundation of Alqueva dam. Division into blocks and internal mesh.

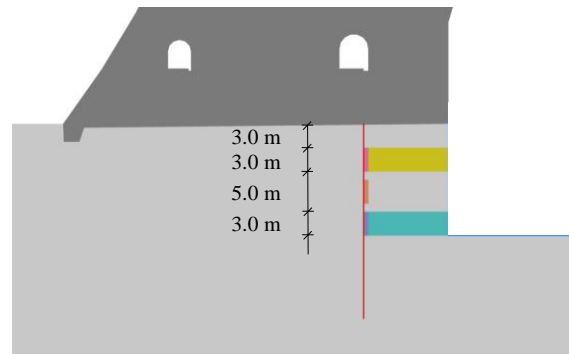


Figure 6.80 – Relative position of the horizontal layers of higher permeability upstream from the piezometer.

6.8.3 Hydraulic boundary conditions

Numerical analysis was carried out assuming the reservoir at an elevation of 143.6 m and the water downstream from the dam at an elevation of 81.95 m. A zero pressure was assumed at the drain head, which corresponds to a hydraulic head of 61.0 m along the drain borehole. The hydraulic head is forced to be constant along each piezometric chamber's length.

6.8.4 Results analysis

In each of the previously mentioned situations, numerical analysis was done in two phases:

- phase 1: it was assumed that the piezometer was open, i.e. working as a drain, and the total discharge was obtained;
- phase 2: it was assumed that the borehole towards which water flows from upstream was closed and both the hydraulic head at the piezometer and the discharge at the adjacent drains were analysed.

In a rock mass of non-uniform permeability, the hydraulic head at the piezometer depends not only on the hydraulic boundary conditions but also on the relative permeability values of the different model areas. Leakage and seepage velocity, however, depend on the absolute values of the different permeabilities (Londe 1973c). In the model presented here, the areas are: the rock mass, the upper and lower layers of higher hydraulic conductivity, and the layers linking the piezometer to the adjacent drains.

6.8.4.1 Analysis of discharges and hydraulic heads

Results of the five situations are presented and analysed below. In order to show the results independent of the assumed hydraulic boundary conditions and permeability values, graphs of percentage of hydraulic head versus relative permeability values are presented.

Situation 1:

The simple case of seepage towards a single borehole through a horizontal confined pervious layer, which is linked to both the adjacent drains, was analysed first. The rock mass was assumed to be impervious and a hydraulic conductivity of 5.0×10^{-7} m/s was assumed at the pervious layer. The permeability of the link between the piezometer and the adjacent drain was varied in such a way that the relative permeability of the link and that of the layer was zero, 0.04, 0.2, 0.4, 0.8, 1.0, 2.0 and 4.0. It was taken into account that, as the cross section of the link is smaller than that of the pervious layer upstream from the piezometer, a link permeability of 25×10^{-7} m/s is required for it to be as pervious as the main layer. Taking into account the cubic law (Snow 1965), the layer of higher permeability simulates a rock discontinuity with a hydraulic aperture of 0.12 mm. The hydraulic aperture of the link between the piezometer and the adjacent drains depends on the link's assumed permeability. Figure 6.81 shows the variation in boreholes' discharges in both phases of analysis and the variation in percentage of hydraulic head at the piezometer, in the second phase of analysis.

Naturally, in phase 1, central drain discharges decrease and there is an increase in adjacent drains' discharge due to increase in the link's permeability. With the previously mentioned boundary conditions, when the link is as pervious as the main layer, the central drain discharge is about half of that when there is no link between the central borehole and the adjacent drains.

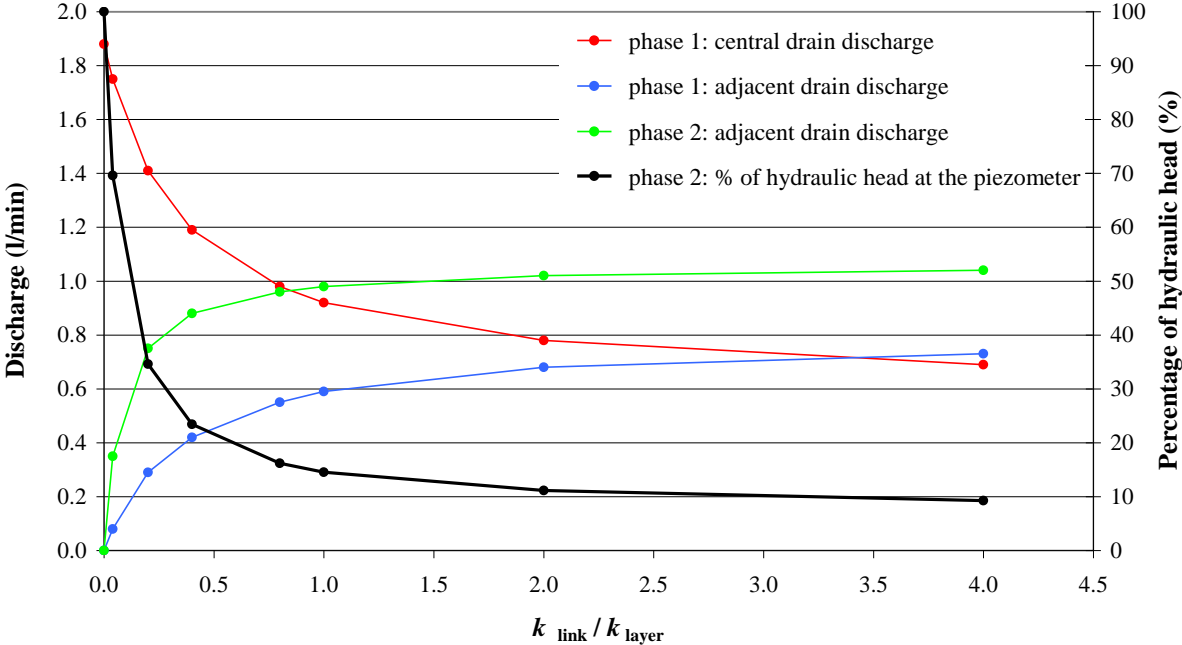


Figure 6.81 – Situation 1: variations in boreholes' discharges and in percentage of hydraulic head at the piezometer for different relative permeability values.

In the second phase of analysis, with the central borehole (piezometer) closed, the reservoir head is obtained at the piezometer when the main layer is not linked to the adjacent drains. However, a link with a very low hydraulic conductivity leads to a sudden loss of water pressure at the piezometer. When the link is as pervious as the main layer, the water pressure at the piezometer is 14.5 % of the hydraulic head. Increasing the link permeability to permeabilities higher than that of the main layer does not significantly alter either the water pressure at the piezometer or the discharge at the adjacent drains.

Figure 6.82 shows the hydraulic head contours in a cross-section through the middle of both the pervious layer and the link, together with block contours, assuming that the link is 5 times less pervious than the main layer (Figure 6.82 a) and as pervious as the main layer (Figure 6.82 b). Figure 6.83 shows the variations in hydraulic head along two perpendicular lines that cross the piezometer in the upstream-downstream direction and along the line of boreholes. The variation in hydraulic head in the upstream-downstream direction is linear except close to the line of boreholes. Along the line of boreholes, the maximum hydraulic head decreases as the link's permeability increases.

In the first phase of analysis, when it is assumed that there is no link between the piezometric borehole and the adjacent drains, a total discharge of $3.54 \times 10^{-5} \text{ m}^3/\text{s}$ (2.12 l/min) would flow out of a hypothetical continuous trench 3 m long with the same vertical length as the drains (Darcy's law):

$$q = k_H i A = 5.0 \times 10^{-7} \times \frac{143.6 - 61.0}{10.5} \times 3.0 \times 3.0 = 3.54 \times 10^{-5} \text{ m}^3/\text{s} \quad (6.18)$$

In a 3D model, this is simulated assuming the same hydraulic head at the line of the boreholes across 3 m of the model's thickness, 1.5 m each side of the central borehole. In the model presented here, in which the boreholes are simulated by their axis, and the same hydraulic head is assumed along the whole borehole's length, the numerical drain discharge is $3.14 \times 10^{-5} \text{ m}^3/\text{s}$ (1.88 l/min), which is 88.8 % of the above-mentioned result. The study presented in chapter 5.2.2, in which seepage in a concrete dam foundation is analysed using a two-dimensional horizontal model, led to the conclusion that the total discharge at a drainage curtain, with drains of diameter 0.076 m located 3.0 m apart, is 87 % of the total discharge at a hypothetical continuous trench with the same depth as the drains. The small difference between these percentages is due to the size of the zones around the drain. In fact, around both the drain and the piezometer the average edge length of the tetrahedral zones is 0.60 m, while, according to the results of both the 2D horizontal model and the 3D model of seepage through a horizontal layer presented in chapter 5, it should be around 0.30 m. Results are coherent, as larger zones lead to greater discharges.

In this first situation, as water flows into the piezometer through one or more discontinuities located in a confined area, simulated by the main pervious layer, the hydraulic pressure measured at the pressure gauge placed at the top of a long single chamber piezometer would be the same as that measured in a piezometer with a small intake crossed by the pervious area.

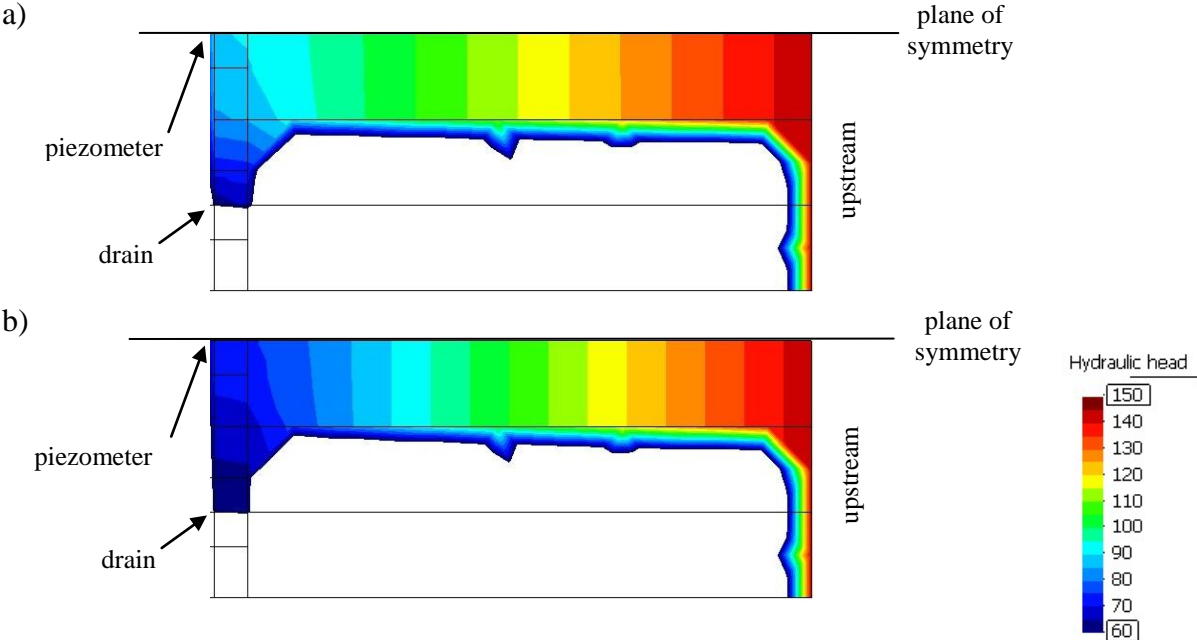


Figure 6.82 – Situation 1: hydraulic head contours with the link a) 5 times less pervious than the main layer and b) as pervious as the main layer. Horizontal cut through the middle of the pervious layers, in the upstream-downstream direction.

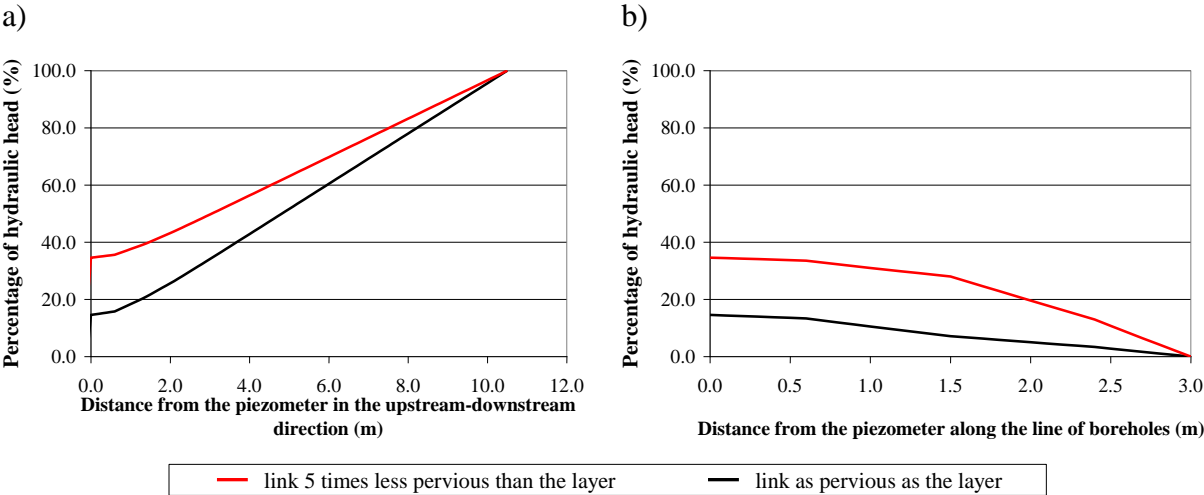


Figure 6.83 – Situation 1: variations in the piezometric head in the middle of the pervious layers along horizontal lines which cross the piezometer a) in the upstream-downstream direction and b) along the plane of the boreholes.

Situation 2:

The model described in situation 1 with the link between the piezometer and the drain as pervious as the main layer was taken as reference, and a new layer of higher permeability was considered at a lower depth. Figure 6.84 shows the variations in discharges and in percentage of hydraulic head at the piezometer for different permeability values of this layer. In phase 1, central drain discharge increases linearly and there is no change in adjacent drains' discharges due to increase in the permeability of the lower layer. When this layer is as pervious as the upper layer, the central drain discharge is about 3 times that when there is no lower layer. In phase 2, an increase in the lower layer's permeability leads to a slight increase in adjacent drains' discharge and to a large increase in the percentage of hydraulic head at the piezometer. In fact, taking the case when there is no lower layer as reference, adjacent drains' discharge increase around 2.8 times (from 0.98 l/min to 2.71 l/min) when the lower layer is 10 times more pervious than the upper layer, and the percentage of hydraulic head at the piezometer increases from 14.5 % to 78.6 %.

Variations in hydraulic head in the middle of the upper layer along two perpendicular lines that cross the piezometer in the upstream-downstream direction and along the line of boreholes are shown in Figure 6.85. The same figure shows the variation in hydraulic head in the middle of the lower layer, in the upstream-downstream direction. Results of two ratios between the permeability of both layers are presented: lower layer either 5 times less pervious or 10 times more pervious than the upper layer. The upper layer is linked to both the adjacent drains, therefore the loss of hydraulic head in this layer is always greater than that in the lower layer, as shown in Figure 6.85 a). The same figure shows that the loss of hydraulic head at the lower layer is smaller for higher permeabilities of this layer and, therefore, there is an increase in the hydraulic head at the piezometer with the increase in the lower layer's permeability. When the permeability of the lower layer is high compared to that of the upper layer, the hydraulic head at the upper layer suddenly increases close to the piezometer. Figure 6.85 b) shows the variation in hydraulic head along the line of boreholes, in the middle of both the upper layer and the link. Figure 6.86 shows the hydraulic head contours in horizontal cuts through the middle of the pervious layers.

In this second situation, if there were two piezometers in the piezometric borehole, each of them with a small intake area, one crossed by the upper layer and the other crossed by the lower one, the hydraulic head at the piezometer at a lower level would be the same as that of the reservoir, while in the upper piezometer the hydraulic head would be 73.0 m, which is 14.3 % of the reservoir head, as mentioned in the results analysis of situation 1. In a piezometer with a long single chamber, the percentage of hydraulic head varies from 14.3 % up to a maximum value which depends on the relative permeabilities of the link between the piezometer and adjacent boreholes, of both the lower and upper layers. Therefore, in this case,

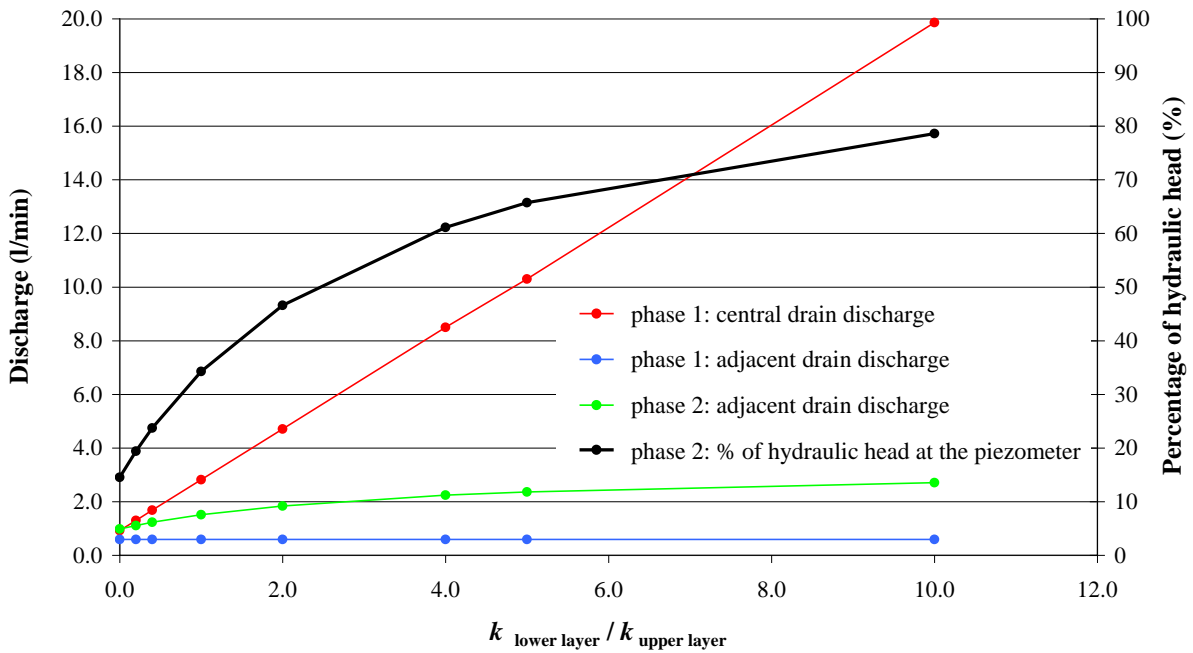


Figure 6.84 – Situation 2: variations in boreholes' discharges and in percentage of hydraulic head at the piezometer for different values of $k_{lower\ layer} / k_{upper\ layer}$, assuming an impervious rock mass.

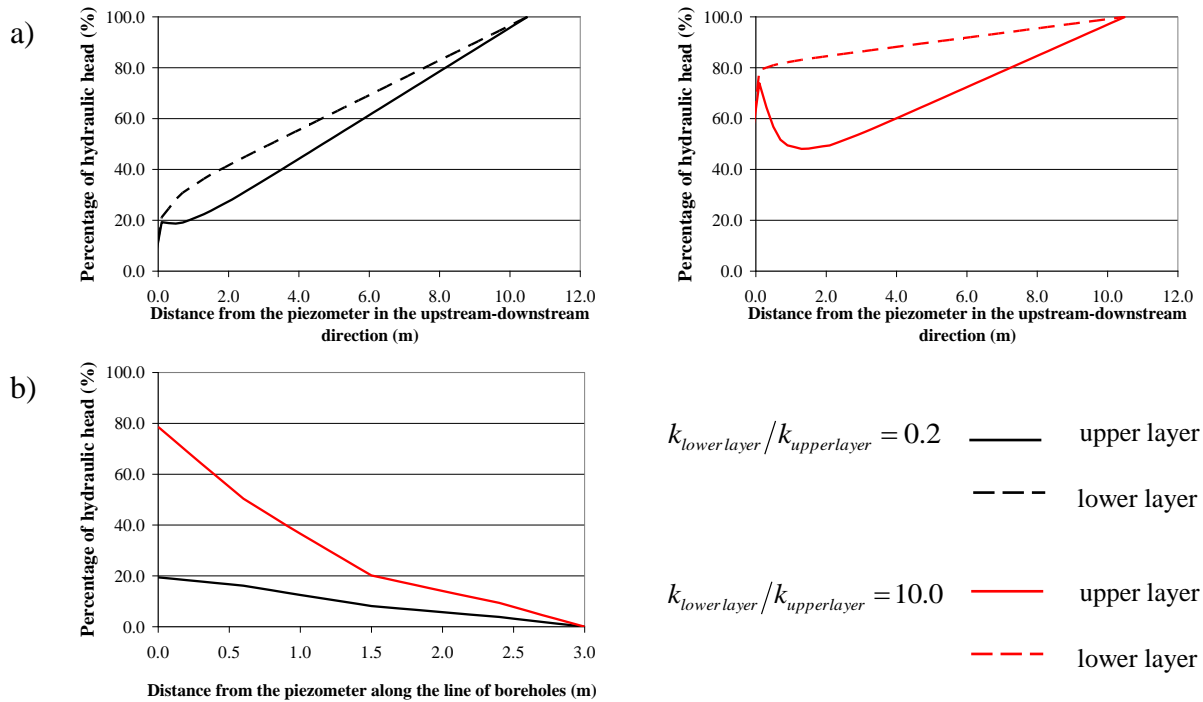
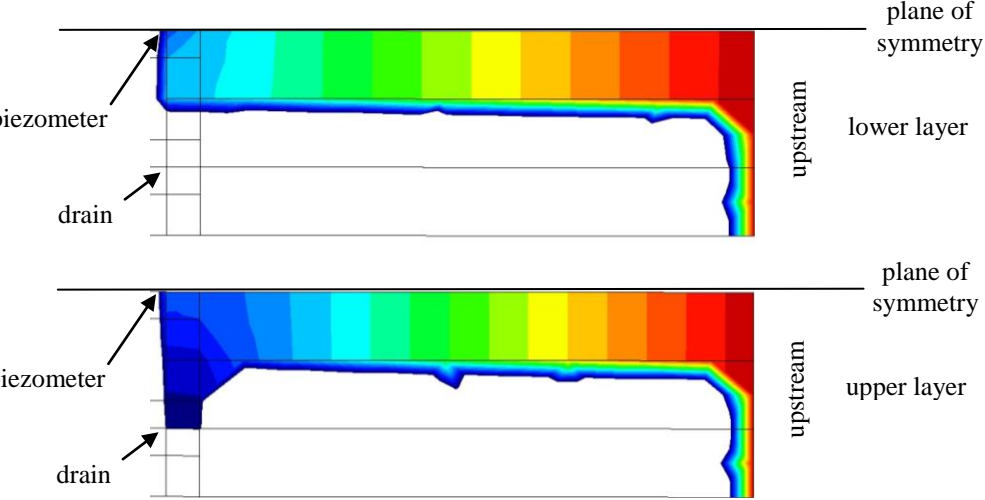


Figure 6.85 – Situation 2: variations in the piezometric head in the middle of the pervious layers along horizontal lines which cross the piezometer a) in the upstream-downstream direction and b) along the boreholes.

multilevel piezometers with the piezometric chambers suitably positioned would provide valuable information, as it would be possible to know that there were one or more discontinuities located at the lower level linked to the reservoir, with high hydraulic pressures. Figure 6.87 shows the variations in discharges and in percentage of hydraulic head at the piezometer for different permeability values of the lower layer, assuming that the rock mass is pervious, with 5.0×10^{-8} m/s of permeability. With a pervious rock mass, the quantity of water flowing into and out of the boreholes increases. Therefore, when compared to the results obtained with an impervious rock mass (Figure 6.84), discharges are greater and the hydraulic head at the piezometer is lower.

a) lower layer 5 times less pervious than the upper layer



b) lower layer 10 times more pervious than the upper layer

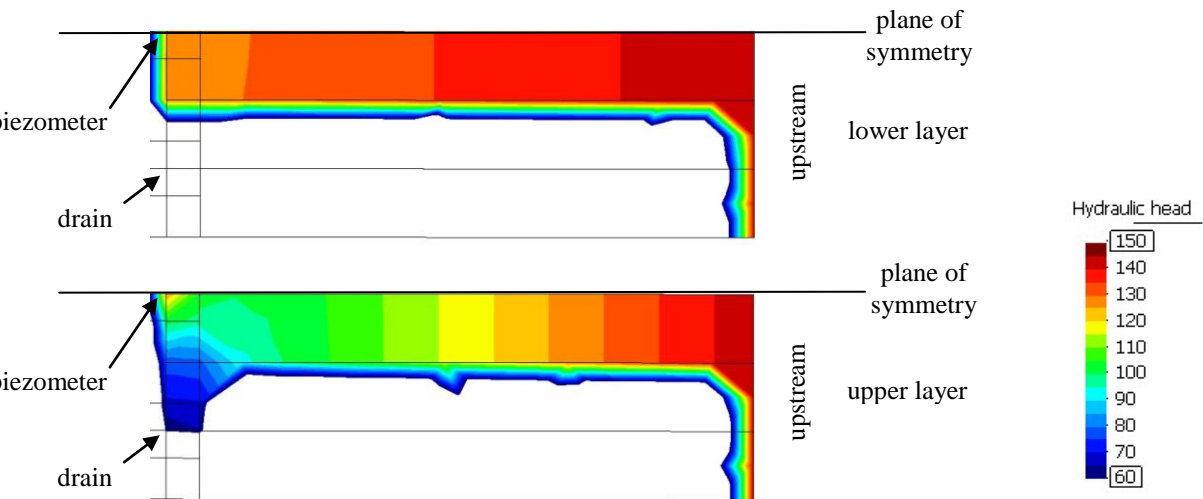


Figure 6.86 – Situation 2: hydraulic head contours with $k_{lower\ layer}/k_{upper\ layer} = 0.2$ and with $k_{lower\ layer}/k_{upper\ layer} = 10.0$. Horizontal cuts through the middle of the pervious layers, in the upstream-downstream direction.

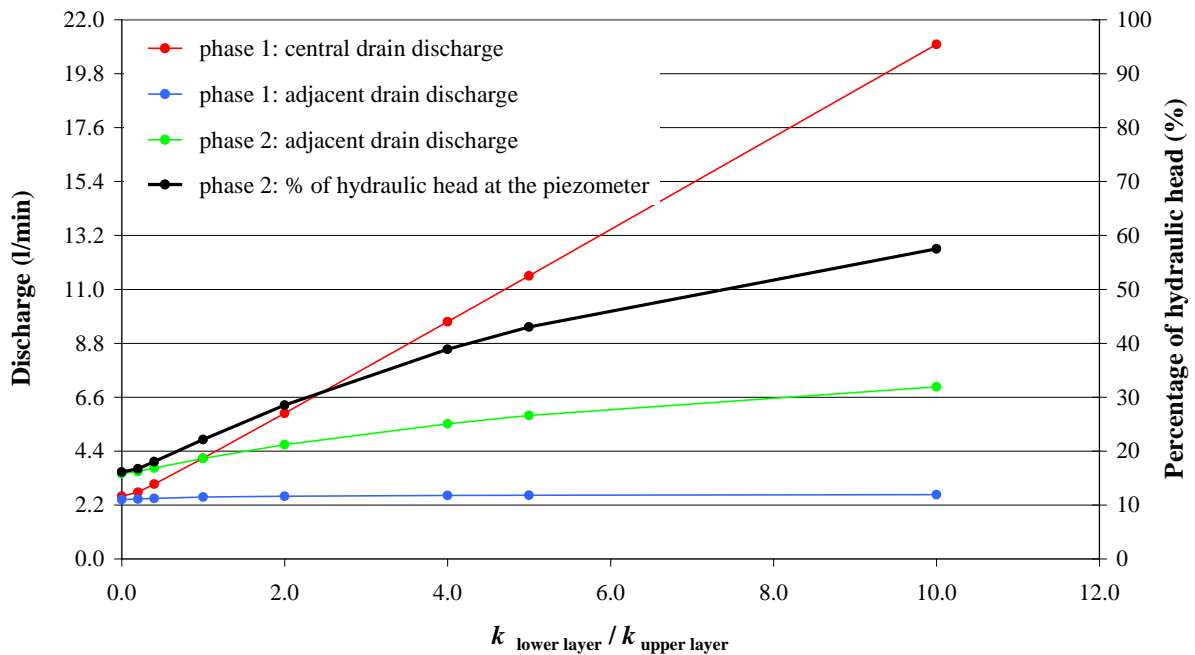


Figure 6.87 – Situation 2: variations in boreholes’ discharges and in percentage of hydraulic head at the piezometer for different values of $k_{\text{lower layer}}/k_{\text{upper layer}}$, assuming a pervious rock mass.

Situation 3:

New numerical analysis was carried out assuming the link between the piezometer and the adjacent drains at mid-way between the pervious layers. The rock mass was assumed to be impervious and the permeability of the upper and lower layers was assumed to be 5.0×10^{-7} m/s and 1.0×10^{-7} m/s, respectively. The permeability of the link was gradually increased and both discharges and water pressures were calculated. Figure 6.88 shows the variations in discharges in both phases of analysis and the variation in percentage of hydraulic head at the piezometer at the second phase of analysis. In the first phase of analysis water flows from the upstream area towards the central borehole through the pervious layers, therefore central drain discharge is constant, not dependent on the link’s permeability, and no water flows out of the adjacent drains. In the second phase of analysis, this situation is similar to situation 1, in which the amount of water flowing towards the adjacent drains gradually increases, and therefore, the curves obtained are similar to those for phase 2 shown in Figure 6.81. However, as the link between the piezometer and the adjacent drains is at a lower level and there is more water flowing towards the piezometer, discharges and water pressures are slightly different.

This situation was not further analysed as, with this model in which the link is located at mid-way between the pervious layers, it would not be possible to compare the hydraulic head with a single chamber to that with two chambers.

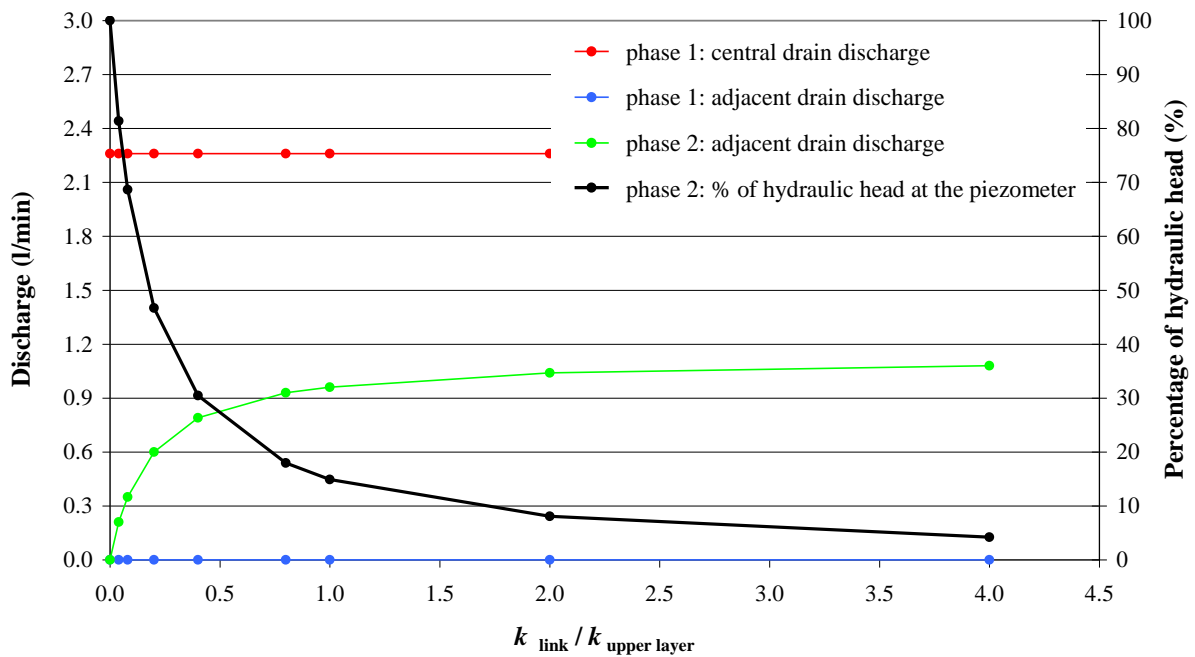


Figure 6.88 – Situation 3: variations in boreholes' discharges and in percentage of hydraulic head at the piezometer for different values of $k_{link}/k_{upper\ layer}$, assuming an impervious rock mass.

Situation 4:

In situation 4, it is assumed that water flows towards the piezometer through two layers of higher permeability and that the piezometer is linked to the adjacent drains by a pervious rock mass. This new situation is similar to the previous one, but has the advantage of allowing the comparison between piezometric heads in a piezometer with a long single chamber and in two piezometers with chambers of different lengths. Variations in discharges in the first phase of analysis have already been analysed in similar situations, either by gradually increasing the permeability of the lower layer (situation 2) or by gradually increasing the permeability of the link between the central and the adjacent boreholes (situation 3), therefore only results of the second phase of analysis are presented here.

It was first assumed that $k_{rock\ mass} = 0.5 \times 10^{-7}$ m/s and $k_{upper\ layer} = 5.0 \times 10^{-7}$ m/s, and the permeability of the lower layer was gradually increased. In order to analyse the way in which water pressures vary along the piezometric borehole, numerical analysis was carried out assuming the piezometer with (Figure 6.89):

- i) a long single chamber;
- ii) two long chambers located 3.0 m apart;
- iii) two long chambers located 5.0 m apart;

- iv) two chambers with a small intake area, defined by the zones where the piezometer is crossed by the pervious layers.

Figure 6.90 shows the variations in discharge and in percentage of hydraulic head at a piezometer with a long single chamber. In this case, discharges in the adjacent drains increase by around 1.8 times, from 3.1 to 5.66 l/min, when $k_{\text{lower layer}}/k_{\text{upper layer}}$ increases from 0.1 to 10, and the percentage of hydraulic head increases from 27.2 % to 66.5 %. A comparison between the percentages of hydraulic head at a piezometer with a long single chamber and those at chambers of different lengths is shown in Figure 6.91. In this case, the maximum difference between percentages of hydraulic head in a long single chamber and in the chamber crossed by the most pervious layer is 12.7 %. The greatest differences are obtained when two short chambers are considered, because the loss of water through the rock mass is smaller. Figure 6.91 a) shows that when the lower layer is as pervious as the upper layer, the percentage of hydraulic head in the lower chamber is smaller than that in the upper one. This is due to the difference in the chambers' length. In fact, as the lower chamber is longer, the quantity of water flowing out of this chamber is greater, which reduces water pressures. Almost the same hydraulic head is obtained in both chambers when they are short. Analysis of numerical results with two long chambers located either 3.0 or 5.0 m apart aimed to check whether there was a link between both chambers, due to zone sizes. It was concluded that isolated chambers are suitably modelled, as almost the same results are obtained in both cases, the difference being lower than 0.3 %.

Figure 6.92 shows the variations in percentage of hydraulic head along the borehole in the above-mentioned cases i), ii) and iv), when the lower layer is either 10 times less pervious or 10 times more pervious than the upper layer. In the first case, the percentage of hydraulic head measured with a long single chamber is around the mean value between hydraulic heads recorded in both chambers. In the second case, it is closer to the higher hydraulic head, recorded in the lower chamber.

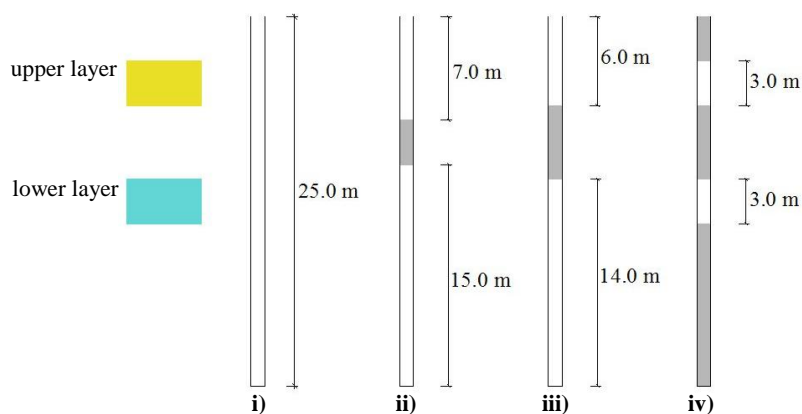


Figure 6.89 – Length of piezometric chambers: i) long single chamber; ii) two long chambers located 3.0 m apart; iii) two long chambers located 5.0 m apart; iv) two chambers 3.0 m long.

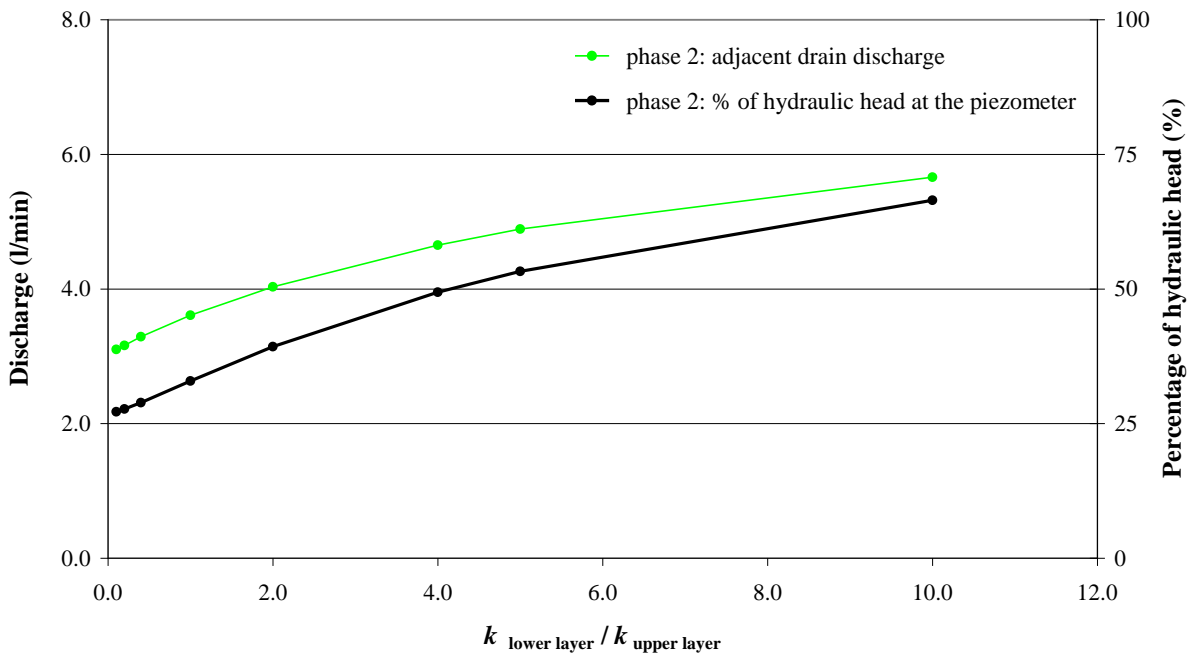
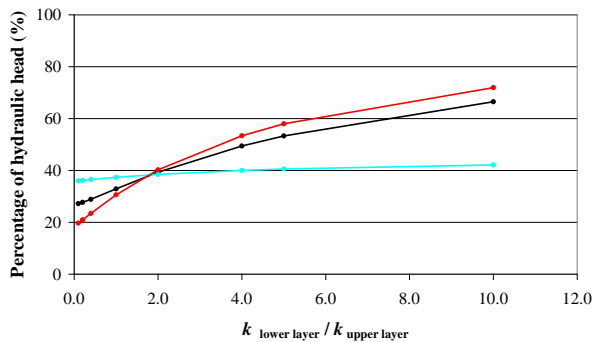
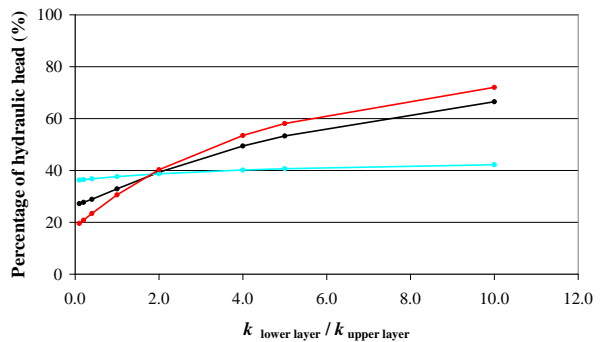


Figure 6.90 – Situation 4: variations in discharge and in percentage of hydraulic head at the piezometer in the second phase of analysis for different values of $k_{\text{lower layer}} / k_{\text{upper layer}}$.

a) two long chambers 3.0 m apart



b) two long chambers 5.0 m apart



c) two short chambers

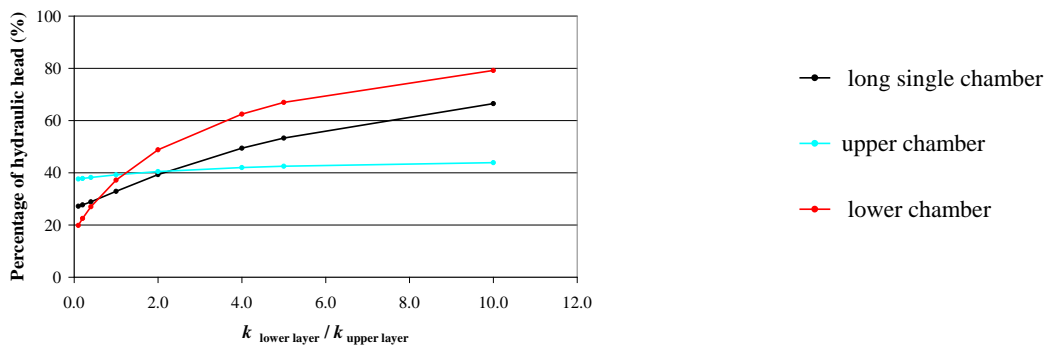


Figure 6.91 – Situation 4: comparison of variations in percentage of hydraulic head at a long single chamber and those at chambers of different lengths.

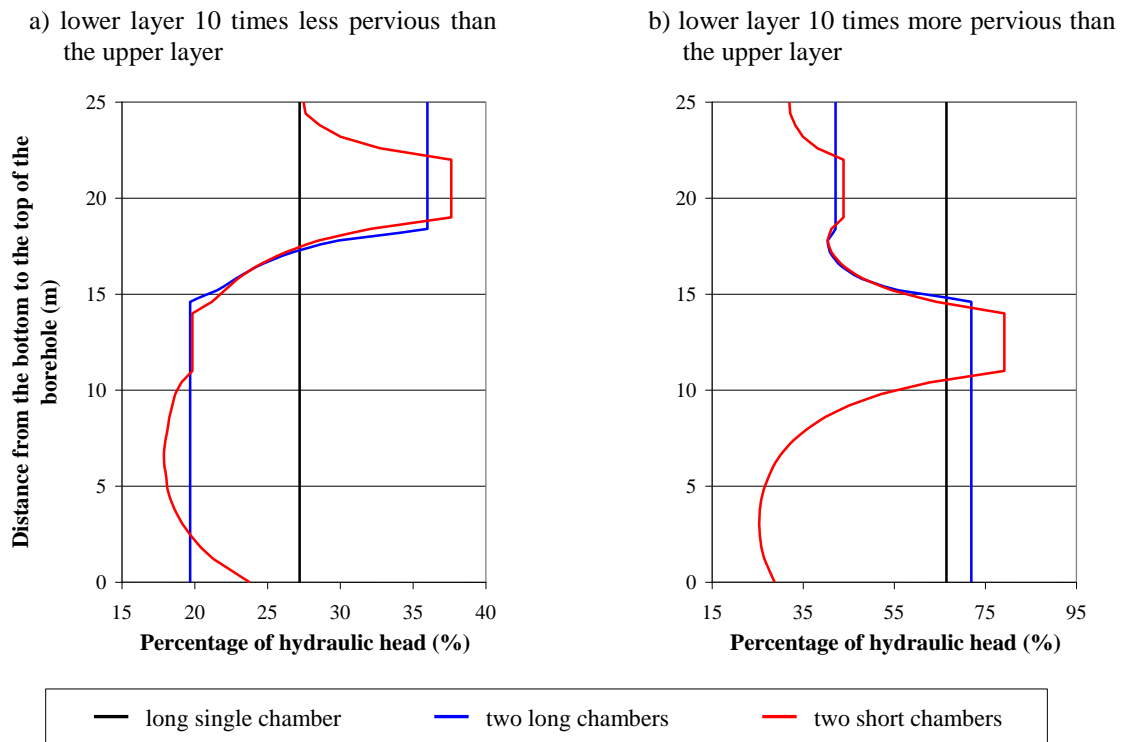


Figure 6.92 – Situation 4: hydraulic head along the borehole assuming different piezometers.

The analysis presented above was repeated assuming different rock mass permeabilities, varying from 0.1 to 3.0×10^{-7} m/s, and four different ratios between the permeability of the lower layer and that of the upper layer:

- i) lower layer two times less pervious than the upper layer ($k_{lower\ layer}/k_{upper\ layer} = 0.5$);
- ii) lower layer as pervious as the upper layer ($k_{lower\ layer}/k_{upper\ layer} = 1$);
- iii) lower layer two times more pervious than the upper layer ($k_{lower\ layer}/k_{upper\ layer} = 2$);
- iv) lower layer twenty times more pervious than the upper layer ($k_{lower\ layer}/k_{upper\ layer} = 20$).

Variations in percentages of hydraulic head for the four different situations at a piezometer with a long single chamber are shown in Figure 6.93. Naturally, higher percentages of hydraulic head are obtained for rock masses with a low permeability. In this case, percentages of hydraulic head of around 57 % to 72 % would be recorded if the permeability of the lower layer were not greater than two times that of the upper one. 95 % of the hydraulic head would be recorded if the lower layer were 20 times more pervious than the upper.

Percentages of hydraulic head at piezometers with two either short or long chambers were compared to those presented in Figure 6.93, for the above-mentioned cases ii) and iv). Results

are shown in Figure 6.94 and Figure 6.95. Figure analysis shows that, in this situation 4, readings taken in a piezometer with a long single chamber would be:

- close to those recorded in both the upper and lower chambers, either short or long, if the lower layer is as pervious as the upper one. In this case, the maximum differences are of around 10 % and are obtained for a low pervious rock mass (Figure 6.94);
- between those taken in the upper and lower chambers, closer to readings taken in the latter, if the lower layer is 20 times more pervious than the upper. The highest differences are obtained when the upper layer is around 10 times more pervious than the rock mass (Figure 6.95).

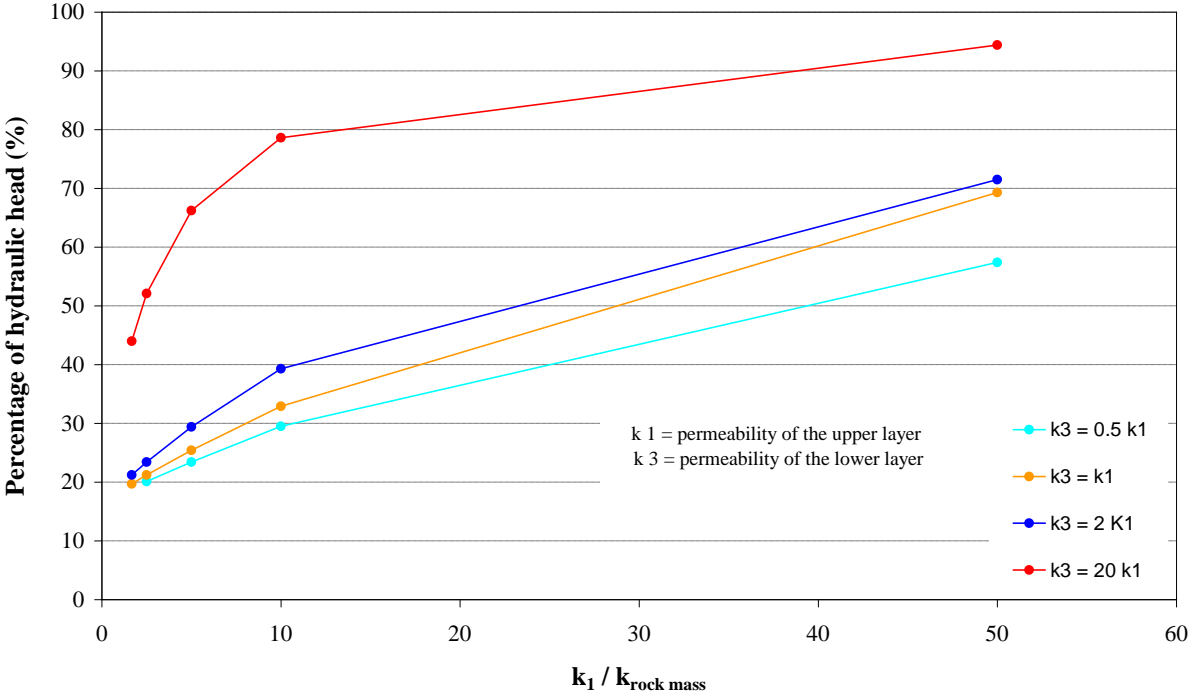
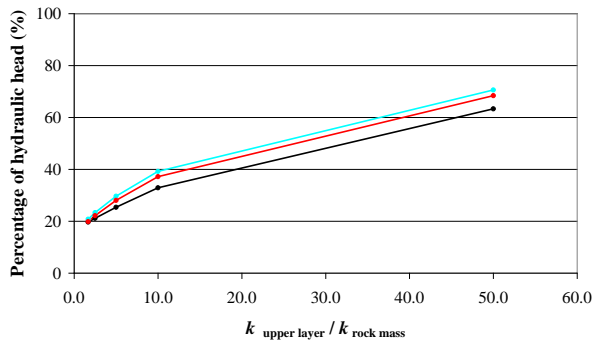


Figure 6.93 – Variations in percentage of hydraulic head at the piezometer for different values of $k_{\text{upper layer}}/k_{\text{rock mass}}$ and $k_{\text{lower layer}}/k_{\text{upper layer}}$.

a) two short chambers



b) two long chambers

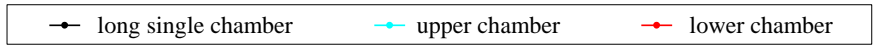
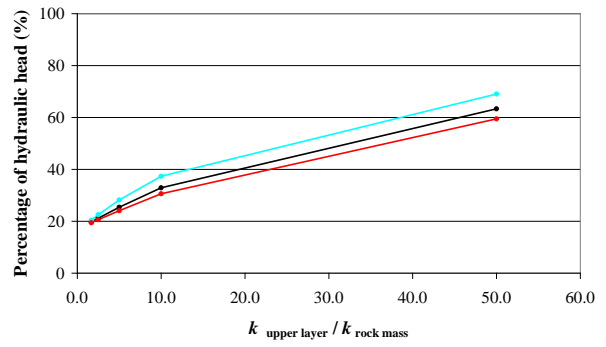
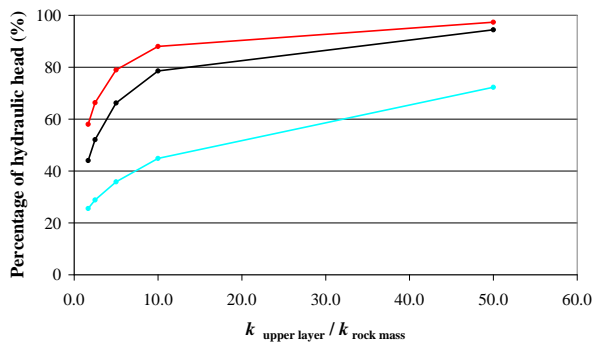


Figure 6.94 – Situation 4 ($k_{\text{lower layer}} = k_{\text{upper layer}}$): comparison of variations in percentage of hydraulic head in a long single chamber and those in chambers of different lengths.

a) two short chambers



b) two long chambers

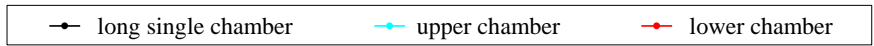
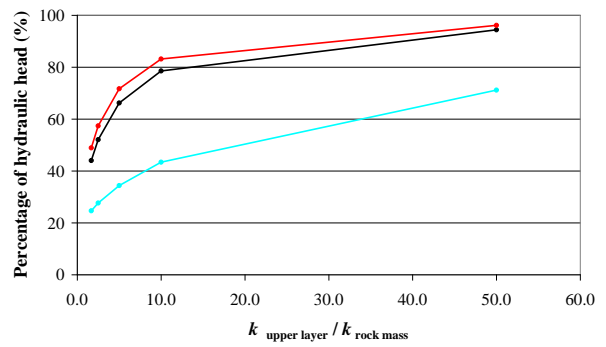


Figure 6.95 – Situation 4 ($k_{\text{lower layer}} / k_{\text{upper layer}} = 20$): comparison of variations in percentage of hydraulic head in a long single chamber and those in chambers of different lengths.

Situation 5:

In situation 5, it is assumed that water flows towards the piezometer through a layer of higher permeability close to the dam/foundation interface, and that there is a link between the piezometer and the adjacent drains at a lower level. A rock mass with a low permeability was considered ($k_{\text{rock mass}} = 1.0 \times 10^{-8}$ m/s) and the permeability of the pervious layer was assumed to be 5×10^{-7} m/s. The permeability of the link between the three boreholes was gradually increased. Figure 6.96 shows the variations in boreholes' discharges and in percentage of hydraulic head at a piezometer with a long single chamber. In the first phase of analysis, as in situation 3, central drain discharge is constant. An invariable quantity of water also flows into the adjacent drains, through the rock mass. In the second phase of analysis, the percentage of hydraulic head decreases from 52.4 %, if the piezometer is linked to the adjacent drains by the pervious rock mass, to 3.9 %, if the link is 4 times more pervious than the main layer. When the link is as pervious as the main layer, the percentage of hydraulic head is 12.8 %.

Figure 6.97 and Figure 6.98 show the hydraulic head contours in a vertical cut through the piezometer and in horizontal cuts through the middle of both the link and the pervious layer, respectively. Figures show that the loss of hydraulic head increases with the increase in the link's permeability.

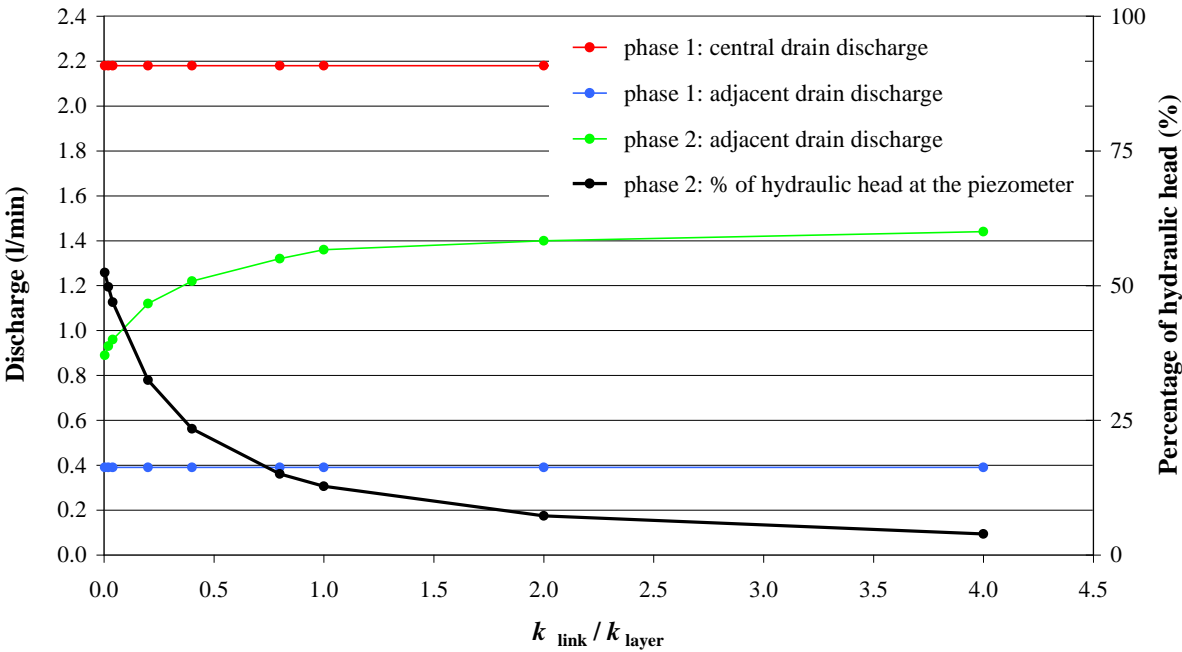
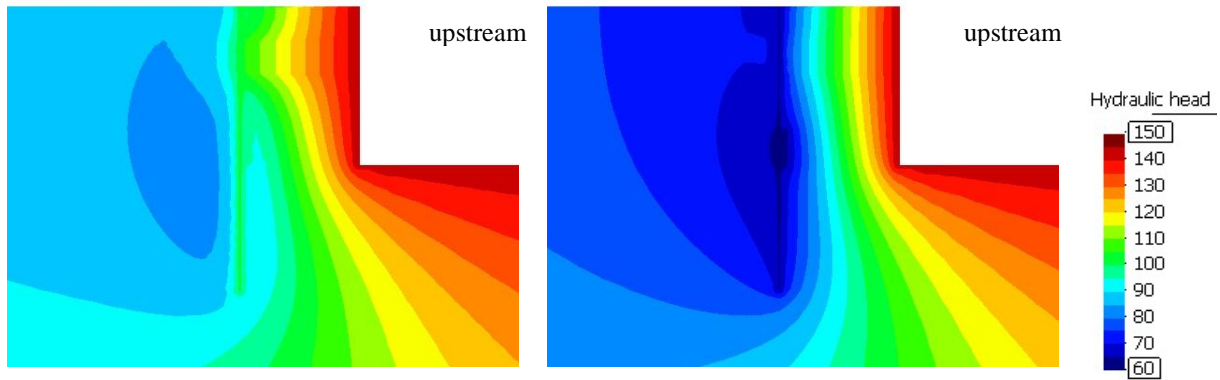


Figure 6.96 – Situation 5: variations in boreholes' discharges and in percentage of hydraulic head at the piezometer for different values of $k_{\text{link}}/k_{\text{layer}}$.

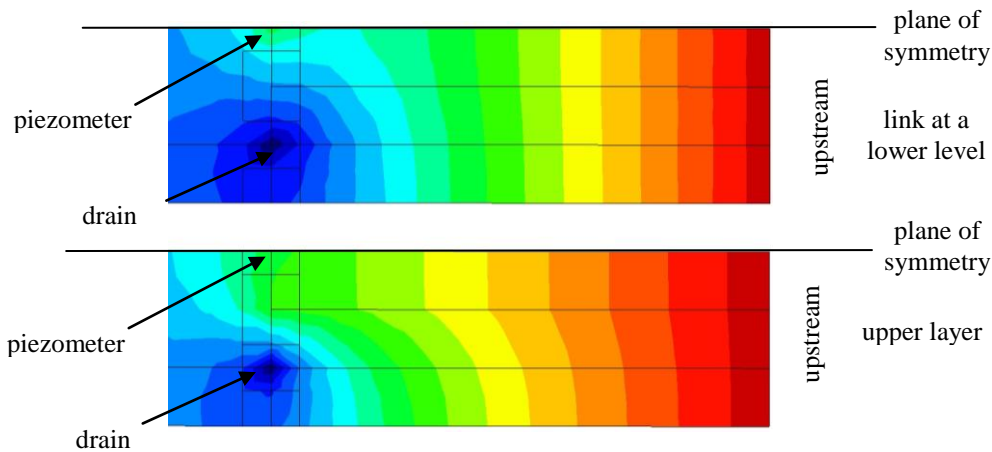


a) piezometer linked to the adjacent drains by the pervious rock mass

b) link 4 times more pervious than the upper layer

Figure 6.97 – Situation 5: hydraulic head contours in a vertical cut through the piezometer.

a) piezometer linked to the adjacent drains by the pervious rock mass



b) link 4 times more pervious than the upper layer

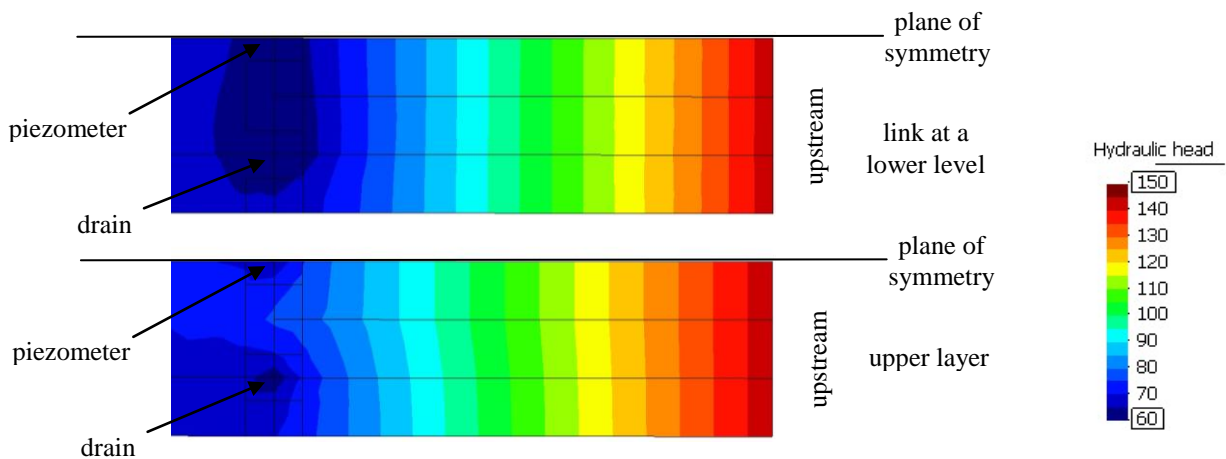


Figure 6.98 – Situation 5: hydraulic head contours in horizontal cuts through the middle of both the link and the pervious layer.

New numerical analysis was carried out, assuming that the piezometric borehole has two long chambers. Figure 6.99 shows a comparison between the percentages of hydraulic head at the long single chamber piezometer and in the two long chambers. Results show that, in this case, if the permeability of the link is the same as or lower than the permeability of the main layer, water pressures lower than 13 % of the hydraulic head will be recorded in a piezometer with a long single chamber, while, in fact, the water pressure within the upper discontinuity is about 66 % of the hydraulic head.

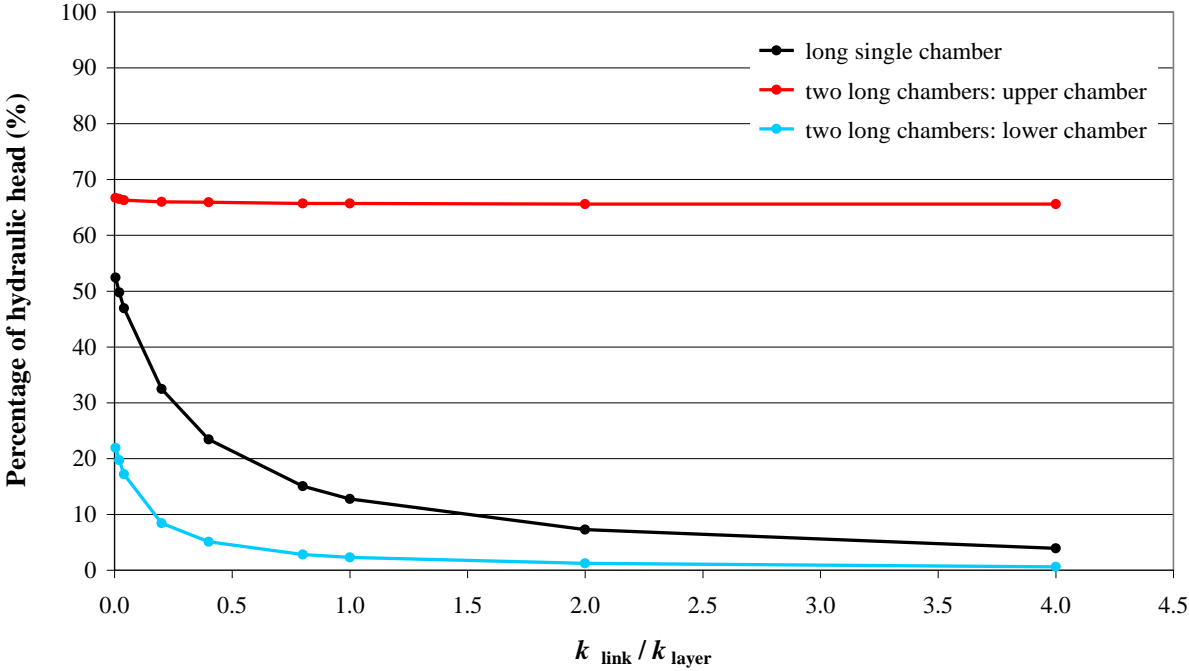


Figure 6.99 – Situation 5: variations in percentage of hydraulic head at a piezometer either with a long single chamber or with two long chambers, for different values of k_{link} / k_{layer} .

6.8.4.2 Analysis of flow through discontinuity networks

Hudson and Harrison (2000) suggest a simple method to study seepage in the complex discontinuity networks that exist in rock masses, taking into account the continuity equation and assuming that the flow in the network is laminar and of low velocity. In this method, the hydraulic heads at nodal points are calculated by solving a set of simultaneous equations. An equation is established for each node, taking into account that the hydraulic head at each of the discontinuity networks' node depends both on the conductance and on the hydraulic head at the beginning of the particular branch of the discontinuities that converge to that node (Figure 6.100). Conductance, c , is given by:

$$c = \frac{g a^3}{12 \nu L} \quad (6.19)$$

where g = acceleration of gravity; a = hydraulic aperture of the discontinuity; ν = kinematic viscosity of the water, and L = length of the discontinuity in the direction of flow.

Jing and Stephansson (2007) present a similar procedure to determine piezometric heads at discontinuity intersections. They mention that the method can also be applied for unconfined flow field, using an iterative procedure with initial head. In this case, a set of additional discrete intersection points on fracture segments where the pressure is equal to the atmospheric pressure is considered, so that the final geometric location of the water table can be obtained.

The horizontal section shown in Figure 6.101 schematically represents the simple set of discontinuities simulated in situation 1, in a 12 m \times 9 m rock mass block, with the same height as the layers (3 m). On the left hand side, the hydraulic head is the reservoir level (H_u), and in both drains is 61.0 m. As seepage occurs in a horizontal level, the solution is independent of the elevation head. It is assumed that there is no variation in flow throughout the thickness of the rock block. The hydraulic head at the piezometer is the only unknown parameter and can be easily obtained, taking into account that the quantity of water flowing into the model is the same as the drains' discharge (continuity equation) and that the flow rate in each network branch (1, 2, and 3) is given by Darcy's law:

$$q_1 = q_2 + q_3 \quad (6.20)$$

where,

$$q_1 = k_1 i_1 A_1 = k_1 \frac{H_u - H_{piezometer}}{L_1} A_1 \quad (6.21)$$

$$q_2 = k_2 i_2 A_2 = k_2 \frac{H_{piezometer} - H_{drain}}{L_2} A_2 \quad (6.22)$$

$$q_3 = k_3 i_3 A_3 = k_3 \frac{H_{piezometer} - H_{drain}}{L_3} A_3 \quad (6.23)$$

and thus,

$$H_{piezometer} = \frac{\frac{k_1 A_1}{L_1} H_u + \left(\frac{k_2 A_2}{L_2} + \frac{k_3 A_3}{L_3} \right) H_{drain}}{\frac{k_1 A_1}{L_1} + \frac{k_2 A_2}{L_2} + \frac{k_3 A_3}{L_3}} \quad (6.24)$$

In this case, $k_1 = 5.0 \times 10^{-7}$ m/s; k_2 varies from 0.0 m/s to 25.0×10^{-7} m/s; $L_1 = 10.5$ m; $L_2 = L_3 = 3.0$ m; $A_1 = 3.0 \times 3.0$ m²; $A_2 = A_3 = 0.6 \times 3.0$ m². Figure 6.102 shows the comparison of the hydraulic head at the piezometer obtained with the 3D model and with the simplified model shown in Figure 6.101 (Equation 6.24). This simple model simulates seepage very accurately, as differences to the numerical result are lower than 7 %. If the link is as pervious as the main layer a hydraulic head of 71.3 m is calculated at the piezometer, which is 97.7 % of the numerical result.

The layer of higher permeability upstream from the piezometer is 3.0 m wide (Figure 6.103), therefore the simplified model would be closer to that analysed with 3DEC if an equivalent permeability were used in Equation 6.24 in branches 2 and 3, instead of the links' permeability. In this case, the equivalent permeability is given by:

$$\frac{1}{k_{equivalent}} = \frac{L_2}{\frac{(L_2/2)}{k_1} + \frac{(L_2/2)}{k_{link}}} \quad (6.25)$$

With this second simplified model, the hydraulic head at the piezometer is equal to or lower than that calculated with the 3D model, and differences to the numerical result are lower than 9 % (Figure 6.104).

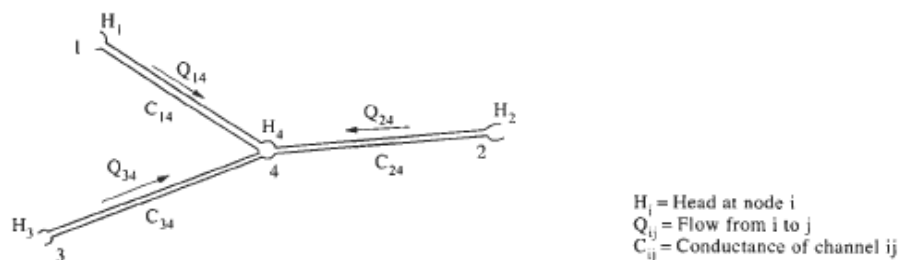


Figure 6.100 – Flow at a network node (after Hudson and Harrison 2000)

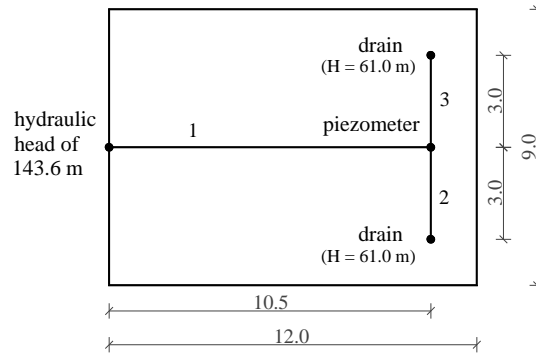


Figure 6.101 – Set of discontinuities simulated in situation 1.

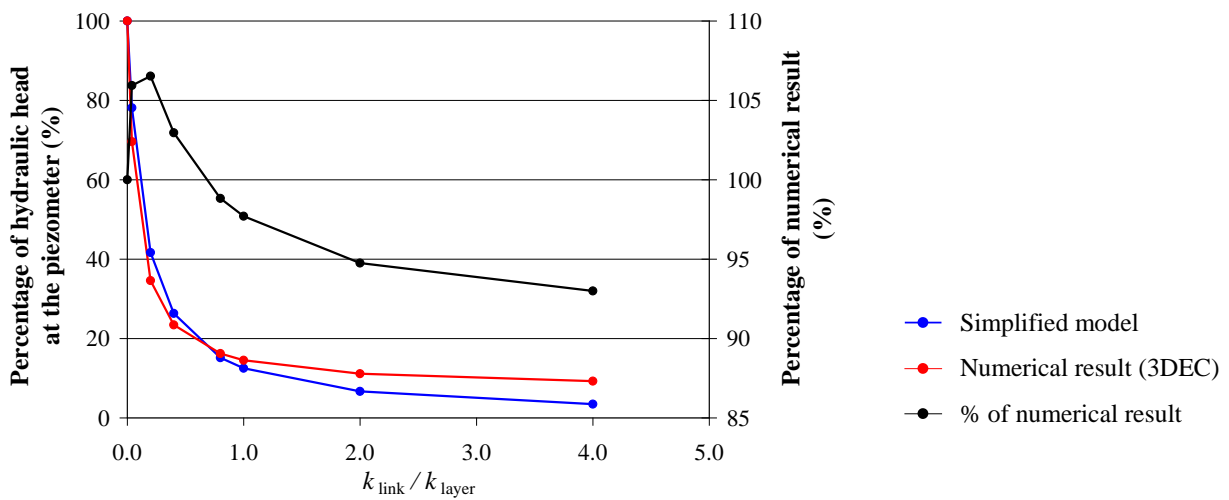


Figure 6.102 – Comparison of the hydraulic head at the piezometer obtained with the 3D model and with the simplified model shown in Figure 6.101 (Equation 6.24).

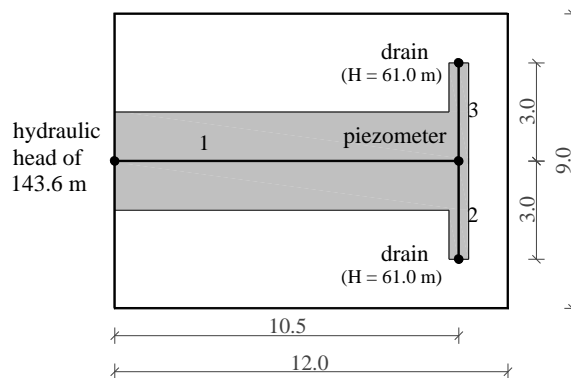


Figure 6.103 – Set of discontinuities simulated in situation 1. Width of the horizontal layer of higher permeability upstream from the piezometer.

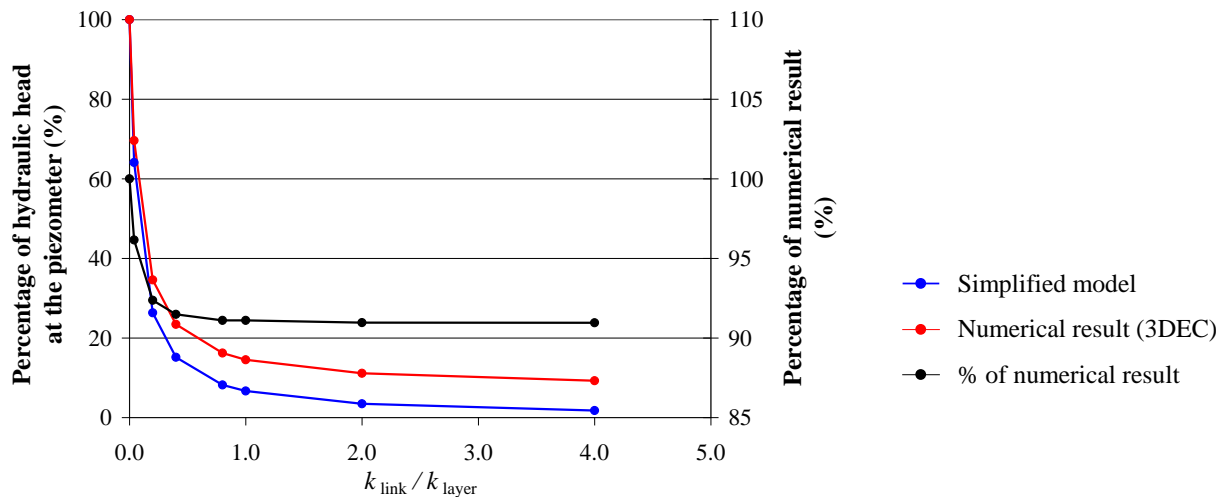


Figure 6.104 – Comparison of the hydraulic head at the piezometer obtained with the 3D model and with the simplified model shown in Figure 6.101 assuming an equivalent permeability in branches 2 and 3.

Although the above-mentioned analysis is for an essentially 2D network, it was also used to study flow in the other situations presented here. In these cases, unlike in the situation previously described, the elevation head must be taken into account, because the set of discontinuities is not horizontal. Hudson and Harrison (2000) highlight that the analysis cannot be simply extended into three dimensions because in 3D two discontinuity planes meet along an intersection line, along which the hydraulic head may vary. Jing and Stephansson (2007) point out that the principle applies also for 3D problems but with much more complexity in handling fracture system geometry and connectivity.

Figure 6.105 shows the set of rock fractures simulated in situations 2, 3 and 5. The mid-level of the lower horizontal layer of higher permeability was taken as reference. In this figure, on the left hand side of each drawing the pressure head is the reservoir level, and the hydraulic head is 61.0 m in both drains. Situation 4, in which it is assumed that water flows towards the drains only through the rock mass, was not taken into account. The hydraulic head at each node as well as the equations established for each situation are also shown in Figure 6.105.

Figure 6.106 shows the comparison of the hydraulic head at the piezometer obtained with the 3D models and with the simplified models shown in Figure 6.105. In situation 2, results are compared to those obtained with an impervious rock mass, shown in Figure 6.84. Here, the difference between the results of the simplified model and those obtained with the 3D model are lower than 12 %. In situation 3, results are very accurate, the difference being lower than 0.5 %. In situation 5, results are not so accurate when k_{link} / k_{layer} is lower than 0.4. However, the difference is lower than 3 % when k_{link} / k_{layer} is greater than 0.4. In this last situation, the difference between 3DEC results and those obtained with the simplified model is due to the

fact that the latter does not simulate the permeability of the rock mass. In fact, the 3DEC model for situation 5 was run again, this time assuming an impervious rock mass, and the results are almost exactly the same as those obtained with the simplified model, as shown in Figure 6.107.

Results show that, in each situation, the hydraulic head at the piezometer, and hence the direction and magnitude of flow in each discontinuity segment, can be easily obtained with very simple models. These models can be very useful in parameter studies, as they provide a very quick means to identify which of the parameters has the greatest influence on the hydraulic head at the piezometer.

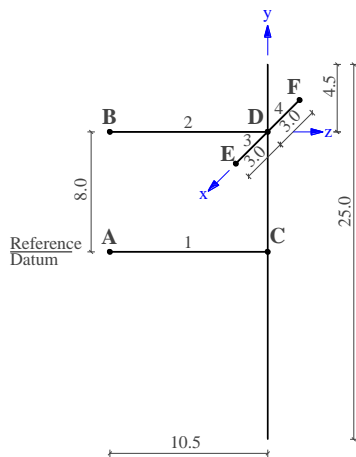
6.8.5 Conclusions and discussion

The majority of the piezometers installed in the foundations of our large concrete dams have a long single chamber. Therefore, the water pressure measured at the pressure gauge is a weighted average pressure, which depends on the hydraulic head at the various discontinuities that cross the borehole. In this study, five different possible situations of water flow patterns created by discontinuities crossing the piezometer were analysed. It was taken into account that in concrete dam foundations the majority of the flow takes place through discontinuities that cross each other and that most of the discontinuities come to an end in another discontinuity.

When the piezometer is crossed by joints through which water flows in a single confined area, as in situation 1, the water pressure recorded at the pressure gauge in a piezometer with a long single chamber is the same as that recorded in one with a small intake crossed by the conductive joints. However, when the piezometer is crossed by conductive joints at different levels, as in the other situations analysed, multilevel piezometers with the piezometric chambers suitably positioned would provide more useful data. It was found that the most serious situation is when water flows into the piezometer at a shallow depth, and flows out at a greater depth. In this case, relatively low water pressures can be measured in a piezometer with a single long chamber, while high water pressures are found within the discontinuities close to the dam/foundation interface, which can affect the dam's stability.

The numerical analysis presented here shows that it is difficult to draw generalized conclusions concerning the advantages and disadvantages of long or short piezometric chambers, as the most appropriate solution depends on local conditions. It has also been shown that it is not possible to establish the length of piezometric chambers in advance as each situation is different.

Situation 2



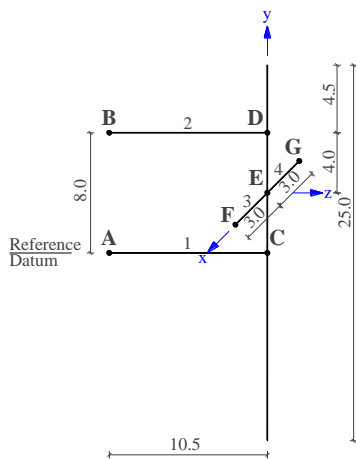
	A	B	C	D	E	F
P/γ_w	143.6	143.6-8	P_C/γ_w	P_D/γ_w	61.0-8	61.0-8
z	0	8	0	8	8	8
H	143.6	143.6	$H_{\text{piezom.}}$	$H_{\text{piezom.}}$	61.0	61.0

$$q_1 + q_2 = q_3 + q_4$$

$$H_C = H_D = H_{\text{piezometer}}$$

$$H_{\text{piezometer}} = \frac{\frac{k_1 A_1}{L_1} H_A + \frac{k_2 A_2}{L_2} H_B + \frac{k_3 A_3}{L_3} H_E + \frac{k_4 A_4}{L_4} H_F}{\frac{k_1 A_1}{L_1} + \frac{k_2 A_2}{L_2} + \frac{k_3 A_3}{L_3} + \frac{k_4 A_4}{L_4}}$$

Situation 3



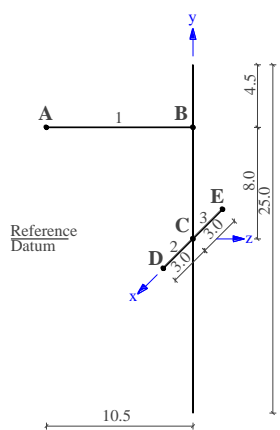
	A	B	C	D	E	F	G
P/γ_w	143.6	135.6	P_C/γ_w	P_D/γ_w	P_E/γ_w	57.0	57.0
z	0	8	0	8	4	4	4
H	143.6	143.6	$H_{\text{piezom.}}$	$H_{\text{piezom.}}$	$H_{\text{piezom.}}$	61.0	61.0

$$q_1 + q_2 = q_3 + q_4$$

$$H_C = H_D = H_E = H_{\text{piezometer}}$$

$$H_{\text{piezometer}} = \frac{\frac{k_1 A_1}{L_1} H_A + \frac{k_2 A_2}{L_2} H_B + \frac{k_3 A_3}{L_3} H_F + \frac{k_4 A_4}{L_4} H_G}{\frac{k_1 A_1}{L_1} + \frac{k_2 A_2}{L_2} + \frac{k_3 A_3}{L_3} + \frac{k_4 A_4}{L_4}}$$

Situation 5



	A	B	C	D	E
P/γ_w	143.6-8	P_B/γ_w	P_C/γ_w	61.0	61.0
z	8	8	0	0	0
H	143.6	$H_{\text{piezom.}}$	$H_{\text{piezom.}}$	61.0	61.0

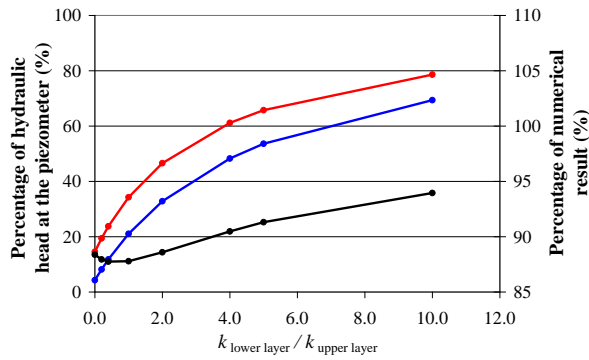
$$q_1 = q_2 + q_3$$

$$H_B = H_C = H_{\text{piezometer}}$$

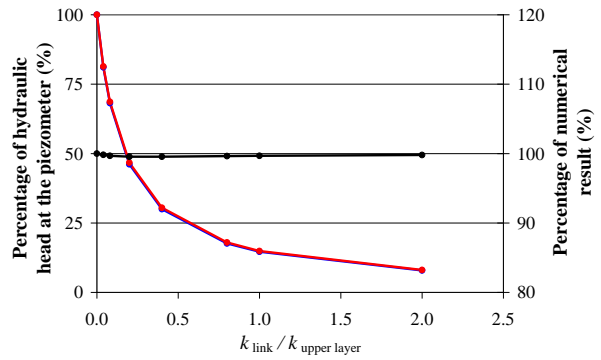
$$H_{\text{piezometer}} = \frac{\frac{k_1 A_1}{L_1} H_A + \frac{k_2 A_2}{L_2} H_D + \frac{k_3 A_3}{L_3} H_E}{\frac{k_1 A_1}{L_1} + \frac{k_2 A_2}{L_2} + \frac{k_3 A_3}{L_3}}$$

Figure 6.105 - Set of discontinuities simulated in situations 2, 3 and 5. Hydraulic head at each node and at the piezometer.

situation 2



situation 3



Situation 5

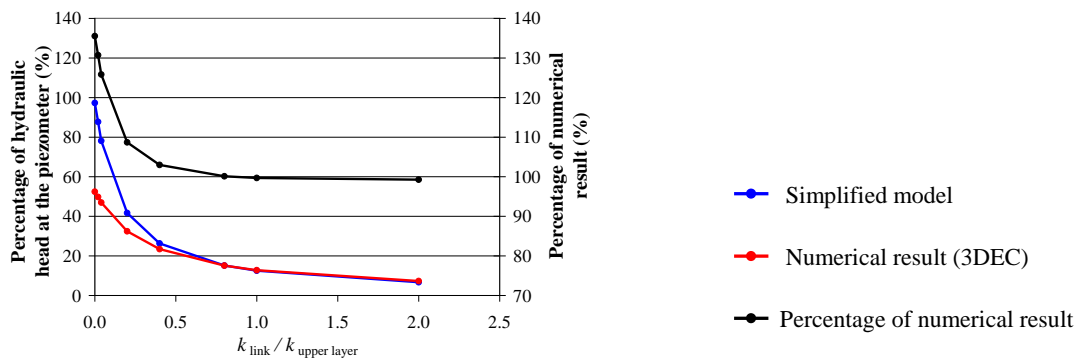


Figure 6.106 – Comparison of the hydraulic head at the piezometer obtained with the 3D model and with the simplified models shown in Figure 6.105.

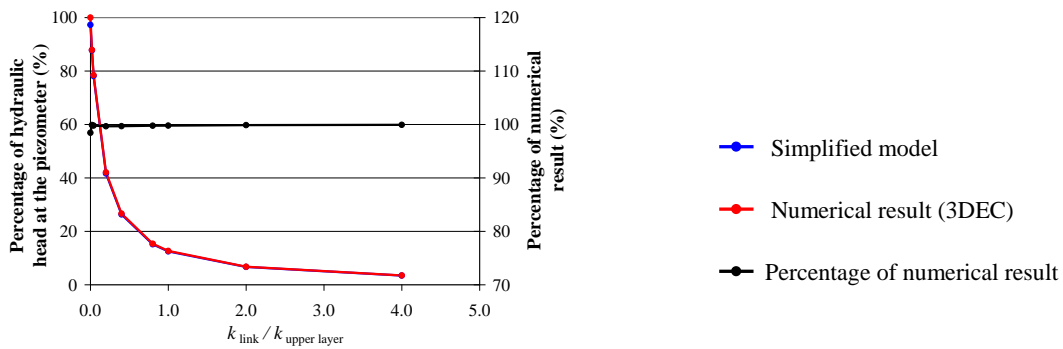


Figure 6.107 – Situation 5 assuming an impervious rock mass: comparison of the hydraulic head at the piezometer obtained with the 3D model and with the simplified model shown in Figure 6.105.

The positioning and length of the piezometric chambers must be defined case by case and should only be specified after obtaining detailed information about the main seepage paths. It is not only relevant to know where the piezometric boreholes are crossed by conductive discontinuities, but also if and how these discontinuities are linked to adjacent drains. Seepage paths, however, can vary with changes in reservoir level or in ambient temperature. It is therefore essential that the geology of the area is well understood, and that borehole logs and results of Lugeon type tests or borehole water-inflow tests are carefully analysed. At the dam site, multilevel piezometers require careful installation, in order to properly isolate the chambers.

Although more detailed data can be obtained with multilevel piezometers, the information they provide is very localized, and can be of little value, unless it can be analysed and understood by means of a suitable numerical model. In fact, results of equivalent continuum models presented thus far show that the hydraulic head varies depending not only on the depth but also on the location in relation to the reservoir and to the grout and drainage curtains (e.g. upstream or downstream from the grout or drainage curtains, in the line of the drains, or in a cross section in the upstream-downstream direction which crosses the drain or which is midway between drains). In practice, the complexity of the rock mass jointing pattern and the fact that water flows only through some of the discontinuities makes it necessary to take into account that piezometric heads can vary significantly from one point to another, even if the two points are very close to each other, and therefore, readings may appear incoherent.

It must be stressed that in the monitoring of concrete dams it is common practice to be concerned with water pressures recorded in piezometers located downstream from the drainage curtain when the percentages of hydraulic head are greater than around 30 %. However, readings taken in piezometers with a long single chamber can be misleading. In addition, as mentioned in the previous paragraph, high percentages of hydraulic head may be localised and therefore not significant regarding the safety of the dam, or may be of concern, when acting on a horizontal discontinuity with a large surface, which encompasses the whole base of a dam block. Therefore, when a high percentage of hydraulic head is recorded at a piezometer, it is important to know whether there exists a horizontal or sub-horizontal discontinuity upon which that pressure is acting (unfavourable to the stability of the dam).

In the majority of our large concrete dams, there is one piezometer per dam block and drains are located 2.5 to 5.0 m apart. In order to understand whether high pressures are localised or over a wider area, the drainage system should be used, and some simple tests carried out, firstly closing the drains close to the piezometer, and then closing the drains located further away:

1. if it is localised, when the drains closer to the piezometer are closed, the water pressure at the piezometric borehole increases and there is no change in the quantity of water that flows through drains located further away from the piezometer. The closure of these latter drains causes no change in the piezometric reading.
2. On the contrary, if there is a horizontal or sub-horizontal discontinuity with a large surface where the water pressure is acting, the pressure in the piezometric borehole increases when the drains closer to the borehole are closed, as do discharges in boreholes located in the vicinity, and increases still further when the drains located further away from the piezometer are closed.

As was seen in chapter 4, valuable additional data can be obtained with borehole water-inflow tests and water electrical conductivity analyses.

High percentages of hydraulic head might be recorded if vertical and/or sub-vertical discontinuities parallel to the river axis and with high heads cross the piezometric borehole. These water pressures, however, are of no concern to the stability of the dam. In Alqueva dam, as mentioned in chapter 4.5.8.3, the gradual closure of all the drains and piezometers located in block 17-18 showed that the high percentage of hydraulic head recorded at drain D25 D while carrying out borehole water-inflow tests was localised.

Finally, regarding the method suggested by Hudson and Harrison (2000) to study seepage in complex discontinuity networks, which was used in the simple flow cases presented here, it must be mentioned that quite accurate results were obtained. However, the method is very difficult to apply in practice, because there is a lack of information about the interconnection between conductive joints.

6.9 Summary and conclusions

The first model presented in this chapter, which was a simplified 2D model of a vertical cross section of the dam foundation, follows the standard practice of assuming that water flows from the bottom of the reservoir, goes down around the grout curtain, so that the majority of the drained water reaches the drainage boreholes at their lower part. However, seepage in the foundation usually differs from the assumed conceptual model as local defects, such as gaps in the grout curtain, change the flow path. Seepage as that assumed in the conceptual model would only be achieved if the watertight curtain were effective. According to Londe (1973), an effective grout curtain must be thick enough, with permeability much lower than that of the surrounding rock mass. In a rock mass of low permeability, such as in Alqueva dam foundation, reducing the permeability from around 10^{-7} m/s down to 5×10^{-8} m/s would be an impressive achievement. Therefore, in these cases, it is very difficult to have an effective

grout curtain because grout only slightly reduces the natural permeability and, as penetration is limited, the curtain is thin.

The tests and field measurements which were required for the assessment of the main seepage paths in an area of the foundation of Alqueva dam were presented in chapter 4. The simulations of borehole water-inflow tests carried out provided a good match of recorded discharges and water pressures for different experimental conditions. These simulations are relevant as the numerical modelling of tests provides a valuable tool for the validation of numerical techniques. The models developed are very simple, and only a few parameters were used, all of them with physical meaning. The study shows the relevance of knowing where the main flow paths are located. Parametric studies carried out showed the importance of assigning proper values to both rock mass equivalent permeability and the permeability of the layers which simulate the main flow paths.

The knowledge of seepage patterns around some boreholes provided by test analysis was essential to develop an effective application of a simplified global model of the dam foundation. Global hydraulic models of dam foundations are useful not only for the assessment of the behaviour of dams in use, comparing the average value of discharges and uplift pressures with numerical results, but also to determine water pressure distributions to take into account in stability analysis.

Global 3D models of dam foundations, which involve large volumes of rock masses, can only be carried out with coarse meshes. In these models, due to zone sizes, the drainage system is represented in a simplified way. As previously mentioned, the model was developed taking into account the results of borehole water-inflow tests and conclusions drawn from the detailed 3D models presented in the previous section. It was concluded that parameters determined using the detailed models cannot be used directly in a global 3D model of the foundation. In the global model zones are larger, and therefore discharges are greater. Comparison of both numerical and recorded discharges and water pressures showed that the model can provide mean water pressures and flow rates for each dam foundation block.

Models of flow in discontinuous rock masses, while representing more closely the physical phenomenon, are difficult to apply in many practical cases because of insufficient data on the hydraulic properties of the various discontinuity sets. Grouting and drainage add to the complexity of flow patterns. However, the analysis presented here shows that the simpler equivalent continuum models can be used successfully to model the hydraulic behaviour of both large and local areas of dam foundations. In equivalent continuum models bands of elements of higher permeability may be assigned to simulate the main seepage paths. These layers, located close to the dam/foundation interface, simulated in both the detailed and global models of the dam foundation may be justified either by the two sub-horizontal sets of rock

joints, shown in Figure 4.10, or by the existence of a more disturbed rock mass zone close to the surface, due to excavation works.

As this study shows, borehole water-inflow tests can be extremely significant in increasing knowledge of the hydraulic behaviour of concrete dam foundations. Not only do these tests provide additional information to the usual monitoring data, they also make it possible to build up a picture of the flow paths and thus, to develop realistic and accurate numerical models, which enables more effective assessment of the safety of concrete dams.

The interdependency between the state of stress and seepage in the foundation of Alqueva dam was studied in an uncoupled way, taking into account the results of the hydraulic model and those from a global mechanical model. The latter takes into account the two areas of different deformability and allows the non-linear behaviour of dam contraction joints and of both dam/foundation interface and grout curtain/foundation interface to be taken into account. The model was validated by comparing the numerical results with monitoring data. A methodology was developed which can be used to establish rules which, from a hydraulic model calibrated for specific water levels in the reservoir and downstream from the dam, allow the calculation of discharges for both higher and lower reservoir levels, taking into account that permeability depends not only on the stress level but also on local geological features.

The study on piezometric measurements presented in the last part of this chapter confirmed that multilevel piezometers provide more accurate data than piezometers with a long single chamber. However, the most appropriate solution depends highly on local conditions and therefore the positioning and length of the piezometric chambers must be defined case by case.

7 Analysis of seepage and stability assessment – the case study of Pedrógão dam

7.1 Introduction

In concrete dam foundations, failure mechanisms are typically defined by natural rock discontinuities, the dam/foundation interface or strata with lower strength. Stability analysis for scenarios of foundation failure is often based on simplified limiting equilibrium procedures. Equivalent continuum models, used in the analysis of seepage presented in the previous two chapters, can be employed to assess the safety of concrete dams, complemented with interface elements to simulate the behaviour of joints, shear zones and faults along which sliding may occur. More advanced analysis, however, is carried out with discrete element techniques, which allow the discontinuous nature of rock to be properly simulated, and which may include fluid flow through the discontinuities. According to Lemos (1999a) they are particularly suitable for stability evaluation of dam foundations, given the importance of sliding and/or separation phenomena on natural joints in failure mechanisms.

This chapter presents a study on seepage in a gravity dam foundation carried out with a view to evaluating dam stability. Pedrógão dam was used as reference and the hydraulic behaviour in some foundation areas was analysed using both two-dimensional continuum and discontinuum models. Firstly, an equivalent continuum model was developed to study seepage in a specific cross section of the dam, where the main seepage paths, identified with the borehole water-inflow tests presented in chapter 4.4, were represented. A discontinuous model of the dam foundation was afterwards developed, using the code UDEC, and a fully coupled mechanical-hydraulic analysis of the water flow through the rock mass discontinuities was carried out. Due to limited data on orientation and spacing between discontinuities within the area being studied, a much idealised fracture pattern was assumed.

The discontinuum model was used to assess water pressures in the dam/foundation interface and along a rock mass horizontal joint of higher hydraulic conductivity, which simulates the main flow path. Results of the coupled hydromechanical analysis were compared with those obtained with a simple hydraulic analysis, in which the joint hydraulic aperture remains constant, and also with those obtained assuming that the drainage system is clogged. Results were afterwards compared with those obtained assuming rock masses with different equivalent deformability. Variations in discharges due to the filling and subsequent emptying of the reservoir were analysed and the influence of joint dilatancy on numerical discharges was also investigated. Numerical water pressures were compared with those recorded *in situ*, at the piezometers located underneath the stilling basin.

Discontinuum models which simulate the hydromechanical interaction provide a means of assessing the stability of the dam, taking into account the actual shear displacements and aperture of discontinuities, and the water pressure pattern within the foundation. The safety for different failure scenarios involving the foundation and the dam body was evaluated using the discontinuum model developed for this study. The method of strength reduction was used to estimate the stability of the dam/foundation system. Analysis was carried out assuming different water pressures at the drainage line, including the scenario of a foundation with no drainage system.

7.2 Two-dimensional model of vertical cross sections based on the hypothesis of an equivalent continuum media

7.2.1 Model description

A two-dimensional model of the foundation of Pedrógão dam was developed to analyse the flow in the rock mass and to support the assessment of the field results (Farinha et al. 2007). The hydraulic properties of an equivalent continuum are considered and the mesh is based on that developed in order to study seepage in Alqueva dam foundation, presented in section 6.2, which has the boundaries quite far away from the dam's area of influence. The mesh was modified in the dam area, in order to be adjusted to the length of the dam/foundation interface along the upstream-downstream direction, and to the position of both the grout curtain and the drainage system. In addition, to take into account the conclusion presented in chapter 6.2.3 concerning the distance at which boundaries should be placed from the area being studied when most of the water flows between the reservoir and the drainage system, zones located further away from the dam were assigned zero permeability. In this way, seepage takes place in a restricted area of about $200 \times 100 \text{ m}^2$. It is assumed that water flows according to Darcy's law, in a homogeneous and isotropic media. The steady state seepage flow is analysed with FLAC 5.0.

The mesh is made up of 1139 zones, and was developed in such a way that it enables the analysis of seepage in different cross sections of the dam, namely in blocks 7-8 and 8-9, of which the base is at a level lower than that of the adjacent blocks. The grout curtain is simulated by a band of elements 1 m wide. The drains and piezometers are modelled at the same position and with the same length as the holes drilled in the foundation.

A detailed study of the hydraulic behaviour of the foundation of block 6B-7, where the highest discharges and percentages of hydraulic head are recorded, was carried out. Taking into account the results of water pressure permeability tests performed before the construction of the dam in the area under study it is assumed that the equivalent permeability of the rock mass is $5.0 \times 10^{-7} \text{ m/s}$. The hydraulic conductivity of the grout curtain is assumed to be

5.0×10^{-8} m/s. The dam body is assumed to be impervious. Figure 7.1 a) shows a detail of the mesh below the dam. The study was carried out comparing the numerical results to the monitoring data collected on 4 April 2006. On this date, the recorded discharge at the drains of block 6B-7 was 2.78×10^{-5} (m³/s)/m (1.67 (l/min)/m).

7.2.2 Hydraulic boundary conditions and numerical results

The lateral and bottom model boundaries are impermeable. The reservoir level is 84.71 m and the tailwater level is 60.0 m. Hydrostatic hydraulic heads are applied along permeable boundaries: a constant pressure is assigned at the bottom of the reservoir corresponding to a water height of 33.71 m and downstream from the dam a constant pressure is assigned corresponding to a water height of 0.5 m. Taking into account the high number of piezodrains installed in the foundation of block 6B-7, it is not adequate to assume zero water pressure at the drains head and therefore the average value of the hydraulic heads recorded at the line of the drains (in drains and piezodrains) is assumed at the drainage curtain (65.24 m).

Taking into account the hydraulic boundary conditions described in the previous paragraph, the numerical value of the discharge at the dam drains is about 40 % of the recorded discharge. To match the observed values an average hydraulic conductivity of 22.5×10^{-7} m/s would be needed (4.8 times higher than the assumed equivalent hydraulic conductivity).

A more accurate model of the foundation of block 6B-7 was developed taking into account the existence of tensile stresses at the heel of the dam, due to the filling of the reservoir, which lead to the opening of vertical fissures. To simulate these vertical fissures, a band of elements of higher permeability was assumed upstream from the grout curtain (Figure 7.1 b). The depth of the band of elements is about 20.0 m and the hydraulic conductivity is assumed to be 10.0×10^{-7} m/s. With this model the average discharge at the dam drains is 45 % of the recorded discharge.

Finally, the results of the borehole-water inflow tests performed were taken into account, simulating the area where the main seepage paths cross the drains. A horizontal layer of higher permeability about 4.5 to 7.5 m down from the drain head was considered, as shown in Figure 7.1 c). The hydraulic conductivity of this horizontal layer is assumed to be 60.0×10^{-7} m/s, and therefore the layer, with a height of 3.0 m, simulates a discontinuity with a hydraulic aperture of 0.28 mm. The layer crosses the grout curtain simulating a hypothetical area of the foundation where the total sealing of discontinuities with very small apertures was not achieved. With this model the average discharge at the drain heads, which is 2.86×10^{-5} (m³/s)/m, is almost the same as the recorded discharge. The difference in hydraulic head at two points located around 7.0 m apart along the horizontal layer of higher permeability was used to calculate the quantity of water flowing through that layer. It was

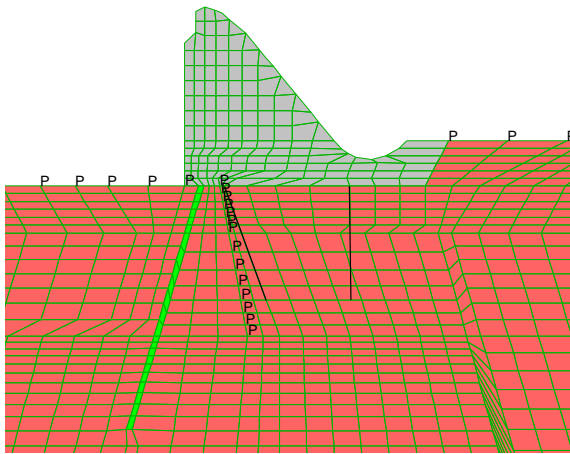
concluded that, with this model, around 40 % of the drain discharge is water that flows through the layer.

The numerical discharges with the three models presented in Figure 7.1 and their difference, in percentage, to the recorded discharge are shown in Table 7.1. Figure 7.2 shows the hydraulic head contours and seepage velocity for the three different models. In the final model, the maximum seepage velocity is about 6.5 times higher than in model b) and around 8.0 times higher than in model a), and therefore, to make the flow patterns visible, the flow vectors are not represented at the same scale. Figure 7.2 shows that there are only changes in the hydraulic head contours close to heel of the dam, with the exception of model c), in which, due to the horizontal layer of higher permeability, the area with a hydraulic head between 64.5 m and 66.0 m extends a little further towards downstream. The seepage pattern, however, changes significantly in model c), in which the highest seepage velocity and the majority of the flow are concentrated in the layer of higher permeability that crosses the grout curtain.

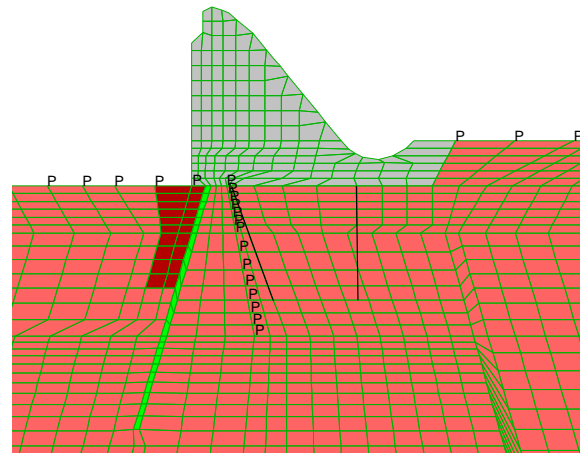
The model shown in Figure 7.1 c) was used to calculate discharges with the reservoir at level 80.67 m. This level was recorded on 1 March 2006, and the average discharge in block 6B-7 was 2.43×10^{-5} (m³/s)/m. It was taken into account that the average value of the hydraulic head recorded on that date was 64.12 m. The numerical discharge is only 1 % higher than that recorded.

The model shown in Figure 7.1 a) was afterwards used to study the hydraulic behaviour of the foundation of blocks 5-6, 6-6A and 6A-6B. No tests were performed in the foundation of these blocks, and therefore it was decided that it would be more adequate to use the simplest model developed. Taking into account the results of water permeability tests it is assumed that the hydraulic conductivity of the rock mass in this area of the foundation is 1.8×10^{-7} m/s. The average value of the hydraulic heads recorded at the line of the drains is 59.15 m. The numerical value of the discharge at the dam drains is 64 % of the recorded discharge. To obtain the recorded discharge, an equivalent hydraulic conductivity of 3.0×10^{-7} m/s would be necessary (1.7 times higher than the assumed equivalent hydraulic conductivity).

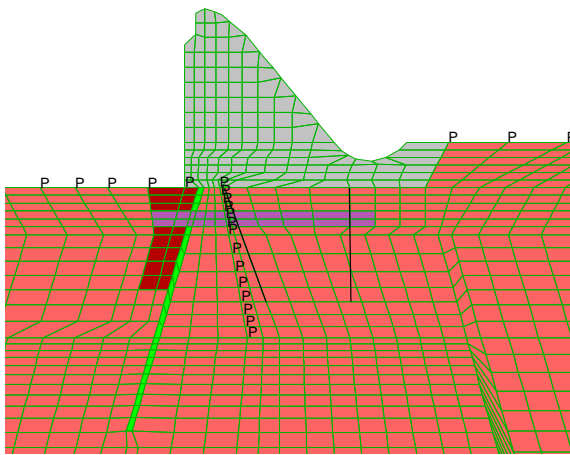
The study presented here shows that the knowledge of the area where the main seepage paths cross the tested boreholes, referred to in chapter 4.4, allowed a more in-depth analysis of the foundation area where both the highest discharges and water pressures are recorded, and the improvement of the developed numerical model.



a) Homogeneous rock mass



b) Homogeneous rock mass with a band of elements of higher permeability upstream from the grout curtain



c) Homogeneous rock mass with bands of elements of higher permeability upstream from the grout curtain and in a horizontal layer about 4.5 to 7.5 m down from the drain head

P – grid points with fixed water pressure

— piezometer

Permeability (cm/s)

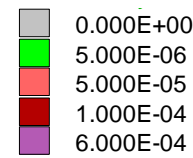


Figure 7.1 – Detail of meshes below the dam for three different models.

Model	Numerical value of the discharge ($\times 10^{-5}$ (m ³ /s)/m)	Percentage of the recorded discharge (%) (2.78×10^{-5} (m ³ /s)/m)
a)	1.11	40
b)	1.24	45
c)	2.86	103

Table 7.1 - Numerical discharges for the three models of Figure 7.1 and comparison to observed value.

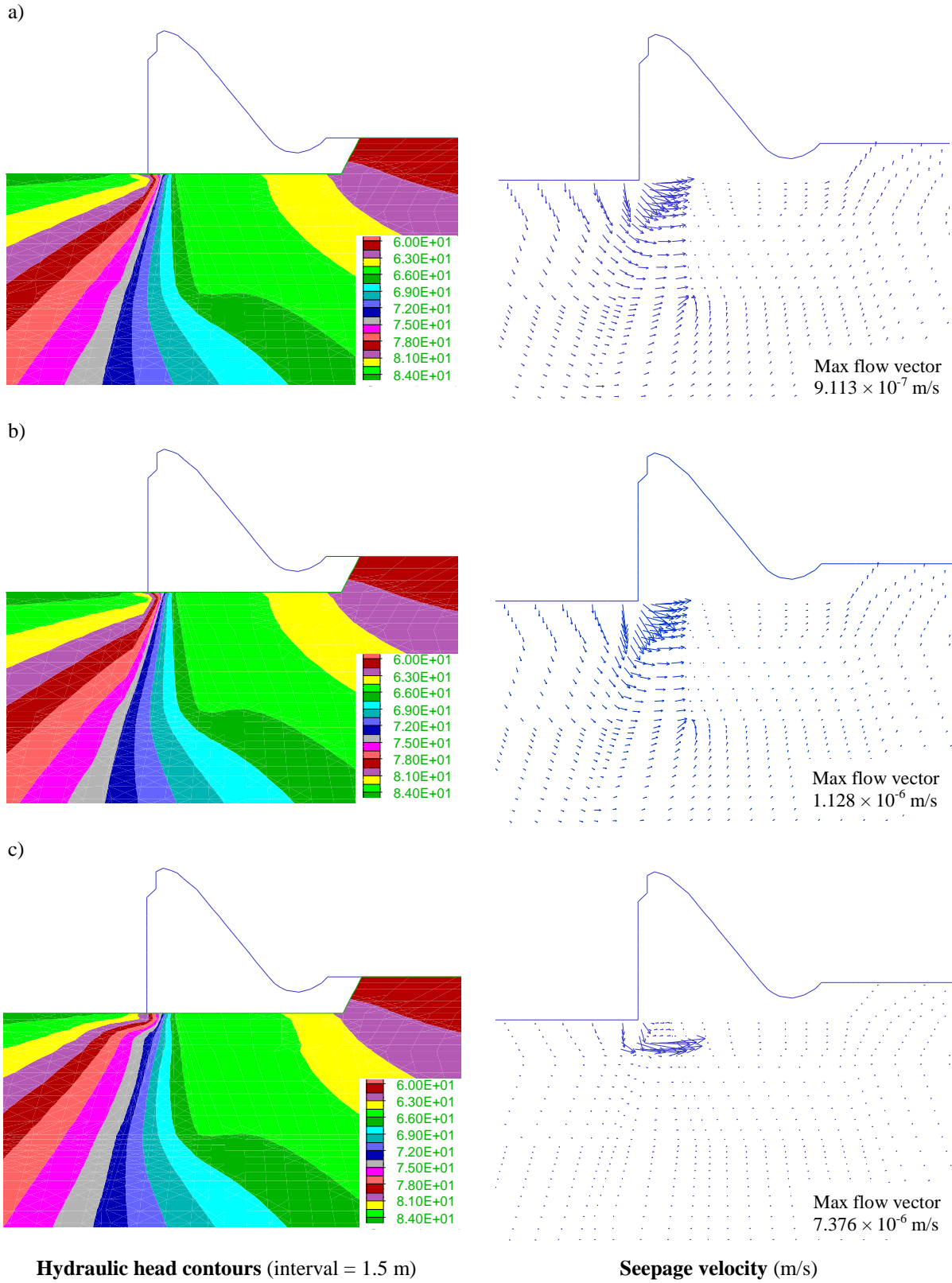


Figure 7.2 – Hydraulic head contours and seepage velocity in the foundation for the three different models shown in Figure 7.1.

7.3 Two-dimensional discontinuum model

7.3.1 Fluid flow analysis with UDEC

UDEC performs a fully-coupled hydromechanical analysis, where fracture conductivity is dependent on mechanical deformation and, conversely, joint water pressures affect the mechanical behaviour (Itasca 2004). Joint apertures and water pressures are updated at every timestep. The algorithm is described by Lemos (1987). It is assumed that rock blocks are impervious and that flow takes place only through the set of interconnecting discontinuities. These are divided into a set of domains, separated by contact points. Each domain is assumed to be filled with fluid at uniform pressure and flow is governed by the pressure differential between adjacent domains.

Flow is modelled by means of the parallel plate model, and the flow rate per unit width is thus expressed by the cubic law. The flow rate through contacts is given by:

$$q = -k_j a^3 \frac{\Delta p}{l} \quad (7.1)$$

where k_j = a joint permeability factor (also called joint permeability constant), whose theoretical value is $1/(12 \mu)$ being μ the dynamic viscosity of the fluid; a = contact hydraulic aperture; l = length assigned to the contact between the domains. The dynamic viscosity of water at 20°C is $1.002 \times 10^{-3} \text{ N}\cdot\text{s}/\text{m}^2$ and therefore the joint permeability factor is $83.3 \text{ Pa}^{-1}\text{s}^{-1}$.

In UDEC, the hydraulic aperture to be used in Equation 7.1 is given by:

$$a = a_0 + \Delta a \quad (7.2)$$

where a_0 = aperture at nominal zero normal stress and Δa = joint normal displacement taken as positive in opening. A minimum value, a_{res} , is assumed for the aperture, below which mechanical closure does not affect the contact permeability. A maximum aperture, a_{max} , is also assumed. Figure 7.3 shows the variation of joint aperture with normal stress, used by default in the code UDEC.

Total stresses are obtained inside the impervious blocks and effective normal stresses at the mechanical contacts. The timestep is limited to a value which is proportional to the domain volume and inversely proportional to the bulk modulus of the fluid and to joint conductivity (Equation 3.3), as explained in section 3.6. In problems in which only the final steady-state condition is of interest, the code UDEC is very efficient, as several simplifications are possible, which accelerate the convergence to the solution.

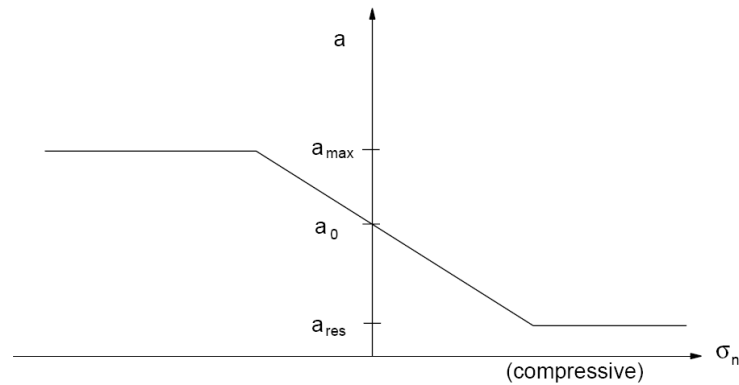


Figure 7.3 – Relation between hydraulic aperture, a , and joint normal stress, σ_n , in UDEC (after Itasca 2004).

7.3.2 Model description

The discontinuous model of Pedrógão dam foundation developed to analyse fluid flow through the rock mass discontinuities is shown in Figure 7.4. A much idealised fracture pattern was assumed. Two sets of discontinuities were simulated: the first joint set is horizontal and continuous, with a spacing of 5.0 m, and the second set is formed by vertical cross-joints, with a spacing of 5.0 m normal to joint tracks and standard deviation from the mean of 2.0 m. The former attempts to simulate the sub-horizontal set of discontinuities **g**) and the latter the sub-vertical set **b**), both of which were referred to in chapter 4 and whose average position in relation to the dam is shown in Figure 4.19. An additional rock mass joint was assumed downstream from the dam dipping 25° towards upstream, necessary to the stability analysis presented in section 7.4.3. The foundation model is 200.0 m wide and 80.0 m deep. The dam has the crest of the uncontrolled spillway 33.8 m above ground level and the base is 44.4 m long in the upstream-downstream direction (Chapter 4.3). In concrete, a set of horizontal continuous discontinuities located 2.0 m apart was assumed to simulate dam construction joints. The numerical model has 611 deformable blocks divided into 2766 zones, and 3451 nodal points.

Both dam concrete and rock mass blocks are assumed to follow elastic linear behaviour, with the properties shown in Table 7.2. Discontinuities are assigned a Mohr-Coulomb constitutive model, complemented with a tensile strength criterion. In a base run, the mechanical properties shown in Table 7.3 were assumed. A construction joint normal stiffness (k_n) of 10 GPa/m corresponds to the assumption that these joints have a width of 3 m of material identical to dam concrete. In the rock mass, the assumed k_n is an average of laboratory test results. A ratio of 0.5 is assumed between normal and shear stiffnesses. Both at the dam construction joints and at the concrete/rock mass interface cohesion and tensile strength were assigned 2.0 MPa. In rock joints, cohesion and tensile strength are assumed to be zero.

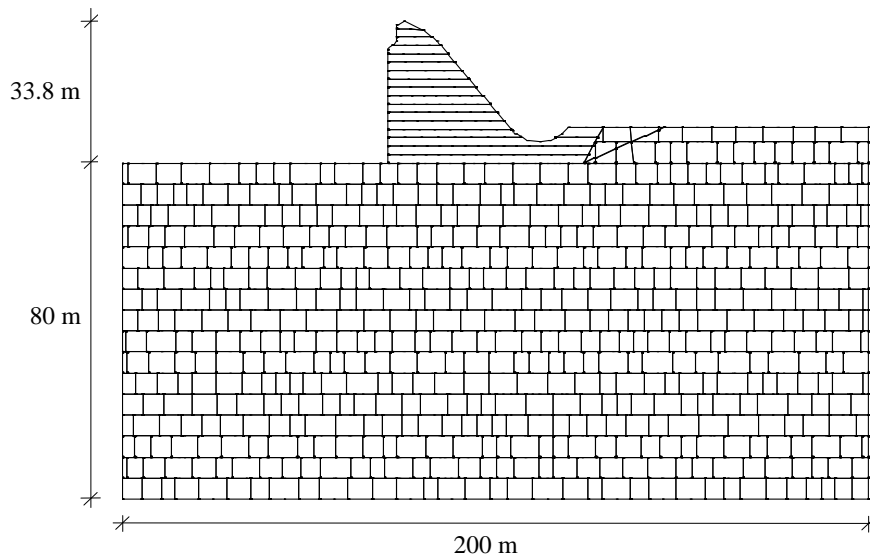


Figure 7.4 – UDEC model of Pedrógão dam foundation.

Material	Density (kg/m ³)	Young's modulus (<i>E</i>) (GPa)	Poisson's ratio -
Dam	2400	30	0.2
Rock blocks	2650	10	0.2

Table 7.2 – Material properties.

Discontinuities	Normal stiffness <i>k_n</i> (GPa/m)	Shear stiffness <i>k_s</i> (GPa/m)	Friction angle <i>φ</i> (°)	Cohesion <i>c</i> (MPa)	Tensile strength <i>σ_t</i> (MPa)
Dam construction joints	10	5	35°	2	2
Rock joints	10	5	35°	0	0
Dam/foundation joint	10	5	35°	2	2

Table 7.3 – Mechanical properties of discontinuities.

7.3.3 Sequence of analysis

Analysis was carried out in two loading stages. Firstly, the mechanical effect of gravity loads with the reservoir empty was assessed. An in-situ state of stress with an effective stress ratio $\sigma_H/\sigma_V = 0.5$ was assumed in the rock mass. The water table was assumed to be at the same level as the rock mass surface upstream from the dam. Secondly, the hydrostatic loading corresponding to the full reservoir was applied to both the upstream face of the dam and

reservoir bottom. Mechanical pressure was first applied, followed by fluid flow analysis. In both stages, vertical displacements at the base of the model and horizontal displacements perpendicular to the lateral model boundaries were prevented. Regarding hydraulic boundary conditions, joint contacts along the bottom and sides of the model were assumed to have zero permeability. On the rock mass surface, the head was 33.8 m upstream from the dam, and 5.0 m downstream.

In order to adjust joint flow properties, the model was first run without grout curtain and with no drainage system and the results were compared with those obtained with a FLAC model similar to that shown in Figure 7.1 a), but with no grout curtain or drains. The UDEC model was slightly changed for this comparison, adopting a regular joint pattern in the whole foundation with the rock mass horizontal joint closest to the dam/foundation interface located 2.5 m away from the interface, instead of 5.0 m. Regular joint patterns do not simulate water flow in dam foundations properly because, in reality, discontinuities are not regular. However, in this way the UDEC model is more similar to a continuum model. The equivalent permeability of the rock mass is assumed to be 5.0×10^{-7} m/s, as in the FLAC model. The correlation between this and the joint coefficient of permeability, k_f , is given by:

$$k_{rock\ mass} = \frac{k_f}{d} \quad (7.3)$$

where d is the spacing of discontinuities and:

$$k_f = \frac{g a^2}{12 \nu} \quad (7.4)$$

The joint coefficient of permeability is thus 25.0×10^{-7} m/s, and the hydraulic aperture of discontinuities is 0.1457 mm. Assuming this as a constant aperture in all the discontinuities (UDEC disregards the interaction between hydraulic and mechanical effects and performs a simple hydraulic analysis if the joint aperture is assigned to a_{res} and (-1) is assigned to a_0), the quantity of water that flows through the UDEC model (0.77×10^{-5} (m³/s)/m) is almost the same as that in the FLAC model (0.78×10^{-5} (m³/s)/m). This result may seem incoherent because the FLAC mesh is finer and therefore drain discharges should be lower. However, in the UDEC mesh, seepage occurs through the domains (in UDEC, a “domain” is a segment of a joint, as explained in section 3.6), so the path through which water must flow is longer. Longer paths lead to greater losses of hydraulic head and, consequently, to lower discharges. In order to analyse seepage in the foundation of Pedrógão dam with the code UDEC a finer mesh should be used. For the safety assessment, however, a coarse mesh with an average zone size of 5.0 m × 5.0 m is sufficient.

The grout curtain was simulated by changing the permeability of the joints in the grouted area, in such a way that it is 10 times less pervious than the surrounding rock mass, as in the FLAC model. In this latter model the grout curtain was simulated by a band of elements 1 m wide. Here, the joint pattern is not regular, and thus the grouted area has different widths at different levels. The joint permeability constant at the grouted area was estimated taking into account the average width of the grout curtain, which is 3.94 m: as the grout curtain is wider than in the FLAC model, the permeability has to be greater. The dam/foundation interface was assumed to be two times less pervious than rock joints, because it involves only to 2.5 m of rock mass foundation in the vertical direction. At the grouted area, the permeability of the dam/foundation interface was also reduced by half. The drainage system was simulated by assigning domain water pressures along the drain axis, equivalent to 1/3 of the sum of the reservoir and tailwater hydraulic heads. Care was taken in order to define the drainage system without including rock mass vertical joints. At this stage of the modelling process, results were compared with those obtained with the FLAC model shown in Figure 7.1 a). In this latter model, the numerical value of the discharge at the dam drains was about 40 % of the recorded discharge whereas in the UDEC model, it is around 49 %. Finally, to simulate the main flow path, the horizontal discontinuity located 5.0 m below the dam/foundation interface was assumed to be more pervious than the other rock mass discontinuities, in the same area as that assumed in the FLAC final model (Figure 7.1 c). In the code UDEC, the permeability of a given joint can be changed either by varying the joint aperture, or by multiplying the theoretical value of the joint permeability factor (k_j) by another factor (α). The latter was used in this analysis and thus the joint permeability factor (k_j) in the layer of higher permeability was adjusted in order for the numerical drain discharge to be the same as that recorded. The adjusted joint permeability factor assumed in the various discontinuities is shown in Table 7.4.

Hydromechanical analysis was afterwards carried out with the following apertures: $a_0 = 0.1668$ mm and $a_{res} = 0.05$ mm, a_0 being the aperture that led to the recorded discharge.

Discontinuities	Joint permeability factor ($\times 10^8 \text{ MPa}^{-1} \text{ s}^{-1}$)
Dam construction joints	0.0
Rock joints	0.83
Rock joints in the grouted area	0.327
Dam/foundation joint	0.415
Dam/foundation joint at the grouted area	0.16351
Horizontal discontinuity of higher permeability	6.8475

Table 7.4 – Joint permeability factor in discontinuities.

To take into account the uncertainty in joint normal stiffness, new analysis was carried out assuming rock masses with different deformability (k_n 5 times higher and 5 times lower than that assumed in the base run). Using equation 6.17, the rock mass in which the normal stiffness of discontinuities is assumed to be 2 GPa/m has an equivalent deformability of 5 GPa, that with $k_n = 10$ GPa/m an equivalent deformability of 8.33 GPa and the stiffest foundation, with $k_n = 50$ GPa/m, an equivalent deformability of 9.6 GPa (Table 7.5). In every run, the same a_{max} and a_{res} were assumed and a_0 was that which, in each analysis, led to the recorded discharge ($a_0 = 0.1313$ mm for $k_n = 50$ GPa/m and $a_0 = 0.4287$ mm for $k_n = 2$ GPa/m). In this way, the same situation is simulated with different models, which enables comparison of water pressures and apertures along the base of the dam or along other rock mass discontinuities.

7.3.4 Results analysis

7.3.4.1 Stresses and displacements due to both rock mass and dam weight

At the first stage of analysis, stresses due to both rock mass and dam weight were obtained (Figure 7.5). Analysis started from a given linear state of stress, close to the *in situ* state of stress due to rock mass weight. It was thus assumed that the vertical *in situ* stress was the weight of the overburden, using the rock mass surface upstream from the dam as the reference level, and that the ratio of horizontal to vertical stresses was 0.5. Results show a realistic stress pattern with vertical stresses increasing with depth. In foundation blocks close to the base of the dam, stresses are higher below the heel of the dam, where an average compressive stress of around 0.83 MPa is determined, which is of the same order as that roughly estimated due to dam weight ($2400 \text{ kg/m}^3 \times 10 \text{ m/s}^2 \times 34 \text{ m} = 0.8 \text{ MPa}$). Displacements at this phase of analysis are shown in Figure 7.6. These displacements are only due to the dam weight and to the weight of the upper part of the rock mass, downstream from the stilling basin (rock mass at an elevation higher than the above-mentioned reference level). The crest of the dam moves downwards and towards upstream, with a displacement of 4.3 mm.

7.3.4.2 Hydrostatic loading

Principal stresses at the second phase of analysis are shown in Figure 7.7 and displacements of the dam/foundation system are shown in Figure 7.8. As expected, stresses on the rock mass surface upstream from the dam increase, as do those in the downstream area of the dam close to the stilling basin. Below the heel of the dam, close to the dam/foundation interface, stresses decrease by around 0.3 MPa, due to dam load and consequent dam rotation towards downstream. Gridpoint displacements were reset at the beginning of this loading stage, thus displacements shown are due only to hydrostatic loading. At the crest of the dam the displacement is practically horizontal and is 1.87 mm.

Joint normal stiffness (kn) (GPa)	Equivalent deformability (GPa)
2	5
10	8.33
50	9.6

Table 7.5 – Equivalent deformability of the assumed rock masses.

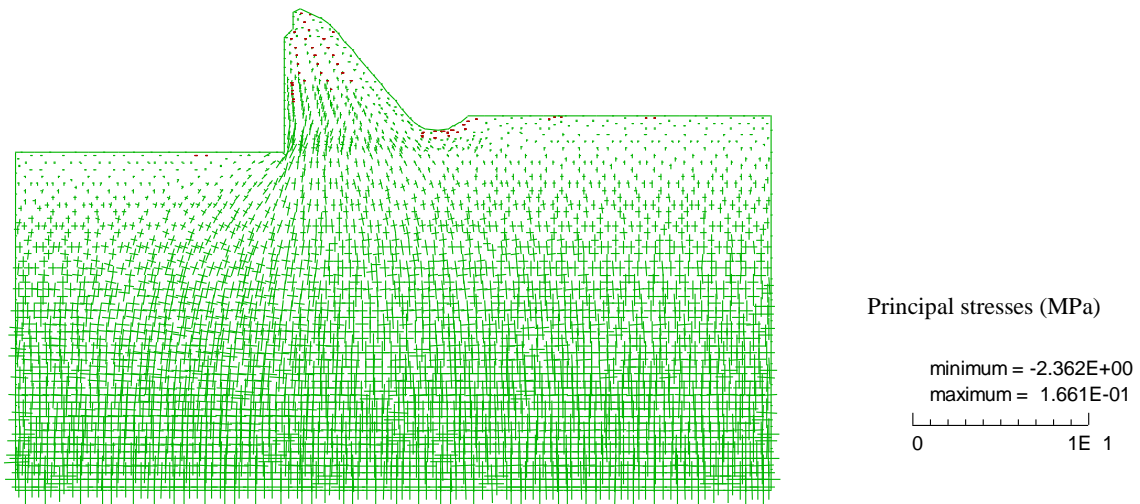


Figure 7.5 – Principal stresses due to both rock mass and dam weight.

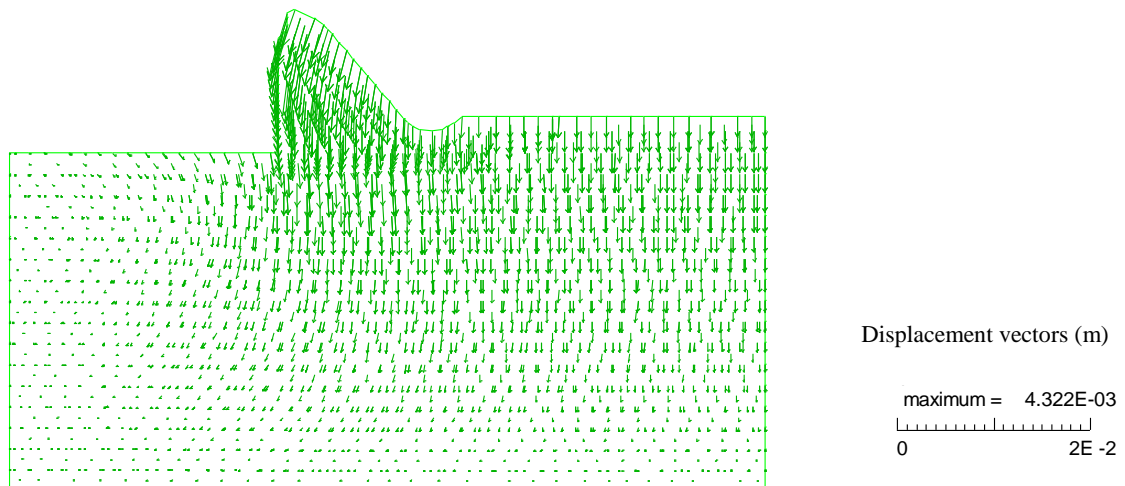


Figure 7.6 – Displacements due to both dam weight and the weight of the upper part of the rock mass, downstream from the stilling basin.

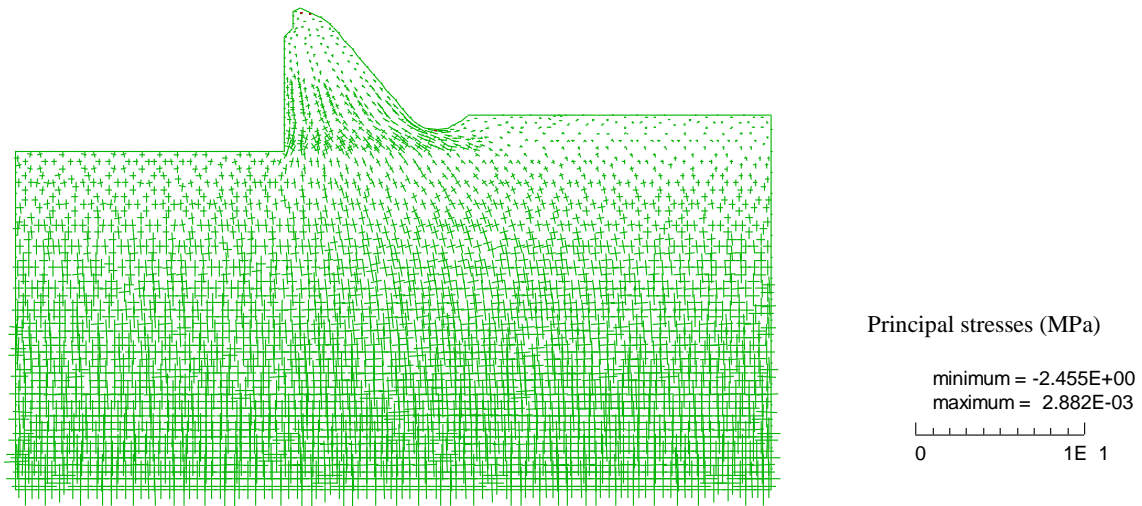


Figure 7.7 – Principal stresses after hydrostatic loading.

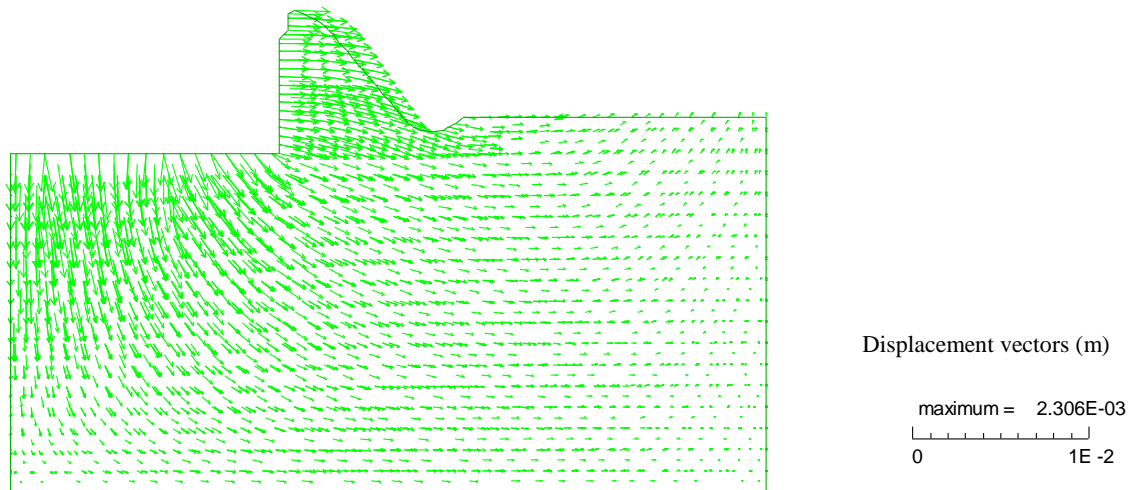


Figure 7.8– Displacements due to hydrostatic loading.

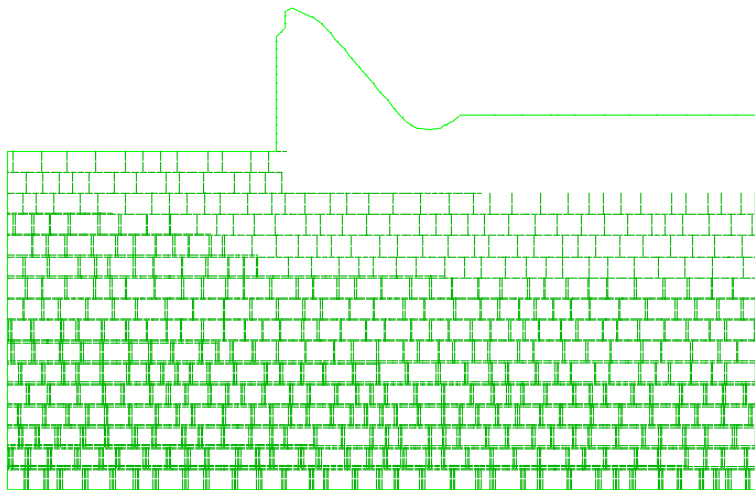
7.3.4.3 Fluid flow analysis

Results of fluid flow analysis both with constant joint hydraulic aperture and taking into account the hydromechanical interaction (HM interaction) are shown in Figure 7.9 and Figure 7.10. In these figures, the line thickness is proportional to the pressure and to the flow rate in the fracture, respectively. When the coupling between stress and flow is taken into account, domain water pressures are higher in the foundation area upstream from the dam and lower in the downstream area, and the maximum water pressure is around 10 % higher (Figure 7.9 a and b). Without drainage, domain pressures increase below the dam (Figure 7.9 c). The flow pattern in steady-state conditions shows that the majority of the flow is concentrated in the first two vertical joints upstream from the heel of the dam, and that this water flows towards

the drain, or towards downstream in the foundation with no drainage system, along the joint of higher permeability that crosses the grout curtain (Figure 7.10). When the HM interaction is taken into account, flow rates are higher at lower levels and a higher quantity of water flows into the model through the second vertical joint upstream from the heel of the dam, rather than through the first as is the case in the run where joint aperture remains constant. This depends on the increase in water pressure in a given vertical joint, which causes the closure of adjacent vertical joints. The maximum flow rate is slightly higher when the interaction is taken into account (it varies from around 1.21 to 1.25 (l/min)/m). Flow rates below 3.0×10^{-6} (m³/s)/m (0.18 (l/min)/m) are not represented. The quantity of water that flows through the model in the analysis with no drainage system and constant joint aperture is 0.57 (l/min)/m. This increases by around 248 %, to 1.40 (l/min)/m, in the case of the most deformable foundation, and decreases by around 26 %, to 0.42 (l/min)/m, in the case of the stiffest foundation. Figure 7.11 shows a detail of dam and foundation deformation due to a) dam weight and the weight of the upper part of the rock mass, downstream from the stilling basin; b) hydrostatic loading and flow; and c) both the above-mentioned effects together. In this figure block deformation is magnified 3000 times.

Figure 7.12 shows the joints that are at shear limit, those with zero normal force or stress and the magnitude of joint separation due to mechanical deformation, for the three foundation models with different deformability, taking into account the HM interaction. Analogous results are shown in Figure 7.13 for the same foundations, this time with no drainage system.

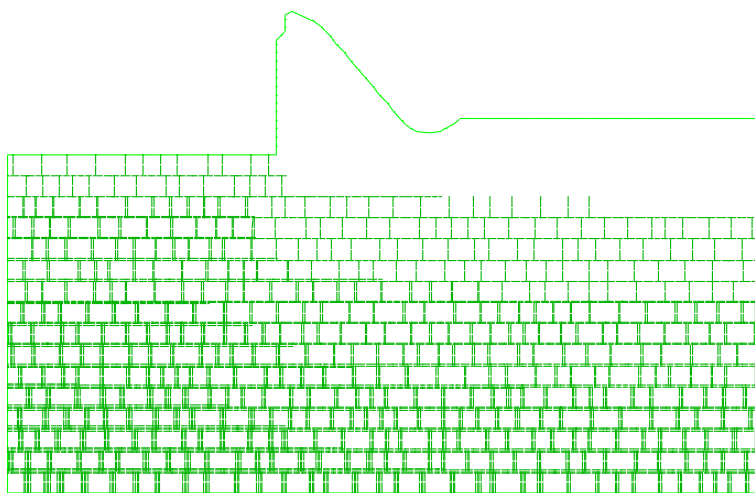
Figure 7.12 shows that some sliding occurs in the upper part of the rock mass joint dipping 25° towards upstream, that the number of vertical joints that are at shear limit increases towards downstream for stiffer foundations, and, as expected, that joint separation is lower for less deformable foundations. In the three different foundation models, the second joint upstream from the heel of the dam has an aperture due to mechanical deformation higher than the first, because it is linked to the two lower vertical joint tracks in a nearly continuous line, as can be seen in Figure 7.4, which makes joint opening easier. Without drainage, the number of vertical joints at shear limit and with zero normal force or stress increases towards downstream and goes down to deeper foundation areas (Figure 7.13). In this case, the first horizontal joint below reservoir bottom, which has an area of higher permeability to simulate the main flow path, is at shear limit below the downstream area of the base of the dam.



a) constant joint aperture

Domain water pressures
(MPa)

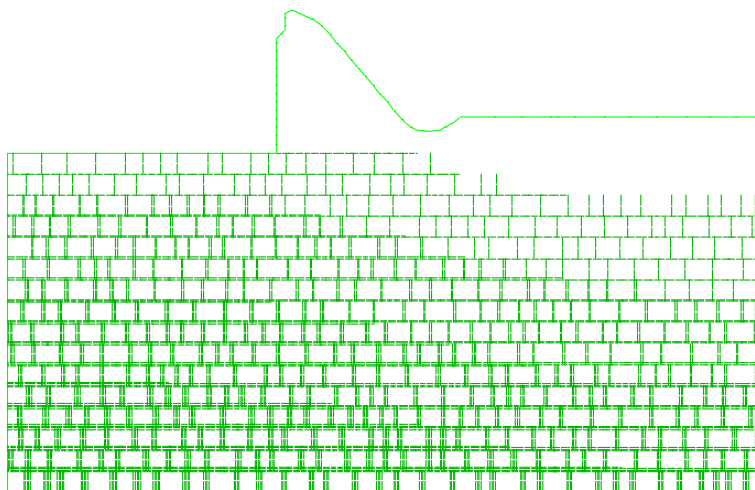
maximum pressure= 1.002E+00
each line thick = 2.200E-01



b) hydromechanical interaction

Domain water pressures
(MPa)

maximum pressure= 1.107E+00
each line thick = 2.200E-01



c) hydromechanical interaction, no drainage system

Domain water pressures
(MPa)

maximum pressure= 1.110E+00
each line thick = 2.200E-01

Figure 7.9 – Domain water pressures for full reservoir with a) constant joint aperture, b) hydromechanical interaction with drainage system and c) without drainage system (pressure is proportional to line thickness).

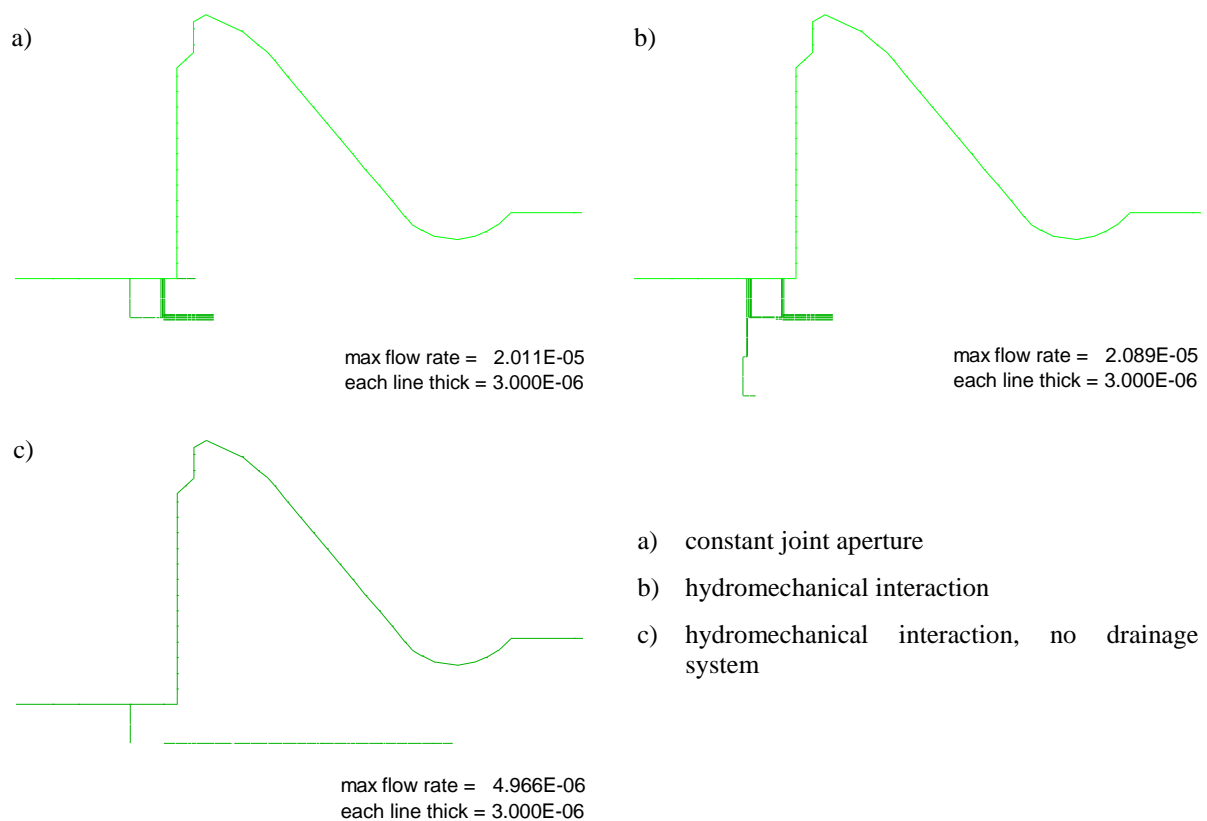


Figure 7.10 – Flow rates for full reservoir (flow rate is proportional to line thickness; flow rates below 3.0×10^{-6} (m³/s)/m (0.18 (l/min)/m) are not represented).

7.3.4.4 Normal displacements and hydraulic aperture along the dam/foundation joint

The normal displacement along the dam/foundation joint in both phases of analysis and for the different rock masses is shown in Figure 7.14. The jagged shape of the curves is due to block rotation, and the magnitude of normal displacement depends on the normal stiffness of discontinuities. In the first phase of analysis the point at which the dam/foundation joint closes more is below the heel of the dam, due to dam weight, as shown in Figure 7.11 a). In the foundation in which the joint normal stiffness is 10 GPa/m, joint closure at this point is 0.221 mm. Taking this as reference, joint closure is around 3.7 times greater in the most deformable foundation, in which $k_n = 2$ GPa/m, and 3.8 times lower in the stiffest foundation. In the second phase of analysis, water pressures cause both a decrease in normal displacements and an increase in blocks rotation. The peaks like those highlighted with *, which are more evident on the chart concerning the stiffest foundation, are due to the numerical discretization, because the upper corners of the foundation blocks do not coincide with the grid-points of the internal mesh of the dam deformable block adjacent to the dam/foundation interface.

Figure 7.15 shows the hydraulic aperture of the dam/foundation joint in the studied situations, given by Equation 7.2, with a_{res} as the minimum value. The initial aperture used for each foundation is also represented. In the most deformable foundations, the contact at the heel of the dam is at a_{res} (0.05 mm), which means that the dam weight is higher than water pressure. This does not happen in the same foundations with no drainage system, due to higher water pressures.

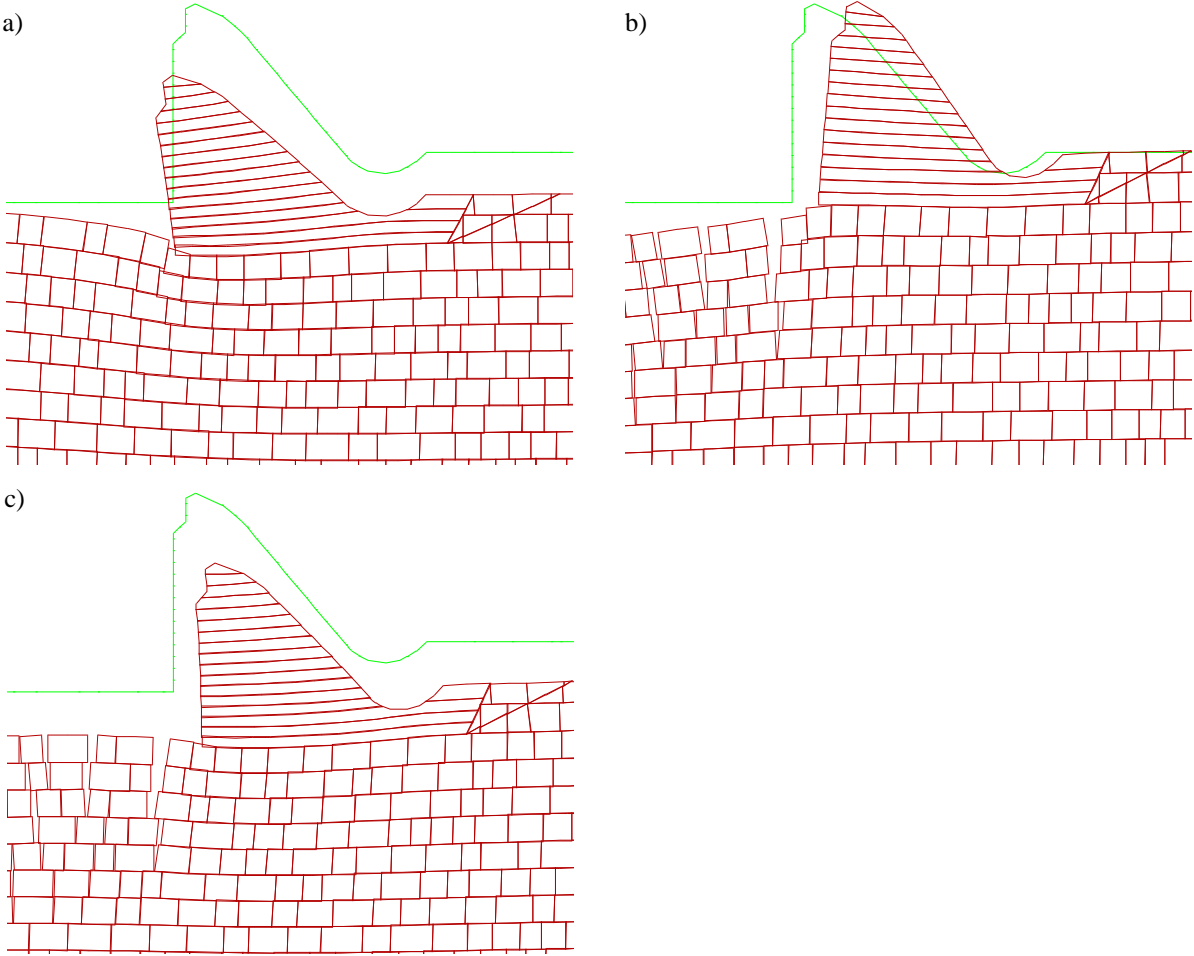
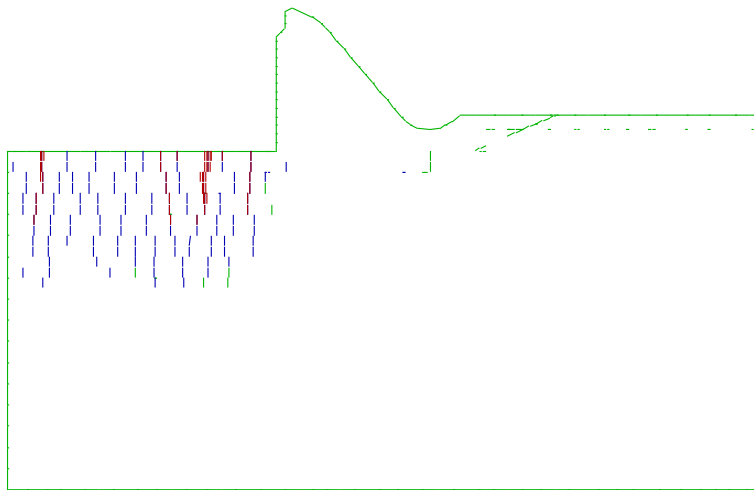
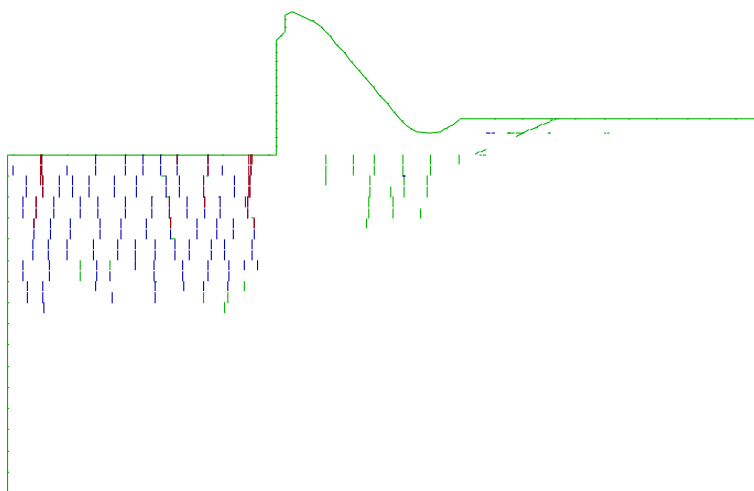


Figure 7.11 – Block deformation (magnified 3000 times) due to: a) both dam weight and the weight of the upper part of the rock mass, downstream from the stilling basin; b) hydrostatic loading and flow; c) both effects shown together.



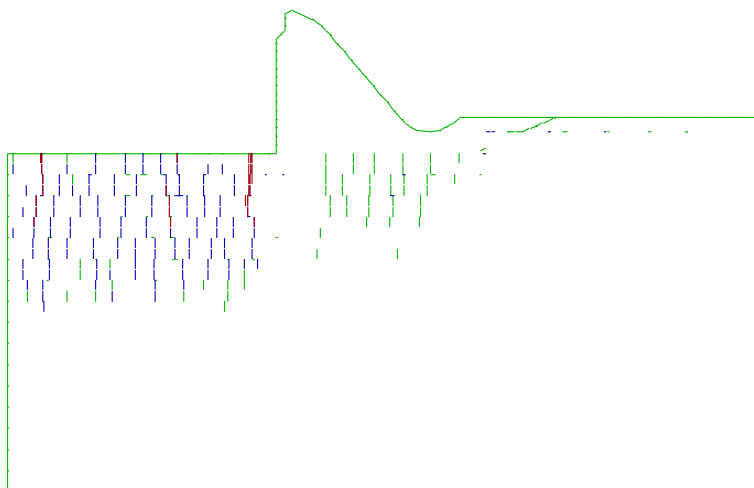
a) $k_n = 2$ GPa/m

joints now at shear limit
 joints with FN or SN = 0.0
 joint opening
 max jnt opening = 1.611E-03
 each line thick = 3.000E-04



b) $k_n = 10$ GPa/m

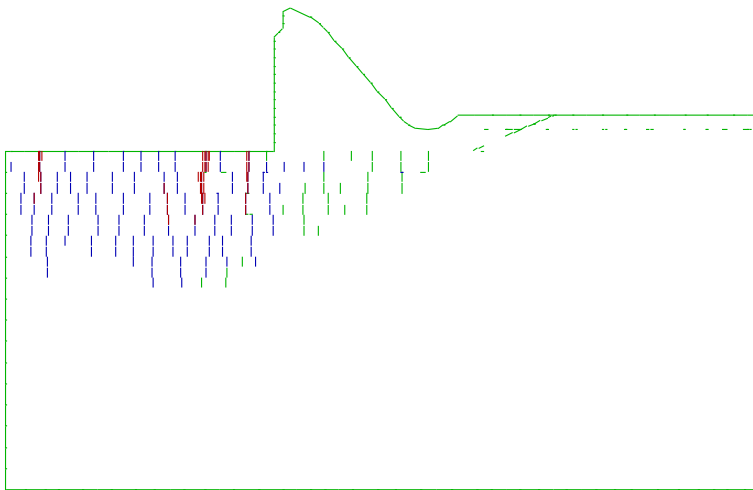
joints now at shear limit
 joints with FN or SN = 0.0
 joint opening
 max jnt opening = 9.359E-04
 each line thick = 3.000E-04



a) $k_n = 50$ GPa/m

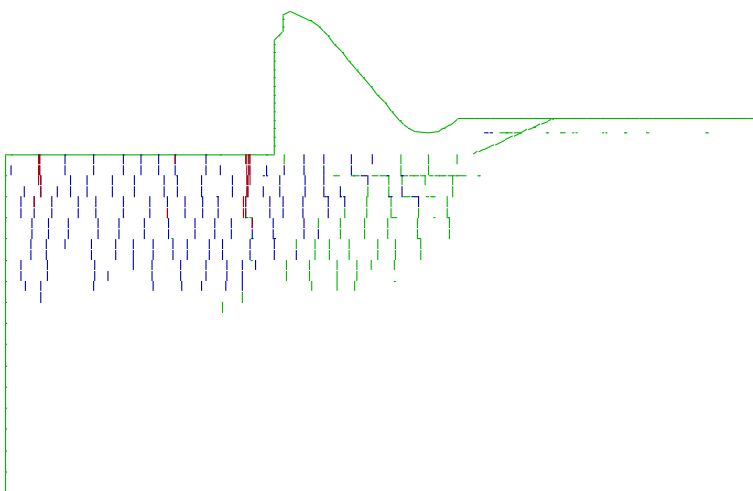
joints now at shear limit
 joints with FN or SN = 0.0
 joint opening
 max jnt opening = 1.100E-03
 each line thick = 3.000E-04

Figure 7.12 – Joints at shear limit (green), joints with zero normal force or stress (blue) and magnitude of joint separation (red), for rock masses with different deformability (joint separation is proportional to line thickness).



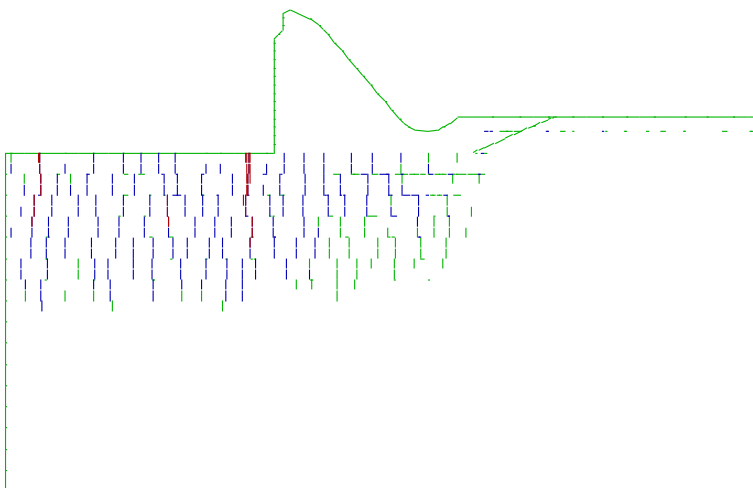
a) $k_n = 2$ GPa/m, no drainage system

joints now at shear limit
 joints with FN or SN = 0.0
 joint opening
 max jnt opening = 1.646E-03
 each line thick = 3.000E-04



b) $k_n = 10$ GPa/m, no drainage system

joints now at shear limit
 joints with FN or SN = 0.0
 joint opening
 max jnt opening = 1.381E-03
 each line thick = 3.000E-04



a) $k_n = 50$ GPa/m, no drainage system

joints now at shear limit
 joints with FN or SN = 0.0
 joint opening
 max jnt opening = 1.345E-03
 each line thick = 3.000E-04

Figure 7.13 - Joints at shear limit (green), joints with zero normal force or stress (blue) and magnitude of joint separation (red), for rock masses with different deformability, with no drainage system (joint separation is proportional to line thickness).

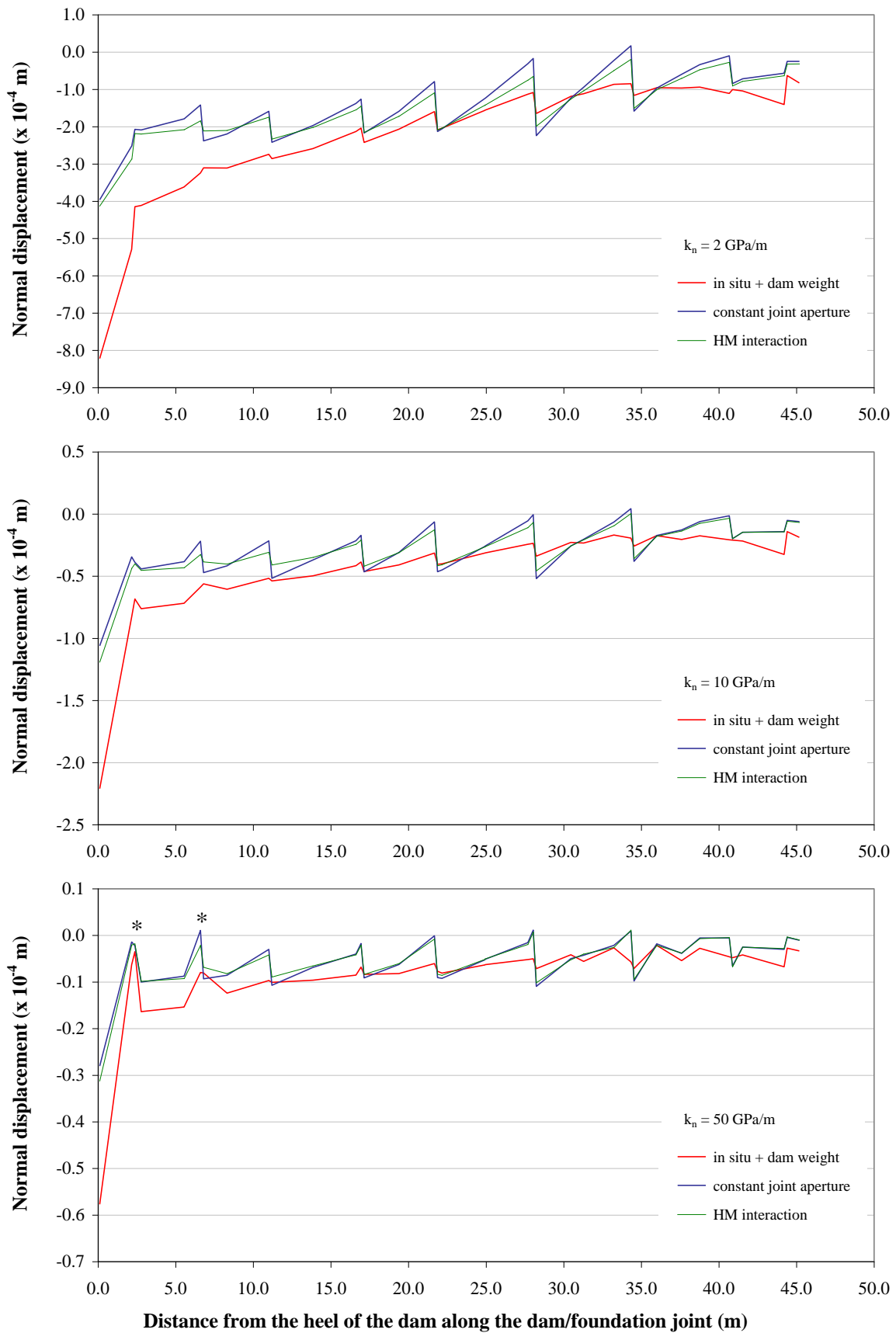


Figure 7.14 – Normal displacement along the dam/foundation joint.

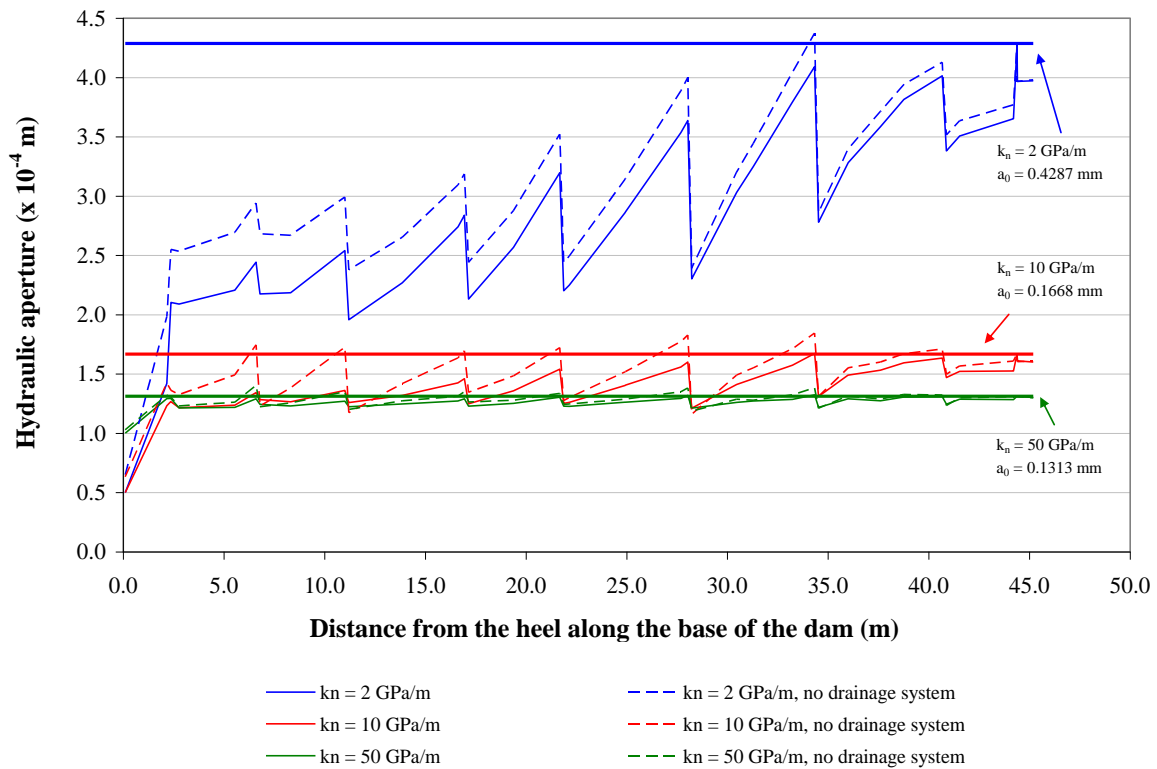


Figure 7.15 – Hydraulic aperture of the dam/foundation joint.

7.3.4.5 Water pressures along the dam/foundation joint and along the joint of higher permeability

The uplift water pressure along the dam base is always of concern to the stability of concrete dams and is usually prescribed in design codes assuming a bi-linear uplift distribution to account for the relief drains. The variation of water pressures along the dam/foundation joint and along the first horizontal joint below the dam in the area of higher permeability is shown in Figure 7.16. Results obtained with the foundations of different deformability are presented. In the hydraulic analysis in which the HM effect is not taken into account, variations in uplift pressures along both the interface and the foundation discontinuities are the same regardless of the foundation deformability, because the joint hydraulic aperture remains constant. Figure 7.16 shows that variations in water pressures are highly dependent on the pressure on the drainage line. Upstream from this line, water pressures are higher for more deformable foundations. Downstream from the drainage line, on the contrary, water pressures are higher for stiffer rock masses. Along the dam/foundation joint, if all the drains are clogged, the highest water pressures are obtained with the stiffest foundation, and the lowest with the most deformable rock mass.

Figure 7.17 shows a comparison of water pressures along the dam/foundation joint with both bi-linear and linear uplift distribution, usually used in stability analysis of dams with and

without drainage systems, respectively. In the case of drained foundations, the water pressure curves are close to the bi-linear distribution. In this case, computed water pressures between the heel of the dam and the drainage line are lower than those given by the bi-linear distribution, whereas between the drainage line and the toe of the dam they are higher, except for the most deformable foundation. In the case of the stiffest foundations with no drainage system, calculated uplift pressures are lower than those obtained with the linear distribution, to a distance of around 8.0 m from the heel of the dam, and downstream from this point they are considerably higher. At the dam/foundation joint end close to the toe of the dam, UDEC water pressures are higher than those assumed with the linear distribution of pressures, due to the presence of the rock wedge downstream from the dam. For the most deformable foundation, the linear distribution of uplift pressures greatly overestimates pressures along the base of the dam, with the exception of an area with a length of around 6.0 m, close to the toe of the dam.

7.3.4.6 Joint dilatancy

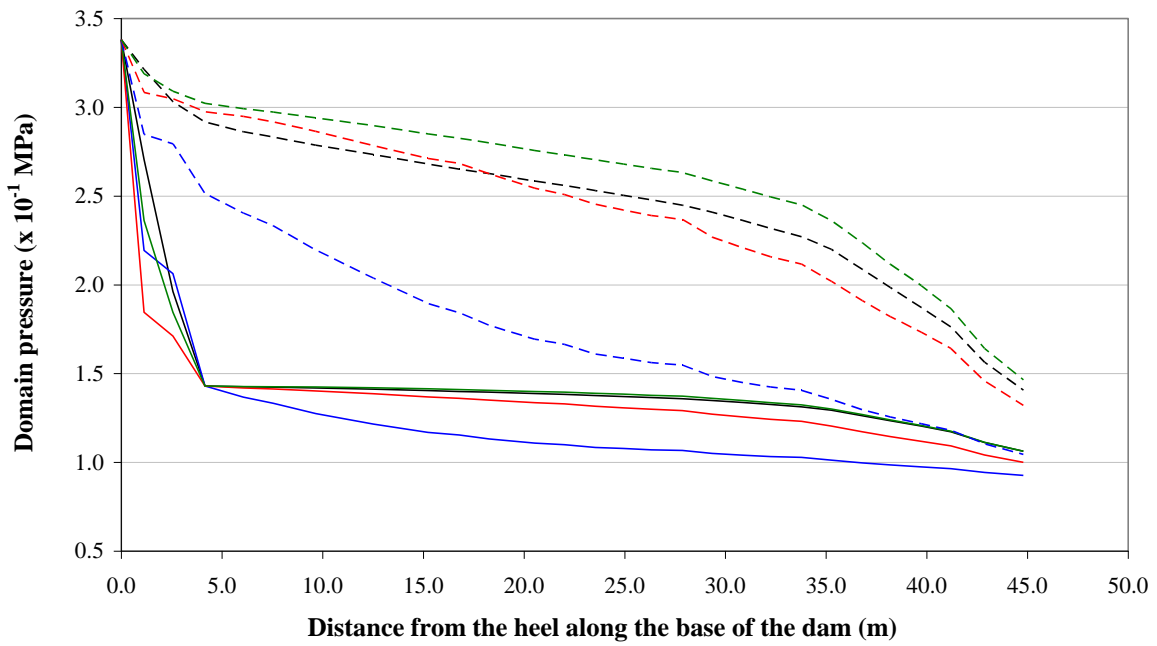
Joint dilation is effective when the joint is slipping and can be modelled in different ways. The simplest way is by specifying a dilation angle and the dilation increases indefinitely irrespective of the joint loading path (Figure 7.18 a). In the UDEC code the normal displacement increment due to dilation, is calculated as:

$$\begin{aligned} \Delta u_n^d &= \tan i \Delta u_s \operatorname{sign} u_s && \text{if } |u_s| < z_{dil} \\ \Delta u_n^d &= 0 && \text{if } |u_s| > z_{dil} \end{aligned} \quad (7.5)$$

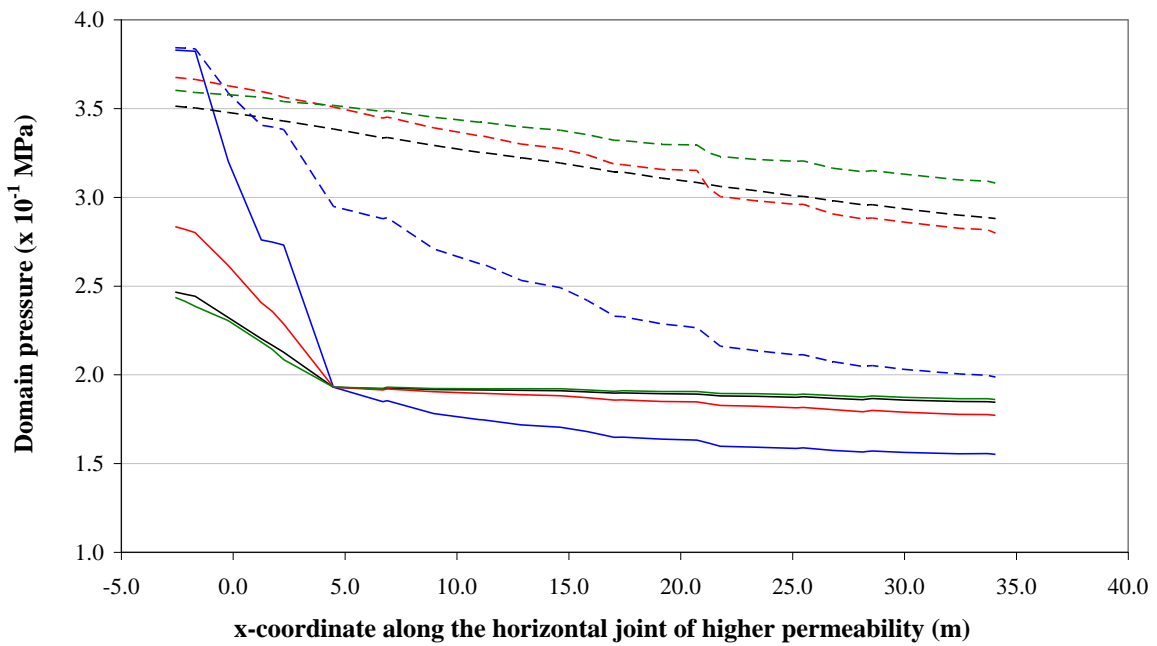
where z_{dil} is a parameter that allows the control of maximum dilation. Dilation is zero for shear displacements higher than z_{dil} (Figure 7.18 b) and is positive if the shear displacement increment (Δu_s) is in the direction of the total shear displacement (u_s), and negative otherwise. As mentioned in Chapter 2, the separation during shear displacement due to dilation causes an increase in joint hydraulic apertures and consequently, an increase in joint permeability.

In the analysis presented in the preceding sections, hydrostatic loading corresponding to full reservoir was applied in a single stage. However, due to the non-linear effects, hydrostatic loading is better applied in small increments, and therefore, to investigate the dilation effect, hydrostatic loading was applied in increments of 5 m. The effect of dilatancy on discharges in a loading cycle was analysed, using a dilatancy angle of 10° . In this case, shear displacements are small and thus the effect of dilatancy is small. Analysis led to the conclusion that the discharge is the same for the full reservoir level in the foundations in which it is assumed that $k_n = 10 \text{ GPa/m}$ and $\varphi = 30^\circ$. However, if a friction angle (φ) equal to 15° is assumed, joint sliding increases and thus the dilation effect is more evident (Figure 7.19). However, a friction angle of 15° is too low, and not likely to occur in practice.

a)



b)



- constant joint aperture
- — — constant joint aperture, no drainage system
- HM interaction (kn = 2 GPa/m)
- HM interaction, no drainage system (kn = 2 GPa/m)
- HM interaction (kn = 10 GPa/m)
- HM interaction, no drainage system (kn = 10 GPa/m)
- HM interaction (kn = 50 GPa/m)
- HM interaction, no drainage system (kn = 50 GPa/m)

Figure 7.16 - Water pressure along the a) dam/foundation joint and b) joint of higher permeability.

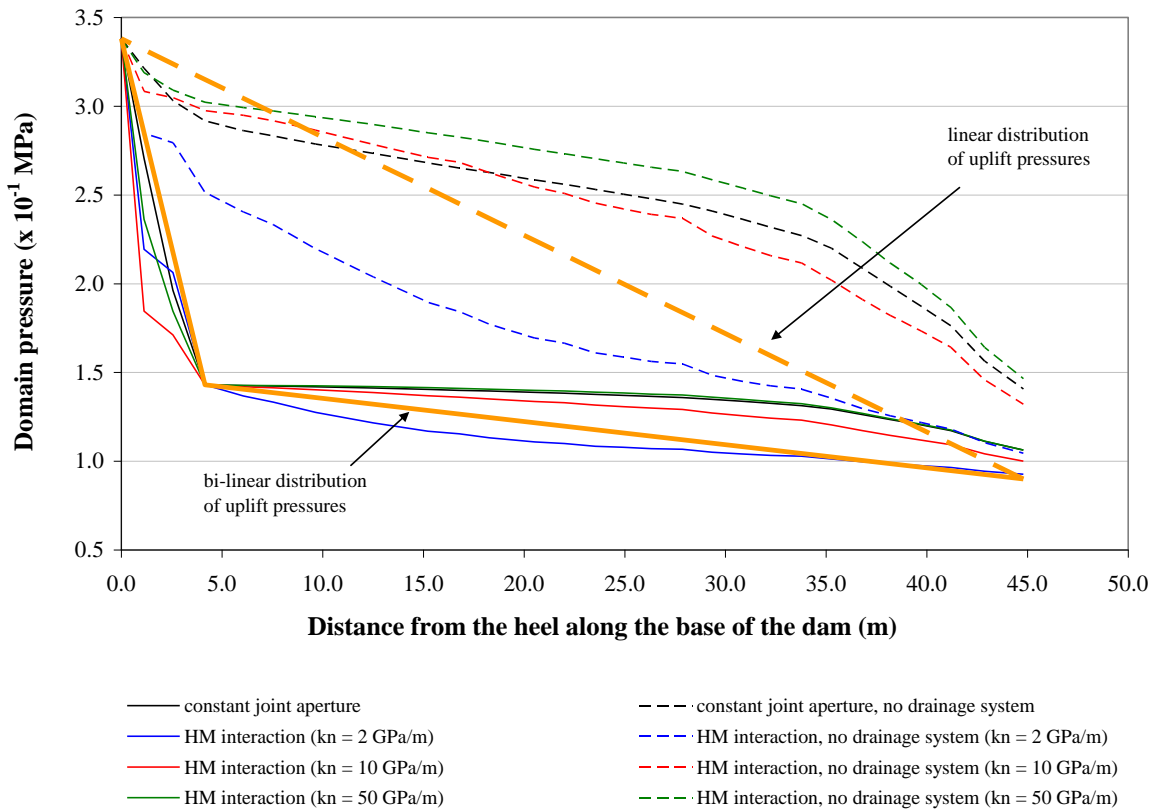


Figure 7.17 – Comparison of water pressures along the dam/foundation joint with both bi-linear and linear distribution of water pressures.

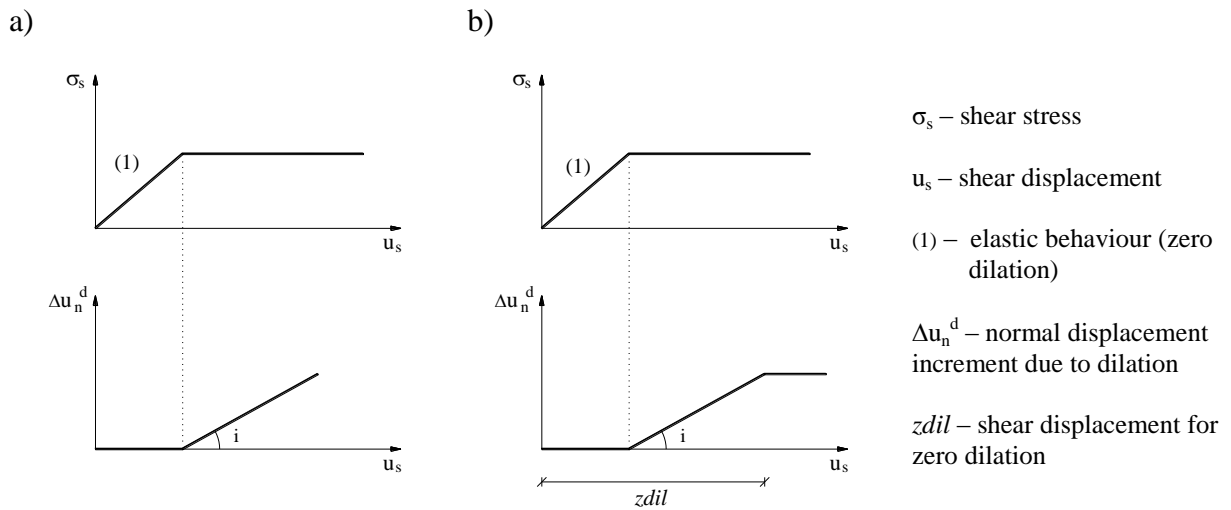


Figure 7.18 – Models for joint dilation: a) the dilation increases indefinitely; b) UDEC model.

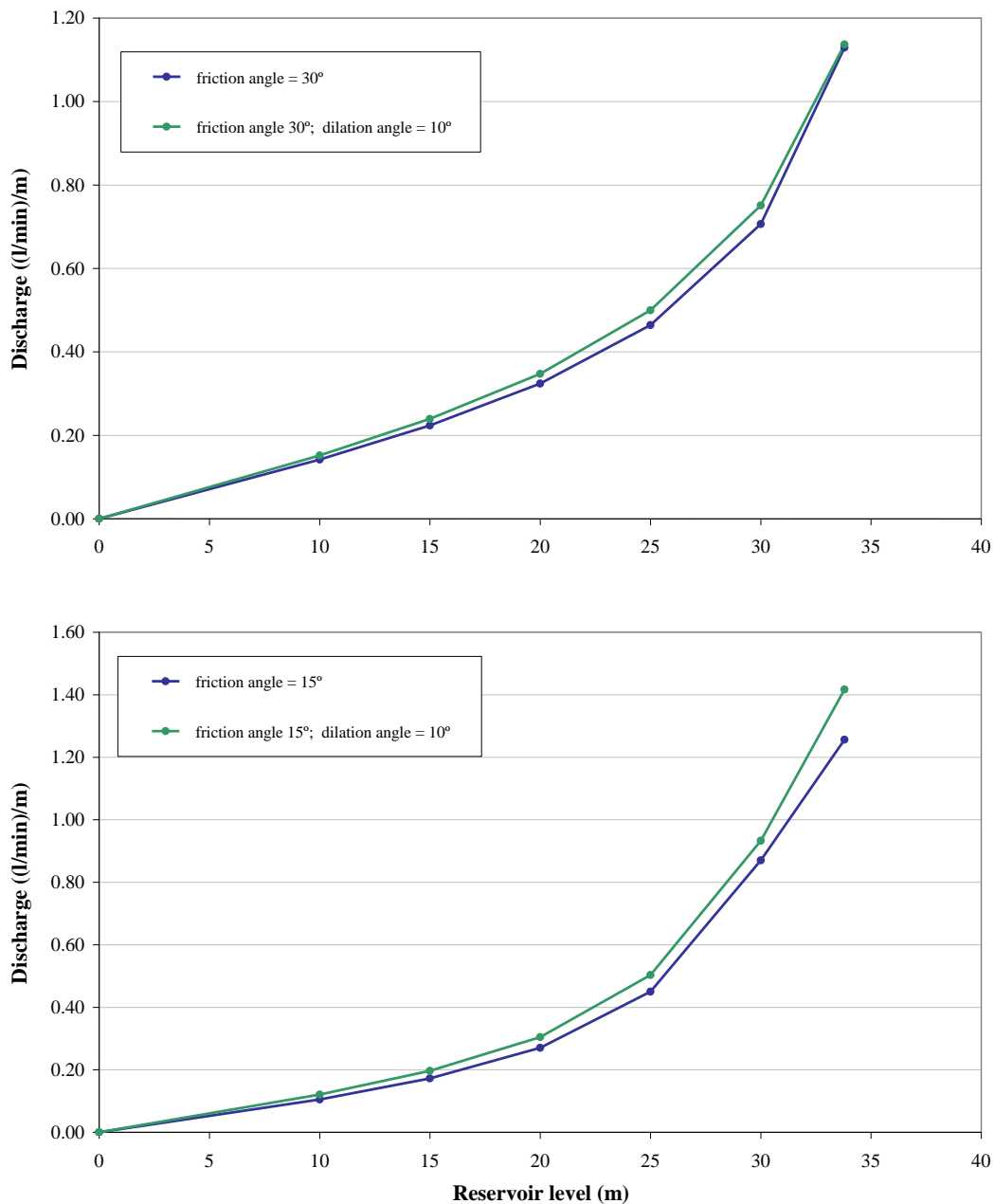


Figure 7.19 – Drain discharges during the filling of the reservoir both without and with joint dilation effect for two different joint friction angles.

7.3.5 Comparison of monitored and numerical hydraulic heads at the piezometers located underneath the stilling basin

There are vertical boreholes with two piezometric chambers located in blocks 4B-5, 5B-6, 6A-6B and 7-8, in the downstream area, underneath the stilling basin (Figure 4.21). Figure 7.20 shows the hydraulic head in these piezometers plotted versus time. The length of piezometric chambers varies from 0.75 m to 2.55 m. Figure analysis shows that the hydraulic

head varies with changes in the reservoir level and that it is higher in the piezometric chambers located at lower levels, further away from the dam/foundation interface. This variation is approximately linear, although readings are widely scattered for the highest reservoir levels (Figure 7.21), for which there are more readings.

The difference between the hydraulic head in the lower chamber and that in the upper one is around 0.5 m in block 4B-5, around 0.8 m in block 7A-8, around 2.0 m in block 5B-6 and is as high as around 4.5 m in block 6A-6B. Results of both FLAC and UDEC models are consistent, showing that the variation in water pressures in the foundation area underneath the stilling basin is hydrostatic (i.e. the hydraulic head is the same at points located at different levels), and this approximately simulates what is observed in blocks 4B-5 and 7A-8. However, the high differences between readings taken in the lower and upper chambers in blocks 5B-6 and 6A-6B show that recorded water pressures are mainly dependent on local conditions, which are not represented in the model. The following paragraph describes the changes introduced into the model in order to try to make numerical results correspond more closely to measurements taken in block 6A-6B, where the differences are higher. Figure 7.22 shows the location of the piezometric chambers underneath the stilling basin in the foundation of this block.

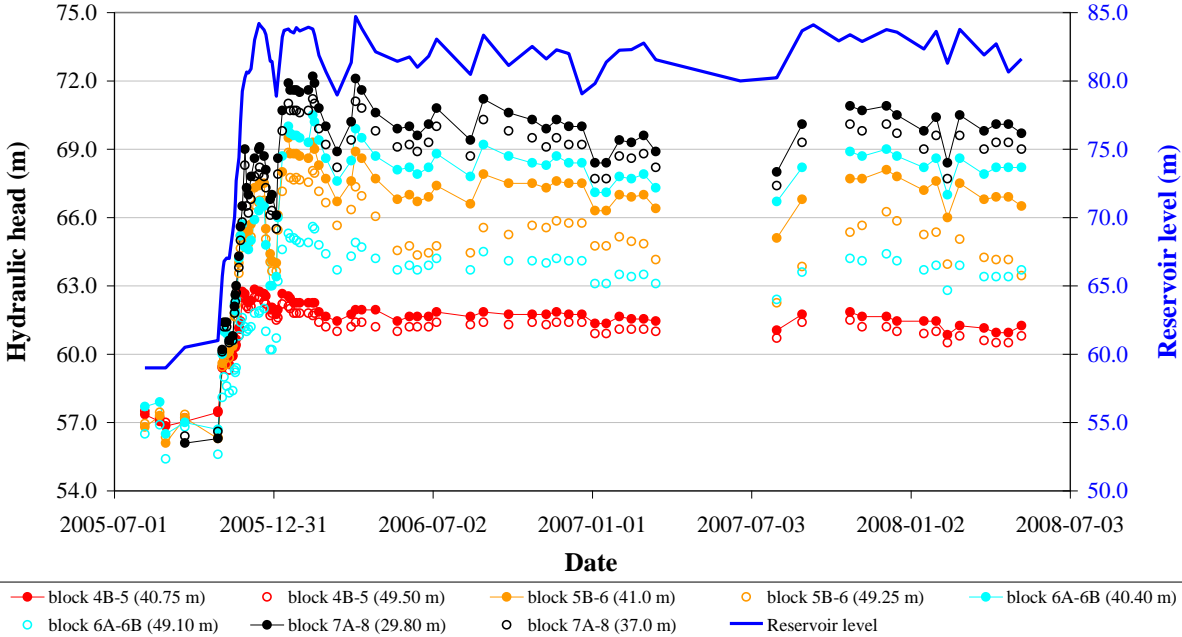


Figure 7.20 – Hydraulic heads at the piezometers located underneath the stilling basin (mid-height level of piezometric chambers shown in brackets).

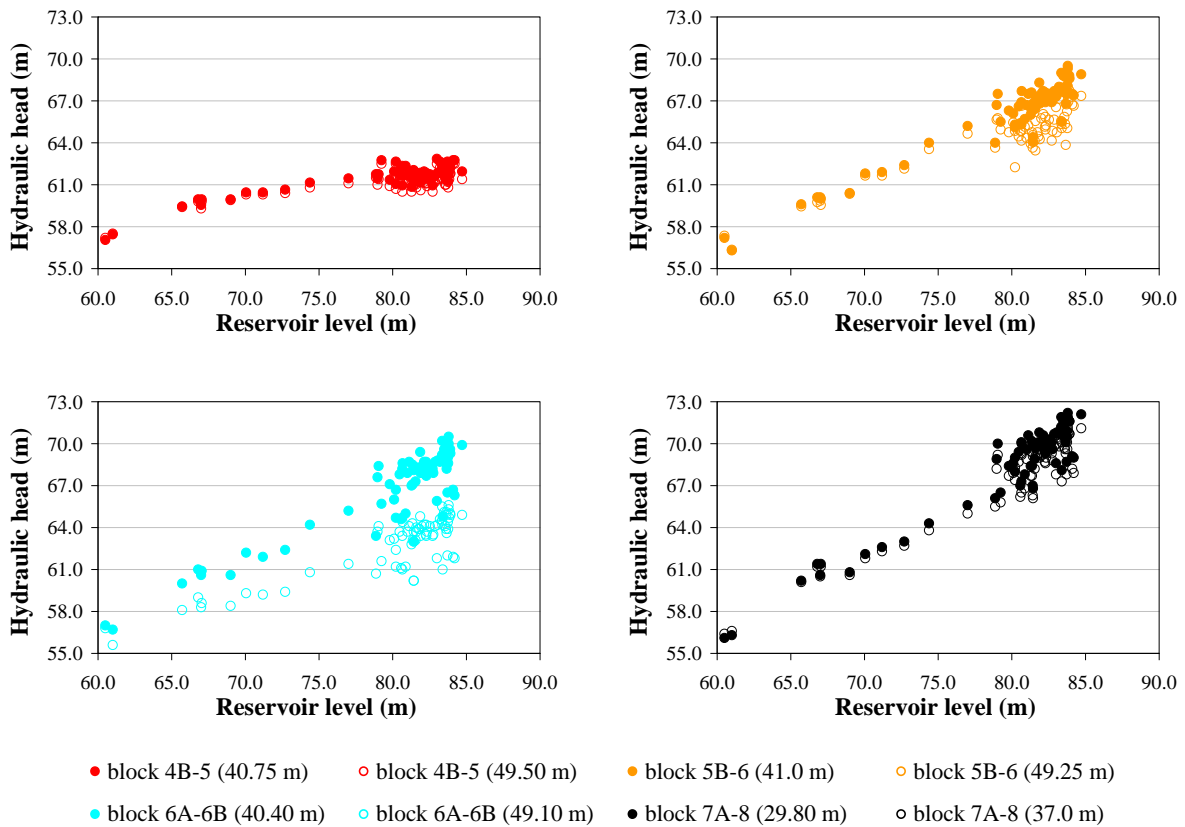


Figure 7.21 – Variations in the hydraulic head at the piezometers located underneath the stilling basin in relation to the reservoir level (mid-height level of piezometric chambers shown in brackets).

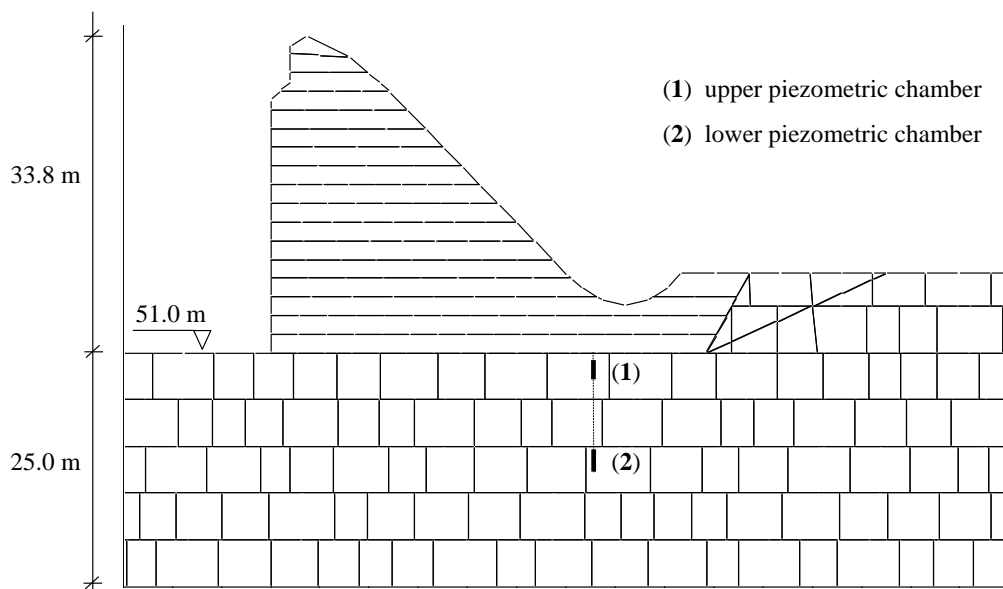


Figure 7.22 – Location of the piezometric chambers in the foundation of block 6A-6B, in the downstream area, underneath the stilling basin.

On 4 April 2006, recorded hydraulic heads in block 6A-6B at the lower and upper piezometric chambers were 69.9 m and 64.9 m, respectively. An attempt was made to obtain hydraulic heads closer to those recorded in this block by changing the developed UDEC model. Firstly, as the lower piezometric chambers are located at around 10.3 m below the dam/foundation interface, the layer of higher permeability was assumed to be located 10.0 m below this interface, instead of the previously assumed 5.0 m. The length of this layer was gradually increased, which led to higher water pressures at the downstream area. These varied from around 66.1 m to 67.9 m, depending on the layer's length. However, below the stilling basin the variation in pressure remained hydrostatic. Secondly, the permeability of the vertical discontinuities was increased 5 times, except in the grouted area, where they remained as pervious as the horizontal ones. This decision was made because the model's vertical discontinuities are not continuous, and therefore the rock mass permeability in the vertical direction is lower. It was concluded that this increase did not alter the rock mass global permeability, because, as vertical joints are discontinuous, water must always flow through the set of horizontal discontinuities. Finally, results analysis led to the conclusion that the lower hydraulic head recorded at the upper piezometric chambers is almost certainly due to leakage through dam vertical joints. To simulate this leakage, the permeability of the downstream area of the dam/foundation joint, close to the toe of the dam, was gradually increased. However, the maximum numerical difference in water pressures between the lower and upper piezometric chambers was 0.8 m (Table 7.6).

Regarding the model, it was concluded that results closer to those recorded might be obtained if it was assumed that the majority of the water flows through sub-horizontal discontinuities that are interconnected only in some areas of the dam foundation.

Joint permeability factor of the downstream area of the dam/foundation joint ($\times 10^8 \text{ MPa}^{-1} \text{ s}^{-1}$)	Numerical hydraulic head (m)		Difference between the numerical hydraulic heads at the lower and upper chambers (m)
	upper chamber	lower chamber	
0.415	67.7	67.7	0.0
6.8475	65.8	66.5	0.7
13.695	65.5	66.2	0.7
27.39	65.3	66.0	0.7
54.78	65.1	65.9	0.8
109.56	65.0	65.8	0.8

Table 7.6 – Difference between numerical hydraulic heads at the lower and upper piezometric chambers for different permeabilities of the downstream area of the dam/foundation joint.

In reality, several springs were identified at the dam site whilst excavating, which are shown on the surface foundation map. The water from these springs was collected in two different wells, but it was not diverted from the base of the dam to the area downstream from the dam. Instead, the wells were covered with a layer of conventional concrete. The water from these springs is probably increasing water pressures within the foundation and, consequently, increasing the hydraulic head. Since the beginning of the first filling of the reservoir, it has been observed that a relatively high quantity of water appears at the downstream sidewall and floor of the gallery close to dam vertical contraction joints 4 to 7. The water probably flows from the dam foundation through the dam contraction joints, due to misplacement of the sealing strips. This can explain the difference in hydraulic head recorded in the lower and upper piezometric chambers in some foundation areas.

7.4 Stability analysis

7.4.1 Introduction

For rock foundations, stability analysis requires that possible sliding block mechanisms which may lead to failure be identified (ICOLD 1993; Londe 1985). These involve the dam/foundation interface, rock mass joints and/or planes of weakness. Wyllie (1999) highlights that in general stability conditions are unfavourable if the discontinuities are continuous and planar, contain a low strength or brittle infilling and have positions and orientations that form a wedge of rock that can slide from the foundation. Instability may occur underneath the dam, in the abutments or in adjacent slopes.

This section starts by briefly describing the main accident scenarios of different dam types and the available stability analysis methods for gravity dams. The safety of Pedrógão dam against dam base sliding is afterwards assessed with the limit equilibrium method, following the Portuguese guidelines for dam design. Water pressures along the dam/foundation joint, shown in Figure 7.16, were used to assess the safety of the stilling basin against upsurge. Finally, the stability of the dam/foundation system was estimated for different possible failure scenarios, using the UDEC model developed and the strength reduction method.

7.4.2 Main accident scenarios of different dam types

7.4.2.1 Gravity dams

The main loads in gravity dams are the self-weight and water pressures (hydraulic pressures and uplift). The dam/foundation interface is very large, therefore, uplift pressures at the base of the dam and hydraulic pressures play an important role, as they reduce the stabilizing effect of the structure weight. Such hydraulic pressures can occur in rock mass discontinuities or

even in the dam body, if there is any deficiency in construction joints, or fissures in contact with the reservoir. Temperature variations are only important during the construction stage. In gravity dams earthquakes can cause various sliding mechanisms in addition to high tensile stresses, particularly close to the crest.

The stresses on the foundations of gravity dams are relatively low so failure of the intact rock material is unlikely and the behaviour of the rock mass is controlled by sliding either along the dam/concrete interface or along sub-horizontal weak layers in the foundation, close to the base of the dam. Depending on the geometrical and mechanical properties of the foundation discontinuities and on uplift distribution on those surfaces, other failure scenarios can occur, such as overturning around a left abutment/right abutment axis.

The failure of Austin dam, in the USA in 1911, is an example of concrete gravity dam failure due to sliding along a layer of shale, which was the weakest zone in the foundation (Greene and Christ 1998). The dam was about 165 m in length and 15 m high. The foundation consisted of horizontally layered sedimentary rocks, principally sandstone and shale. Prior to concreting, excavation was very shallow and only 1.2 m of shale needed to be excavated to reach the sandstone. However, the thickness of the sandstone layer was only 0.6 m, which was only discovered after the dam failure. The dam designer had planned a foundation cutoff wall that was to be taken to a sufficient depth into bedrock to prevent underseepage, but this had not been built. According to Greene and Christ (1998) had the dam's foundation been taken deeper into bedrock, below the shale layer, the dam's stability would have been significantly enhanced.

7.4.2.2 Buttress dams

In buttress dams the water load is transmitted to triangular buttresses parallel to the direction of the river flow. These resistant elements are isolated blocks, which theoretically work in an isolated way, allowing fitting to different geotechnical conditions along the foundation. The continuity of the upstream face can be assured either by a thickening of the buttress' heads or by small arches. The spaces between buttresses allow the discharge of water seeping through the foundation, thus greatly reducing uplift pressures. The dam/foundation interface is much smaller than in massive gravity dams and stresses on the foundation are higher; therefore failure scenarios related to block sliding are more likely to occur. Failure scenarios are similar to those mentioned for gravity dams, but failure of an isolated block is more likely to occur, due to the less effective linking three-dimensional effect and because this type of dam is often built in valleys with heterogeneous foundation rock masses. In addition to these failure scenarios, problems related to slenderness shall also be taken into account, such as the instability of buttresses or connecting structures.

7.4.2.3 Arch dams

Arch dams are curved structures, with their convexity towards upstream, designed to transmit water thrust mainly to the abutments and not to the valley bottom, taking advantage both of concrete and foundation rock mass compression strength (Veltrop 1988). Therefore, in the safety assessment of these dams it is essential to know the maximum stresses and the mechanical resistance of concrete and rock mass foundation, particularly in the slopes. In arch dams the dam/foundation interface is relatively small when compared to gravity dams and uplift pressures do not in general affect safety. However it is of major importance to reduce seepage under the dam in order to reduce erosion. The main accident scenarios are: 1) sliding along weaker surfaces in the foundation area where the arches rest, particularly in the valley sides and in the abutments; ii) crushing of the upper central arch area, where high compression stresses can occur and shear scenarios can develop; and iii) seepage in the valley bottom, which leads to erosion of discontinuities.

There are some reported cases of arch dam failure due to the rock mass foundation behaviour of which the most well-known case is the failure of the 61 m high Malpasset dam, in France in 1959, which is briefly described in chapter 2, section 2.5.3.

7.4.2.4 Other types of dams

In addition to gravity, buttress and arch dams, other types are also built, which combine the characteristics of those previously mentioned: arch-gravity, multiple arch and composite dams. Arch-gravity dams take advantage of a significant curvature in plan, although they are very thick in order to reduce stresses on the foundation. Multiple arch dams consist of a number of arches bearing on buttresses and the foundation (Pedro 1977). Multiple arch dams of large span are usually built in valleys where the ratio span-height is very large. Composite dams include not only the dams with linked concrete and embankment areas but also dams which join different types of concrete structures. In arch gravity dams and in large-span multiple arch dams the failure scenarios to consider are, basically, the failure scenarios of the main types of dams. Therefore, taking into account specific features of each structure, in arch-gravity dams, failure scenarios associated with both gravity and arch dams must be considered, and in large-span multiple arch dams special attention must be given to failure scenarios associated with both arch and buttresses dams. In composite dams special attention must be given to the part where the different structural areas are linked.

An example of concrete arch-gravity dam failure is that of the 64 m high St. Francis dam, in the USA in 1928. Analysis carried out immediately after the disaster pointed to piping of material along a fault, about halfway up the right abutment, as being the cause of failure.

Subsequent studies suggested that dam failure involved the partial reactivation of an ancient bedrock landslide which comprised the dam's entire left abutment (Rogers 2006).

7.4.3 Stability analysis methods for gravity dams

The limit equilibrium approach has been widely used to evaluate dam foundation stability, and considerable experience has been accumulated with its application. The dam is assumed to be a rigid body and the method consists of assuming a simplified failure mode and calculating the driving and resisting forces acting on the sliding surface, with the ratio of these two forces being the safety factor (F). Regarding the stability evaluation of gravity dams, different criteria have been adopted by different bodies, and great effort has been made in order to analyse the differences in the results (CFBR 2006; European Club of ICOLD 2004a; European Club of ICOLD 2004b; FERC 2002; USACE 2000; USACE 2005). These differences are mainly related with different ways of simulating the distribution of uplift pressures along the base of the dam, the possibility of crack formation and propagation along the dam/foundation interface and stability criteria, expressed in terms of either minimum values for the safety factors or maximum allowable stresses. A comprehensive computer program to perform both static and seismic stability evaluation of gravity dams was developed at the École Polytechnique de Montréal, with the aim of providing learning support and a basis for research and development on the subject (Leclerc et al. 2003). The program, CADAM, which is freely available, includes a large number of modelling options, as it is possible to carry out stability analysis using different worldwide published dam safety guidelines.

Two-dimensional analysis is generally adequate for most gravity dams (Rocha 1980a; Rocha 1980b), though with some exceptions including cases where the dam height is variable along its axis and some in which the geotechnical conditions are not uniform (Bustamante and Radisic 2006; Lombardi 2007). However, for arch dams 3D analysis is always required, as, in this case, failure mechanisms involve intersecting planes which can not be modelled two-dimensionally. Lemos (1999b) highlights that a significant difference with respect to the 2D case is that the failure surfaces for arch dam foundations tend to intercept the concrete structure, and various local mechanisms need to be examined. The limit equilibrium method allows estimates of the margin of safety to be obtained but does not give an indication of the magnitude of shear displacements as instability is approached. Analysis carried out with the Finite Element Method (FEM), may be used to estimate both shear deformations and margin of safety (e.g. Alonso et al. 1994; Shahkarami et al. 2004; Wittke 1990; Wittke and Polczyk 2002; Wittke et al. 2003). In this type of analysis, discontinuities along which sliding may take place can be modelled using special interface elements. Continuum codes not based on the FEM, such as FLAC, can also be used to assess both static and dynamic stability of gravity dams (e.g. Bureau 2006). However, stability analysis of dam foundations is better

carried out with block models, which may or may not include fluid flow through the discontinuities.

Stability evaluation using the DEM may be carried out applying suitable water pressures on potential sliding surfaces, calculated with a simple uncoupled flow analysis, in order to provide worst case scenarios (Lemos 1999b). The reliability of the application of the DEM to the study of sliding in jointed rock masses has been proven by comparing numerical results with both analytical solutions and experimental data. Studies which addressed failure of gravity dams on multiple discontinuities were carried out, as shown in Figure 7.23 (Pereira da Costa et al. 1993; Pereira Gomes et al. 1997; Pina et al. 1993). The collapse mechanism of arch dams calculated with 3DEC was also compared with experimental results (Lemos 1999a; Lemos 1999b; Lemos et al. 1995). Comparisons for dynamic analysis in seismic failure scenarios, using experimental results of a scale model of a gravity dam tested on LNEC's shaking table are presented in Pereira Gomes (2006) and in Lemos and Pereira Gomes (2007). Additional data for validation of numerical models for failure scenarios is provided by a series of shear tests and shake table sliding tests recently carried out by Rochon-Cyr and Léger (2009).

Stability analysis using discontinuum models that take into account the coupling between hydraulic and mechanical effects have been applied mainly for gravity dams. Some of these studies are briefly referred to in the following paragraphs.

Lemos (1987) implemented a series of new features in UDEC necessary for both hydromechanical and dynamic analysis of jointed rock masses and studied the behaviour and stability of a 100 m high hypothetical gravity dam on a rock mass with 2 joint sets. A parametric study was carried out in order to investigate the influence of different factors on numerical results. Results of seismic analysis carried out with this model (Lemos and Cundall 1999) were coherent with results of laboratory experiments which were later carried out by Javanmardi et al. (2005a; 2005b) regarding transient water pressures inside a crack created in a concrete specimen subjected to a cyclic dynamic movement.

Mostyn et al. (1997) carried out stability analysis of Chichester gravity dam, located in New South Wales, Australia, and the UDEC results were used to assess the accuracy of the Hoek-Brown empirical rock mass failure criterion.

Barla et al. (2004) used the code UDEC to investigate the seepage conditions through the rock mass foundation of a 73 m high gravity dam in Italy, which was going to be built on a granitic foundation, and to assess its stability. The flow patterns and pressure distributions under the

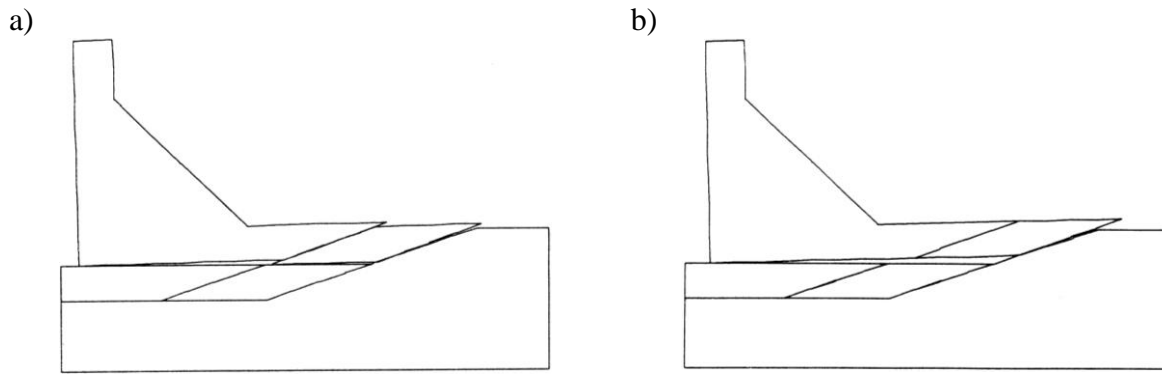


Figure 7.23 – Physical model tests of a gravity dam on a discontinuous foundation. Failure mechanisms: a) same friction angle on all joints; and b) reduced friction on lower joint (after Pereira Gomes et al. 1997).

dam were compared with those usually assumed in static analysis of gravity dams. Comparisons of results showed that the safety factors obtained using UDEC were lower than those obtained in FLAC analysis, in similar loading conditions.

Gimenes (2000) and Gimenes and Fernández (2006) performed stability analysis of Albigna gravity dam. The dam had a fairly complete foundation monitoring system (Kovari et al. 1989) which allowed measured field data to be compared with UDEC results. The behaviour of both dam/foundation interface and rock mass discontinuities during reservoir filling was simulated and the safety of the dam was evaluated for different failure scenarios.

Concerning the safety factor, several definitions have been proposed as referred to in Kovari and Fritz (1989; 1993) and in Alonso et al. (1996). In all cases, it provides a measure of the distance from the limit equilibrium, but generally, uncertainty about water pressure distribution and shear strength parameters (cohesion and friction angle) along the slip surfaces, for the relevant level of normal effective stresses, requires parametric studies to be carried out. Two alternative approaches may be employed: partial safety factors and probabilistic procedures. The first allows the consideration of the different levels of uncertainty attached to the various actions and material properties (Lemos 1999b), as lower safety factors may be used for better defined loads or material properties. This is a semi-probabilistic approach and is the method prescribed in Eurocode 7 for geotechnical engineering (Maranha das Neves 1994). The second would allow us to estimate a probability of failure, taking into account the uncertainties in the different parameters (ICOLD 1993). However, as discussed in Lemos (1999b), the calculation of probabilities of failure in rock engineering presents serious difficulties, mainly due to the usual lack of knowledge concerning the probability distribution functions of the material properties, and to our current inability to reproduce in numerical models statistical descriptions of the joint patterns. Approximate solutions of the probability of failure can be obtained with the reliability

analysis method, briefly described in Lemos (1999b), based on simplifying assumptions about the distributions of the random parameters involved in the limit state equation. Bernstone et al. (2009) have recently used this method to assess the safety of an operating concrete dam, taking into account recorded uplift data.

7.4.4 Stability analysis of Pedrógão dam

7.4.4.1 Limit equilibrium approach

In a stability analysis using the limit equilibrium method the loads to take into account are the weight of the dam; the reservoir and tailwater loads; uplift water pressures; silt pressures, if applicable; and seismic loads. To assess safety against dam base sliding, usual and extreme loading combinations were used, as set out in the Portuguese guidelines for dam design (RSB 2007). Usual combinations encompass different situations which may occur in normal operating conditions, while extreme loading combinations cover the conditions that may lead to possible failure scenarios. The available shear strength is expressed by a Mohr-Coulomb criterion. The peak values of friction angle and cohesion should be used for the usual loading combinations, and residual values for the extreme loading combinations.

The stability analysis was carried out with given minimum shear-friction safety factors at the concrete/rock mass interface for the following different hypotheses:

- i) hydraulic head at the drainage line equal to 1/3 of the sum of the reservoir and tailwater pressures or dam with no drains (linear distribution of the uplift pressure);
- ii) cohesion c in the dam/foundation interface of 0.2 MPa or zero; and
- iii) including and not including the resistance from the rock wedge close to the toe of the dam (assuming that downstream from the dam the river bottom is at its actual elevation or at the same level as the base of the dam).

Silt pressure was not taken into account. The following unit weights were used for the concrete, foundation rock mass and water: $\gamma_c = 24 \text{ kN/m}^3$; $\gamma_r = 25 \text{ kN/m}^3$; and $\gamma_w = 10 \text{ kN/m}^3$. Regarding seismic loads, the same accelerations as those used in the dam design (HIDRORUMO 2001) were employed: $a = 0.06 g$ for the Operational Basis Earthquake (OBE) and $a = 0.143 g$ for the Maximum Design Earthquake (MDE). For the latter, analysis was also carried out with a higher value, $a = 0.35 g$, which is slightly higher than the acceleration for a surface magnitude of 6.0 at a distance of 1 km from a fault with a square failure area with sides 7.5 km long (Câmara 2007). The effect of seismic loads is simulated by applying two additional external forces to the structure: the first is applied through the centre

of gravity of the structure in a downstream direction and is equal to the product of the dam weight and a seismic coefficient; the second is the hydrodynamic force exerted by the water on the dam. In a first analysis the reservoir is at the level of the spillway crest (84.8 m) and the tailwater at level 60.0 m. This is the most probable situation, as the dam has an uncontrolled spillway. A second analysis was carried out considering the maximum operating level (91.8 m) and a tailwater at level 67.8 m. This situation could arise during a flood. Figure 7.24 shows the water static loads on block 6-7.

The hydrodynamic force on the reservoir/concrete interface, which occurs during an earthquake, is calculated with the Westergaard simplified model (Figure 7.25). In this model, it is assumed that: i) the dam is not deformable; ii) the reservoir is semi-infinite; iii) the water is incompressible; iv) the surface waves can be neglected; and v) there are only horizontal vibrations along the upstream-downstream direction. The pressure distribution is parabolic and the hydrodynamic equivalent force, whose line of action is 0.4 H above the reservoir bottom, is added to the static water pressure force to get the total water force on the structure. USACE (2005) stresses that it is necessary to be aware of the limitations and the simplifying assumptions made with respect to hydrodynamic pressures and their distribution on the structure, as this method can lead to significant error. However, if the primary aim of the analysis is the foundation behaviour, the model is adequate.

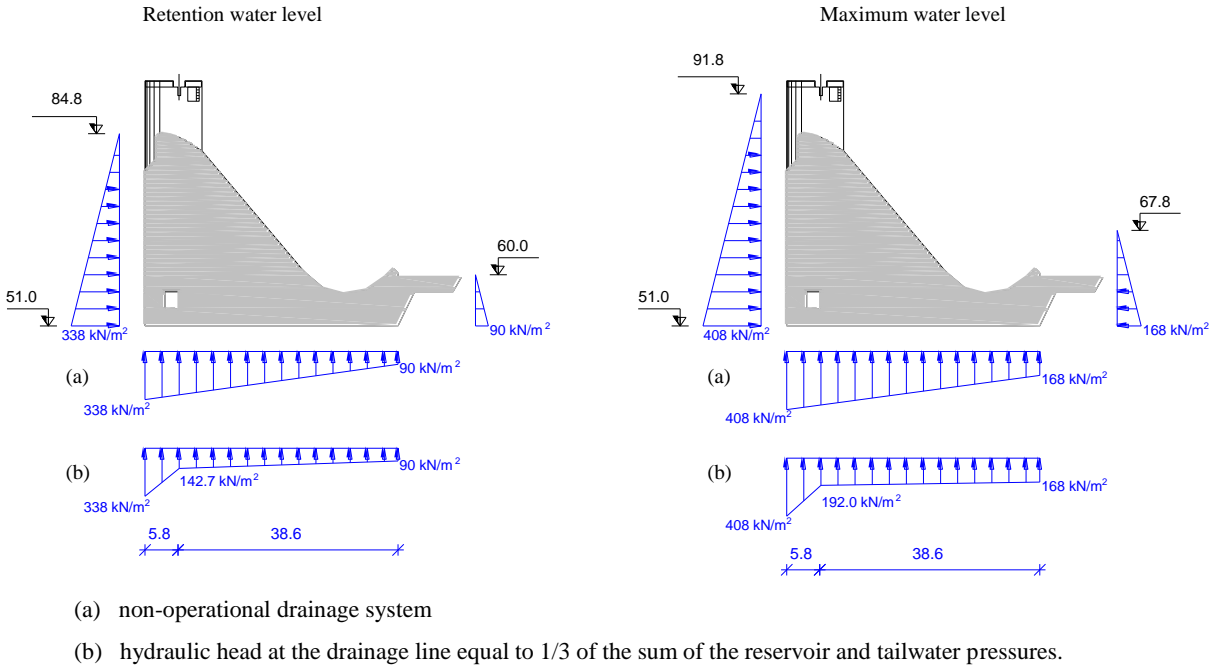
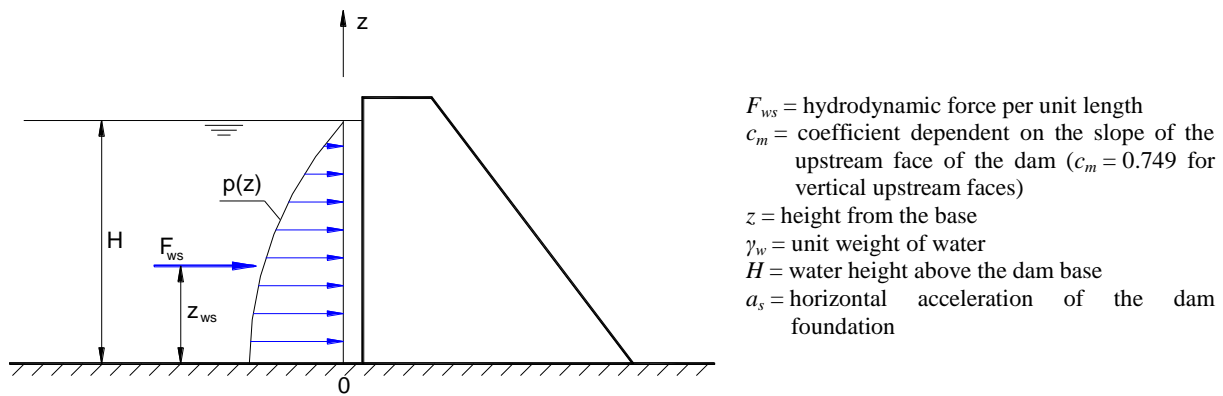


Figure 7.24 – Water static loads on block 6-7 of Pedrógão dam.



$$p(z) = \frac{1}{2} c_m \left(1 - \frac{z^2}{H^2} + \sqrt{1 - \frac{z^2}{H^2}} \right) H \gamma_w a_s$$

$$F_{ws} = \frac{8 + 3\pi}{24} c_m H^2 \gamma_w a_s \qquad z_{ws} = \frac{7}{8 + 3\pi} H = 0.4 H$$

Figure 7.25 – Hydrodynamic pressures. Westergaard simplified model.

Table 7.7 shows the different loading combinations used in the analysis presented here, and Table 7.8 shows the requirements necessary to ensure safety against sliding, according to the Portuguese Regulation; with 3.0, 1.5 and 1.2 as minimum safety factors relative to cohesion, to the peak friction angle, and to the residual friction angle of the dam/foundation interface, respectively. In this table, destabilising actions are shown on the left hand side of each formula, while both stabilising actions and the shear resistance, which develops on the concrete/rock mass interface, are shown on the right hand side.

Table 7.9 shows the results of the stability analysis carried out. Although high flow rates and uplift pressures are recorded in the foundation of the dam block 6-7, the conclusion is drawn that the base sliding stability of the dam is ensured for usual load conditions, when the reservoir is at the level of the spillway crest. At the maximum operating level, stability is not guaranteed when cohesion of the dam/foundation interface is neglected. For extreme load conditions stability is not guaranteed if drains are inoperable. In the case of seismic combination using $a = 0.143 g$, stability is not ensured if drains are inoperable and if the resistance from the rock wedge at the toe of the dam is not included in the analysis. If it is assumed that the MDE is $0.35 g$ some shear displacement could occur during the earthquake. Therefore it can be concluded that care must be taken in order to maintain the existing drainage system in good condition.

Usual scenarios	Static loads (retention water level)	Cross section weight, static loads of water for the retention water level (hydrostatic pressure and uplift) and part of the passive force downstream from the dam
	Seismic combination (retention water level and OBE)	Cross section weight, static loads of water for the retention water level (hydrostatic pressure and uplift), part of the passive force downstream from the dam and OBE (inertia forces on the concrete section and hydrodynamic pressures)
Failure scenarios	Static loads (maximum water level)	Cross section weight, static loads of water for the maximum water level (hydrostatic pressure and uplift) and part of the passive force downstream from the dam
	Seismic combination (retention water level and MDE)	Cross section weight, static loads of water for the retention water level (hydrostatic pressure and uplift), part of the passive force downstream from the dam and MDE (inertia forces on the concrete section and hydrodynamic pressures)

Table 7.7 – Loading combinations to take into account in the safety assessment against dam sliding for both usual and failure scenarios.

Usual scenarios	Static loads (retention water level)	$F_w \leq (W - V) \frac{\text{tg } \varphi}{\gamma_\varphi} + L \frac{c}{\gamma_c} + F_{wd} + \frac{F_p}{3}$
	Seismic combination (retention water level and OBE)	$F_w + F_{ws} + F_b \leq (W - V) \frac{\text{tg } \varphi}{\gamma_\varphi} + L \frac{c}{\gamma_c} + F_{wd} + \frac{F_p}{3}$
Failure scenarios	Static loads (maximum water level)	$F_w \leq (W - V) \frac{\text{tg } \varphi_r}{\gamma_{\varphi_r}} + F_{wd} + \frac{F_p}{3}$
	Seismic combination (retention water level and MDE)	$F_w + F_{ws} + F_b \leq (W - V) \frac{\text{tg } \varphi_r}{\gamma_{\varphi_r}} + F_{wd} + \frac{F_p}{3}$

W = weight of the concrete cross-section
 V = resultant of uplift pressures at the horizontal dam/foundation interface
 F_w = horizontal resultant of the hydrostatic pressure on the upstream face of the dam
 F_{wd} = horizontal resultant of the hydrostatic pressure on the downstream face of the dam
 F_p = passive (resisting) force in the area of the downstream face below the river bottom
 F_{ws} = hydrodynamic pressure on the upstream face of the dam
 F_b = inertia force due to the seismic load on the concrete section

φ = peak friction angle on the dam/foundation joint
 c = cohesion
 φ_r = residual friction angle on the dam/foundation joint
 L = length of the dam/foundation interface in the upstream-downstream direction
 γ_φ = safety factor relative to the peak friction angle
 γ_c = safety factor relative to cohesion
 γ_{φ_r} = safety factor relative to the residual friction angle

Table 7.8 – Safety assessment against sliding at the dam/foundation interface for both usual and failure scenarios.

Hu (m)	Hd (m)	Drainage system	Cohesion <i>c</i> (MPa)	River bottom down- stream from the dam	Usual scenarios		Failure scenarios		
					Peak friction angle (minimum value)		Residual friction angle (minimum value)		
					$c = 0.2 \text{ MPa}; \gamma_c = 3.0;$ $\gamma_\phi = 1.5$		$c = 0; \gamma_{\phi r} = 1.2$		
					Static loads	Seismic loads (retention water level and OBE)	Static loads (maximum water level)	Seismic loads (retention water level and MDE)	
								0.143 g	0.35 g
84.8	60.0	not operative	0.0	1)	-	-	-	47°	60°
			0.2	1)	19°	30°	-	-	-
			0.0	2)	-	-	-	43°	58°
			0.2	2)	10°	23°	-	-	-
		operative	0.0	1)	-	-	-	38°	52°
			0.2	1)	14°	23°	-	-	-
			0.0	2)	-	-	-	35°	49°
			0.2	2)	8°	17°	-	-	-
91.8	67.8	not operative	0.0	1)	-	-	51°	-	-
			0.0	2)	-	-	46°	-	-
		operative	0.0	1)	-	-	37°	-	-
			0.0	2)	-	-	33°	-	-

Downstream from the dam the river bottom is: 1) at the same level as the concrete/rock mass interface (51.0 m)
2) at its actual level (59.5 m)

Table 7.9 – Minimum values of the friction angle in discontinuities close to the dam/foundation interface which ensure safety against sliding.

Analysis shows that the dam is very stable. For the usual scenarios, in which it is assumed that cohesion in the dam/foundation interface is not zero, the dam is stable even when the drainage system is not operative. For failure scenarios, during a flood, stability is still ensured if the drainage system is working properly. This is not the case if the drainage system is inoperative, as the calculated friction angles are very high. Thus, in this case, stability is not ensured. For the MDE, with the acceleration assumed in the dam design ($a = 0.143 \text{ g}$), the dam is stable if the drains are operative. For the larger seismic loads ($a = 0.35 \text{ g}$), some shear displacement could occur. The magnitude of these displacements, however, can not be obtained with the limit equilibrium approach. A step by step time domain analysis would be required.

Additional analysis was carried out in order to evaluate the stability of the stilling basin of Pedrógão dam, which was concreted separately from the dam body, as a series of individual blocks, as shown in Figure 7.26. Therefore it is necessary to assess its stability against upsurging due to water pressure. Figure 7.16 a) shows the variation in uplift pressures along the base of the dam, for different foundations, with and without drainage system. These pressures were used to determine the force acting upwards in the area of the stilling basin/foundation interface, and this force was compared with the weight of the stilling basin. Analysis was carried out for the worst scenario, of foundation with no drainage system (Table 7.10). Results lead to the conclusion that the stability of the stilling basin against upsurging is ensured both when the drainage system is working properly and when there is no drainage system but the foundation is very deformable. In situations with no drainage system, stability is at its limit in the case of a foundation with joint normal stiffness of 10 GPa/m and is not guaranteed in the case of the stiffest foundation.



Figure 7.26 – Construction of Pedrógão dam stilling basin.

Model: HM interaction, no drainage system	Force due to uplift pressure on the stilling basin/foundation interface (kN/m)	Percentage of stilling basin weight (%) (stilling basin weight = 2904 kN/m)
$k_n = 2 \text{ GPa/m}$	1990	40
$k_n = 10 \text{ GPa/m}$	2890	99.5
$k_n = 50 \text{ GPa/m}$	3320	114.3

Table 7.10 – Force due to uplift pressures acting upwards on the stilling basin/foundation interface and comparison with the weight of the stilling basin.

7.4.4.2 Strength reduction method

The UDEC model developed, with joint normal stiffness of 10 GPa/m, was used to assess the stability of the dam/foundation system for the five different possible failure scenarios shown in Figure 7.27. Scenarios a) and e) concern only the dam/foundation joint. Sliding along this interface is the most probable failure scenario in dam foundation rock masses containing widely spaced discontinuities, none of which are unfavourably oriented. Pedrógão dam is embedded in the foundation, and therefore the resistance to sliding is high. Scenario e) neglects the resistance of the rock wedge at the toe of the dam, in order to take into account a possible excavation downstream, close to the toe of the dam. Scenario b) involves both the dam/foundation joint and the rock mass joint dipping 25° towards upstream, which was purposely included in the model for stability analysis. This hypothetical situation may simulate a combined mode of failure, where the failure path occurs both along the dam/foundation interface and through intact rock, in geology where the rock is horizontally or near horizontally bedded and the intact rock is weak (USACE 1994). In scenario c), sliding along the inclined rock mass joint is prevented, assuming that the behaviour of this joint is elastic. Finally, scenario d) concerns sliding through the dam body, along a construction joint.

Analysis was carried out with the method of strength reduction, typically applied in foundation design. The model was first run until equilibrium, then the fluid flow analysis was switched off and, for each failure scenario, the friction angle of the highlighted discontinuities was gradually reduced until failure (the reduction coefficient was applied to $\tan \phi$). Each analysis started with the same water pressures, which were obtained assuming the reservoir at the retention water level. In cases a), b), c) and e), zero cohesion and zero tensile strength were assigned to the dam/foundation joint, involved in the failure mode. In case d), zero cohesion was assigned to a dam construction joint, in order to allow sliding and to simulate failure along that discontinuity. In this latter case, additional analysis was carried out, which consisted of applying a gradually increasing water pressure along the dam joint, instead of reducing the joint friction angle. The failure indicator was the horizontal crest displacement. Results obtained with an initial friction angle of 35° were compared with those obtained with an initial friction angle of 30° (friction angles assumed on rock joints, on the dam/foundation joint and on the dam horizontal joints), in order to assess differences in the results due to variations in joint shear strength. With the exception of case d), analysis was also carried out assuming no drainage system in the dam foundation.

Stability analysis results are shown in Figure 7.28 to Figure 7.30, in which, for ease of analysis, friction angles in the x-axis are shown in reverse order. The first of these figures shows the results of scenarios a), b) and c), which may be compared with one another. In both scenarios a) and c) stability was assessed for friction angles as low as around 9.5° , and the dam/foundation system remained stable ($F > 4.2$ for $\phi = 35^\circ$ and $F > 3.5$ for $\phi = 30^\circ$).

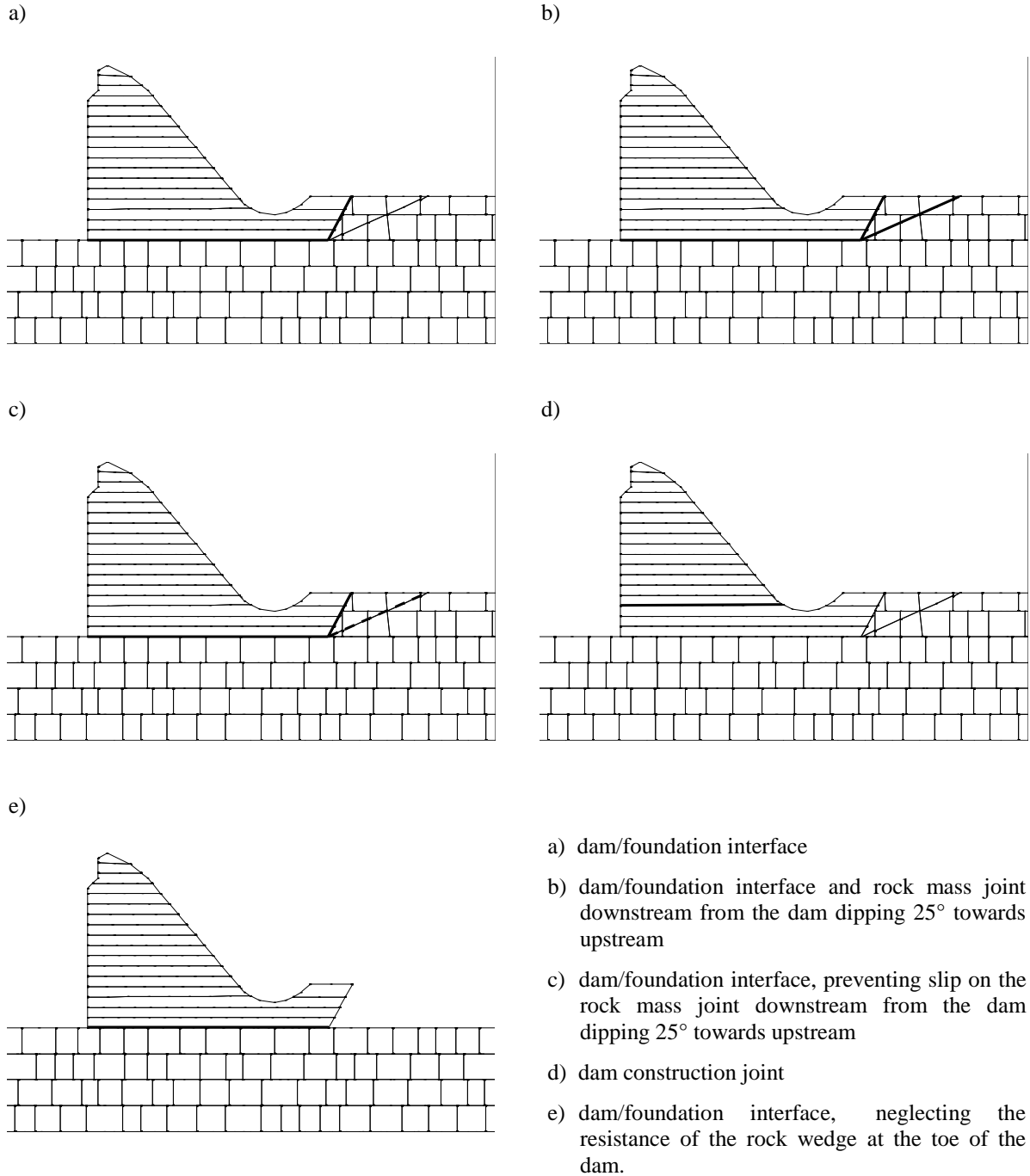


Figure 7.27 – Analysed failure modes.

Although stable, displacements in scenario a) are considerably higher when the initial friction angle is 30° . Displacements are much lower in scenario c), in which sliding along the inclined rock mass joint is prevented. Indeed, in this case, it is as if the inclined rock mass joint were not there. In scenario a), the presence of this joint can make larger displacements occur. In scenario b), with the drainage system operating well, the dam is unstable for friction angles lower than around 15° ($F = 2.6$ for $\varphi = 35^\circ$ and $F = 2.1$ for $\varphi = 30^\circ$). Without drainage, the dam is not stable for friction angles lower than 19° and 21° , for the initial angles of 35° and 30° , respectively ($F = 2.0$ and 1.5). In the cases of no drainage system, water pressures are higher and therefore the initial elastic displacement is also higher.

In scenario d), whose results are shown in Figure 7.29, sliding along the highlighted dam construction joint only occurs for friction angles lower than around 18° ($F = 2.1$ for $\varphi = 35^\circ$ and $F = 1.8$ for $\varphi = 30^\circ$). Water pressures can go up to 0.21 MPa, for a joint friction angle of 35° , and 0.16 MPa, for a joint friction angle of 30° . These water pressures are equivalent to 21 and 16 m of water column, respectively. The joint along which sliding is being analysed is 6 m above the reservoir bottom, therefore, when the reservoir is at crest level, there is a water column of 27.8 m above the joint, which is higher than the water column that may cause sliding.

Increasing the passive wedge resistance is one of the available methods for increasing gravity dam resistance to sliding, and therefore scenario e), in which this resistance is neglected, is the most unfavourable of the four analysed failure modes which involve the dam/foundation interface. Analysis was carried out assuming that the drainage system is working properly, that the water pressure at the drainage line is 60 % of the reservoir head, as that recorded in some cross sections of blocks 6-7 and 7-8 (Figure 4.23), and also assuming that the drains are all clogged. Stability analysis results for $\varphi = 35^\circ$ (Figure 7.30) show that the dam is unstable for friction angles lower than 22.4° , in the former case ($F = 1.7$), for friction angles lower than around 26° , in the second case ($F = 1.4$), and is unstable for friction angles lower than 34.5° in foundations without drainage system ($F = 1.02$).

In scenarios a) and c), if failure were to occur, sliding would be along the dam/foundation interface. In scenarios d) and e) failure is obviously along the highlighted discontinuities. Scenario b) deserves further analysis in order to understand how the dam/foundation system fails. Figure 7.31 shows that close to failure the sliding path is along the base of the dam and along the inclined rock mass joint. The interface between the foundation and the downstream face of the stilling basin is opened at its upper part, as are the vertical discontinuities which intercept this interface. The downstream area of the base of the dam is also opened, as is the last vertical discontinuity that meets this interface.

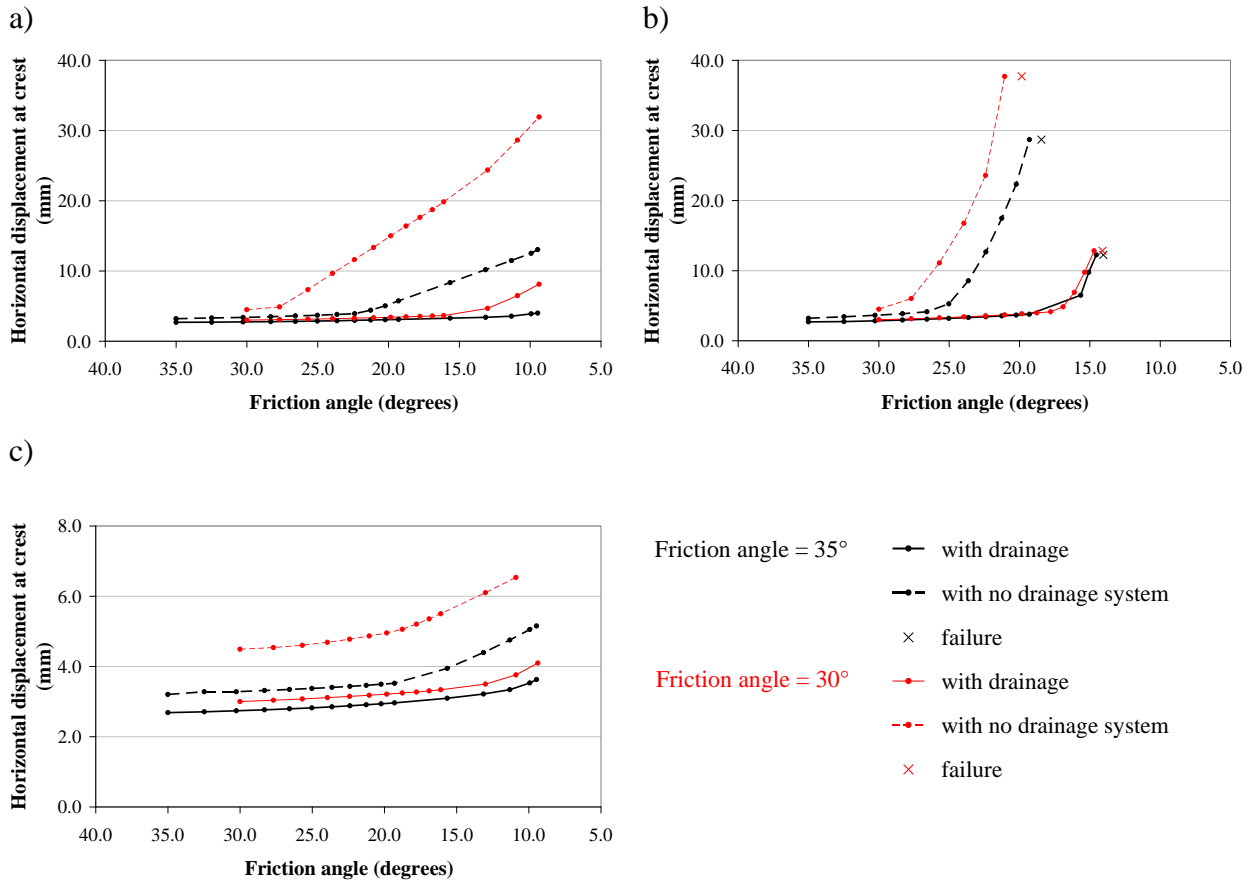


Figure 7.28 – Variation in crest horizontal displacement due to reduction of the friction angle on highlighted joints, for failure modes a), b), and c), shown in Figure 7.27.

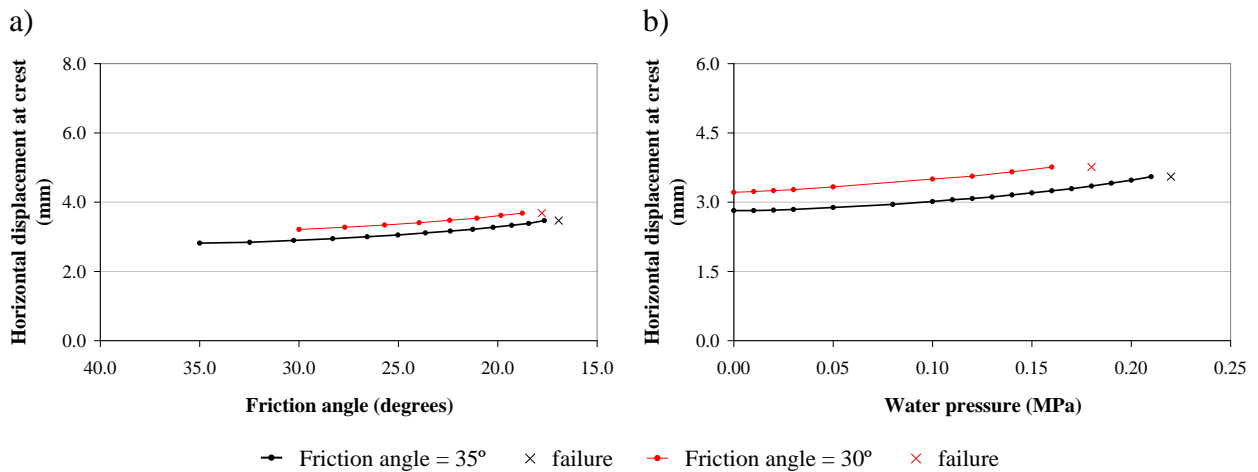


Figure 7.29 – Failure mode through the dam construction joint shown in Figure 7.27 d): horizontal displacement at crest for a) decreasing friction angle and b) increasing water pressure at the dam joint.

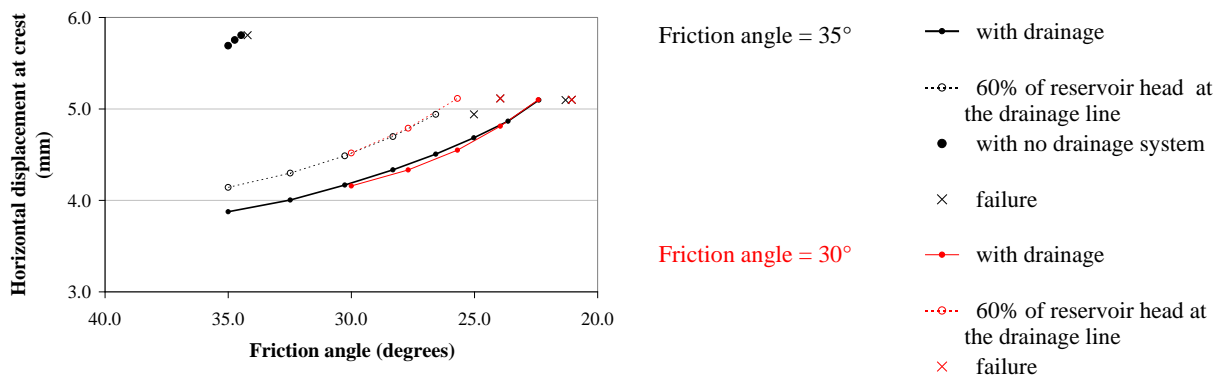


Figure 7.30 – Variation in crest horizontal displacement due to reduction of the friction angle on the dam/foundation interface, for failure mode e) shown in Figure 7.27.

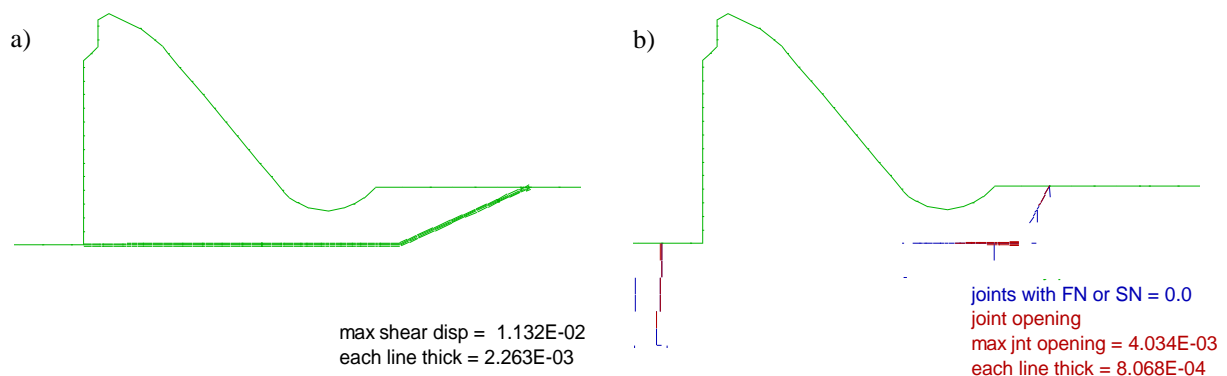


Figure 7.31 – Joints at shear limit (green), joints with zero normal force or stress (blue) and magnitude of joint separation (red), for failure mode b) (joint separation is proportional to line thickness).

Figure 7.28 to Figure 7.30 show the great influence that water pressure in the drainage line has both on horizontal crest displacements and safety factors, as does the joint friction angle.

Results analysis shows that in all the analysed failure modes involving the dam/foundation interface, sliding starts in its downstream area. In the failure mode through the dam construction joint, sliding begins close to the downstream face of the dam and extends towards upstream.

7.4.4.3 Comparison of the UDEC results with those obtained using the limit equilibrium method

The UDEC results concerning the different failure scenarios involving the dam foundation presented in the previous section were compared with those obtained using the limit equilibrium approach. To simplify the comparisons new equilibrium analysis was carried out,

assuming only the case of zero cohesion in the dam/foundation interface. Analysis was done assuming either full development of passive pressure, which is improbable as it requires large structure displacements, or the development of one-third of the passive pressure, which is more realistic. No minimum safety coefficients were considered, in contrast to what was done in section 7.4.4.1, in which the limit equilibrium analysis was done according to the Portuguese Regulation. Results, presented in Table 7.11, show that the dam is stable when the reservoir is at the retention water level, even when the drainage system is inoperative. When the reservoir is at the maximum water level, the safety factor is lower than 1 when: i) the drainage system is inoperative and the resistance from the rock wedge downstream from the dam is neglected ($F = 0.69$); and ii) the drainage system is inoperative and only one third of the passive force is considered in the analysis ($F = 0.82$).

Results of the UDEC analysis with the reservoir at both the retention water level and the maximum water level are shown in Figure 7.32, Figure 7.33 and in Table 7.12.

Hu (m)	Hd (m)	Drainage system	River bottom downstream from the dam	Passive force due to the rock wedge close to the toe of the dam	Friction angle (minimum value)	Safety factor (F)
84.8 (retention water level)	60.0	not operative	1)	-	27.8°	1.33
			2)	full	11.1°	3.57
			1/3	22.6°	1.68	
		operative	1)	-	21.2°	1.81
			2)	full	8.2°	4.86
			1/3	17.1°	2.28	
91.8 (maximum water level)	67.8	not operative	1)	-	45.6°	0.69
			2)	full	27.8°	1.33
			1/3	40.6°	0.82	
		operative	1)	-	32.4°	1.10
			2)	full	18.2°	2.13
			1/3	28.1°	1.31	

Downstream from the dam the river bottom is: 1) at the same level as the concrete/rock mass interface (51.0 m)
2) at its actual level (59.5 m)

Table 7.11 – Limit equilibrium method. Minimum values of the friction angle in discontinuities close to the dam/foundation interface which ensure safety against sliding, and corresponding safety factors.

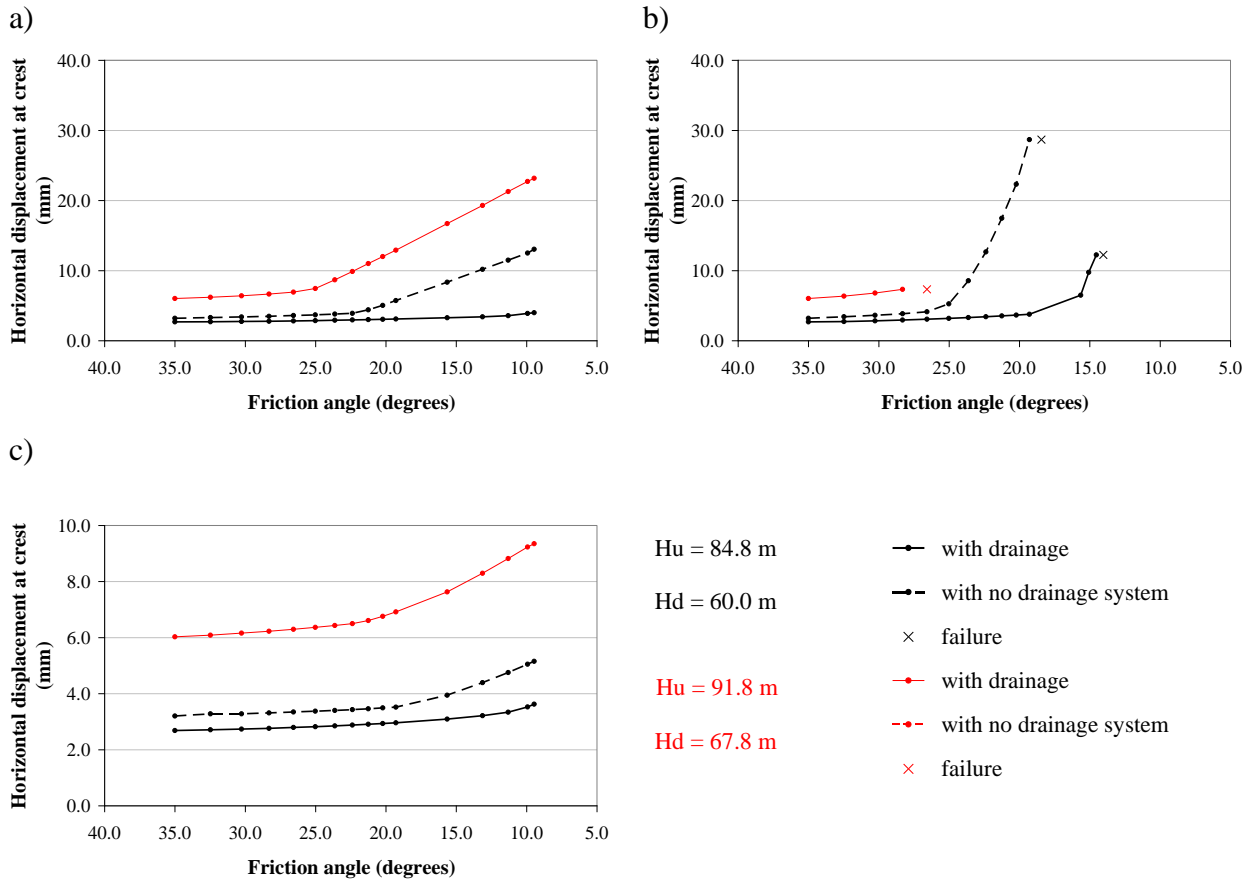


Figure 7.32 – Variation in crest horizontal displacement due to reduction of the friction angle on highlighted joints, for failure modes a), b), and c), shown in Figure 7.27.

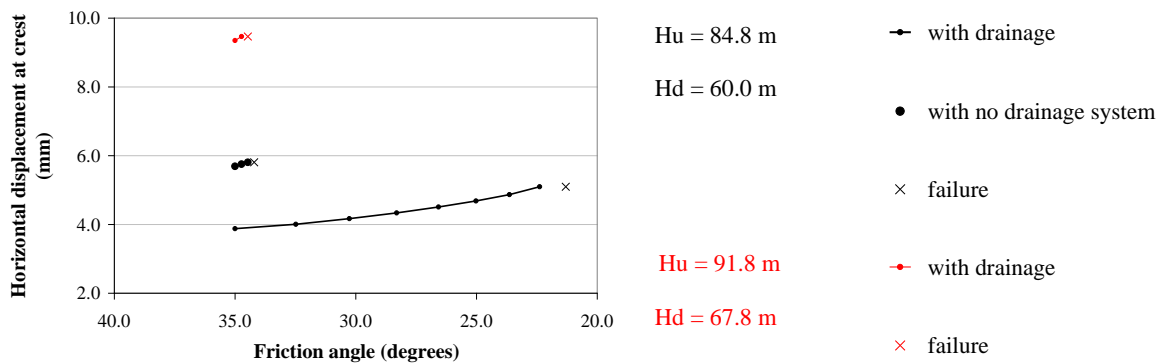


Figure 7.33 – Variation in crest horizontal displacement due to reduction of the friction angle on the dam/foundation interface, for failure mode e) shown in Figure 7.27.

Hu (m)	Hd (m)	Failure scenario	Drainage system	Friction angle		Safety factor (F)
				last stable	failure	
84.8 (retention water level)	60.0	a)	not operative	stable *		> 4.2
			operative	stable *		> 4.2
		b)	not operative	19.30°	18.44°	2.0
			operative	14.54°	14.04°	2.6
		c)	not operative	stable *		> 4.2
			operative	stable *		> 4.2
e)	not operative	34.47°	34.21°	1.02		
	operative	22.39°	21.30°	1.7		
91.8 (maximum water level)	67.8	a)	not operative	unstable		
			operative	stable *		> 4.2
		b)	not operative	unstable		
			operative	28.31°	26.57°	1.4
		c)	not operative	unstable		
			operative	stable *		> 4.2
e)	not operative	unstable				
	operative	34.73°	34.47°	1.01		

* Stable for friction angles as low as around 9.5°.

Table 7.12 – UDEC analysis. Friction angle in discontinuities close to the dam/foundation interface which ensure safety against sliding and for which failure occurs, and corresponding safety factors (failure scenarios shown in Figure 7.27).

In the four failure scenarios analysed, the dam/foundation system is unstable when the reservoir is at the maximum water level and the drainage system is inoperative, and thus these situations are not shown in Figure 7.32 and Figure 7.33. For the same reservoir level, in both scenarios a) and c) the dam/foundation system remains stable when the drainage system is working properly, while in scenario b) failure occurs for a friction angle of around 27.5° (F = 1.4) (Figure 7.32). In scenario e), of which the results are shown in Figure 7.33, the dam is unstable for friction angles lower than 34.47° when the reservoir is at the maximum water level (F = 1.01).

Table 7.12 shows that, of failure scenarios a), b) and c), the results of scenario b) are the ones which can be compared with those obtained using the limit equilibrium analysis. For ease of comparison, results presented in Table 7.11 and in Table 7.12 are summarized in Table 7.13.

Failure mode e) is the only one which enables UDEC analysis to be verified, as the same results must be obtained for similar loads with both the UDEC and limit equilibrium analysis. Indeed, when the reservoir is at the retention water level and the drainage system is operative almost the same friction angles were obtained (21.2° in the limit equilibrium analysis and between 21.3° and 22.39° in the UDEC analysis). A difference as low as around 2° is

obtained in similar conditions, but with the reservoir at the maximum water level (32.4° in the limit equilibrium analysis and between 34.47° and 34.73° in the UDEC analysis). However, when the drainage system is inoperative, the friction angles obtained in the UDEC analysis (34.21° - 34.47°) are higher than that given by the limit equilibrium method (27.8°). This difference can be explained by the higher uplift pressures obtained in the UDEC analysis, when compared with those given by the linear distribution of water pressures between the reservoir and the tailwater, assumed in the limit equilibrium analysis. This difference in water pressures is shown in Figure 7.34. A limit equilibrium analysis carried out assuming a resultant of the uplift pressure 24 % higher than that given by the linear distribution of water pressures would lead to the same friction angle at failure as the UDEC analysis (assuming that in the UDEC model failure occurs for a friction angle of 34.3°).

In the analysis in which it is assumed that downstream from the dam the reservoir is at its actual level, the UDEC results are within the range of friction angles given by the limit equilibrium method, when only part or full passive force is considered, but are closer to those obtained for one third passive force.

7.5 Conclusions

This chapter presents a study on seepage in Pedrógão dam foundation using both continuum and discontinuum models. Information provided from borehole water-inflow tests presented in chapter 4 was essential to develop both models. Analysis of seepage using the UDEC model, which takes into account the coupled hydromechanical behaviour of rock masses, shows that results depend mainly on the joint normal stiffness and on joint aperture. Stability analysis was carried out with different assumptions about uplift pressures and joint shear strength. Results allowed us to quantify the influence of water pressures on the stability of the dam. This result draws attention to the importance of using recorded water pressures for the sliding safety assessment of existing dams, as recommended by the European Club of ICOLD (2004b).

Discontinuum models are difficult to apply in most practical cases, because jointing patterns are very complex and there is usually a lack of data on hydraulic properties of the discontinuity sets. Among these parameters are the orientation and spacing of discontinuities, and the hydromechanical characterization data, namely joint normal stiffness, joint apertures and residual aperture, which is not readily available. However, such models which simulate the hydromechanical interaction are relevant in stability analysis, and the uncertainty in the different parameters, can be overcome by performing stability analysis assuming that each parameter may vary within a credible range.

Hu (m)	Hd (m)	Drainage system	River bottom downstream from the dam	Limit equilibrium	Friction angle	
					failure	UDEEC last stable
84.8 (retention water level)	60.0	not operative	1)	27.8°	34.21°	34.47°
			2)	11.1° - 22.6°	18.44°	19.30°
		operative	1)	21.2°	21.30°	22.39°
			2)	8.2° - 17.1°	14.04°	14.54°
91.8 (maximum water level)	67.8	not operative	1)	45.6°	unstable	
			2)	27.8° - 40.6°	unstable	
		operative	1)	32.4°	34.47°	34.73°
			2)	18.2° - 28.1°	26.57°	28.31°

Downstream from the dam the river bottom is: 1) at the same level as the concrete/rock mass interface (51.0 m)
2) at its actual level (59.5 m)

Table 7.13 – Comparison between the UDEC results and those from the limit equilibrium method.

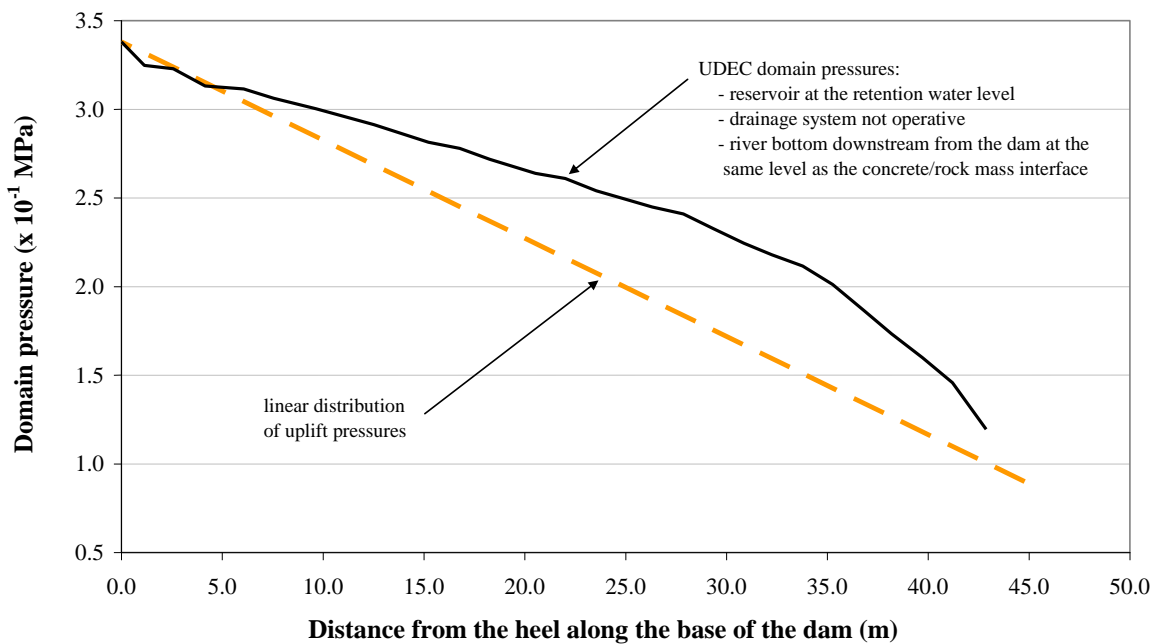


Figure 7.34 – Comparison of water pressures along the dam/foundation joint obtained in the UDEC analysis with the linear distribution of water pressures.

The main limitation of the UDEC fluid flow analysis is that it is carried out in 2D. As flow in fractured rock masses is mainly three-dimensional, 2D flow modelling can be highly misleading because water can not flow in other directions, out of the plane of the model. However, in dam foundations the flow is mainly in the upstream-downstream direction, and therefore 2D analysis may be considered adequate in most cases. For arch dams, 3D analysis is necessary, but coupled fracture flow modelling of an arch dam foundation would imply representing a network of joints from various sets, which would be computationally prohibitive.

In dam stability evaluation, the main advantage of using the 2D code UDEC instead of the limit equilibrium method is that it allows the study of a wider range of failure modes. This was the case in section 7.4.3.2, in which five different failure modes involving the dam/foundation interface, rock joints and a dam construction joint were effectively analysed. In addition, UDEC enables displacements to be calculated in seismic analysis, in contrast to what happens with the limit equilibrium approach. Stability analysis is also easily done in 3D, assuming water pressures obtained with equivalent continuum models. In the case of Alqueva dam, presented in the previous chapter, water pressures calculated with the global hydraulic model could be transferred to the global mechanical model, in which other interface elements could be included, so as to evaluate stability. In 3D, discontinuum models are particularly adequate for scenarios of foundation failure, as limiting equilibrium procedures, like those proposed by Londe (1973a), make basic assumptions about the forces acting on the independent volumes of rock that may become kinematically unstable, and are thus much simplified.

As stated in USACE (2005), advanced analytical analysis, such as that carried out with UDEC, can be used to gain a better understanding of structural behaviour. It is, however, highlighted that the results obtained from such analysis must be used in conjunction with traditional analysis methods, and that the advanced analytical methods can be difficult to perform and evaluate. This type of analysis is particularly useful when the foundation contains more than one material or is made up of a combination of intact rock, jointed rock and sheared rock, as, in these cases, the overall strength of the foundation depends on the stress-strain characteristics and compatibility of the various materials. It is also relevant in those cases in which controls of maximum displacement, needed to ensure proper function and safety, may prevail over safety factor requirements.

8 Conclusions

8.1 Summary and conclusions

The main objective of this research was to validate and justify the application of numerical models for the analysis of hydromechanical behaviour of concrete dam foundations in normal operating conditions. The effective use of these models is necessary to make the analysis of the monitoring data and safety control of these structures more efficient. The study explored the possibility of using simplified statistical models, traditionally employed in analysis of dam displacements, in the analysis of recorded discharges. A series of *in situ* tests was carried out so as to understand the way in which seepage occurs in some areas of the foundation of two large concrete dams. Taking into account test results and hydraulic and geomechanical characterization of the rock mass, different numerical hydraulic and hydromechanical models were afterwards developed to simulate both local and global effects. These models were then validated against the flow rates and water pressures recorded *in situ*.

The main scientific contribution of this thesis is not only the validation of hypotheses assumed in recently developed numerical codes, by comparison of numerical results with both experimental and field data, but also the development of methodologies to calibrate models for the specific geological and geotechnical conditions of a given dam foundation. This research has made relevant contributions in the following areas:

- the viability of using simplified statistical methods of quantitative interpretation in the analysis and prediction of foundation behaviour;
- the use of *in situ* tests, particularly borehole water-inflow tests, to complement the usual monitoring data;
- the development of numerical models adequate for the assessment of concrete dam foundations' hydraulic and hydromechanical behaviour in normal operating conditions, using available data together with the results of the proposed *in situ* tests;
- the application of numerical models for both the simulation of borehole water-inflow tests and the analysis of piezometers' readings; and
- the assessment of the safety of concrete dams for failure scenarios involving the foundation.

Regarding the viability of using simplified statistical methods of quantitative interpretation in the analysis and prediction of foundation behaviour, addressed in the third chapter, a study

was carried out to experiment applying methods customarily employed in the analysis of mechanical factors in the analysis of discharges. In this study, the shape of the influence line of the hydrostatic pressure on discharges in a concrete dam foundation was first established with a numerical model that has the required capabilities for simulating the hydromechanical process. Using polynomial functions of which the graph adequately follows the shape of the above-mentioned influence line, a series of quantitative interpretation analysis was carried out. The most significant conclusions were that the effect that variations in reservoir level have on discharges is adequately simulated by polynomials of the type $h^3 + h$ or $h^4 + h$, and that it is not possible to predict discharges recorded in single drains, as they are largely due to local effects and do not represent the permeability of the rock mass. This means that discharges recorded in seepage weirs, collected in relatively large areas, rather than discharges in single drains should be analysed. The study presented here shows that statistical models based on the simplified methods of quantitative interpretation, which can be an accurate and powerful tool in the analysis of concrete dam displacements, are not so accurate when used in the analysis of the hydraulic behaviour. Although more limited when used in the analysis of discharges, this type of method may be useful to approximately predict discharges in short periods of time.

Borehole water-inflow tests, carried out in drains and piezometric boreholes, are introduced as an innovative means of obtaining more detailed information on the hydraulic activity in dam foundations. These tests, which are conducted with single and double packers, allow measurement of discharges and water pressures in isolated sections of the holes. Analysis of test results in conjunction with other available information, such as geological and geotechnical data of the dam site, boreholes logs and results of other complementary tests, can be extremely significant in increasing knowledge of the hydraulic behaviour of concrete dam foundations. The information provided by these tests can be used not only to validate hydraulic models and to improve numerical models that take into account the existence of rock mass discontinuities, but also to choose the best place to locate piezometric chambers or to choose suitable remedial or supplementary seepage control measures in areas of the foundation where the discharges and/or the uplift pressures are excessive.

Borehole water-inflow test procedures were established in this thesis, and are presented as a basis for other studies. These test procedures were progressively improved during the weeks in which tests were carried out in the foundations of two large Portuguese concrete dams and proved to be practical and effective. Analysis of water-inflow test results together with data recorded with water electrical conductivity analysis and, in some cases, with additional simple tests that include closure and opening of boreholes within a given area of the dam foundation, proved to be appropriate to obtain knowledge of seepage patterns underneath concrete dams.

The tests carried out in both Pedrógão and Alqueva dam led to some conclusions about the depth at which the seepage paths cross each one of the tested boreholes, about the distribution of discharges and water pressures along the boreholes, and about seepage paths linking various boreholes. Results analysis showed that tests are better carried out with both single and double packers, as the two sets of results provide different and additional information. The simultaneous analysis of water pressures and discharges at each test interval can give information about the aperture of the discontinuities through which water flows. The knowledge obtained from the use of borehole water-inflow tests and water electrical conductivity analysis is relevant when identifying possible failure modes, and can thus help in the development of a suitable monitoring programme, which indirectly contributes to a better safety assessment of the dam.

Concerning modelling, different approaches were used to simulate both local and global effects and to assess the stability of dam foundations. Modelling was carried out using a step-by-step procedure, starting from simple models and gradually adding complexity, in order not only to detect possible errors in parameters, loads or boundary conditions, but also to make it clear how each change in the model affected the numerical outcome. Equivalent continuum models with regions of different permeability were employed to analyse both local and global effects, as an alternative to discontinuum modelling. Fracture flow models were used in the case of the gravity dam, for which the stability for different foundation failure scenarios was also evaluated.

Appropriate ways to represent individual drains were analysed in detail, taking into account the computational difficulties of three-dimensional models. In fact, while the drain's cylindrical surface is easily represented in simple 2D meshes, this is not the case in large 3D models. The alternative, employed in this study, is to represent the drain as a line, i.e. by its axis, however in such cases the mesh around the drain must be carefully selected. Comparison of different mesh sizes in this study showed that finer meshes do not improve the numerical solution, but tend to amplify the line singularity. Modelling the drain by its axis allows the use of coarser meshes which, consequently, leads to shorter run times. Particularly relevant is the conclusion that, with the type of elements used in both codes FLAC and 3DEC, when the drain is modelled by its axis the optimal size of the elements in the vicinity of the drain is in the order of three and a half times the borehole diameter.

In this study, borehole water-inflow tests carried out *in situ* were simulated using a detailed three-dimensional model which allowed each drain to be modelled individually, taking into account the results of rock mass permeability tests and identified areas where seepage paths cross each borehole. This detailed 3D model required a fine mesh, and thus, with a view to using adequate element sizes and faster analysis, numerical experiments with different meshes were carried out, from very fine meshes to coarser meshes. Back-analysis techniques are

sometimes used to determine unknown or little-known physical parameters; however, in this case, even with the low number of parameters considered in each model, this would have presented significant difficulties, namely due to the excessive run-times required. Therefore, during the model's development, a trial-and-error estimating procedure was carried out to continually adjust parameters.

The borehole water-inflow tests provided more details about seepage in the foundation of both Alqueva and Pedrógão dams. The simulations of borehole water-inflow tests presented in chapter 6 provided a good match of recorded discharges and water pressures for different experimental conditions. These simulations are relevant as the numerical modelling of tests provides a valuable tool for the validation of numerical techniques. Parametric studies carried out showed the importance of assigning proper values to both rock mass equivalent permeability and the permeability of the layers which simulate the main flow paths. The knowledge of seepage patterns around particular boreholes gained from test analysis was essential to develop an effective application of a simplified global model of the dam foundation.

The difficulties in simulating tests carried out in one of the boreholes draw attention to two relevant issues, both concerning numerical modelling. The first is the fact that numerical results can be highly sensitive to boundary conditions, and therefore great care must be taken in order to use the most appropriate boundary conditions for the problem to be solved. In fact, it was impossible to simulate results of tests carried out in one of the dam drains until the existence of a small leakage through the floor of a gallery located downstream from where the tests were carried out was taken into account. This leakage was almost imperceptible, and only detectable by personnel with great experience in the task of dam inspection. This fact leads to the second relevant issue, that those involved in numerical modelling of test results should follow up the tests carried out. This may not be so relevant in tests carried out in the laboratory, of which the procedures are well established. However, in tests carried out *in situ*, every detail can be relevant for accurate numerical modelling. Even details concerning the equipment and the way tests were carried out can help and be significant in numerical modelling of test results. This also applies to the numerical modelling of dam behaviour, which means that the modeller always profits from visiting the dam site and carefully observing relevant aspects. This greatly helps in choosing appropriate boundary conditions and in deciding the relevant aspects to be taken into account and included in the model.

Global 3D foundation models involve large volumes of the rock masses, thus can only be carried out with coarse meshes, in which it is not possible to model each one of the drains. As a consequence the drainage system is represented in a simplified way. The study presented here shows that modelling the drainage system by a hypothetical continuous trench with the same depth as the drains is practical. In this case, if the average value of the hydraulic head at

the line of the drains is assumed, the total discharge at the trench is almost the same as the total discharge in a 3D model, and the difference in piezometric heads is only significant close to the line of the drains. Global models may not be able to simulate local effects but can provide mean water pressures and flow rates for each dam foundation block, which is significant in stability analysis.

The interdependency between the state of stress and seepage in the foundation of Alqueva dam was studied in an uncoupled way, taking into account the results of global hydraulic and mechanical models, which were both validated against monitoring data. A methodology was developed that can be used to establish rules which, from a hydraulic model calibrated for specific water levels in the reservoir and downstream from the dam, allow the calculation of discharges for different water levels, taking into account that permeability depends not only on the stress level but also on local geological features. The simplicity of the method makes it very useful in the safety assessment of concrete dams.

Several conclusions are drawn regarding the suitability and limitations of the adopted numerical models. Concerning the study of both local and global hydraulic behaviour of dam foundations, it is concluded that although discontinuum models provide a more natural representation of flow in jointed rock masses, equivalent continuum models can also be used successfully. In fact, realistic and efficient models were developed with only a few parameters, all of them with physical meaning. These simpler models were employed as an alternative to discontinuum modelling and proved to be an effective analysis tool to assess concrete dam foundations' behaviour in normal operating conditions. These models have the advantage of making it possible to avoid the difficulties of characterizing the behaviour of individual joints and the complications of explicitly representing the discontinuities in large models of dam foundations. Hydraulic equivalent continuum models require the permeability of the different foundation areas to be properly measured and the main seepage paths to be clearly identified. In these models, flow through specific higher conductivity features may be approximated, as in this study, with bands of elements of higher permeability. Due to uncertainty about geomechanical and hydraulic properties, it is essential to assess the key parameters.

Regarding monitoring of the dam foundation, the *in situ* tests used in this study (borehole water-inflow tests, water electrical conductivity analysis and simple tests that involve the closing and opening of drainage and piezometric boreholes) could in future be used in other dams as a supplement to the usual seepage information available from drains and piezometers, as they allow the assessment of seepage patterns underneath the dam. The numerical study on piezometric measurements presented in the last part of chapter 6 highlights the significance of using small intake areas to measure uplift pressures or pressures within discontinuities. The most appropriate solution for piezometric measurements depends highly on local conditions

and therefore the positioning and length of the piezometric chambers must be decided case by case, in order to provide the most accurate information. This can be easily done in the majority of the Portuguese concrete dams.

For those whose work involves the modelling of concrete dams, especially arch dams, the code 3DEC is particularly suitable to carry out stability analysis, considering some discontinuities in the foundation. In this case, failure mechanisms involve the rock mass discontinuities and the dam/foundation interface. 3DEC allows the study of the dam-foundation system, as it allows the modelling of the dam as a shell structure, represented by the FEM, and the foundation as a group of blocks. Hydraulic analysis with the code 3DEC presented in this thesis was carried out with a new version of the numerical code, which allows both equivalent continuum and fracture flow models. The validation of the equivalent continuum possibility of this new version, by comparing its results with analytical solutions, is relevant as it is very useful to study the hydraulic behaviour of the dam foundation with the same code which is used to carry out stability analysis. In mechanical modelling, the consideration of a few selected discontinuities is often sufficient to assess the safety conditions. Fluid flow analysis of global 3D foundation models based on equivalent continuum concepts, like those presented in this thesis, may provide an adequate approximation of the water pressures on the discontinuities, necessary for the mechanical stability analysis.

In order to improve current ability to assess the safety of concrete dams for failure scenarios involving the foundation, a detailed study on seepage in a gravity dam foundation was carried out, using a discontinuum model. While the evaluation of dam behaviour can be done accurately with equivalent continuum models, dam stability analysis is better carried out with models in which the discontinuities are explicitly represented. The results of these models, however, depend mainly on the fracture pattern and on hydromechanical characterization data, namely joint normal stiffness, joint apertures and residual aperture. Therefore, stability analysis must be carried out assuming that each parameter may vary within a credible range. The study presented in Chapter 7 uses the code UDEC, which allows the hydromechanical behaviour of jointed rock masses to be accurately simulated. Stability analysis was carried out with different assumptions about uplift pressures, joint shear strength and joint hydraulic properties. Results allowed us to quantify the influence of water pressures on the stability of the dam.

8.2 Further developments

Concerning the observation and analysis of dam foundation behaviour, additional studies can be done, namely quantitative interpretations carried out for different periods of time, gradually longer, but using the same functions to represent the two main effects, which could be a way of quantifying phenomena such as clogging of the rock mass, and more detailed analysis of the results obtained in quantitative interpretations of discharges collected in measuring weirs, taking into account that for different reservoir levels the water may be collected from a different number of drains. Another area for further investigation concerns the hypothesis regarding the fact that in both Alto Lindoso and Alqueva dams, for a given water level, the highest discharges are recorded when that level is reached for the first time. The suggestion made in this study is that this could be due to the higher rate of variation of the reservoir level.

Further developments in the experimental field include the simplification of test procedures and the implementation of an automatic data collection system. Test procedures could be simplified, depending on the information required, by taking readings in transient conditions. This may significantly decrease the time taken to carry out tests in a large number of cases. More detailed and accurate information on variations in water pressures during tests could be easily obtained via a data logger linked to a laptop. As a basis for other studies, it would be very interesting to have multilevel piezometers or piezodrains continuously monitored by automatic recording systems. This would provide valuable data, which analysed in conjunction with records of variations in both reservoir level and ambient temperature, could provide important information about hydromechanical interaction in some areas of a concrete dam foundation.

Regarding numerical modelling, the procedures presented for analysis of observed behaviour by means of global continuum models may be developed in order to represent the hydromechanical interaction more consistently. To carry out hydromechanical analysis, an iterative procedure may be implemented, as the developed hydraulic and mechanical models are essentially the same. It is therefore possible to transfer the uplift and seepage forces obtained from the seepage flow analysis to the mechanical analysis. Firstly, the hydraulic problem can be solved using initial hydraulic parameters and boundary conditions, which provide the seepage and uplift forces. Secondly, the mechanical model may be run and the final states of stress and strain allow the new permeability coefficients to be calculated. The iterative procedure ends when the difference in displacements and hydraulic heads in successive iterations is not significant. As was shown in the case studied, this coupled analysis may require different laws to be attributed to the foundation of each dam block. The meshes of the hydraulic and mechanical models may not be exactly the same. This is the case of the global hydraulic and mechanical models presented in chapter 6, developed for Alqueva

dam. It is therefore necessary to develop a procedure to interpolate the different variables which have to be transferred from one model to another.

In this study, stability analysis was carried out only for gravity dams, however these procedures can be extended to 3D, for analysis of arch dam foundations or even gravity dams with more complex jointing patterns. These more elaborate models will require better characterization of both fracture geometry and hydraulic properties. In addition, they will also require the application of adequate methodologies and the use of 3D joint generators, particularly discrete fracture network (DFN) generators, in order to realistically reproduce statistical descriptions of joint patterns. DFN generators for flow simulations in fractured hard rocks, which only represent the void space of the connected fractures and exclude the rock blocks between the fractures, are practical and have been applied in different engineering fields. Their use in 3D in the particular case of dam foundations could be a basis for further study.

Analysis in steady state conditions, such as that presented in this study, is adequate in most fluid flow analysis of dam foundations. However, there are circumstances in which the time dependent effect transient flow may be important. This was the case in chapter 3, in which it was found useful to determine flow times. However, the small timesteps required by UDEC make transient fluid flow analysis impractical in relatively large domains and with very small joint apertures, such as those necessary to analyse flow in dam foundations. It is therefore necessary to develop new procedures, based on algorithms that use larger timesteps.

Another field that merits further attention is concerned with the foundation treatment, namely regarding characterization, for more accurate modelling. In this study, grouted rock mass areas were simulated by regions of lower permeability, of which the width in the upstream-downstream direction was roughly estimated. According to the Committee on Fracture Characterization and Fluid Flow (1996), limited analytical prediction is possible and much of the grouting procedure is based on experience and on careful application of the adaptable/observational approach. In this regard, *in situ* permeability tests are usually carried out during foundation treatment, before deciding on further grouting, and this gives an indication of the permeability of the grouted area. *In situ* tests, such as those based on geophysical methods, for example, may be used to map the spreading of grout in dam foundations, for better characterization. Regarding modelling, further analysis of grout flow and solidification could be carried out.

References

- Alonso, E. 2005. Las catástrofes y el progreso de la geotecnia. Lección Inaugural del Año Académico 2005. Real Academia de Ingeniería, Madrid, Spain, 18 January 2005.
- Alonso, E., Carol, I., Delahaye, C., Gens, A., and Prat, P. 1996. Evaluation of safety factors in discontinuous rock. *International Journal of Rock Mechanics and Mining Science & Geomechanics Abstracts*, **33**(5): 513-537.
- Alonso, E.E., Gens, A., Carol, I., Prat, P., and Herrero, E. 1994. Three-dimensional failure mechanisms in arch dam abutments. A safety study. *In Proceedings of the 18th International Congress on Large Dams*. Durban, South Africa, 7-11 November 1994. ICOLD, Paris, pp. 471-484.
- Andrade, R.M. 1982. A drenagem na fundação das estruturas hidráulicas. Análise e interpretação prática. Engevix, S.A. - Estruturas e Projectos de Engenharia, Rio de Janeiro, Brasil.
- Andrade, R.M. 1983. O controle da subpressão pela drenagem horizontal. Base teórica e experimental. Engevix, S.A. - Estruturas e Projectos de Engenharia, Rio de Janeiro, Brasil.
- Andrade, R.M. 1984. Hidrogeotecnia nas barragens. Método de análise. Engevix, S.A. - Estruturas e Projectos de Engenharia, Rio de Janeiro, Brasil.
- Andrade, R.M. 1988. Mechanics of flow in fractured rock masses applied to dams. Engevix, S.A. - Estruturas e projectos de Engenharia, Rio de Janeiro, Brasil.
- Asgian, M. 1989. A numerical model of fluid-flow in deformable naturally fractured rock masses. *International Journal of Rock Mechanics and Mining Science & Geomechanics Abstracts*, **26**(3/4): 317-328.
- Ask, D., Cornet, F.H., Fontbonne, F., Nilsson, T., Jönsson, L., and Ask, M.V.S. 2009. A quadruple packer tool for conducting hydraulic stress measurements in mines and other high stress settings. *International Journal of Rock Mechanics and Mining Sciences*, **46**(6): 1097-1102.
- Bandis, S.C., Lumsden, A.C., and Barton, N.R. 1983. Fundamentals of rock joint deformation. *International Journal of Rock Mechanics and Mining Science & Geomechanics Abstracts*, **20**(6): 249-268.
- Barla, G., Bonini, M., and Cammarata, G. 2004. Stress and seepage analyses for a gravity dam on a jointed granitic rock mass. *In Proceedings of the First International UDEC/3DEC Symposium*. Bochum, 29 September - 1 October 2004. A.A. Balkema Publishers, Rotterdam, pp. 263-268.

- Barton, N., and de Quadros, E.F. 1997. Joint aperture and roughness in the prediction of flow and groutability of rock masses. *International Journal of Rock Mechanics and Mining Science & Geomechanics Abstracts*, **34**(3-4): 252e251-252e214.
- Barton, N., Bandis, S., and Bakhtar, K. 1985. Strength, deformation and conductivity coupling of rock joints. *International Journal of Rock Mechanics and Mining Science & Geomechanics Abstracts*, **22**(3): 121-140.
- Batista, A.L. 1998. Análise do comportamento ao longo do tempo de barragens abóbada. Ph.D. thesis, Departamento de Engenharia Civil e Arquitectura, IST, Universidade Técnica de Lisboa, Lisboa, Portugal.
- Bawden, W.F., Curran, J.H., and Roegiers, J.-C. 1980. Influence of fracture deformation on secondary permeability - A numerical approach. *International Journal for Rock Mechanics and Mining Sciences and Geomechanical Abstracts*, **17**: 265-279.
- Bear, J. 1988. *Dynamic of fluids in porous media*. Dover Publications, Inc., New York.
- Bedmar, A.P., and Araguás, L.A. 2002. *Detection and prevention of leaks from dams*. A.A. Balkema Publishers, Rotterdam.
- Bernstone, C., Westberg, M., and Jeppsson, J. 2009. Structural assessment of a concrete dam based on uplift pressure monitoring. *Journal of Geotechnical and Geoenvironmental Engineering*, **135**(1): 133-142.
- Bonaldi, P., Fanelli, M., and Giuseppetti, G. 1977. Displacement forecasting for concrete dams. *Water Power and Dam Construction*, **September 1977**: 42-50.
- Bonaldi, P., Fanelli, M., Giuseppetti, G., and Riccioni, R. 1980a. Automatic observation and instantaneous control of dam safety. Part two: a priori, deterministic models, and a posteriori models. *In ISMES*. Vol. 133, pp. 1-69.
- Bonaldi, P., Fanelli, M., Giuseppetti, G., and Riccioni, R. 1980b. Automated safety control procedures and management of surveillance for concrete dams in Italy. *In ISMES*. Vol. 139.
- Bonaldi, P., Fanelli, M., Giuseppetti, G., and Riccioni, R. 1982. Safety control of concrete dams: the role of automated procedures and management of surveillance. *In Proceedings of the 14th International Congress on Large Dams*. Rio de Janeiro, Brazil, 3-7 May 1982. ICOLD, France, Vol.I, Q52-R56, pp. 943-969.
- Bonelli, S. 2004. Analyse retard des mesures d'auscultation de barrages. *Revue Française de Géotechnique*, **108**(3): 31-45.
- Bordes, J.L., and Debeuille, P.J. 1987. Instrumentation practice for short term monitoring of civil works. *Water Power and Dam Construction*, **June 1987**: 45-47.
- Breitenstein, F., Köhler, W., and Widmann, R. 1985. Safety control of the dams of the Glockner-Kaprun hydro-electric development. *In Proceedings of the 15th International*

- Congress on Large Dams Lausanne, Switzerland, 18-23 June 1985. ICOLD, Paris, Vol.I, Q56-R59, pp. 1121-1134.
- Brown, E.T., and Bray, J.W. 1982. Rock support interaction calculations for pressure shafts and tunnels. *In Proceedings of the International Symposium on Rock Mechanics, Caverns and Pressure Shafts*, pp. 555-566.
- Bulut, F., Boynukalm, S., Tarhan, F., and Dilek, R. 1996. A new approach to the evaluation of water-pressure test results obtained in bedrock by the US Bureau of Reclamation Method. *Engineering Geology*, **44**(1-4): 235-243.
- Bureau, G.J. 2006. Use of FLAC for seismic analysis of concrete gravity dams. *In Proceedings of the 4th International Symposium on Numerical Modelling in Geomechanics*. Madrid, Spain, 29-31 May 2006. Itasca Consulting Group, Inc, Minneapolis, pp. 141-148.
- Bustamante, L., and Radisic, A. 2006. Structural design and RCC zoning in Ralco dam. *In Proceedings of the 22nd International Congress on Large Dams*. Barcelona, Spain, 18-23 June 2006. ICOLD, Paris, Vol.1, Q84-R3, pp. 33-45.
- Cadei, M., Lazzari, M., and Salvaneschi, P. 1990. Safety management of civil structures using knowledge based systems. *In Proceedings of the 3rd International Conference on Industrial and Engineering Applications of Artificial Intelligence and Expert Systems*. Charleston, South Carolina, United States. ACM, Vol.2, pp. 618-627.
- Câmara, R. 2007. Radiação sísmica numa falha para uma barragem abóbada. Relatório 264/2007 - NMMF, LNEC, Lisboa.
- Cammarata, G., Fidelibus, C., Cravero, M., and Barla, G. 2007. The hydro-mechanically coupled response of rock fractures. *Rock Mechanics and Rock Engineering*, **40**(1): 41-61.
- Cappa, F., Guglielmi, Y., Fénart, P., Merrien-Soukatchoff, V., and Thoraval, A. 2005. Hydromechanical interactions in a fractured carbonate reservoir inferred from hydraulic and mechanical measurements. *International Journal of Rock Mechanics and Mining Sciences*, **42**(2): 287-306.
- Cappa, F., Guglielmi, Y., Rutqvist, J., Tsang, C.F., and Thoraval, A. 2006. Hydromechanical modelling of pulse tests that measure fluid pressure and fracture normal displacement at the Coaraze Laboratory site, France. *International Journal of Rock Mechanics and Mining Sciences*, **43**(7): 1062-1082.
- Carmo Vaz, A. 1979. Programa de cálculo automático para estudo de escoamentos tridimensionais em meios contínuos pelo método dos elementos finitos, LNEC, Lisboa.
- Carrère, A.J., Colson, M., Goguel, B., and Noret, C. 2000. Modelling: a means of assisting interpretation of readings. *In Proceedings of the 20th International Congress on Large Dams*. Beijing, China, 19-22 September 2000. ICOLD, Paris, Vol.III, Q78-R63, pp. 1005-1037.

- Casagrande, A. 1961. Control of seepage through foundations and abutments of dams. First Rankine Lecture. *Géotechnique*, **XI**(3): 161-182.
- Castro, A.T. 1997. Métodos de retroanálise na interpretação do comportamento de barragens de betão. Ph.D. thesis, Departamento de Engenharia Civil e Arquitectura, IST, Universidade Técnica de Lisboa, Lisboa, Portugal.
- CFBR 2006. Recommandations pour la justification de la stabilité des barrages-poids.
- Chen, Y., Zhou, C., and Sheng, Y. 2007. Formulation of strain-dependent hydraulic conductivity for a fractured rock mass. *International Journal of Rock Mechanics and Mining Sciences*, **44**(7): 981-996.
- Chen, Z., Narayan, S.P., Yang, Z., and Rahman, S.S. 2000. An experimental investigation on hydraulic behaviour of fractures and joints in granitic rock. *International Journal of Rock Mechanics and Mining Sciences*, **37**: 1061-1071.
- CIMNE 2006. GID - The personal pre and post processor. Version 8.0.2. GID User Manual. International Center for Numerical Methods in Engineering, Barcelona, Spain.
- Committee on Fracture Characterization and Fluid Flow 1996. Rock fractures and fluid flow. Contemporary understanding and applications. National Academy Press, Washington, D.C.
- Cook, N.G.W. 1992. Natural joints in rock: mechanical, hydraulic and seismic behaviour and properties under normal stress. *International Journal of Rock Mechanics and Mining Science & Geomechanics Abstracts*, **29**(3): 198-223.
- Cornet, F.H., Li, L., Hulin, J.P., Ippolito, I., and Kurowski, P. 2003. The hydromechanical behaviour of a fracture: an in situ experimental case study. *International Journal of Rock Mechanics and Mining Sciences*, **40**(7-8): 1257-1270.
- Crépon, O., and Lino, M. 1999. An analytical approach to monitoring. *International Water Power and Dam Construction*, **June 1999**: 52-54.
- Da Silva, J.F. 2005. Influence of the geometry of the drainage system and of the foundation anisotropy on the uplift pressures under concrete dams. *In Proceedings of the 5° Brazilian Symposium on Applications of Computational Mechanics in Geotechnical Engineering*. Belo Horizonte, Brazil, May 2005, pp. 165-174.
- Da Silva, J.F. 2006. Optimization of concrete gravity dams foundation drainage systems. *In Proceedings of the XXII International Congress on Large Dams*. Barcelona, Spain, 18-23 June 2006. Taylor & Francis Group, Balkema, London, UK, pp. 633-639.
- Da Silva, J.F., and Da Gama, E.M. 2003. A three-dimensional model for seepage analysis of concrete dam foundations. *In Proceedings of the 4th International Workshop on Applications of Computational Mechanics in Geotechnical Engineering*. Ouro Preto, Brazil, 17-20 August 2003, pp. 337-357.

- Damjanac, B. 1996. A three-dimensional numerical model of water flow in a fractured rock mass. Ph.D. thesis, University of Minnesota, Minneapolis, USA.
- De Sortis, A., and Paoliani, P. 2007. Statistical analysis and structural identification in concrete dam monitoring. *Engineering Structures*, **29**(1): 110-120.
- DGRAH 1978. Sistema Odelouca-Funcho. Barragem do Funcho. Volume IV. Estudos geológicos e geotécnicos, Lisboa.
- Doboz, W. 1982. Model estimating displacement of a dam point as a function of loading and temperature history. *In Proceedings of the 14th International Conference on Large Dams*. Rio de Janeiro, Brazil, 3-7 May 1982. ICOLD, Paris, Vol.I, Q52-R35.
- Dunnicliff, J. 1988. Geotechnical instrumentation for monitoring field performance. John Wiley & Sons, Inc., New York, USA.
- EDP 1988. Aproveitamento do rio Guadiana. Escalão de Alqueva. Projecto, EDP, Porto, Portugal.
- EDP 1994. Aproveitamento do rio Guadiana. Escalão de Alqueva. Revisão do projecto de Março de 1988, Porto, Portugal.
- EDP 2003. Aproveitamento hidroeléctrico do empreendimento de fins múltiplos de Alqueva. Escalão de Alqueva. Planta geológica-geotécnica da fundação. Nota Técnica, Porto.
- EDP 2004. Aproveitamento hidroeléctrico de fins múltiplos de Alqueva. Escalão de Pedrógão. Cartografia geológica-geotécnica das superfícies escavadas. Nota Técnica, Porto.
- EDP 2006. Aproveitamento hidroeléctrico do Alqueva. Arquivo técnico. Relatório síntese, Porto, Portugal.
- Esaki, T., Du, S., Mitani, Y., Ikusada, K., and Jing, L. 1999. Development of a shear-flow test apparatus and determination of coupled properties for a single rock joint. *International Journal of Rock Mechanics and Mining Sciences*, **36**(5): 641-650.
- European Club of ICOLD 2004a. Uplift pressures under concrete dams - Final Report. Report of the European Working Group. *In Proceedings of the ICOLD European Symposium Dams in a European Context*. Geiranger, Norway, June 2001. A.A. Balkema, The Netherlands.
- European Club of ICOLD 2004b. Sliding safety of existing gravity dams - Final Report. Report of the European Working Group.
- Fanelli, M. 1979. Automatic observation and instantaneous control of dam safety. Part one: an approach to the problem. *Water Power and Dam Construction*, **Special Issue**(November-December 1979).
- Fanelli, M.A., Giuseppetti, G., and Riccioni, R. 1979. Experience gained during control of static behaviour of some large Italian dams. *In Proceedings of the 13th International*

- Congress on Large Dams. New Delhi, India, November 1979. ICOLD, Paris, Vol.II, Q49-R44, pp. 663-682.
- Farinha, M.L.B., and Lemos, J.V. 2006. Representação em modelos numéricos do comportamento hidráulico de fundações de barragens de betão. Relatório 419/2006 - NO/NMMF, LNEC, Lisboa.
- Farinha, M.L.B., Castro, A.T., and Pina, C.A.B. 2004. Definição e exploração de sistemas de recolha automática de dados da observação de barragens de betão. Relatório 175/04 - NO, LNEC, Lisboa.
- Farinha, M.L.B., Lemos, J.V., and Castro, A.T. 2006. Modelação numérica do comportamento hidráulico de fundações de barragens de betão. *In* Proceedings of the 10º Congresso Nacional de Geotecnia. Lisboa, Portugal, 22-26 May 2006. Sociedade Portuguesa de Geotecnia, Lisboa, Vol.2, pp. 553-562.
- Farinha, M.L.B., Lemos, J.V., and Castro, A.T. 2007. Analysis of seepage in the foundation of Pedrógão dam. *In* Proceedings of the 5th International Conference on Dam Engineering. Lisbon, Portugal, 14-16 February 2007. LNEC, Lisboa, pp. 195-202.
- Fell, R., MacGregor, P., Stapledon, D., and Bell, G. 2005. Geotechnical engineering of embankment dams. Taylor and Francis Group, London, UK.
- FERC 2002. Engineering guidelines for the evaluation of hydropower projects. Chapter 3 - Gravity dams.
- Ferry, S., and Willm, G. 1958. Méthode d'analyse et de surveillance des déplacements observés par le moyen de pendules dans les barrages. *In* Proceedings of the 6th International Congress on Large Dams. New York, USA, 15-20 September 1958. ICOLD, Paris, Vol.II, Q21-R118, pp. 1179-1201.
- Florentino, C.A. 1983. O controlo de segurança de barragens de betão. Research Programme, LNEC, Lisboa, Portugal.
- Florentino, C.A., Leite Pinto, L.V., and Mascarenhas, A.T. 1971. Interpretação quantitativa dos resultados de observação de barragens de betão. Relatório final, LNEC, Lisboa.
- Florentino, C.A., Matos, M.E.C., Silva, A.F., and Rocha, M.E.M. 1985. Basic principles of dams observation in Portugal. The Aguieira dam example. *In* Proceedings of the 15th International Congress on Large Dams. Lausanne, Switzerland, 18-23 June 1985. ICOLD, Paris, Vol.I, Q.56-R37, pp. 721-735.
- Franciss, F.O. 1970. Contribution à l'étude du mouvement de l'eau à travers les milieux fissurés. Ph.D. thesis, Faculté des Sciences de l'Université de Grenoble, Grenoble, France.
- Gale, J.E., Dillabough, G., and Butt, S. 1994. Comparison of coupled stress-flow numerical simulations to experimental data from shear permeability tests. *In* Proceedings of the 2nd International Conference on Applications of Computational Mechanics in Geotechnical Engineering. Rio de Janeiro, Brazil, 3-5 November 1994, pp. 125-148.

- Gallego, J.D., Olias, E.M., Lopez, D.S., and Aguilar, J.P. 2007. Automatic system for the management of monitoring information in 16 dams in the South of Spain. *In Proceedings of the 5th International Conference on Dam Engineering*. Lisbon, Portugal, 14-16 February 2007 pp. 179-186.
- Ghobadi, M.H., Khanlari, G.R., and Djalaly, H. 2005. Seepage problems in the right abutment of the Shahid Abbaspour dam, southern Iran. *Engineering Geology*, **82**(2): 119-126.
- Giacomel, A., and Rowe, C. 1992. Inflatable packer fundamentals. *In Proceedings of the International Conference Drill '92*. Perth, Australia, October 1992.
- Giacomini, A., Buzzi, O., Ferrero, A.M., Migliazza, M., and Giani, G.P. 2008. Numerical study of flow anisotropy within a single natural rock joint. *International Journal of Rock Mechanics and Mining Sciences*, **45**(1): 47-58.
- Gicot, H. 1964. The deformations of the Rossens arch dam during fourteen years service. *In Proceedings of the 8th International Congress on Large Dams*. Edinburgh, UK, 4-8 May 1964. ICOLD, Paris, Vol.II, Q29-R24, pp. 419-429.
- Gicot, H. 1976. Une méthode d'analyse des déformations des barrages. *In Proceedings of the 12th International Congress on Large Dams*. Mexico City, Mexico, 29 March - 2 April 1976. ICOLD, Paris, Vol.IV, C1, pp. 787-790.
- Gimenes, E.Á. 2000. Hydromechanical evaluation of flow behaviour in rock foundations of concrete gravity dams. Ph.D. thesis, Department of Civil Engineering, University of Illinois at Urbana-Champaign, Urbana, Illinois, USA.
- Gimenes, E.Á., and Fernández, G. 2006. Hydromechanical analysis of flow behaviour in concrete gravity dam foundations. *Canadian Geotechnical Journal*, **43**(3): 244-259.
- Gomes, A.F.S. 1981. Automatização das actividades de observação de barragens e análise quantitativa de resultados. Tese para obtenção do grau de Especialista. LNEC, Lisboa, Portugal.
- Gomes, A.F.S., and Matos, D.S. 1985. Quantitative analysis of dam monitoring results. State of the art, applications and prospects. *In Proceedings of the 15th International Congress on Large Dams*. Lausanne, Switzerland, 18-23 June 1985. ICOLD, Paris, Vol.I, Q56-R39, pp. 749-761.
- Goodman, R.E. 1974. The mechanical properties of joints. *In Proceedings of the 3rd International Congress of the International Society for Rock Mechanics*. Denver, USA, 1-7 September 1974, Vol.I, pp. 127-140.
- Goodman, R.E., Amadei, B., and Sitar, N. 1983. Uplift pressure in a crack below a dam. *Journal of Energy Engineering*, **109**(4): 207-221.
- Greene, B., and Christ, C.A. 1998. Mistakes of man: the Austin dam disaster of 1911. *Pennsylvania Geology*, **29**(2/3): 7-14.

- Guedes, Q.M., and Coelho, P.S.M. 1985. Statistical behaviour model of dams. *In Proceedings of the 15th Congress on Large Dams*. Lausanne, Switzerland, 18-23 June 1985. ICOLD, Paris, Vol.I, Q.56-R16, pp. 319-334.
- Hamm, S.-Y., Kim, M., Cheong, J.-Y., Kim, J.-Y., Son, M., and Kim, T.-W. 2007. Relationship between hydraulic conductivity and fracture properties estimated from packer tests and borehole data in a fractured granite. *Engineering Geology*, **92**(1-2): 73-87.
- Hans, J., and Boulon, M. 2003. A new device for investigating the hydro-mechanical properties of rock joints. *International Journal for Numerical and Analytical Methods in Geomechanics*, **27**(6): 513-548.
- Harr, M.E. 1962. *Ground water and seepage*. MacGraw Hill Book Co., New York, USA.
- Hasegawa, T., and Murakami, A. 1988. Technique of monitoring for dam safety and its application. *In Proceedings of the 16th International Congress on Large Dams*. San Francisco, USA, 13-17 June 1988. ICOLD, Paris, Vol.II, C2, pp. 929-954.
- HIDRORUMO 1999. Aproveitamento Hidroeléctrico do Empreendimento de Fins Múltiplos do Alqueva. Escalão de Pedrógão. Projecto-Base, Porto.
- HIDRORUMO 2001. Aproveitamento hidroeléctrico do empreendimento de fins múltiplos de Alqueva. Escalão de Pedrógão. Projecto, Porto.
- Hoek, E. 2001. Rock mass properties for underground mines. *In Underground Mining Methods: Engineering Fundamentals and International case studies*. Edited by W.A. Hustrulid and R.L. Bullock. Society for Mining, Metallurgy, and Exploration (SME), Littleton, Colorado, USA. pp. 467-474.
- Hoek, E., and Brown, E.T. 1980. *Underground excavations in rock*. Institution of Mining and Metallurgy, London.
- Hoek, E., and Bray, J.W. 1981. *Rock slope engineering*. Institution of Mining and Metallurgy, London, UK.
- Houlsby, A.C. 1976. Routine interpretation of the Lugeon water test. *Quarterly Journal Engineering Geology*, **9**: 303-312.
- Huai-Zhi, S., and Zhi-Ping, W. 2005. Intelligent early-warning system of dam safety. *In Proceedings of the International Conference on Machine Learning and Cybernetics*, Vol.3, pp. 1868-1877.
- Hudson, J.A., and Cosgrove, J.W. 1997. Integrated structural geology and engineering rock mechanics approach to site characterization. *International Journal of Rock Mechanics and Mining Sciences*, **34**(3-4): 136.e131-136.e115.
- Hudson, J.A., and Harrison, J.P. 2000. *Engineering rock mechanics. An introduction to the principles*. Imperial College of Science, Technology and Medicine. University of London, London, UK.

- Hvorslev, M.J. 1951. Time lag and soil permeability in ground-water observations. Report to the Waterways Experiment Station, Corps of Engineers, Vicksburg, Mississippi. Bulletin n° 36.
- ICOLD 1974. Lessons from dam incidents. International Commission on Large Dams, Paris.
- ICOLD 1983. Deterioration of dams and reservoirs. Examples and their analysis. International Commission on Large Dams, Paris.
- ICOLD 1993. Rock foundations for dams. Bulletin 88. International Commission on Large Dams, Paris.
- ICOLD 1994. Ageing of dams and appurtenant works. Review and recommendations. International Commission on Large Dams, Paris.
- ICOLD 1995. Dam failures. Statistical analysis. International Commission on Large Dams, Paris.
- ICOLD 2005. Dam foundations - Geologic considerations. Investigation methods. Treatment. Monitoring. Bulletin 129. International Commission on Large Dams, Paris.
- ISRM 1978. Suggested methods for the quantitative description of discontinuities in rock masses. International Journal of Rock Mechanics and Mining Science & Geomechanics Abstracts, **15**(6): 319-368.
- ISRM 1981. Basic geotechnical description of rock masses. International Journal of Rock Mechanics and Mining Science & Geomechanics Abstracts: 85-110.
- ISRM 2007. The complete ISRM suggested methods for rock characterization, testing and monitoring: 1974-2006. ISRM Turkish National Group, Ankara, Turkey.
- Itasca 2002. FLAC - Fast Lagrangean Analysis of Continua, Version 4.0, User's Manual. Itasca Consulting Group, Minneapolis, USA.
- Itasca 2003. 3DEC - 3-Dimensional Distinct Element Code, Version 3.0, User's Manual. Itasca Consulting Group, Minneapolis, USA.
- Itasca 2004. UDEC - Universal Distinct Element Code, Version 4.0, User's Manual. Itasca Consulting Group, Minneapolis, USA.
- Itasca 2005. FLAC - Fast Lagrangean Analysis of Continua, Version 5.0, User's Manual. Itasca Consulting Group, Minneapolis, USA.
- Javanmardi, F., Léger, P., and Tinawi, R. 2005a. Seismic structural stability of concrete gravity dams considering transient uplift pressures in cracks. Engineering Structures, **27**(4): 616-628.
- Javanmardi, F., Léger, P., and Tinawi, R. 2005b. Seismic water pressure in cracked concrete gravity dams: experimental study and theoretical modelling. Journal of Structural Engineering ASCE, **131**(1): 139-150.

- Jing, L. 2003. A review of techniques, advances and outstanding issues in numerical modelling for rock mechanics and rock engineering. *International Journal of Rock Mechanics and Mining Sciences*, **40**(3): 283-353.
- Jing, L., and Hudson, J.A. 2002. Numerical methods in rock mechanics. *International Journal of Rock Mechanics and Mining Sciences*, **39**(4): 409-427.
- Jing, L., and Stephansson, O. 2007. *Fundamentals of discrete element methods for rock engineering: theory and applications*. Elsevier, Rotterdam.
- Jinping, H., and Zhenzhao, L. 1988. The mathematical model of dam safety monitoring based on multiple survey points. *In Proceedings of the International Conference on New Trends and Guidelines on Dam Safety*. Barcelona, Spain, 17-19 June 1988. Balkema, Rotterdam, Vol.2, pp. 989-995.
- Kovari, K., and Köppel, J. 1987. Head distribution monitoring with the sliding piezometer system "piezodex". *In Proceedings of the 2nd International Symposium Field measurements in Geomechanics*. Kobe, Japan, 6-9 April 1987, Vol.1, pp. 255-267.
- Kovari, K., and Koppel, J. 1987. Field studies of coupled mechanical and hydraulic processes in the foundation rock of large dams. *In Coupled Processes Associated with Nuclear Waste Repositories*. Academic Press, pp. 739-757.
- Kovari, K., and Fritz, P. 1989. Re-evaluation of the sliding stability of concrete structures on rock with emphasis on European experience. Technical Report REMR-GT-12, U.S. Army Research Development and Standardization Group, London, UK.
- Kovari, K., and Fritz, P. 1993. Reevaluation of the stability of large concrete structures on rock. *In Comprehensive rock engineering: principles, practice and projects (Vol. 5)*. Edited by John A. Hudson. Pergamon Press, Oxford. pp. 653-700.
- Kovari, K., Arn, T., and Gmünder, C. 1989. Groundwater flow through fissured rock: field investigations and interpretation in the Albigna dam area, Graubünden, Switzerland, Nationale Genossenschaft für die Lagerung Radioaktiver Abfälle (Nagra), Baden, Switzerland.
- Kulatilake, P.H.S.W., Park, J., Balasingam, P., and Morgan, R. 2008. Quantification of aperture and relations between aperture, normal stress and fluid flow for natural single rock fractures. *Geotechnical and Geological Engineering*, **26**(3): 269-281.
- Lamas, L.N. 1993. Contributions to understanding the hydromechanical behaviour of pressure tunnels. Ph.D. thesis, Imperial College of Science, Technology and Medicine, University of London, London, UK.
- Lambe, T.W. 1973. Thirteenth Rankine Lecture: Predictions in soil engineering. *Géotechnique*, **23**(2): 149-202.
- Lancaster-Jones, P.F.F. 1975. The interpretation of the Lugeon water-test. *Quarterly Journal Engineering Geology*, **8**: 151-154.

- Leclerc, M., Léger, P., and Tinawi, R. 2003. Computer aided stability analysis of gravity dams-CADAM. *Advances in Engineering Software*, **34**(7): 403-420.
- Léger, P., and Leclerc, M. 2007. Hydrostatic, temperature, time-displacement model for concrete dams. *Journal of Engineering Mechanics*, **133**(3): 267-277.
- Leitão, N.S., and Lamas, L.N. 2006. Modeling of the high pressure circuit of the Venda Nova hydroelectric scheme. *In Proceedings of the 4th International FLAC Symposium. Madrid, Spain, 29-31 May 2006. Itasca Consulting Group, Inc., Minneapolis*, pp. 131-137.
- Lemos, J.V. 1987. A distinct element model for dynamic analysis of jointed rock with application to dam foundations and fault motion. Ph.D. thesis, University of Minnesota, Minneapolis, USA.
- Lemos, J.V. 1996. Modelling of arch dams on jointed rock foundations. *In Proceedings of the International Conference EUROCK'96. Torino, Italy, 2-5 September 1996. Balkema, Rotterdam, The Netherlands, Vol.1*, pp. 519-526.
- Lemos, J.V. 1998. Development of an arch dam analysis module for the program 3DEC. Relatório 316/98 - NDE/NEE, LNEC, Lisboa.
- Lemos, J.V. 1999a. Discrete element analysis of dam foundations. *In Distinct Element Modelling in Geomechanics. Edited by V.M. Sharma, K.R. Saxena and R.D. Woods. Oxford and IBH Publishing, New Delhi*. pp. 89-115.
- Lemos, J.V. 1999b. Modelling and failure analysis in rock engineering. Research Programme, LNEC, Lisbon, Portugal.
- Lemos, J.V., and Cundall, P. 1999. Earthquake analysis of concrete gravity dams on jointed rock foundations. *In Distinct element modelling in geomechanics. Edited by V.M. Sharma, K.R. Saxena and R.D. Woods. Oxford and IBH Publishing, New Delhi*. pp. 117-143.
- Lemos, J.V., and Pereira Gomes, J. 2007. Modeling seismic failure scenarios of concrete dam foundations. *In Proceedings of the 5th International Workshop on Applications of Computational Mechanics in Geotechnical Engineering. Guimarães, Portugal, 1-4 April 2007*, pp. 341-349.
- Lemos, J.V., Pina, C.A.B., Pereira da Costa, C., and Pereira Gomes, J. 1995. Experimental study of an arch dam on a jointed foundation. *In Proceedings of the Eighth ISRM Congress. Edited by T. Fujii. Tokyo, Japan. Rotterdam: Balkema, Vol.III*, pp. 1263-1266.
- Lemos, J.V., Batista, A.L., Dias, I., and Câmara, R. 2006. Análise sísmica da barragem de Chicamba (Moçambique). *In Proceedings of 4as Jornadas Portuguesas de Engenharia de Estruturas. Lisboa, LNEC, 13-16 Dezembro 2006*, pp. 130-131.
- Lévy, M.M. 1895. Quelques considérations sur la construction des grands barrages. *Comptes Rendus des Séances de l'Académie des Sciences*, **CXXI**(6): 288-300.

- Li, B., Jiang, Y., Koyama, T., Jing, L., and Tanabashi, Y. 2008. Experimental study of the hydro-mechanical behavior of rock joints using a parallel-plate model containing contact areas and artificial fractures. *International Journal of Rock Mechanics and Mining Sciences*, **45**(3): 362-375.
- Liberal, O., Miranda, P., Monteiro, P., Paixão, J., Lima, C., and Moreira, A.P. 2002. Tratamento de uma zona de falha de grande possança na margem esquerda da barragem de Alqueva. *In XII Congresso Brasileiro de Mecânica de solos e Engenharia Geotécnica*. S. Paulo, Brasil (in Portuguese).
- Liu, E. 2005. Effects of fracture aperture and roughness on hydraulic and mechanical properties of rocks: implication of seismic characterization of fractured reservoirs. *Journal of Geophysics and Engineering*, **2**(2005): 38-47.
- LNEC 1961. Observação da barragem da Venda Nova. Relatório final, LNEC, Lisboa.
- LNEC 1970. Prospeção geofísica no local da barragem de Alqueva. 1º Relatório, LNEC, Lisboa.
- LNEC 1973. Estudo das fundações da barragem de Alqueva. Relatório. Volumes I, II, III, LNEC, Lisboa.
- LNEC 1975. Prospeção geofísica no local da barragem de Alqueva. 3º Relatório, LNEC, Lisboa.
- LNEC 1984. Estudo das características de deslizamento de diaclases do maciço de fundação da barragem de Alqueva. Relatório 272/84 - NFR, LNEC, Lisboa.
- LNEC 1986. Ensaios geofísicos, por métodos sísmicos, na caracterização do maciço de fundação da barragem de Alqueva. Relatório, LNEC, Lisboa.
- LNEC 1990. Comportamento hidráulico actual da fundação da barragem do Funcho. Nota Técnica, LNEC, Lisboa.
- LNEC 1995. Fundações da barragem de Alqueva. Caracterização do material da falha. Relatório 245/95 - NOS, LNEC, Lisboa.
- LNEC 1997a. Plano de observação do escalão de Alqueva. Barragem, fundação, maciço envolvente, albufeira e obras anexas. Relatório 244/97 - NO, LNEC, Lisboa.
- LNEC 1997b. Complemento da componente piezométrica do sistema de observação da barragem de Santa Águeda (Marateca). Relatório 147/97 - NF, LNEC, Lisboa.
- LNEC 1998a. Fundações da barragem de Alqueva. Caracterização do material da falha (no estado natural e consolidado). Relatório 141/98 - NOS, LNEC, Lisboa.
- LNEC 1998b. Reforço do tratamento da fundação da barragem do Funcho (2ª Fase). Relatório 272/98 - NO/NF, LNEC, Lisboa.

- LNEC 1999a. Estudo do comportamento da barragem de Vilarinho das Furnas. Relatório 221/99 - NO; NDE/NEE, LNEC, Lisboa.
- LNEC 1999b. Ensaios de caracterização do material da falha da barragem do Alqueva. Nota Técnica 4/99 - NF, LNEC, Lisboa.
- LNEC 1999c. Barragem de Alqueva. Caracterização do material da falha 22. Ensaios de placa. Relatório 209/99 - NOS, LNEC, Lisboa.
- LNEC 1999d. Prospeção geofísica complementar, por métodos sísmicos, no local de implantação do açude de Pedrógão. Relatório 260/99 - NP, LNEC, Lisboa.
- LNEC 2002. Tomografias sísmicas nas fundações da barragem de Alqueva. Fases 1 (pré-tratamento) e 2 (pós-tratamento). Relatório 147/2002 - NP, LNEC, Lisboa.
- LNEC 2003. Barragem de Alqueva. Caracterização do material da falha 22. Ensaios de dilatómetro. Relatório 350/03 - NFOS, LNEC, Lisboa.
- LNEC 2004. Ensaios de caracterização geomecânica do maciço de fundação da barragem de Pedrógão. Relatório 44/04 - NFOS, LNEC, Lisboa.
- LNEC 2005a. Análise do comportamento estrutural da barragem do Funcho com base na observação até 2004. Relatório 215/2005-NO/DBB, LNEC, Lisboa.
- LNEC 2005b. Análise do comportamento hidráulico da fundação do muro-barragem jusante de Alqueva. Relatório 312/05 - NO/NFOS, LNEC, Lisboa.
- LNEC 2008. Barragem de Alqueva. Comportamento observado durante o primeiro enchimento da albufeira. Relatório 435/2008 - DBB/NO, LNEC, Lisboa.
- LNEC 2009. Barragem de Alqueva. Interpretação do comportamento durante o 1º enchimento da albufeira. Relatório DBB/NO, LNEC, Lisboa.
- Lombardi, G. 2007. 3-D analysis of gravity dams. *Hydropower and Dams(One)*: 98-102.
- Lombardi, G., Amberg, F., and Darbre, G.R. 2008. Algorithm for the prediction of functional delays in the behaviour of concrete dams. *The International Journal on Hydropower and Dams*, **15**(Issue Three, 2008): 111-116.
- Londe, P. 1973a. Analysis of the stability of rock slopes. *The Quarterly Journal of Engineering Geology*, **6**(1): 93-124.
- Londe, P. 1973b. The role of rock mechanics in the reconnaissance of rock foundations. *The Quarterly Journal of Engineering Geology*, **6**(1): 56-74.
- Londe, P. 1973c. Water seepage in rock slopes. *The Quarterly Journal of Engineering Geology*, **6**(1): 75-92.

- Londe, P. 1985. The Malpasset dam failure. *In Proceedings of the International workshop on dam failures*. Purdue University, West Lafayette; Indiana, 6-8 August 1985. Elsevier, N.Y.
- Londe, P. 1993. Safety evaluation using reliability analysis. *In Proceedings of the International Workshop on Dam Safety Evaluation*. Grindelwald, Switzerland, 26-28 April 1993, Vol.4, pp. 171-188.
- Londe, P., and Sabarly, F. 1966. La distribution des perméabilités dans la fondation des barrages voûtes en fonction du champ de contrainte. *In Proceedings of the 1st International Congress on Rock Mechanics*. Lisboa, Portugal, 25 September - 1 October 1966, Vol.II, pp. 517-522.
- Lopez, P., Thoraval, A., Buzzi, O., Rahmani, I., and Boulon, M. 2007. Advances in constitutive modelling of jointed rock hydro mechanical interactions at laboratory scale. *In Proceedings of the 18^{ème} Congrès de Mécanique*. Grenoble, France, 27-31 August 2007.
- Louis, C. 1969. A study of groundwater flow in jointed rock and its influence on the stability of rock masses. Ph.D. thesis, University of Karlsruhe (in German), English translation, Imperial College Rock Mechanics Research Report n°10, London, UK.
- Louis, C., and Maini, Y.N. 1970. Determination of in situ hydraulic parameters in jointed rock. *In Proceedings of the 2nd International Congress on Rock Mechanics*. Belgrade, USA, 21-26 September 1970, Vol.I, pp. 235-245.
- Lugeon, M. 1932. Barrages et géologie. *Bulletin technique de la Suisse Romande*.
- Marache, A., Riss, J., and Gentier, S. 2008. Experimental and modelled mechanical behaviour of a rock fracture under normal stress. *Rock Mechanics and Rock Engineering*, **41**(6): 869-892.
- Maranha das Neves, E. 1994. Estados limites e segurança em geotecnia. *Geotecnia*, **72**: 5-62.
- Mascarenhas, A.T. 1979. Percolação na fundação de barragens de betão. LNEC thesis, Lisboa, Portugal.
- Mascarenhas, A.T. 1991. Comportamento hidromecânico e deteriorações em fundações de barragens de betão. Research Programme, LNEC, Lisbon, Portugal.
- Mascarenhas, A.T., and Silva, H.S. 1990. Estudo da eficiência das obras de impermeabilização e drenagem no controlo da percolação nas fundações de barragens de betão. LNEC, Lisboa, Memória n° 747.
- Mascarenhas, A.T., Sousa, L.R., and Martins, C.S. 1985. Uplift, seepage control and observed behaviour of Aguieira dam foundation. LNEC, Lisboa, Memória n° 656.
- Mata, J. 2007. Aplicação de redes neuronais ao controlo de segurança de barragens de betão. M.Sc. thesis, Departamento de Engenharia Civil e Arquitectura, IST, Universidade Técnica de Lisboa, Lisboa, Portugal.

- Mendonça, T.G. 1989. Modelo de elementos finitos tridimensionais para estudo do comportamento hidromecânico de fundações de barragens de betão, LNEC, Lisboa.
- Miike, R., and Kobayashi, I. 1989. Safety control of arch dams by regression model. *In* Proceedings of the 2nd International Symposium on Design of Hydraulic Structures. Fort Collins, USA, 26-29 June 1989. Balkema, Rotterdam, pp. 91-96.
- Miranda, M.P., and Maia, M.C. 2004. Main features of the Alqueva and Pedrógão Projects. *The International Journal on Hydropower and Dams* **11**(Issue Five, 2004): 95-99.
- Mostyn, G., Helgstedt, M.D., and Douglas, K.J. 1997. Towards field bounds on rock mass failure criteria. *International Journal of Rock Mechanics and Mining Sciences*, **34**(3-4): 208.e201-208.e218.
- Moura, G.M.G. 2005. Determinação de tensões a partir de extensões observadas em barragens de betão. M.Sc. thesis, FEUP Porto, Portugal.
- Moye, D.G. 1967. Diamond drilling for foundation exploration. *Civil Engineering Transactions*, **CE** **9**(1): 95-100.
- Muralha, J., Leitão, N.S., and Castro, A.T. 2003. Observação do tratamento da falha 22 da barragem de Alqueva. *In* Proceedings of the 1as Jornadas Hispano-Lusas sobre Obras Subterrâneas. Madrid, Spain, 15-16 September 2003 pp. 507 - 516.
- Muskat, M. 1946. *The flow of homogeneous fluids through porous media*. Edwards Brothers, Inc, Michigan, U.S.A.
- Neiva, J.M.C., Neves, J., and Lima, C. 2004. Geology and geotechnics of Alqueva and Pedrógão dam sites and their importance on the foundation zoning. *In* Proceedings of the 2nd International Conference on Site Characterization (ISC-2). Porto, Portugal. 20-22 September 2004. Millpress, Rotterdam, Vol.2, pp. 1067-1073.
- Neiva, J.M.C., Matos, D.S., Lima, C., and Ferreira, F. 1997. Geology and geotechnics of Alqueva dam site in the Guadiana river. *In* Proceedings of 6º Congresso Nacional de Geotecnia. IST, Lisboa, Vol.2/3, pp. 615-626.
- Neuzil, C.E., and Tracy, J.V. 1981. Flow through fractures. *Water Resources Research*, **17**: 191-199.
- Neves, J., and Gonçalves, L. 2002. Reconhecimento geológico e geotécnico da zona de falha 22 durante a fase de construção da barragem de Alqueva. *In* 12º Congresso Brasileiro de Mecânica dos Solos e Engenharia Geotécnica. S. Paulo, Brasil, 20-24 Outubro 2002.
- Neves, J., Neiva, J.M.C., and Lima, C. 2000. Geology and Geotechnics of Pedrógão dam site in the Guadiana River. *In* Proceedings of the 7º Congresso Nacional de Geotecnia. Porto, Portugal, 10-13 April 2000, pp. 263-272.
- Nguyen, H.P. 2003. Trends and technologies for monitoring dams (at Hydro-Quebec). *Hydro Review*, **22**(June 2003).

- Noorishad, J., Ayatollahi, M.S., and Witherspoon, P.A. 1982. A finite-element method for coupled stress and fluid flow analysis in fractured masses. *International Journal of Rock Mechanics and Mining Science & Geomechanics Abstracts*, **19**: 185-193.
- Noorishad, J., Tsang, C.F., and Witherspoon, P.A. 1992. Theoretical and field studies of coupled hydromechanical behaviour of fractured rocks - 1. Development and verification of a numerical simulator. *International Journal of Rock Mechanics and Mining Sciences and Geomechanics Abstracts*, **29**(4): 401-409.
- Oliveira, S. 2000. Modelos para análise do comportamento de barragens de betão considerando a fissuração e os efeitos do tempo. Formulações de dano. Ph.D. thesis, FEUP, Porto, Portugal.
- Olsson, R., and Barton, N. 2001. An improved model for hydromechanical coupling during shearing of rock joints. *International Journal of Rock Mechanics and Mining Sciences*, **38**(3): 317-329.
- Pedro, J.O. 1999a. Safety and performance of arch dams. *In Arch dams. Designing and monitoring for safety. Edited by J.O. Pedro. Springer. pp. 27-42.*
- Pedro, J.O. 1999b. Observação de obras. LNEC, Lisboa, Memória nº 821.
- Pedro, J.O. 2001. Segurança e funcionalidade das barragens. LNEC, Lisboa, Memória nº 824.
- Pedro, J.O., Gomes, A.F.S., and Câmara, R.C. 1984. Stress evaluation in concrete dams: the example of Varosa dam. *In Proceedings of the International Conference on Safety of Dams. Coimbra, Portugal, 23-28 April 1984. A. A. Balkema, Rotterdam, pp. 179-187.*
- Pedro, J.O., Mascarenhas, A.T., Sousa, L.R., Rodrigues, L.F., Silva, H.S., and Castro, A.T. 1989. Rock mass foundation deterioration of portuguese concrete dams. Some case histories. Report 58/89 - Chefia, LNEC, Lisboa.
- Penot, I., Daumas, B., and Fabre, J.P. 2005. Monitoring behaviour. *Water Power and Dam Construction*, **57**(12): 24-27.
- Pereira da Costa, C., Pereira Gomes, J., Lemos, J.V., and Pina, C.A.B. 1993. Estudo em modelo geomecânico da rotura de uma barragem gravidade por deslizamento ao longo da fundação. Relatório 85/93 - NDE/NEE, LNEC, Lisboa, Portugal.
- Pereira Gomes, J. 2006. Análise experimental de cenários de rotura em fundações de barragens de betão. Ensaio estáticos e dinâmicos. Ph.D. thesis. Universidade Federal do Rio de Janeiro.
- Pereira Gomes, J., Pereira da Costa, C., Lemos, J.V., and Pina, C.A.B. 1997. Study on a geomechanical model of the failure of a gravity dam due to sliding along the foundation. LNEC, Lisboa, Memória nº 810.
- Perner, F., Koehler, W., and Oberhuber, P. 2001. Interpretation of Schlegeis dam crest displacements. *In Proceedings of the 6th International Benchmark Workshop on Numerical Analysis of Dams. Salzburg, Austria, 17-19 October 2001.*

- Pina, C.A.B., and Portela, E.A. 2006. Tecnologias de informação no controlo de segurança de barragens de betão. *Construção Magazine. Revista Técnico-Científica de Engenharia Civil*, **15**(Dossier "Grandes Obras"): 18-25.
- Pina, C.A.B., Pereira da Costa, C., Lemos, J.V., and Pereira Gomes, J. 1993. An experimental study of failure of a gravity dam on a jointed rock foundation. *In Proceedings of Computational Methods and Experimental Measurements VI*. Sienna, Italy, 3-5 May 1993. Elsevier, Vol.2, pp. 293-301.
- Pina, C.A.B., Lemos, J.V., Leitão, N.S., Câmara, R., Centeno, F.V., Cevallos, F.G., Rodriguez, L.C., and Tejada, J.O. 2006. Seismic analysis of El Frayle arch dam considering the non-linear behaviour of the rock mass joints. *In Proceedings of the 22nd International Congress on Large Dams*. Barcelona, Spain, 18-23 June 2006. ICOLD, Paris, Vol.I, Q84-R22, pp. 345-356.
- Pinto, A.V., Quintela, A., Gomes, A.S., and Coelho, A.M. 1991. Beliche dam. Study of a foundation leakage. *In Proceedings of the 17th International Congress on Large Dams*. Wien, Austria, 16-21 June 1991. ICOLD, Paris, Vol.III, Q66-R66, pp. 1241-1257.
- Pinto, P.S.S., and Maranha das Neves, E. 1987. Analysis of the foundations of Crestuma and Coimbra dams. *In Proceedings of the 9th European Conference on Soil Mechanics and Foundation Engineering*. Dublin, 31 August - 3 September 1987. A.A. Balkema, Rotterdam, pp. 485-490.
- Piroddi, L., and Spinelli, W. 2003. Long-range nonlinear prediction: a case study. *In Proceedings of the 42nd IEEE Conference on Decision and Control*. Maui, Hawaii, USA, December 2003, pp. 3984-3989.
- Plesha, M.E. 1987. Constitutive models for rock discontinuities with dilatancy and surface degradation. *International Journal for Numerical and Analytical Methods in Geomechanics*, **11**: 345-362.
- Portela, E.A. 2001. Novas metodologias de apoio ao controlo de segurança de barragens de betão. Uma abordagem através dos sistemas periciais. Ph.D. thesis, Departamento de Engenharia Civil e Arquitectura, IST, Universidade Técnica de Lisboa, Lisboa, Portugal.
- Portela, E.A., Pina, C., Silva, A.R., Galhardas, H., and Barateiro, J. 2005. A modernização dos sistemas de informação de barragens: o sistema GestBarragens. *In Proceedings of the Seminário Barragens, Tecnologia, Segurança e Interação com a Sociedade*. Lisboa, Portugal, 27-29 Outubro 2005, pp. 467-482.
- Post, G. 1985. Dams and foundation monitoring. General Report Q. 56. *In Proceedings of the 15th International Congress on Large Dams*. Lausanne, Switzerland, 24-28 June 1985. ICOLD, Paris, Vol.1, pp. 1623-1727.
- Pyrak-Nolte, L.J., and Morris, J.P. 2000. Single fractures under normal stress: The relation between fracture specific stiffness and fluid flow. *International Journal of Rock Mechanics and Mining Sciences*, **37**(1-2): 245-262.

- Ramos, J.M. 1985. Consideração da reologia do betão no comportamento de barragens. LNEC thesis, Lisboa.
- Ramos, J.M. 2008. Deterioração e reabilitação de barragens de betão. Aspectos estruturais. Casos de obra. LNEC, Lisboa, Memória nº 838.
- Resende, R., Lemos, J.V., and Dinis, P.B. 2004. Application of a discontinuity model with softening to the analysis of dam foundations using the Discrete Element Method. *In* Proceedings of the First International UDEC/3DEC Symposium. Bochum, 29 September - 1 October 2004. A.A. Balkema Publishers, Rotterdam, pp. 249-255.
- Rocha, M. 1956. Nota sobre a interpretação dos resultados da observação de barragens, LNEC, Lisboa, Portugal.
- Rocha, M. 1964. Assessment of observation techniques used in Portuguese concrete dams. *In* Proceedings of the 8th International Congress on Large Dams. Edinburgh, UK, 4-8 May 1964, Vol.II, Q29-R42, pp. 757-790.
- Rocha, M. 1980a. Comportamento e segurança das fundações das barragens de betão (2ª parte). *Geotecnia*, **30**(Dezembro): 63-91.
- Rocha, M. 1980b. Comportamento e segurança das fundações das barragens de betão (1ª parte). *Geotecnia*, **29**(Julho): 83-114.
- Rocha, M., and Franciss, F. 1977. Determinação da permeabilidade dos maciços rochosos anisotrópicos a partir de amostras integrais. *Geotecnia*, **19**: 23-56.
- Rocha, M., Serafim, J.L., and Silveira, A.F. 1958a. A method of quantitative interpretation of the results obtained in the observation of dams. *In* Proceedings of the 6th International Congress on Large Dams. New York, USA, 15-20 September 1958. ICOLD, Paris, Vol.II, Q21-R36, pp. 371-396.
- Rocha, M., Serafim, J.L., and Silveira, A.F. 1960. Um método de interpretação quantitativa dos resultados obtidos na observação de barragens. LNEC, Lisboa, Memória nº 128.
- Rocha, M., Serafim, J.L., Silveira, A.F., and Guerreiro, M.Q. 1958b. Observation of concrete dams. Results obtained in Cabril dam New York, USA, 15-20 September 1958. ICOLD, Paris, Vol.II, Q21-R83, pp. 877-926.
- Rochon-Cyr, M., and Léger, P. 2009. Shake table sliding response of a gravity dam model including water uplift pressure [online]. *Engineering Structures*(2009): doi: 10.1016/j.engstruct.2009.1003.1001.
- Rogers, J.D. 2006. Lessons learned from the St. Francis dam failure. *Geo-Strata*, **6**(March/April 2006): 14-17.
- Romana, M. 2004. DMR (an adaptation of RMR), a new geomechanics classification for use in dams foundations. *In* Proceedings of the II Congresso Luso-Brasileiro de Geotecnia. Aveiro, Portugal, pp. 175-188.

- Rowe, C.J. 2000. Inflatable packers for grouting. AEG Developments, Perth W.A., Australia.
- Rowe, C.J. 2001. The inflatable packer - a most versatile tool. *In* Proceedings of the International Conference Drill 2001. Perth W.A., Australia, October 2001.
- RSB 2007. Regulamento de Segurança de Barragens e correspondentes portarias: I - Normas de projecto de barragens; II - Normas de observação e de inspecção de barragens. Decreto-Lei 344/2007 de 15 de Outubro, Diário da República, Lisboa.
- Rutqvist, J., and Stephansson, O. 2003. The role of hydromechanical coupling in fractured rock engineering. *Hydrogeology Journal*, **11**(1): 7-40.
- Rutqvist, J., Noorishad, J., Stephansson, O., and Tsang, C.F. 1992. Theoretical and field studies of coupled hydromechanical behaviour of fractured rocks - 2. Field experiment and modelling. *International Journal of Rock Mechanics and Mining Sciences and Geomechanics Abstracts*, **29**(4): 411-419.
- SCD 2003. Methods of analysis for the prediction and the verification of dam behaviour. Edited by the Swiss Committee on Dams (SCD) on the occasion of the 21st International Congress on Large Dams. *Wasser Energie Luft*, **95**(3/4): 73-110.
- Schnitter, N.J. 1994. A history of dams. The useful pyramids. A.A. Balkema, Rotterdam, Netherlands.
- Serafim, J.L. 1954. A subpressão nas barragens. LNEC thesis, Lisboa, Portugal.
- Serafim, J.L. 1968. Influence of interstitial water on the behaviour of rock masses. *In* *Rock Mechanics in Engineering Practice*. Edited by K.G. Staag and O.C. Zienkiewicz John Wiley & Sons, London. pp. 55-97.
- Serafim, J.L., and Del Campo, A. 1965. Interstitial pressures on rock foundations of dams. *Journal of the Soil Mechanics and Foundations Division*. Proceedings of the American Society of Civil Engineers.
- Serafim, J.L., Silveira, A.F., and Pedro, J.O. 1962. Interpretação quantitativa dos resultados obtidos na observação de barragens de betão. Aplicação às barragens de Castelo do Bode e Venda Nova, LNEC, Lisboa.
- Service Construction Aménagements Hydroélectriques du Groupe Edison-Milan 1958. Analyse des déplacements de la clé de l'arc de couronnement du barrage de Santa Giustina, relevés pendant les six premières années d'observation. *In* Proceedings of the 6th International Congress on Large Dams. New York, USA, 15-20 September 1958. ICOLD, France, Vol.II, Q21-R67, pp. 627-641.
- Shahkarami, A., Delforouzi, M., and Salari, H. 2004. Study of the compression and tension factors of safety with a 3D FEM model for an arch dam and rock foundation: a case study of the Karun III Arch Dam in Iran. *International Journal of Rock Mechanics and Mining Sciences*, **41**(3): 479-483.

- Silva, H.S. 1988. Estudo do comportamento hidromecânico das fundações de barragens de betão. Aplicação à barragem de Cahora Bassa. Trabalho de síntese, LNEC, Lisboa, Portugal.
- Silveira, A.F. 1965. Quantitative interpretation of results obtained in the observation of concrete dams. LNEC, Lisboa, Memória nº 253.
- Silveira, A.F., and Pedro, J.O. 1964. Quantitative interpretation of results obtained in the observation of concrete dams. *In* Proceedings of the 8th International Congress on Large Dams. Edinburgh, UK, 4-8 May 1964. ICOLD, Paris, Vol.2, Q29-R43, pp. 791-809.
- Silveira, A.F., Florentino, C.A., and Freitas, C.M.S. 1981. LNEC experience in the field of concrete dam observation and of in situ tests. LNEC, Lisboa, Memória nº 548.
- Sisavath, S., Al-Yaarubi, A., Pain, C.C., and Zimmerman, R.W. 2003. A simple model for deviations from the cubic law for a fracture undergoing dilation or closure. *Pure and Applied Geophysics*(160): 1009-1022.
- Smith, N. 1971. A history of dams. Peter Davies, London, UK.
- Snow, D.T. 1965. A parallel plate model of fractured permeable media. Ph.D. thesis, University of California, Berkeley, USA.
- Sousa, L.R., and Mascarenhas, A.T. 1984. Analysis and observation of the behaviour of the Agueira dam foundation. LNEC, Lisboa, Memória nº 621.
- Stateler, J.N. 2006. Instrumented monitoring of dams: the ideal situation, and the current realities in 2006. *In* Proceedings of the III Simpósio Sobre Instrumentação de Barragens. São Paulo, Brasil, 12-14 Setembro 2006. Comité Brasileiro de Barragens, pp. 3-29.
- Tecnasol FGE 2007. Barragem de Pedrógão. Empreitada de tratamento de fundações e de implementação do Plano de Observação. Relatório final.
- Teles, M. 1985. Comportamento térmico de barragens de betão. Ph.D. thesis, FEUP, Porto, Portugal.
- Tremmel, E. 1958. Analysis of pendulum measurements. *In* Proceedings of the 6th International Congress on Large Dams New York, USA, 15-20 September 1958. ICOLD, Paris, Vol.II, Q21-R15, pp. 233-248.
- Tsang, Y.W., and Witherspoon, P.A. 1981. Hydromechanical behavior of a deformable rock fracture subject to normal stress. *Journal of Geophysical Research*, **86**(B10): 9287-9298.
- USACE 1984. Geotechnical investigations. Engineer Manual 1110-2-1804. Washington, DC.
- USACE 1993. Seepage analysis and control for dams. Engineer Manual 1110-2-1901. Washington, DC.

- USACE 1994. Rock foundations. Engineer Manual 1110-1-2908. Washington, DC.
- USACE 2000. Evaluation and comparison of stability analysis and uplift criteria for concrete gravity dams by three Federal Agencies. ERDC/ITL TR-00-1. Washington, DC.
- USACE 2005. Stability analysis of concrete structures. Engineer Manual 1110-2-2100. Washington, DC.
- Veltrop, J.A. 1988. Concrete arch dams. *In* Development of dam engineering in the United States. *Edited by* E.B. Kollgaard and W.L. Chadwick. U.S. Committee on Large Dams. Pergamon Press, New York. pp. 219-318.
- Wang, M., Kulatilake, P.H.S.W., Um, J., and Narvaiz, J. 2002. Estimation of REV size and three-dimensional hydraulic conductivity tensor for a fractured rock mass through a single well packer test and discrete fracture fluid flow modeling. *International Journal of Rock Mechanics and Mining Sciences*, **39**(7): 887-904.
- Wei, L., and Hudson, J.A. 1990. Permeability variation around underground openings in jointed rock masses: a numerical study. *In* Proceedings of the International Symposium on Rock Joints. Loen, Norway, pp. 565-569.
- Wei, L., and Hudson, J.A. 1998. A hybrid discrete-continuum approach to model hydro-mechanical behaviour of jointed rocks. *Engineering Geology*, **49**(3-4): 317-325.
- Widmann, R. 1967. Evaluation of deformation measurements performed at concrete dams. *In* Proceedings of the 9th International Congress on Large Dams. Istanbul, Turkey, 4-8 September 1967. ICOLD, Paris, Vol.III, Q34-R38, pp. 671-676.
- Willm, G., and Beaujoint, N. 1967. Les méthodes de surveillance des barrages au service de la production hydraulique d'Électricité de France. Problèmes anciens et solutions nouvelles. *In* Proceedings of the 9th International Congress on Large Dams. Istanbul, Turkey, 4-8 September 1967. ICOLD, France, Vol.III, Q34-R30, pp. 529-550.
- Witherspoon, P.A., Wang, J.S.Y., Iwai, K., and Gale, J.E. 1980. Validity of cubic law for fluid flow in a deformable rock fracture. *Water Resources Research*, **16**(6): 1016-1024.
- Wittke, W. 1990. Rock Mechanics. Theory and applications with case histories. Springer-Verlag, Berlin, Germany.
- Wittke, W., and Polczyk, H. 2002. The Urft masonry dam, three-dimensional stability analyses, monitoring and comparison of results. *In* Proceedings of the First Iranian Rock Mechanics Symposium. Tehran, Iran, 29-30 January 2002.
- Wittke, W., Schröder, D., and Polczyk, H. 2003. Upgrading the stability of three masonry dams in different ways. *In* Proceedings of the 10th International Congress of the International Society for Rock Mechanics (ISRM). Johannesburg, South Africa. South African Institute of Mining and Metallurgy, pp. 1321-1327.
- Wyllie, D.C. 1999. Foundations on rock. E & FN Spon, London, UK.

- Xerez, A.C., and Lamas, J.F. 1958. Methods of analysis of arch dam behaviour. *In* Proceedings of the 6th International Congress on Large Dams. New York, USA, 15-20 September 1958. ICOLD, Paris, Vol.II, Q21-R39, pp. 407-431.
- Yeo, I.W., de Freitas, M.H., and Zimmerman, R.W. 1998. Effect of shear displacement on the aperture and permeability of a rock fracture. *International Journal of Rock Mechanics and Mining Sciences*, **35**(8): 1051-1070.
- Yoshinaka, R., Yoshida, J., Arai, H., and Arisaka, S. 1993. Scale effects on shear and deformability of rock joints. *In* Proceedings of the International Symposium on Scale Effects in Rock Masses 93. Lisbon, Portugal, 25 June 1993. Balkema, Rotterdam, pp. 143-149.
- Zimmerman, R.W., and Bodvarsson, G.S. 1996. Hydraulic conductivity of rock fractures. *Transport in porous media*, **23**: 1-30.

Appendix 1

A1.1 Equipment required to carry out borehole water-inflow tests

1. Borehole checking

- “blind device” (piece of metal with the same diameter as the equipment to check for and remove, if possible, any obstructions, to make sure that the equipment will fit).

2. Packer

- a single rubber packer and a double packer with extension pipes (which allow test intervals of different lengths);
- a water pump, to inflate the packer;
- two flexible inflation hoses, one for water and the other for air;
- an air pump, to deflate the packers.

3. Placing and keeping in position the packer in the borehole

- steel cable, to hold the packer;
- a cover to close the test interval, with a hook to attach the steel cable;
- a series of pipes which allow the placing of the packers at the pre-established depth and which link the test interval to the borehole head, so that the flow rate into the test interval can be measured (in the study carried out, the equipment used to conduct tests has PVC pipes (38 units 2 m long and 5 units 1 m long), with a diameter of 1”, a weight per metre of 0.52 kg/m and trapezoidal grooves;
- device to link the packer to the pipes, with a hook to hold the steel cable;
- “o-rings” to avoid leaks in the pipes’ joints;
- vaseline, used to make the “o-rings” more flexible.

- adhesive tape or cramps to secure the hoses, the cable that links the pressure transducer to the recording device and the steel cable along the pipes;
- a reel to extend and withdraw the steel cable.

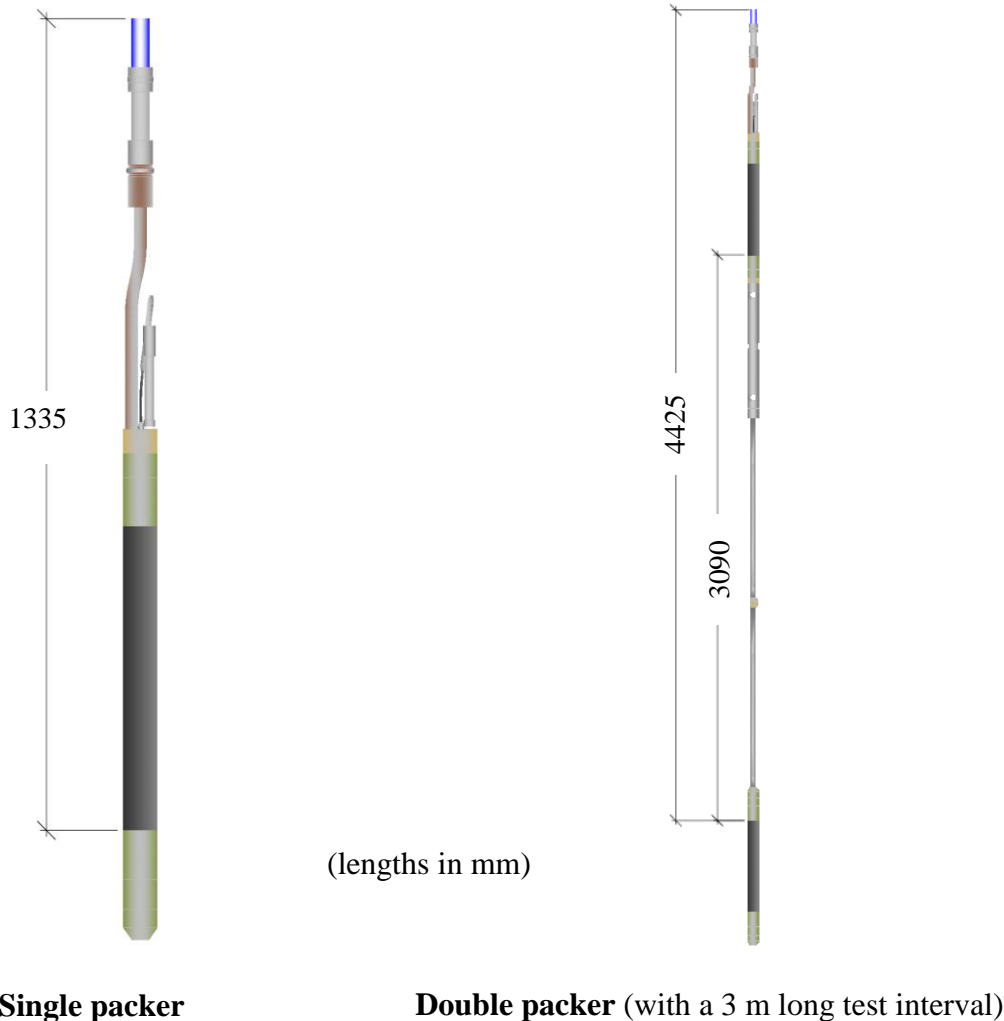
4. Measurement of discharge and water pressure

- measuring cylinders, to measure flow rates (of different sizes between 0.125 l and 20 l);
- a pressure transducer to measure and transmit water pressure data, calibrated for readings from 0 to the expected maximum water pressure (maximum hydraulic load when the reservoir is full), and a cable linking the transducer to the recording device;
- recording device for the electric transducer;
- a PVC “T-pipe”, placed at the borehole head, so that the flow rate into the borehole area above the test interval can be measured;
- a metallic “T-pipe”, placed at the borehole head, linked to a spherical valve tap and an outflow water pipe, to measure the flow rate into the test interval, and linked to a pressure gauge, which measures, at the borehole head, the water pressure at the test interval;
- precisely calibrated pressure gauges, with scales suitable for the expected maximum water pressure in the boreholes which are going to be tested;
- a depth measure with an electric contact meter to measure static water levels, when water does not reach the top of the pipes.

5. Other

- pipe-wrenches;
- a sturdy tripod to hold the pipes while packers are placed in or removed from vertical drainage or piezometric boreholes;
- table and chairs.
- water conductivity measuring device;
- borehole TV camera.

A1.2 Equipment geometry. Total length of pipes in each test interval



The total length of pipes (l) inside the borehole is given by:

$l = x - l_s + c$ - when testing with a single packer, to define a test interval down from a depth of x m.

$l = x_2 - l_d + c$ - when testing with a double packer, to define a test interval from a depth of x_1 m down to x_2 m.

in which:

- x – depth of the top of the test interval, when testing with a single packer;
- x_2 – depth of the bottom of the test interval, when testing with a double packer;
- l_s – length of the equipment assembled as a single packer ($l_s = 1.335$ m);
- l_d – length of the equipment assembled as a double packer ($l_d = 4.425$ m, for a 3 m long test interval);
- c – length of the pipe at the borehole’s head, measured from the floor to the borehole’s head.

A1.3 Test procedures

1. Measure water level in the reservoir.
2. Measure flow rates (l/min) and water pressures (bar), not only in the borehole which is going to be tested but also in the drainage and piezometric boreholes located in an area larger than that expected to be the borehole's area of influence ("reference values"). If there is no water flowing out of any of these boreholes, measure, with a depth measure with an electric contact meter, the static water level.
3. Insert a piece of metal with the same diameter as the equipment (blind device) into the borehole. Measure the borehole's length. If any obstruction which can not be removed is found **tests are not carried out in that borehole** and are restarted in another borehole where tests are planned to be carried out.
4. Assemble the packer as a **single packer**.
5. Place the single packer, with the aid of the pipes and held by the steel cable, for the test interval to be defined between the packer and the bottom of the borehole, with minimum and maximum lengths of 1 m and 3 m. **The "blind device" is not the same length as the packer; therefore, even if it is inserted into the borehole without finding any obstruction, it still may not be possible to insert the packer, if the borehole has not been drilled straight. If any difficulty is found whilst inserting the packer, it should not be forced through, tests are not carried out in that borehole**, and the process is restarted in any other borehole where tests are planned to be carried out.
6. Prepare the water pump: i) remove the air from the hydraulic circuit that links the pump to the pressure valve; ii) link the hose to the water pump; iii) remove the air from the hose; iv) link the water hose to the packer. Link the outflow to the air pump hose (in which the "deflation system" is inserted) to the air pump.
7. Inflate the packer, to seal off the test interval.
8. Measure the following, in pre-defined time intervals so as to observe the development until steady-state conditions are achieved:
 - a. Flow of water into the test interval, if water reaches the pipes' head.

- b. The static water level inside the pipes, if water does not reach the pipes' head.
- c. Water pressure in the test interval, if the packer is equipped with a pressure transducer in the test interval (a pressure gauge should be installed at the pipes' head, to check the water pressure recorded by the transducer: the water pressure at the transducer must correspond to the water pressure recorded at the pressure gauge plus the weight of a water column with a height equal to the distance between the manometer and the pressure transducer).
- d. Quantity of water flowing at above the packer (while tests are being carried out this borehole's area works as a drain). If water flowing at above the packer does not reach the borehole's head, use a depth measure with an electric transducer to measure the depth of the static water level.

Measure, after stabilization of the previous values:

- a. Discharges in all the drains located in the vicinity of the borehole being tested (water pressure and discharges, in the case of piezodrains). If water does not reach any borehole's head, use a depth measure with an electric contact meter to measure the depth of the static water level.
- b. Water pressure in piezometers installed in the vicinity of the borehole being tested.
- c. Taking into account recorded values try to establish the borehole's area of influence.

If values have not stabilized after 15 minutes repeat the same measurements every 15 minutes. If after an hour values are not stabilized, this test phase ends. If water does not reach the pipes' head test continues from step 11.

- 9. Close the test interval, not allowing water to flow out of the pipes.
- 10. Measure the following, in pre-defined time intervals so as to observe the development until steady-state conditions are achieved:
 - a. Test interval water pressure.
 - b. Discharge flowing at above the packer.

Then measure, after values have stabilized:

- a. Water pressure recorded in piezometers located in the area of influence of the borehole being tested.
- b. Water pressures and discharges in piezodrains located in the area of influence of the borehole being tested.

If values have not stabilized after 15 minutes repeat the same measurements every 15 minutes. If after an hour values are not stabilized, this test phase ends.

11. Deflate the packer, allowing a sufficient time interval so that the packer diameter returns to its initial value.
12. Take measurements again in the equipment installed in the area of influence of the borehole being tested (to check if reference values are achieved).
13. Raise the single packer 3 m (so that the same test intervals are considered both with the single and the double packer). Measure the water pressure at the recording device before inflating the packer.
14. Repeat steps 7 to 13 until the upper packer reaches the borehole's head.
15. Remove the equipment from the borehole.
16. With the single packer outside the borehole and when steady-state conditions have been achieved, measure discharges and water pressures in all the equipment installed in the area of influence of the borehole being tested.
17. Assemble the packer as a **double packer** with a 3 m long test interval.
18. Place the double packer, with the aid of the pipes and held by the steel cable, to define the test interval at 3 m above the first test interval defined with the single packer. **Neither the “blind device” nor the single packer used in the previous steps was the same length as the double packer, therefore, even if it was possible to insert the blind device into the borehole and carry out tests with the single packer without finding any obstruction, it may be not possible to insert the double packer. If any difficulty is found whilst inserting the packer, it should not be forced through, tests are not carried out in that borehole, and the process is restarted in any other borehole where tests are planned to be carried out.**
19. Repeat steps 6 to 15.

20. Remove the double packer from the borehole.
21. When tests are concluded, with the double packer out of the borehole and when steady state conditions have been achieved, measure flow rates and water pressures in all the equipment installed in the area of influence of the borehole being tested.

While tests are being carried out, the time at which measurements are taken should be registered.

A1.4 Measurements taken while carrying out borehole water-inflow tests in both Pedrógão and Alqueva dams

Test step	Time when readings began	D22 D	PZB 13-2	D23 D	PZB 13-1	D24 D	D25 D					D26 D	D27 D	PZB 12	D28 D	PZB 13-3	Total discharge
		discharge	water pressure	discharge	water pressure	discharge	diacharge (l/min)			water pressure (bar)		discharge	discharge	water pressure	discharge	water pressure	(l/min)
		(l/min)	(bar)	(l/min)	(bar)	(l/min)	total	test interval	above test interval	at pipes head	pressure transducer	(l/min)	(l/min)	(bar)	(l/min)	(bar)	(l/min)
1. Reference values (16 Oct. 2006)	15h 45min	0.05	1.30	0.03	0.55	0.03	1.92	-	-	-	-	1.04	0.73	0.50	0.26	0.50	4.06
2. Drain D25 D closed	16h 10min	0.06	1.60	0.05	1.40	0.03	-	-	-	4.825	-	1.29	0.82	0.60	0.28	0.60	2.50
3. Check if reference values were re-established after opening drain D25 D	18h 05min	0.05	1.35	0.03	0.55	0.03	1.94	-	-	-	-	1.05	0.74	0.50	0.27	0.50	4.11
(17 Oct. 2006)	9h 30 min	0.05	1.30	0.03	0.50	0.04	2.01	-	-	-	-	1.03	0.73	0.50	0.26	0.50	4.15
4. Lowest test interval (22.0 – 23.57 m)	10h 55min	0.05	1.30	0.03	0.50	0.04	1.96	-	1.96	-	1.99	1.06	0.73	0.50	0.27	0.50	4.14
5. 19.0 m – 23.57 m	12h 00min	0.05	1.30	0.03	0.50	0.03	1.97	-	1.97	-	1.73	1.03	0.75	0.50	0.26	0.50	4.12
6. 16.0 m – 23.57 m	12h 40min	0.05	1.30	0.03	0.50	0.04	1.97	-	1.97	-	1.47	1.01	0.71	0.50	0.26	0.50	4.07
7. 13.0 m – 23.57 m	13h 20min	0.05	1.30	0.03	0.50	0.03	1.99	-	1.99	-	1.19	0.99	0.71	0.50	0.26	0.50	4.06
8. 10.0 m – 23.57 m	13h 50min	0.05	1.30	0.03	0.50	0.04	1.96	-	1.96	-	0.92	0.97	0.71	0.50	0.26	0.50	4.02
9. 7.0 m – 23.57 m	14h 45min	0.05	1.30	0.03	0.50	0.04	1.97	0.14	1.83	-	0.79	1.01	0.71	0.50	0.27	0.50	4.08
10. 7.0 m – 23.57 m. Pipes closed	15h 30min	0.05	1.30	0.03	0.525	0.02	1.93	-	1.93	1.90	2.72	0.99	0.72	0.50	0.26	0.50	3.99
11. Check if reference values were re-established	16h 55min				0.50	0.04	1.98	-	1.98	-	-						4.07
12. 4.0 m – 23.57 m	17h 00min	0.05	1.30	0.03	0.55	0.04	1.96	1.81	0.15	-	0.52	1.00	0.72	0.50	0.26	0.50	4.06
13. 4.0 m – 23.57 m. Pipes closed	17h 40min	0.05	1.45	0.04	0.95	0.04	0.85	-	0.85	2.95	3.46	1.12	0.75	0.55	0.27	0.55	3.12
14. Check if reference values were re-established	19h 25min	0.05	1.35	0.03	0.50	0.03	1.97	-	-	-	-	1.01	0.71	0.50	0.27	0.55	4.07
15. 1.0 m – 23.57 m	19h 40min	0.05	1.35	0.03	0.55	0.04	1.92	1.92	-	-	0.23	1.00	0.72	0.50	0.27	0.55	4.03
16. Check if reference values were re-established	9h 20min	0.05	1.30	0.03	0.50	0.03	2.01	-	-	-	-	1.00	0.71	0.50	0.27	0.50	4.10
(18 Oct. 2006)																	
17. 7.0 m – 10.0 m	10h 20min	0.05	1.30	0.03	0.50	0.04	2.04	0.13	1.91	-	0.81	0.98	0.71	0.50	0.26	0.50	4.11
18. 7.0 m – 10.0 m. Pipes closed	11h 03min	0.05	1.30	0.03	0.50	0.04	2.02	-	2.02	1.90	2.70	0.99	0.72	0.50	0.27	0.50	4.12
19. Check if reference values were re-established	12h 40min	0.05	1.30	0.03	0.50	0.04	2.00	-	2.00	-	-	1.00	0.72	0.50	0.26	0.50	4.10
20. 4.0 m – 7.0 m	13h 10min	0.05	1.30	0.03	0.60	0.04	1.84	1.81	0.03	-	0.51	1.02	0.72	0.50	0.27	0.50	3.97
21. 4.0 m – 7.0 m. Pipes closed	13h 30min	0.05	1.60	0.05	1.35	0.03	0.19	-	0.19	4.35	4.85	1.20	0.78	0.60	0.28	0.60	2.57
22. Check if reference values were re-established	16h 15min	0.05	1.40	0.03	0.50	0.04	2.02	-	2.02	-	-	1.04	0.72	0.50	0.27	0.55	4.17

Test step	Time when readings began	D20 D	D21 D	D22 D	PZB 13-2	D23 D	PZB 13-1	D24 D	D25 D	D26 D					D27 D	PZB12	D28 D	D29 D	D30 D	D31 D	D32 D	PZB11	PZB 13-3	Total discharge
		discharge (l/min)	discharge (l/min)	discharge (l/min)	water press. (bar)	discharge (l/min)	water press. (bar)	discharge (l/min)	discharge (l/min)	discharge (l/min)			water pressure (bar)		discharge (l/min)	Water press. (bar)	discharge (l/min)	discharge (l/min)	discharge (l/min)	discharge (l/min)	discharge (l/min)	water pressure (bar)	water pressure (bar)	(l/min)
										total	test interval	above test interval	at pipes head	pressure transducer										
1. Reference values (21 Mar. 2007)	9h 50min	0.91	0.11	0.07	1.55	0.04	0.50	0.03	2.18	1.33	-	-	-		1.11	0.60	0.30	0.09	0.29	0.07	0.76	0.0	0.60	7.29
2. 7.0 m – 26.0 m		0.91	0.11	0.07	1.55	0.04	0.50	0.03	2.18	1.33	-	1.33	-		1.11	0.60	0.30	0.09	0.29	0.07	0.76	0.0	0.60	7.29
3. 6.0 m – 26.0 m		0.91	0.11	0.07	1.55	0.04	0.50	0.03	2.18	1.33	-	1.33	-		1.11	0.60	0.30	0.09	0.29	0.07	0.76	0.0	0.60	7.29
4. 5.0 m – 26.0 m		0.91	0.11	0.07	1.55	0.04	0.50	0.03	2.18	1.00	-	1.00	-		1.11	0.60	0.30	0.09	0.29	0.07	0.76	0.0	0.60	6.96
5. 4.0 m – 26.0 m		0.92	0.11	0.07	1.55	0.04	0.50	drops	2.25	0.92	0.92	-	-	0.48	1.19	0.675	0.32	0.09	0.30	0.07	0.76	0.0	0.60	7.04
6. 4.0 m – 26.0 m. Pipes closed	19h 10min	0.92	0.11	0.07	1.60	0.04	0.50	drops	2.42	-	-	-	4.475	4.88	1.33	0.80	0.33	0.09	0.30	0.07	0.76	0.0	0.60	6.44
7. Check if reference values were re-established	20h 30min	0.93	0.11	0.07	1.55	0.04	0.50	drops	2.15	1.42	-	-	-	-			No measurements were taken					0.60	-	

Note: In steps 2, 3 and 4 readings were only taken in drain D26 D. Readings shown for the other drains and piezometers are reference values.

Test step	Time when readings began	D20 D	D21 D	D22 D	PZB 13-2	D23 D	PZB 13-1	D24 D	D25 D	D26 D	D27 D					PZB12	D28 D	D29 D	D30 D	D31 D	D32 D	PZB11	PZB 13-3	Total discharge
		discharge	discharge	discharge	water pressu.	discharge	water pressu.	discharge	discharge	discharge	discharge (l/min)					water pressu.	discharge	discharge	discharge	discharge	discharge	water pressu.	water pressu.	(l/min)
		(l/min)	(l/min)	(l/min)	(bar)	(l/min)	(bar)	(l/min)	(l/min)	(l/min)	total	test interval	above test interval	at pipes head	press. Transducer	(bar)	l/min	l/min	l/min	l/min	l/min	(bar)	(bar)	(l/min)
1. Reference values (15 Mar. 2007)	10h 00min	0.91	0.10	0.06	1.50	0.04	0.60	drops	2.15	1.33	0.94	-	-	-	0.70	0.31	0.09	0.11 ⁽¹⁾	0.07	0.73	0.0	0.60	6.84	
2. D27 D closed (16 Mar. 2007)	10h 00min	0.90	0.11	0.07	1.50	0.04	0.60	drops	2.17	1.34	-	-	-	0.40	0.80	0.38	0.10	0.11 ⁽¹⁾	0.06	0.74	0.0	0.60	6.02	
3. Reference values (20 Mar. 2007)	13h 00 min	0.88	0.10	0.07	1.50	0.04	0.60	drops	2.21	1.31	1.15	-	-	-	0.65	0.31	0.09	0.30 ⁽²⁾	0.07	0.74	0.0	0.60	7.27	
4. Lowest test interval (19.0 m – 23.0 m)	16h 45min	0.88	0.10	0.07	1.50	0.04	0.60	drops	2.21	1.31	1.15	-	1.15	-	1.71	0.65	0.31	0.09	0.30	0.07	0.74	0.0	0.60	7.27
5. 16.0 m – 23.0 m	17h 00min	0.88	0.10	0.07	1.50	0.04	0.60	drops	2.21	1.31	1.15	-	1.15	-	1.44	0.65	0.31	0.09	0.30	0.07	0.74	0.0	0.60	7.27
6. 13.0 m – 23.0 m	17h 30min	0.88	0.10	0.07	1.50	0.04	0.60	drops	2.21	1.31	1.15	-	1.15	-	1.18	0.65	0.31	0.09	0.30	0.07	0.74	0.0	0.60	7.27
7. 10.0 m – 23.0 m	17h 45min	0.88	0.10	0.07	1.50	0.04	0.60	drops	2.21	1.31	1.15	-	1.15	-	0.89	0.65	0.31	0.09	0.30	0.07	0.74	0.0	0.60	7.27
8. 7.0 – 23.0 m	18h 00min	0.88	0.10	0.07	1.50	0.04	0.60	drops	2.21	1.31	1.15	-	1.15	-	0.62	0.65	0.31	0.09	0.30	0.07	0.74	0.0	0.60	7.27
9. 4.0 m – 23.0 m	18h 35min	0.88	0.10	0.07	1.50	0.04	0.60	drops	2.21	1.31	1.11	0.59	0.52	-	0.39	0.65	0.31	0.09	0.30	0.07	0.74	0.0	0.60	7.27
10. 4.0 m – 23.0 m Pipes closed	19h 10min	0.90	0.11	0.07	1.50	0.03	0.50	drops	2.18	1.33	1.04	-	1.04	0.25	0.61	0.65	0.31	0.09	0.29	0.07	0.75	0.0	0.60	7.17
11. 1.0 m – 23.0 m	16h 45min																							
12. 0.66 – 23.0m Pipes closed	20h 15min	0.91	0.11	0.07	1.55	0.04	0.50	drops	2.19	1.35	0.22	-	0.22	0.55	0.58	0.75	0.34	0.09	0.30	0.07	0.76	0.0	0.60	6.45
13. Check if reference values were re-established (21 Mar. 2007)	9h 50min	0.91	0.11	0.07	1.55	0.04	0.50	0.03 ⁽³⁾	2.18	1.33	1.11	-	-	-	0.60	0.30	0.09	0.29	0.07	0.76	0.0	0.6	7.29	

⁽¹⁾ Looses water close to the T pipe

⁽²⁾ drain D30 D repaired

⁽³⁾ drain D24 D with obstructions removed

Test step	Time when readings began	D16 D	D17 D	PZB 14-2	D18 D	PZB 14-1	D19 D	D20 D					D21 D	D22 D	PZB 13-2	D23 D	PZB 13-1	D24 D	D25 D	PZB 13-3	Total discharge	
		Discharge (l/min)	discharge (l/min)	water pressure (bar)	discharge (l/min)	water pressure (bar)	discharge (l/min)	discharge (l/min)			water pressure (bar)		discharge (l/min)	discharge (l/min)	water pressure (bar)	discharge (l/min)	water pressure (bar)	discharge (l/min)	discharge (l/min)	water pressure (bar)	(l/min)	
								total	test interval	above test interval	at pipes head	transducer										
1. reference values	20h 30min 21 Mar 07	1.07	1.39	0.80	0.05	5.85	0.21	0.93	-	-	-	-	0.11	0.07	1.55	0.04	0.50	drops	2.15	0.60	6.02	
2. D20 D closed with a pressure gauge at its head	9h 30min 22 Mar 07	1.06	1.42	0.80	0.06	6.0	0.46	-	-	-	1.20	-	0.44	0.07	1.60	0.04	0.50	drops	2.15	0.80	5.70	
3. check if reference values were re-established	15h 00min	1.06	1.45	0.80	0.05	5.85	0.21	0.95	-	-	-	-	0.10	0.06	1.50	0.04	0.50	drops	2.19	0.60	6.11	
Single packer	4. 16.0 m – 22.25 m	16h 30min	1.06	1.45	0.80	0.05	5.85	0.21	0.96	-	0.96	-	1.50	0.10	0.06	1.50	0.04	0.50	drops	2.19	0.60	6.12
	5. 13.0 m – 22.25 m	16h 40min	1.06	1.45	0.80	0.05	5.85	0.21	0.96	-	0.96	-	1.21	0.10	0.06	1.50	0.04	0.50	drops	2.19	0.60	6.12
	6. 10.0 m – 22.25 m		1.06	1.45	0.80	0.05	5.85	0.21	0.96	-	0.96	-		0.10	0.06	1.50	0.04	0.50	drops	2.19	0.60	6.12
	7. 7.0 m – 22.25 m	18h 40min	1.06	1.45	0.80	0.05	5.85	0.21	0.96	0.24	0.72	-	0.78	0.10	0.06		0.04	0.50	drops	2.19	0.60	6.12
	8. 7.0 m – 22.25 m Pipes closed	19h 15min	1.02	1.42	0.80	0.05	5.95	0.53	0.83	-	0.83	1.80	2.50	0.12	0.07	1.55	0.04	0.50	drops	2.20	0.60	6.28
	9. 4.0 m – 22.25 m	19h 45 min	1.06	1.45	0.80	0.05		0.21	0.79	0.79	-	-	0.49	0.10	0.06		0.04		drops	2.19		5.95
	10. 4.0 m – 22.25 m Pipes closed	20h 30m 22 Mar 07	1.05	1.44	0.80	0.06	6.00	0.46	0.09	-	0.09	0.9	1.33	0.43	0.07	1.60	0.04	0.55	drops	2.20	0.70	5.84
		9h 30min 23 Mar 07	1.04	1.44	0.82	0.06	6.00	0.46	0.06	-	0.06	1.0	1.4	0.44	0.07	1.60	0.04	0.55	drops	2.18	0.80	5.79
	11. 1.0 m – 22.25 m								0.77	0.77	drops	-										
	12. 1.0 m – 22.25 m Pipes closed	11h 15min	1.05	1.45	0.80	0.06	6.00	0.47	-	-	-	1.1	1.14	0.45	0.07	1.60	0.04	0.55	drops	2.15	0.75	5.74
	Double packer	13. 4.0 m – 7.0 m	12h 30min						0.67	0.67	-		0.52									
		14. 4.0 m – 7.0 m Pipes closed	13h 00min	1.05	1.47	0.80	0.06	6.00	0.46	-	-	-	0.95	1.31	0.45	0.07	1.60	0.04	0.55	drops	2.16	0.75
15. 7.0 m – 10.0 m Pipes closed								0.97	0.23	0.74	1.20	1.84										

Note: In test steps 4, 5, 6 and 7 readings were only taken in drain D20 D. Readings shown for the other drains and piezometers are measurements taken in test step 3.

Test step	Time when readings began	D16 D	D17 D	PZB 14-2	D18 D	PZB 14-1	D19 D	D20 D					D21 D	D22 D	PZB 13-2	D23 D	PZB 13-1	D24 D	D25 D	PZB 13-3	Total discharge	
		discharge (l/min)	discharge (l/min)	water pressu. (bar)	discharge (l/min)	water pressu. (bar)	discharge (l/min)	discharge (l/min)			water pressure (bar)		discharge (l/min)	discharge (l/min)	water pressure (bar)	discharge (l/min)	water pressure (bar)	discharge (l/min)	discharge (l/min)	water pressure (bar)	(l/min)	
								total	test interval	above test interval	at pipes head	pressu. transducer										
1. Reference values (3 Set. 07)	17h 00min	1.14	1.34	0.65	0.04	3.40	0.14	0.58	-	-	-	-	0.04	0.05	1.35	drops	0.40	drops	1.75	0.60	5.08	
2. D20 D closed	20h 00min	1.16	1.30	0.65	0.04	3.55	0.31	-	-	-	0.75 ⁽¹⁾	-	0.24	0.06	1.35	drops	0.40	drops	1.71	0.70	4.82	
3. Check if reference values were re-established (4 Set. 07)	9h 40min	1.15	1.29	0.70	0.04	3.25	0.14	0.62	-	-	-	-	0.04	0.05	1.35	drops	0.40	drops	1.73	0.60	5.06	
Single packer	4. 10.0 m – 22.5 m							0.62	-	0.62	-	-										
	5. 9.0 m – 22.5 m							0.61	-	0.61	-	-										
	6. 8.0 m – 22.5 m	12h 20min						0.13	0.62	0.14	0.48	-	-	0.03								
	7. 8.0 m – 22.5 m Pipes closed	15h 15min	1.15	1.30	0.65	0.04	3.42	0.14	0.48	-	0.48	1.50 ⁽⁷⁾	3.36 ⁽²⁾	0.04	0.05	1.35	drops	0.40	drops	1.75	0.60	5.10
	8. Check if reference values were re-established	15h 30min							0.63	0.15	0.48											
	9. 7.0 m – 22.5 m	15h 45 min							0.13	0.63	0.15	0.48	-	-	0.03							5.08
	10. 7.0 m – 22.5 m Pipes closed (4 e 5 Set. 07)	17h 30m	1.19	1.29	0.65	0.04	3.45	0.14	0.53	-	0.53	1.45 ⁽⁷⁾	2.39 ⁽³⁾	0.04	0.05	1.35	drops	0.40	drops	1.73	0.60	5.01
		8h 50min	1.15	1.27	0.65	0.04	3.45	0.13	0.54	-	0.54	1.50 ⁽⁷⁾	3.25 ⁽⁴⁾	0.04	0.05	1.35	drops	0.40	drops	1.73	0.60	4.98
	11. Check if reference values were re-established	10h 00min							0.62	0.15	0.47	-										
	12. 6.0 m – 22.5 m	10h 25min							0.62	0.12	0.50	-	-									
	13. 5.0 m – 22.5 m	11h 30min							0.60	0.43	0.17	-	-									
	14. 5.0 m – 22.5 m Pipes closed	12h 05min	1.17	1.30	0.65	0.04	3.40	0.19	0.41	-	0.41	0.25 ⁽⁷⁾	1.82 ⁽⁵⁾	0.14	0.05	1.35	drops	0.40	drops	1.75	0.60	5.05
	15. Check if reference values were re-established								0.63													
	16. 4.0 m – 22.5 m								0.13	0.57	0.57	0.0			0.04							
	17. 4.0 m – 22.5 m Pipes closed	17h 15min	1.18	1.31	0.65	0.04	3.55	0.32	0.0	-	0.0	0.675 ⁽⁷⁾	2.15 ⁽⁶⁾	0.25	0.06	1.35	0.05	0.40	drops	1.74	0.70	4.95

(next test steps in the following page)

Double packer	18. 5.0 m – 6.0 m	19h 10min							0.54	0.37	0.17	-	-										
	19. 5.0 – 6.0 m Pipes closed (6 Set. 07)	9h 15min	1.15	1.33	0.65	0.04	3.40	0.20	0.37	-	0.37	0.24 ⁽⁷⁾	1.79 ⁽⁸⁾	0.14	0.05	1.35	drops	0.40	drops	1.74	0.60	5.39	
	20. Check if reference values were re-established	10h 30min					3.25	0.13	0.62	-	-	-	-	0.03									
	21. 4.0 m – 5.0 m	11h 00min						0.20	0.33	0.33	0.0	-	-	0.15									
	22. 4.0 m – 5.0 m Pipes closed	15h 30min	1.14	1.28	0.65	0.05	3.50	0.32	-	-	-	0.65 ⁽⁷⁾	2.12 ⁽⁹⁾	0.25	0.05	1.35	0.03	0.40	drops	1.75	0.70	4.87	
	23. 4.0 m – 7.0 m	18h 00min							0.48	0.48	-	-	-										
	24. 4.0 m – 7.0 m Pipes closed (6 e 7 Set. 2007)	22h 00m	1.16	1.28	0.65	0.04	3.60	0.31	-	-	-	0.60 ⁽⁷⁾	2.07 ⁽¹⁰⁾	0.24	0.05	1.35	0.03	0.40	drops	1.73	0.725	4.84	
		9h 40min	1.14	1.27	0.65	0.04	3.60	0.30	-	-	-	0.625 ⁽⁷⁾	2.08 ⁽¹¹⁾	0.24	0.05	1.40	0.03	0.40	drops	1.74	0.725	4.81	
25. Check if reference values were re-established	11h 00min	1.15	1.27	0.65	0.04	3.20	0.19	0.57	-	-	-	-	0.04	0.05	1.35	0.03	0.40	drops	1.75	0.60	5.09		

(1) pressure gauge at level 61.20 m

(2) 3.36 – 1.81 = 1.53 bar

(3) 2.39 – 1.72 = 0.67 bar

(4) 3.25 – 1.72 = 1.53 bar

(5) 1.82 – 1.53 = 0.29 bar

(6) 2.15 – 1.43 = 0.72 bar

(7) pressure gauge at level 61.92 m

(8) 1.79 – 1.53 = 0.26 bar

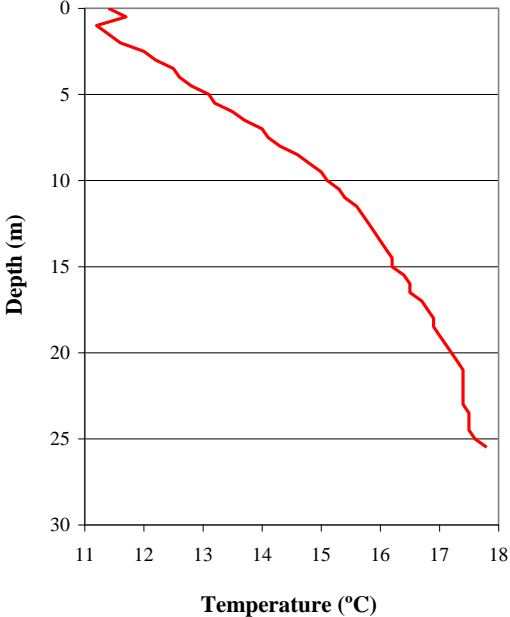
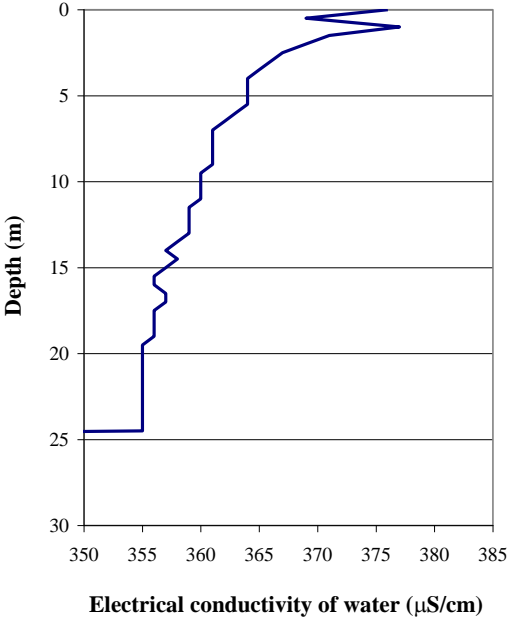
(9) 2.12 – 1.43 = 0.69 bar

(10) 2.07 – 1.43 = 0.64 bar

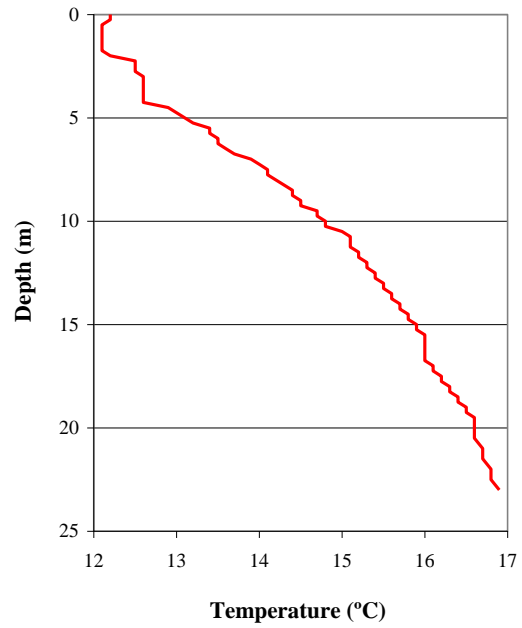
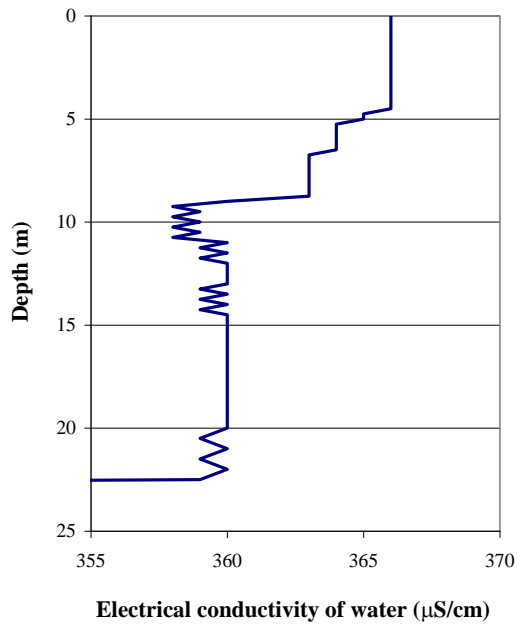
(11) 2.08 – 1.43 = 0.65 bar

A1.5 Electrical conductivity of water and temperature profiles

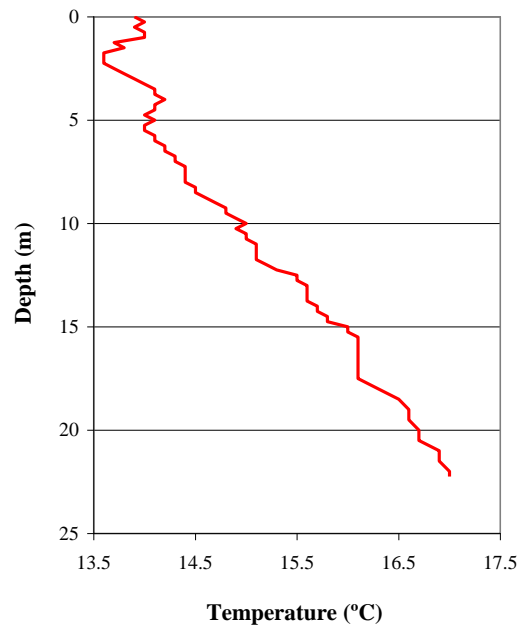
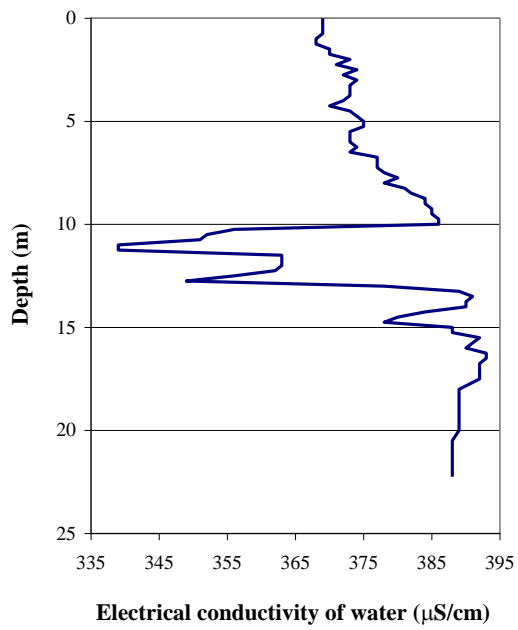
The depth at which the concrete/rock mass interface occurs is shown in gray or green in each graph, with the exception of those regarding boreholes where rotary-percussive drilling was used because no information is available about the section of the borehole which goes through concrete.



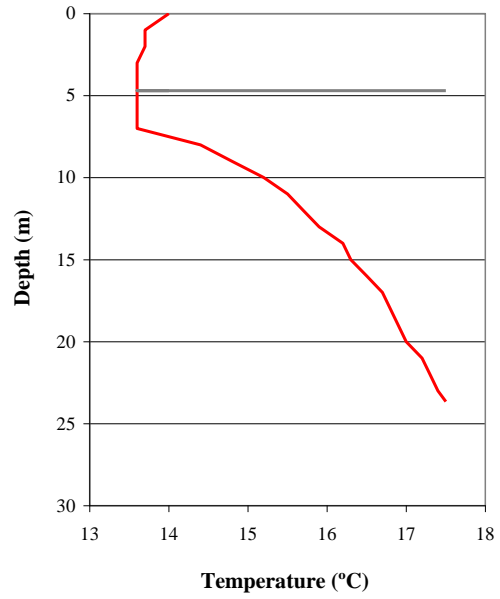
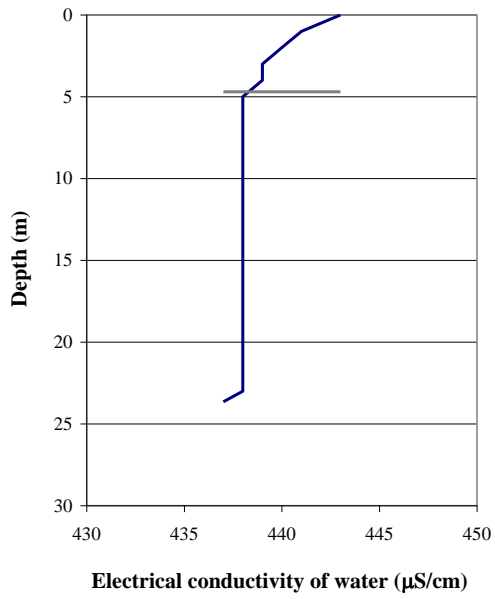
Electrical conductivity of water and temperature profiles along drain **D26 D** (1.33 l/min)



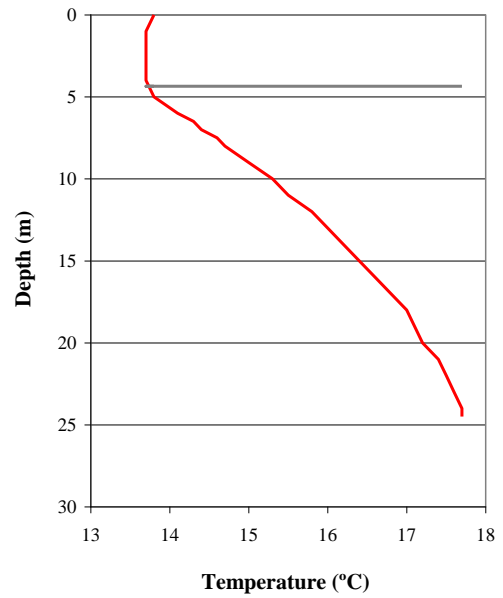
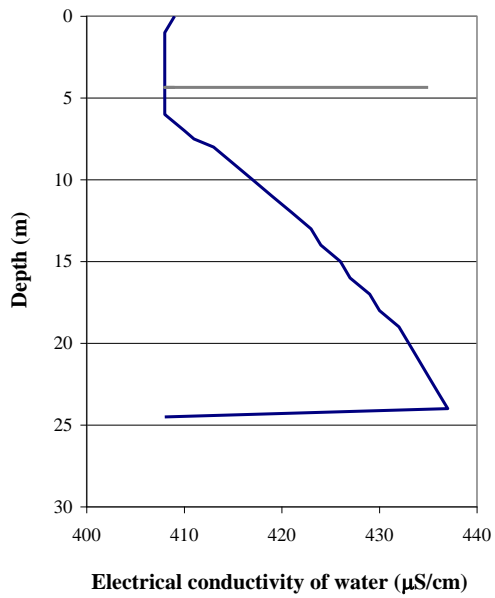
Electrical conductivity of water and temperature profiles along drain **D27 D** (0.94 l/min)



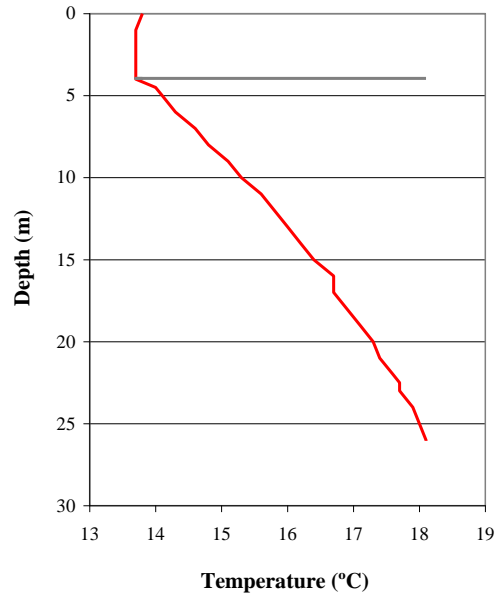
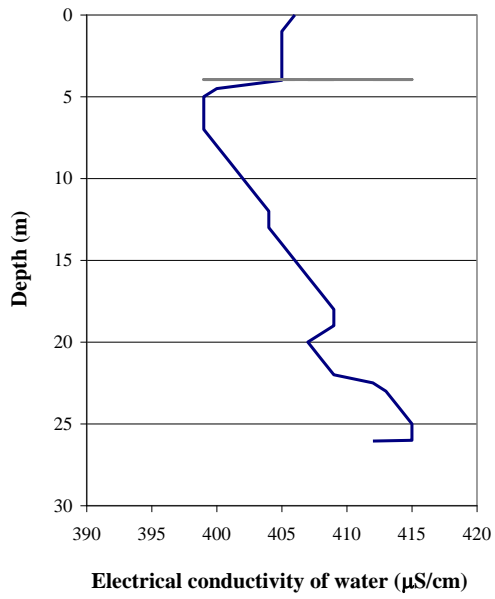
Electrical conductivity of water and temperature profiles along drain **D20 D** (0.93 l/min)



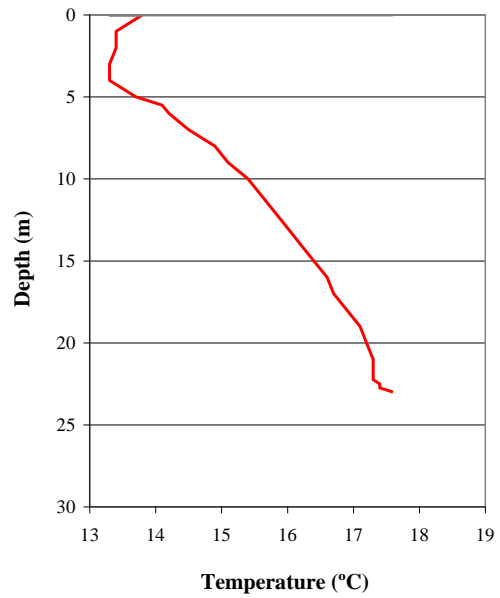
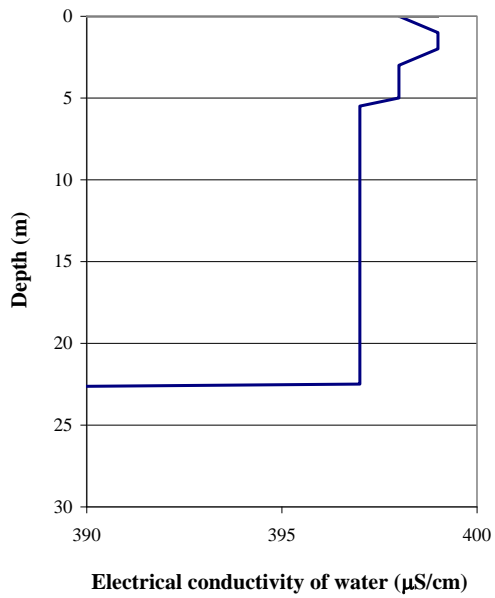
Electrical conductivity of water and temperature profiles along drain **D32 D** (0.76 l/min)



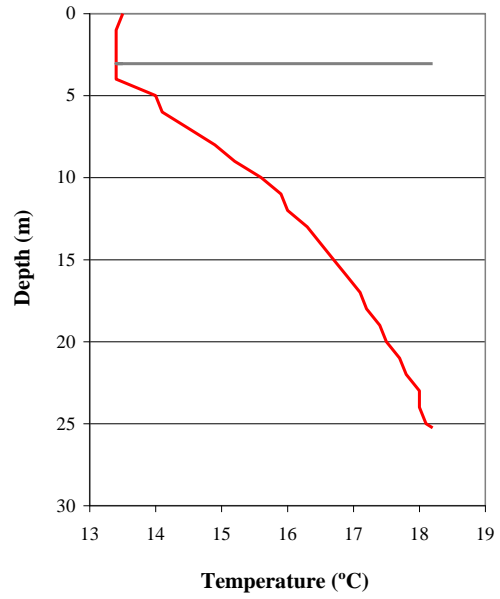
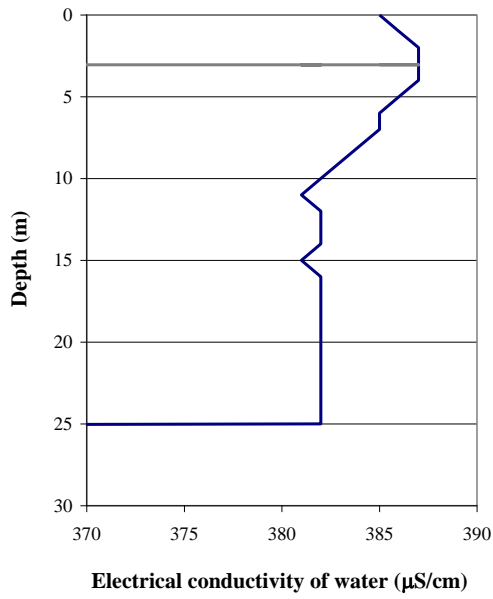
Electrical conductivity of water and temperature profiles along drain **D30 D** (0.29 l/min)



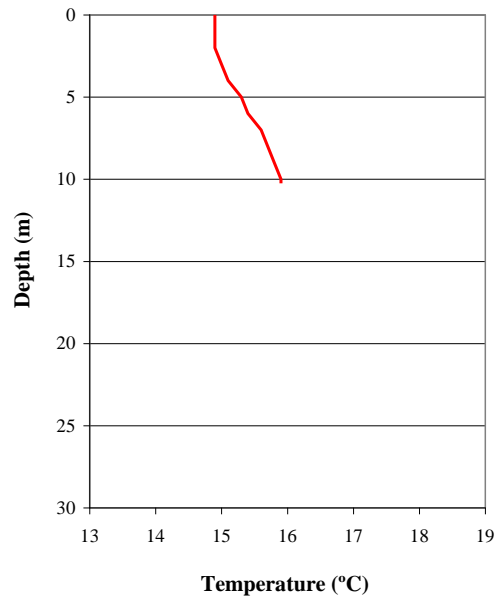
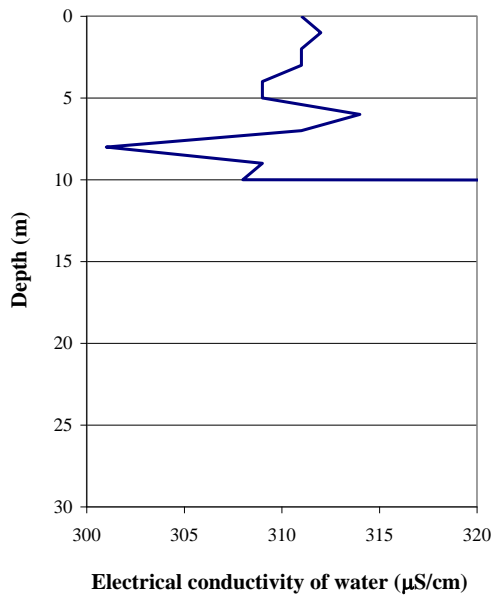
Electrical conductivity of water and temperature profiles along drain **D28 D** (0.32 l/min)



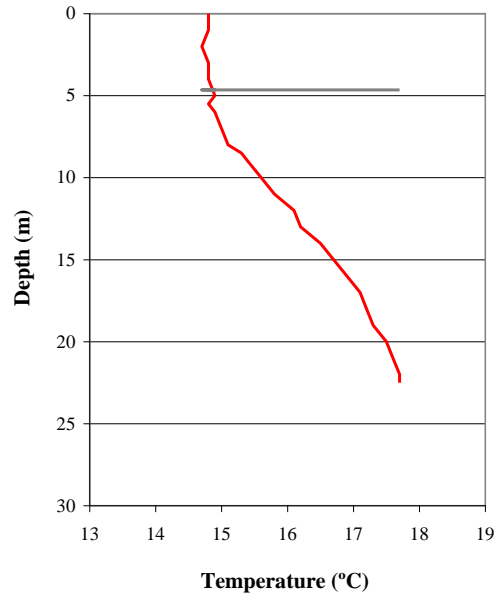
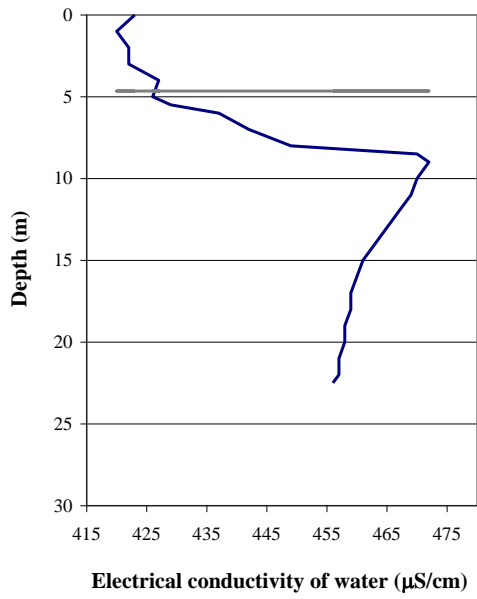
Electrical conductivity of water and temperature profiles along drain **D27 D** (1.01 l/min)



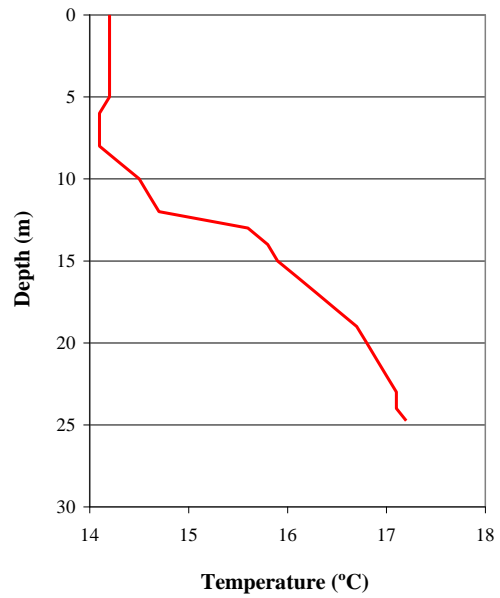
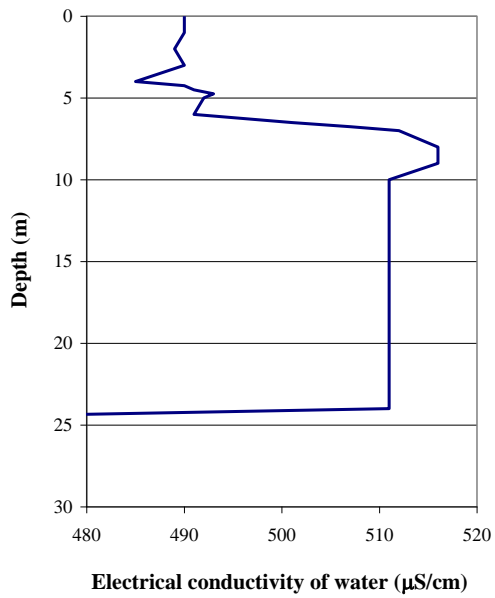
Electrical conductivity of water and temperature profiles along drain **D26 D** (1.26 l/min)



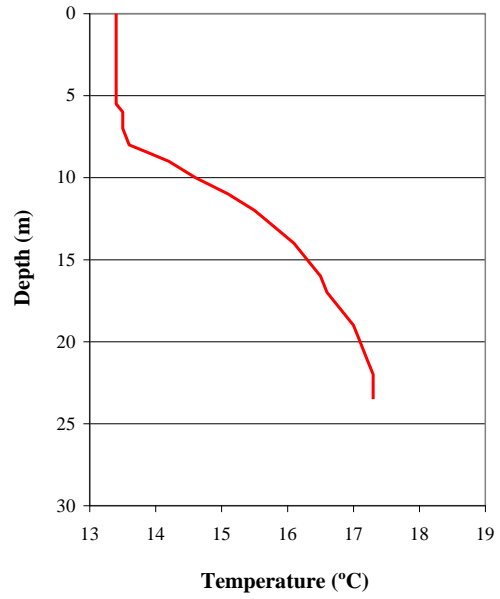
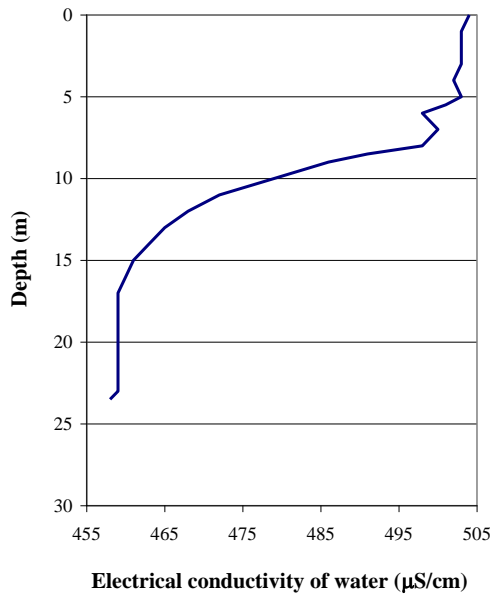
Electrical conductivity of water and temperature profiles along drain **D23 D** (0.04 l/min)



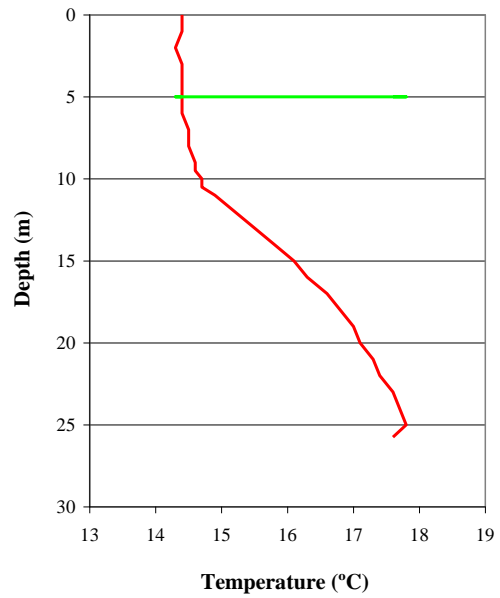
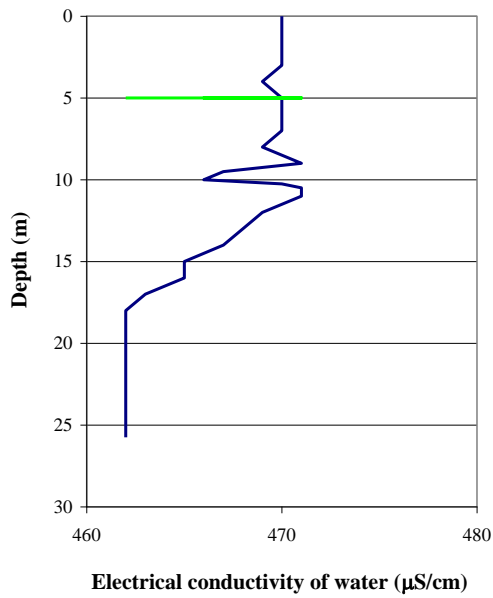
Electrical conductivity of water and temperature profiles along drain **D20 D** (0.90 l/min)



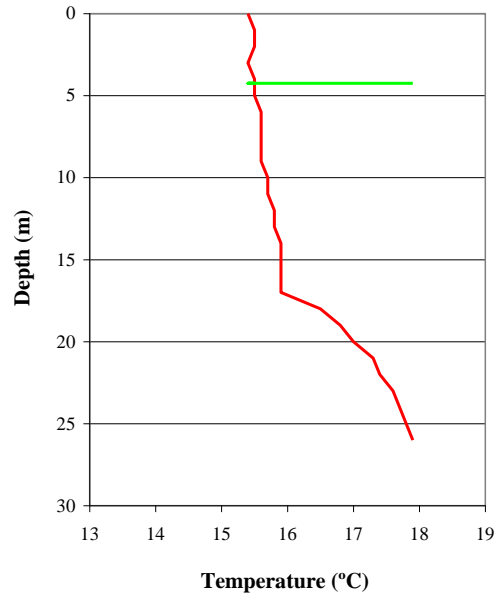
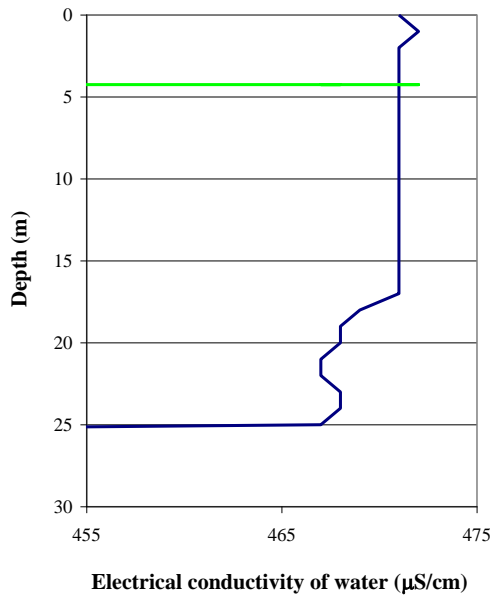
Electrical conductivity of water and temperature profiles along drain **D19 D** (0.19 l/min)



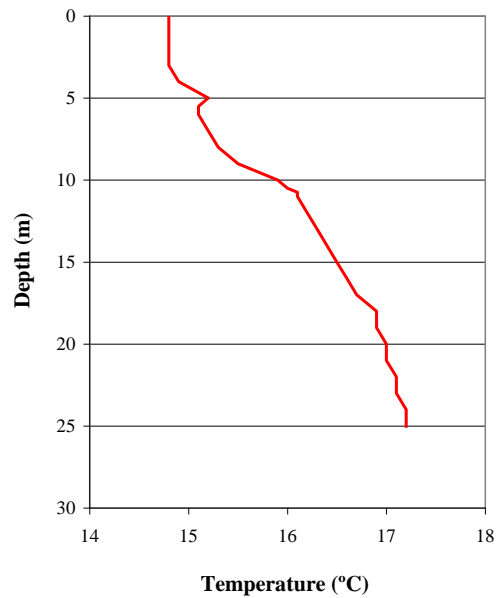
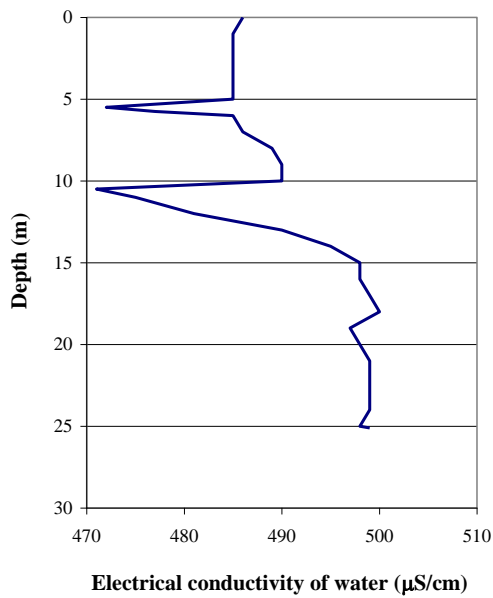
Electrical conductivity of water and temperature profiles along drain **D17 D** (1.38 l/min)



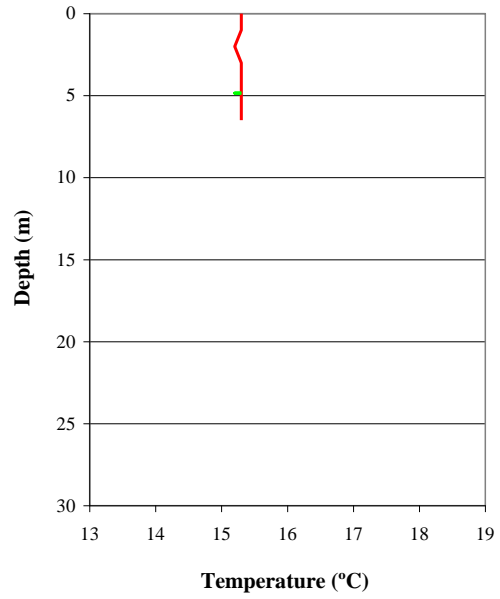
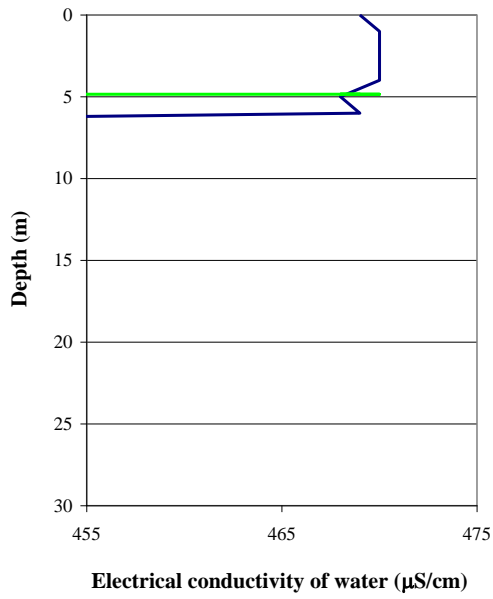
Electrical conductivity of water and temperature profiles along drain **D16 D** (1.09 l/min)



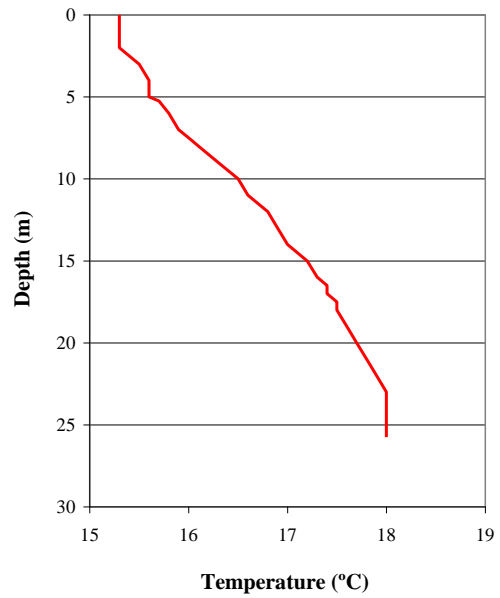
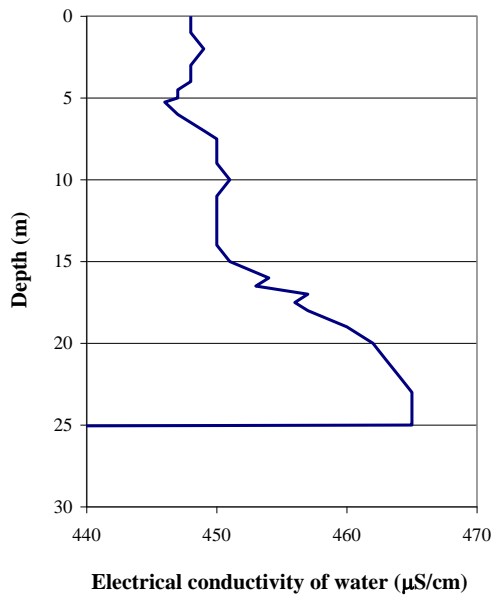
Electrical conductivity of water and temperature profiles along drain **D14 D** (1.53 l/min)



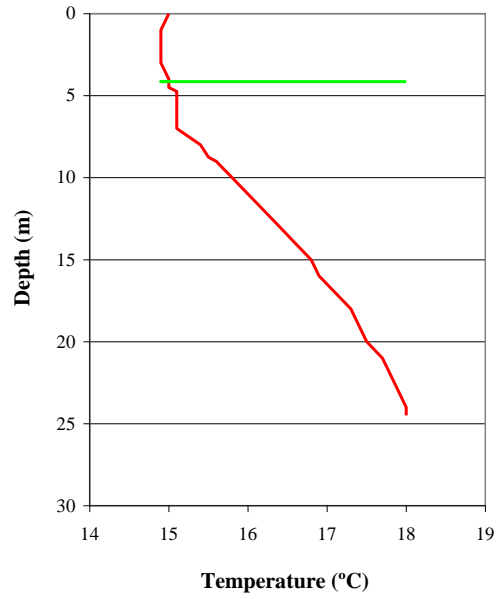
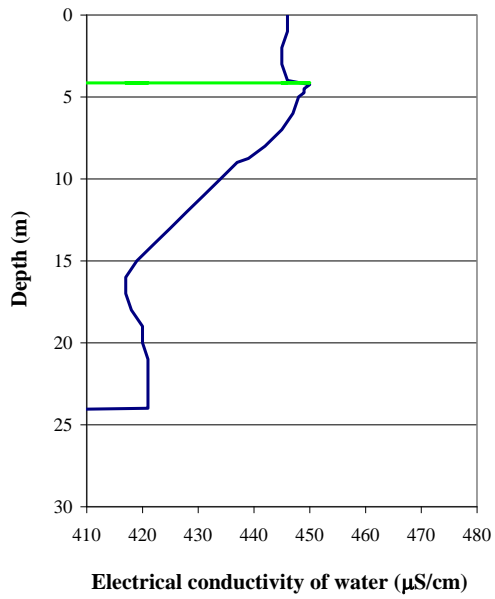
Electrical conductivity of water and temperature profiles along drain **D13 D** (0.35 l/min)



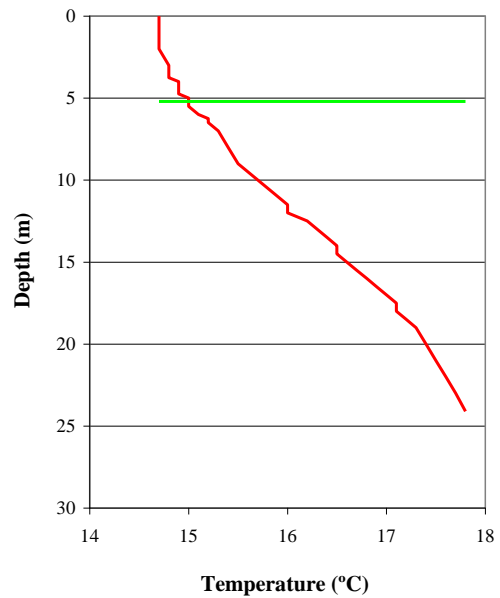
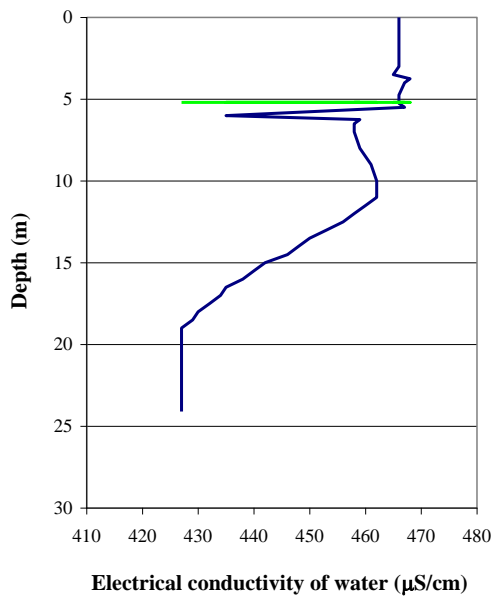
Electrical conductivity and temperature profiles along drain **D12 D** (1.50 l/min)



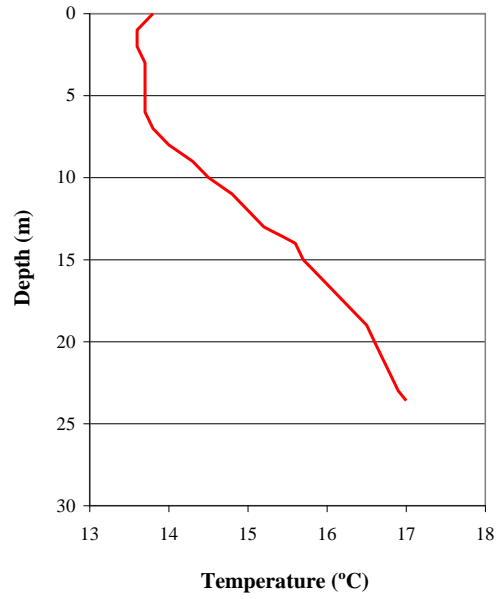
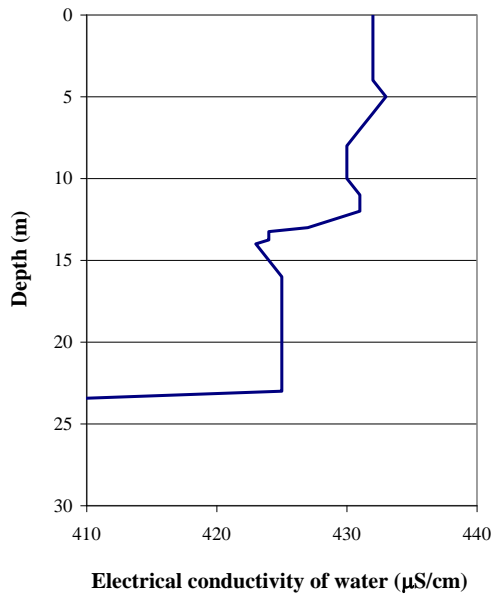
Electrical conductivity of water and temperature profiles along drain **D11 D** (0.32 l/min)



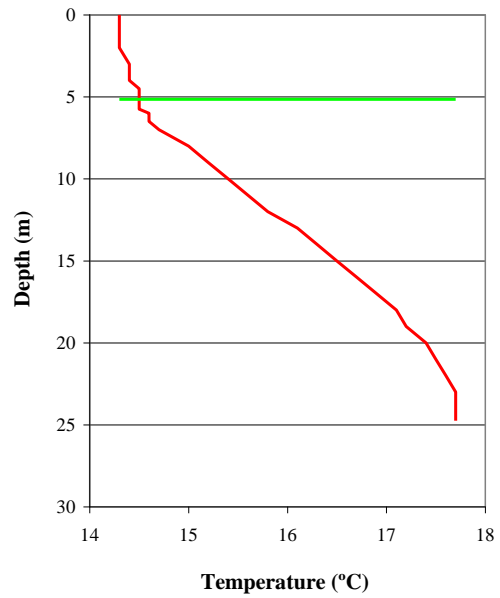
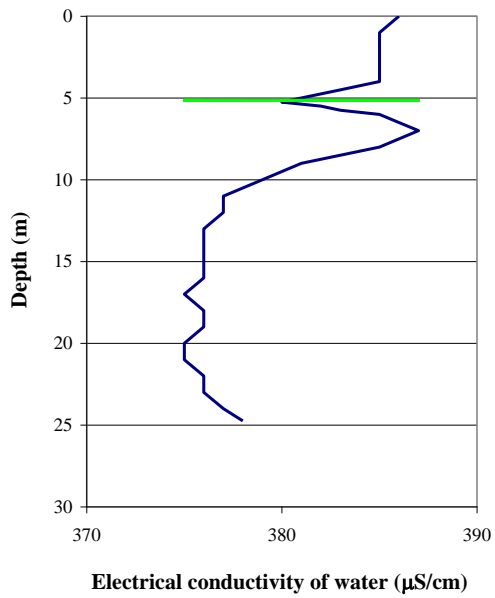
Electrical conductivity of water and temperature profiles along drain **D10 D** (0.57 l/min)



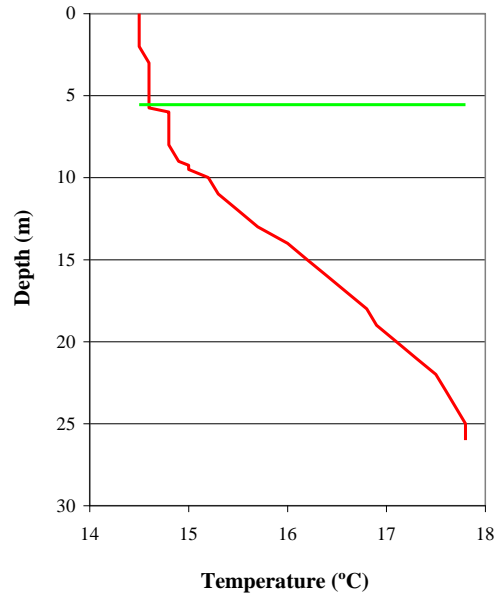
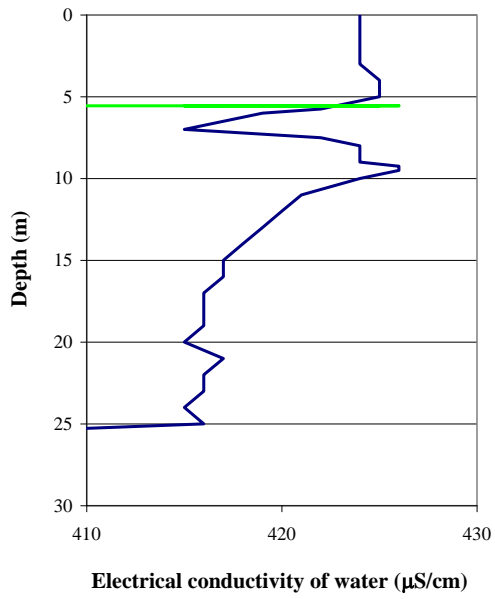
Electrical conductivity of water and temperature profiles along drain **D8 D** (0.20 l/min)



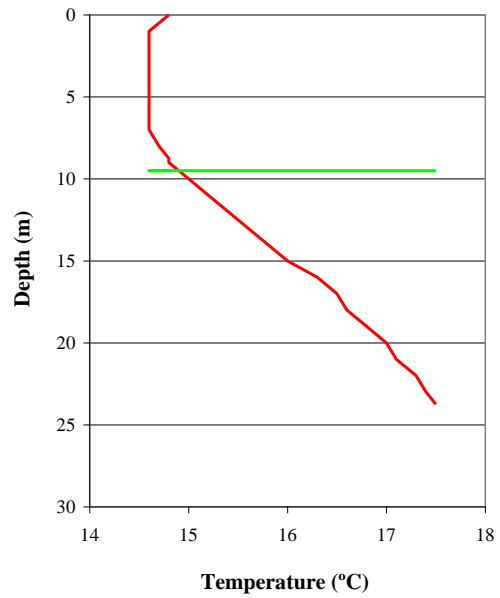
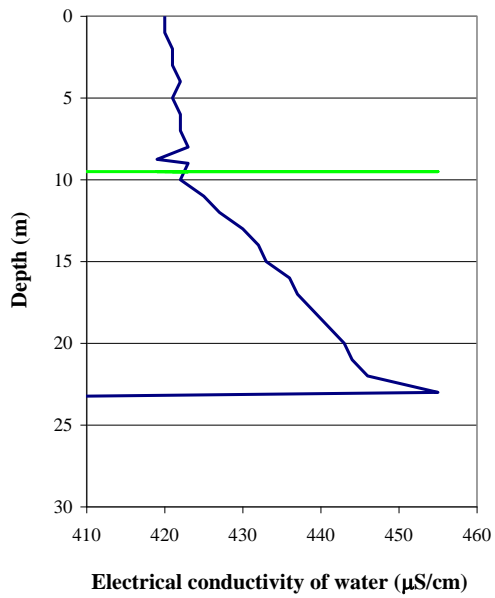
Electrical conductivity of water and temperature profiles along drain **D7 D** (0.50 l/min)



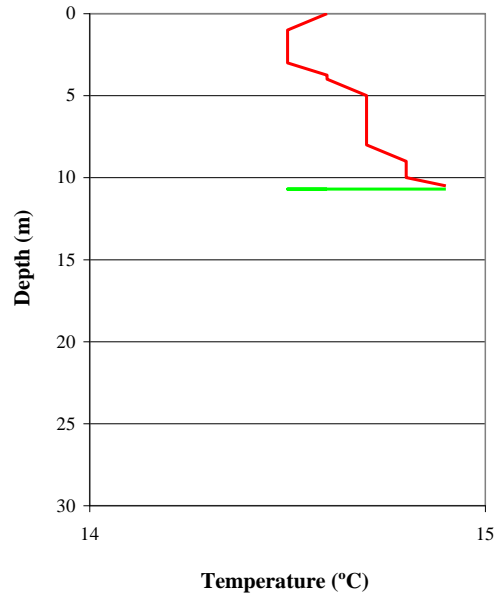
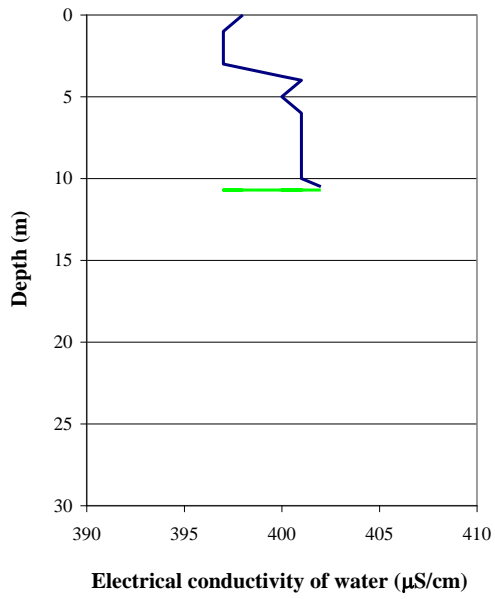
Electrical conductivity of water and temperature profiles along drain **D6 D** (0.26 l/min)



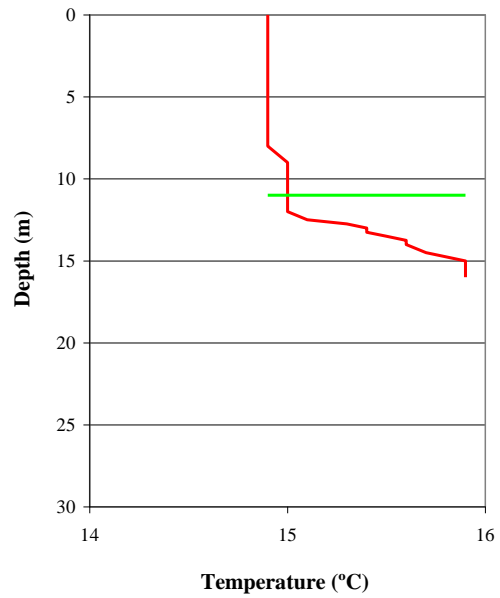
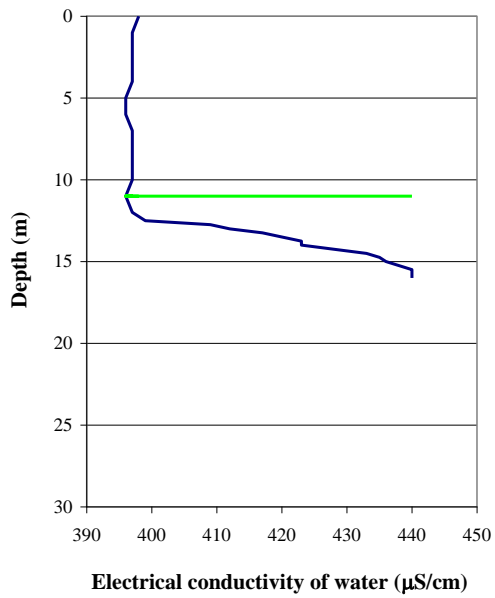
Electrical conductivity of water and temperature profiles along drain **D4 D** (0.16 l/min)



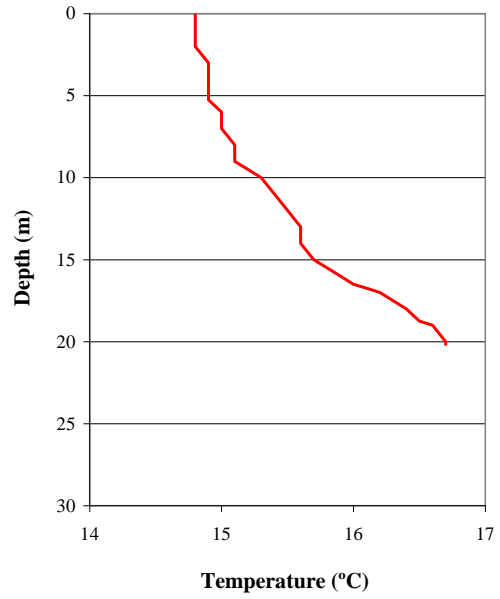
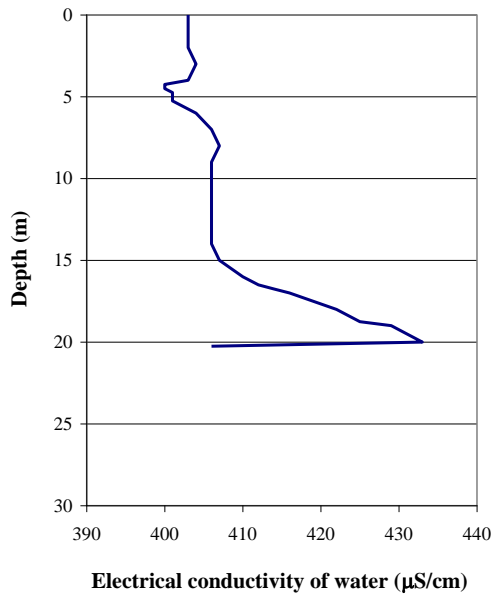
Electrical conductivity of water and temperature profiles along drain **D2 D** (0.29 l/min)



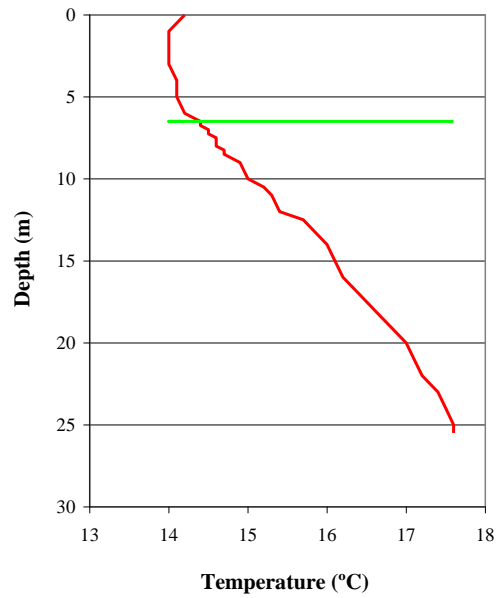
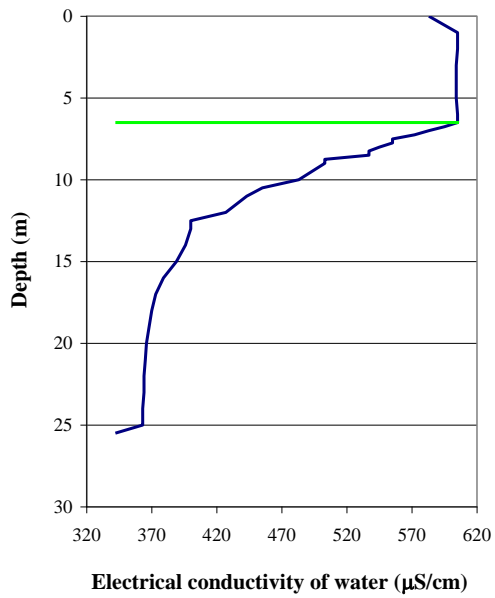
Electrical conductivity of water and temperature profiles along drain **D1 E** (0.16 l/min)



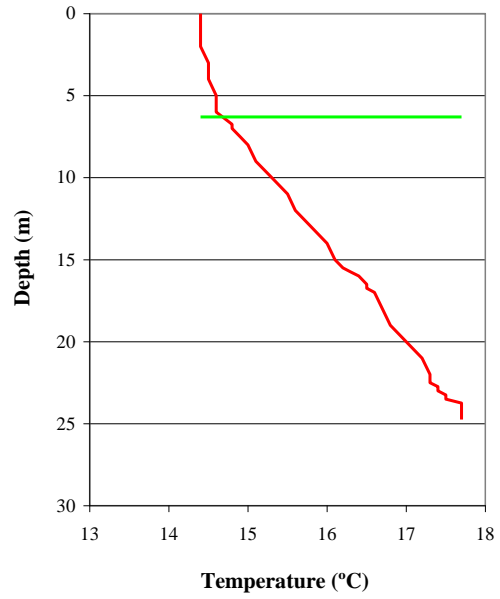
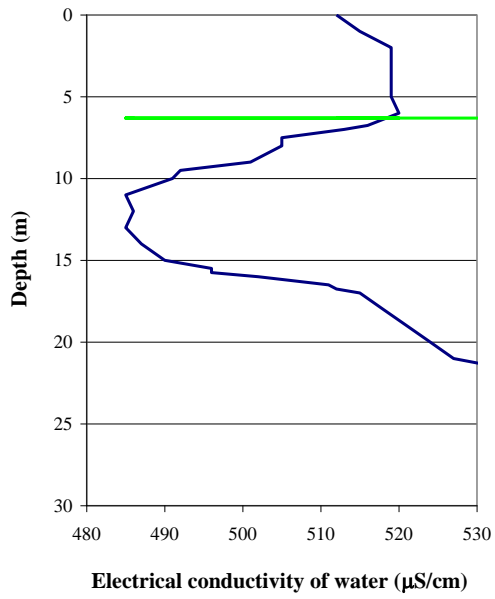
Electrical conductivity of water and temperature profiles along drain **D3 E** (1.00 l/min)



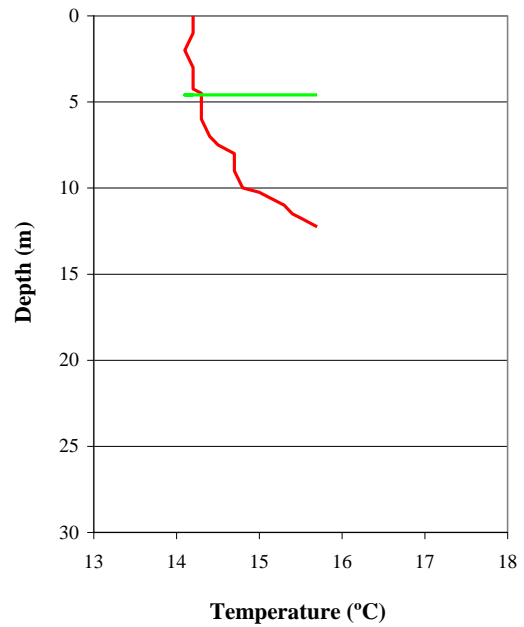
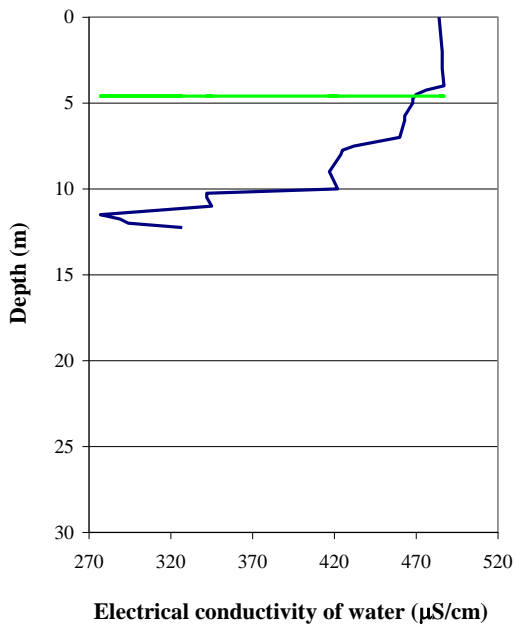
Electrical conductivity of water and temperature profiles along drain **D4 E** (0.74 l/min)



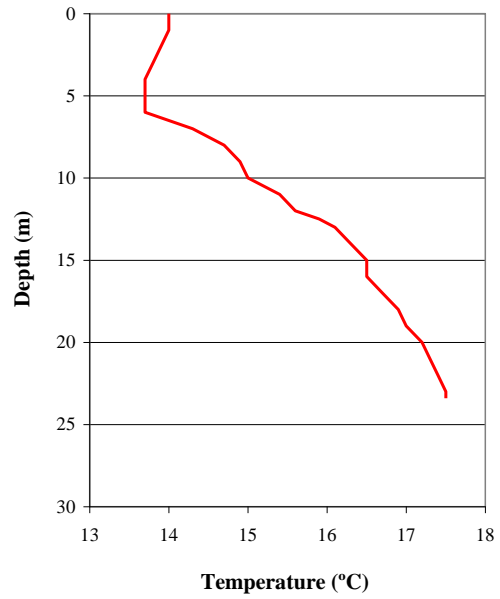
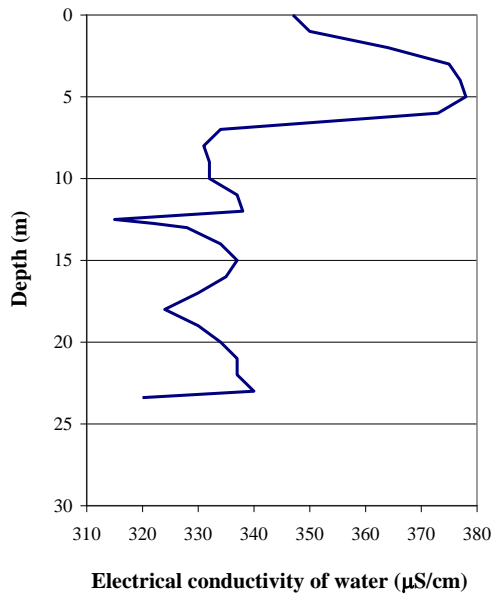
Electrical conductivity of water and temperature profiles along drain **D7 E** (0.18 l/min)



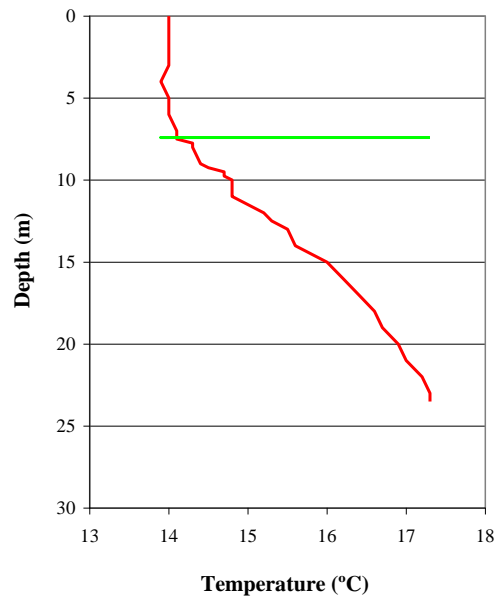
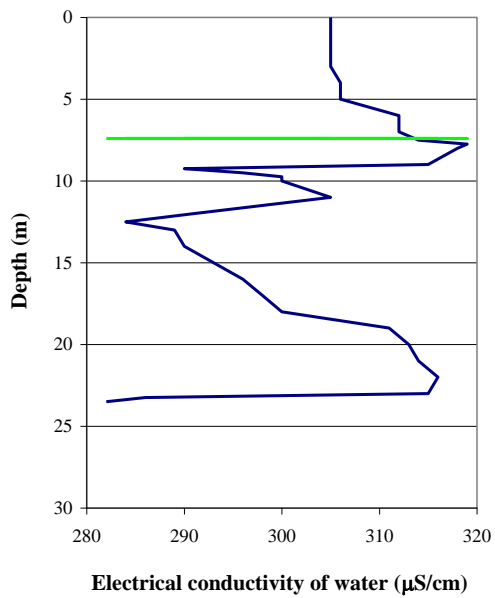
Electrical conductivity of water and temperature profiles along drain **D9 E** (0.21 l/min)



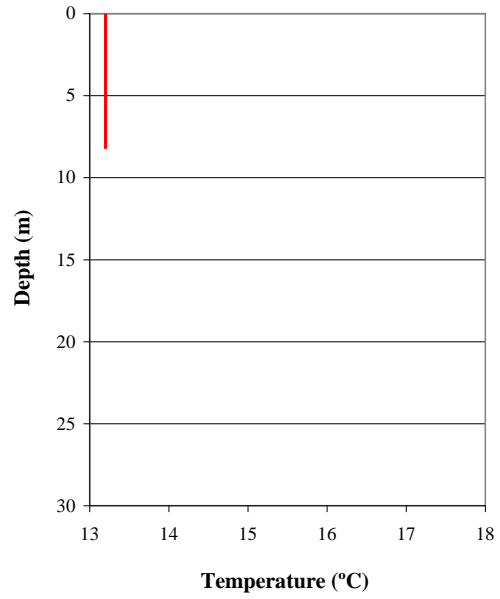
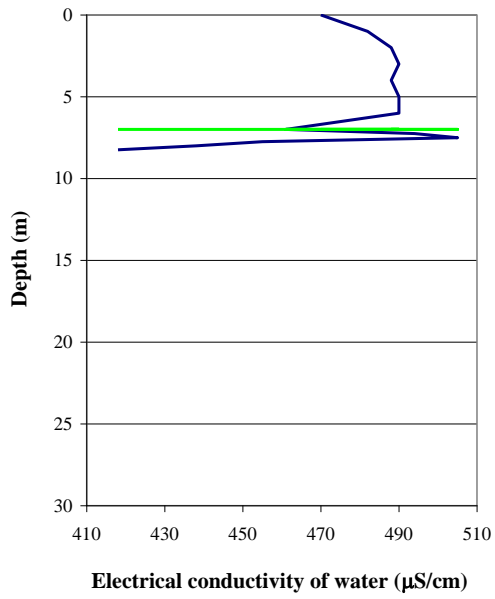
Electrical conductivity of water and temperature profiles along drain **D11 E** (1.12 l/min)



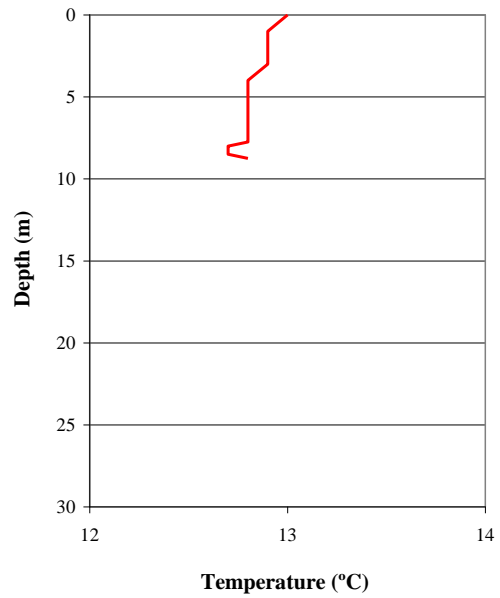
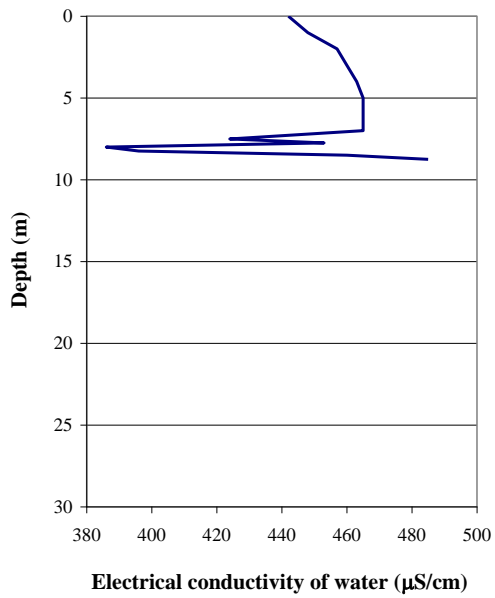
Electrical conductivity of water and temperature profiles along drain **D16 E** (0.90 l/min)



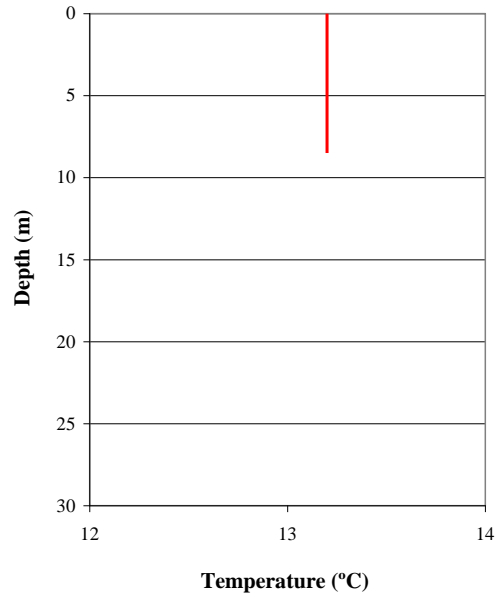
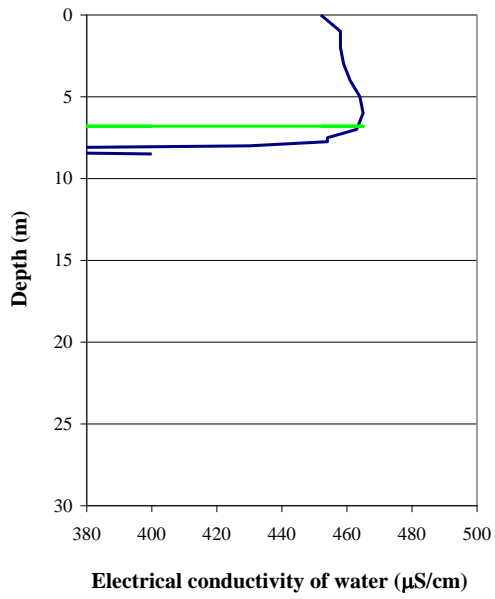
Electrical conductivity of water and temperature profiles along drain **D17 E** (0.13 l/min)



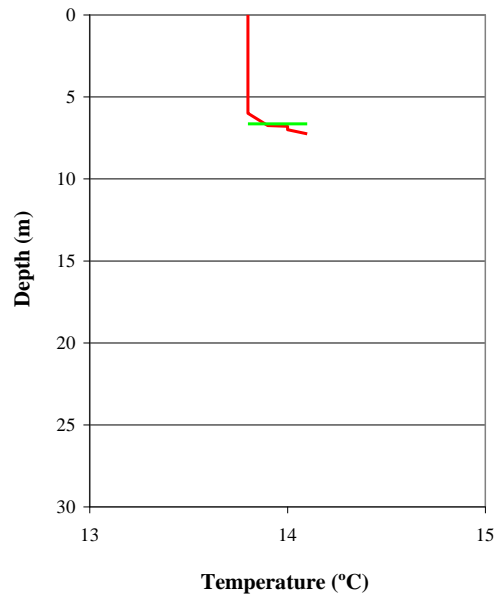
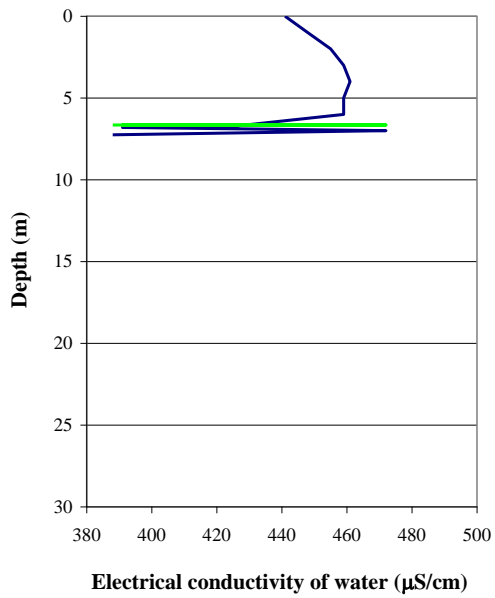
Electrical conductivity of water and temperature profiles along drain **D19 E** (0.99 l/min)



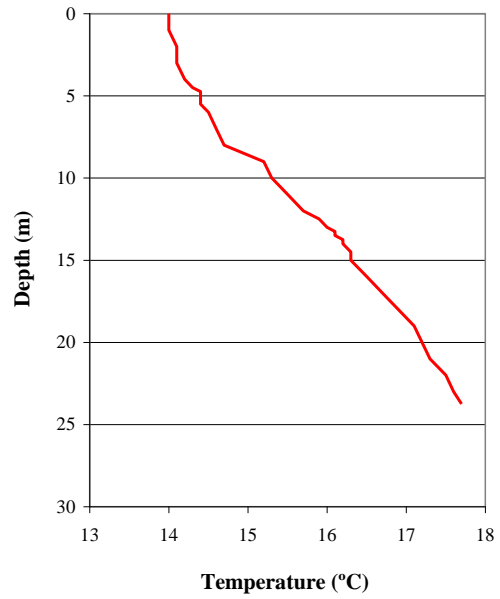
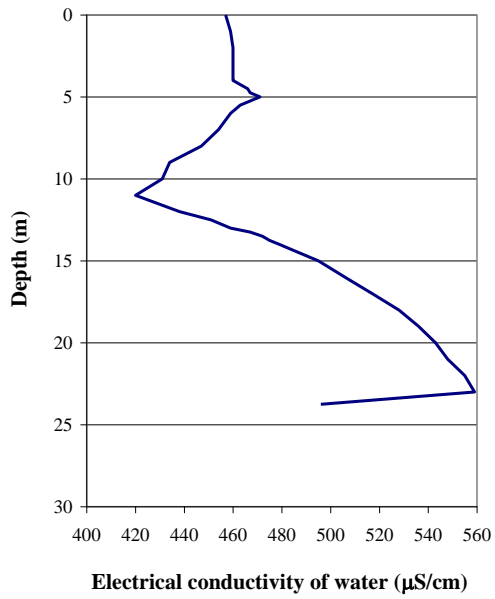
Electrical conductivity of water and temperature profiles along drain **D20 E** (1.05 l/min)



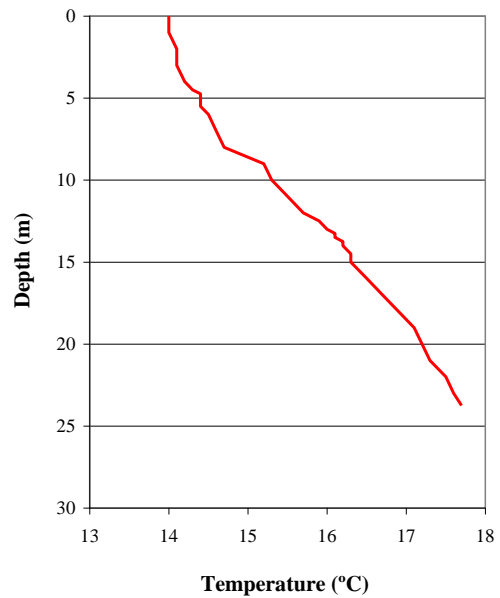
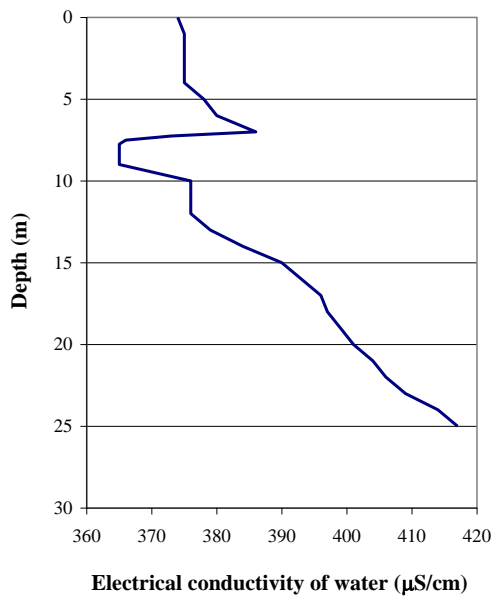
Electrical conductivity of water and temperature profiles along drain **D21 E** (1.53 l/min)



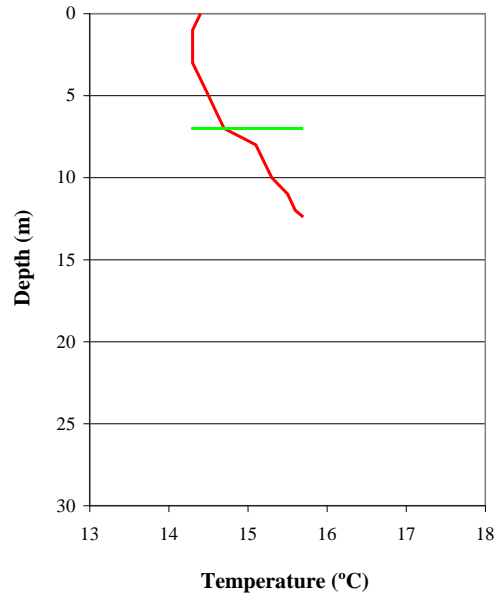
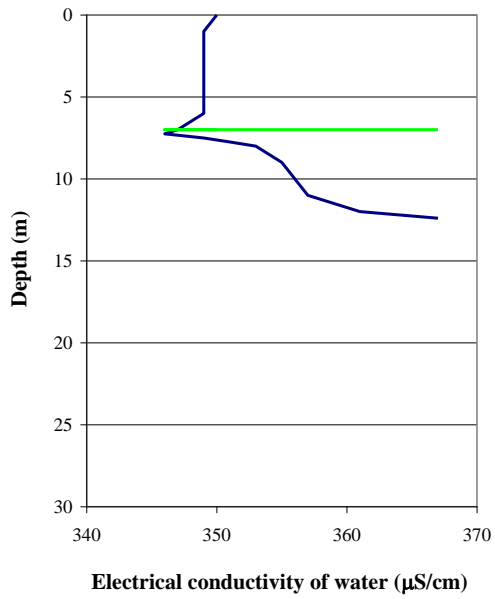
Electrical conductivity of water and temperature profiles along drain **D23 E** (0.16 l/min)



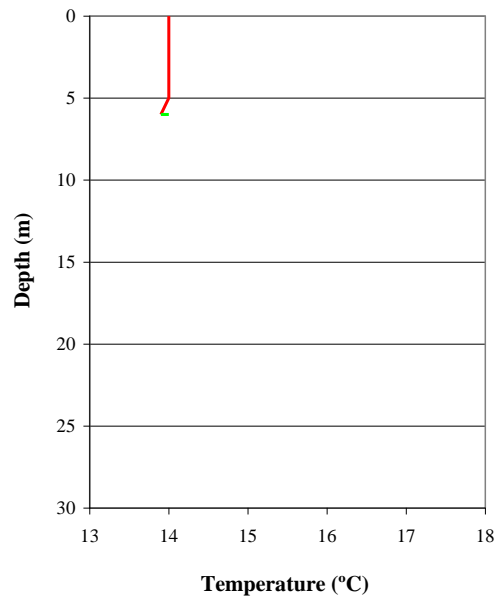
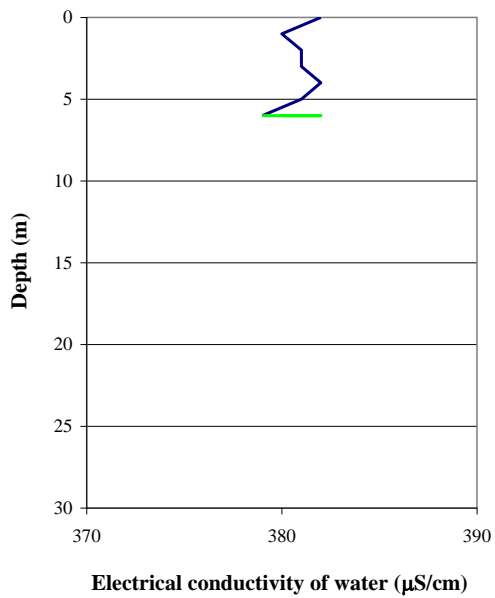
Electrical conductivity of water and temperature profiles along drain **D24 E** (0.16 l/min)



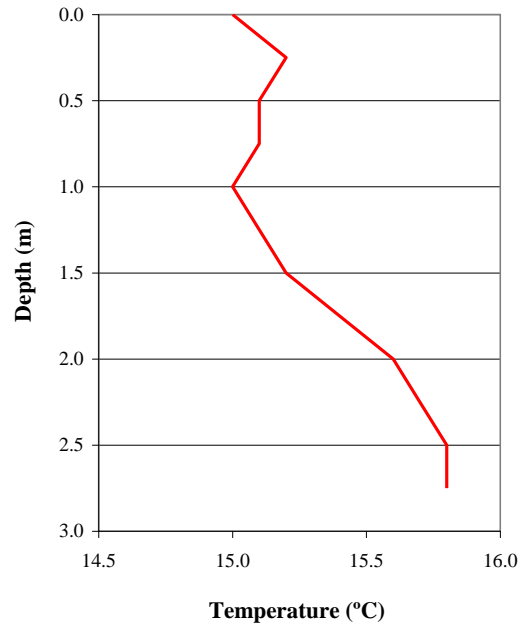
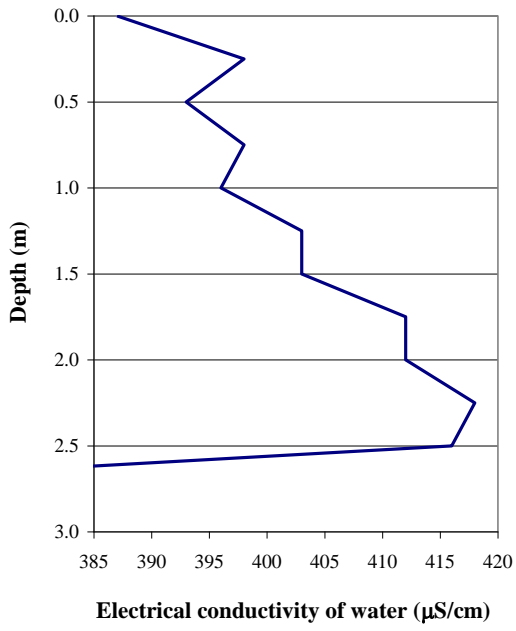
Electrical conductivity of water and temperature profiles along drain **D24 E-1** (0.48 l/min)



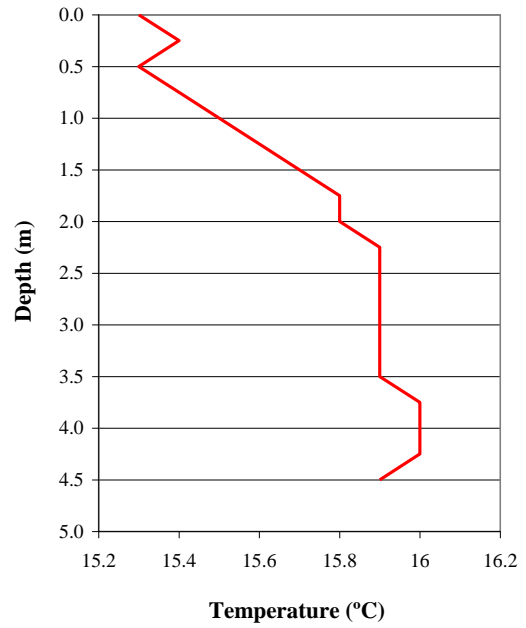
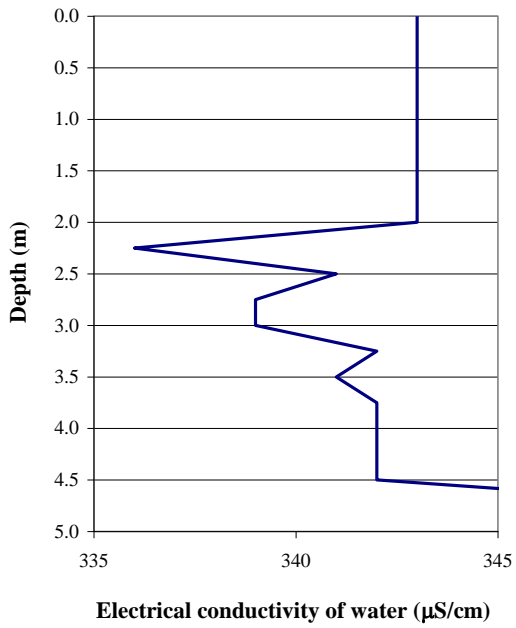
Electrical conductivity of water and temperature profiles along drain **D25 E** (0.19 l/min)



Electrical conductivity of water and temperature profiles along drain **D25 E-1** (1.34 l/min)



Electrical conductivity of water and temperature profiles along drain **DGDJI-5D** (0.41 l/min)



Electrical conductivity of water and temperature profiles along drain **DGDJI-2D** (0.05 l/min)

A1.6 Measurements taken when all the drains and piezometers located in block 17-18 were closed

Borehole	Block	Normal operating conditions	Drains D25 D and D26 D closed	Drains D21 D to D26 D closed	Total discharge in the three different situations (l/min)
		Water pressure (bar) or discharge (l/min)	Water pressure (bar) or discharge (l/min)	Water pressure (bar) or discharge (l/min)	
D16 D	16-17	1.16 l/min	1.17 l/min	1.17 l/min	i) 3.23
D17 D		1.29 l/min	1.29 l/min	1.29 l/min	ii) 3.26
PZB 14-2		0.75 bar	0.75 bar	0.75 bar	iii) 3.34
D18 D		0.04 l/min	0.03 l/min	0.03 l/min	
PZB 14-1		3.90 bar	3.90 bar	3.90 bar	
D19 D		0.15 l/min	0.16 l/min	0.17 l/min	
D20 D		0.59 l/min	0.61 l/min	0.68 l/min	
D21 D	17-18	0.04 l/min	0.04 l/min	0.275 bar	i) 1.63
D22 D		0.04 l/min	0.05 l/min	1.975 bar	ii) 0.21
PZB13-2		1.21 bar	1.85 bar	2.225 bar	iii) 0.05
D23 D		0.03 l/min	0.04 l/min	1.6 bar	
PZB13-1		0.35 bar	1.21 bar	1.75 bar	
D24 D		drops	0.04 l/min	2.7 bar	
D25 D		1.50 l/min	5.60 bar	5.6 bar	
PZB13-3		0.55 bar	0.75 bar	0.80 bar	
Leakage through the floor		0.02 l/min	0.04 l/min	0.05 l/min	
D26 D		18-19	1.07 l/min	5.05 bar	5.15 bar
D27 D	0.98 l/min		1.27 l/min	1.27 l/min	ii) 2.02
PZB 12	0.60 l/min		1.0 bar	1.0 bar	iii) 1.94
D28 D	0.31 l/min		0.42 l/min	0.35 l/min	
D29 D	0.07 l/min		0.06 l/min	0.06 l/min	
D30 D	0.26 l/min		0.27 l/min	0.26 l/min	
D31 D	19-20		0.04 l/min	0.03 l/min	0.03 l/min
D32 D		0.55 l/min	0.57 l/min	0.58 l/min	ii) 0.60 iii) 0.61

Recorded discharges and water pressures in blocks 16-17, 17-18, 18-19 and in two drains located in block 19-20: i) in normal operating conditions; ii) with both drains D25 D and D26 D closed, and iii) with drains D21 D to D26 D closed ($H_u = 148.0$ m; $H_d = 81.6$ m)